PACIFIC EARTHQUAKE ENGINEERING RESEARCH CENTER

Comparison of NGA-Sub Ground-Motion Models

Nicholas Gregor
Consultant

Kofi Addo
BC Hydro

Linda Al Atik
Consultant

Gail M. Atkinson
University of Western Ontario

David M. Boore
Geophysicist

Yousef Bozorgnia
University of California, Los Angeles

Kenneth W. Campbell
Core Logic

Brian S.-J. Chiou
California Department of Transportation

Zeynep Gülerce
Middle East Technical University

Behzad Hassani
BC Hydro

Tadahiro Kishida
Khalifa University of Science and Technology

Nico Kuehn
University of California, Los Angeles

Saburoh Midorikawa
Tokyo Institute of Technology

Silvia Mazzoni
University of California, Los Angeles

Grace A. Parker*
University of California, Los Angeles
*Now at the U.S. Geological Survey,
Moffett Field, California

Hongjun Si
Seismological Research Institute Inc.

Jonathan P. Stewart
University of California, Los Angeles

Robert R. Youngs
Wood Environmental and Infrastrucure
Solutions, Inc.

PEER Report 2020/07
Pacific Earthquake Engineering Research Center
Headquarters, University of California at Berkeley

November 2020

PEER 2020/07
November 2020

Comparison of NGA-Sub Ground-Motion Models

Nicholas Gregor
Consultant

Linda Al Atik
Consultant

David M. Boore
Geophysicist

Kenneth W. Campbell
Core Logic

Zeynep Gülerce
Middle East Technical University

Tadahiro Kishida
Khalifa University of Science and Technology

Saburoh Midorikawa
Tokyo Institute of Technology

Grace A. Parker*
University of California, Los Angeles

*Now at the U.S. Geological Survey, Moffett Field, California

Jonathan P. Stewart
University of California, Los Angeles

Kofi Addo
BC Hydro

Gail M. Atkinson
University of Western Ontario

Yousef Bozorgnia
University of California, Los Angeles

Brian S.-J. Chiou
California Department of Transportation

Behzad Hassani
BC Hydro

Nico Kuehn
University of California, Los Angeles

Silvia Mazzoni
University of California, Los Angeles

Hongjun Si
Seismological Research Institute Inc.

Robert R. Youngs
Wood Environmental and Infrastrucure Solutions, Inc.

PEER Report 2020/07
Pacific Earthquake Engineering Research Center
Headquarters at the University of California, Berkeley

November 2020

ABSTRACT

Ground-motion models (GMMs) for subduction earthquakes recently developed as part of the NGA-Subduction (NGA-Sub) project are compared in this report. The three models presented in this comparison report are documented in their respective PEER reports. Two of the models are developed for a global version and as well regionalized models. The third model is developed based on earthquakes contain in the NGA-Sub dataset only from Japan and as such is applicable for Japan. As part of the comparisons presented in this report, deterministic calculations are provided for the global and regional cases amongst the models. The digital values and additional plots from these deterministic comparisons are provided as part of the electronic supplement for this report. In addition, ground-motion estimates are provided for currently published subduction GMMs. Two example probabilistic seismic hazard analysis calculations are also presented for two sites located in the Pacific Northwest Region in the state of Washington. Based on the limited comparisons presented in this report, a general understanding of these new GMMs can be appreciated with the expectation that the implementation for a specific seismic hazard study should incorporate similar and additional comparisons and sensitivity studies similar to the ones presented in this report.

ACKNOWLEDGMENTS

This study was supported by FM Global, United States Geological Survey (USGS), California Department of Transportation (Caltrans), and the Pacific Earthquake Engineering Research Center (PEER). Any opinions, findings, conclusions, or recommendations expressed in this publication are those of the authors and do not necessary reflect those of the sponsoring agencies.

Following the tradition of previous NGA projects, the ground-motion modeling teams as well as database developers have had continuous technical interactions, which resulted in a higher quality of the final products than each researcher could achieve individually. Acknowledgments and thanks should be given to the over 32 junior and senior researchers who worked on various parts of the NGA-Sub research program. Their contribution, dedication, and teamwork are greatly acknowledged.

CONTENTS

LIST OF TABLES

LIST OF FIGURES

1 Overview

The Next generation attenuation (NGA) research program for subduction earthquakes (NGA-Sub) is the latest component of the NGA research series. NGA-Sub is a large multidisciplinary and multi-researcher research initiative to develop a comprehensive ground-motion database and multiple ground-motion models (GMMs) for subduction earthquakes. In the NGA-Sub project, a database of ground-motions recorded in worldwide subduction events [Bozorgnia and Stewart 2020] is developed. This database includes the processed recordings and supporting source, path, and site metadata from Japan, Taiwan, the U.S. Pacific Northwest, Alaska, Mexico and Central America, South America, and New Zealand. The NGA-Sub database includes 1570 events with moment magnitudes ranging from 4.0 to 9.1. The subduction events are classified as interface, intraslab, or outer-rise events. The NGA-Sub ground-motion database has over 210,000 individual ground-motion components. This is by far the largest ground-motion database that we have developed in any NGA project. Multiple GMMs have been developed by NGA-Sub developer teams using this empirical ground-motion database and supporting ground-motion simulations.

This report discusses and compares the currently developed NGA-Sub GMMs from three developer teams. Additional GMMs are expected to be developed from other developer teams, and the digital files provided with this report will allow for the inclusion of these additional models in the future. The current comparisons will be presented in the form of attenuation curves and response spectra for selected scenario cases. Note that only a selected subset of the full suite of comparison plots are presented in this report with the additional plots in the associated electronic documents; see Appendix A for the full description of the files. Given the wide range of applicability of the GMMs, a complete and exhaustive set of scenario cases would not be practical. However, the selected scenario cases are based on commonly determined controlling scenario cases in seismic hazard analyses, especially for sites located in the Pacific Northwest. It is recommended that prior to implementing and using these new NGA-Sub GMMs for a seismic hazard study, an assessment of their relative comparison and predictive features should be performed by the user, in addition to the comparisons presented in this report.

As part of the comparisons of the three new NGA-Sub models and their features, comparisons will also be provided relative to currently published and commonly used subduction GMMs. Similar to selection of a limited number of scenario cases, this comparison of the three new models with current models is not meant to be a complete comparison of all currently available subduction models. Rather it is a comparison with those models that have been considered in the USGS National Seismic Hazard Map [Petersen et al. 2014; 2020] and are commonly used in seismic hazard studies. More information about other models not selected for the comparison can be reviewed from the global database of GMMs maintained by

J. Douglas (*http://www.gmpe.org.uk*). In addition to the comparisons of median ground motion estimates, a summary comparison of the aleatory sigma models will be presented.

Given the importance of these new GMMs for application to the Pacific Northwest region, an example PSHA calculation is performed for two representative sites. These sites were selected based on their relative contribution from the deeper slab events and the Cascadia interface source in the region. The USGS [2014] seismic-source model is used for the PSHA, and sensitivity calculations are presented based on the previously published GMMs and the newly developed GMMs. These results illustrate the differences in the median predictions as well as the differences in the aleatory sigma models from the different GMMs.

The development and larger presentation of each of the three GMMs are provided in the individual PEER report from each developer team [Kuehn et al. 2020; Parker et al. 2020; and Si et al. 2020]. As such, this report will focus on the comparison of the results between the models and not discuss the technical decisions and choices used by the individual developer teams for the development of each model. For those decisions, the reader is referred to the individual PEER reports for each model.

2 GMM Regionalization and Applicability

Each developer team was provided the NGA-Sub database [Bozorgnia and Stewart 2020] from which their GMM would be developed. The selection criteria for the culling of the full database is presented for each developer team in their respective PEER reports. The NGA-Sub models presented in this comparison report are from the following three developer teams:

- Kuehn, N., Bozorgnia, Y., Campbell, K. and Gregor, N. [KBCG]
- Parker, G., Stewart, J., Hassani, B., Atkinson, G. and Boore, D. [PSHAB]
- Si, H., Midorikawa, S., and Kishida, T. [SMK]

The acronym for each of the three models is indicated in the brackets and will be used throughout this report to identify the three models. The full PEER report for the three developer teams are Kuehn et al. [2020], Parker et al. [2020], and Si et al. [2020].

Given the global distribution of empirical data from subduction earthquakes in the NGA-Sub database, two of the developer teams (KBCG and PSHAB) have developed a global as well as regionalized GMMs. Overall, the same functional form is used for both the global and regional versions of the models, with the difference being a regionalization in the constant, site response amplification scaling and linear attenuation coefficients. In addition, for these two models the magnitude-scaling break point is variable based on the subduction zone within a given region. These magnitude-scaling break points are based on the studies by Ji and Archuleta [2018] for slab events and Campbell [2020] for interface events. The SMK model is developed only from Japanese data and is therefore a model developed specifically for application for Japan.

Based on the station metadata information from sites located in Japan and the Pacific Northwest (i.e., Cascadia), all three models include a basin-amplification component. For KBCG and PSHAB, this component is further differentiated into sites located within and outside of the Seattle Basin, and is dependent on the depth to the 2.5 km/sec shear-wave velocity boundary ($Z_{2.5}$). Similarly, all three models parameterize the basin amplification for Japan based on the $Z_{2.5}$ values.

Table 2.1 provides a summary of the applicable range in magnitude, distance, and V_{S30} values for each of the three models. The use of these models outside of these defined applicability ranges should be performed with caution and—at a minimum—an analyses for the behavior of the models should be performed prior to the application of these models outside of their recommended applicable range. The regional versions of the KBCG and PSHAB models are listed in Table 2.2 along with the magnitude-scaling break points. Both models are defined for the same regions except that the PSHAB model does not have a New Zealand regional model whereas the KBCG model does. Note that the functional parameterization between the KBCG and PSHAB models are different; however, the overall feature of a change in magnitude scaling below and above the magnitude-scaling break points is a common feature of both models. For the SMK model, the magnitude scaling in Japan changes above **M**8.3. Comparisons will be presented later in this report showing the differences in the magnitude-scaling break points.

The parameterization and functional model development for each of the three GMMs is presented in the associated PEER reports for each model [Kuehn et al. 2020; Parker et al. 2020; and Si et al. 2020]. Table 2.3 summarizes the model parameters used in each of the three models.

Table 2.1 Model applicability of the three GMMs for magnitude, distance, and V_{S30}.

	KBCG	PSHAB	SMK
Magnitude	$5 \leq M \leq 9.5$ (interface) $5 \leq M \leq 8.5$ (slab)	$4.5 \leq M \leq 9.5$ (interface) $4.5 \leq M \leq 8.5$ (slab)	$5.5 \leq M \leq 9.1$ (interface) $5.6 \leq M \leq 8.3$ (slab)
Distance (km)	$10 \leq R_{rup} \leq 1000$	$20 \leq R_{rup} \leq 1000$ (interface) $35 \leq R_{rup} \leq 1000$ (slab)	$14 \leq R_{rup} \leq 300$ (interface) $18 \leq R_{rup} \leq 300$ (slab)
V_{S30} (m/sec)	$150 \leq V_{S30} \leq 1500$	$150 \leq V_{S30} \leq 2{,}000$	$100 \leq V_{S30} \leq 1{,}900$
Source depth (km)	$Z_{tor} \leq 50$ (interface) $Z_{tor} \leq 200$ (slab)[1]	$Z_{hyp} \leq 40$ (interface) $0 \leq Z_{hyp} \leq 200$ (sab)	$4 \leq$ focal depth ≤ 50 (interface) $18 \leq$ focal depth ≤ 100 (slab)
Region	Global and region	Global and region	Japan

[1] For Columbia, $Z_{tor} \leq 150$ km for slab events.

Table 2.2 Regionalized models and magnitude-scaling break point values.

Region	KBCG/interface	KBCG/slab	PSHAB/interface	PSHAB/slab
Global	7.9	7.6	7.9	7.6
Alaska	8.6	7.2	8.6	7.2
Alaska - Aleutian	8.0	8.0	8.0	7.98
Cascadia	8.0	7.2	7.7	7.2
Northern Central America and Mexico	7.4	7.4	7.4	7.4
Southern Central America and Mexico	7.5	7.6	7.4	7.6
Japan – Pacific Plate	8.5	7.6	8.5	7.65
Japan – Philippine Plate	7.7	7.6	7.7	7.55
Northern South America	8.5	7.3	8.5	7.3
Southern South America	8.6	7.2	8.6	7.25
Taiwan	7.1	7.7	7.1	7.7
New Zealand	8.3	7.6	---	---

The parameterization and functional model development for each of the three GMMs is presented in the associated PEER reports for each model [Kuehn et al. 2020; Parker et al. 2020; and Si et al. 2020]. Table 2.3 summarizes the model parameters used in each of the three models.

Table 2.3 Functional model parameters used for the three NGA-Sub GMMs.

Parameter	KBCG	PSHAB	SMK
Moment magnitude	**M**	**M**	**M**
Closest distance to rupture plane (km)	R_{rup}	R_{rup}	R_{rup}
Depth to top of rupture (km)	Z_{tor}	---	---
Hypocentral depth (km)	---	Z_{hyp}[1] (only Slab)	D
Moho depth (km)	---	---	Moho depth
Average shear-wave velocity in top 30 m (m/sec)	V_{S30}	V_{S30}	V_{S30}
Depth to 2.5 km/sec boundary (km)	$Z_{2.5}$ (only for Cascadia and Japan Basins)	$Z_{2.5}$ (only for Cascadia and Japan Basins)	$Z_{2.5}$ (only for Japan Basins)
Depth to 1.0 km/sec boundary (km)	$Z_{1.0}$ (only for Taiwan and New Zealand Basins)	---	---
Interface/slab classification	0 = interface/1 = slab	0 = interface/1 = slab	0 = interface/1 = slab
Magnitude-scaling break point	(see Table 2.2)	(see Table 2.2)	8.3

3 Median Value Comparisons

This section presents the comparison of the median value estimates from the three NGA-Sub GMMs. Comparisons will be made for the two global models (KBCG and PSHAB) compared to other previous subduction GMMs and the individual regionalized models from the two new models, noting that the SMK model is only defined for Japan. Comparisons will be presented for attenuation curves, magnitude-scaling, depth to top of rupture, and basin amplifications. For all comparisons except the basin amplifications, these comparisons will be separated based on interface and slab events. Note that the basin-amplification effects are independent of the type of subduction earthquake. For both the attenuation curves and spectra, comparison plots will be presented for two V_{S30} values of 760 m/sec and 400 m/sec. The first value is representative of the common reference condition corresponding to NEHRP B/C boundary site conditions. The second and lower value is more consistent with soft-rock site conditions.

For the global comparisons, the following published models are presented:

- Atkinson and Boore [2003; 2008] (AB08)
- Atkinson and Macias [2009] (AM09)
- Zhao et al. [2006] (Zea06)
- Zhao et al. [2016a, b] (Zea16)
- BCHydro [Abrahamson et al. 2016] (BCH)
- BCHydro Update for USGS [Abrahamson et al. 2018] (BCHU)

The AM09 model was developed for Cascadia interface events only and is defined for a V_{S30} of 760 m/sec. Based on these limitations, the AM09 model is only compared for interface events with V_{S30} of 760 m/sec. For the AB08 model, the site conditions are defined based on NEHRP categories [Building Seismic Safety Council 2009] and for the V_{S30} of 760 m/sec, the average of NHERP B and C site conditions for which ground motions are computed. For the lower V_{S30} value of 400 m/sec, the AB08 ground motions are presented for NHERP C site conditions. Both the Zea06 and Zea16 are also defined based on a binned site classification. For the V_{S30} value of 760 m/sec, the average of the ground motions from the hard soil and rock-site conditions is computed; for the V_{S30} value of 400 m/sec, the hard-soil site conditions is selected for the comparisons. Both the BCH and BCHU models are defined as a continuous function of V_{S30} values.

The AB08 model was developed as a global model with two additional regionalized versions, specifically for Cascadia and Japan. Since these previously published models presented in this report are compared with global versions of the new models, the comparison with AB08 is based on the global version of that model. Although the AM09 model was developed specifically for Cascadia events, it is compared to the global version of the two new

NGA-Sub models. The Zea06 and Zea16 are both based on predominately Japanese data; however, because the application of these models has typically been applied globally, the comparisons will be presented with the global models.

The BCH global model is presented in the comparisons. For the attenuation curve plots, only the forearc ground motions are computed even though for the larger distances up to 1000 km one would expect that the sites would be located in the backarc region. Finally, the BCHU model was developed specifically for application by the USGS for Cascadia earthquakes rather than a global application. Similar to the inclusion of the AM09 model with the global models, the BCHU model is also included in the global-model comparisons. For both the BCH and BCHU models, the upper and lower versions of these models to account for epistemic uncertainty are also included in the comparison figures.

As noted earlier, the comparisons presented in this report (i.e., both in the report and as well in the associated electronic files) do not fully span the wide range of applicable comparisons. However, through the observations and understanding of these new NGA-Sub GMMs and with any additional comparison studies, it is anticipated that the evaluation and application of these new models can be technically informed.

3.1 INTERFACE EVENTS

For the interface event comparisons, the selected input parameters are listed in Table 3.1. Results are calculated for magnitudes 7, 8, and 9 and for distances of 10–1000 km for the attenuation curves and two specific distances of 75 and 200 km for the response spectra. Two V_{S30} values of 760 and 400 m/sec are selected along with the previously described site classifications for the older GMMs. A separate section will be presented for the basin-amplification results from the models and all other comparisons are for non-basin sites.

Table 3.1 Input parameters for interface global GMM comparisons.

Parameter	KBCG	PSHAB	SMK
Moment magnitude	7, 8, and 9	7, 8, and 9	7, 8, and 9
Closest distance torupture plane (km)	10.0–1000.0[1] 75.0[2] 200.0[2]	10.0–1000.0[1] 75.0[2] 200.0[2]	10.0–1000.0[1] 75.0[2] 200.0[2]
Depth to top of rupture (km)	10.0	---	---
Hypocentral depth (km)	---	---	20.0
Moho depth (km)	---	---	30.0
Average shear-wave velocity in top 30 m (m/sec)	760.0 400.0	760.0 400.0	760.0 400.0
Depth to 2.5 km/sec boundary (km)	---	---	---
Depth to 1.0 km/sec boundary (km)	---	---	---
Interface/slab classification	0 = interface	0 = Interface	0 = Interface
Magnitude-scaling break point	7.9 (Global)	7.9 (Global)	8.3

[1] Distance range for attenuation curve plots.

[2] Distance values for spectra plots.

3.1.1 Interface Attenuation Curves

Attenuation curves are compared for both the global versions and regional versions of the models. For the global model, the comparisons are presented with the previous suite of subduction GMMs. For the regional models, the comparison is presented between the global version and regional version of only the NGA-Sub GMMs. Attenuation curves are computed for spectral periods of 0.01 (i.e., to represent an approximate PGA), 0.2, 1, 3, and 5 sec. Representative attenuation curve plots for the **M**8 case for PGA (T = 0.01 sec), 0.2, 1.0, and 3.0 sec spectral periods are plotted in Figure 3.1 to Figure 3.32. The full suite of attenuation curves (i.e., both digital data and plots) are contained in the associated electronic files; see Appendix A.

In general, there is good agreement between the new NGA-Sub GMMs and the previous models for distances in the 100–200 km range. At shorter and longer distances, however, the dispersion of the models increases. These observations are not unexpected given the different datasets used in each GMM development as well the range of focus and applicability of each model. For example, calculating ground motions for distances out to 1000 km is beyond the applicable range of previous models (e.g., AB08). At these large distances, it would be expected that the sites would fall into the back-arc category and have lower ground motions for the shorter period ground motions and higher ground motions for the longer spectral period ground motions (e.g., BCH).

The regional comparisons for seven regions are plotted in Figure 3.5 through Figure 3.32. For the Japan region, the KBCG and PSHAB models have a Pacific Plate and Philippine Plate model based on the different magnitude-scaling break points associated with these two tectonic features (i.e., see Table 2.2). In addition, the SMK model is presented in these comparisons for the Japan region. Overall, variations between the global model and the individual regional models are noted based on the differences in the regional features of each model (e.g., constant, magnitude-scaling break point, site response, and anelastic attenuation).

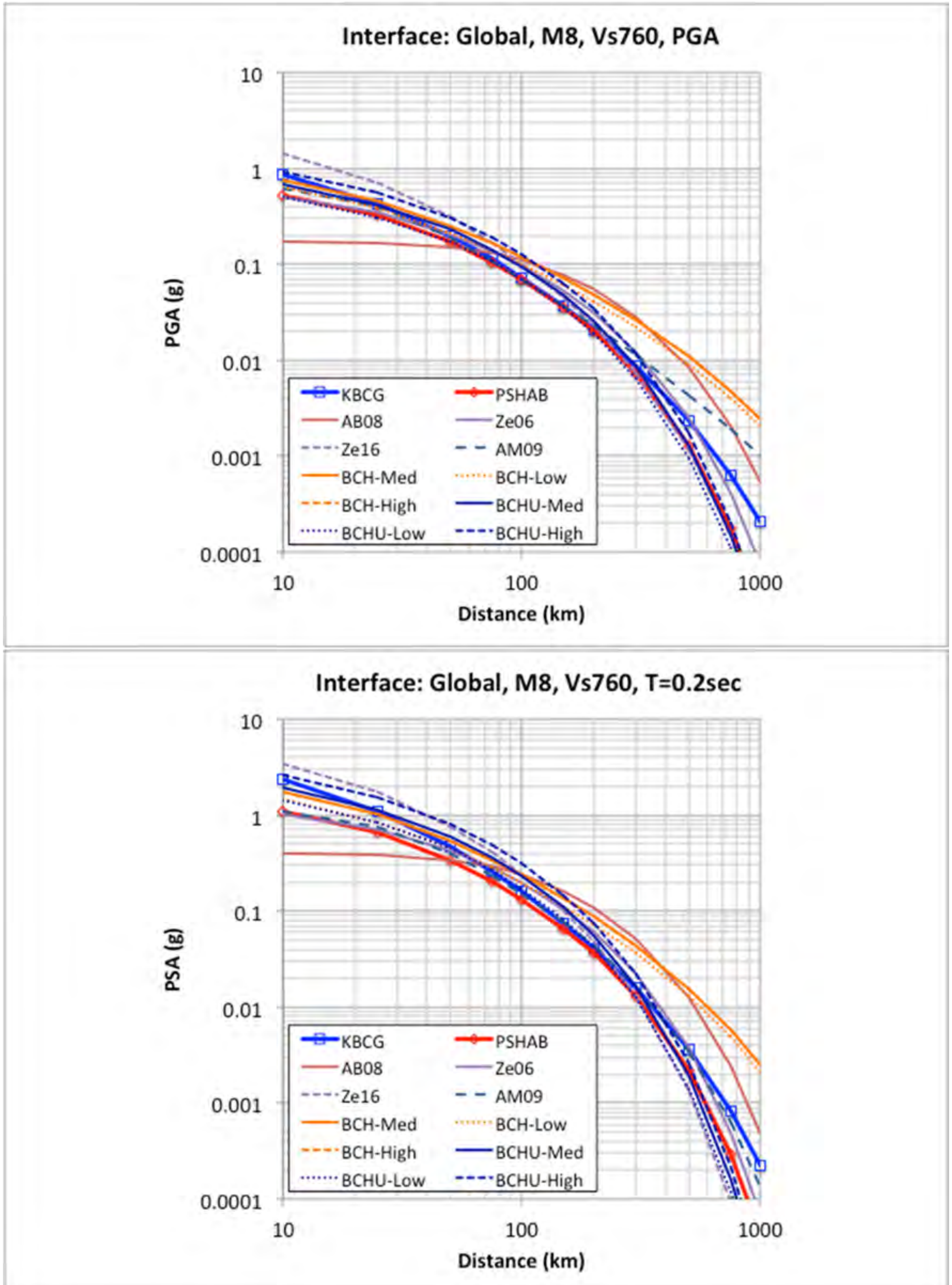

Figure 3.1 **Comparison of global M8 (interface) for PGA (*T* = 0.01 sec) (top) and 0.2 sec (bottom) attenuation curves for V_{S30} = 760 m/sec.**

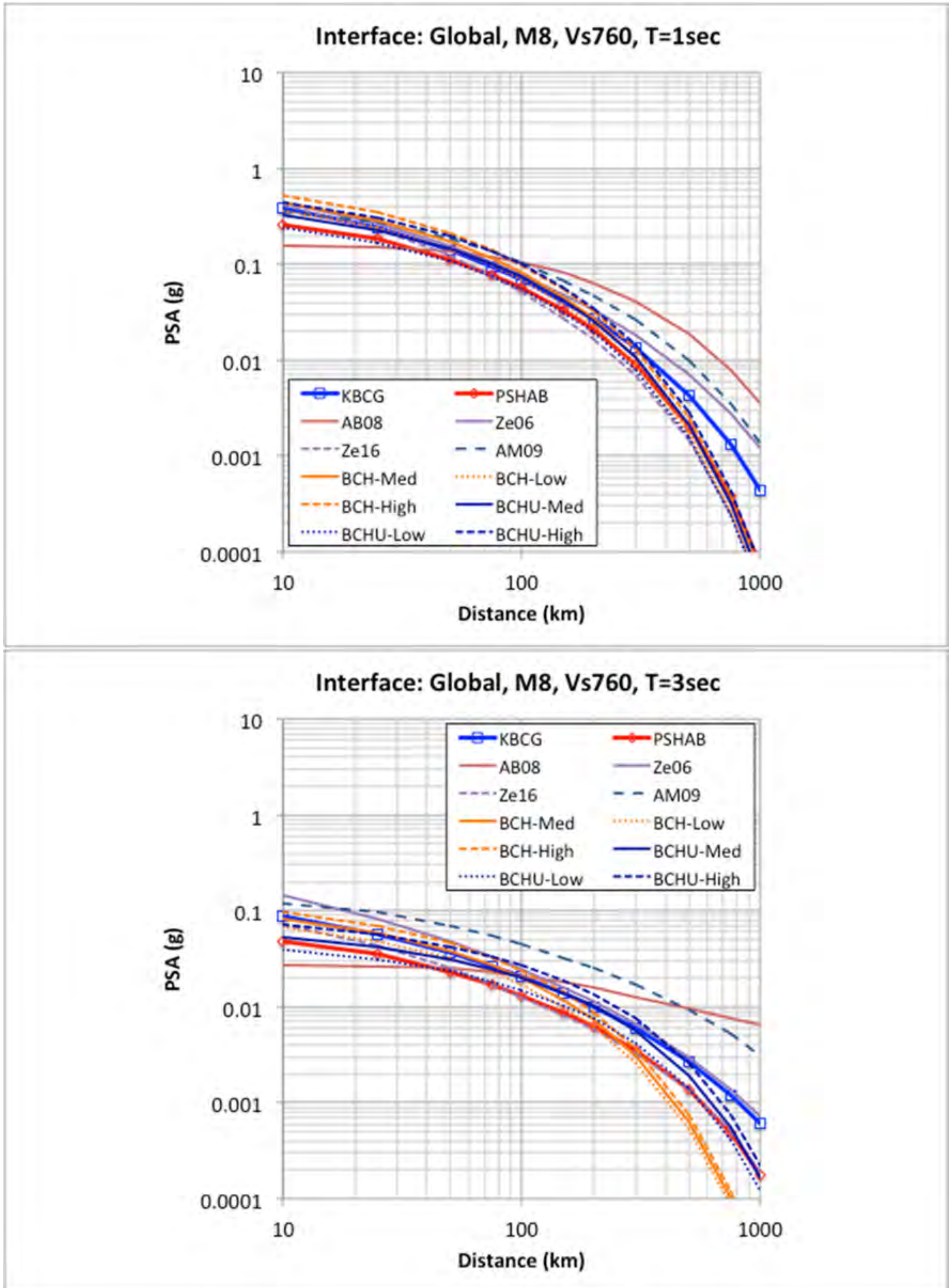

Figure 3.2 **Comparison of global M8 (interface) for 1.0 (top) and 3.0 sec (bottom) attenuation curves for V_{S30} = 760 m/sec.**

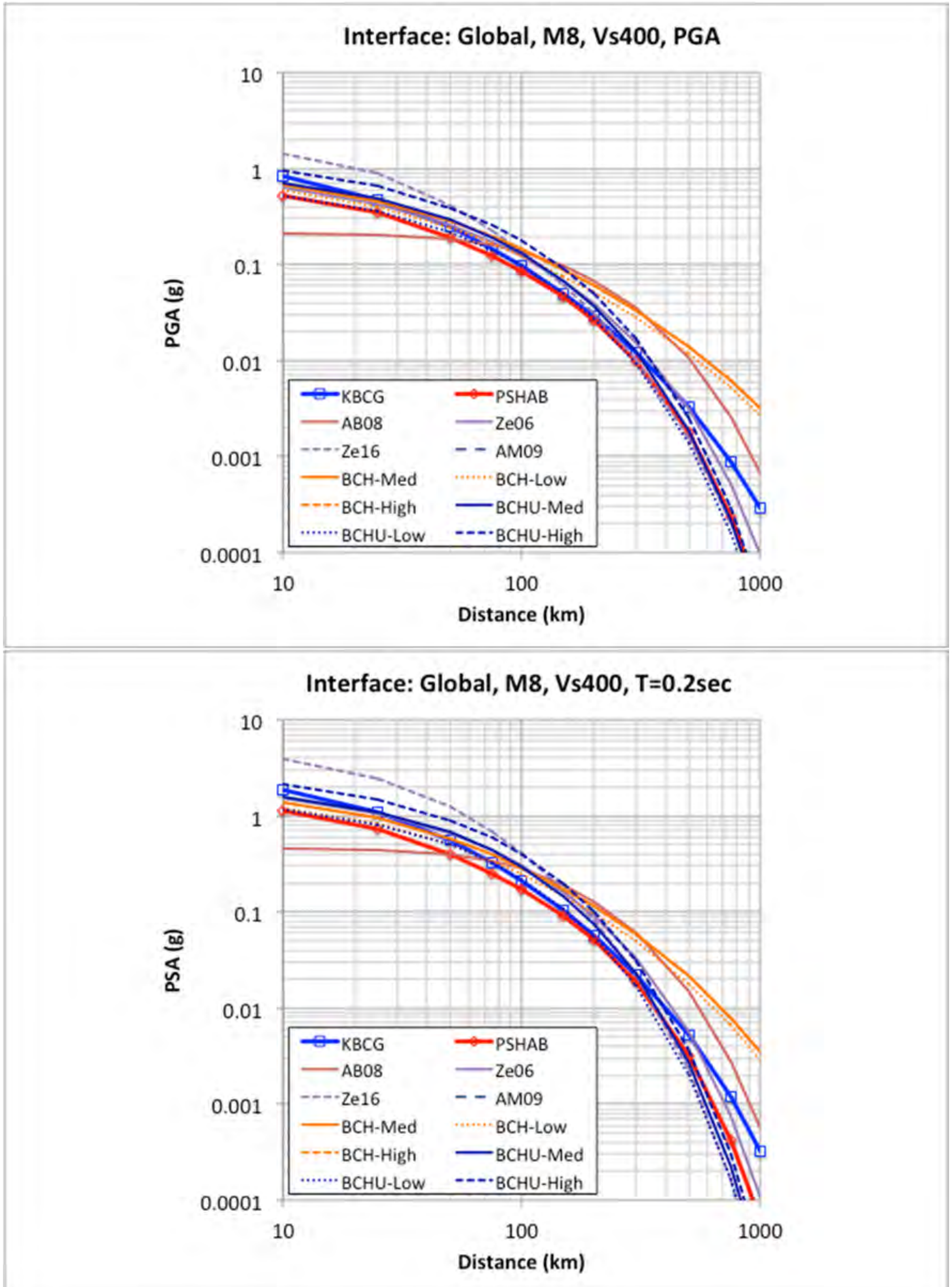

Figure 3.3 **Comparison of global M8 (interface) for PGA (*T* = 0.01 sec) (top) and 0.2 sec (bottom) attenuation curves for V_{S30} = 400 m/sec.**

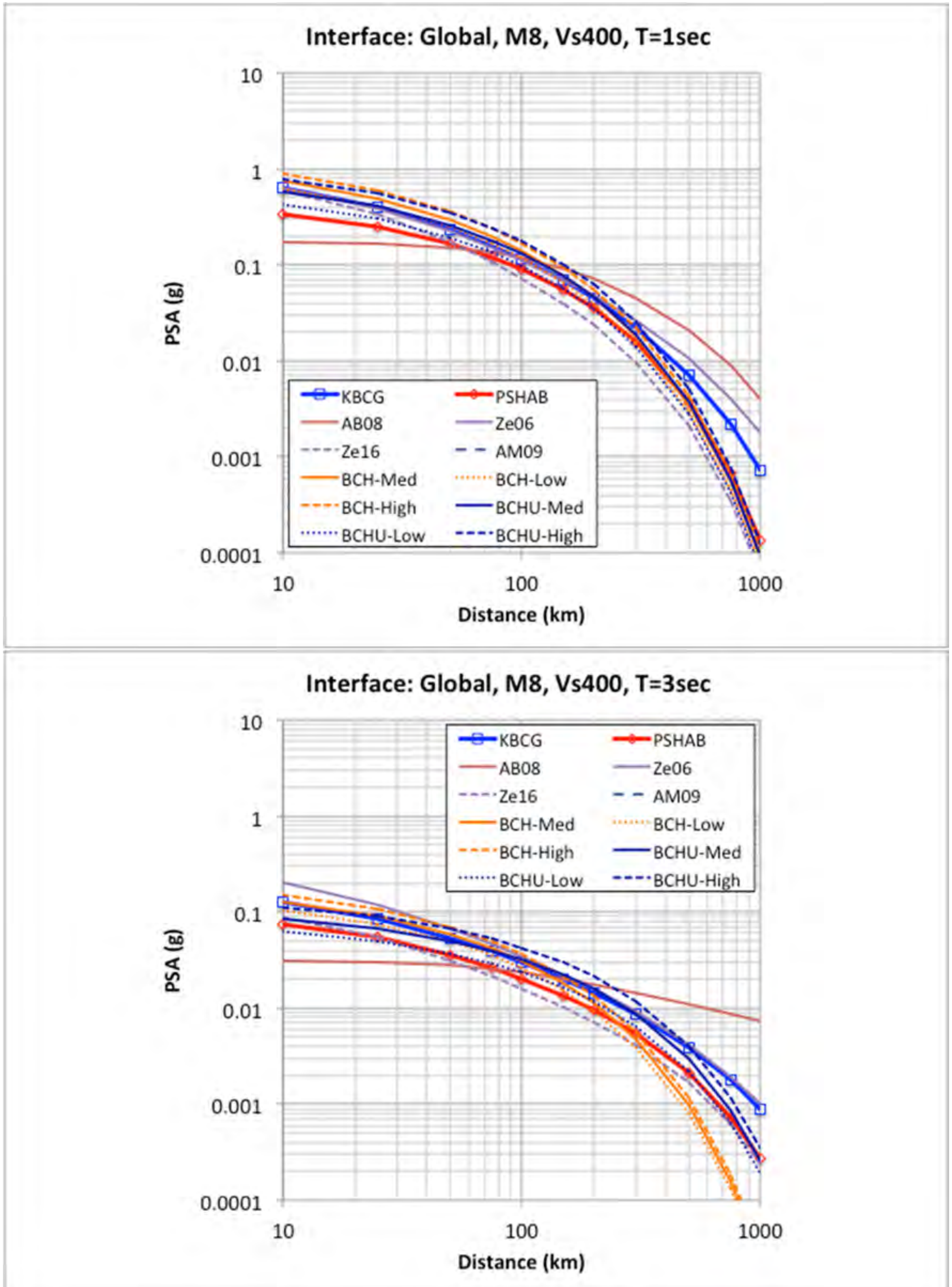

Figure 3.4 **Comparison of global M8 (interface) for 1.0 (top) and 3.0 sec (bottom) attenuation curves for V_{S30} = 400 m/sec.**

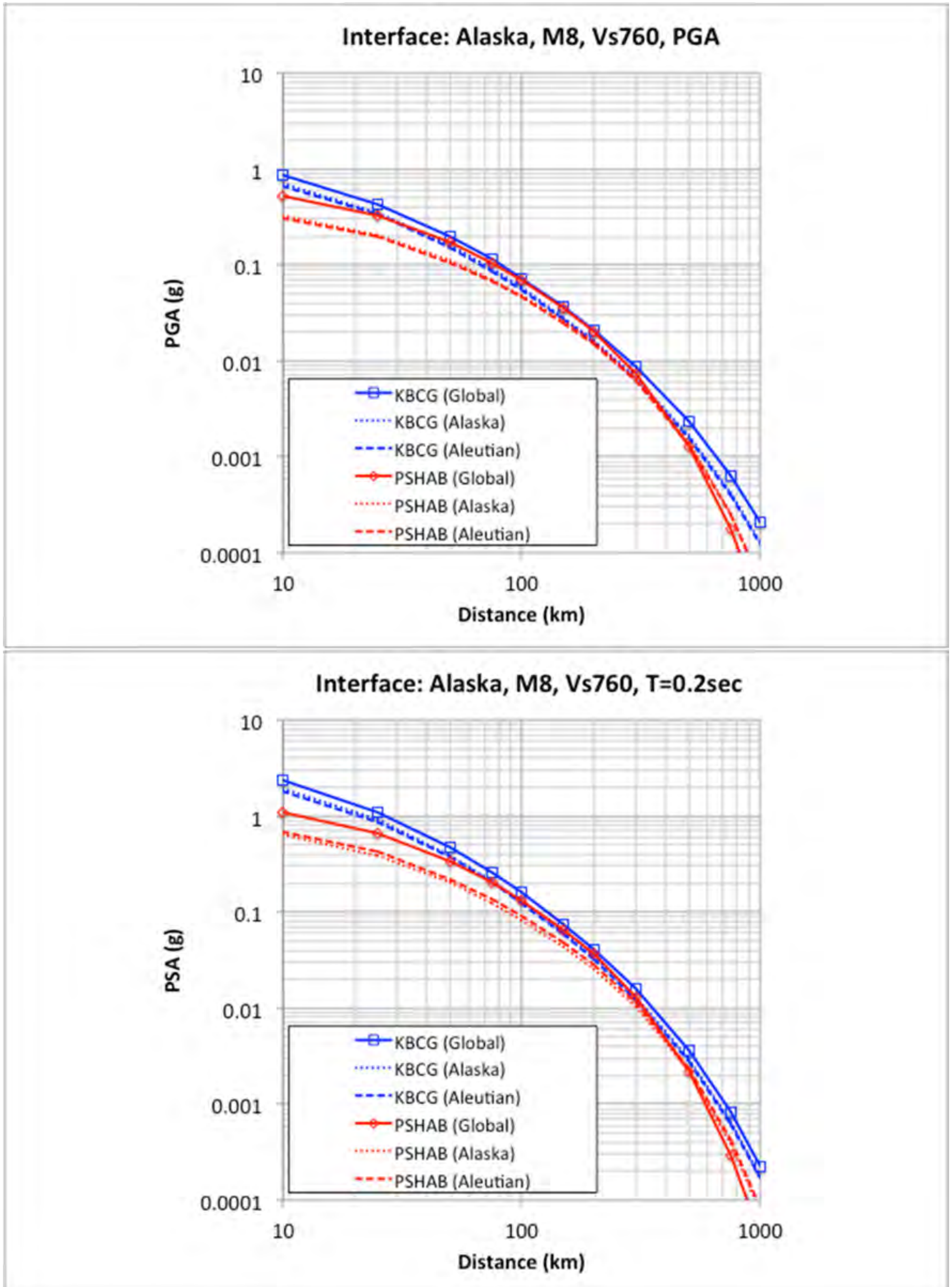

Figure 3.5 Comparison of Alaska regional M8 (interface) for PGA (*T* = 0.01 sec) (top) and 0.2 sec (bottom) attenuation curves for V_{S30} = 760 m/sec.

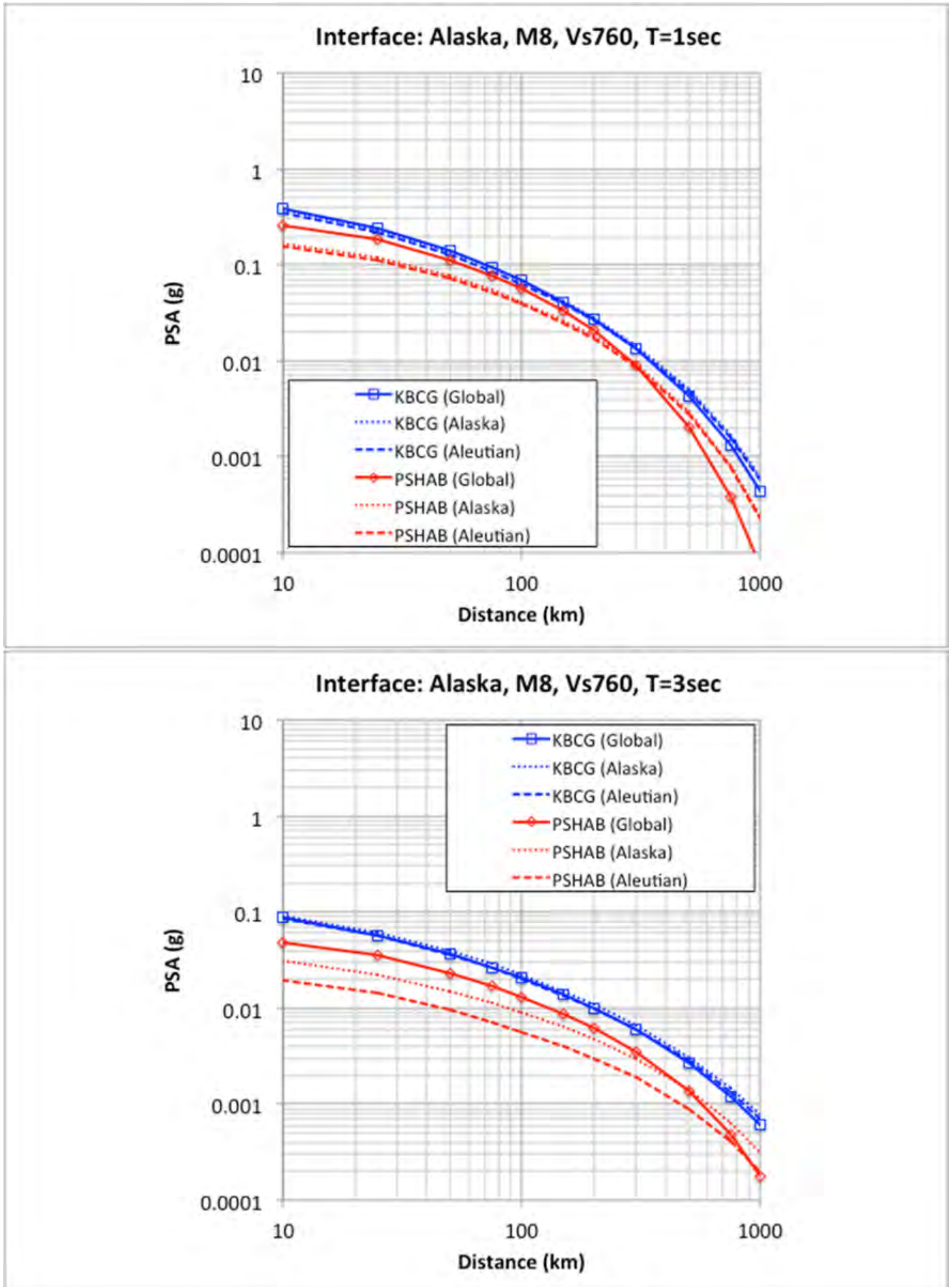

Figure 3.6 **Comparison of Alaska regional M8 (interface) for 1.0 (top) and 3.0 sec (bottom) attenuation curves for V_{S30} = 760 m/sec.**

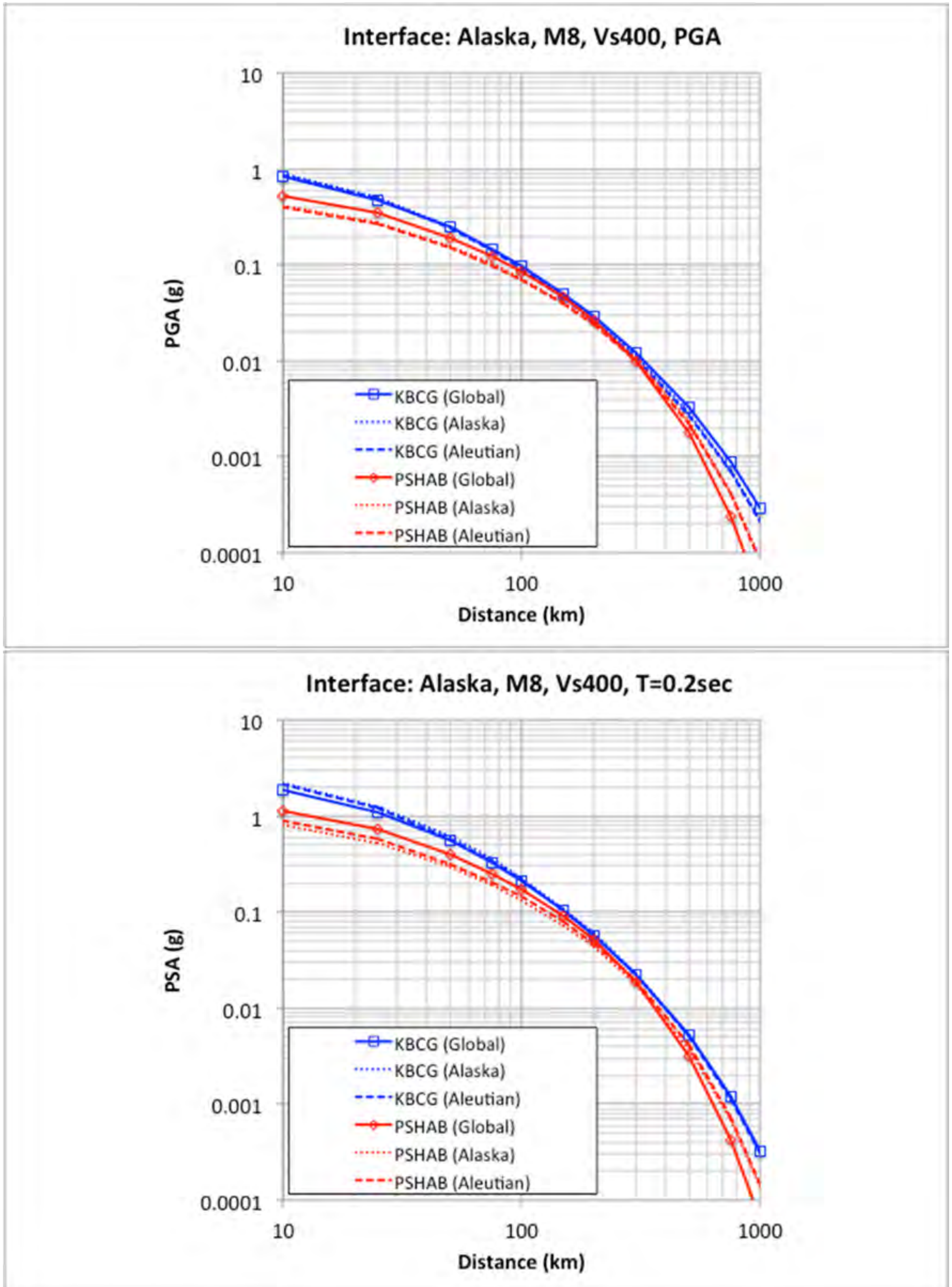

Figure 3.7 Comparison of Alaska regional M8 (interface) for PGA (*T* = 0.01 sec) (top) and 0.2 sec (bottom) attenuation curves for V_{S30} = 400 m/sec.

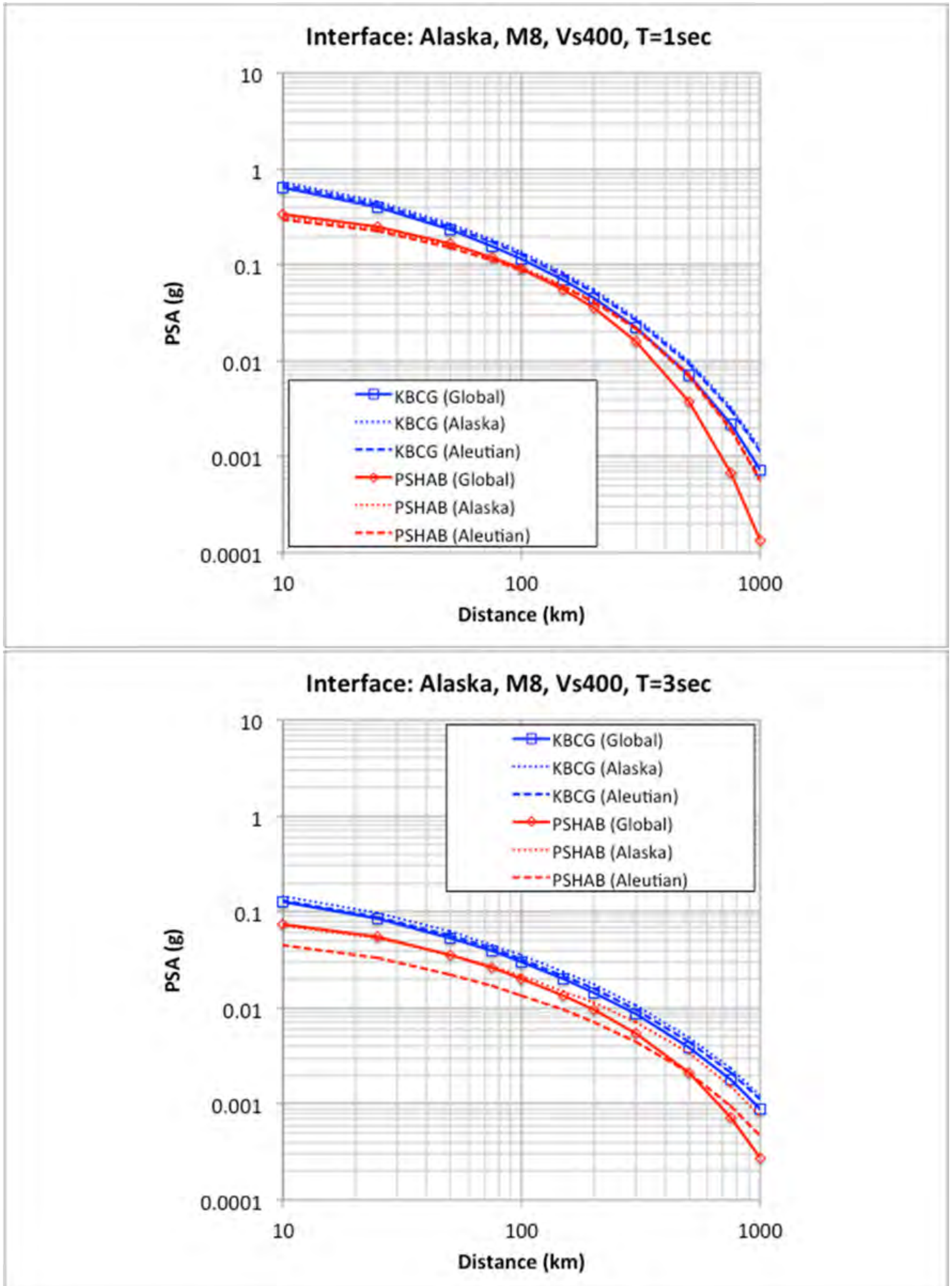

Figure 3.8 **Comparison of Alaska regional M8 (interface) for 1.0 (top) and 3.0 sec (bottom) attenuation curves for V_{S30} = 400 m/sec.**

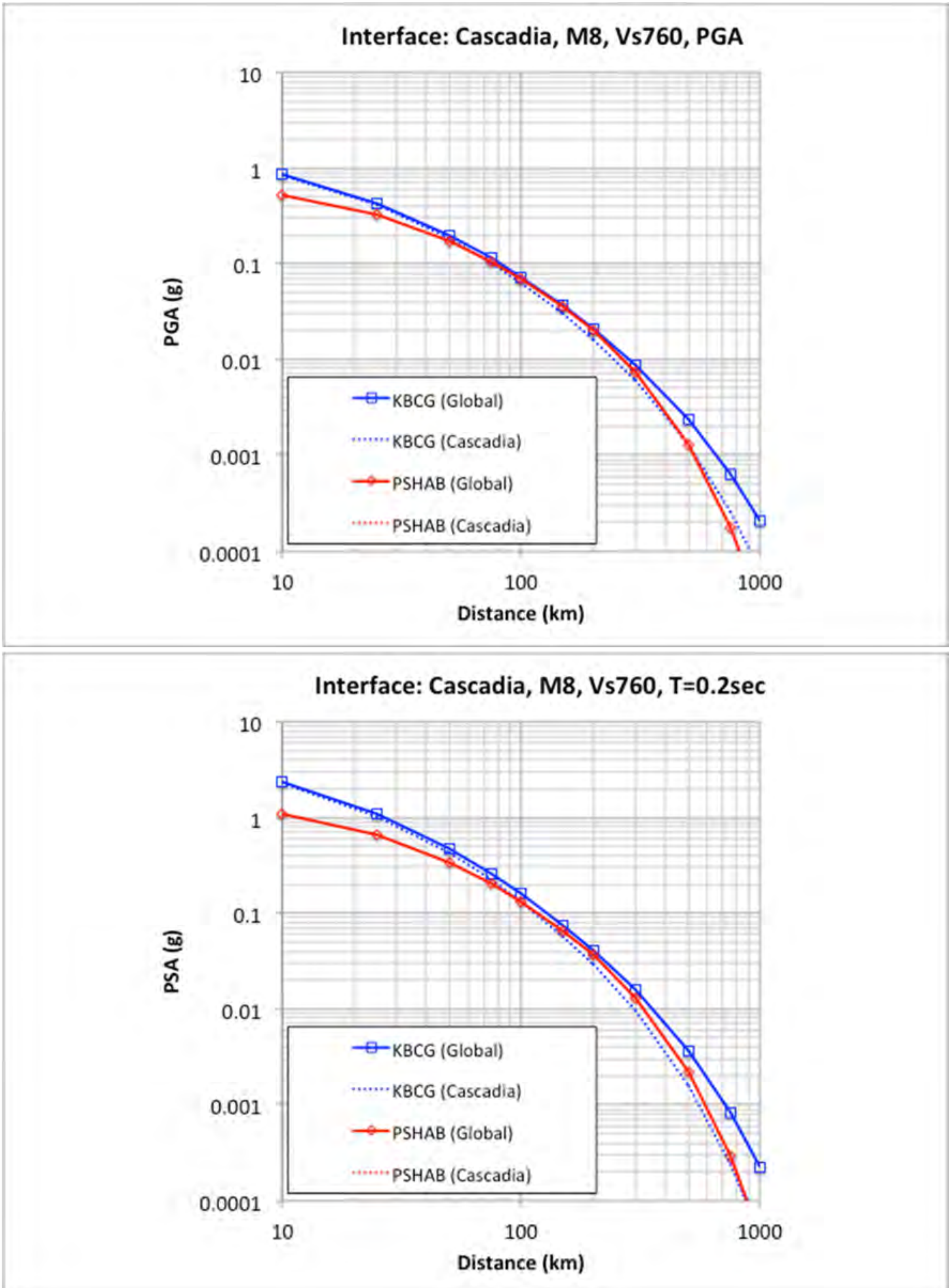

Figure 3.9 **Comparison of Cascadia regional M8 (interface) for PGA (*T* = 0.01 sec) (top) and 0.2 sec (bottom) attenuation curves for V_{S30} = 760 m/sec.**

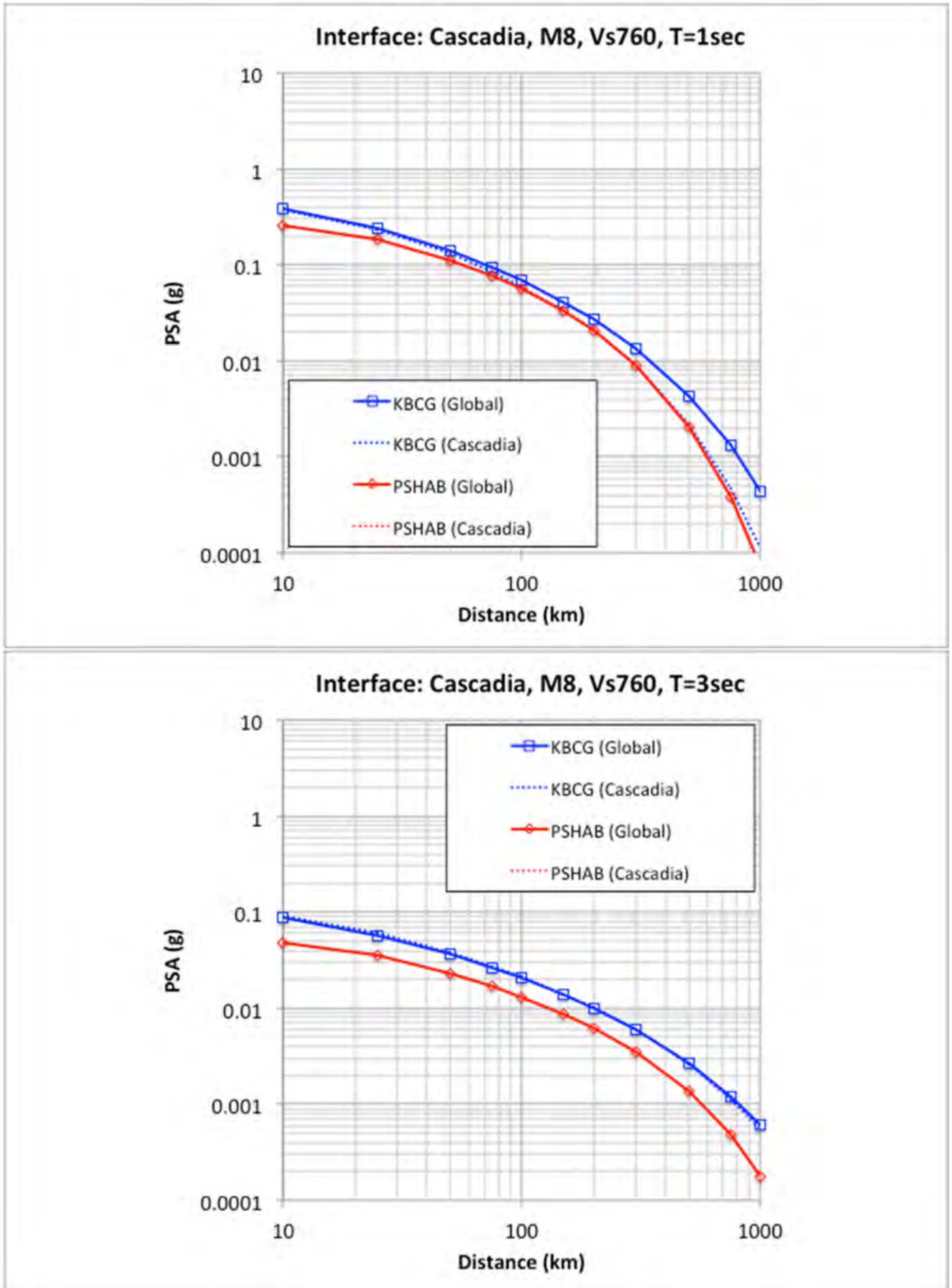

Figure 3.10 Comparison of Cascadia regional M8 (interface) for 1.0 (top) and 3.0 sec (bottom) attenuation curves for V_{S30} = 760 m/sec.

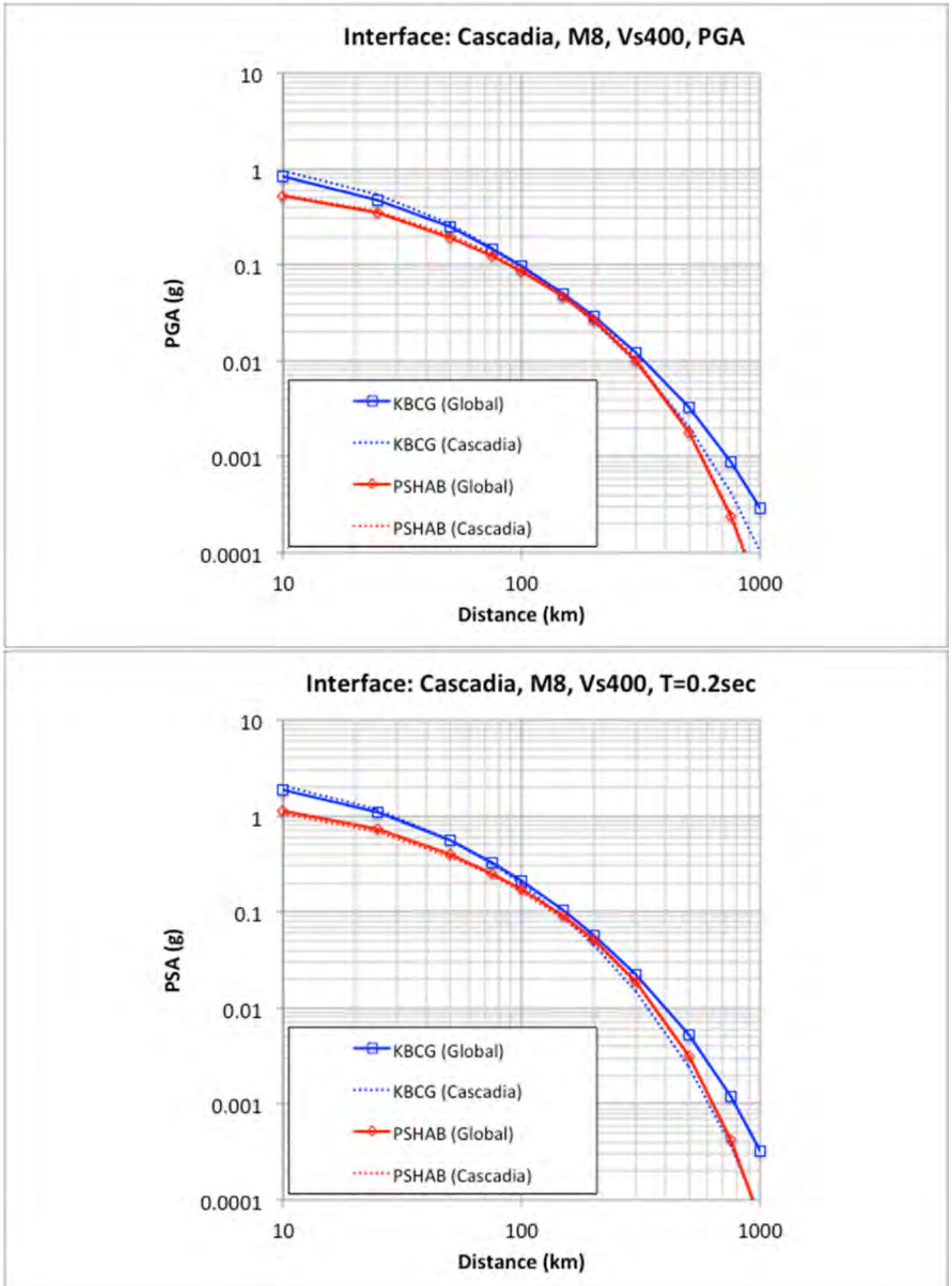

Figure 3.11 Comparison of Cascadia regional M8 (interface) for PGA (*T* = 0.01 sec) (top) and 0.2 sec (bottom) attenuation curves for V_{S30} = 400 m/sec.

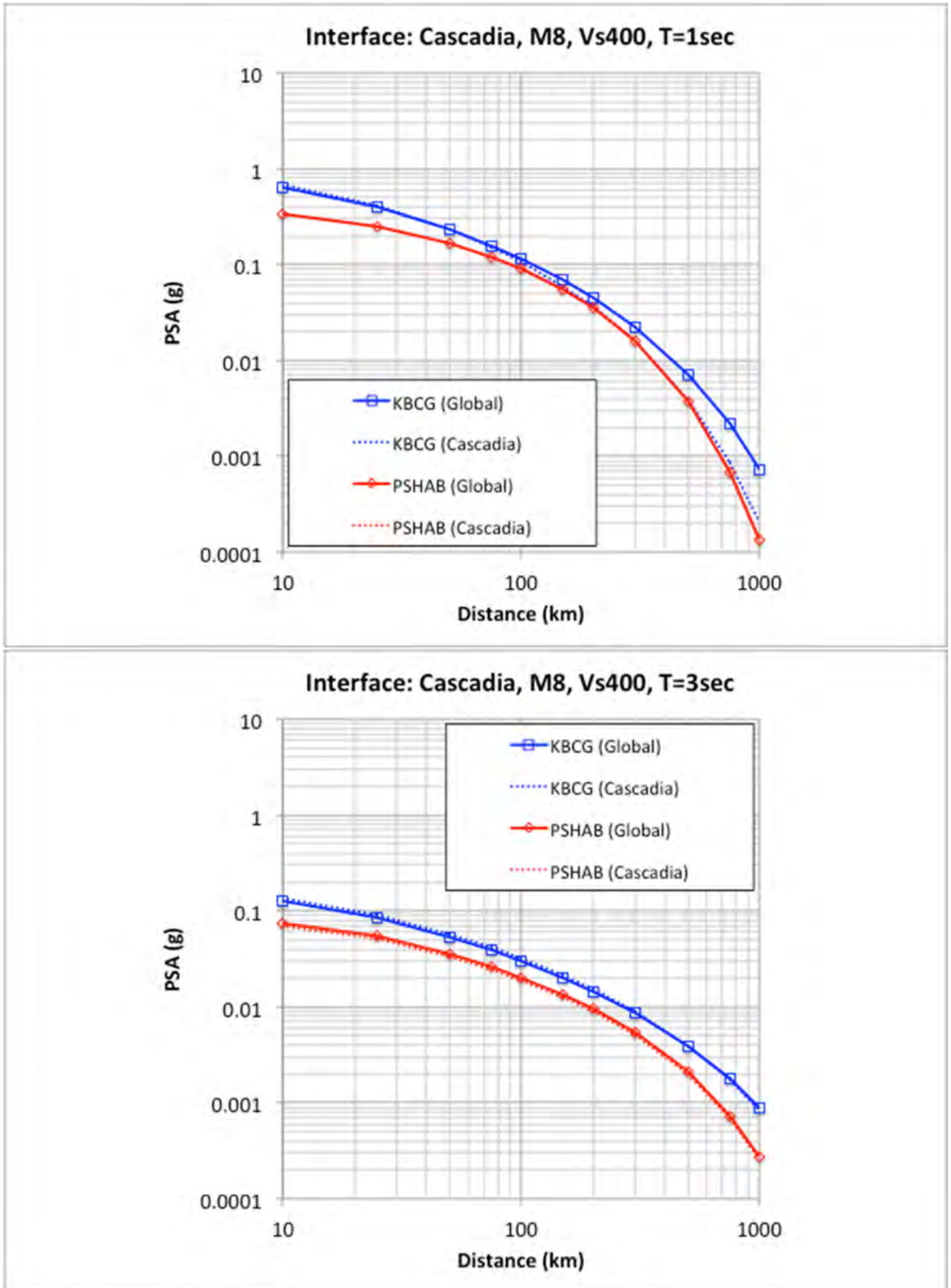

Figure 3.12 **Comparison of Cascadia regional M8 (interface) for 1.0 (top) and 3.0 sec (bottom) attenuation curves for V_{S30} = 400 m/sec.**

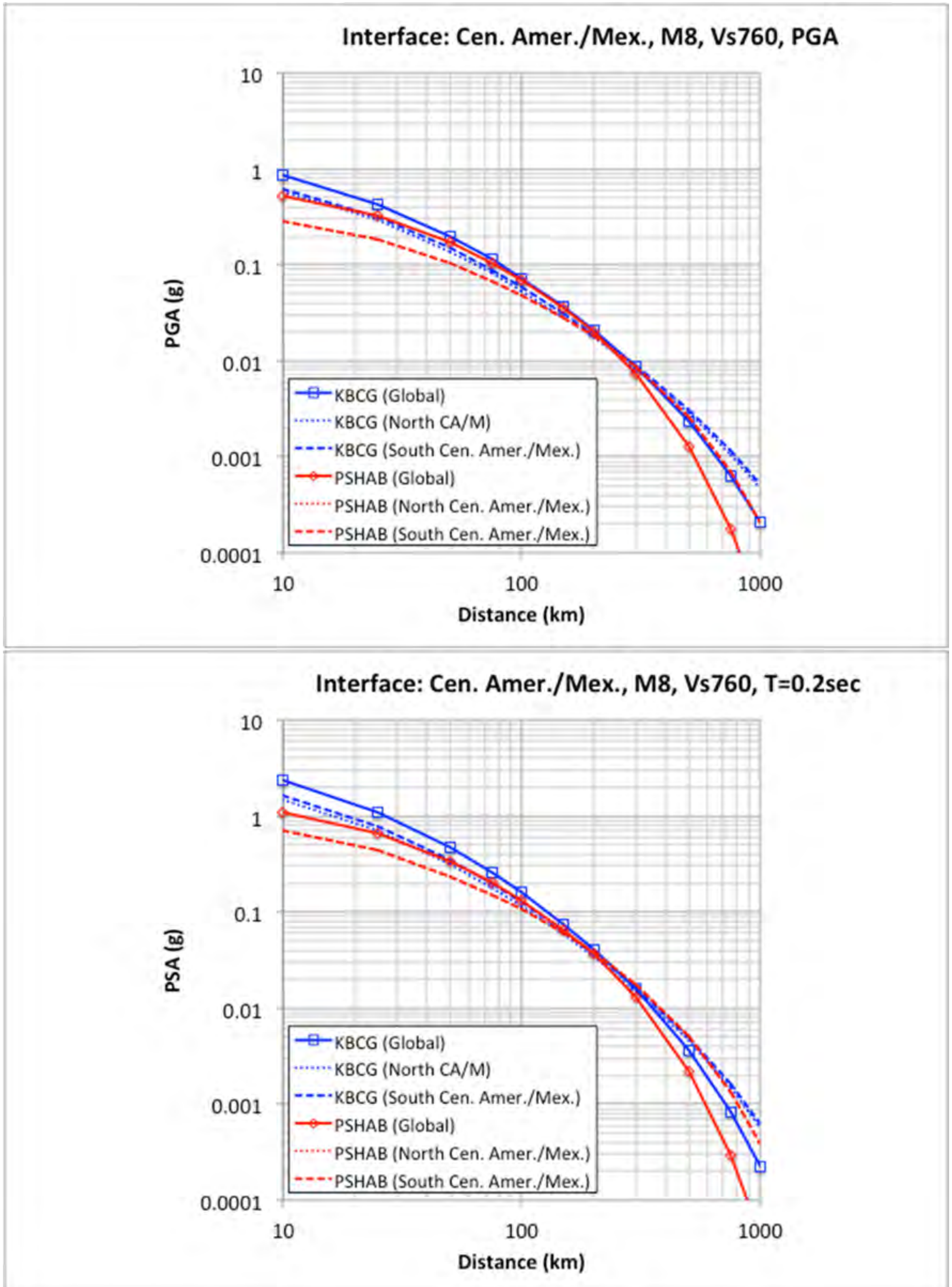

Figure 3.13 Comparison of Central America and Mexico regional M8 (interface) for PGA (*T* = 0.01 sec) (top) and 0.2 sec (bottom) attenuation curves for V_{S30} = 760 m/sec.

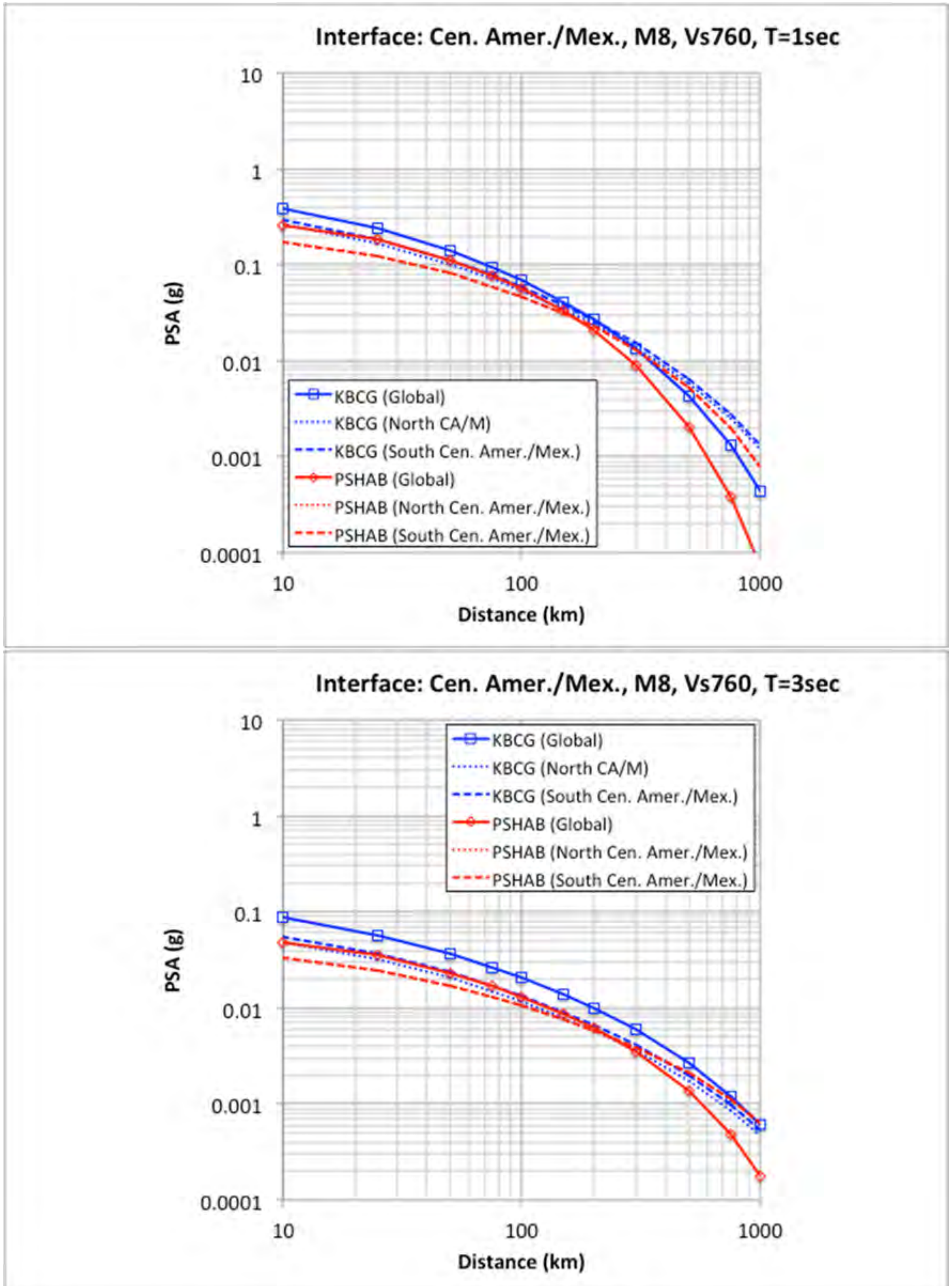

Figure 3.14 Comparison of Central America and Mexico regional M8 (interface) for 1.0 (top) and 3.0 sec (bottom) attenuation curves for V_{S30} = 760 m/sec.

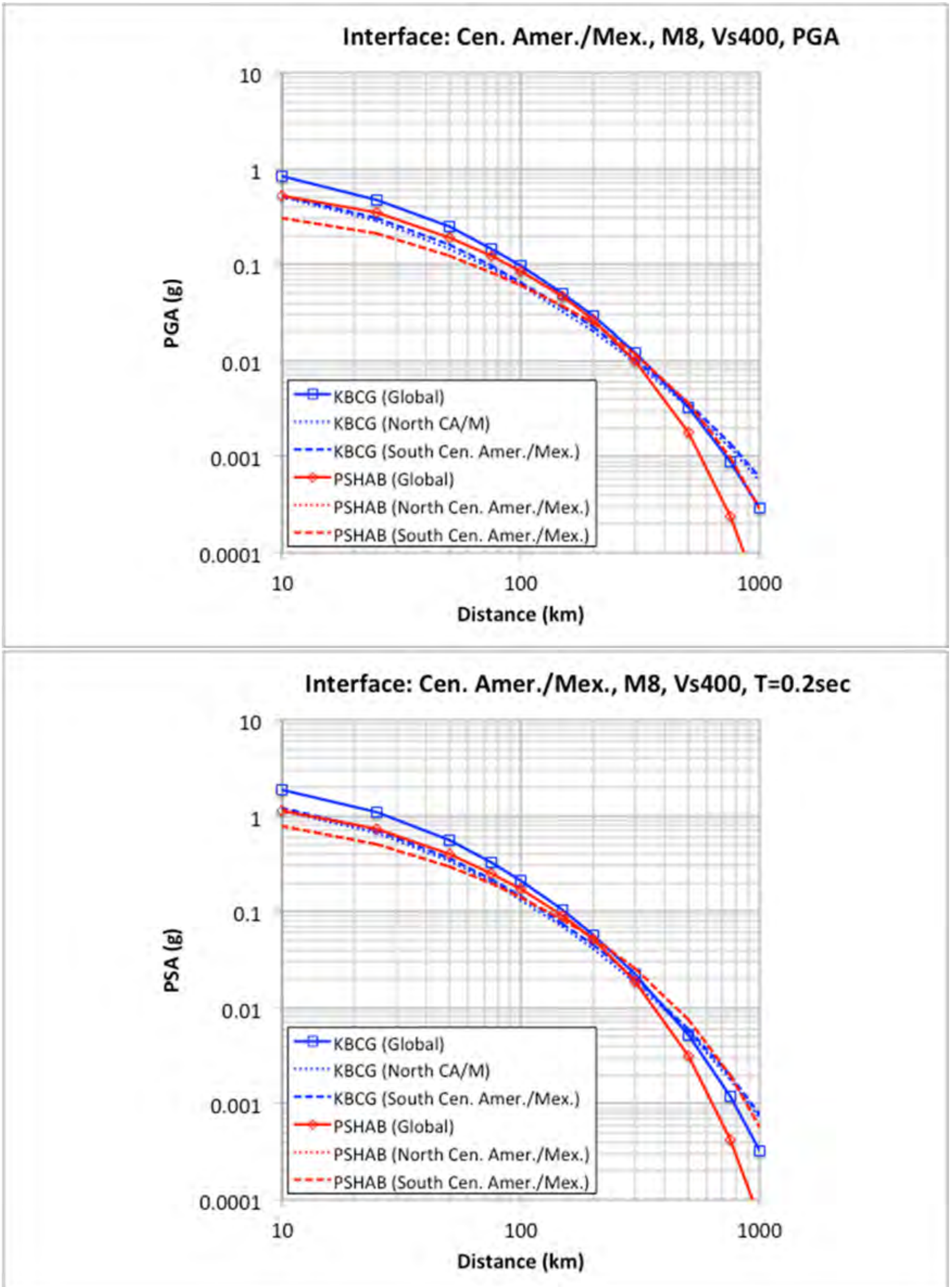

Figure 3.15 **Comparison of Central America and Mexico regional M8 (interface) for PGA (*T* = 0.01 sec) (top) and 0.2 sec (bottom) attenuation curves for V_{S30} = 400 m/sec.**

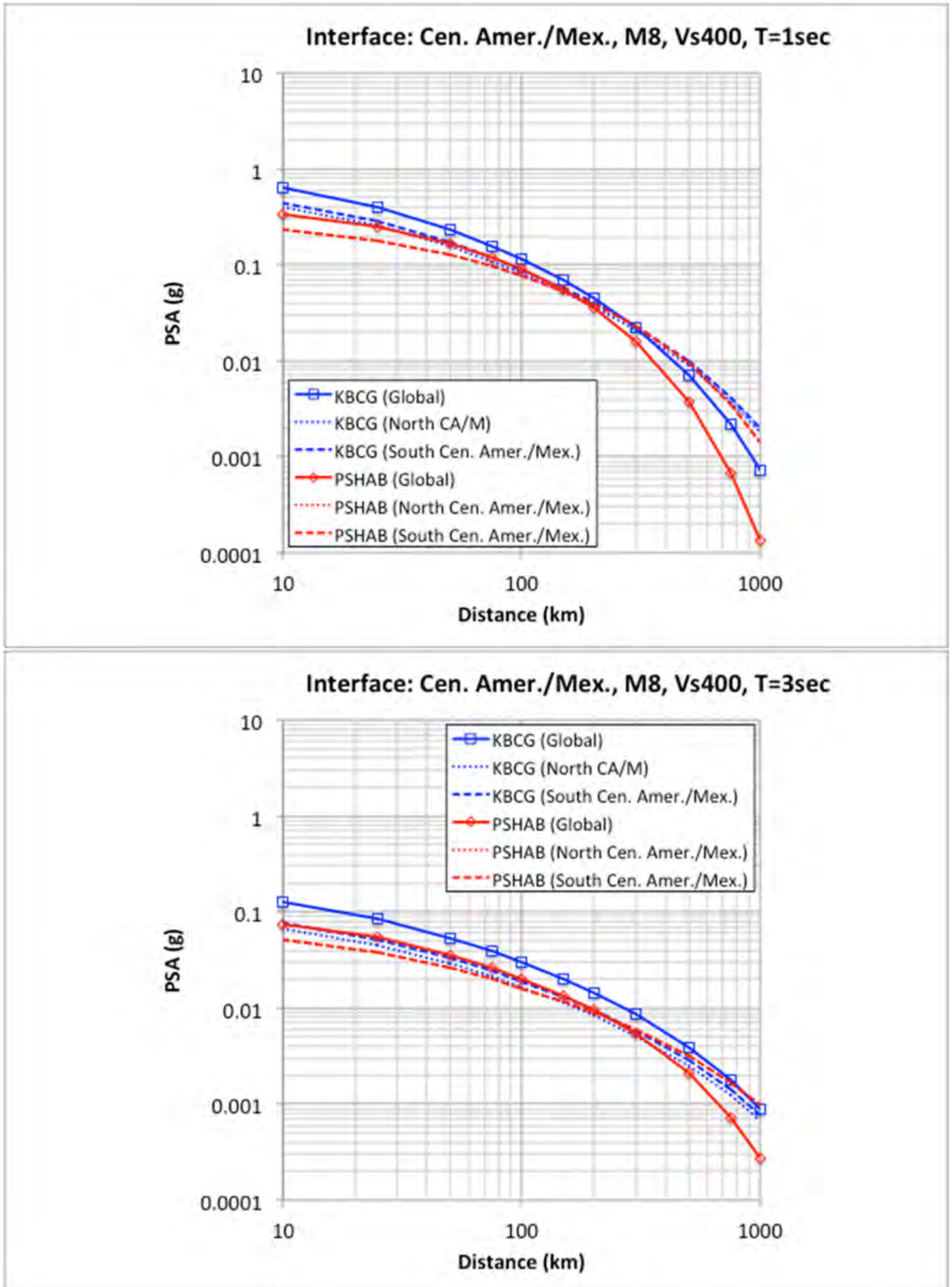

Figure 3.16 **Comparison of Central America and Mexico regional M8 (interface) for 1.0 (top) and 3.0 sec (bottom) attenuation curves for V_{S30} = 400 m/sec.**

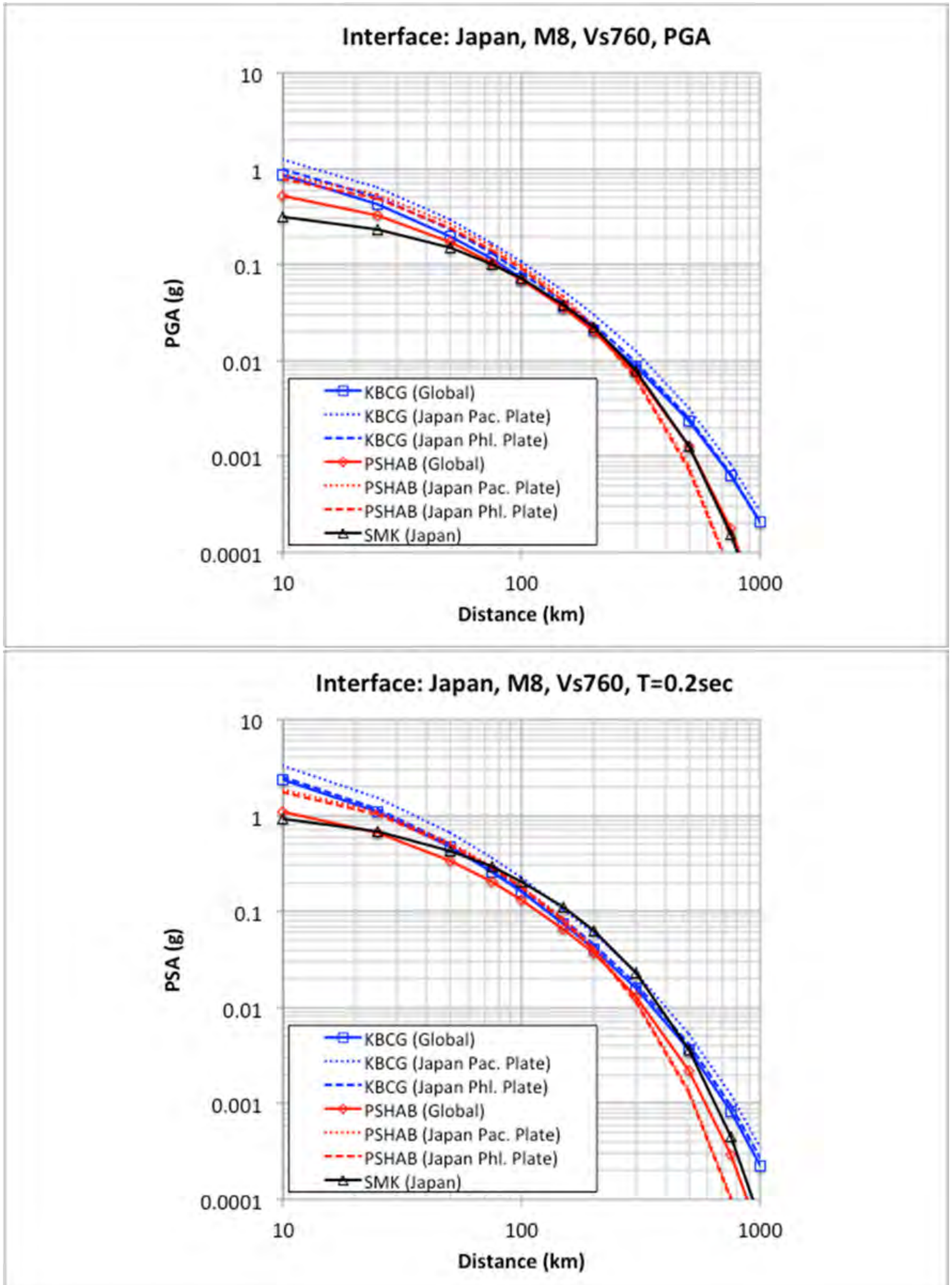

Figure 3.17 **Comparison of Japan regional M8 for (interface) PGA (*T* = 0.01 sec) (top) and 0.2 sec (bottom) attenuation curves for V_{S30} = 760 m/sec.**

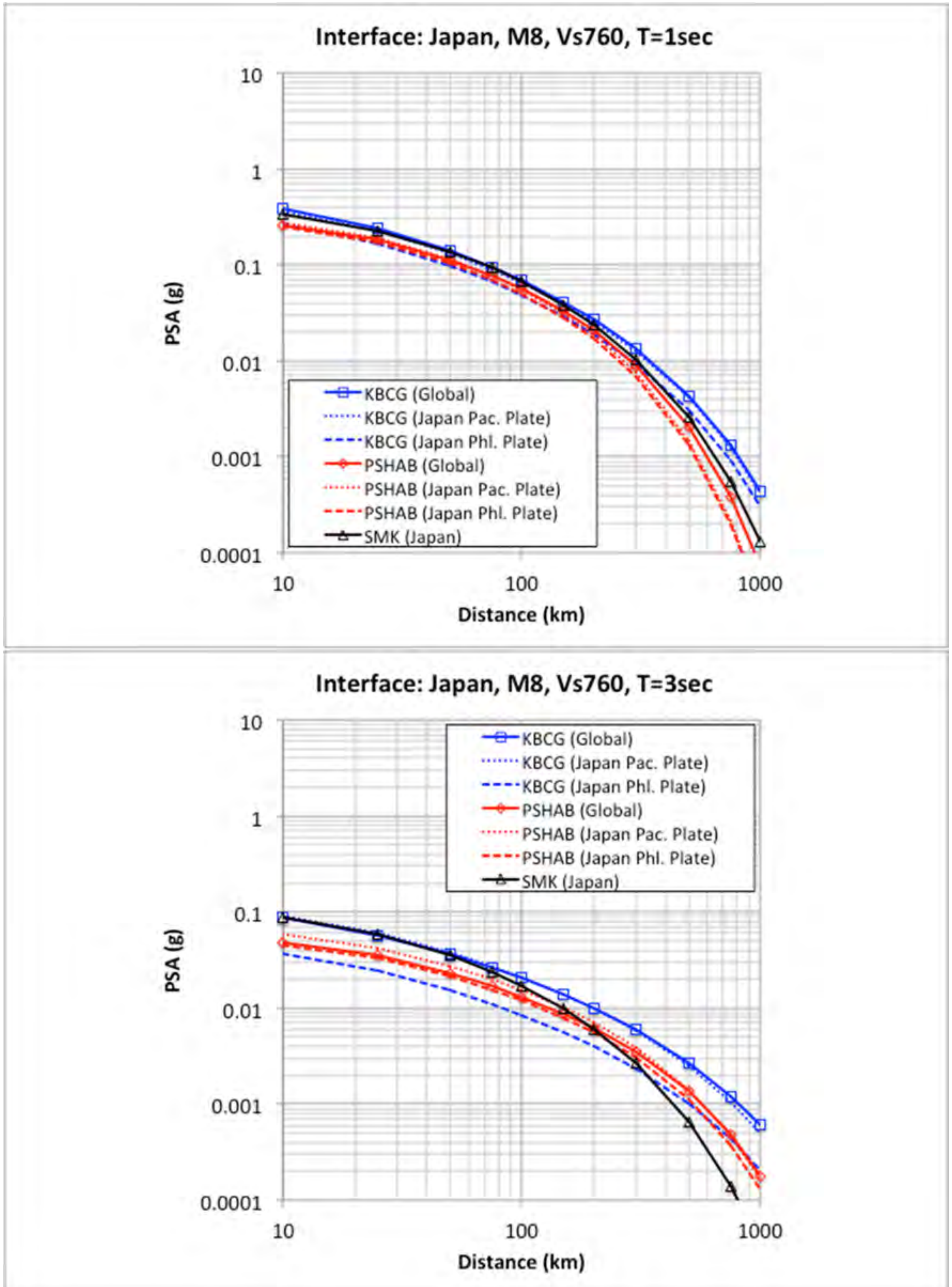

Figure 3.18 Comparison of Japan regional M8 (interface) for 1.0 (top) and 3.0 sec (bottom) attenuation curves for V_{S30} = 760 m/sec.

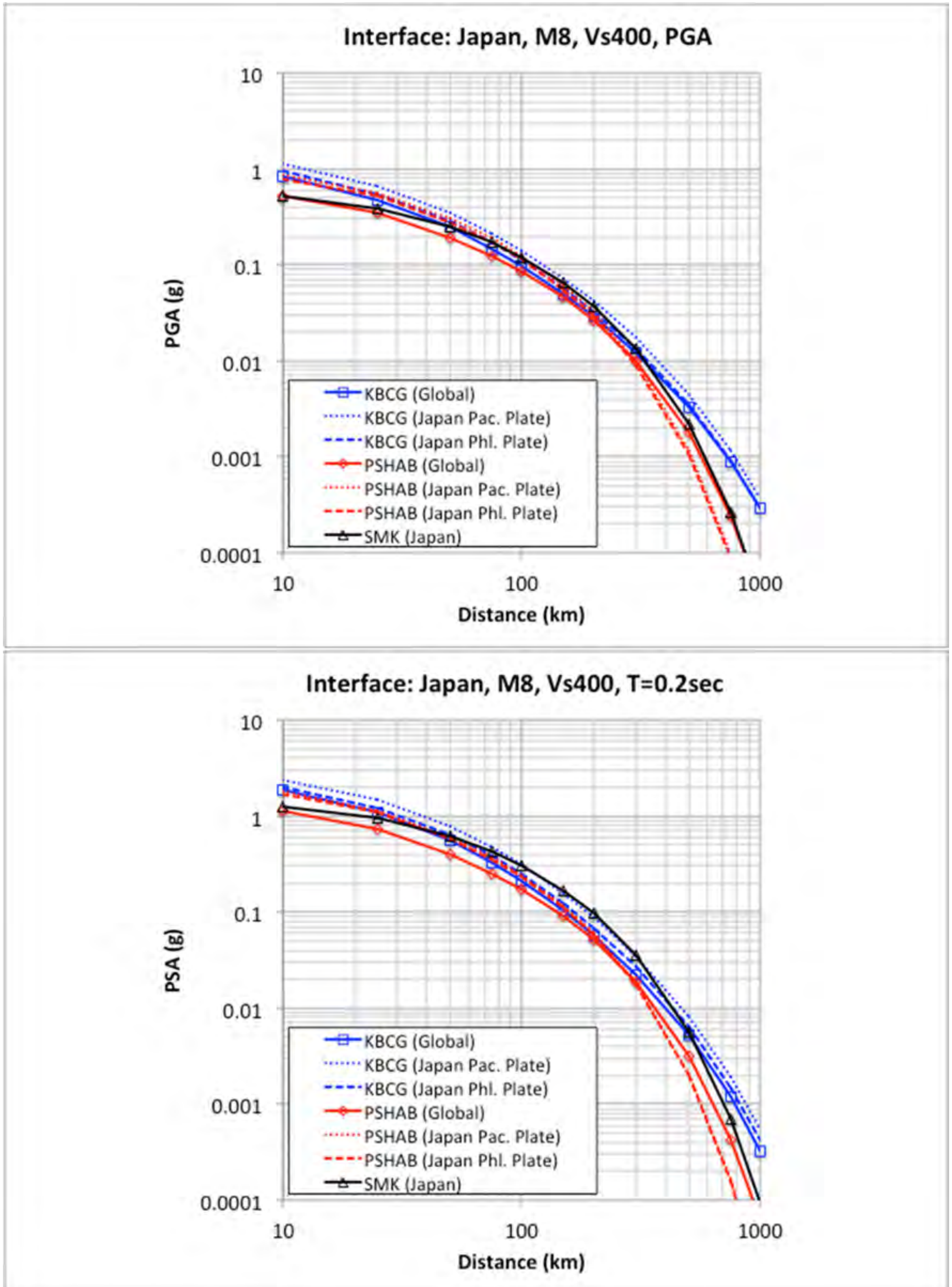

Figure 3.19 **Comparison of Japan regional M8 (interface) for PGA (*T* = 0.01 sec) (top) and 0.2 sec (bottom) attenuation curves for V_{S30} = 400 m/sec.**

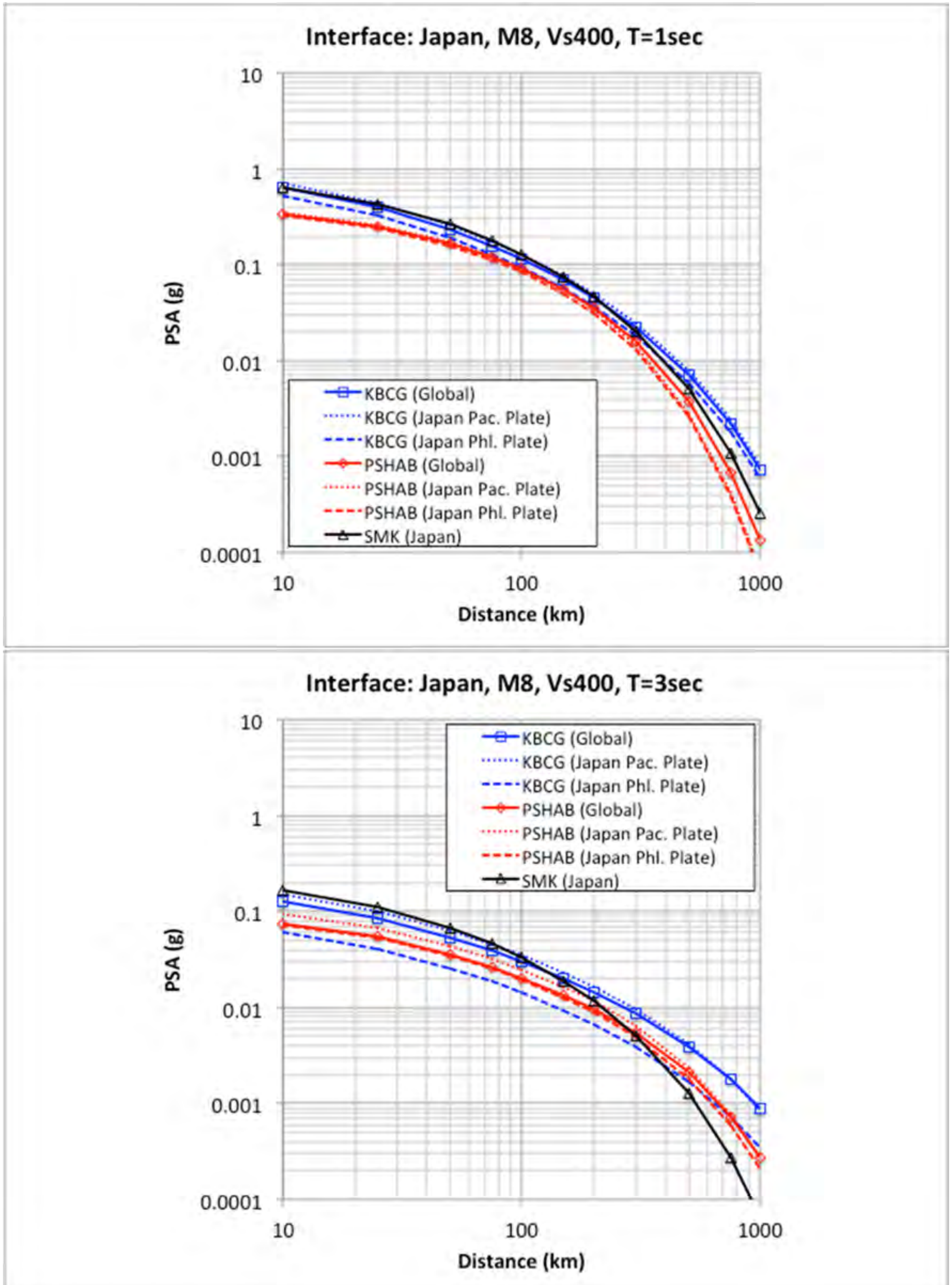

Figure 3.20 **Comparison of Japan regional M8 (interface) for 1.0 (top) and 3.0 sec (bottom) attenuation curves for V_{S30} = 400 m/sec.**

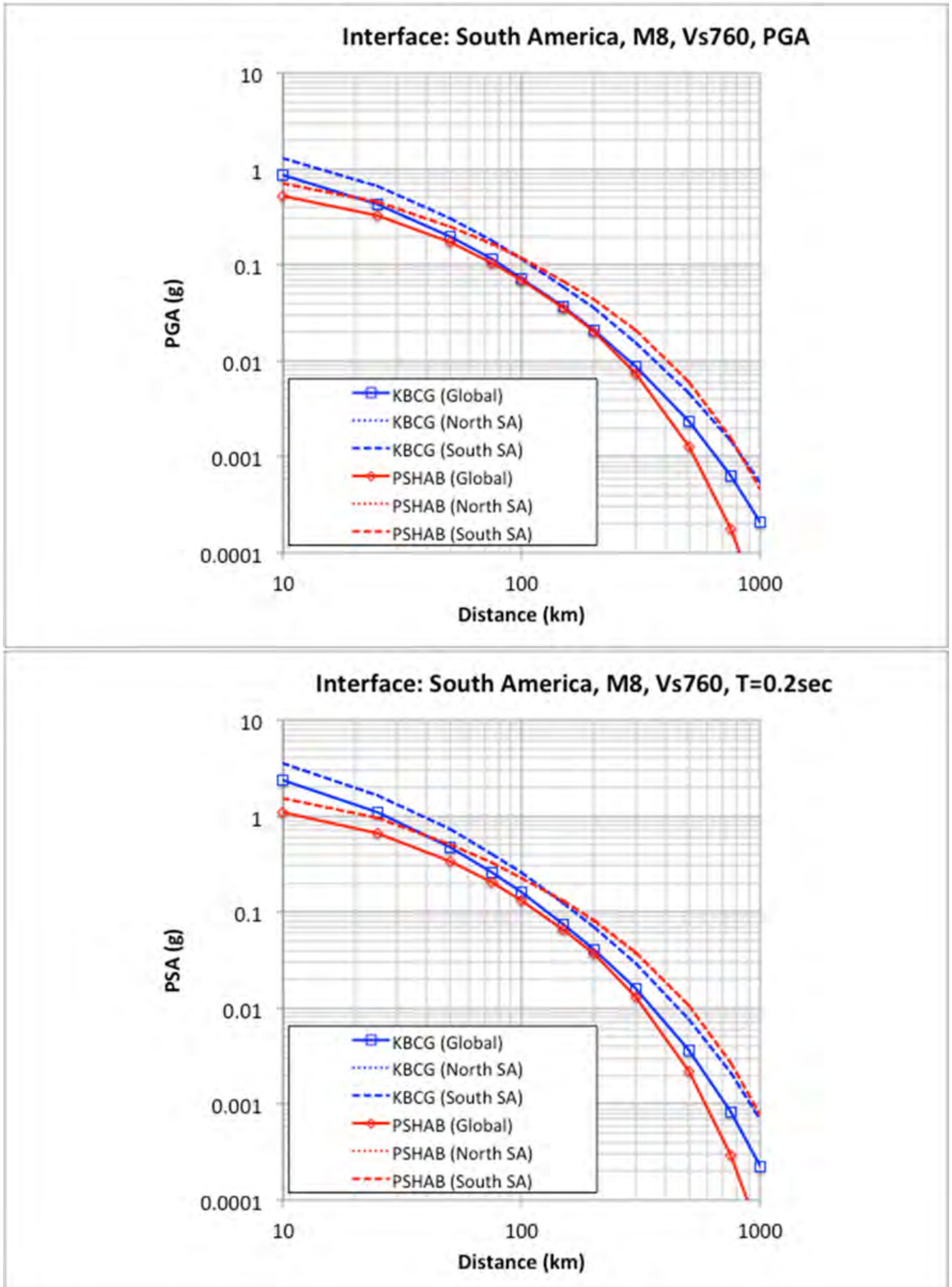

Figure 3.21 **Comparison of South America regional M8 (interface) for PGA (*T* = 0.01 sec) (top) and 0.2 sec (bottom) attenuation curves for V_{S30} = 760 m/sec.**

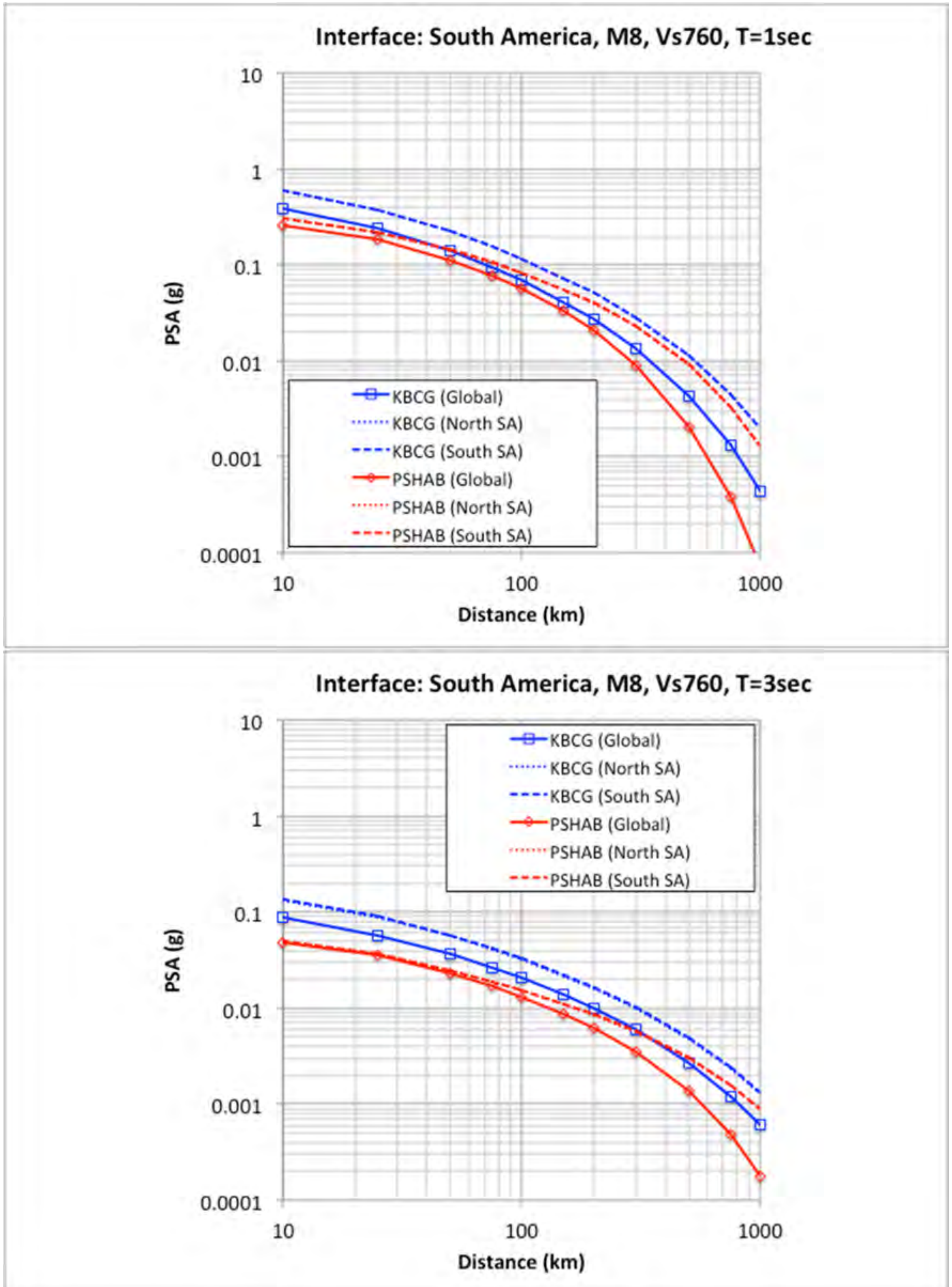

Figure 3.22 **Comparison of South America regional M8 (interface) for 1.0 (top) and 3.0 sec (bottom) attenuation curves for V_{S30} = 760 m/sec.**

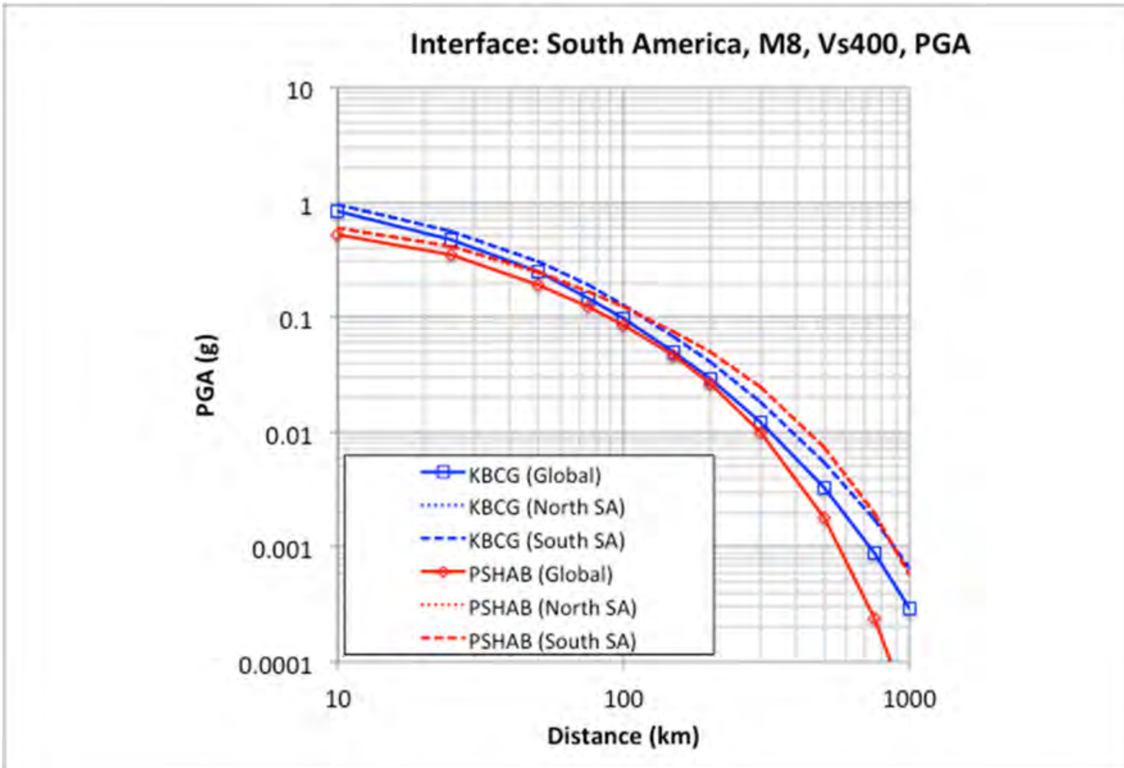

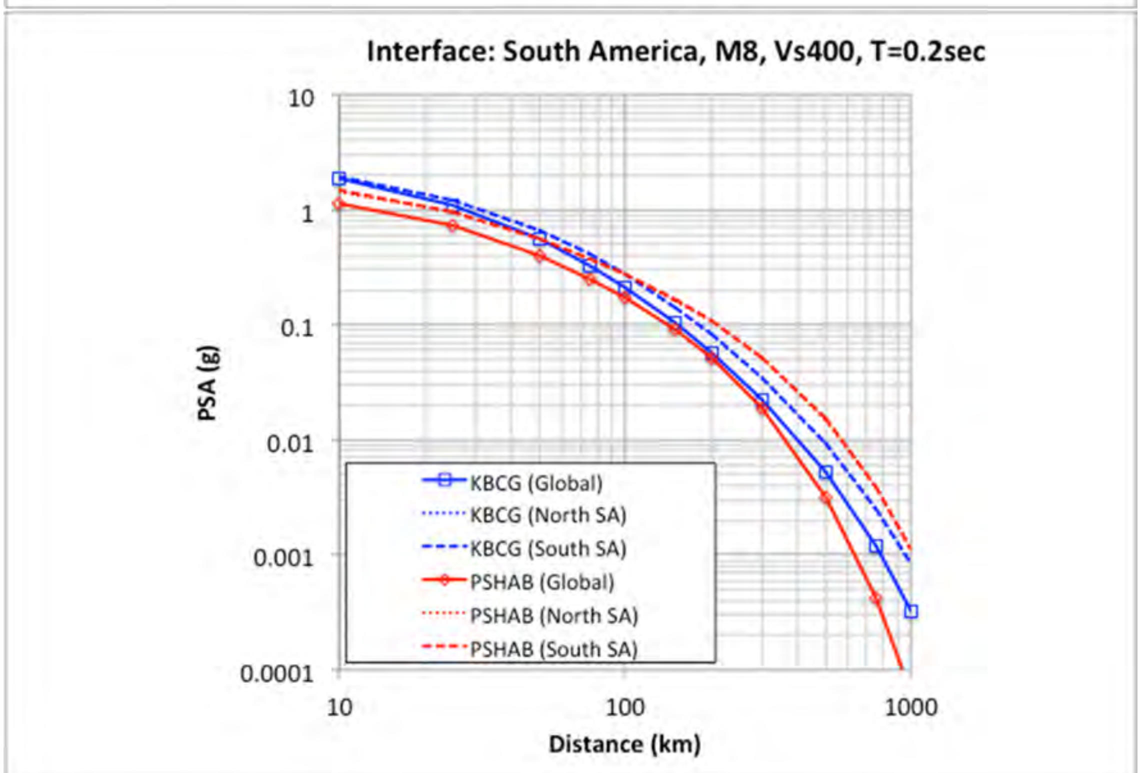

Figure 3.23 **Comparison of South America regional M8 (interface) for PGA (*T* = 0.01 sec) (top) and 0.2 sec (bottom) attenuation curves for V_{S30} = 400 m/sec.**

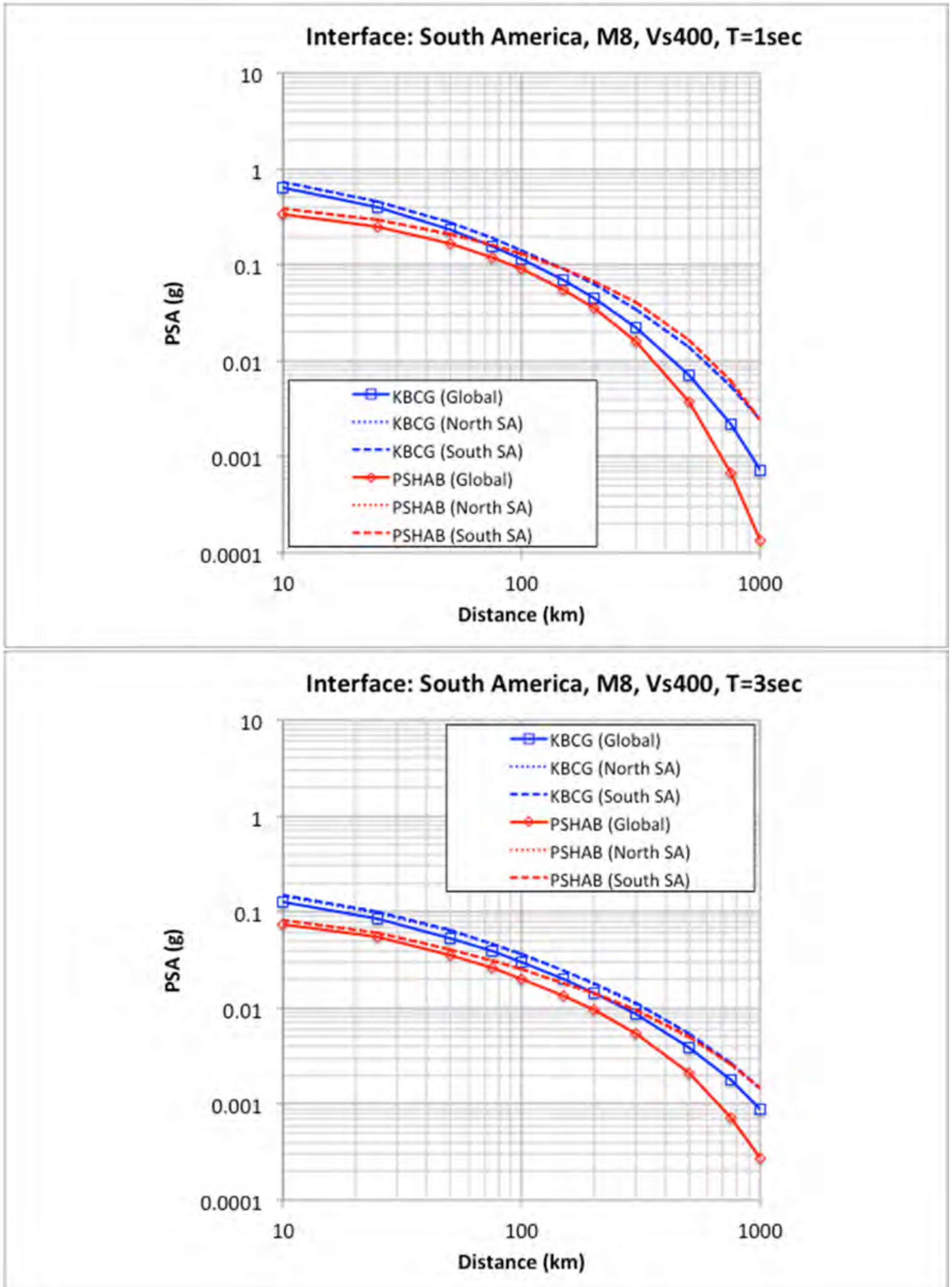

Figure 3.24 Comparison of South America regional M8 (interface) for 1.0 (top) and 3.0 sec (bottom) attenuation curves for V_{S30} = 400 m/sec.

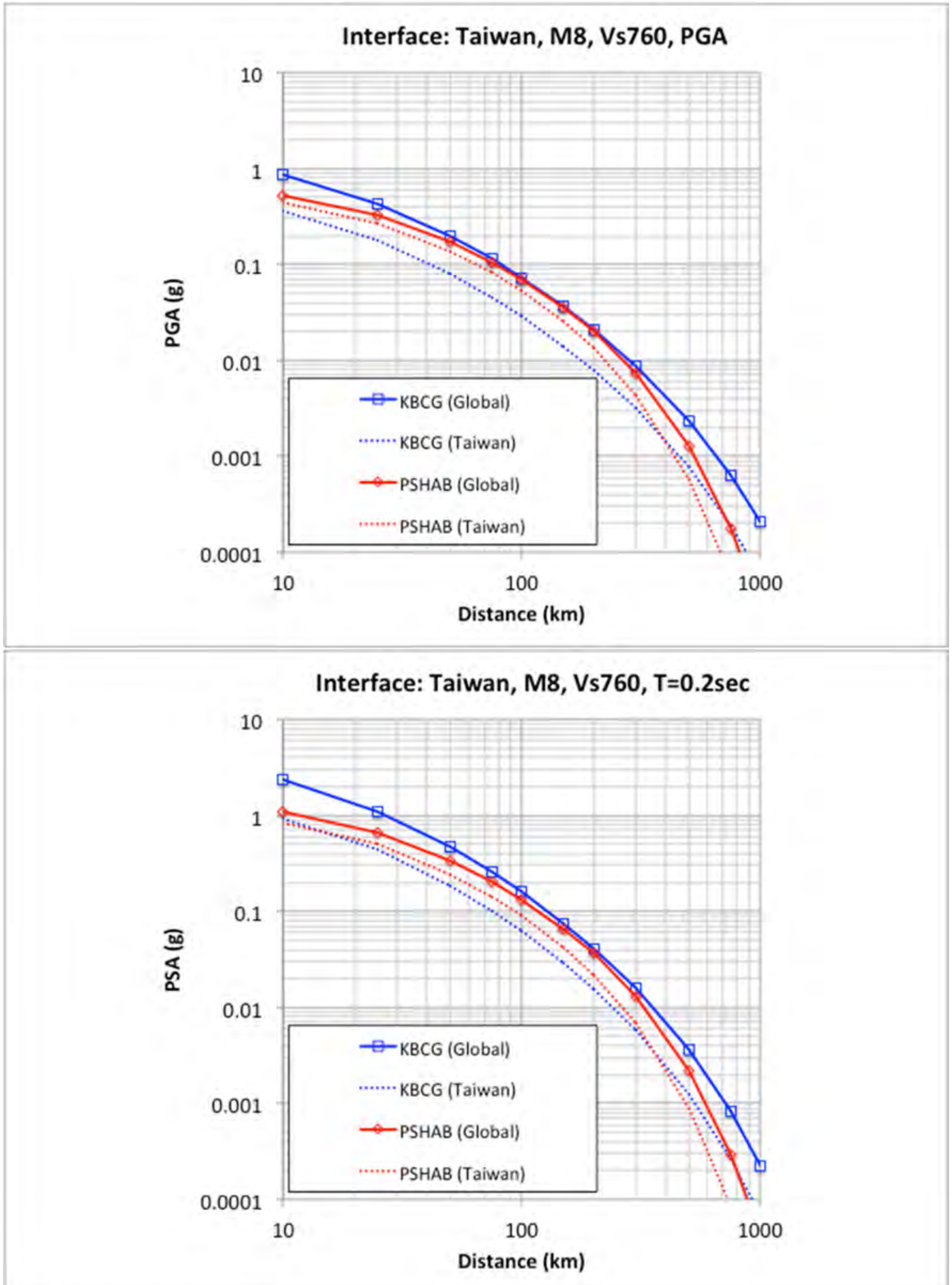

Figure 3.25 **Comparison of Taiwan regional M8 (interface) for PGA (*T* = 0.01 sec) (top) and 0.2 sec (bottom) attenuation curves for V_{S30} = 760 m/sec.**

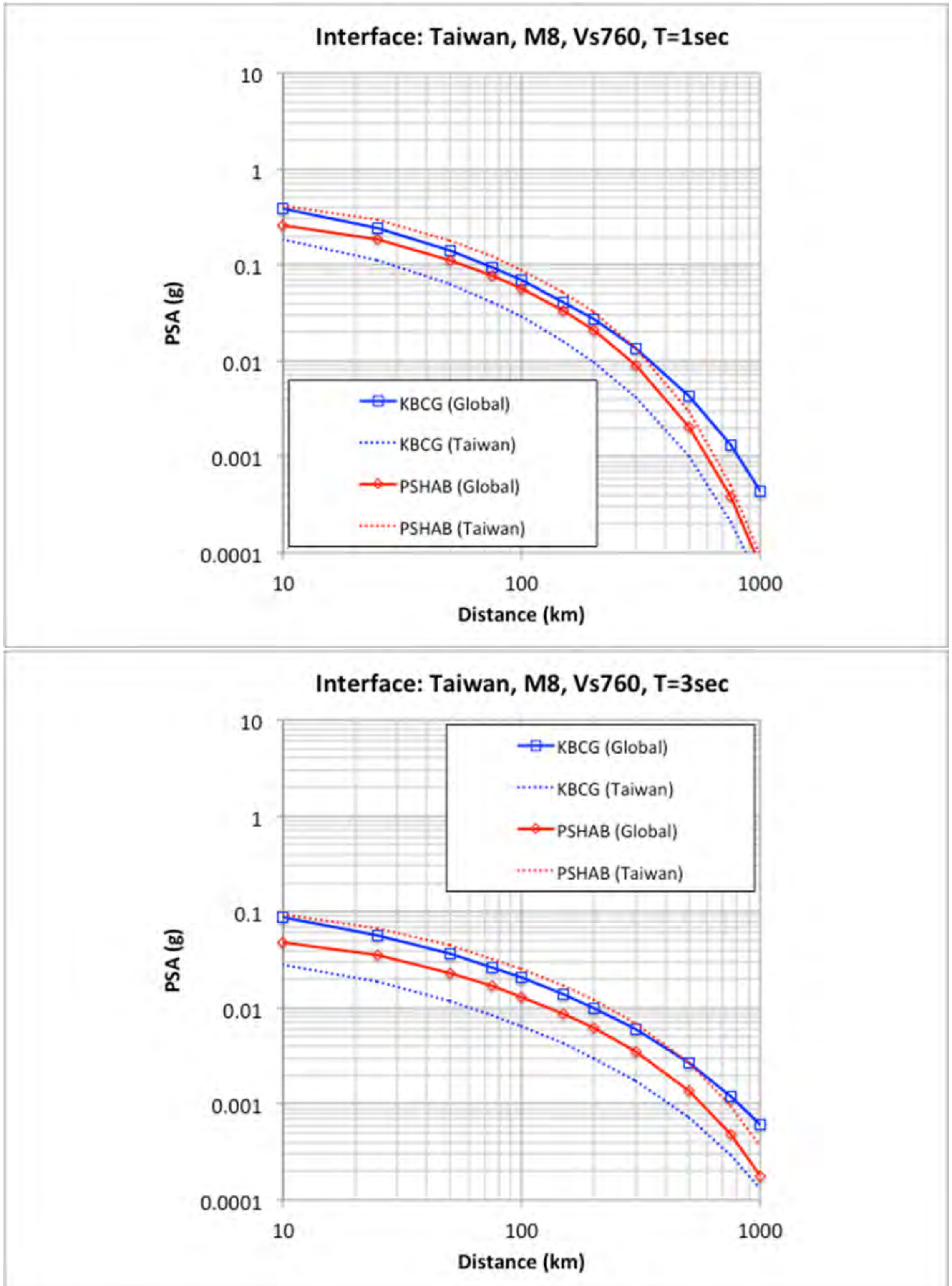

Figure 3.26 **Comparison of Taiwan regional M8 (interface) for 1.0 (top) and 3.0 sec (bottom) attenuation curves for V_{S30} = 760 m/sec.**

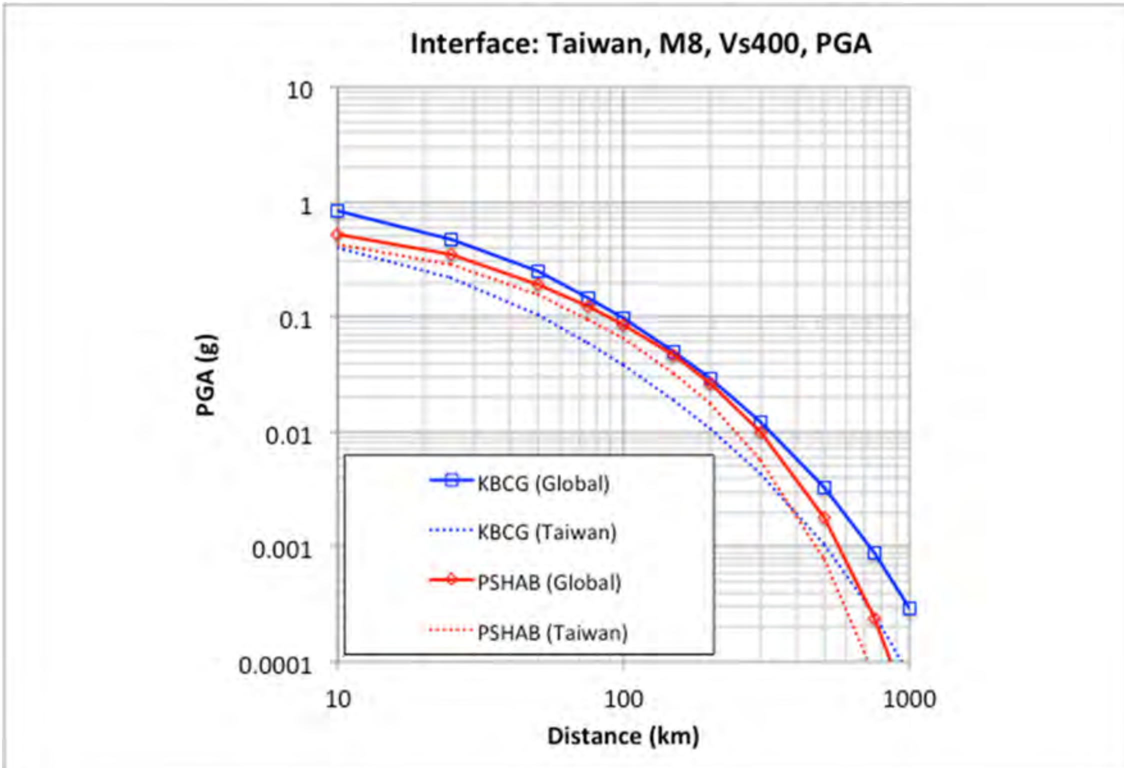

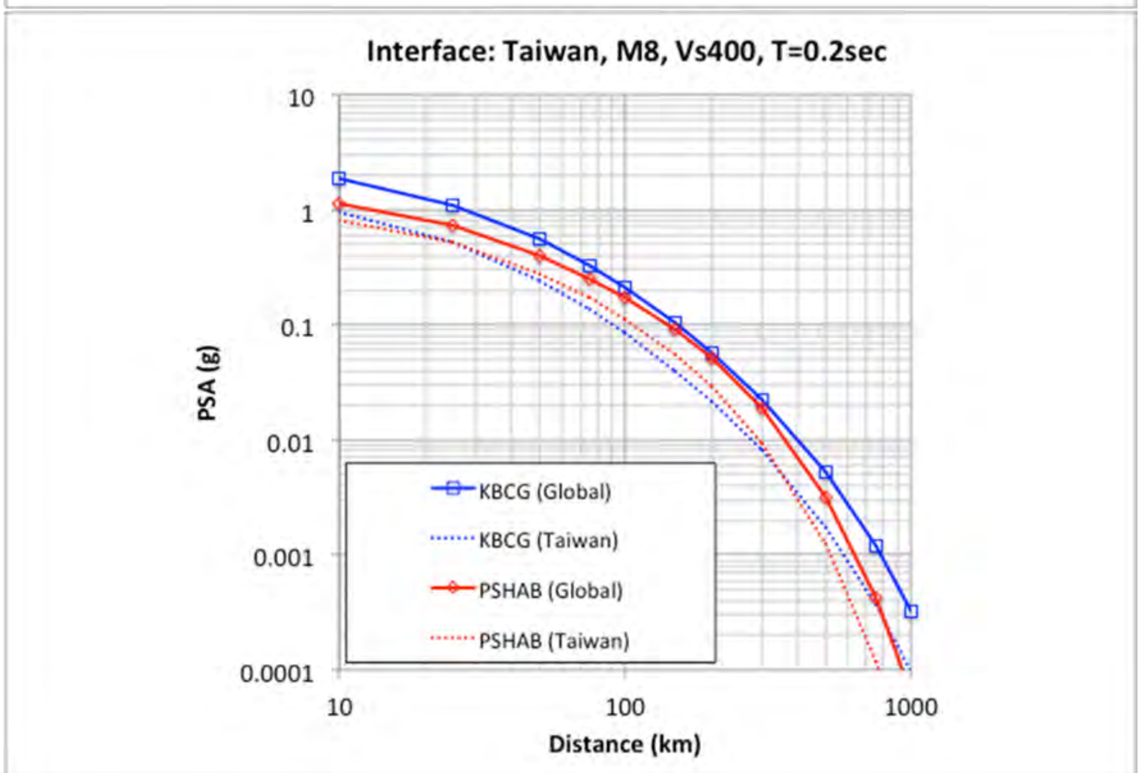

Figure 3.27 **Comparison of Taiwan regional M8 (interface) for PGA *(T* = 0.01 sec) (top) and 0.2 sec (bottom) attenuation curves for V_{S30} = 400 m/sec.**

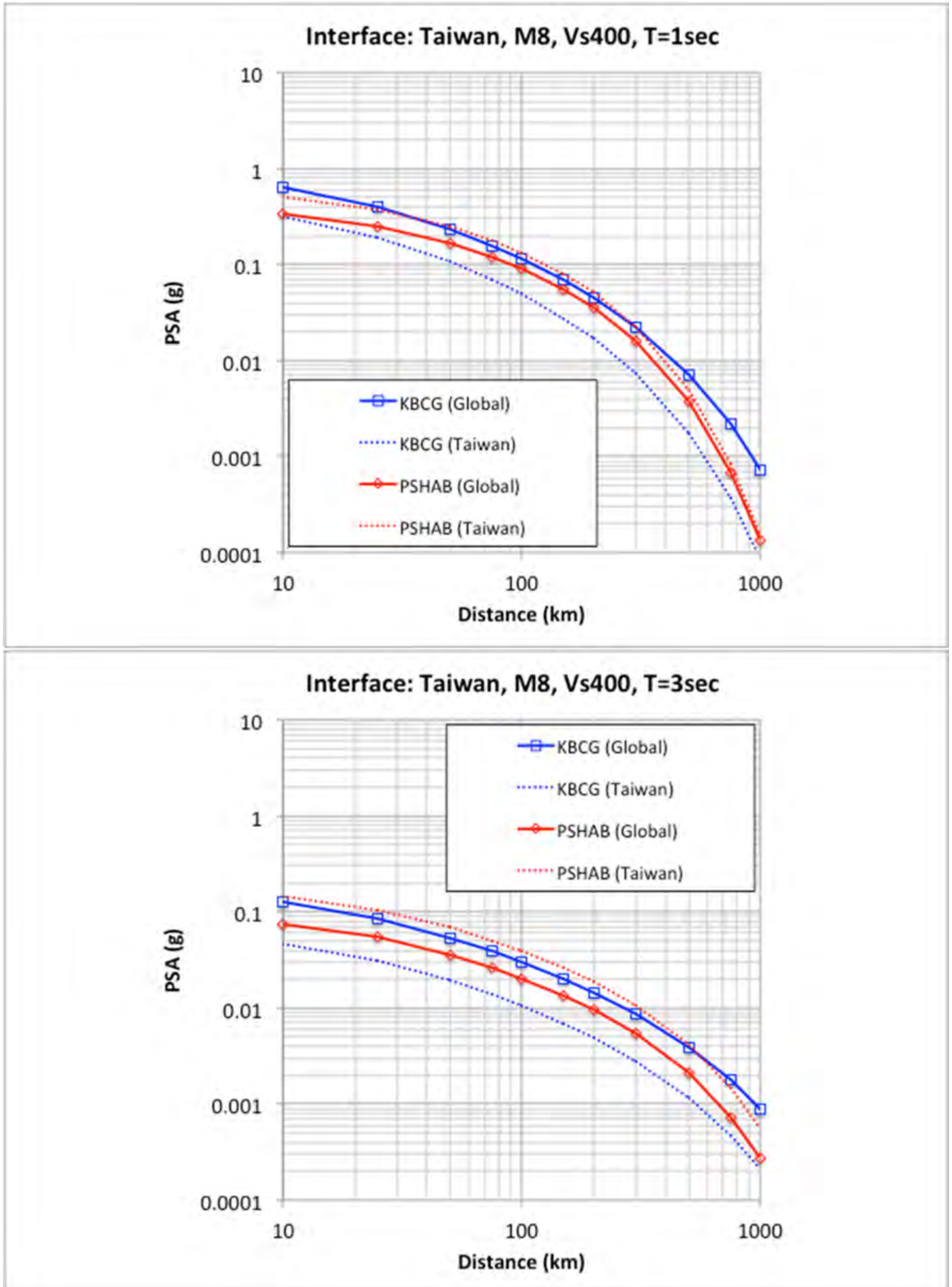

Figure 3.28 **Comparison of Taiwan regional M8 (interface) for 1.0 (top) and 3.0 sec (bottom) attenuation curves for V_{S30} = 400 m/sec.**

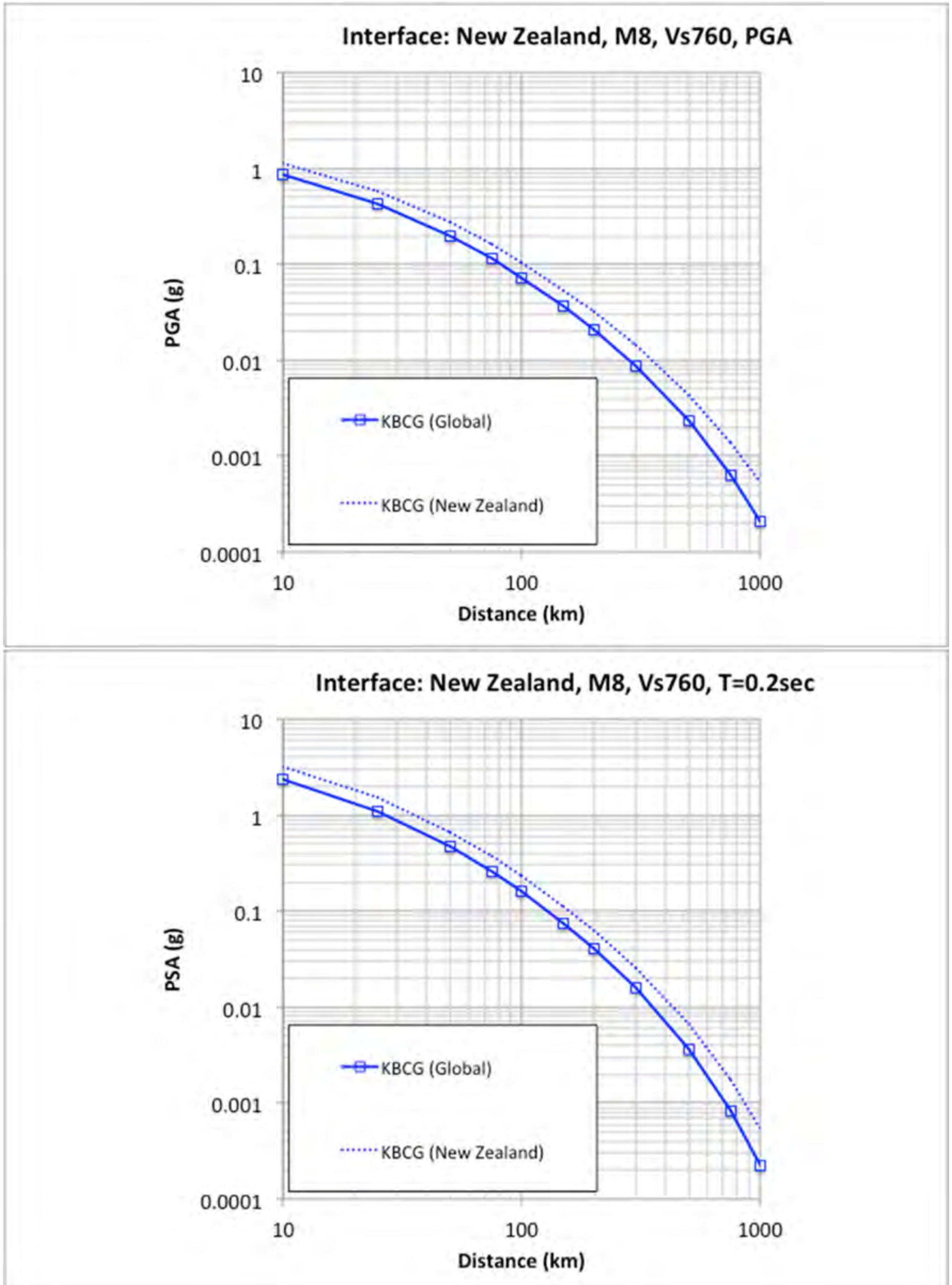

Figure 3.29 **Comparison of New Zealand regional M8 (interface) for PGA (*T* = 0.01 sec) (top) and 0.2 sec (bottom) attenuation curves for V_{S30} = 760 m/sec.**

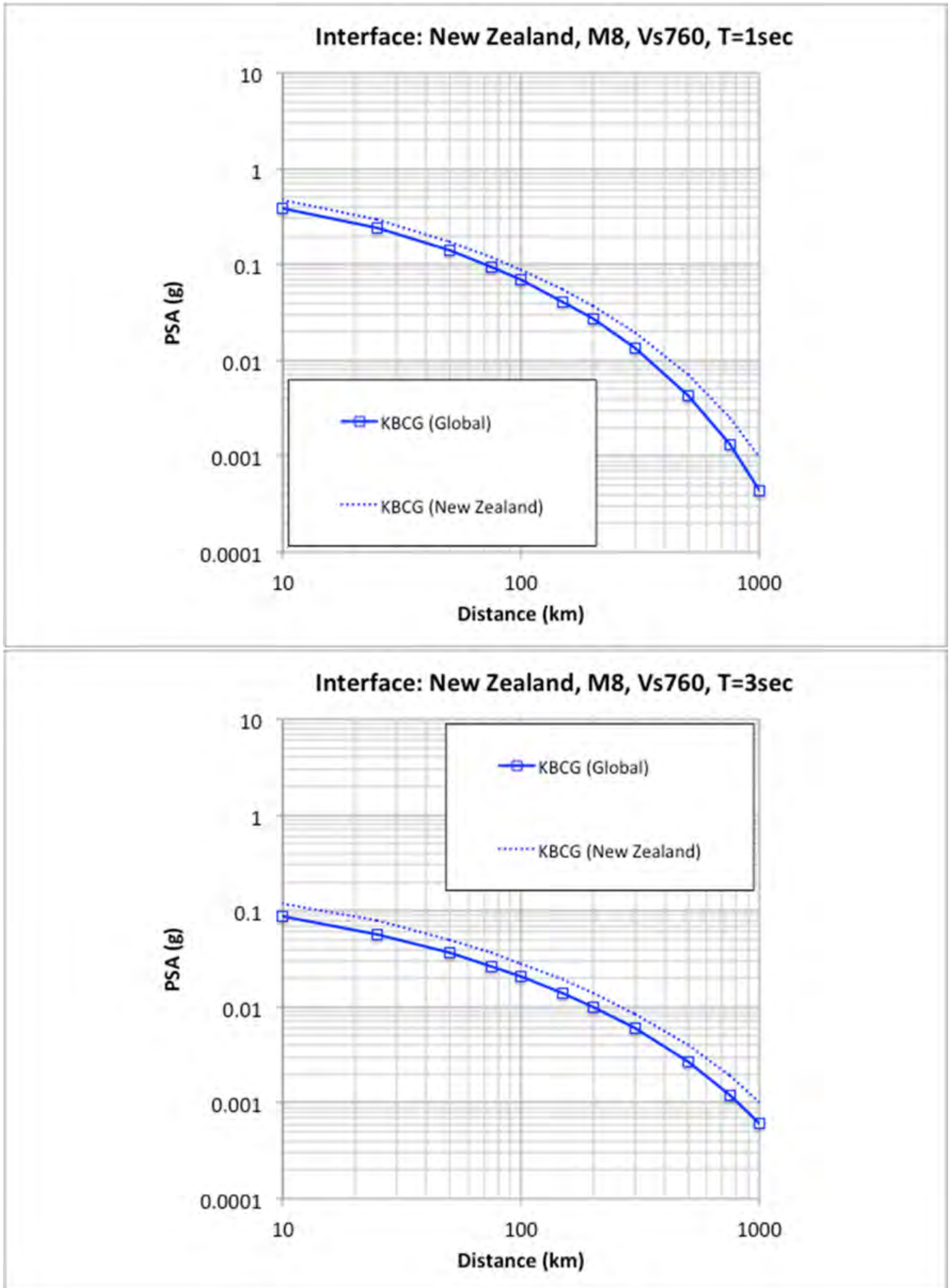

Figure 3.30 **Comparison of New Zealand regional M8 (interface) for 1.0 (top) and 3.0 sec (bottom) attenuation curves for V_{S30} = 760 m/sec.**

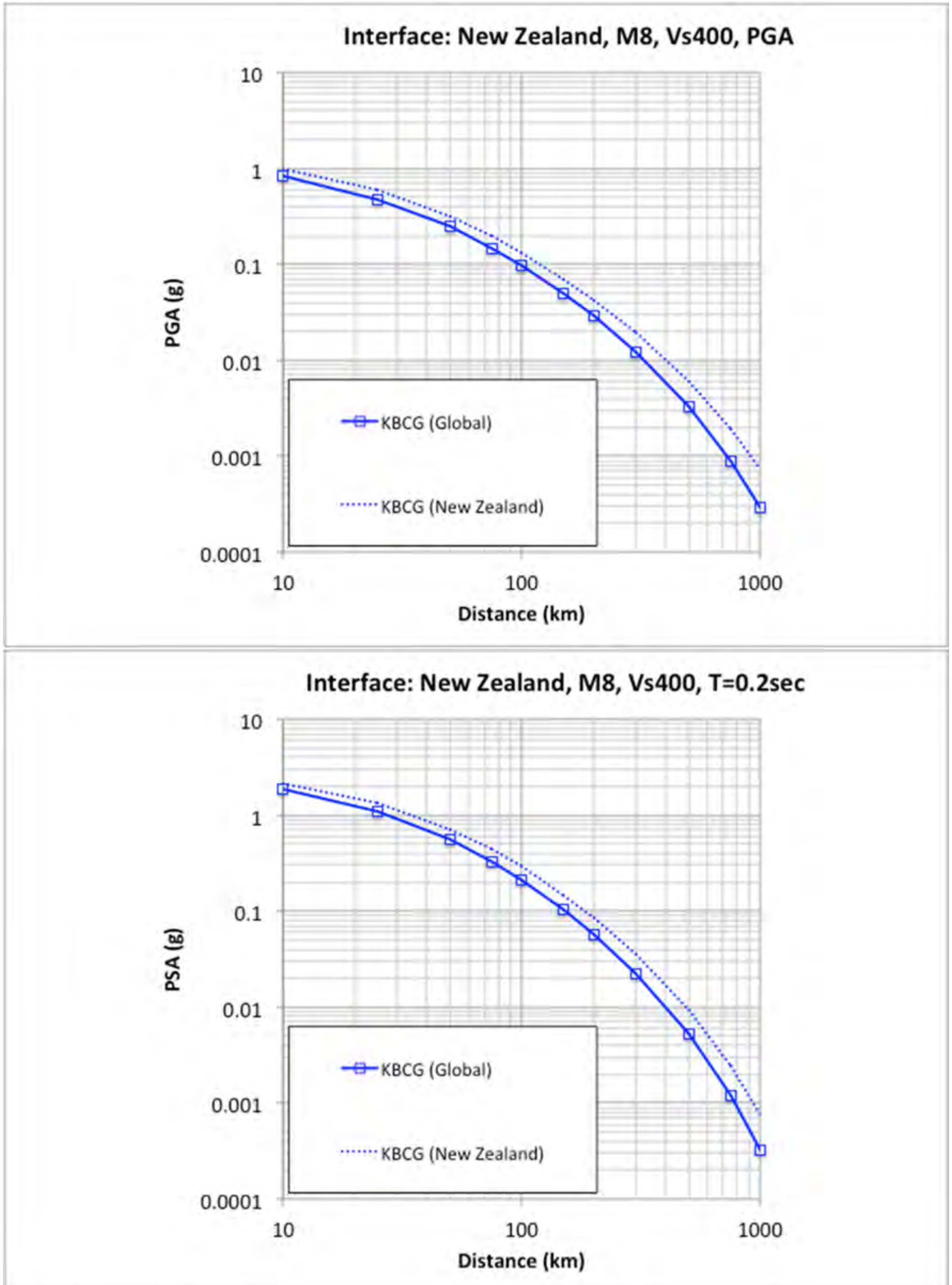

Figure 3.31 Comparison of New Zealand regional M8 (interface) for PGA (T = 0.01 sec) (top) and 0.2 sec (bottom) attenuation curves for V_{S30} = 400 m/sec.

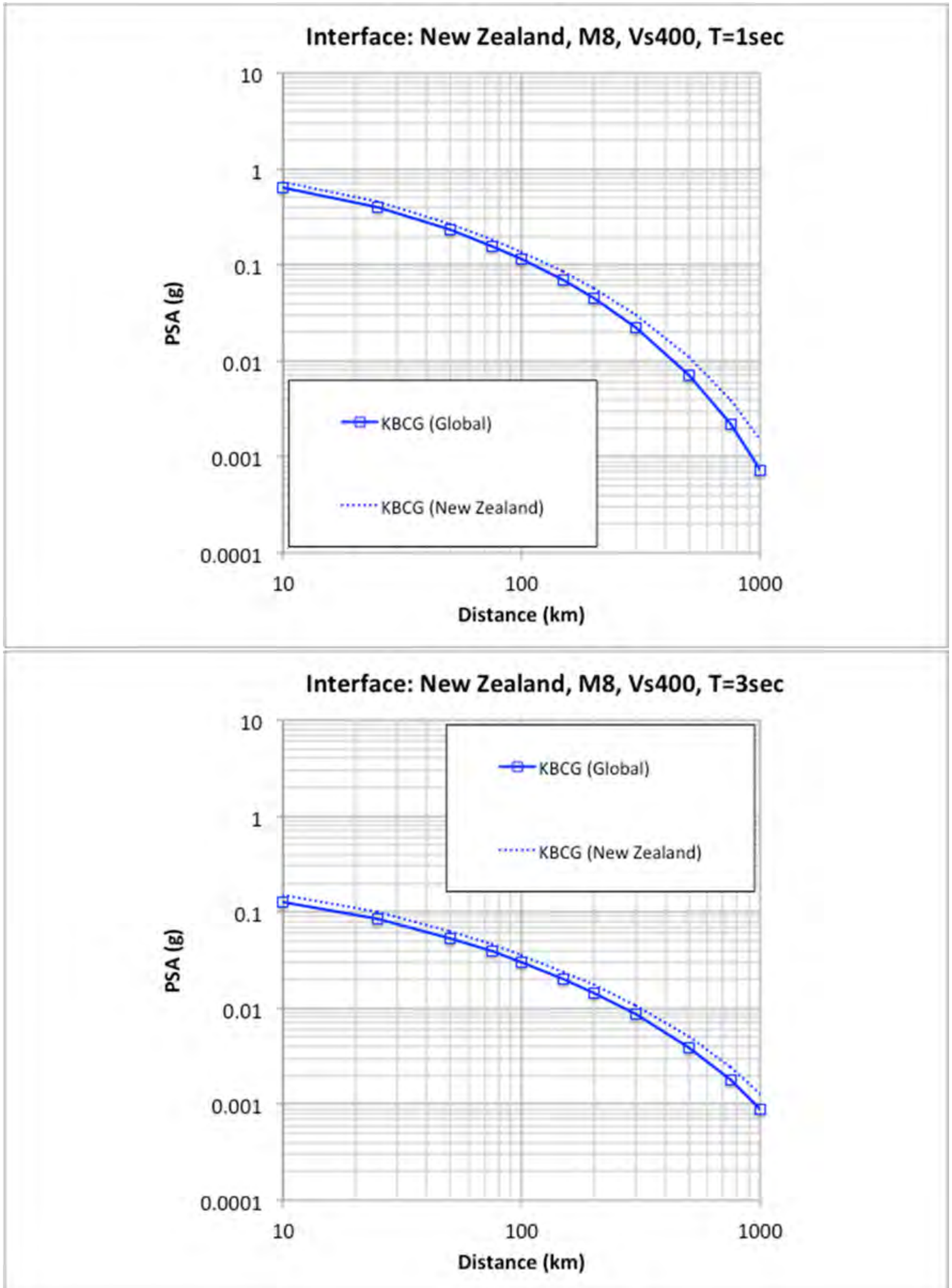

Figure 3.32 **Comparison of New Zealand regional M8 (interface) for 1.0 (top) and 3.0 sec (bottom) attenuation curves for V_{S30} = 400 m/sec.**

3.1.2 Interface Spectra

Interface event spectra are computed for magnitudes 7, 8, and 9 at two distances of 75 and 200 km; see Table 3.1. Ground motions are computed for the full spectral period range of 0.01 to 10 sec for the two selected V_{S30} values of 760 and 400 m/sec. For the global case, the computed spectra from the NGA-Sub GMMs are compared with the previously developed GMMs. For each of the individual regional cases, the comparison is presented between the NGA-Sub GMM global model and the specific regional models. Representative spectra plots for the **M**8 case for both distances of 75 and 200 km are plotted in Figure 3.33 to Figure 3.48. The full suite of spectra plots (i.e., both digital data and plots) are contained in the associated electronic files; see Appendix A.

In general, similar results are observed with the spectra comparisons as is noted for the attenuation curves. For the two NGA-Sub GMM global models, there are similar ground-motion spectra for the selected cases especially when compared to the previous GMMs, which show a larger distribution of ground-motion values. In comparing the regional models with the global models, the results for Alaska, South America, and Taiwan show the largest change from the global models.

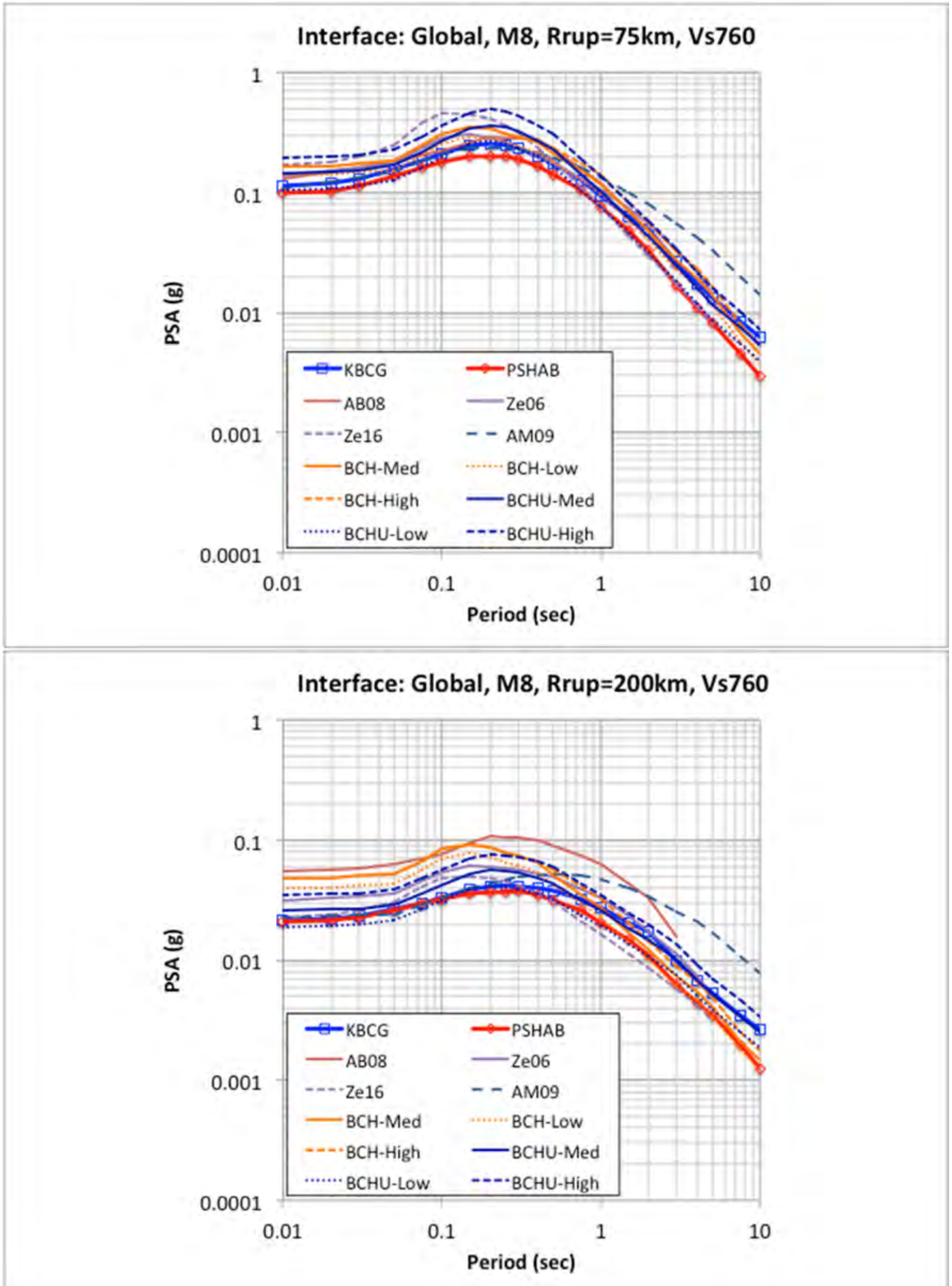

Figure 3.33 **Comparison of global M8 (interface) for distances of 75 km (top) and 200 km (bottom) spectra for V_{S30} = 760 m/sec.**

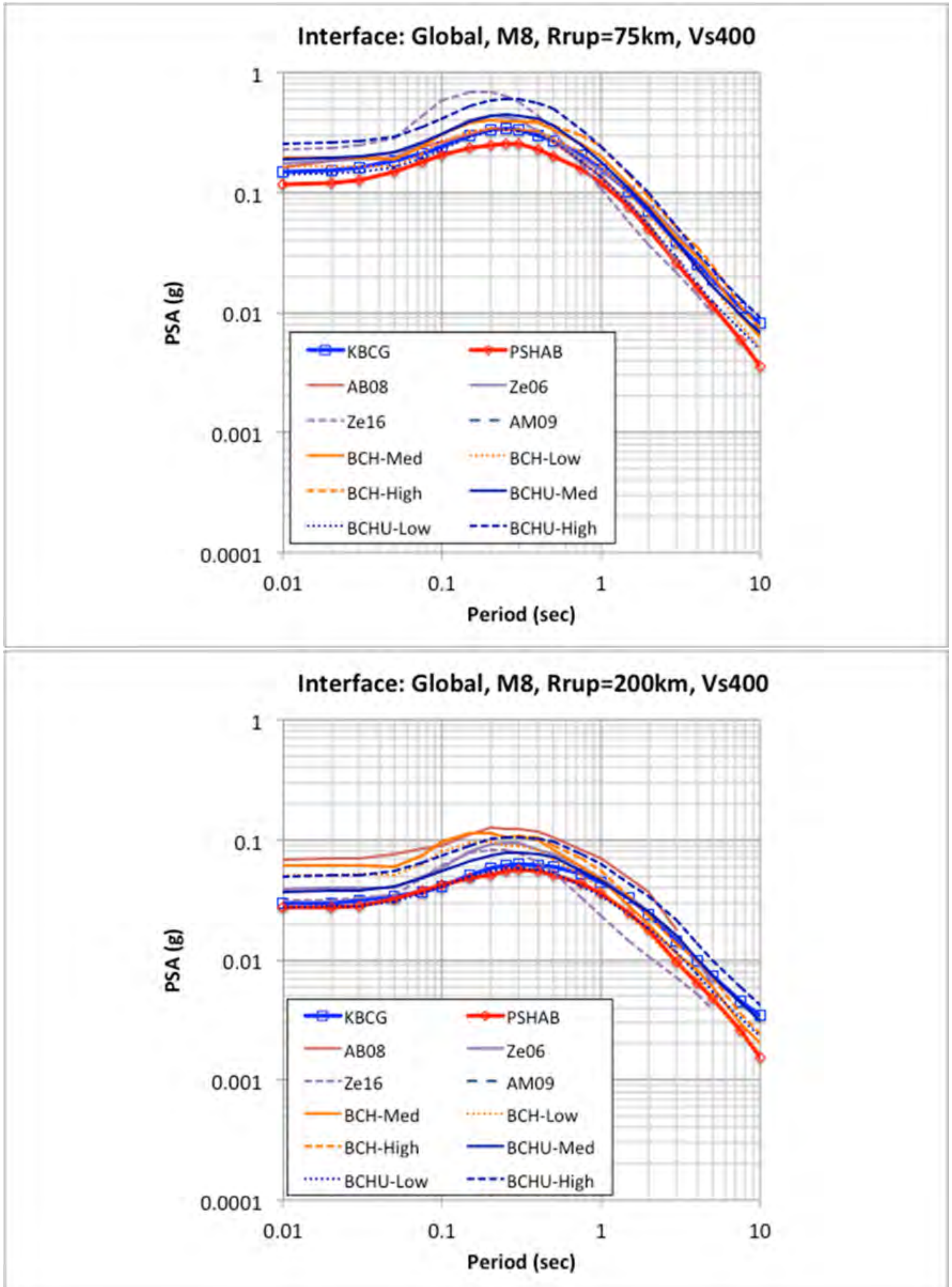

Figure 3.34 **Comparison of global M8 (interface) for distances of 75 km (top) and 200 km (bottom) spectra for V_{S30} = 400 m/sec.**

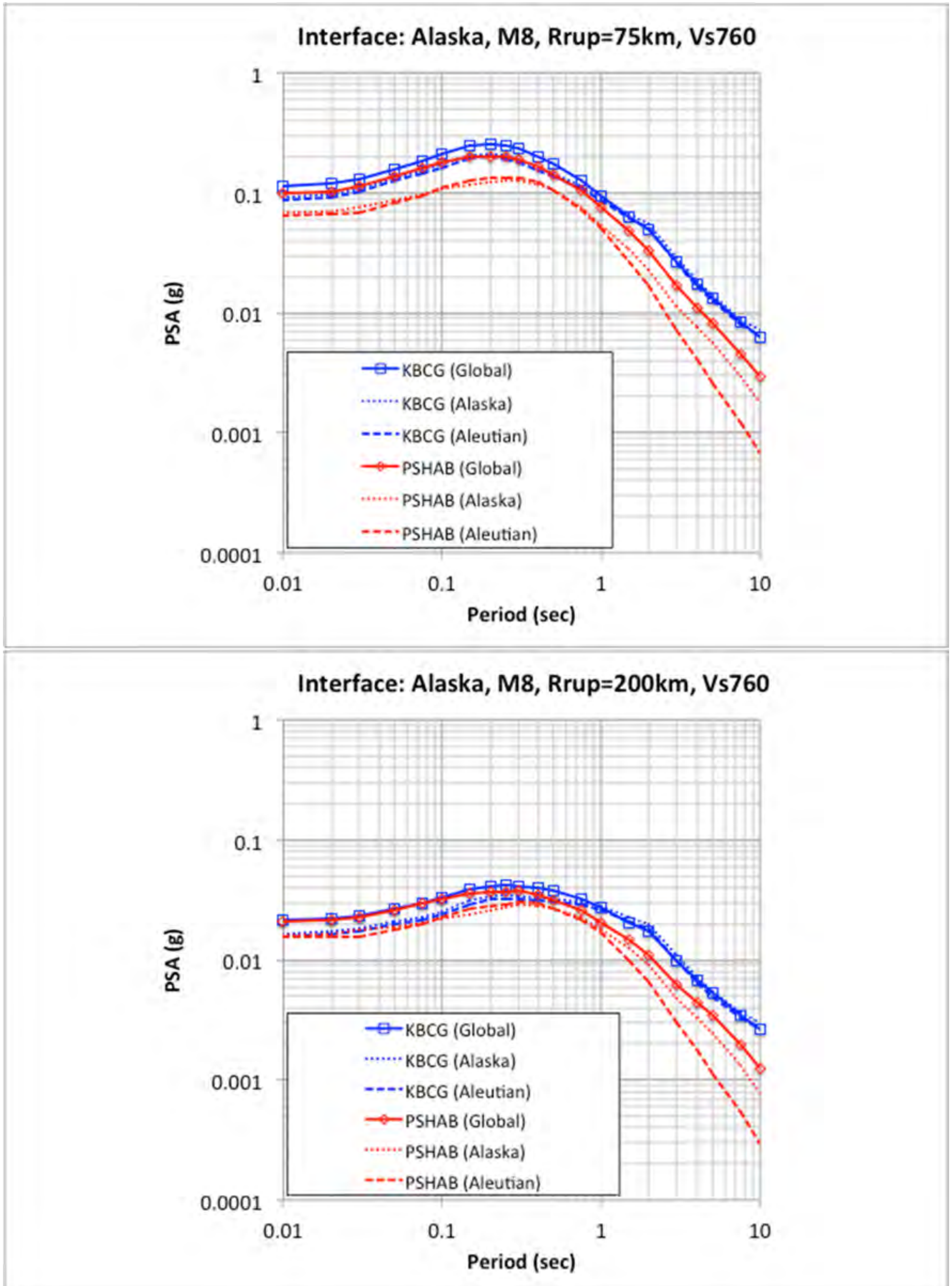

Figure 3.35 **Comparison of Alaska regional M8 (interface) for distances of 75 km (top) and 200 km (bottom) spectra for V_{S30} = 760 m/sec.**

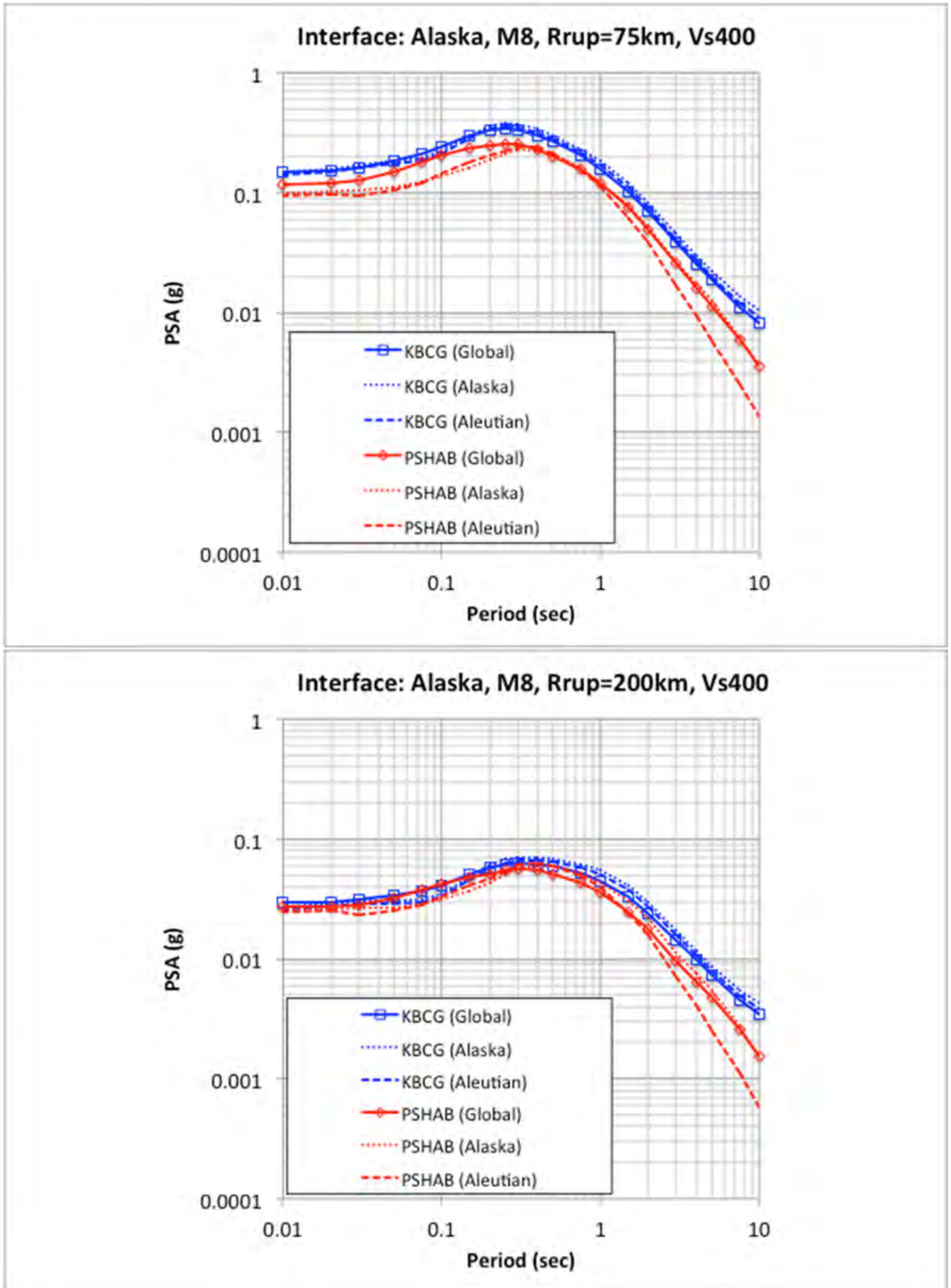

Figure 3.36 **Comparison of Alaska regional M8 (interface) for distances of 75 km (top) and 200 km (bottom) spectra for V_{S30} = 400 m/sec.**

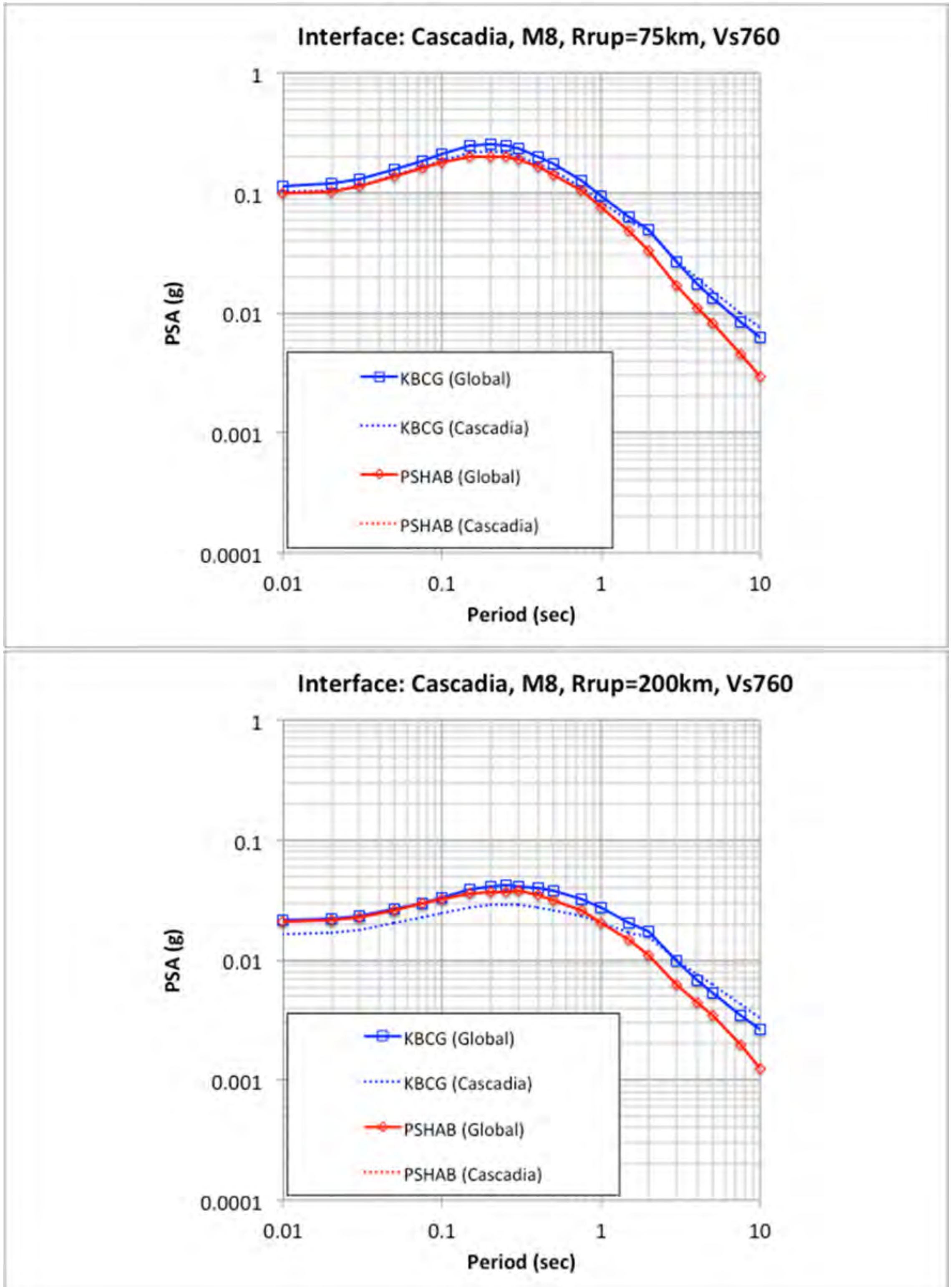

Figure 3.37 Comparison of Cascadia regional M8 (interface) for distances of 75 km (top) and 200 km (bottom) spectra for V_{S30} = 760 m/sec.

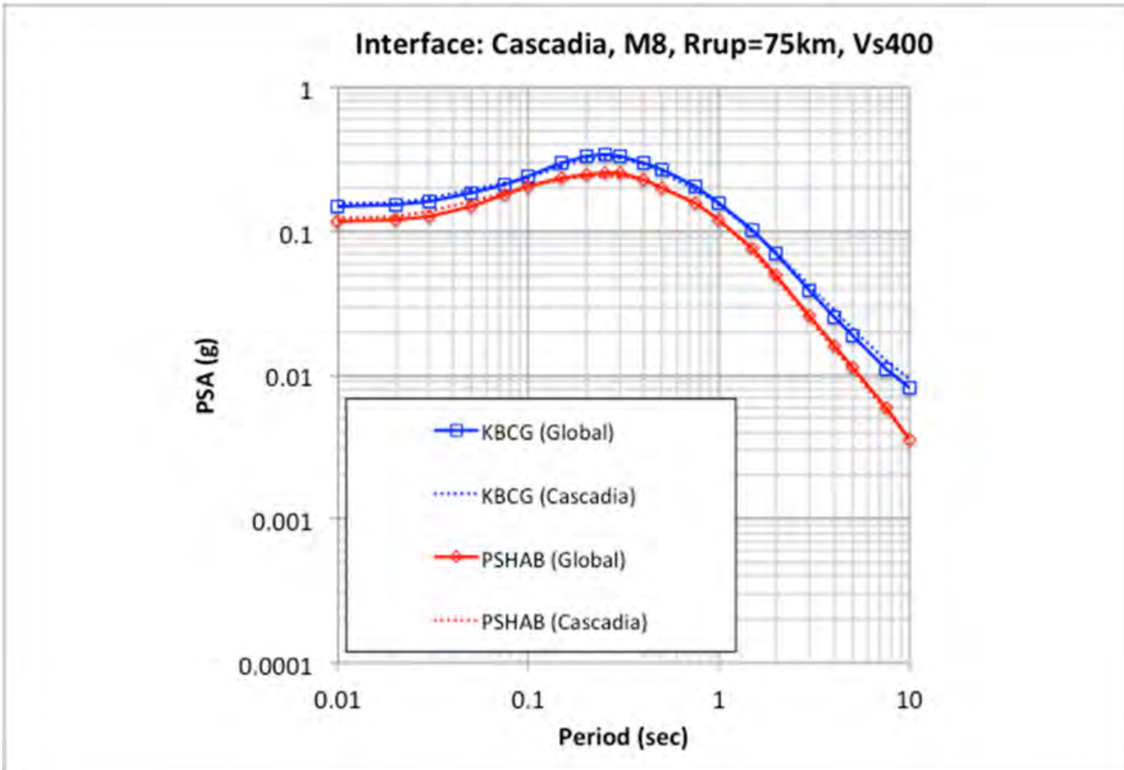

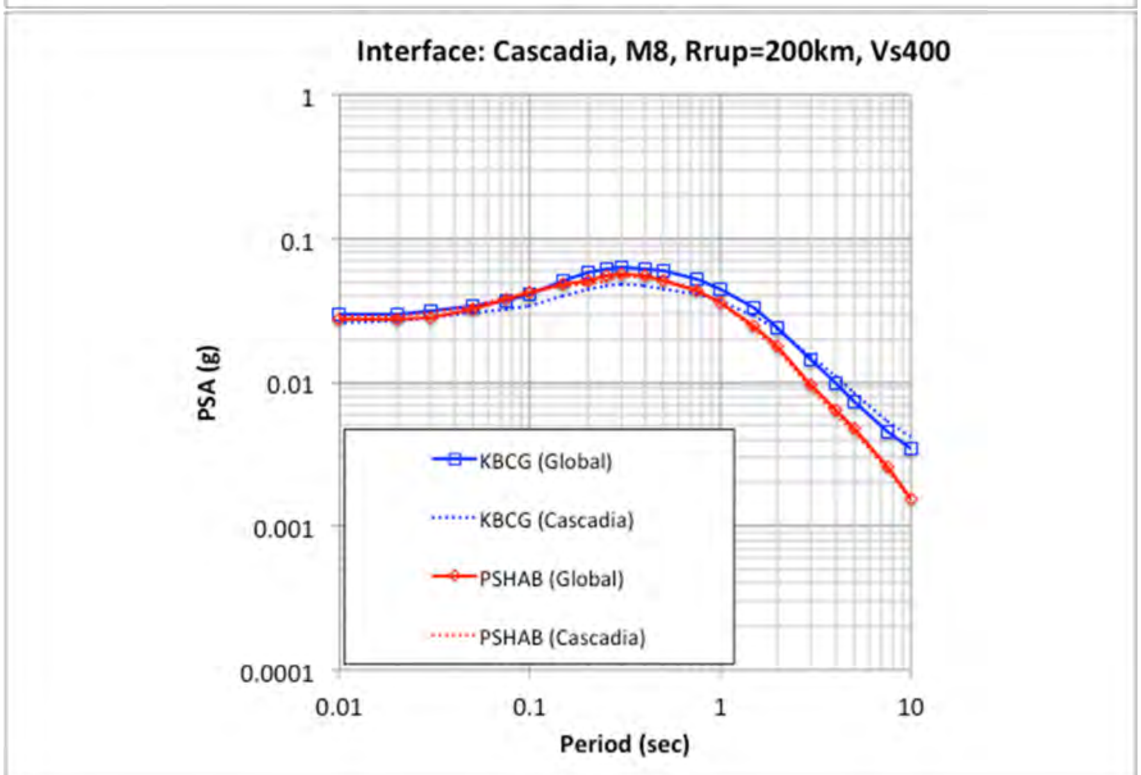

Figure 3.38 Comparison of Cascadia regional M8 (interface) for distances of 75 km (top) and 200 km (bottom) spectra for V_{S30} = 400 m/sec.

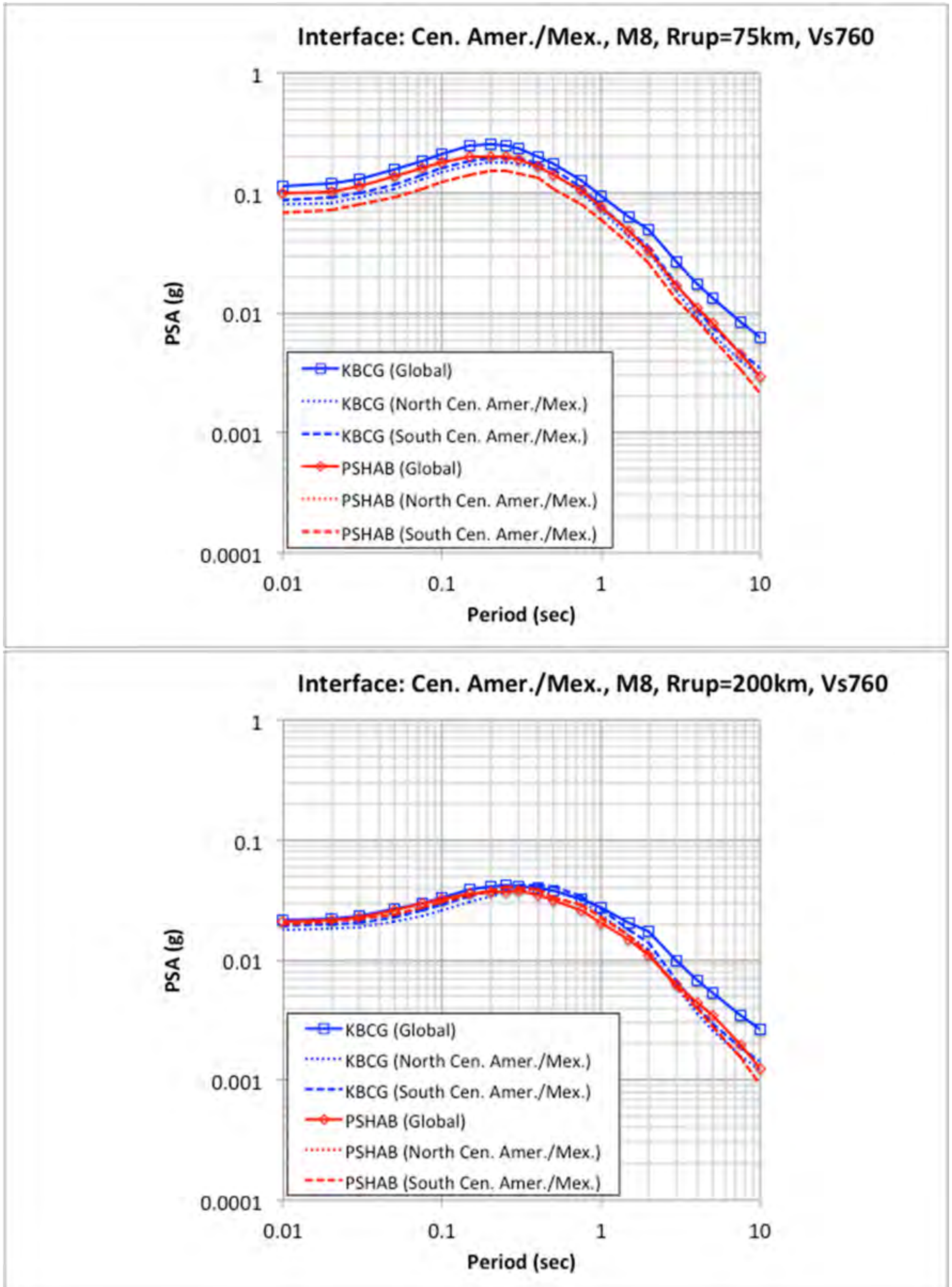

Figure 3.39 **Comparison of Central America and Mexico regional M8 (interface) for distances of 75 km (top) and 200 km (bottom) spectra for V_{S30} = 760 m/sec.**

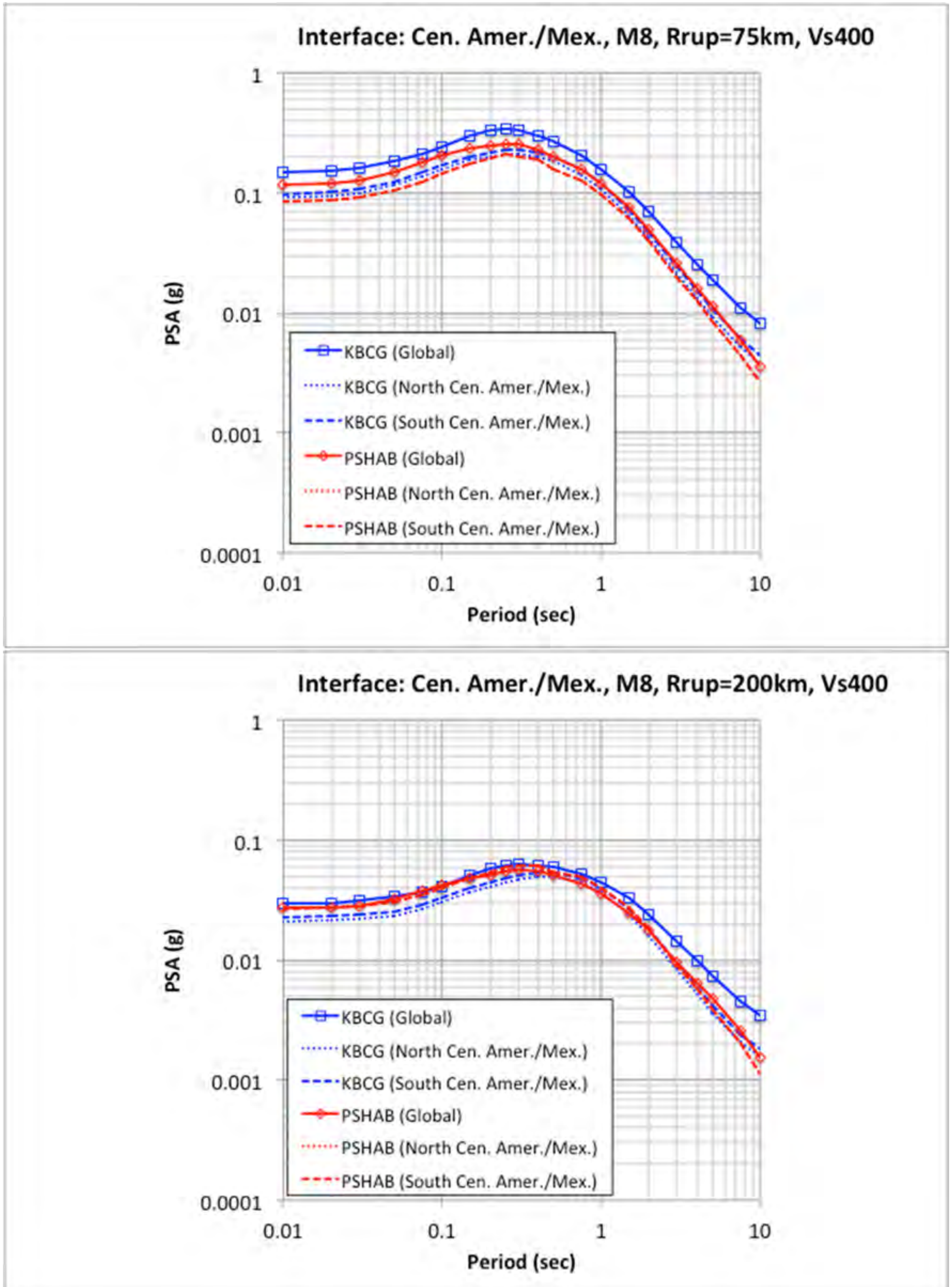

Figure 3.40 Comparison of Central America and Mexico regional M8 (interface) for distances of 75 km (top) and 200 km (bottom) spectra for V_{S30} = 400 m/sec.

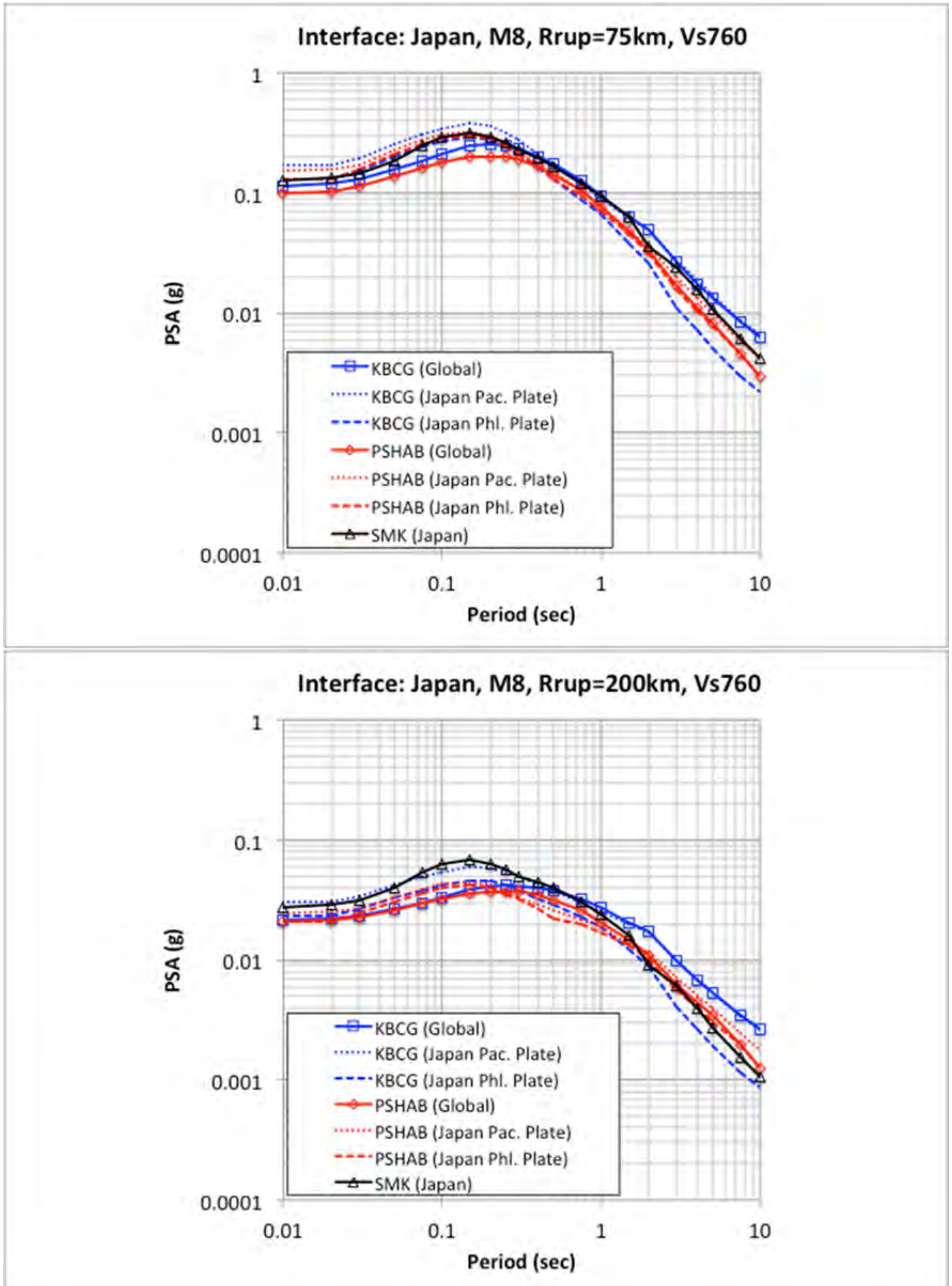

Figure 3.41 **Comparison of Japan regional M8 (interface) for distances of 75 km (top) and 200 km (bottom) spectra for V_{S30} = 760 m/sec.**

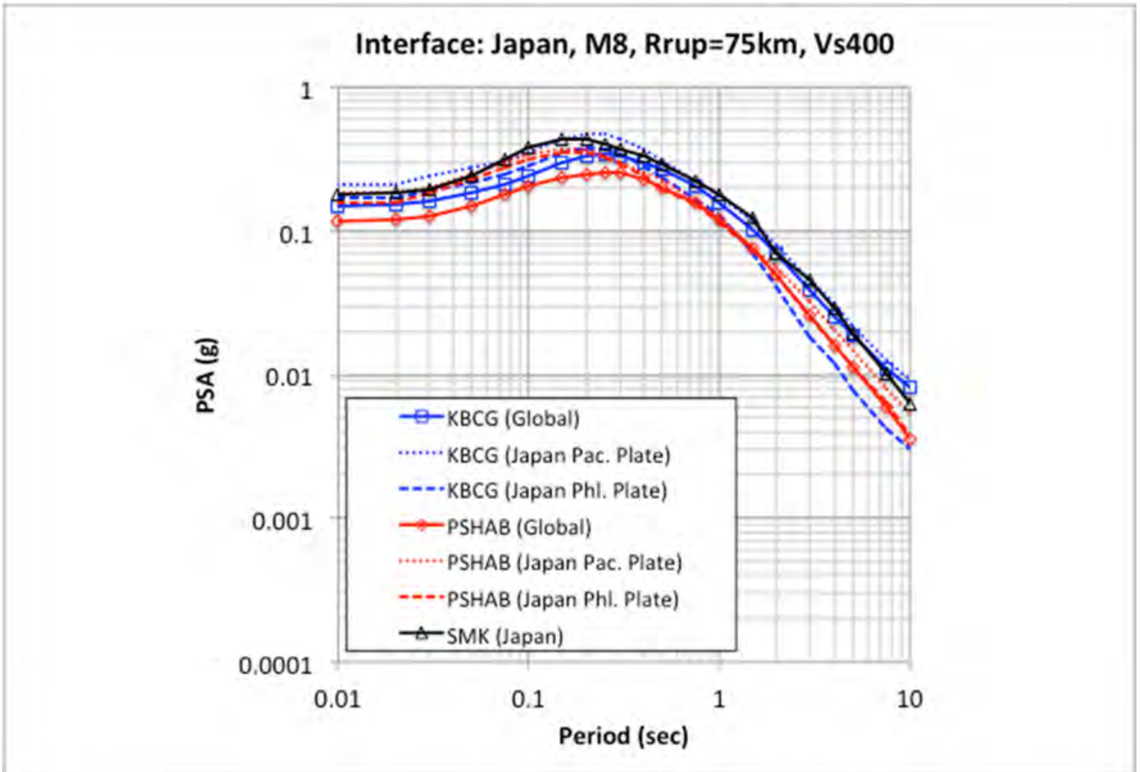

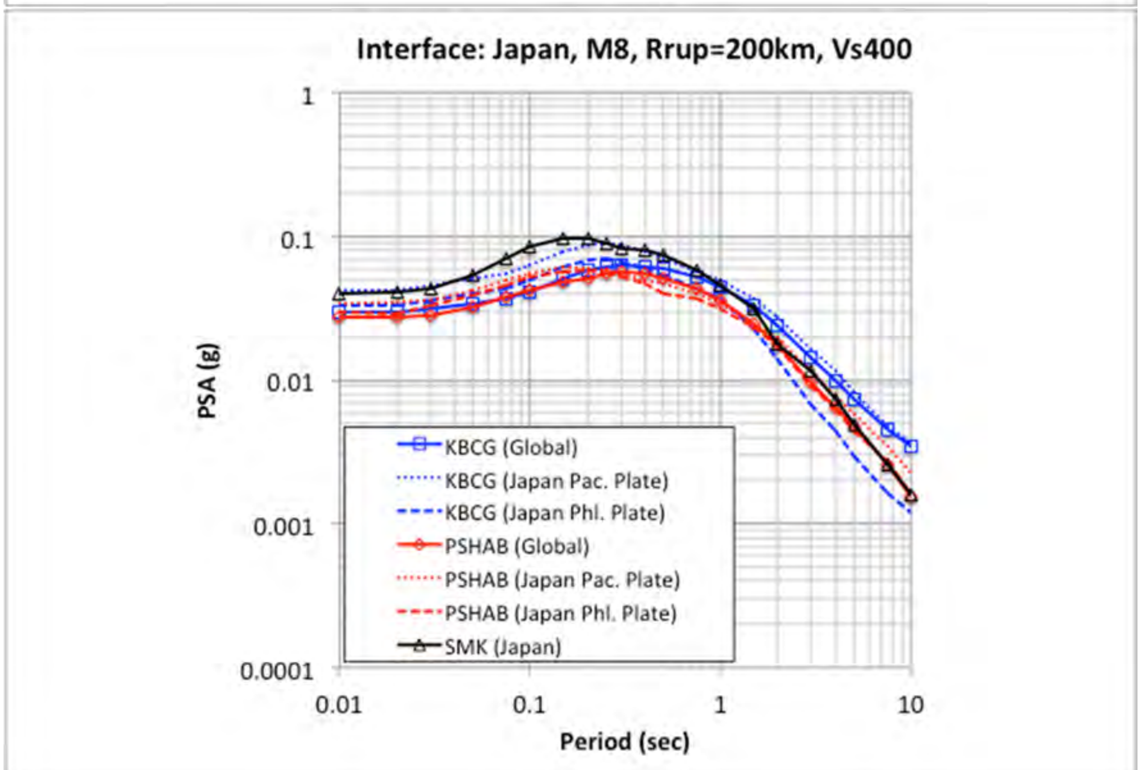

Figure 3.42 **Comparison of Japan regional M8 (interface) for distances of 75 km (top) and 200 km (bottom) spectra for V_{S30} = 400 m/sec.**

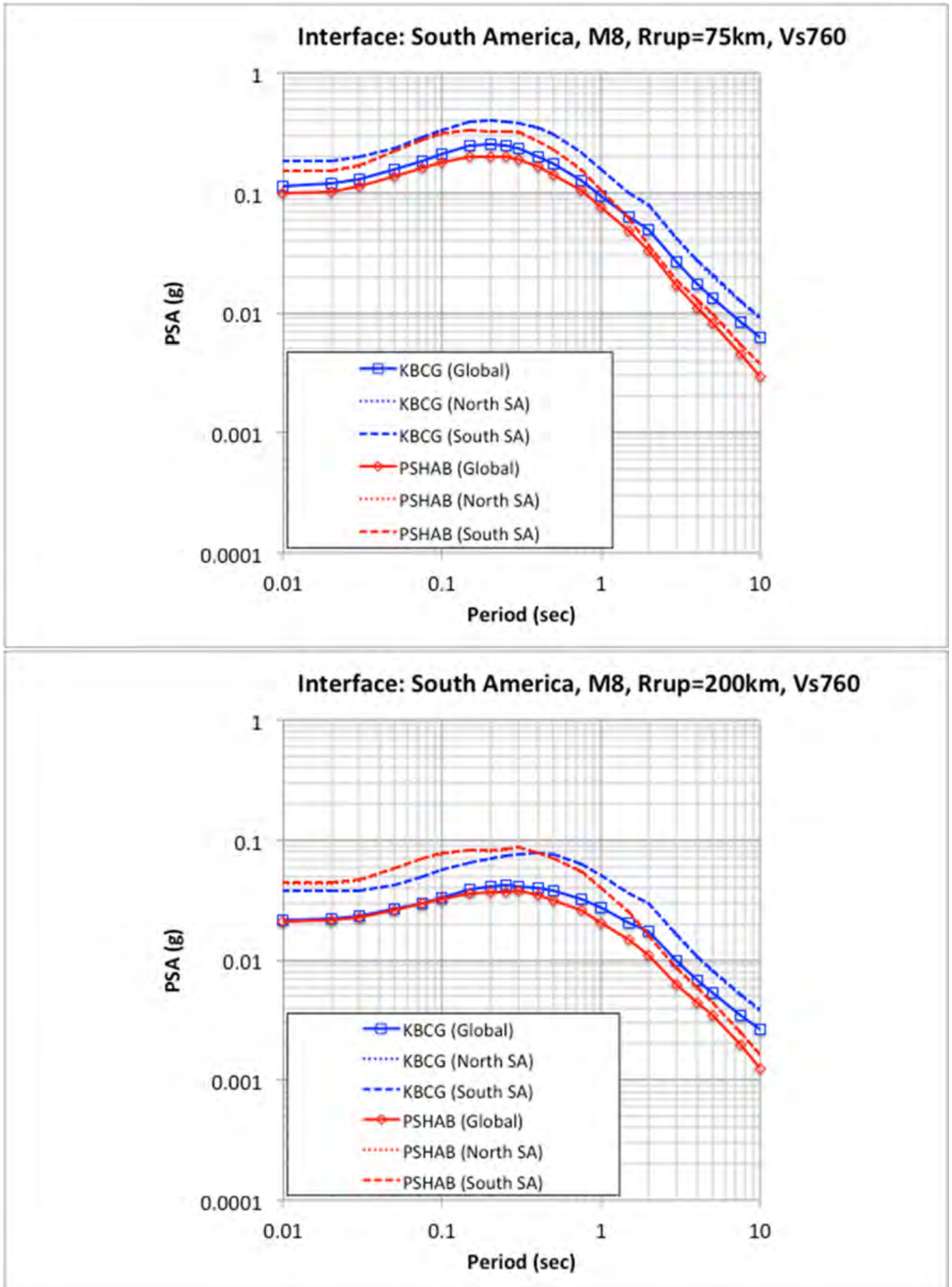

Figure 3.43 **Comparison of South America regional M8 (interface) for distances of 75 km (top) and 200 km (bottom) spectra for V_{S30} = 760 m/sec.**

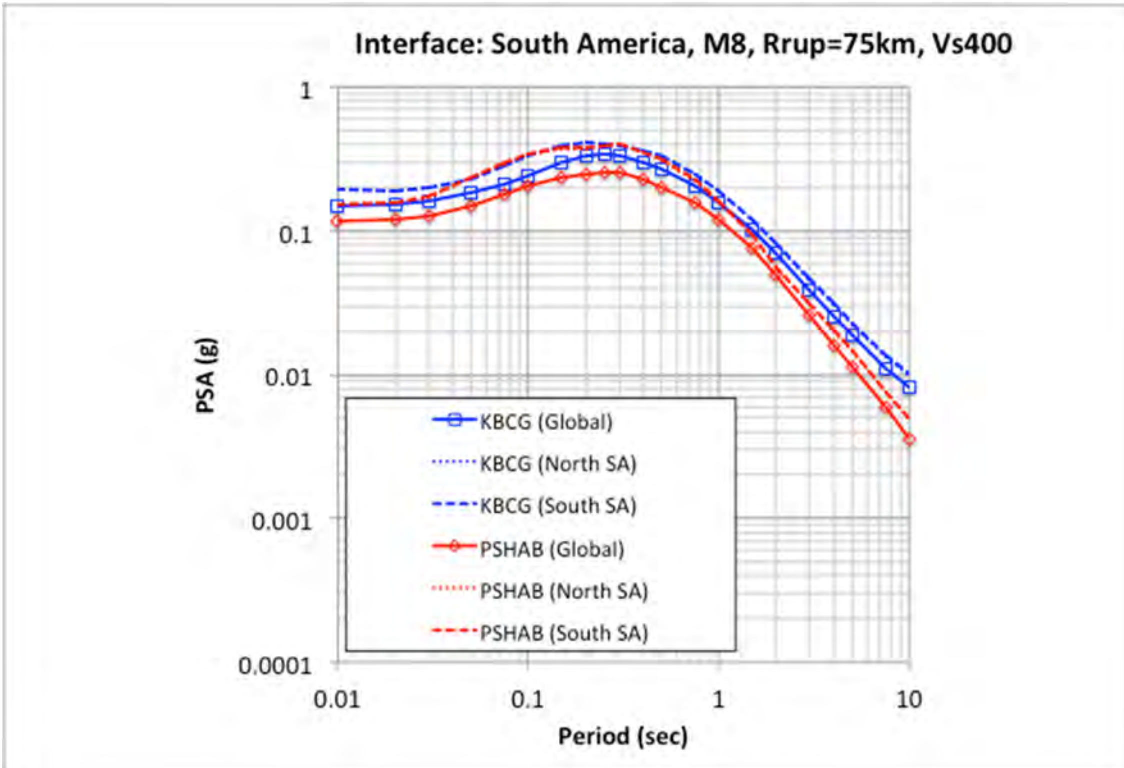

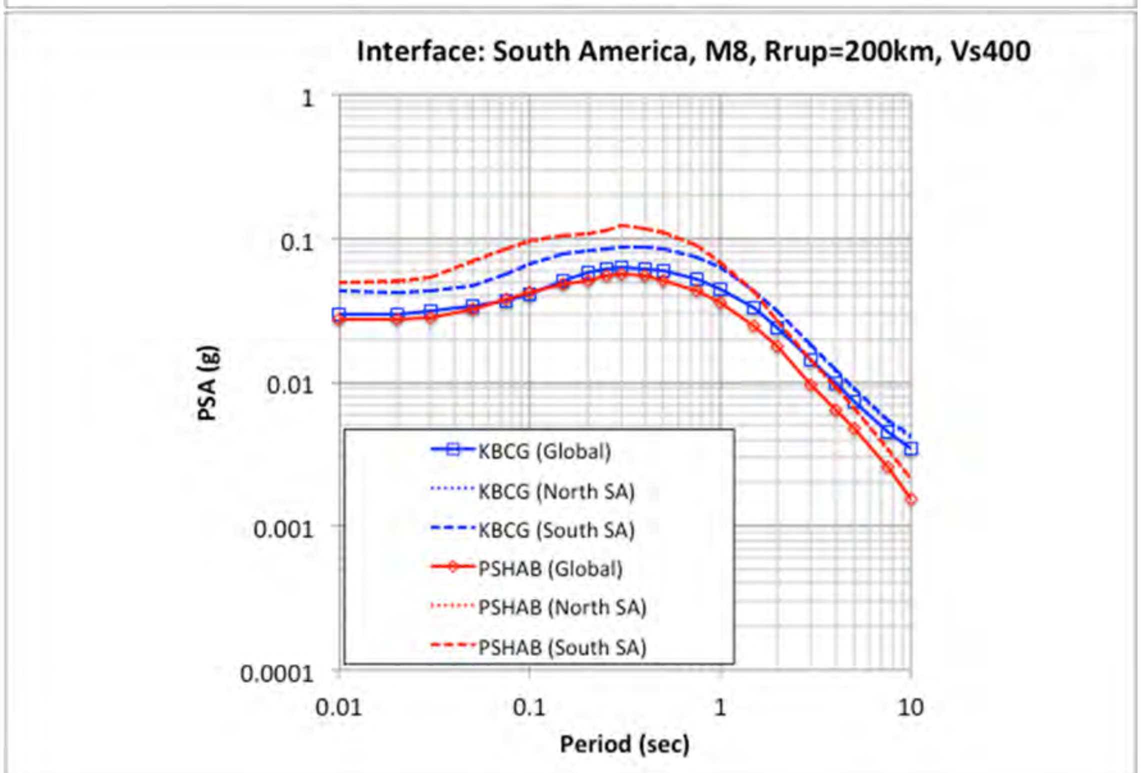

Figure 3.44 **Comparison of South America regional M8 (interface) for distances of 75 km (top) and 200 km (bottom) spectra for V_{S30} = 400 m/sec.**

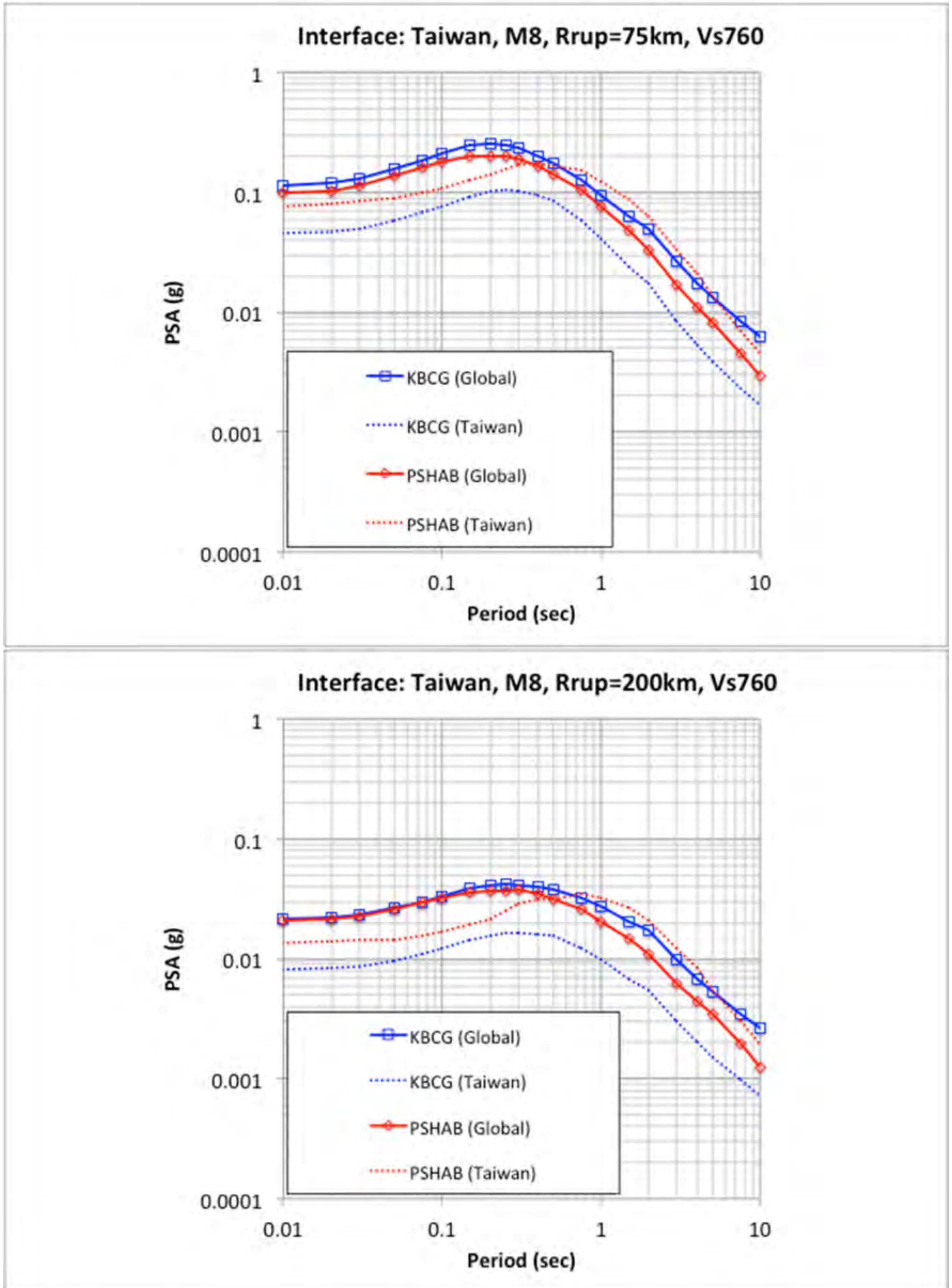

Figure 3.45 **Comparison of Taiwan regional M8 (interface) for distances of 75 km (top) and 200 km (bottom) spectra for V_{S30} = 760 m/sec.**

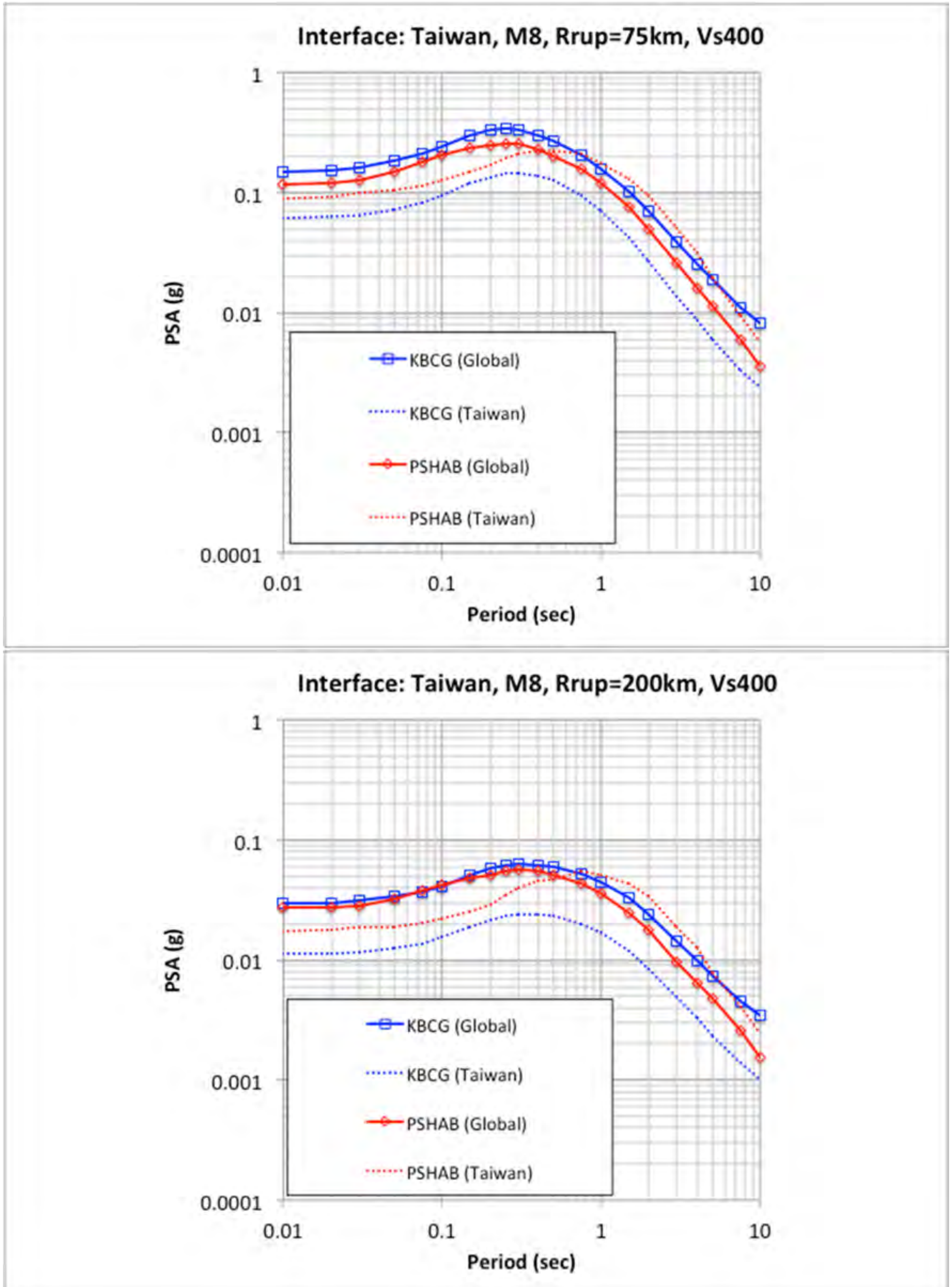

Figure 3.46 **Comparison of Taiwan regional M8 (interface) for distances of 75 km (top) and 200 km (bottom) spectra for V_{S30} = 400 m/sec.**

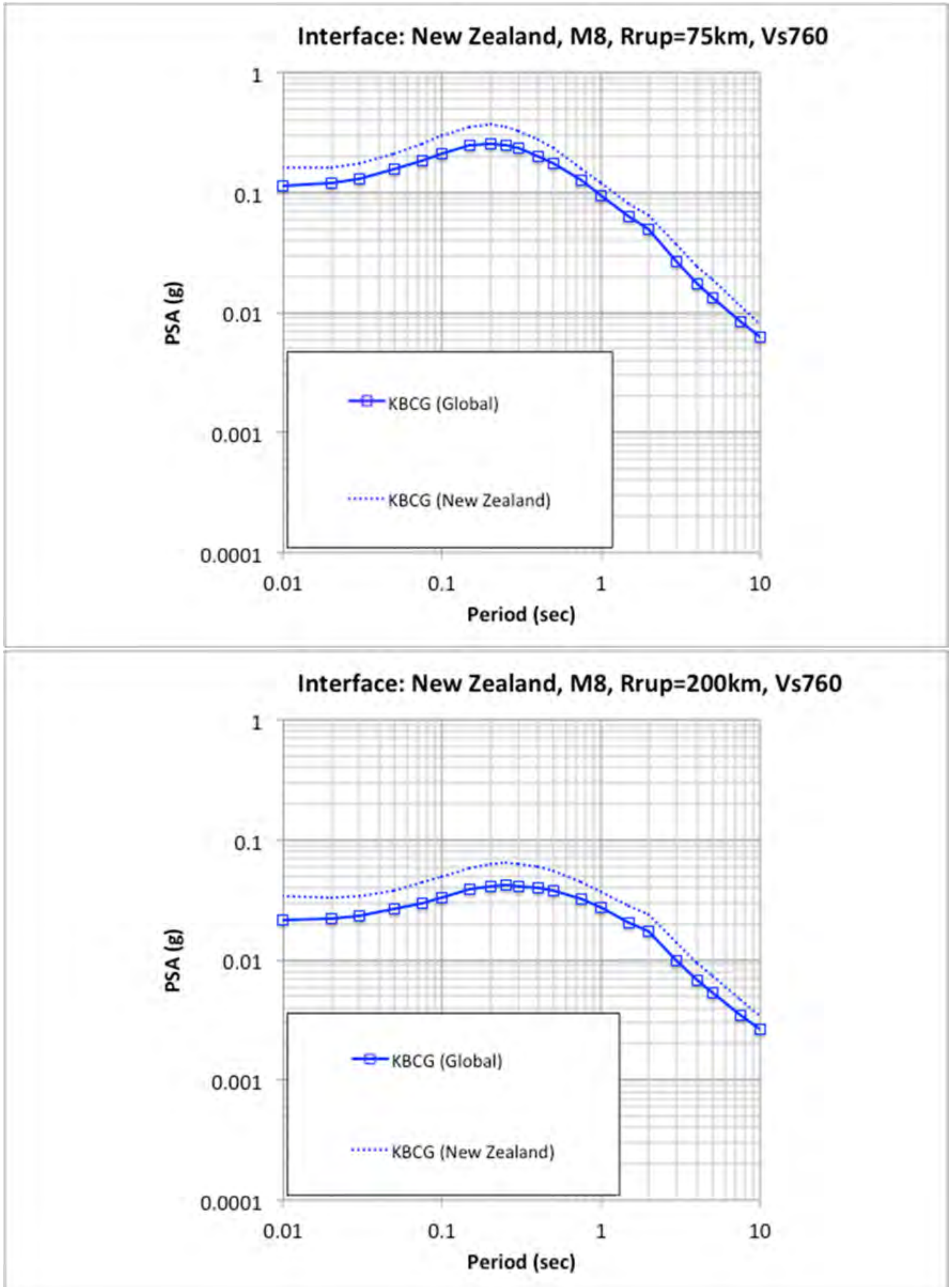

Figure 3.47 **Comparison of New Zealand regional M8 (interface) for distances of 75 km (top) and 200 km (bottom) spectra for V_{S30} = 760 m/sec.**

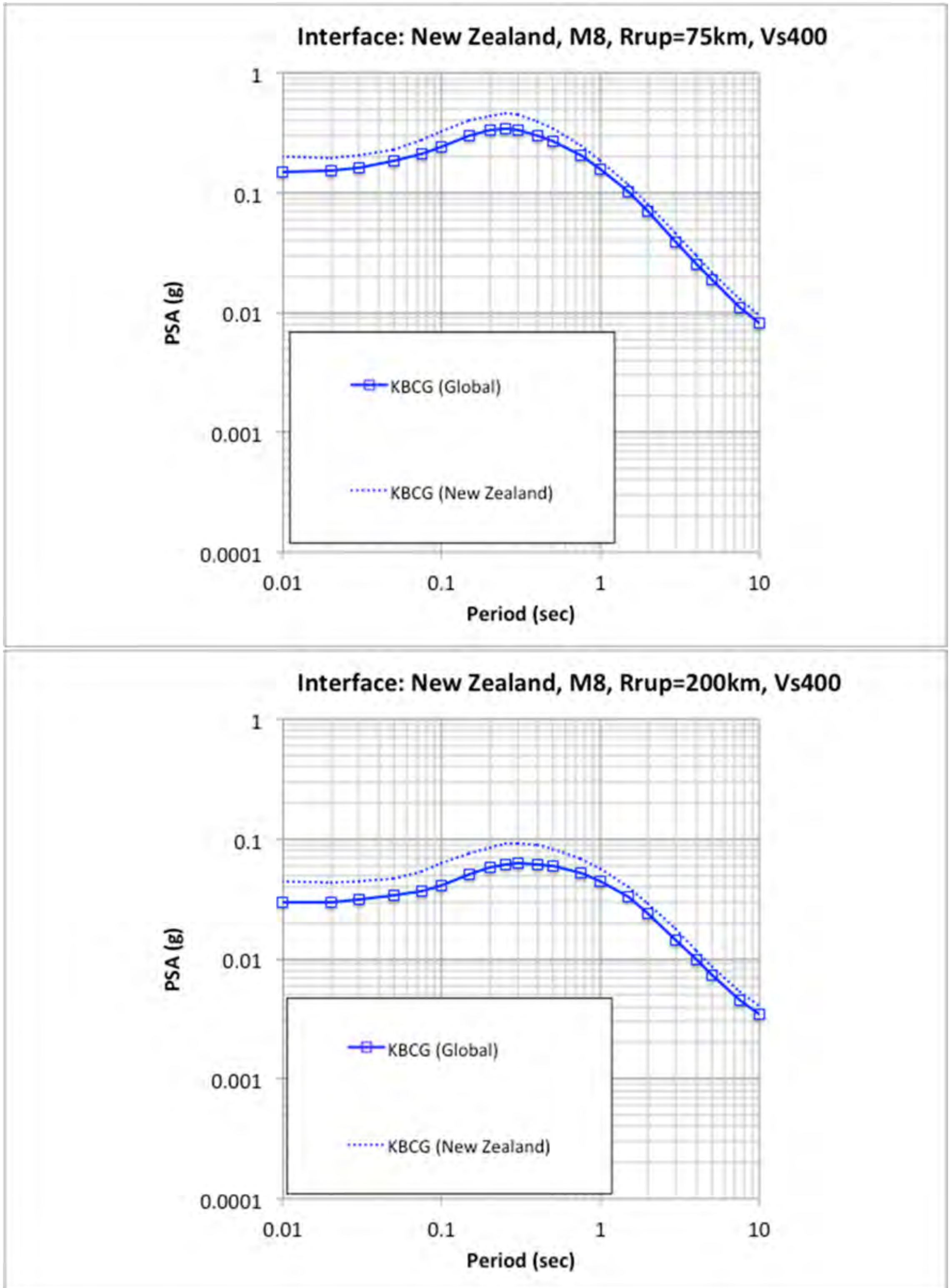

Figure 3.48 **Comparison of New Zealand regional M8 (interface) for distances of 75 km (top) and 200 km (bottom) spectra for V_{S30} = 400 m/sec.**

3.1.3 Interface Magnitude Scaling

A common feature in all three of the NGA-Sub GMMs is the change in magnitude scaling at the magnitude-scaling break points listed in Table 2.2. This magnitude-scaling change is also a feature of previous GMMs—including the BCH and BCHU models—and is also modeled in crustal GMMs (e.g., see Gregor et al. [2014]). Although the magnitude-scaling break point is based on a single magnitude value, the impact on the calculated ground motions depends on spectral period. Both the KBCG and PSHAB model assign a global magnitude-scaling break point of 7.9 although the functional formulation within each model is different.

Comparisons of the median ground motions from an interface earthquake at a distance of 75 km for a V_{S30} value of 760 m/sec are plotted in Figure 3.49 to Figure 3.53 for PGA (T = 0.01 sec) and spectral periods of 0.2, 1.0, 3.0, and 5.0 sec. The results from the KBCG and PSHAB model are for the global version of their models. The SMK results are also included in these comparison figures along with the results from the suite of previously developed GMMs.

In general, there is relative agreement between the results from the three NGA-Sub GMMs and the other published models with a few noted exceptions. Both the AM09 and AB09 models fall outside of the range of the other models for the smaller magnitude and shorter spectral periods (i.e., 1.0 sec and less). It should be noted that these smaller magnitude values are outside of the range of applicability for these models based on their respective datasets used in their development. For the longer spectral periods (e.g., 3.0 and 5.0 sec), the AB08 is more consistent with the other GMMs even at the lower magnitude range. The AM09 model has a more similar shape in the magnitude scaling for these longer spectral periods, but it is also offset from the other models, which can be related to other parts of the model.

For the large magnitude values exceeding the magnitude-scaling break point, the AB08 and SMK models predict complete saturation (i.e., constant ground motion values for increasing magnitudes). For the SMK model, this is true for the short spectral periods (i.e., 1.0 sec and less) but for the longer spectral period, the SMK model predicts an increase in the ground motions as a function of these larger magnitude values.

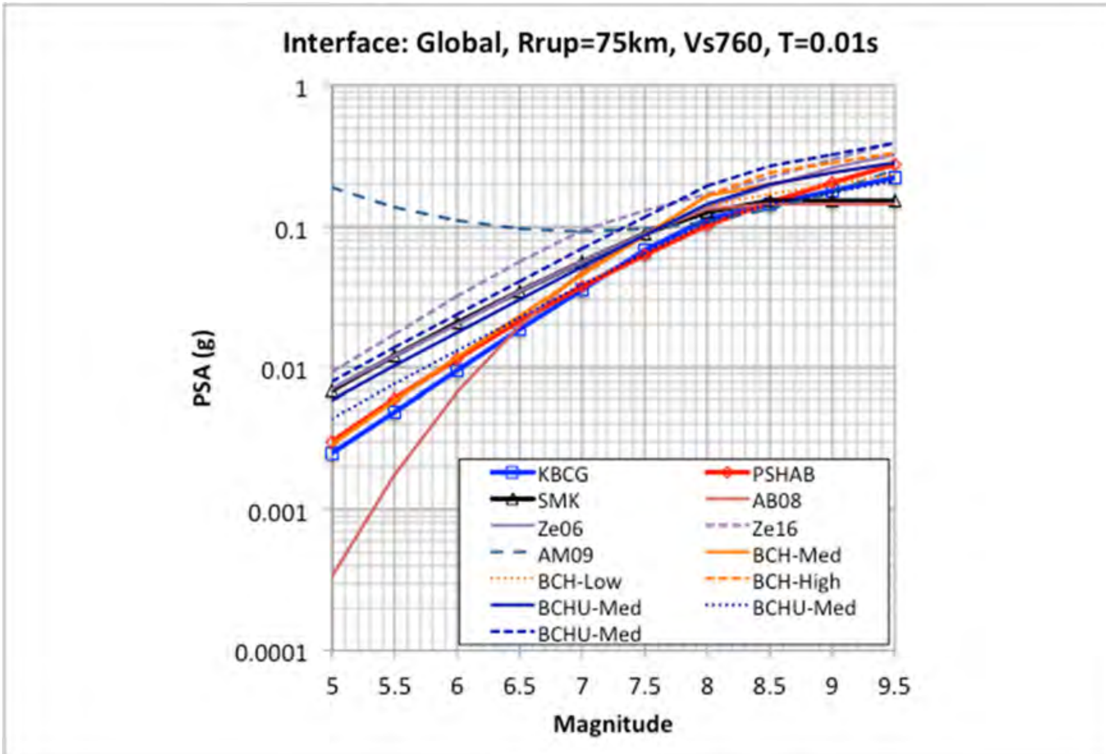

Figure 3.49 Comparison of PGA magnitude scaling for interface events at a distance of 75 km for V_{S30} = 760 m/sec.

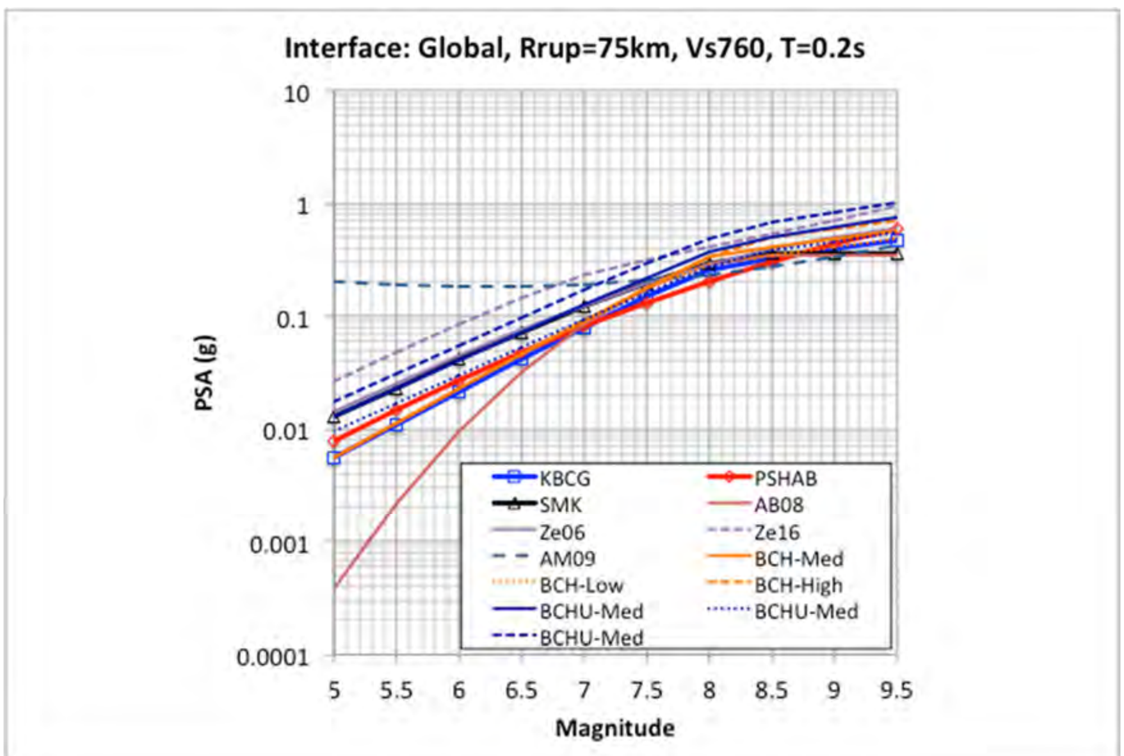

Figure 3.50 Comparison of T = 0.2 sec spectral acceleration magnitude scaling for interface events at a distance of 75 km for V_{S30} = 760 m/sec.

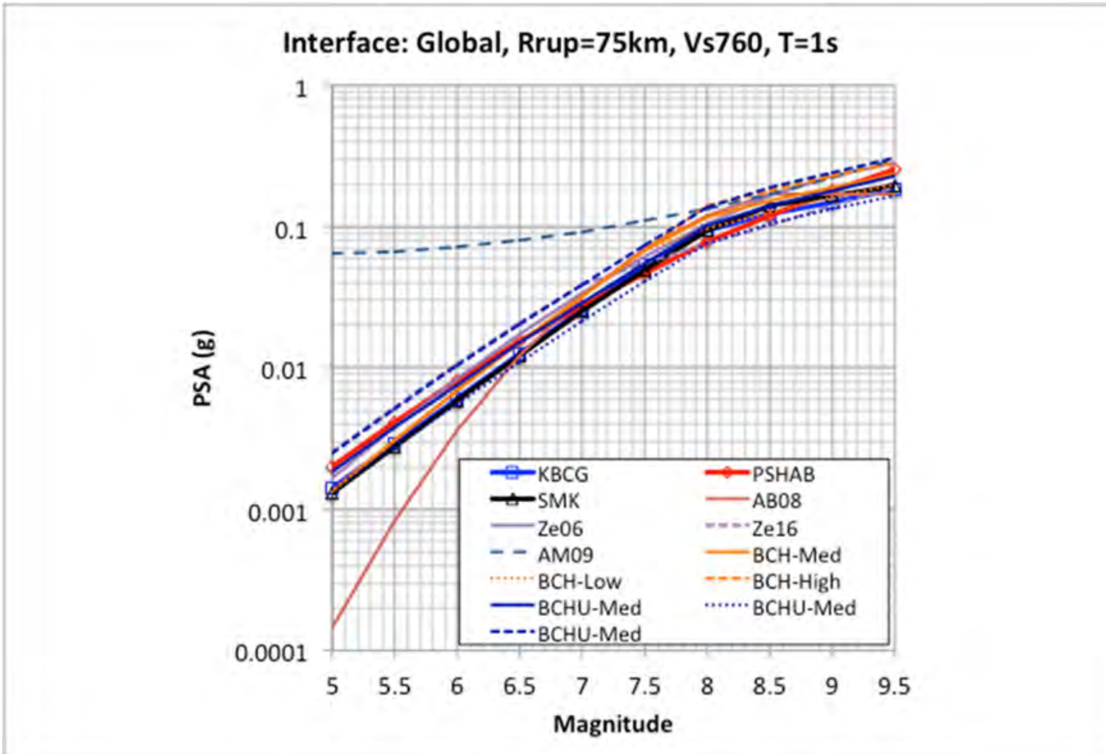

Figure 3.51 **Comparison of *T* = 1.0 sec spectral acceleration magnitude scaling for interface events at a distance of 75 km for V_{S30} = 760 m/sec.**

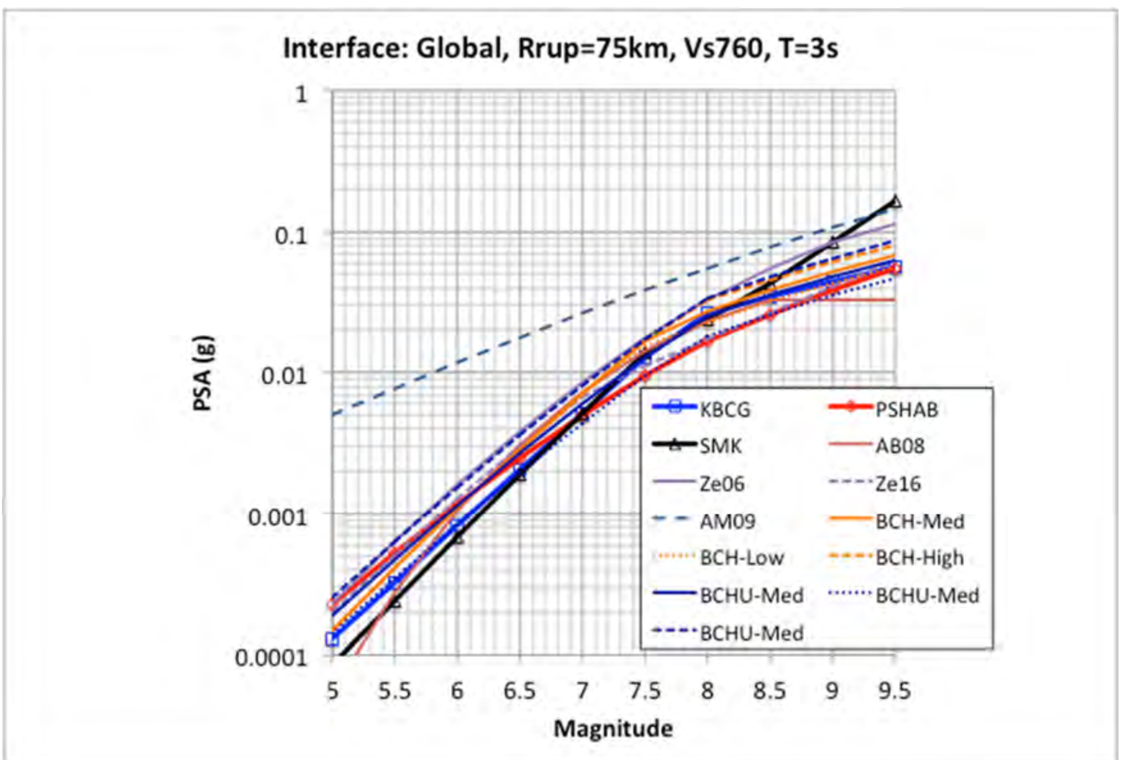

Figure 3.52 **Comparison of *T* = 3.0 sec spectral acceleration magnitude scaling for interface events at a distance of 75 km for V_{S30} = 760 m/sec.**

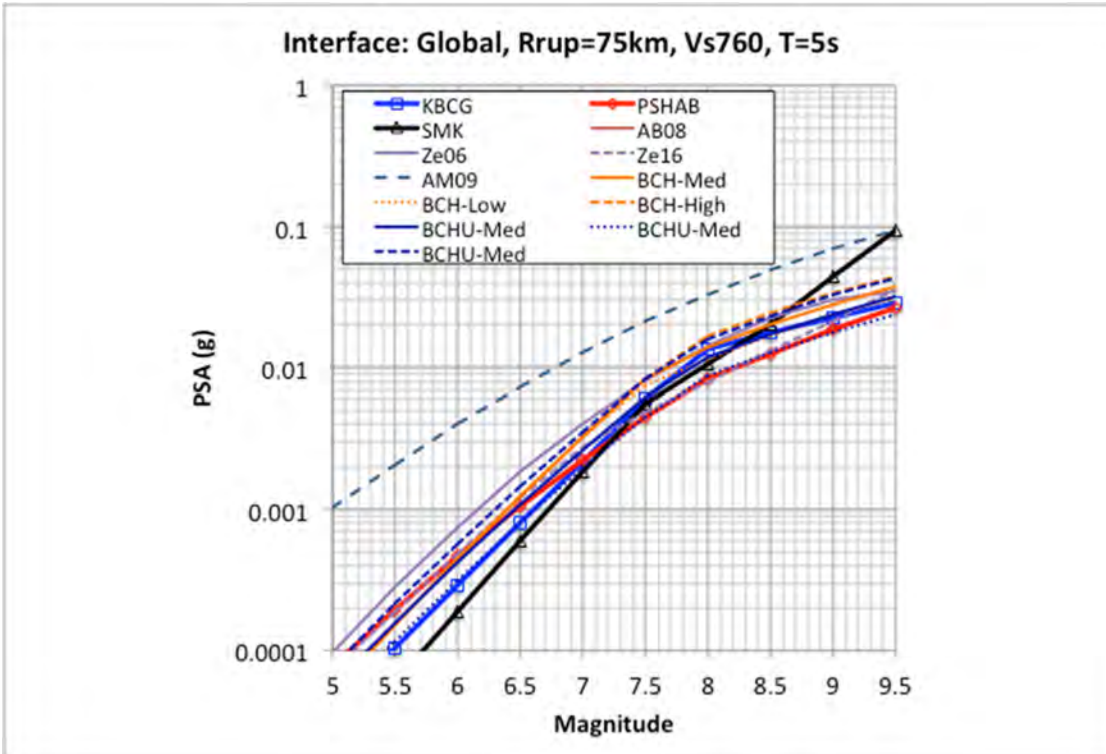

Figure 3.53 Comparison of *T* = 5.0 sec spectral acceleration magnitude scaling for interface events at a distance of 75 km for V_{S30} = 760 m/sec.

3.1.4 Interface Depth Dependence

For interface events only the KBCG model includes a depth to the top of rupture (Z_{tor}) term. Note that both the KBCG and PSHAB model as well as previous models include a Z_{tor} term for slab events. This aspect of the KBCG model shows a strong period dependence, with the shorter spectral periods showing a larger increase in ground motions with increasing Z_{tor} values. A comparison with the KBCG global model and the other models is provided in Figure 3.54 through Figure 3.58 for PGA (*T* = 0.01 sec), 0.2, 1.0, 3.0, and 5.0 sec. These results are for a **M**8 interface earthquake at a distance of 75 km, with a V_{S30} value of 760 m/sec. For the low and intermediate spectral period cases of PGA (*T* = 0.01 sec) and 0.2 sec, the Z_{tor} scaling associated with the KBCG model is strong, leading to relatively low ground-motion estimates for the shallowest Z_{tor} values starting at 5 km and high ground-motion values for the deeper Z_{tor} values up to 40 km when compared to the other models, which are not dependent on Z_{tor}. At the longer spectral periods, the Z_{tor} dependency is reduced, and the estimated ground motions from the KBCG model are within the range of ground motions estimated from the other models.

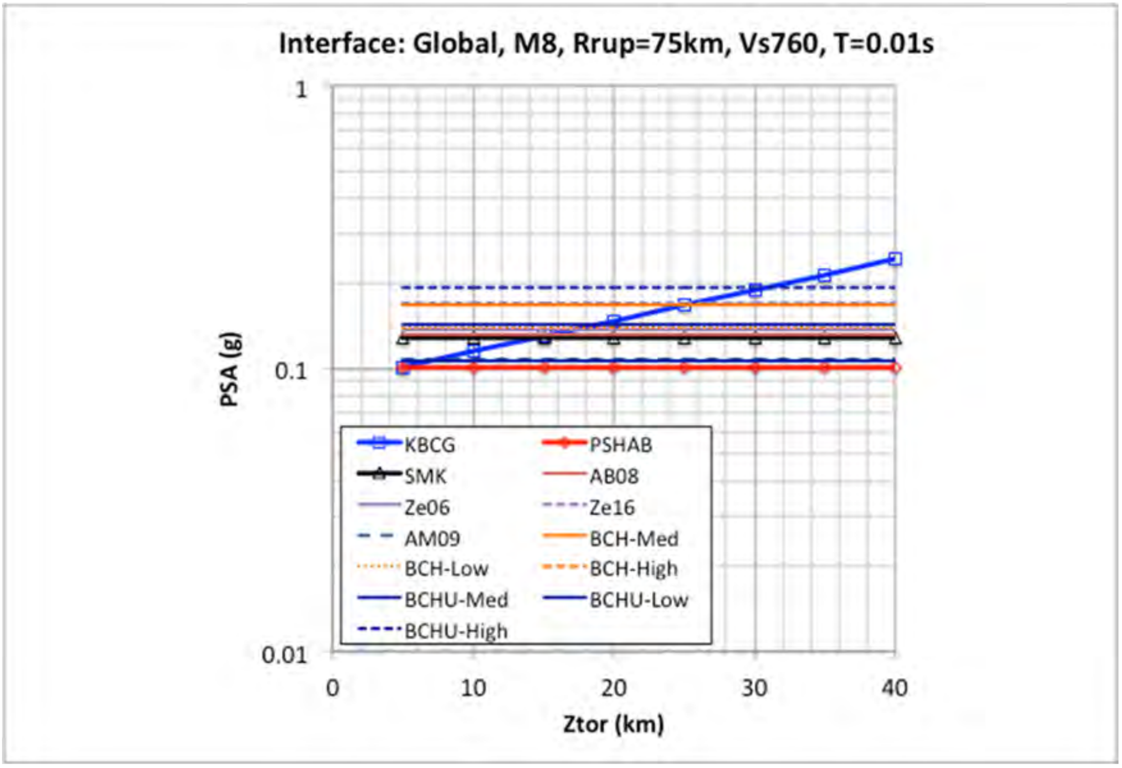

Figure 3.54 **Comparison of PGA (*T* = 0.01 sec) Z_{tor} scaling for a M8 interface event at a distance of 75 km for V_{S30} = 760 m/sec.**

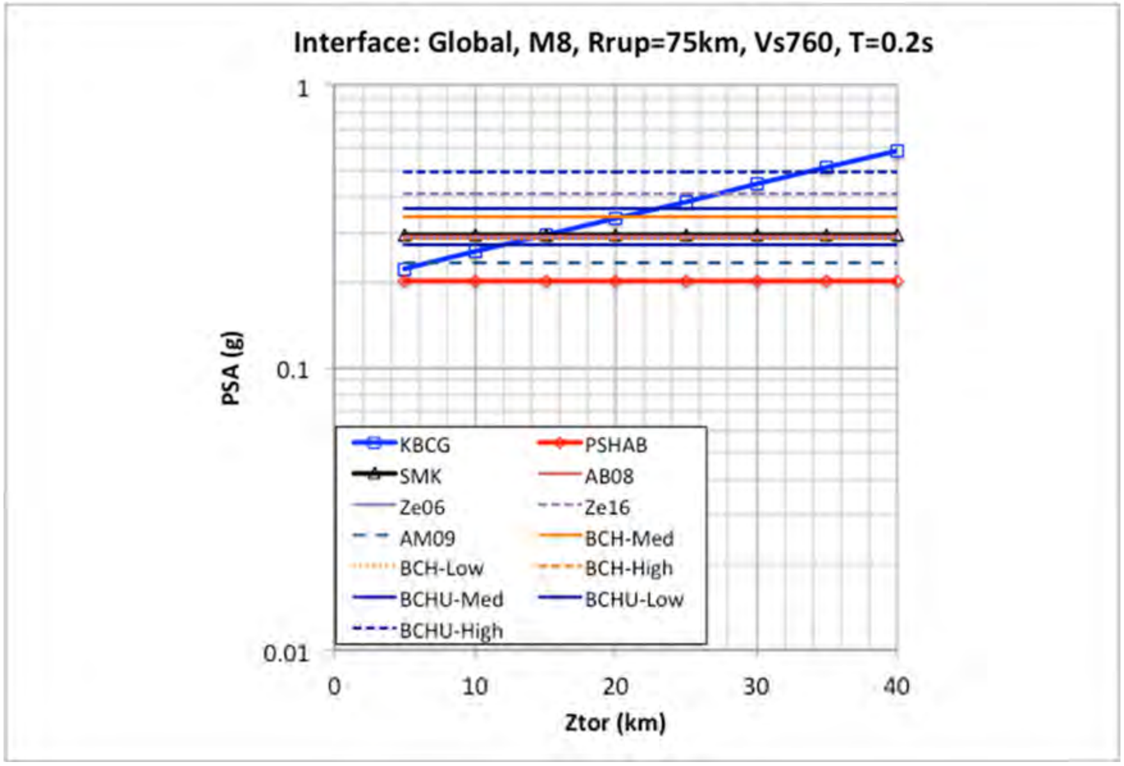

Figure 3.55 **Comparison of *T* = 0.2 sec Z_{tor} scaling for a M8 interface event at a distance of 75 km for V_{S30} = 760 m/sec.**

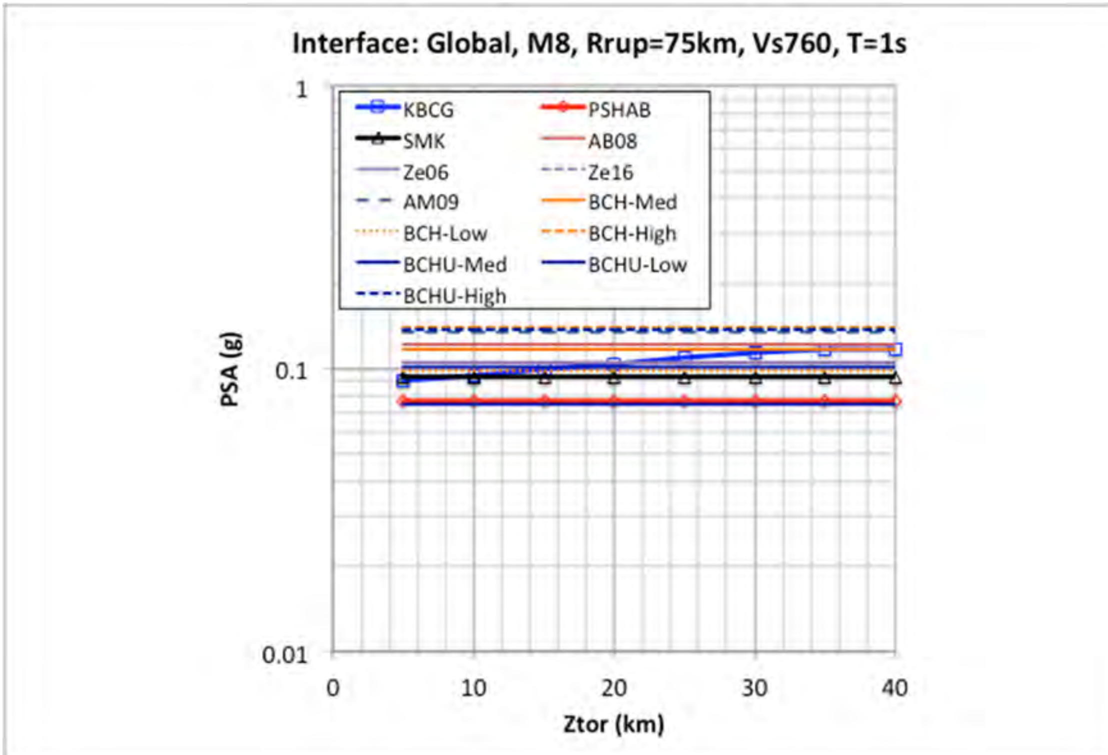

Figure 3.56 **Comparison of T = 1.0 sec Z_{tor} scaling for a M8 interface event at a distance of 75 km for V_{S30} = 760 m/sec.**

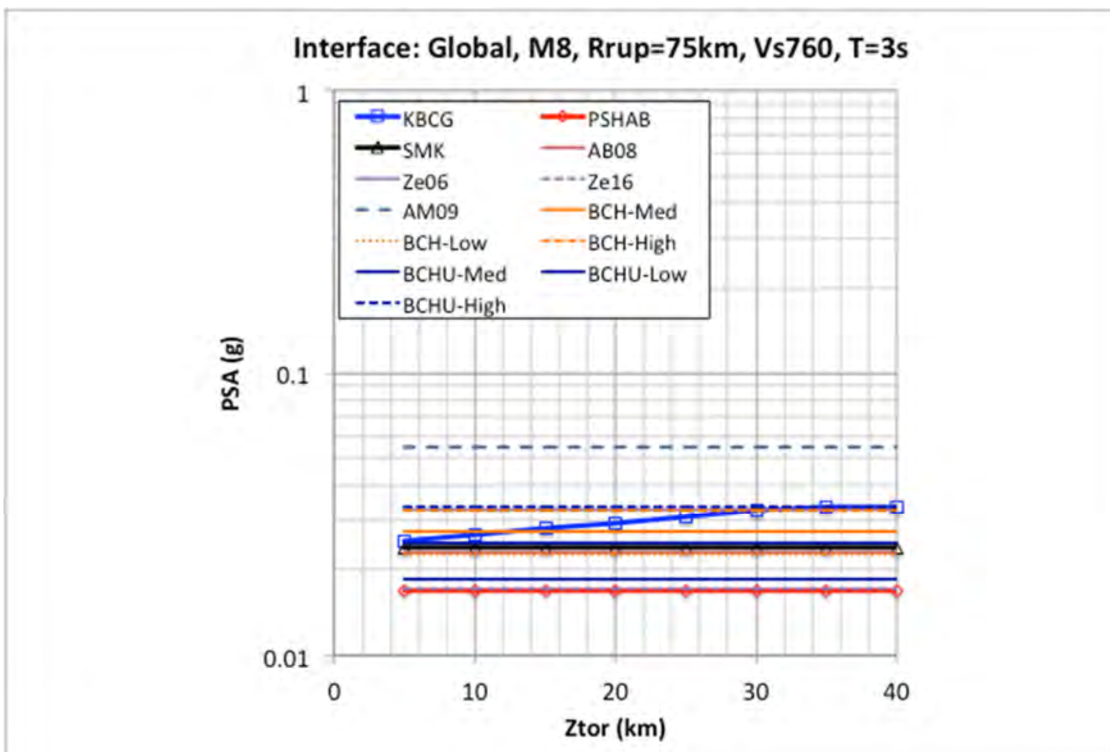

Figure 3.57 **Comparison of T = 3.0 sec Z_{tor} scaling for a M8 interface event at a distance of 75 km for V_{S30} = 760 m/sec.**

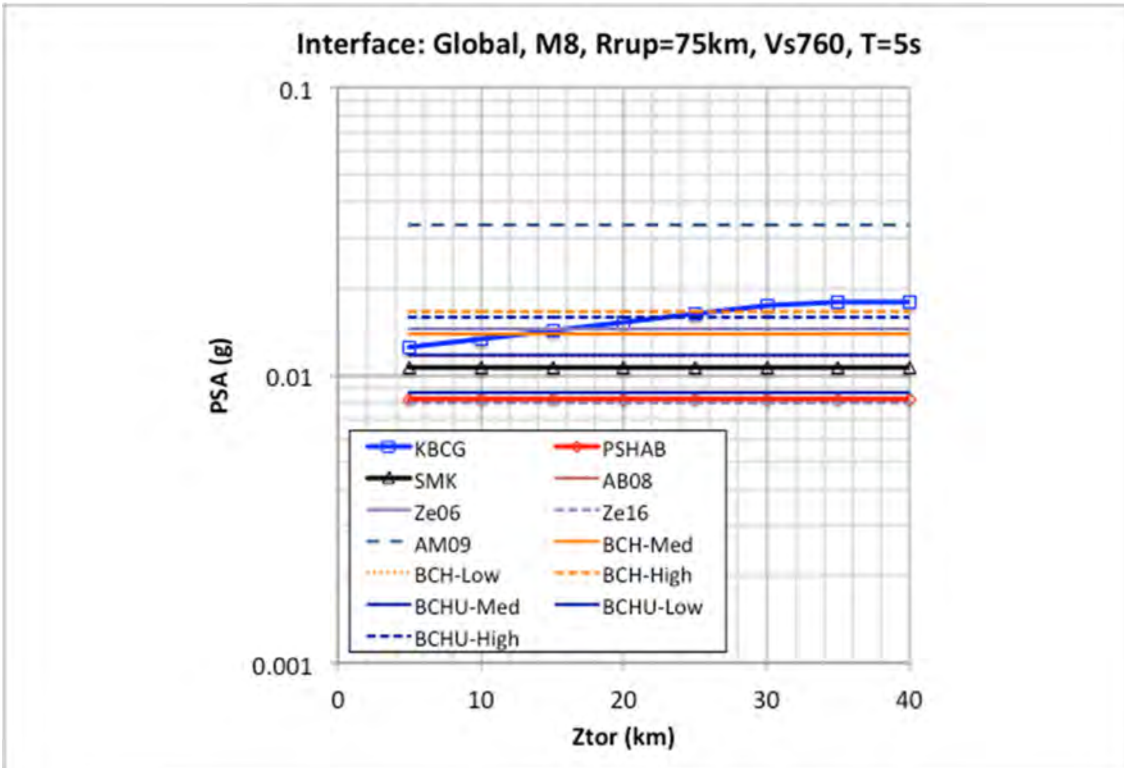

Figure 3.58 Comparison of T = 5.0 sec Z_{tor} scaling for a M8 interface event at a distance of 75 km for V_{S30} = 760 m/sec.

3.2 SLAB EVENTS

For the slab event comparisons, the selected input parameters are listed in Table 3.2. Results are calculated for magnitudes 6, 7, and 8 and for distances of 50–1000 km for the attenuation curves and distances of 75 and 200 km for the spectra. Distances smaller than 50 km are not considered geometrically acceptable, with the depth of the slab source being a minimum of 50 km. Two V_{S30} values of 760 and 400 m/sec are selected along with the previously described site classifications for the other older GMMs. A separate section will be presented for the basin-amplification results from the models and all other comparisons are for non-basin sites.

Table 3.2 Input parameters for slab global GMM comparisons.

Parameter	KBCG	PSHAB	SMK
Moment magnitude	6, 7, and 8	6, 7, and 8	6, 7, and 8
Closest distance to rupture plane (km)	50.0–1000.0[1] 75.0[2] 200.0[2]	50.0–1000.0[1] 75.0[2] 200.0[2]	50.0–1000.0[1] 75.0[2] 200.0[2]
Depth to top of rupture (km)	50.0	---	---
Hypocentral depth (km)	---	50.0 (**M**6.0) 60.0 (**M**7.0) 70.0 (**M**8.0)	50.0 (**M**6.0) 60.0 (**M**7.0) 70.0 (**M**8.0)
Moho depth (km)	---	---	30.0
Average shear-wave velocity in top 30 m (m/sec)	760.0 400.0	760.0 400.0	760.0 400.0
Depth to 2.5 km/sec boundary (km)	---	---	---
Depth to 1.0 km/sec boundary (km)	---	---	---
Interface/slab classification	1 = slab	1 = slab	1 = slab
Magnitude-scaling break point	7.6 (global)	7.6 (global)	8.3

[1] Distance range for attenuation curve plots.

[2] Distance values for spectra plots.

3.2.1 Slab Attenuation Curves

Attenuation curves are compared for both the global versions and regional versions of the models. For the global model, the comparisons are presented with the previous suite of subduction GMMs. For the regional models, the comparison is presented between the global version and regional version of only the NGA-Sub GMMs. Attenuation curves are computed for PGA (T = 0.01 sec) and spectral periods of 0.2, 1.0, 3.0, and 5.0 sec. Representative attenuation curve plots for the **M**7 case for PGA (T = 0.01 sec), 0.2, 1.0, and 3.0 sec spectral periods are plotted in Figure 3.59 to Figure 3.90. The full suite of attenuation curves (i.e., both digital data and plots) are contained in the associated electronic files; see Appendix A.

Based on the comparisons presented in these figures, both the KBCG and PSHAB global models are relatively similar and consistent with the other previous models for distances less than about 200 km. The one exception to this is observed for the BCHU model, which is offset and lower than the suite of GMMs for the shorter spectral period cases. At the longer spectral periods, this model is more consistent with the other GMMs. It should again be noted that the BCHU model is an update to the BCH model with specific application for Cascadia; hence, the comparison with other global models such as the KBCG and PSHAB models is not direct. It is also observed that for the Cascadia regional model, the KBCG model estimates ground motions that are lower than the global model for these low spectral periods and are more consistent with the BCHU model. The PSHAB Cascadia regional model has the opposite effect in estimating slightly larger ground motions for shorter distances. Given the stronger regional attenuation for the Cascadia region, the ground motions are lower than the global estimates at longer distances. The global and Cascadia region-specific comparisons for the KBCG and PSHAB models are provided in Figure 3.67 through Figure 3.70.

Another observation for these slab attenuation curves is the more rapid attenuation for the AB08, BCH, BCHU, and SMK models for distances greater than about 200–300 km. This observed increase in the attenuation rate impacts the intermediate to shorter spectral periods (i.e., 1.0 sec and less) for the AB08 model, the longer spectral periods (i.e., 1.0 sec and longer) for the BCH model, and across all spectral periods for the BCHU and SMK models. The faster attenuation rate for the SMK model is shown in Figure 3.75 through Figure 3.78, which compares the SMK model, the global, and two Japan region-specific estimates to the KBCG and PSHAB models. Given the recommended applicability of the SMK model (see Table 2.1) of distances less than 300 km and the selection of the database for only these shorter distances used in its development, the attenuation curves shown in the comparison figures are based on the extrapolation of the model and may not be well constrained for these larger distances, especially when compared to the other models that did include more distant data in their development.

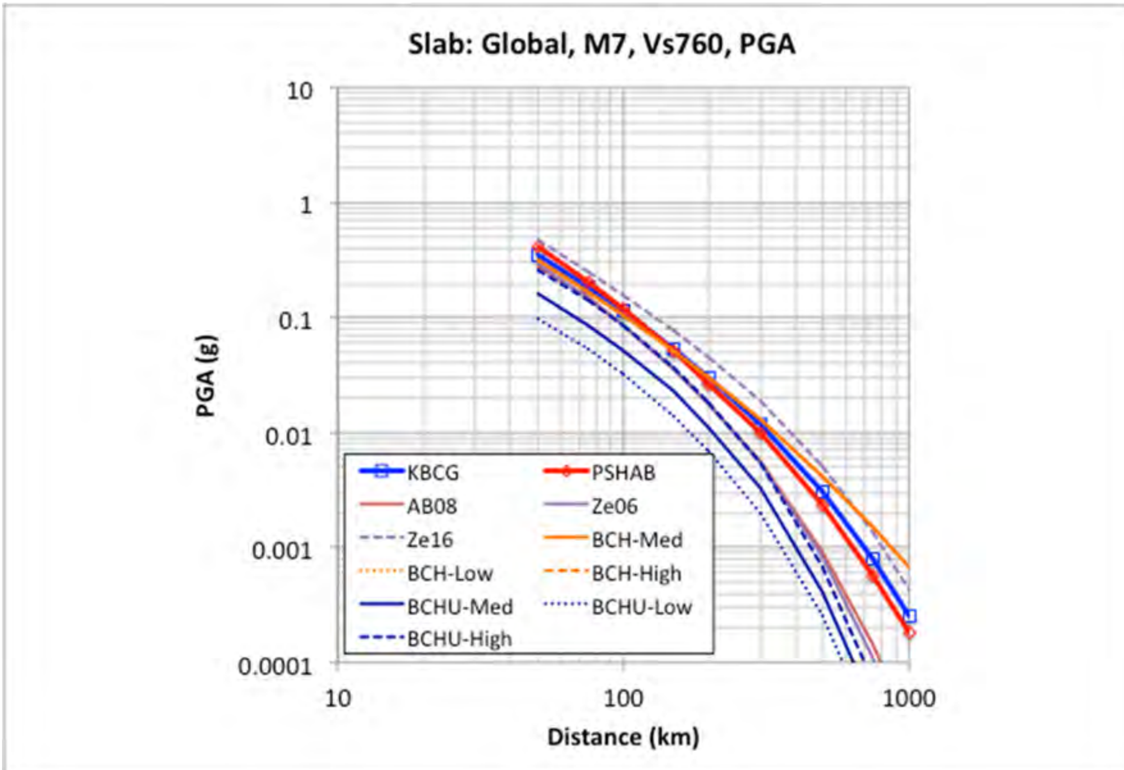

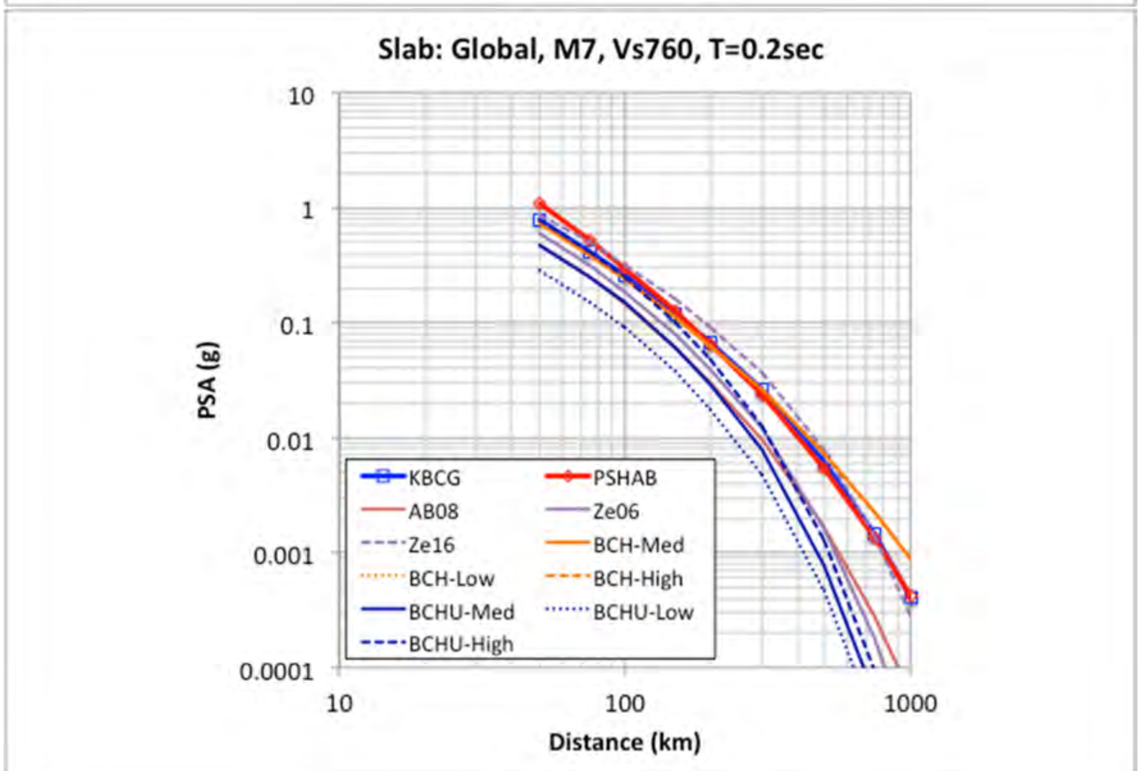

Figure 3.59 **Comparison of global M7 (slab) for PGA (*T* = 0.01 sec) (top) and 0.2 sec (bottom) attenuation curves for V_{S30} = 760 m/sec.**

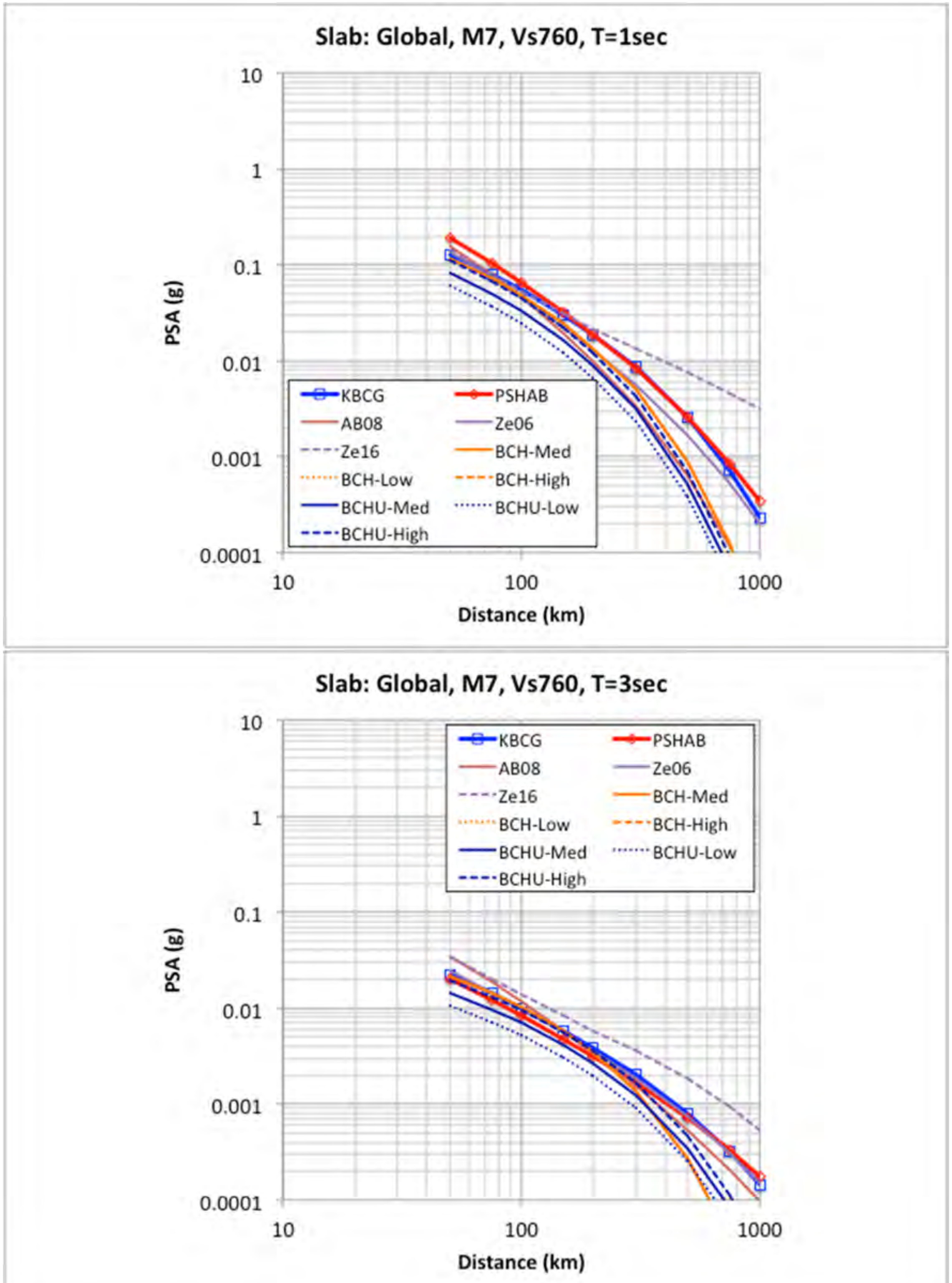

Figure 3.60 **Comparison of global M7 (slab) for 1.0 (top) and 3.0 sec (bottom) attenuation curves for V_{S30} = 760 m/sec.**

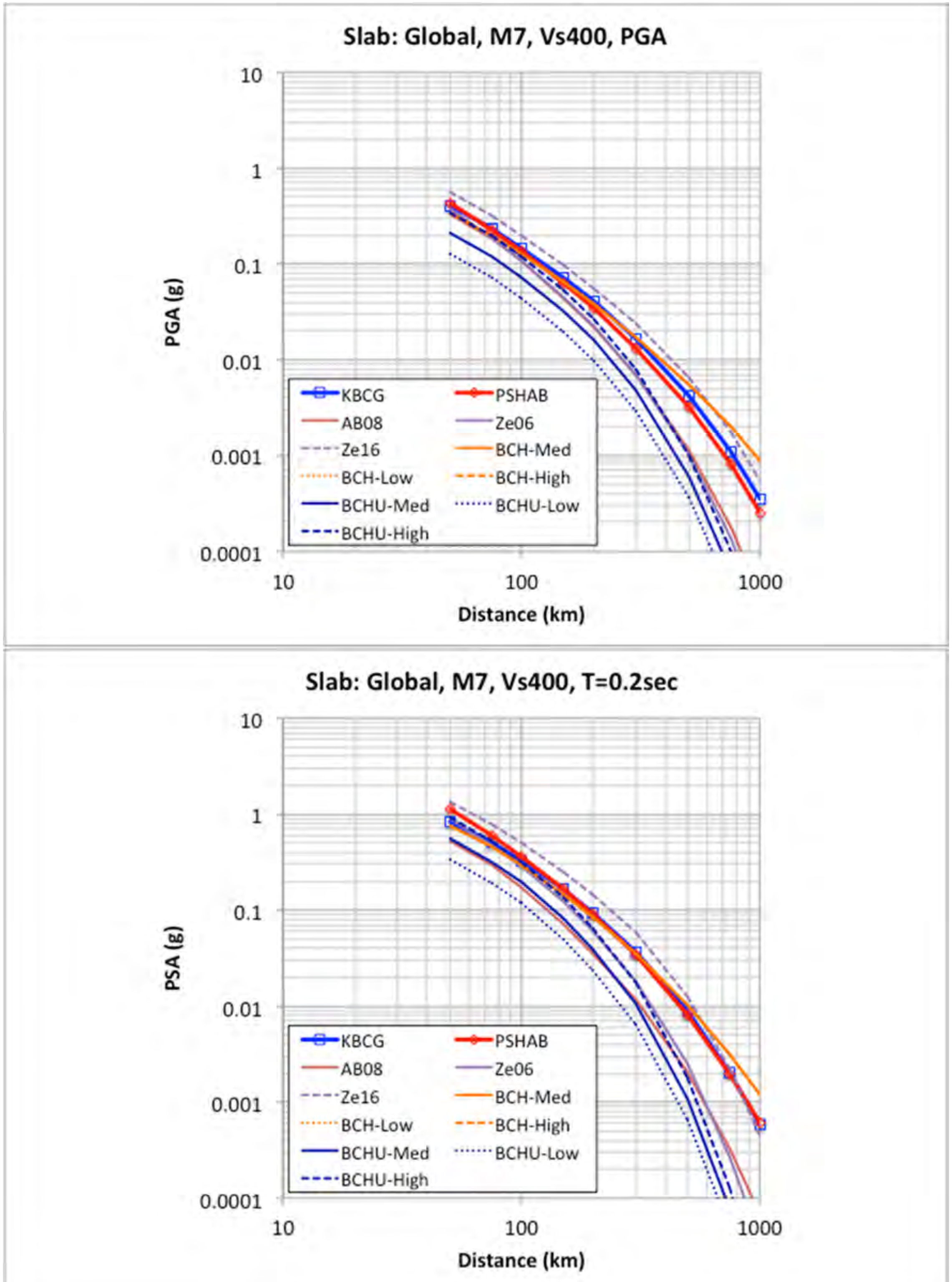

Figure 3.61 **Comparison of global M7 (slab) for PGA (*T* = 0.01 sec) (top) and 0.2 sec (bottom) attenuation curves for V_{S30} = 400 m/sec.**

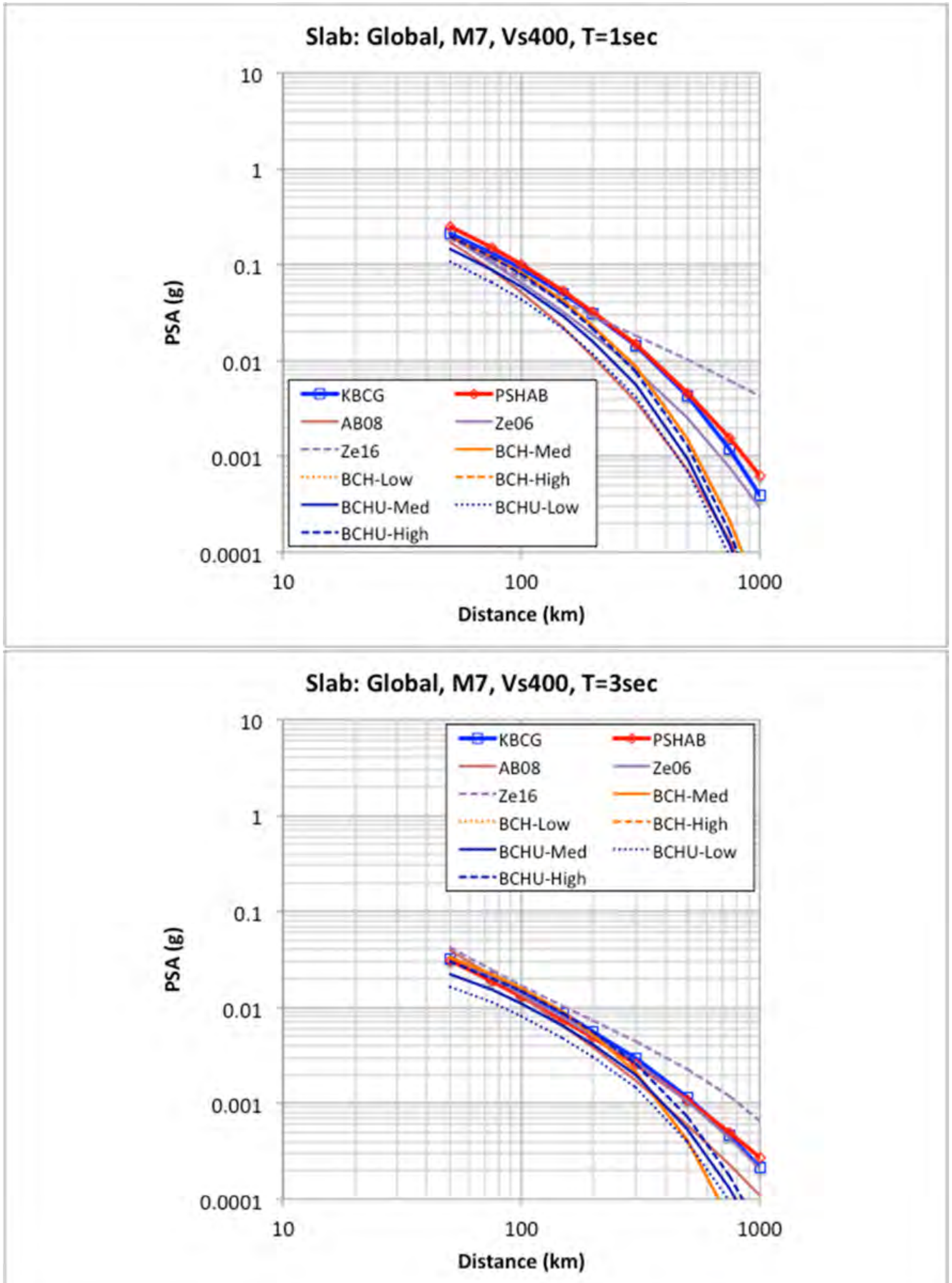

Figure 3.62 **Comparison of global M7 (slab) for 1.0 (top) and 3.0 sec (bottom) attenuation curves for V_{S30} = 400 m/sec.**

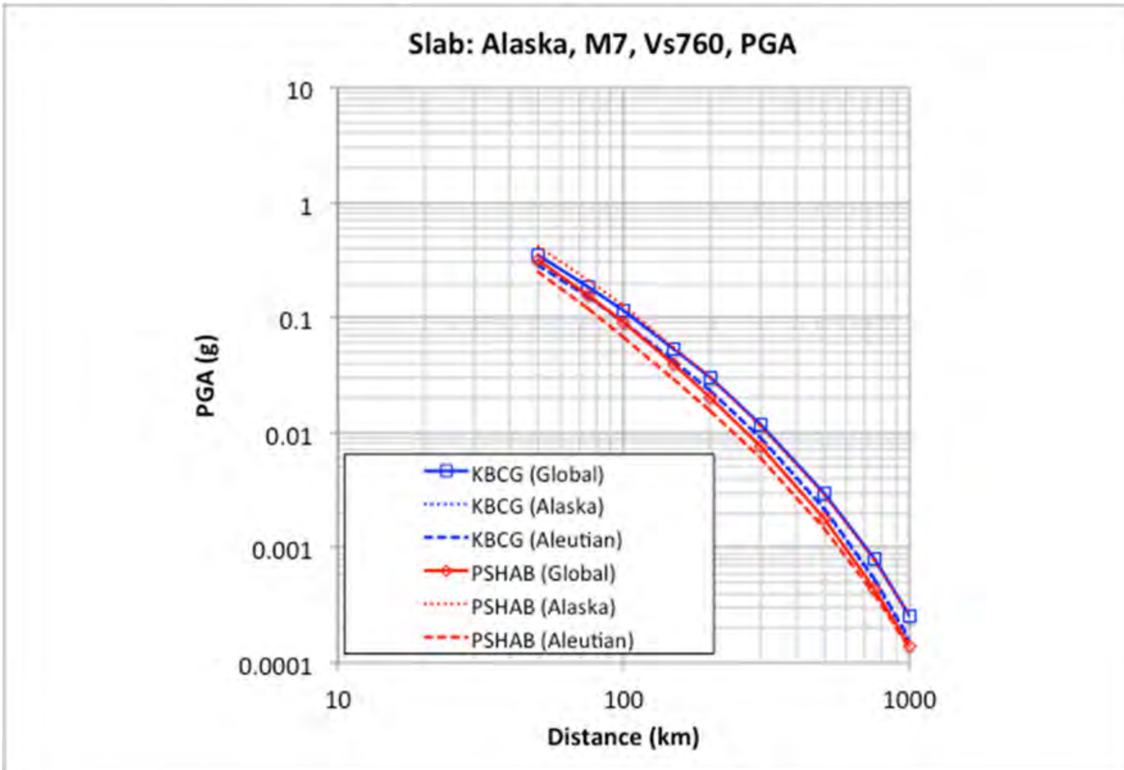

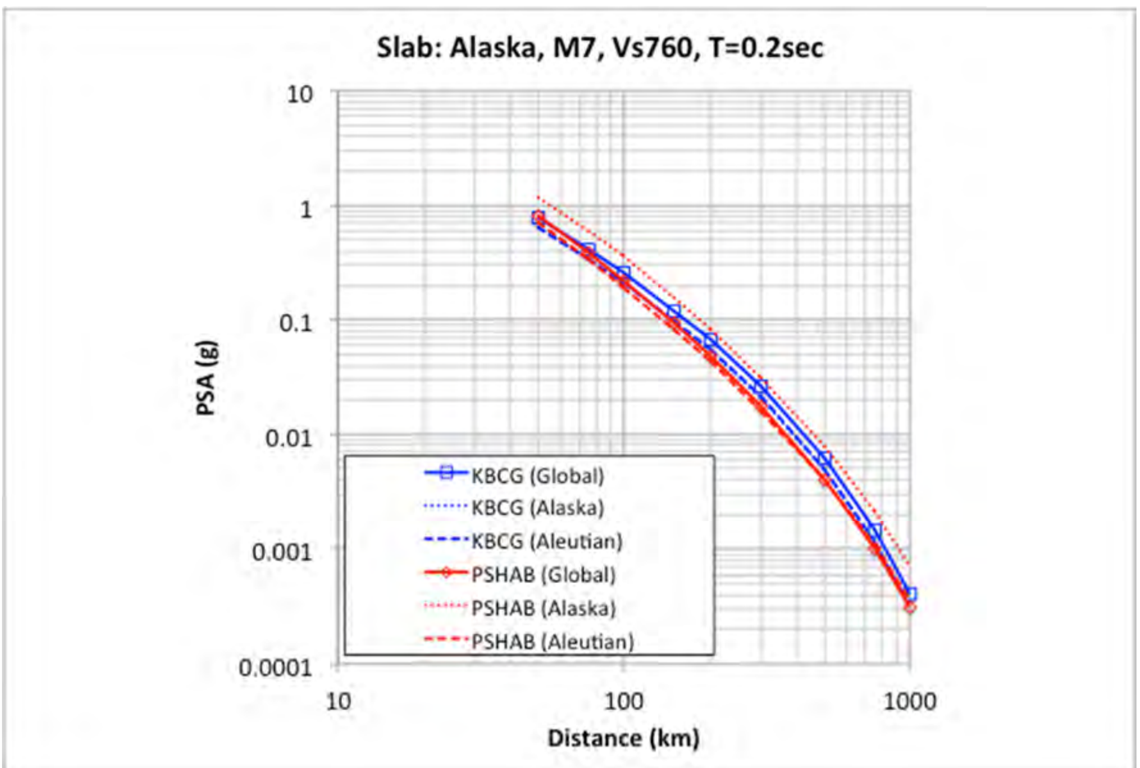

Figure 3.63 Comparison of Alaska regional M7 (slab) for PGA (*T* = 0.01 sec) (top) and 0.2 sec (bottom) attenuation curves for V_{S30} = 760 m/sec.

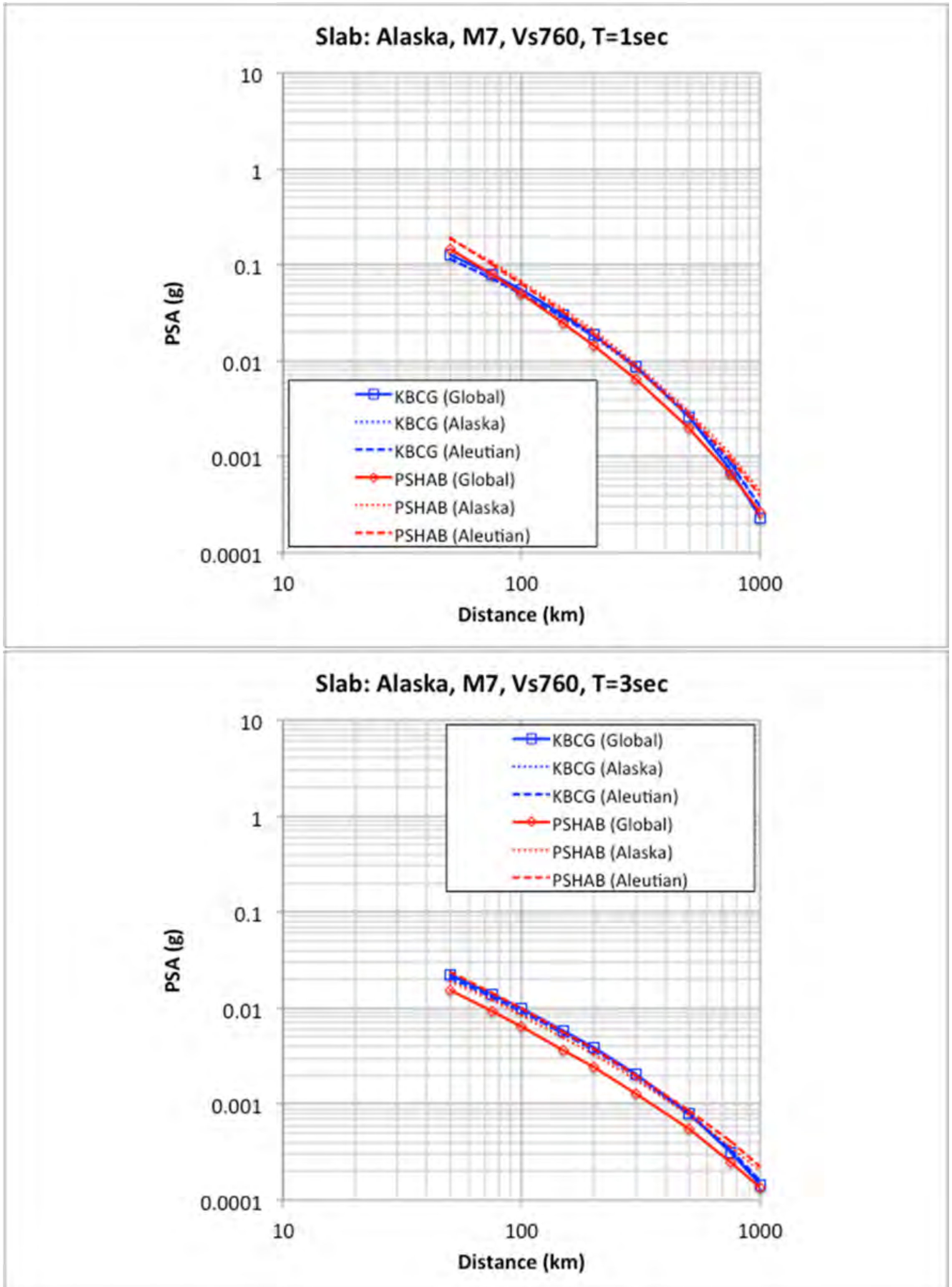

Figure 3.64 **Comparison of Alaska regional M7 (slab) for 1.0 (top) and 3.0 sec (bottom) attenuation curves for V_{S30} = 760 m/sec.**

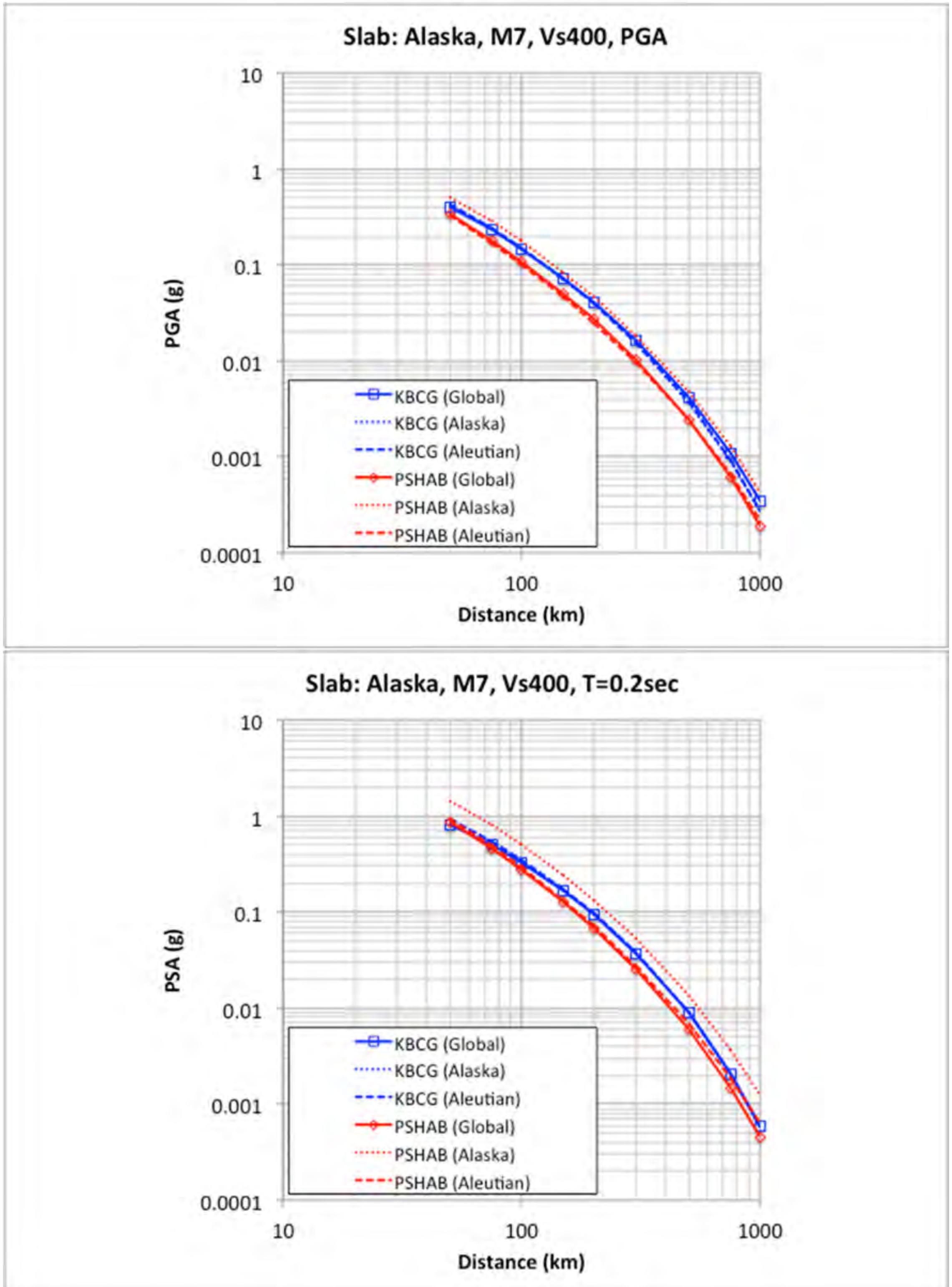

Figure 3.65 Comparison of Alaska regional M7 (slab) for PGA (T = 0.01 sec) (top) and 0.2 sec (bottom) attenuation curves for V_{S30} = 400 m/sec.

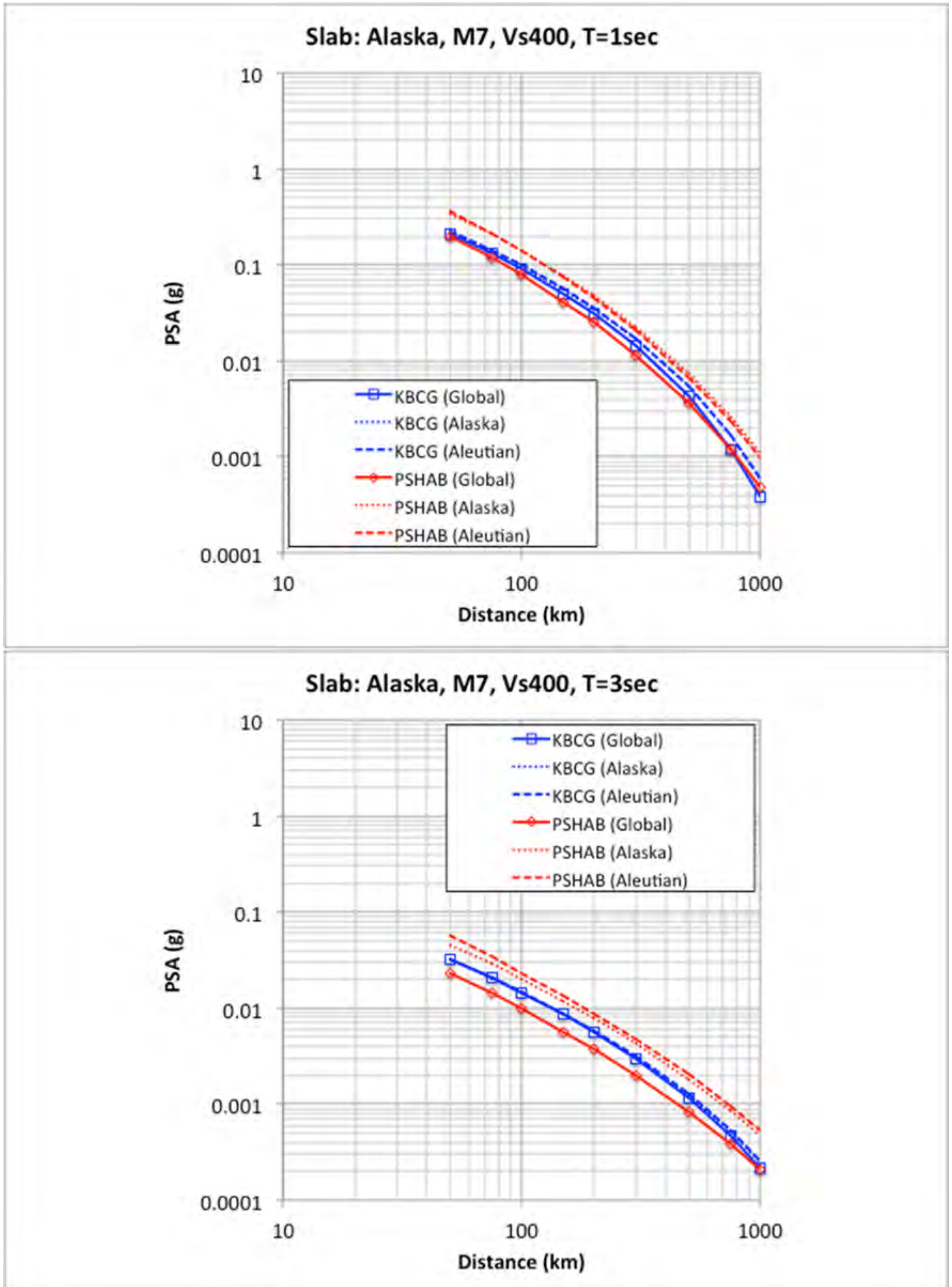

Figure 3.66 Comparison of Alaska regional M7 (slab) for 1.0 (top) and 3.0 sec (bottom) attenuation curves for V_{S30} = 400 m/sec.

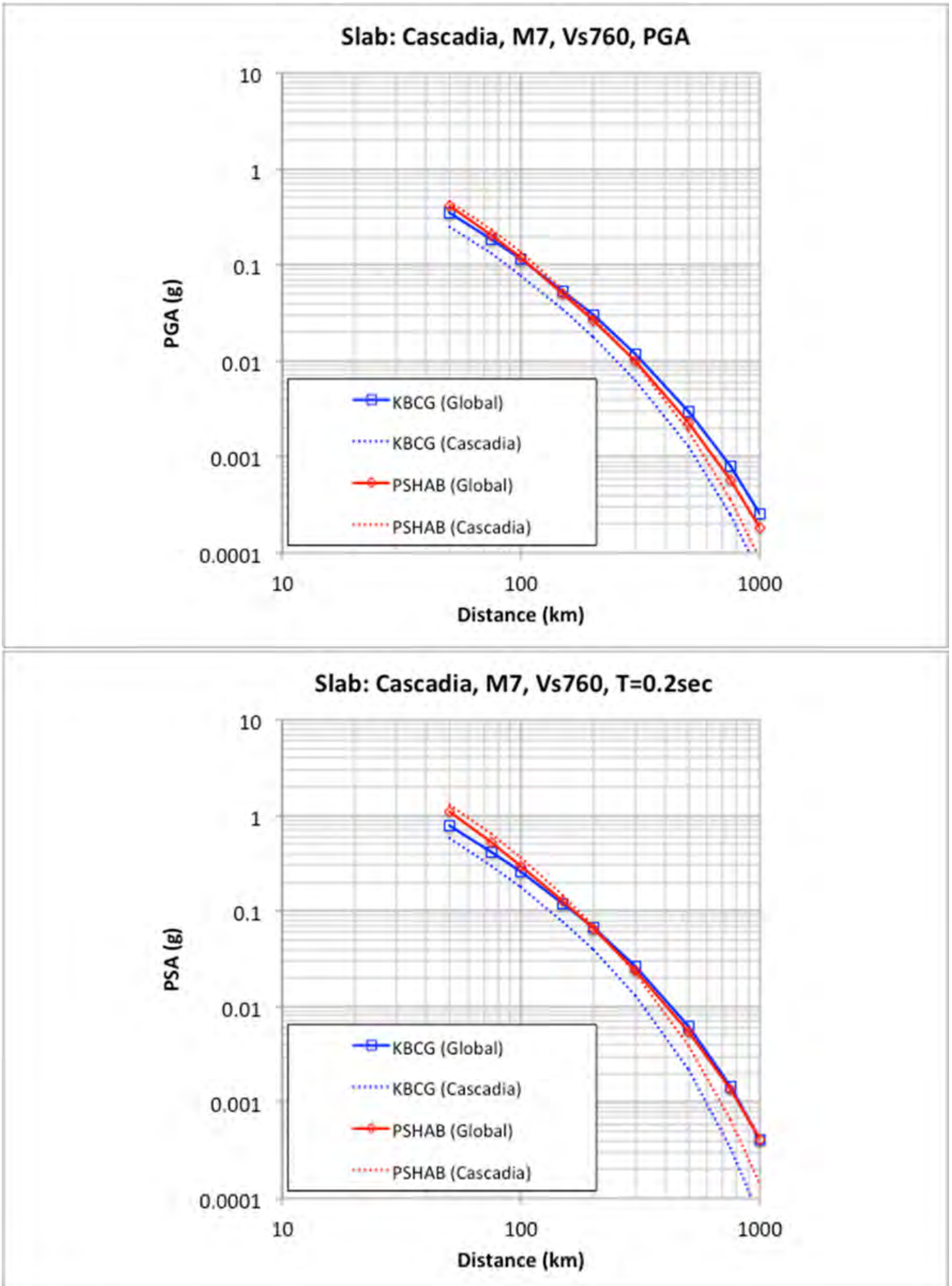

Figure 3.67 **Comparison of Cascadia regional M7 (slab) for PGA (*T* = 0.01 sec) (top) and 0.2 sec (bottom) attenuation curves for V_{S30} = 760 m/sec.**

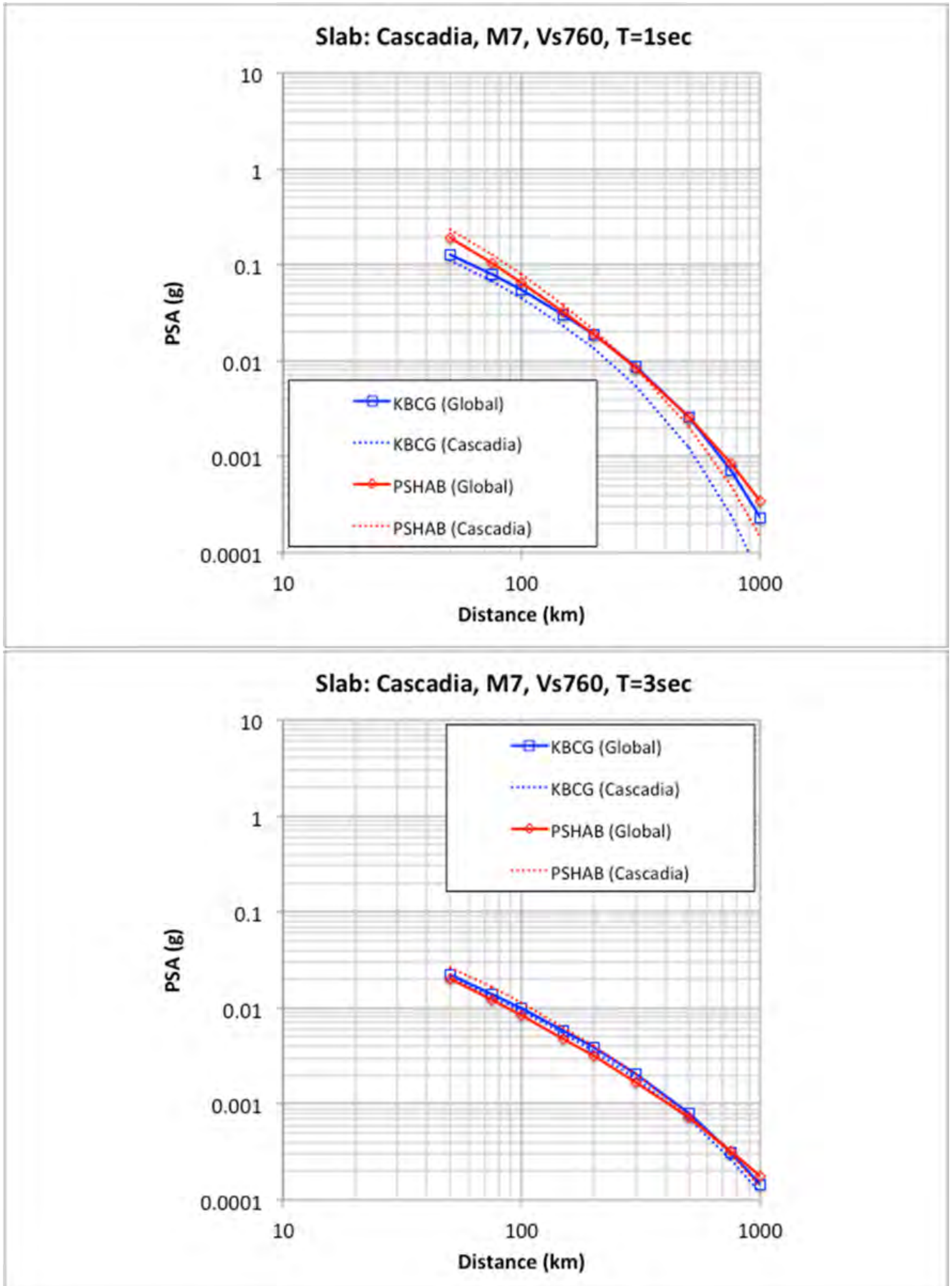

Figure 3.68 **Comparison of Cascadia regional M7 (slab) for 1.0 (top) and 3.0 sec (bottom) attenuation curves for V_{S30} = 760 m/sec.**

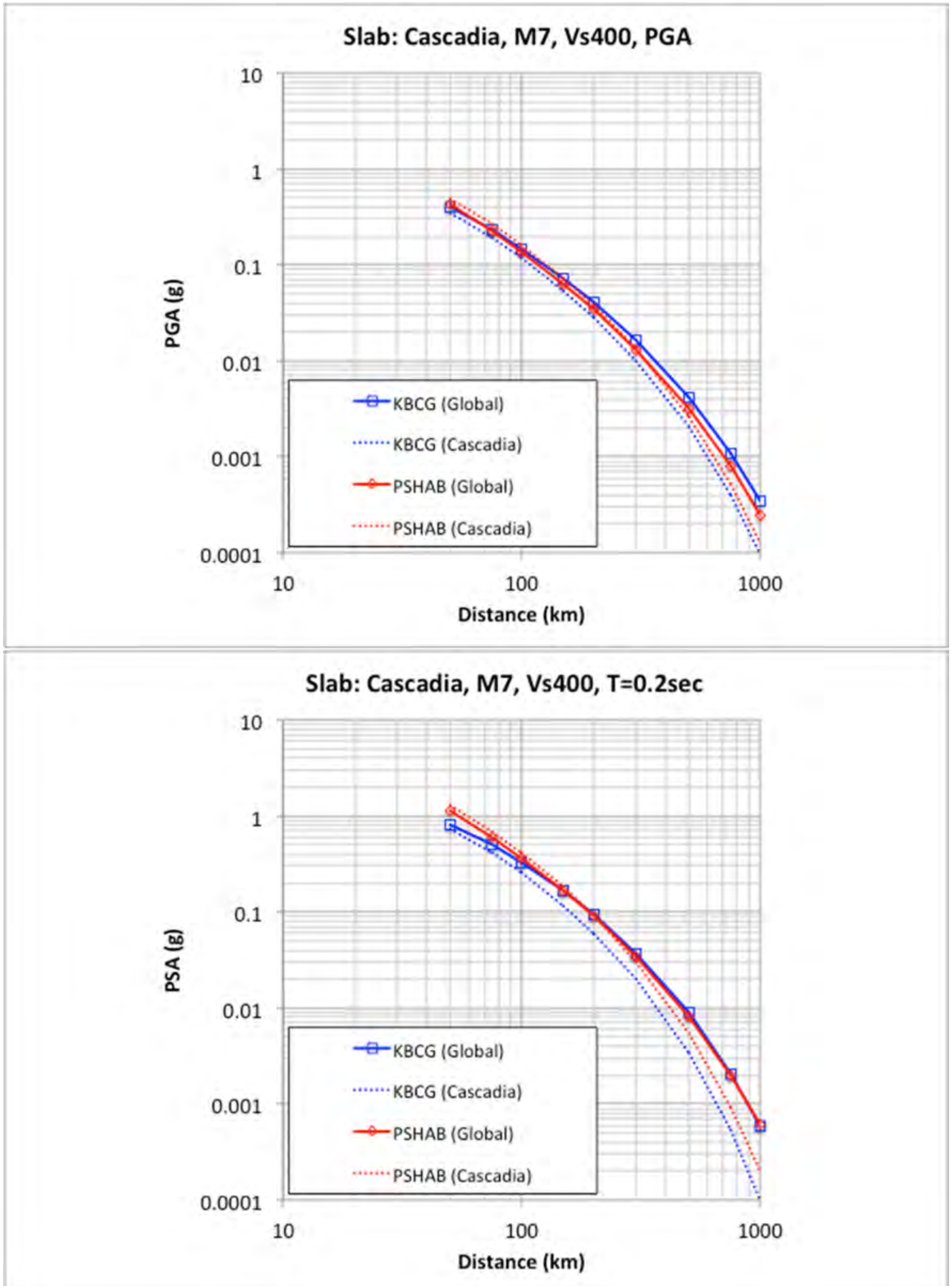

Figure 3.69 **Comparison of Cascadia regional M7 (slab) for PGA (T = 0.01 sec) (top) and 0.2 sec (bottom) attenuation curves for V_{S30} = 400 m/sec.**

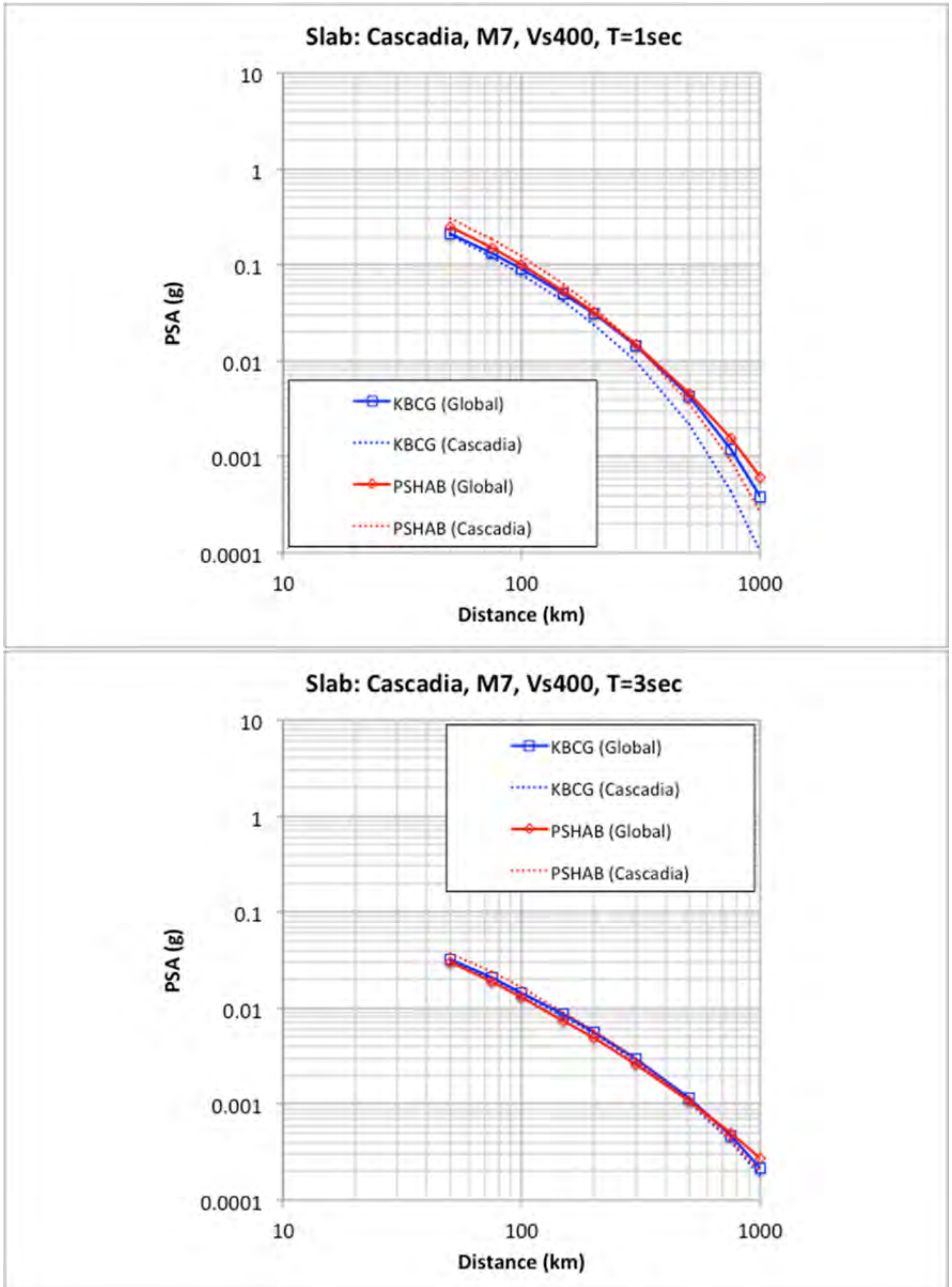

Figure 3.70 Comparison of Cascadia regional M7 (slab) for 1.0 (top) and 3.0 sec (bottom) attenuation curves for V_{S30} = 400 m/sec.

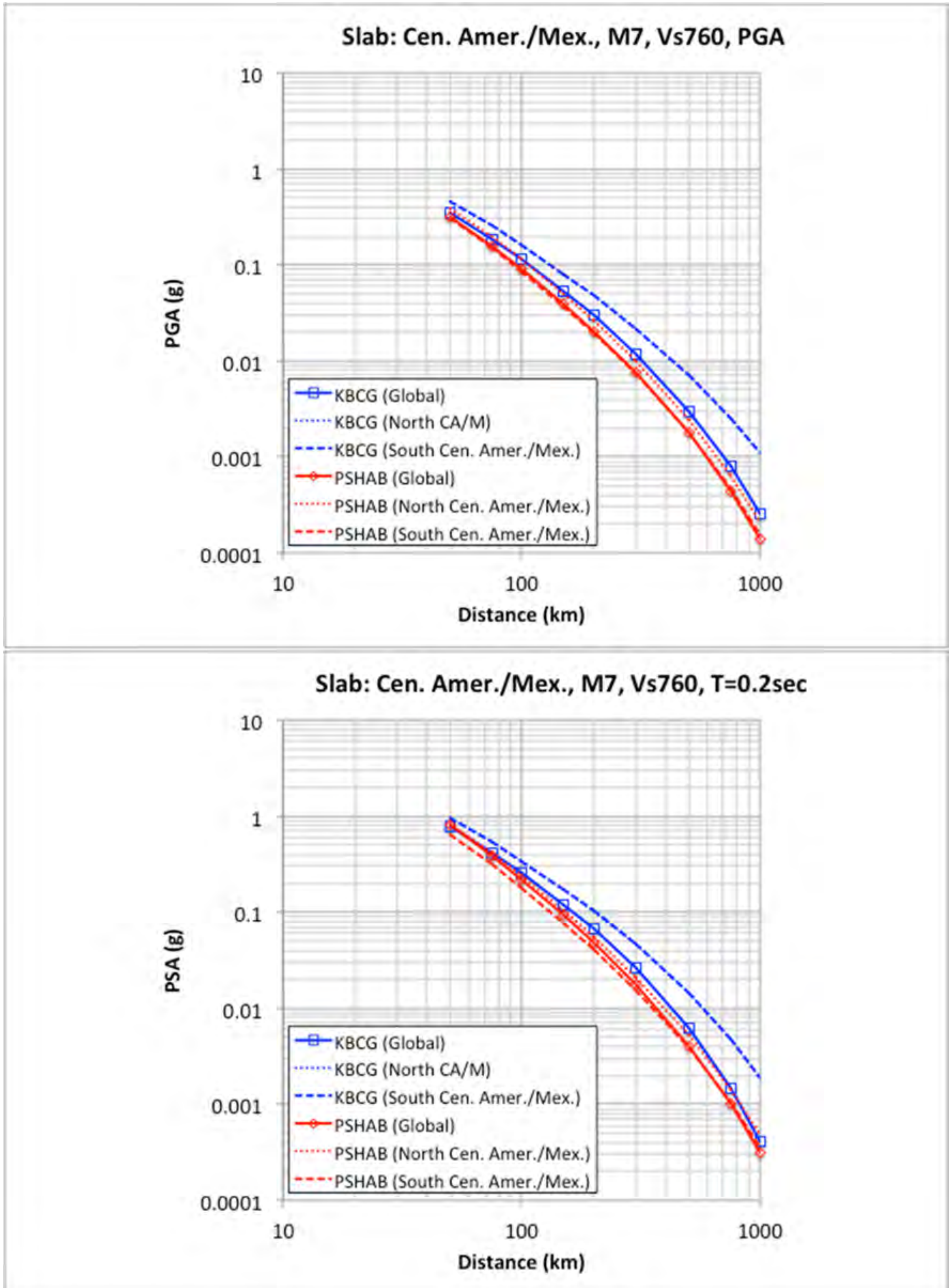

Figure 3.71 Comparison of Central America and Mexico regional M7 (slab) for PGA (T = 0.01 sec) (top) and 0.2 sec (bottom) attenuation curves for V_{S30} = 760 m/sec.

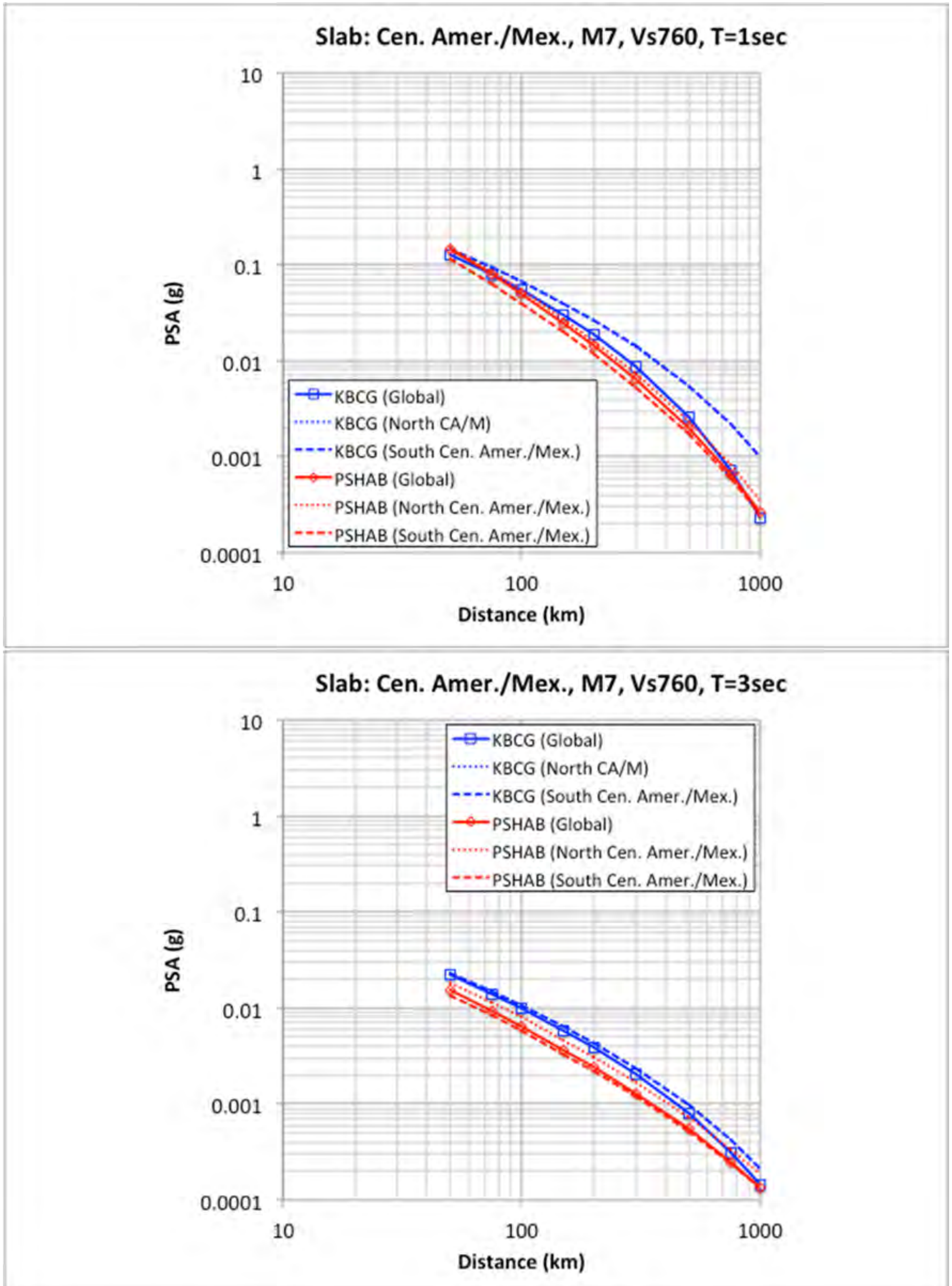

Figure 3.72 **Comparison of Central America and Mexico regional M7 (slab) for 1.0 (top) and 3.0 sec (bottom) attenuation curves for V_{S30} = 760 m/sec.**

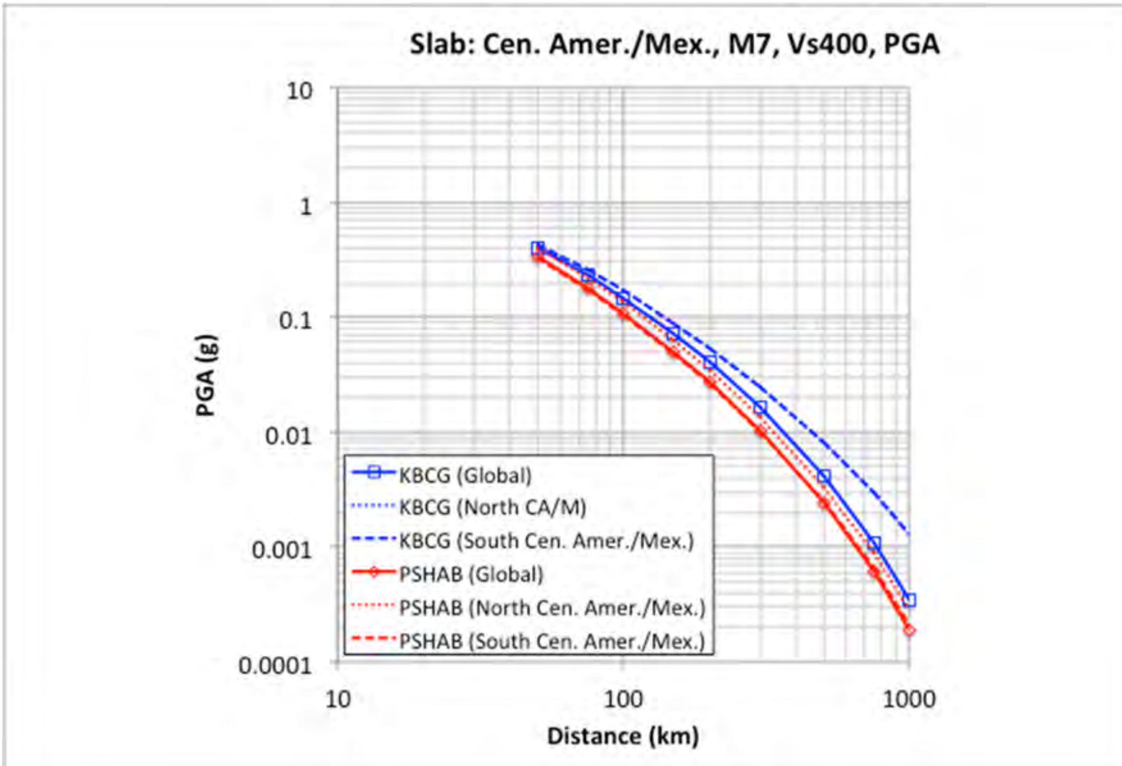

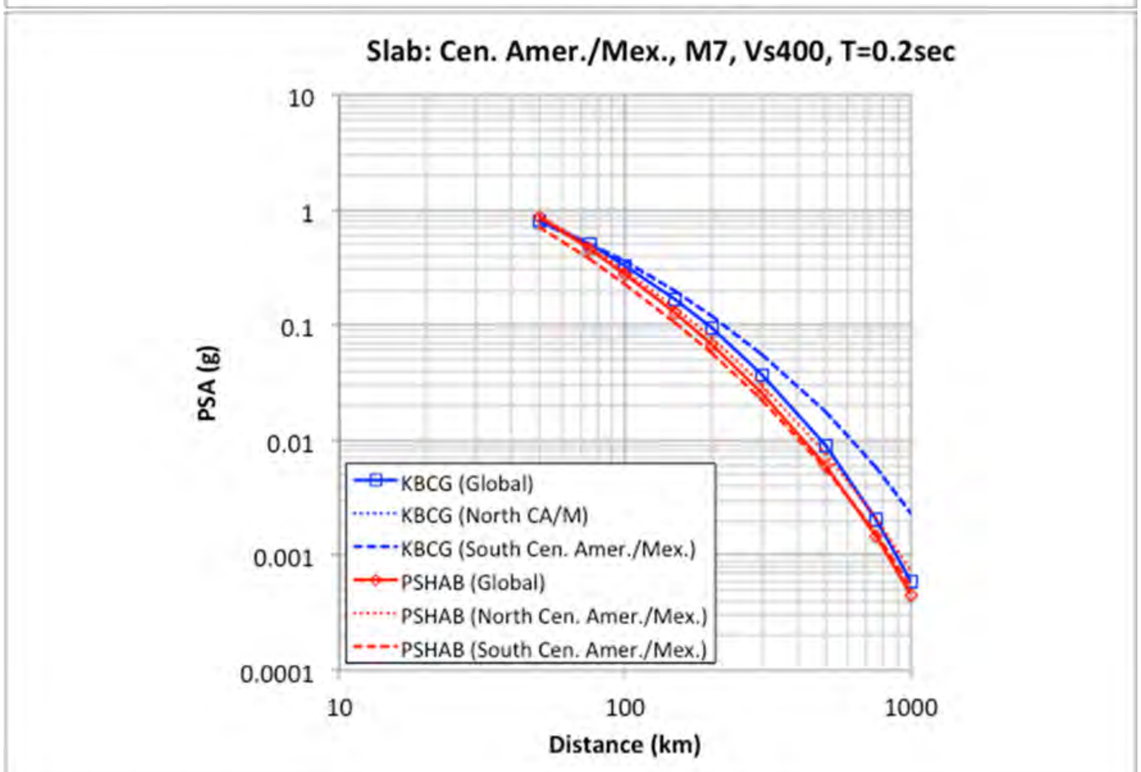

Figure 3.73 Comparison of Central America and Mexico regional M7 (slab) for PGA (*T* = 0.01 sec) (top) and 0.2 sec (bottom) attenuation curves for V_{S30} = 400 m/sec.

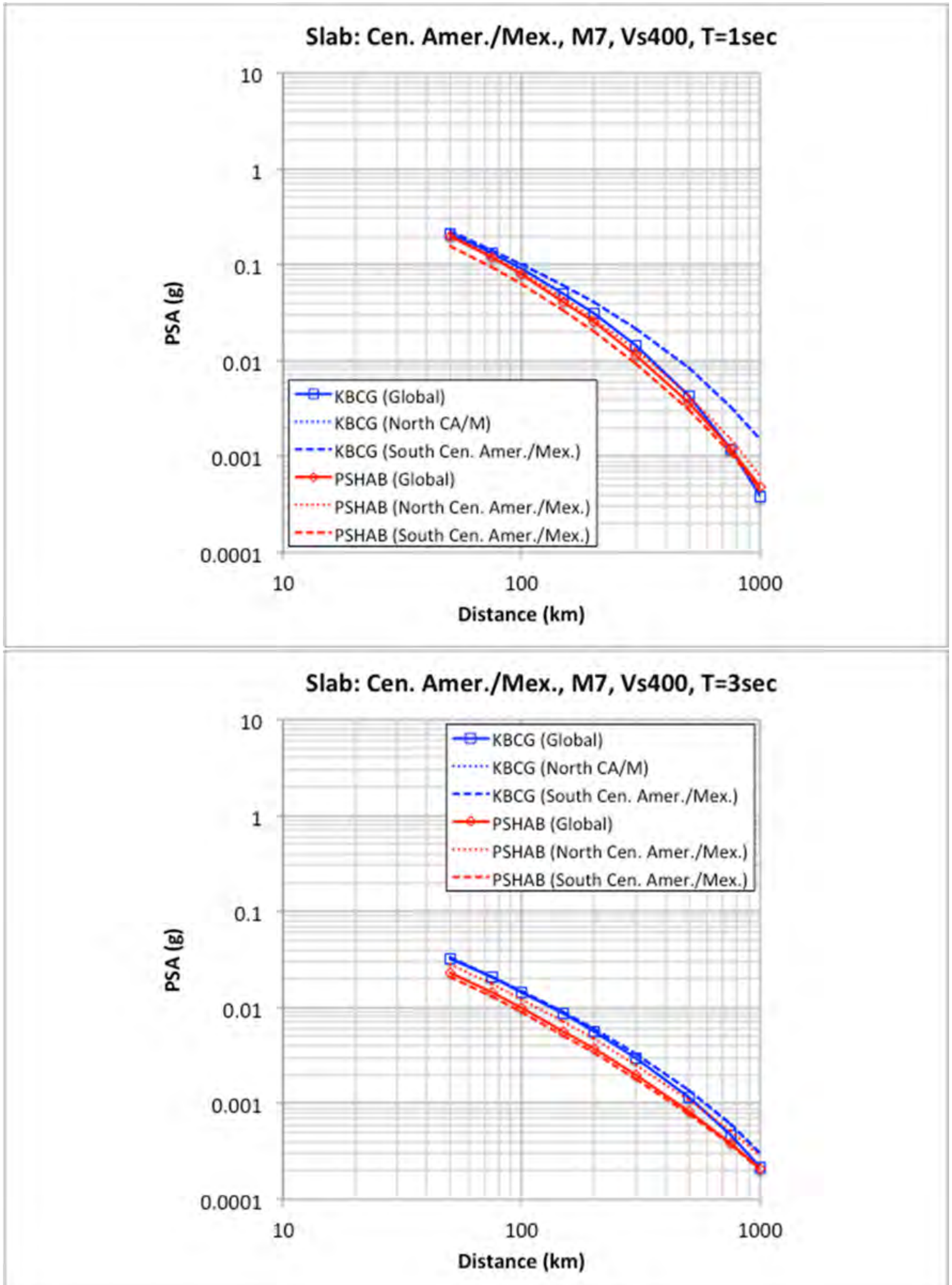

Figure 3.74 **Comparison of Central America and Mexico regional M7 (slab) for 1.0 (top) and 3.0 sec (bottom) attenuation curves for V_{S30} = 400 m/sec.**

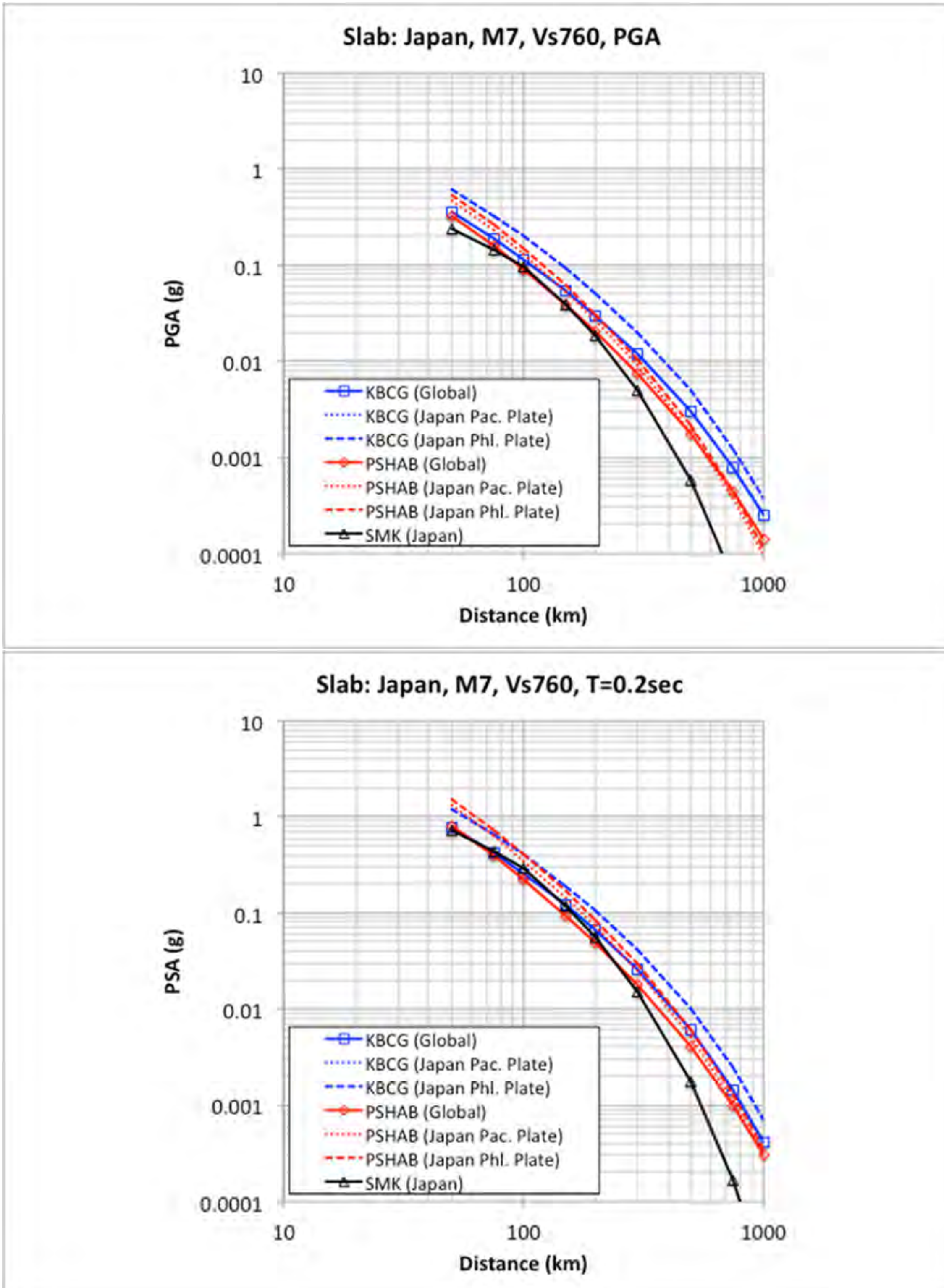

Figure 3.75 **Comparison of Japan regional M7 (slab) for PGA (*T* = 0.01 sec) (top) and 0.2 sec (bottom) attenuation curves for V_{S30} = 760 m/sec.**

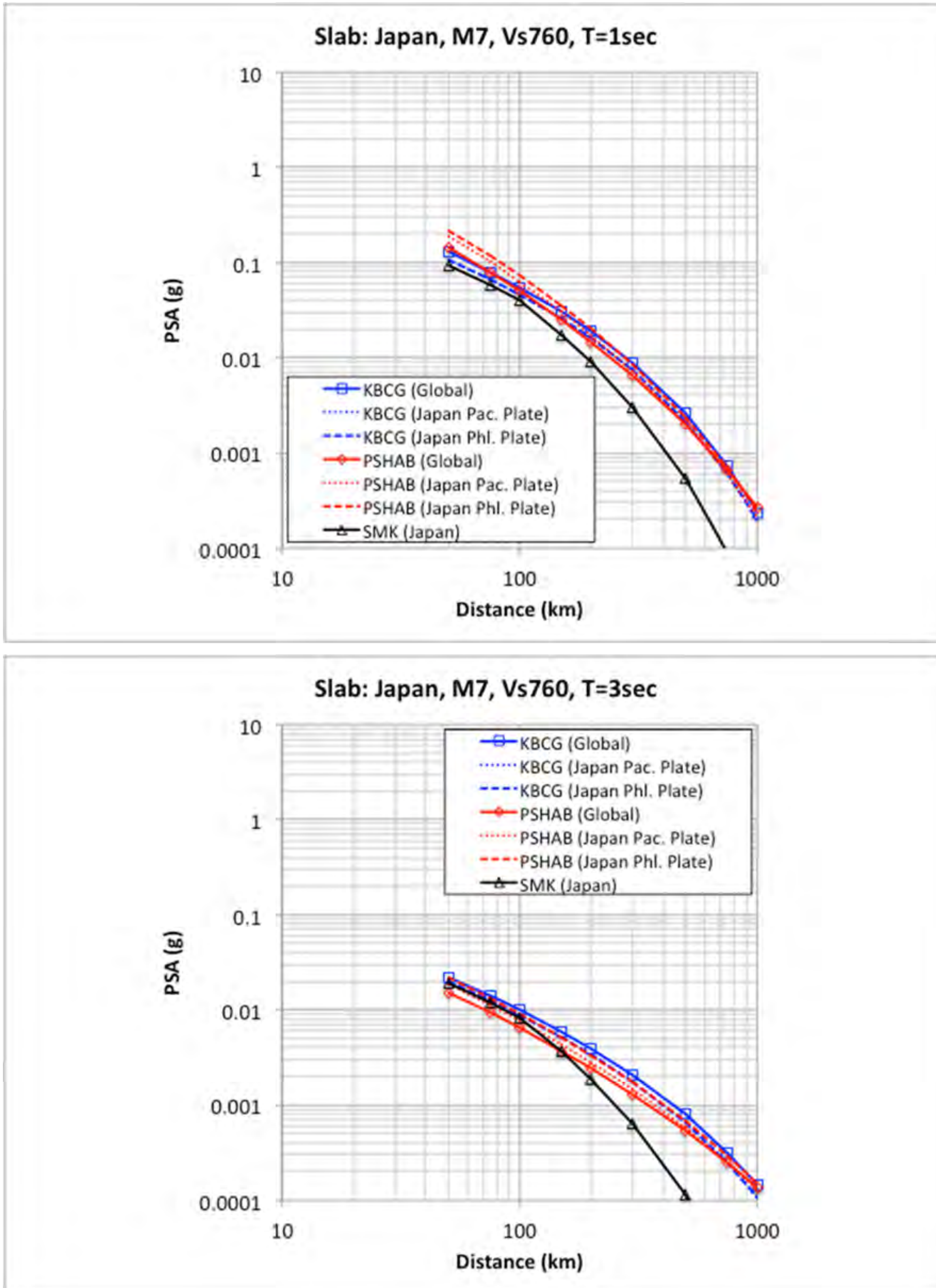

Figure 3.76 Comparison of Japan regional M7 (slab) for 1.0 (top) and 3.0 sec (bottom) attenuation curves for V_{S30} = 760 m/sec.

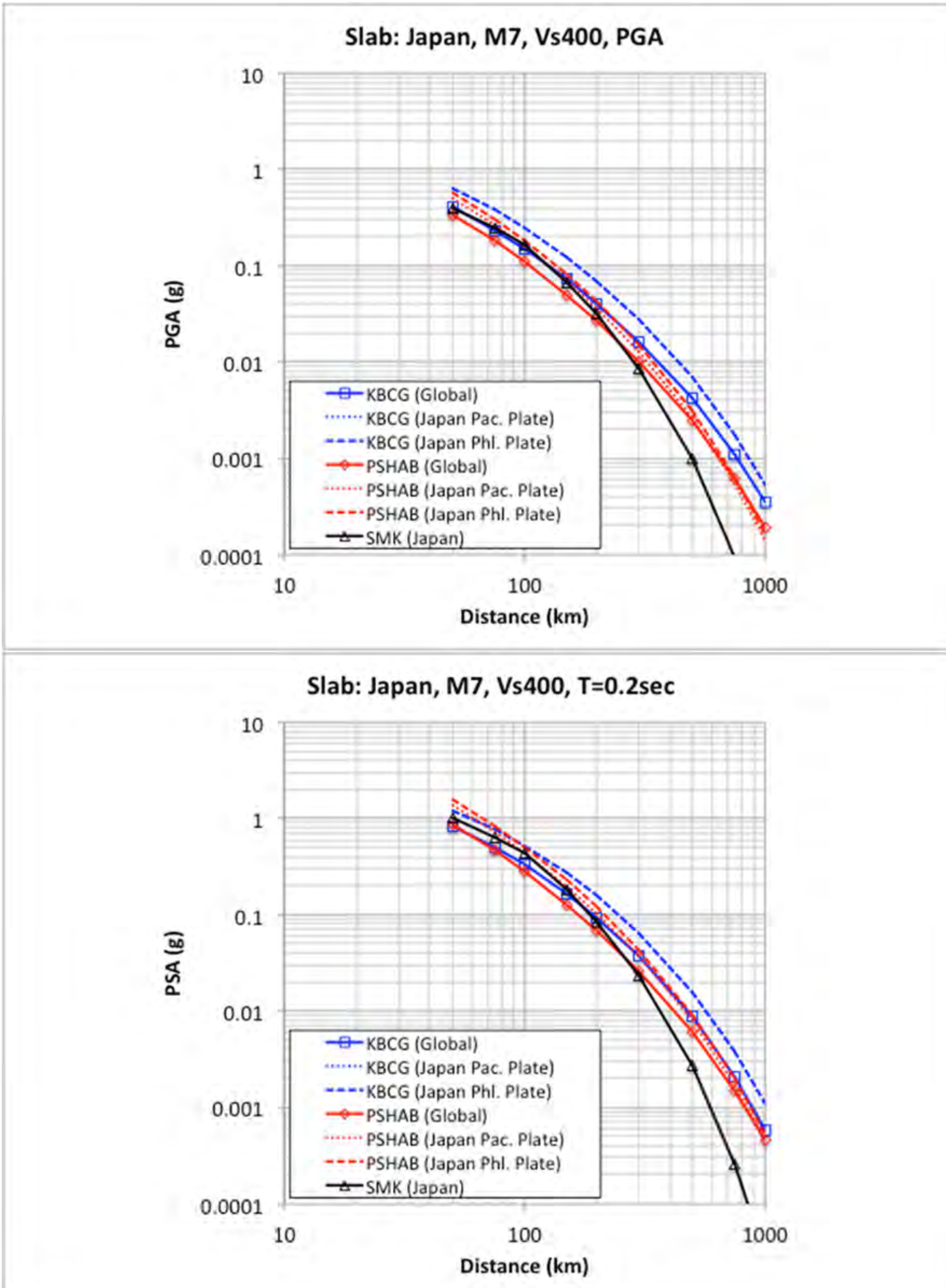

Figure 3.77 Comparison of Japan regional M7 (slab) for PGA (*T* = 0.01 sec) (top) and 0.2 sec (bottom) attenuation curves for V_{S30} = 400 m/sec.

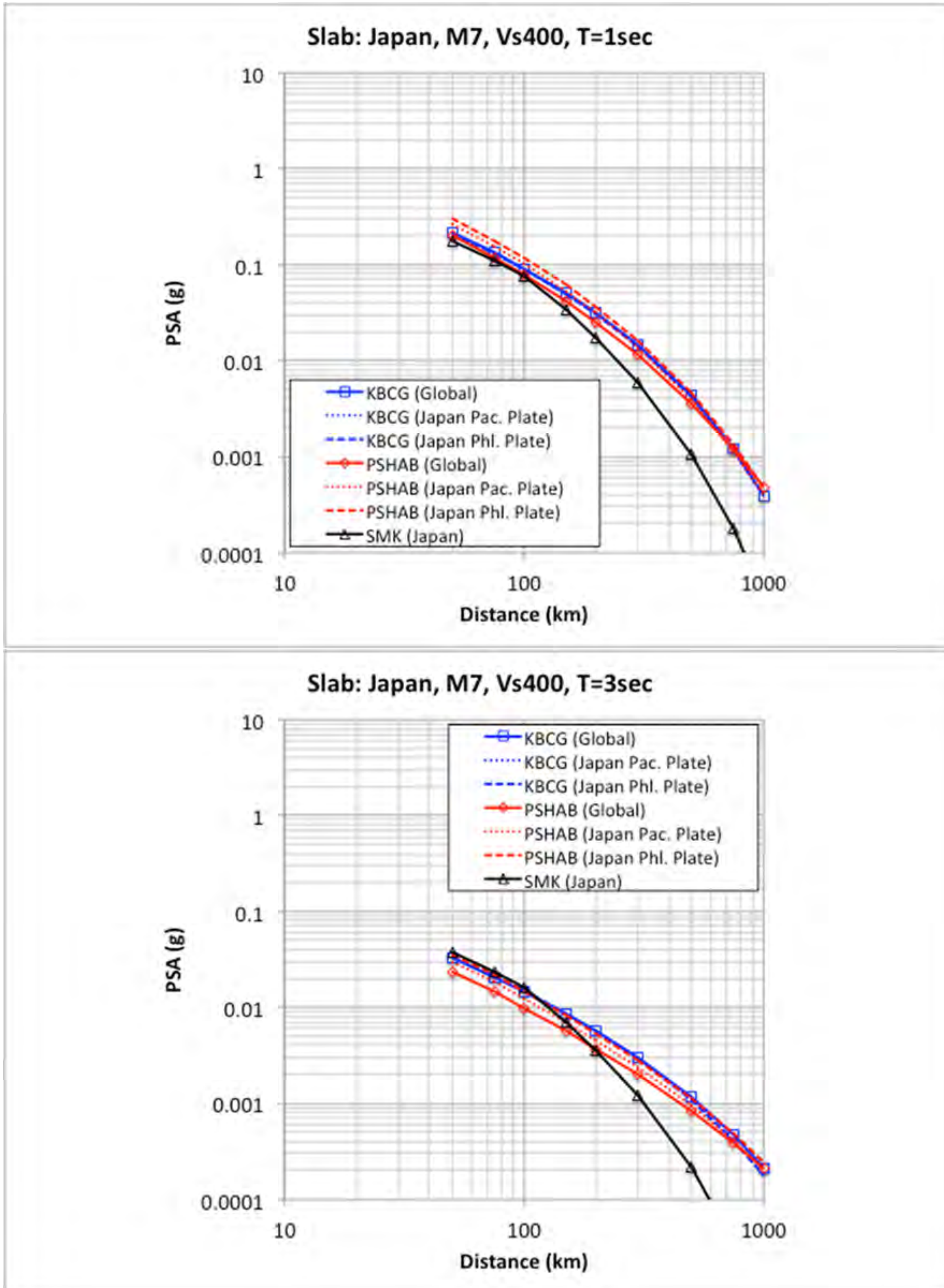

Figure 3.78 Comparison of Japan regional M7 (slab) for 1.0 (top) and 3.0 sec (bottom) attenuation curves for V_{S30} = 400 m/sec.

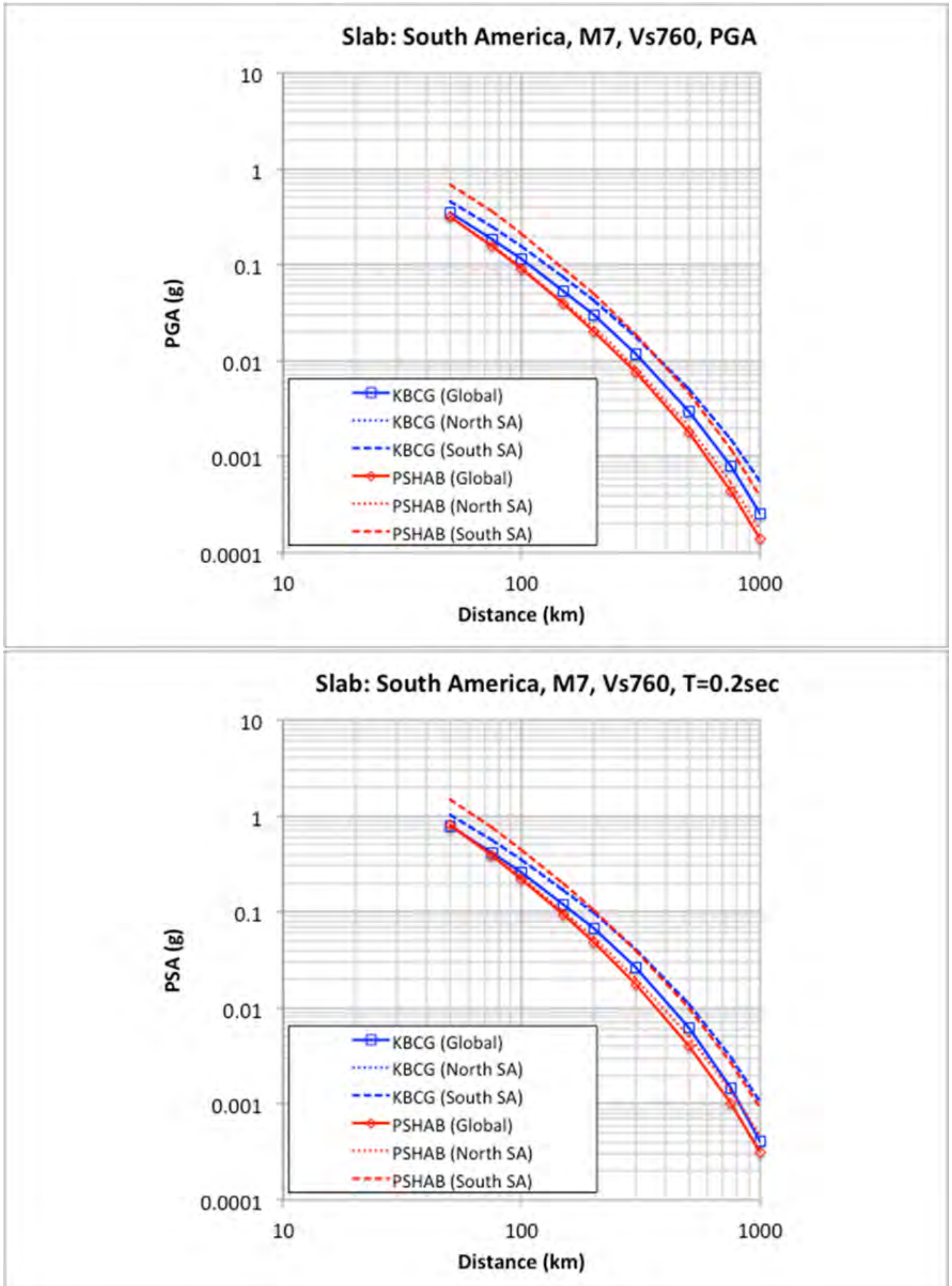

Figure 3.79 Comparison of South America regional M7 (slab) for PGA (T = 0.01 sec) (top) and 0.2 sec (bottom) attenuation curves for V_{S30} = 760 m/sec.

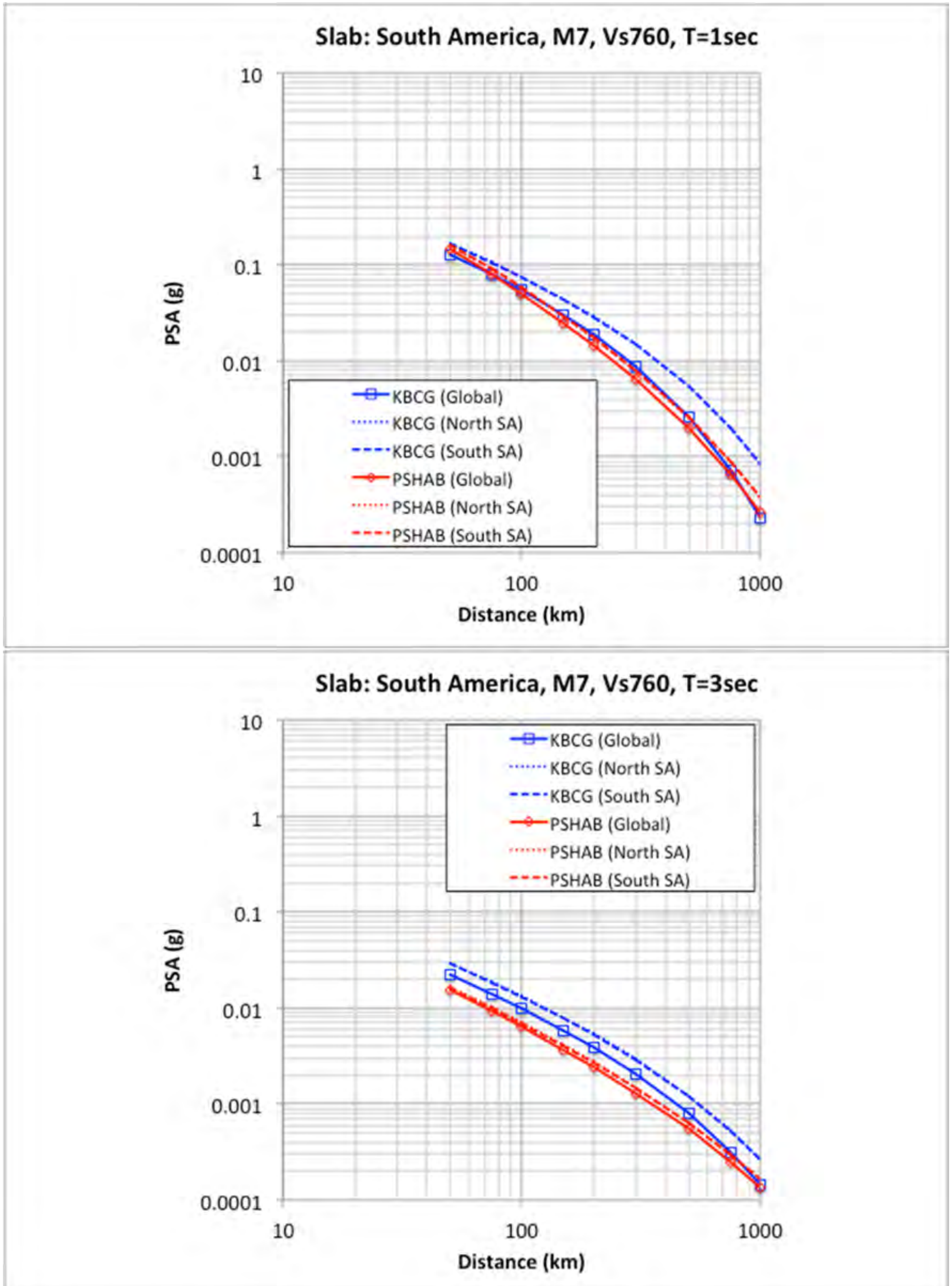

Figure 3.80 Comparison of South America regional M7 (slab) for 1.0 (top) and 3.0 sec (bottom) attenuation curves for V_{S30} = 760 m/sec.

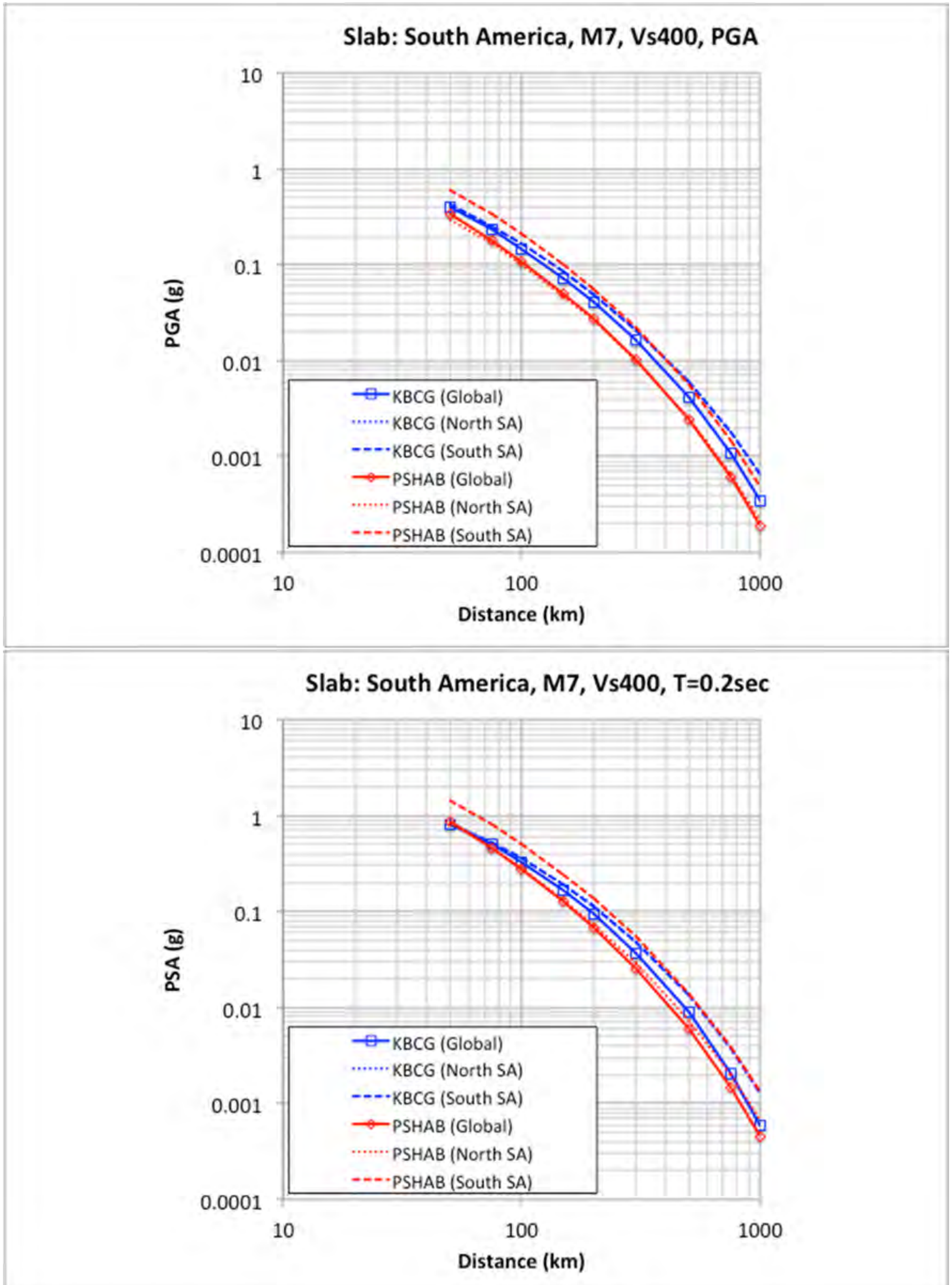

Figure 3.81 **Comparison of South America regional M7 (slab) for PGA (T = 0.01 sec) (top) and 0.2 sec (bottom) attenuation curves for V_{S30} = 400 m/sec.**

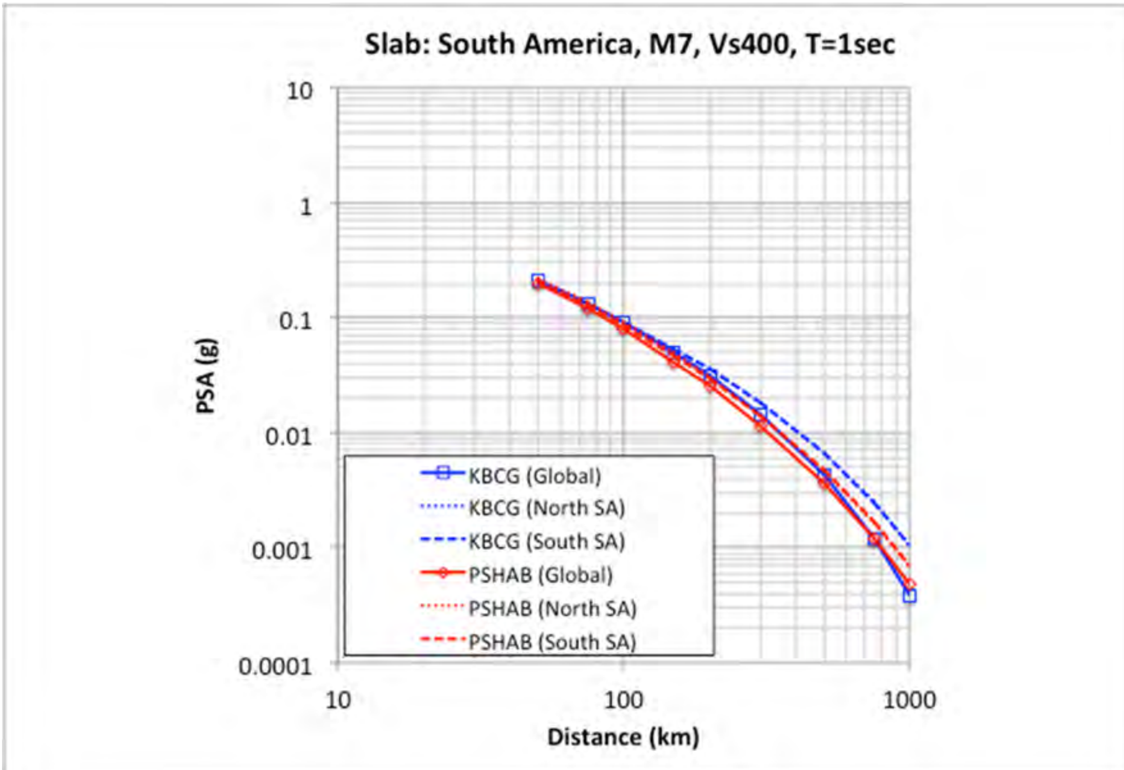

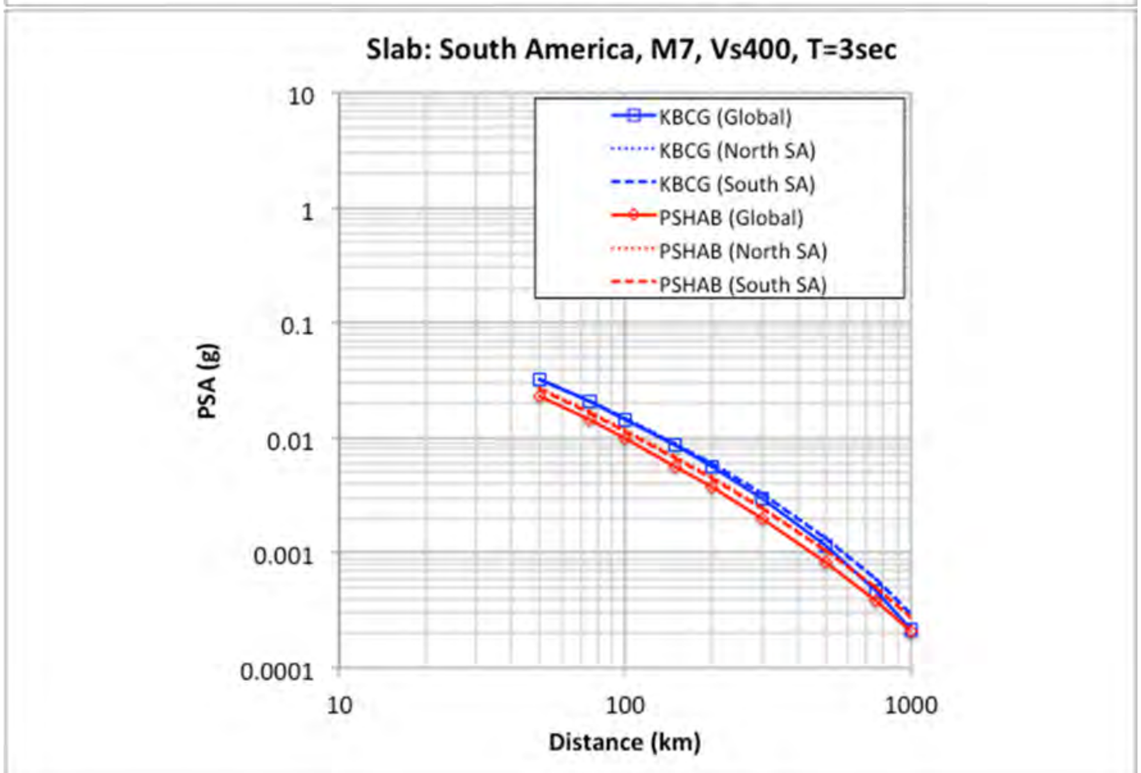

Figure 3.82 **Comparison of South America regional M7 (slab) for 1.0 (top) and 3.0 sec (bottom) attenuation curves for V_{S30} = 400 m/sec.**

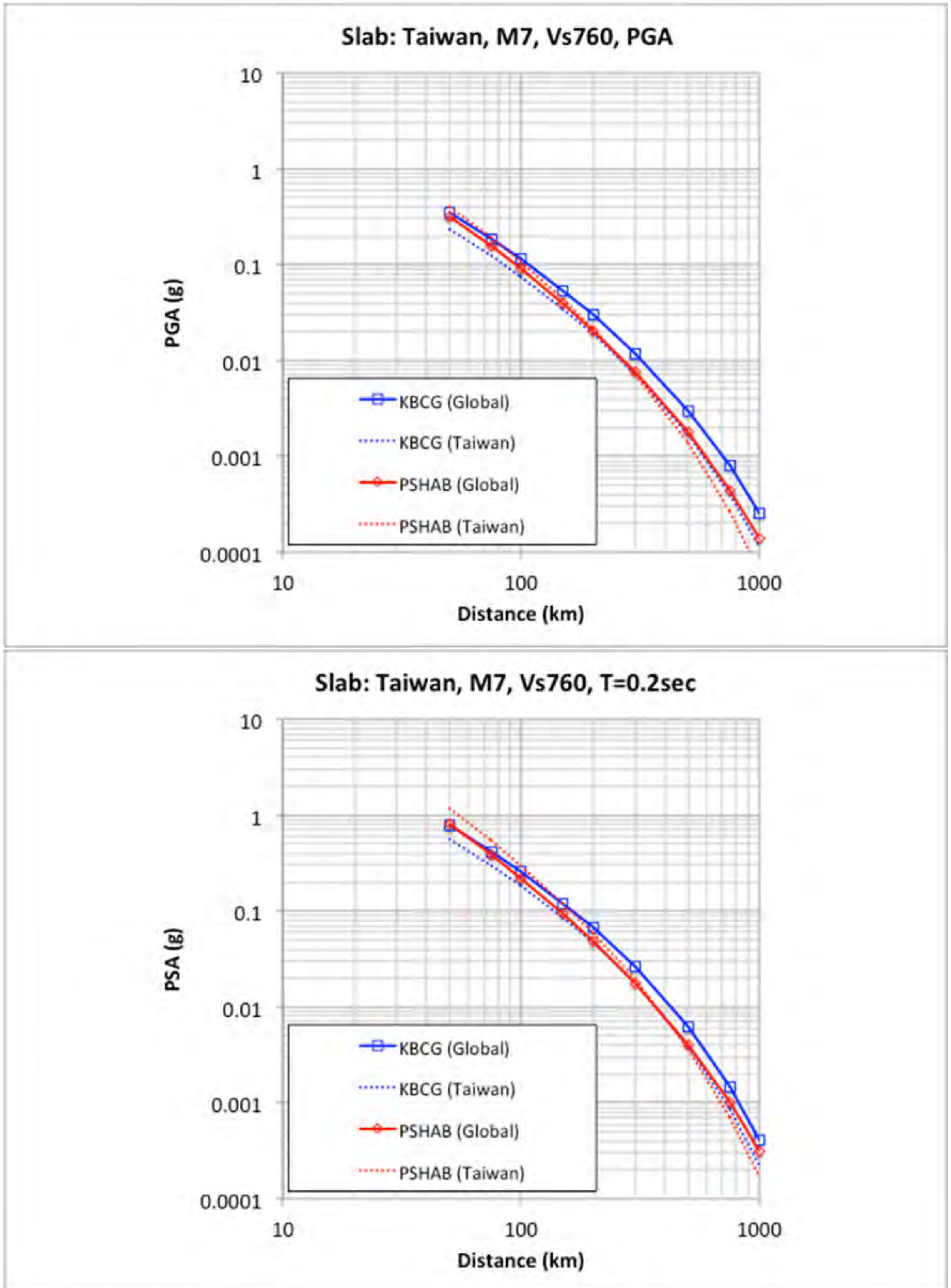

Figure 3.83 **Comparison of Taiwan regional M7 (slab) for PGA (*T* = 0.01 sec) (top) and 0.2 sec (bottom) attenuation curves for V_{S30} = 760 m/sec.**

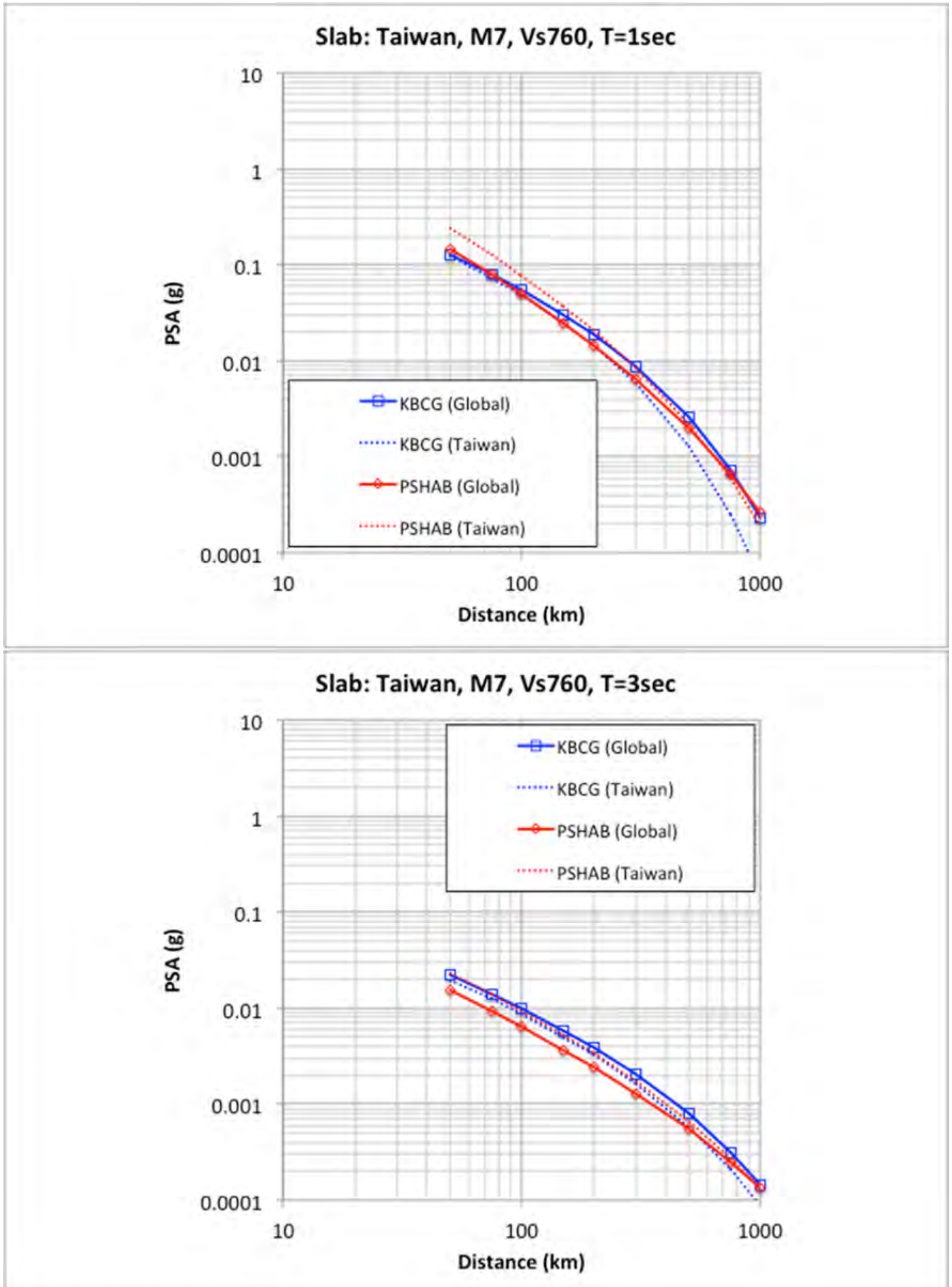

Figure 3.84 **Comparison of Taiwan regional M7 (slab) for 1.0 (top) and 3.0 sec (bottom) attenuation curves for V_{S30} = 760 m/sec.**

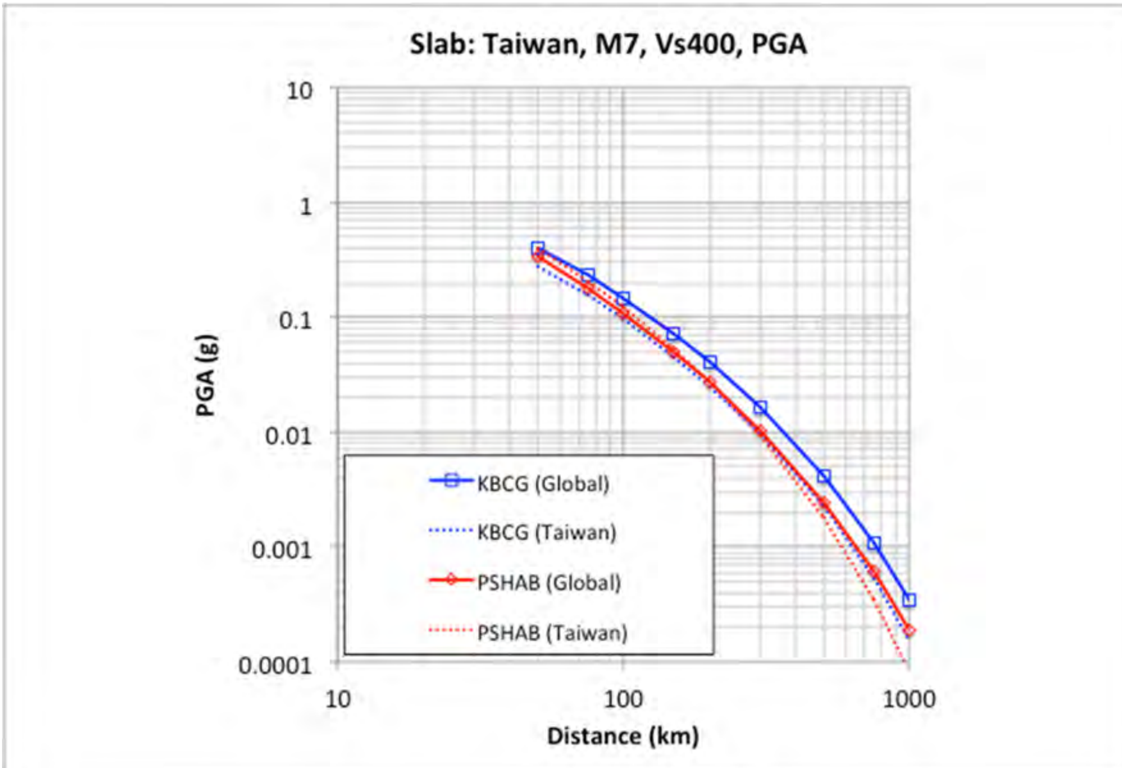

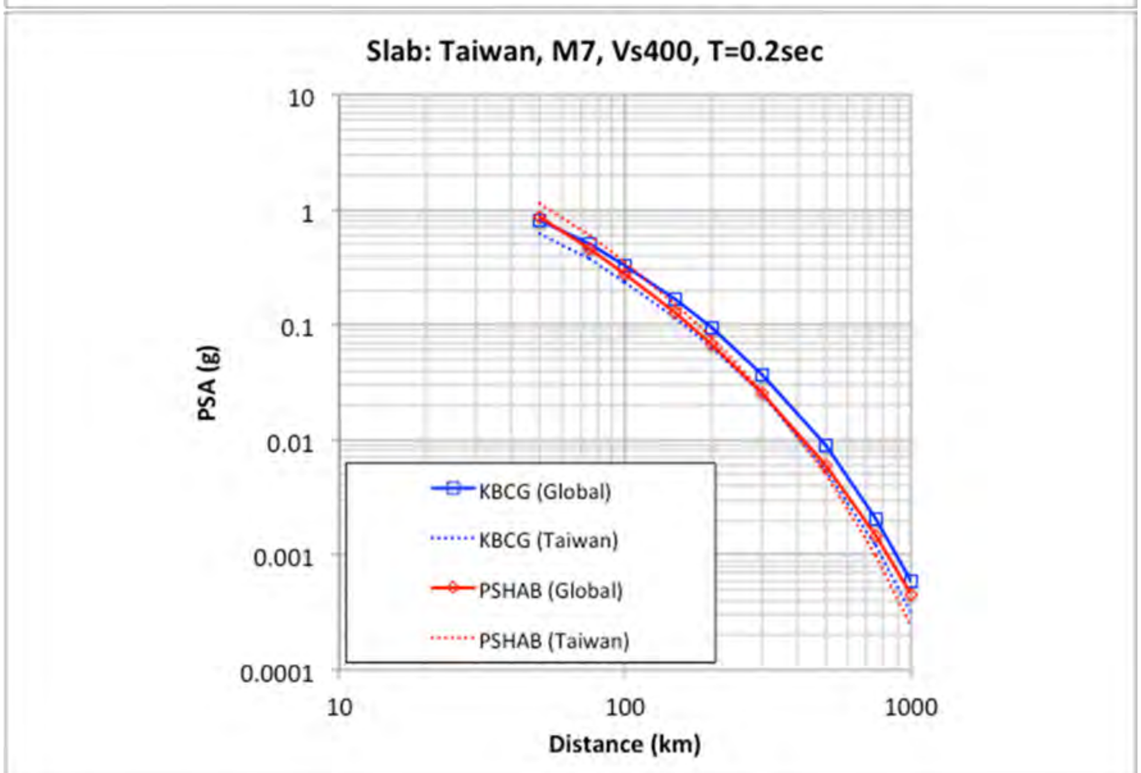

Figure 3.85 **Comparison of Taiwan regional M7 (slab) for PGA (T = 0.01 sec) (top) and 0.2 sec (bottom) attenuation curves for V_{S30} = 400 m/sec.**

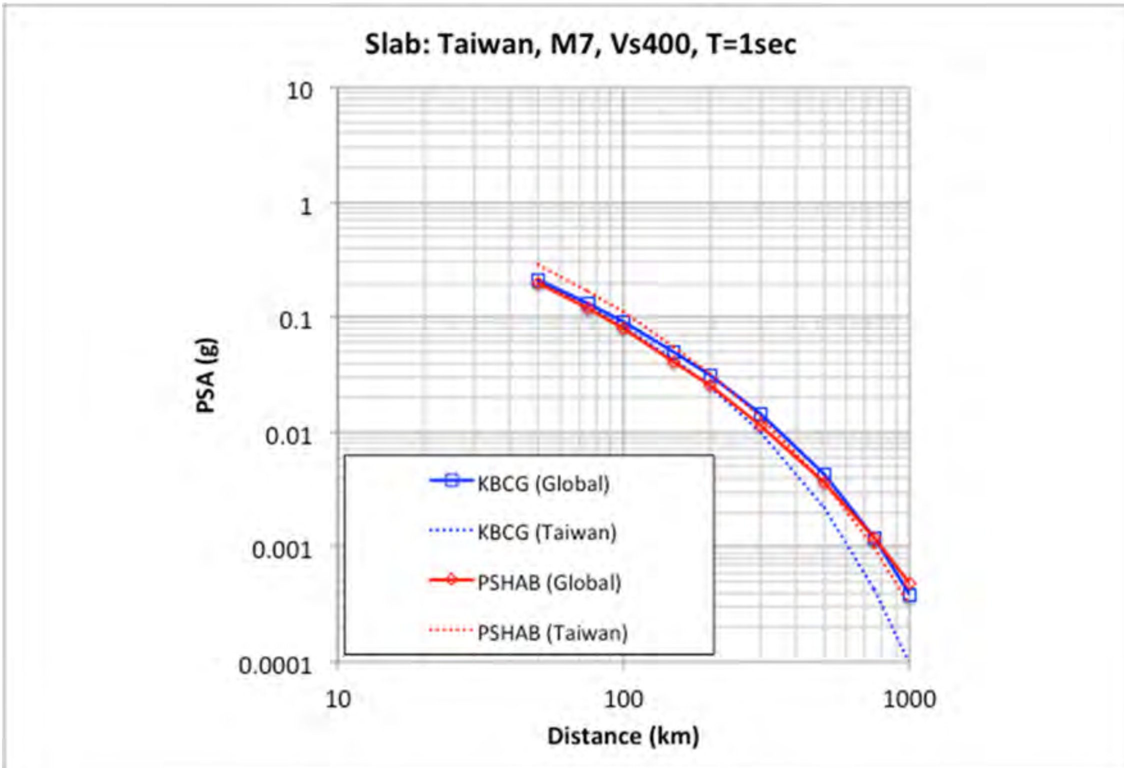

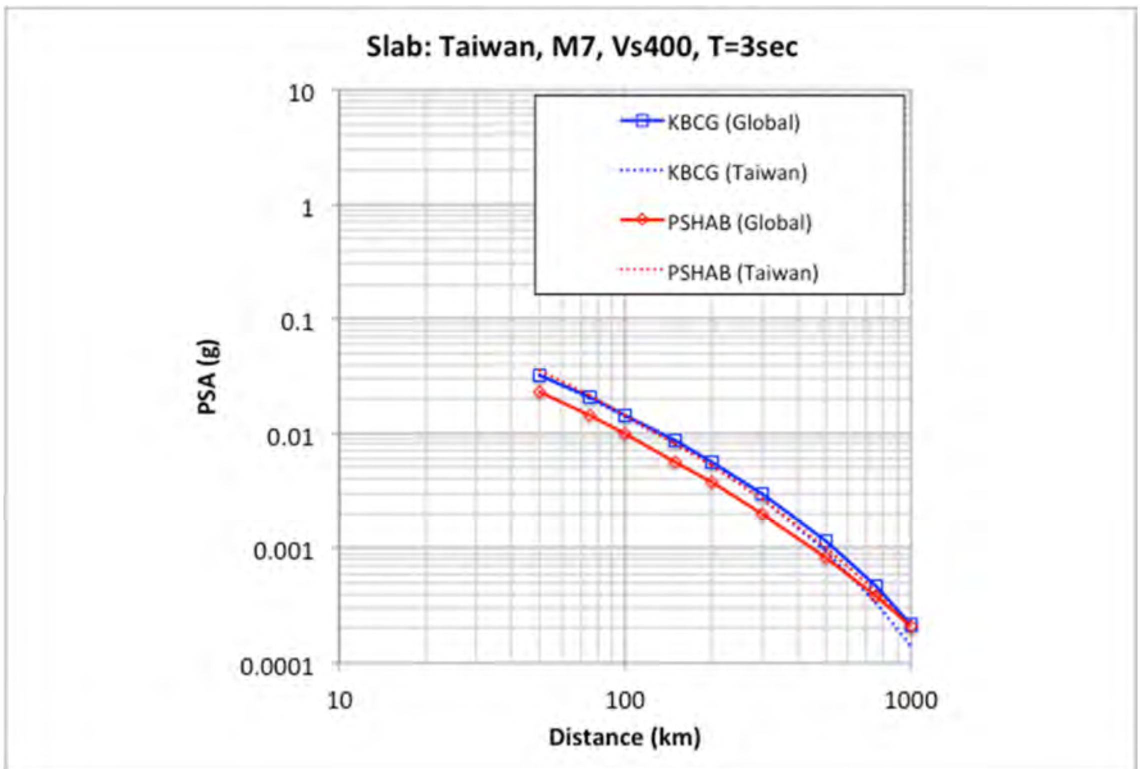

Figure 3.86 **Comparison of Taiwan regional M7 (slab) for 1.0 (top) and 3.0 sec (bottom) attenuation curves for V_{S30} = 400 m/sec.**

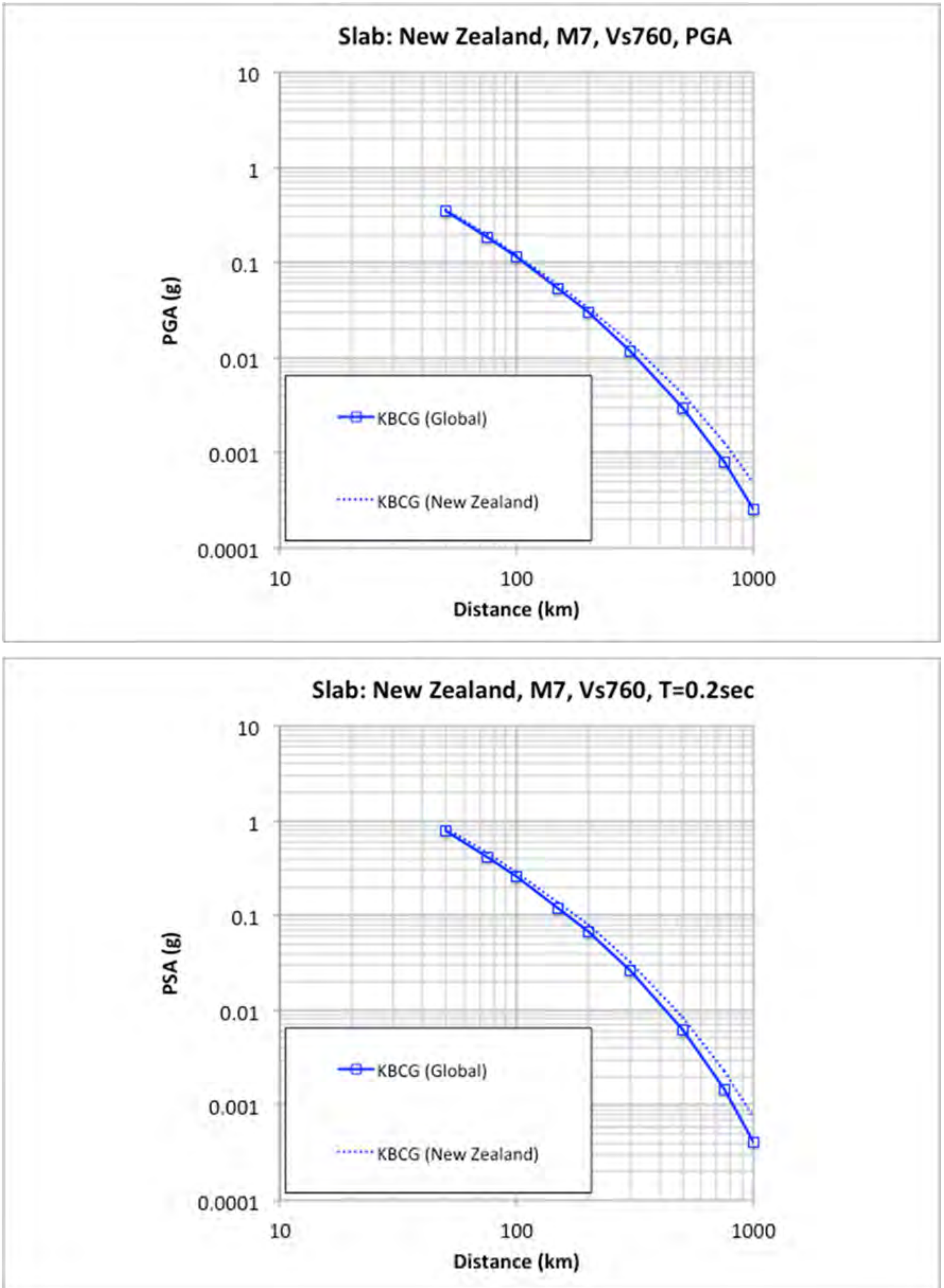

Figure 3.87 Comparison of New Zealand regional M7 (slab) for PGA (T = 0.01 sec) (top) and 0.2 sec (bottom) attenuation curves for V_{S30} = 760 m/sec.

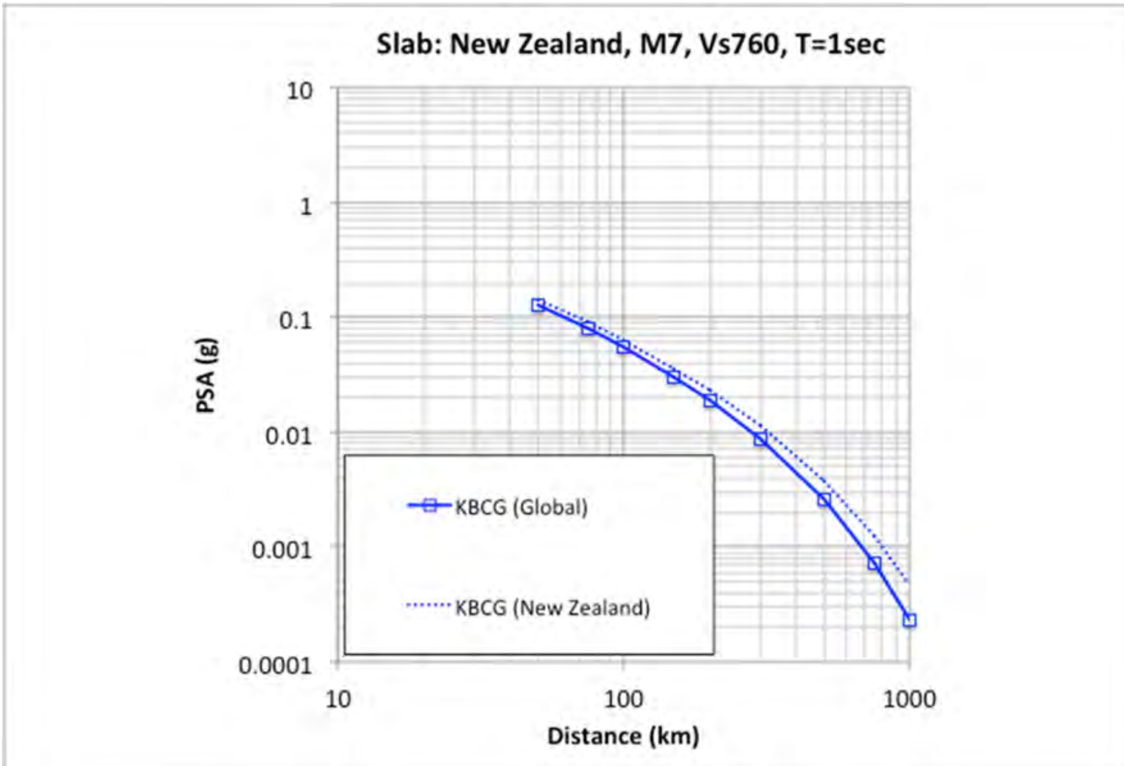

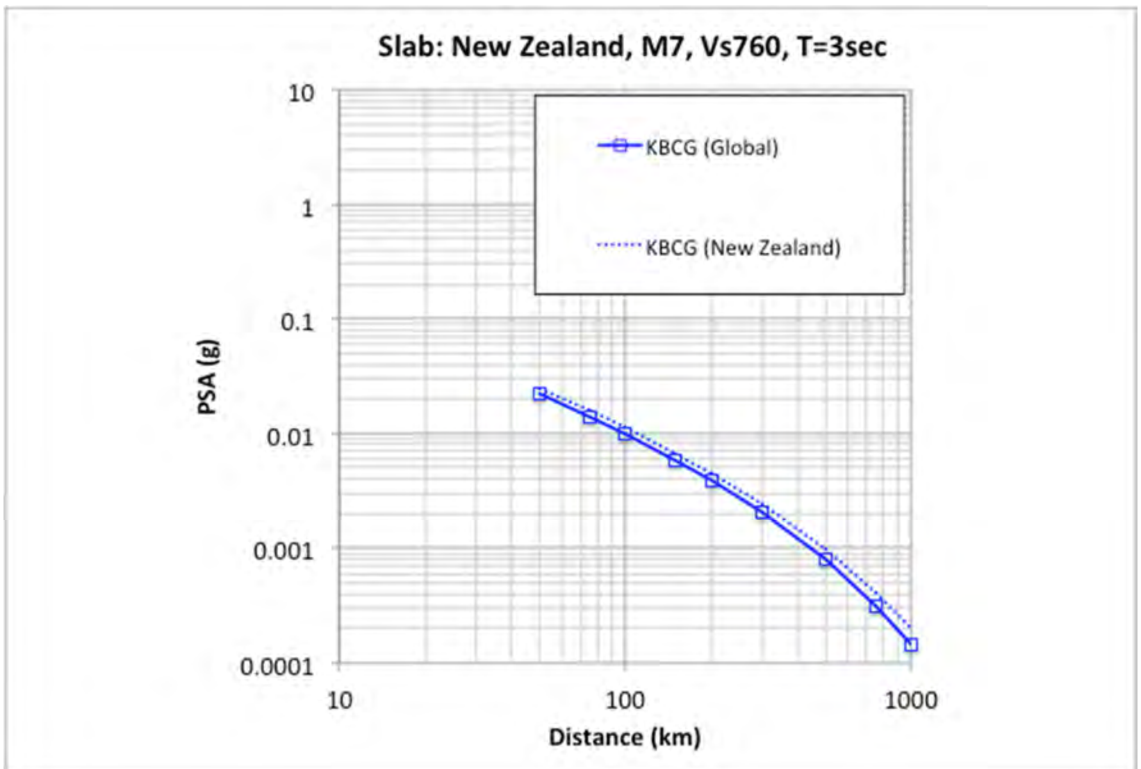

Figure 3.88 Comparison of New Zealand regional M7 for 1.0 (top) and 3.0 sec (bottom) attenuation curves for V_{S30} = 760 m/sec.

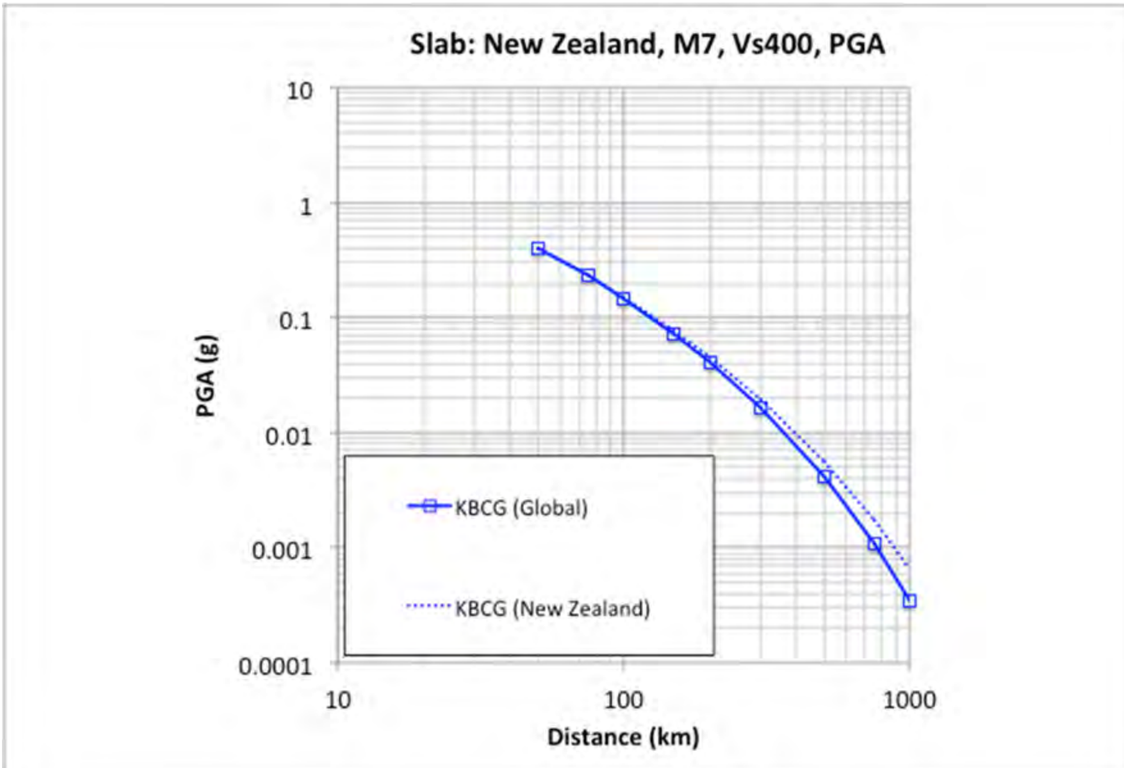

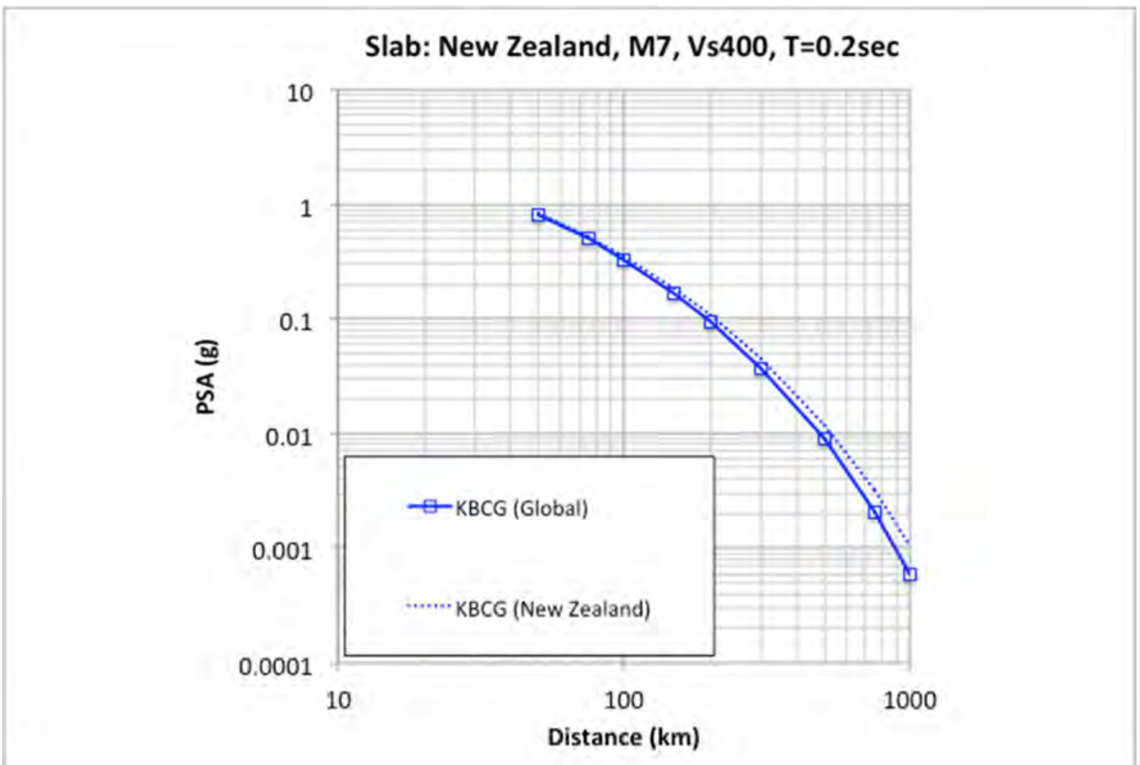

Figure 3.89 Comparison of New Zealand regional M7 (slab) for PGA (T = 0.01 sec) (top) and 0.2 sec (bottom) attenuation curves for V_{S30} = 400 m/sec.

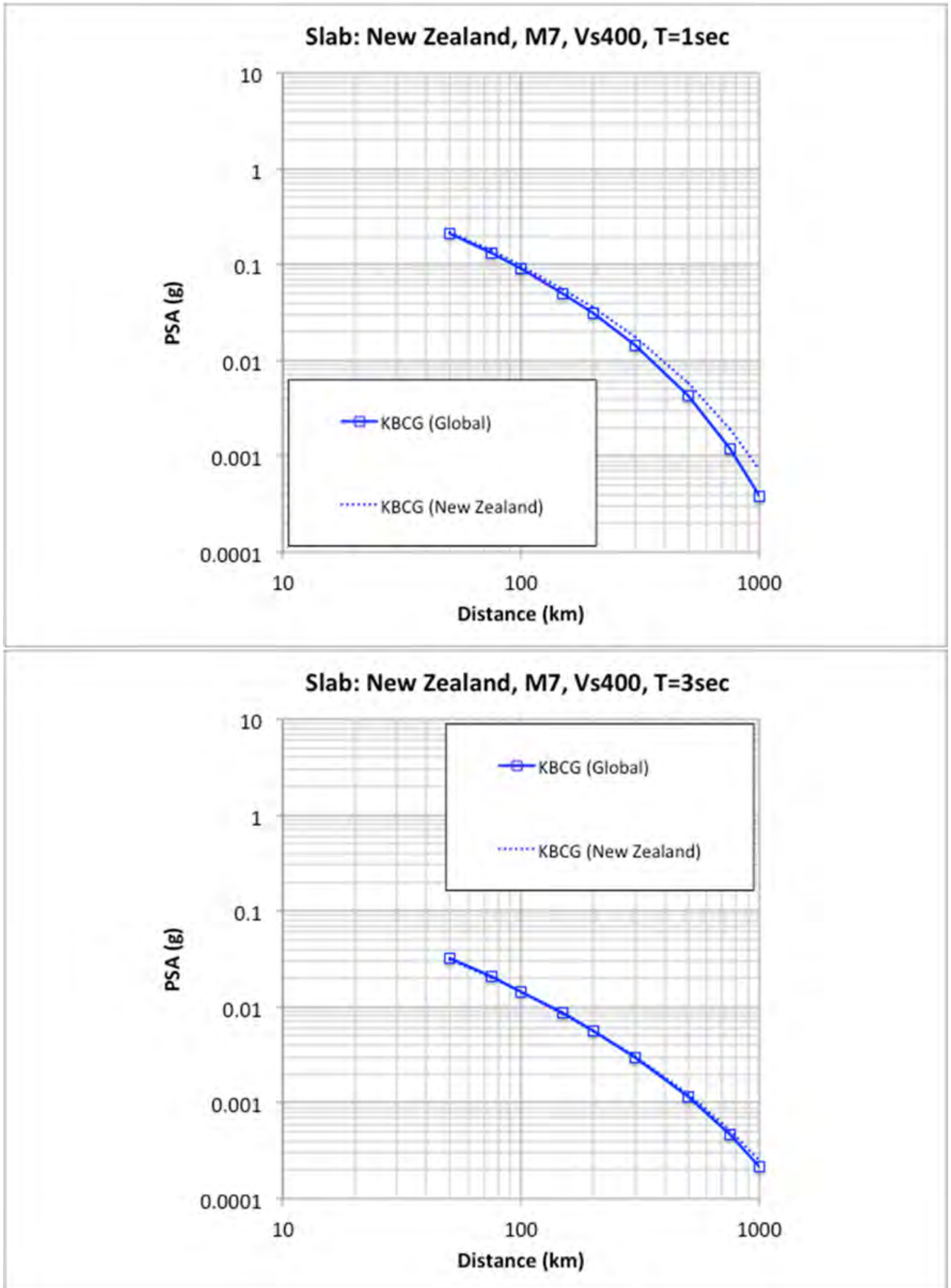

Figure 3.90 **Comparison of New Zealand regional M7 (slab) for 1.0 (top) and 3.0 sec (bottom) attenuation curves for V_{S30} = 400 m/sec.**

3.2.2 Slab Spectra

Slab event response spectra are computed for magnitudes 6, 7, and 8 at two distances of 75 and 200 km; see Table 3.2. Ground motions are computed for the full spectral period range of 0.01 to 10 sec for the two selected V_{S30} values of 760 and 400 m/sec. For the global case, the computed spectra from the NGA-Sub GMMs are compared with the previously developed GMMs. For each of the individual regional cases, the comparison is presented between the NGA-Sub GMM global model and the specific regional models. Representative spectra plots for the **M**7 case for both distances of 75 and 200 km are plotted in Figure 3.91 to Figure 3.106. The full suite of spectra plots (i.e., both digital data and plots) are contained in the associated electronic files; see Appendix A.

Overall, the comparison between the KBCG and PSHAB global models indicate similar ground motions from the two models. For comparison with the other previous GMMs, the BCHU and AB08 models tend to estimate lower ground motions than the other models, including the KBCG and PSHAB global models in the intermediate and lower spectral period range. The agreement between all models improves in the longer spectral period range.

As noted in the attenuation plots, the regional comparisons for Cascadia (see Figure 3.95 and Figure 3.96) indicate a reduction in the KBCG model. This reduction for the KBCG is observed for spectral periods of less than about 1.0 sec. For longer spectral periods, the Cascadia regional model is consistent with the KBCG global model. For the PSHAB model, the spectra are slightly higher at the shorter 75 km distance case and similar for the 200 km distance case between the global model and Cascadia model for the **M**7 events plotted in the comparisons. For the smaller **M**6 provided in the electronic files, the Cascadia spectra is larger than the global model at both distances, with the opposite effect for the **M**8 case (i.e., approximately equal or smaller Cascadia ground motions than the global estimates).

For the Japan region comparisons (see Figure 3.99 and Figure 3.100), the SMK model is only slightly lower or approximately equal to the other GMMs; however, as observed in the comparison of the attenuation curves, the SMK model would be expected to estimate lower ground motions for distances greater than the 200 km shown in the spectra comparisons. Additional regional differences are noted in the various comparisons between the global and regional versions of the KBCG and PSHAB models.

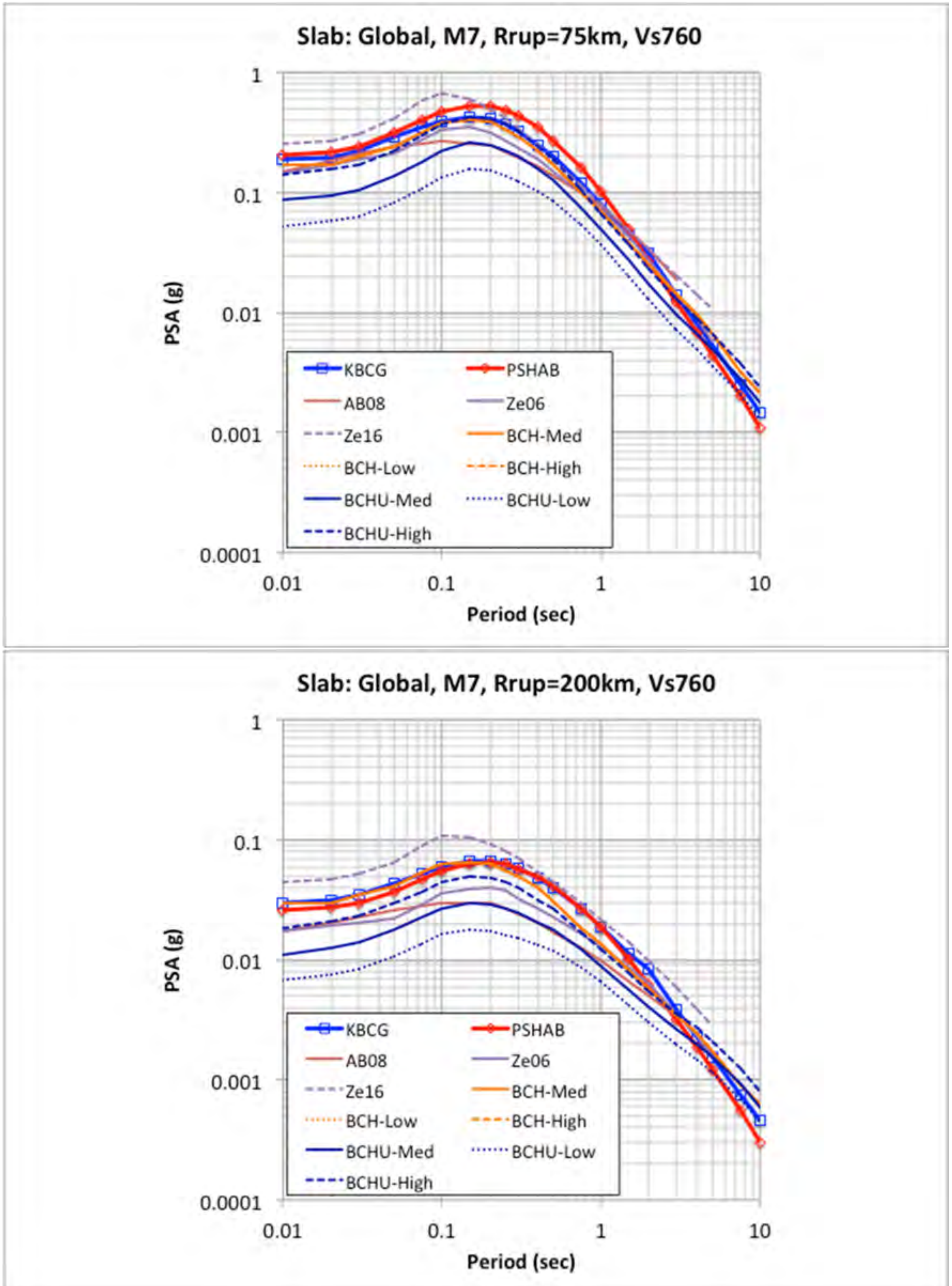

Figure 3.91 **Comparison of global M7 (slab) for distances of 75 km (top) and 200 km (bottom) spectra for V_{S30} = 760 m/sec.**

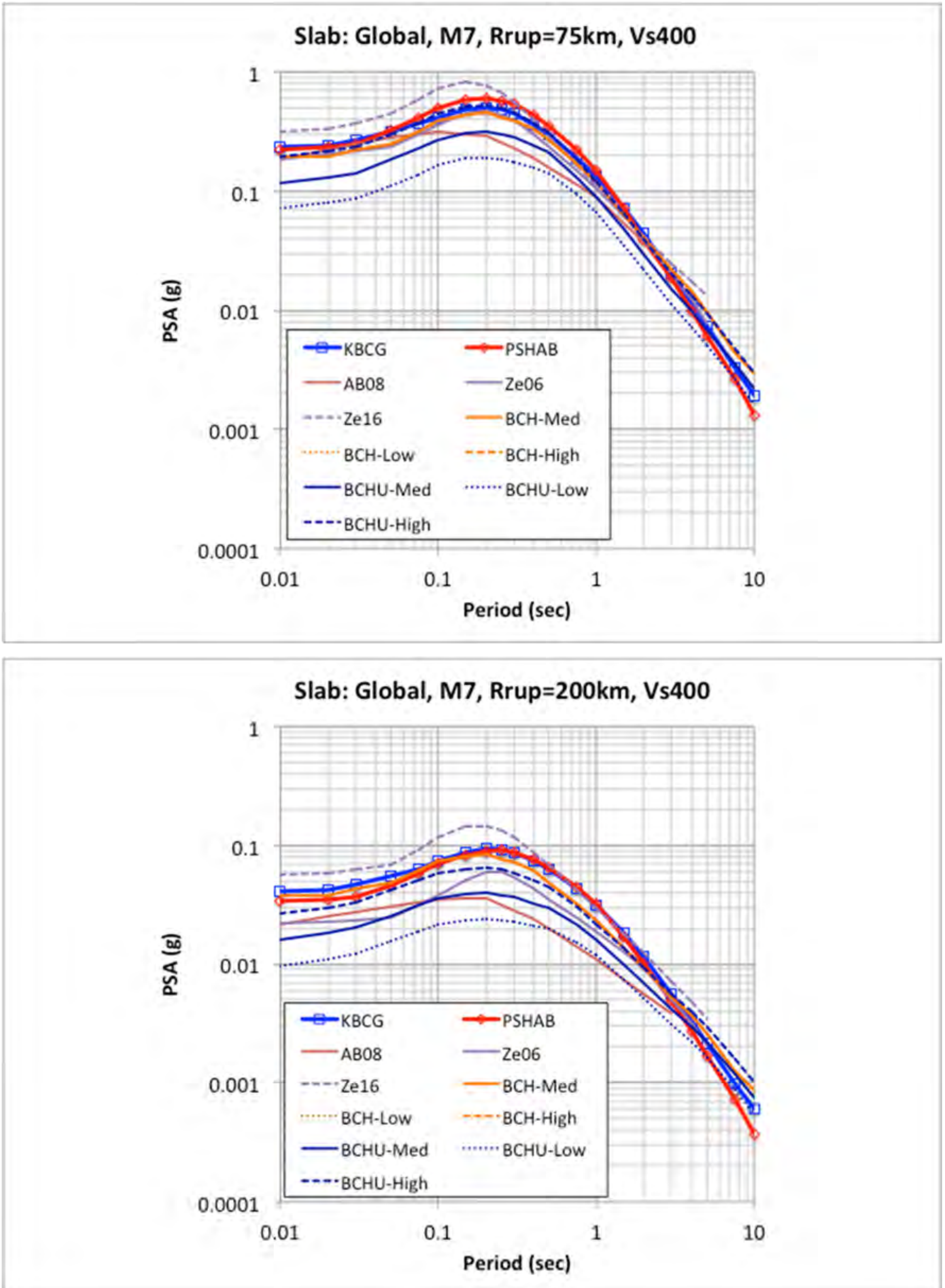

Figure 3.92 **Comparison of global M7 (slab) for distances of 75 km (top) and 200 km (bottom) spectra for V_{S30} = 400 m/sec.**

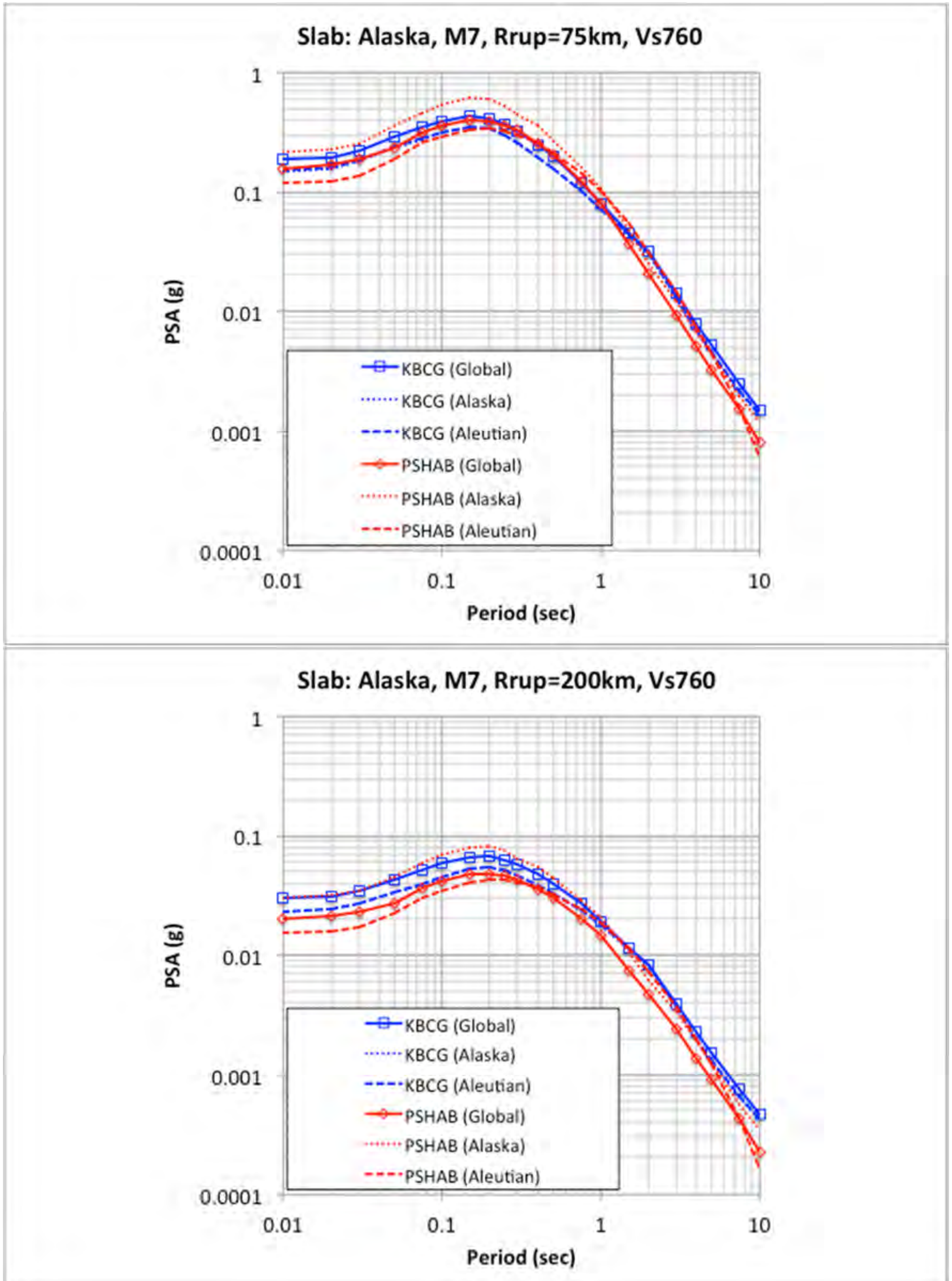

Figure 3.93 Comparison of Alaska regional M7 (slab) for distances of 75 km (top) and 200 km (bottom) spectra for V_{S30} = 760 m/sec.

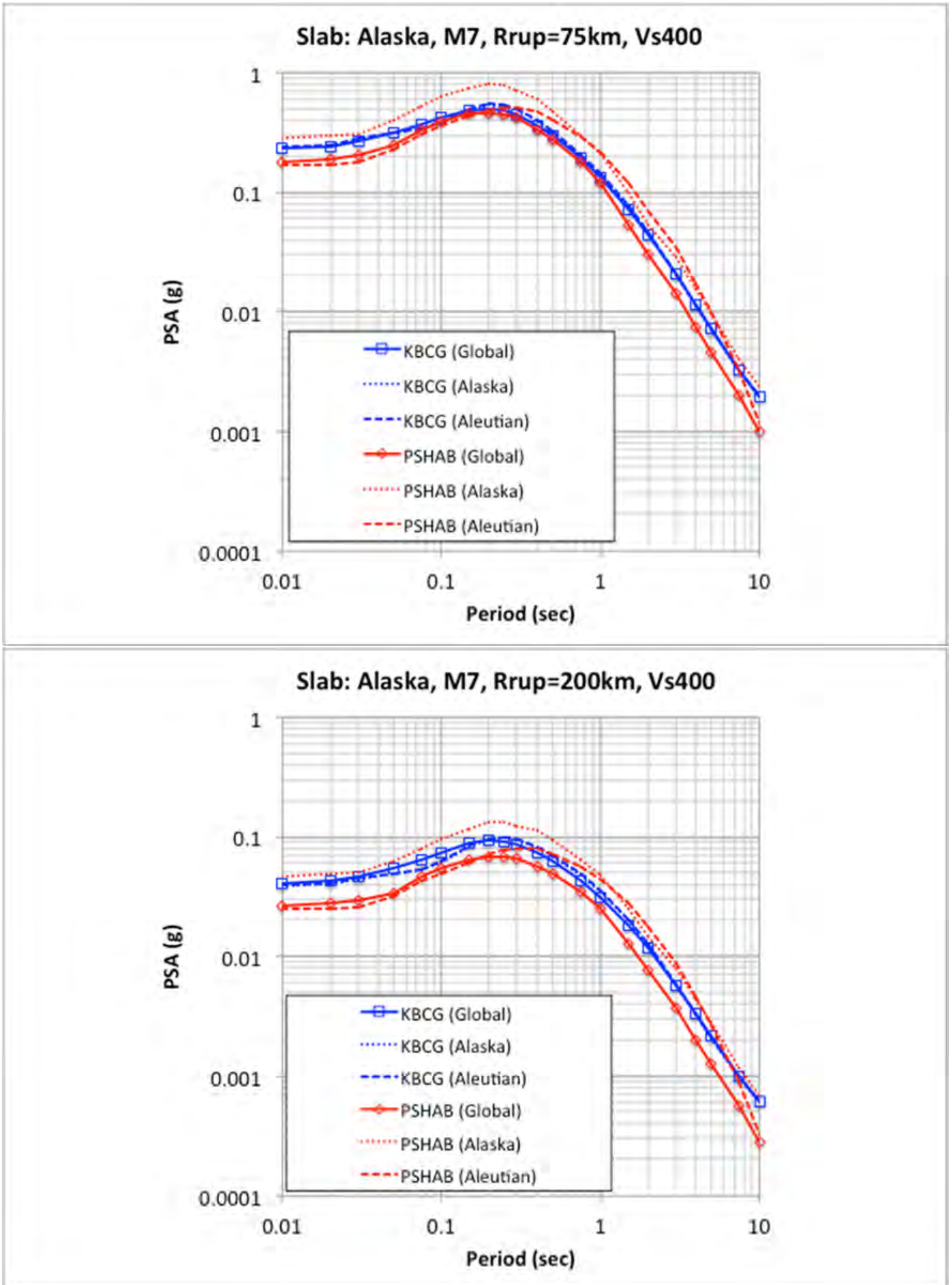

Figure 3.94 **Comparison of Alaska regional M7 (slab) for distances of 75 km (top) and 200 km (bottom) spectra for V_{S30} = 400 m/sec.**

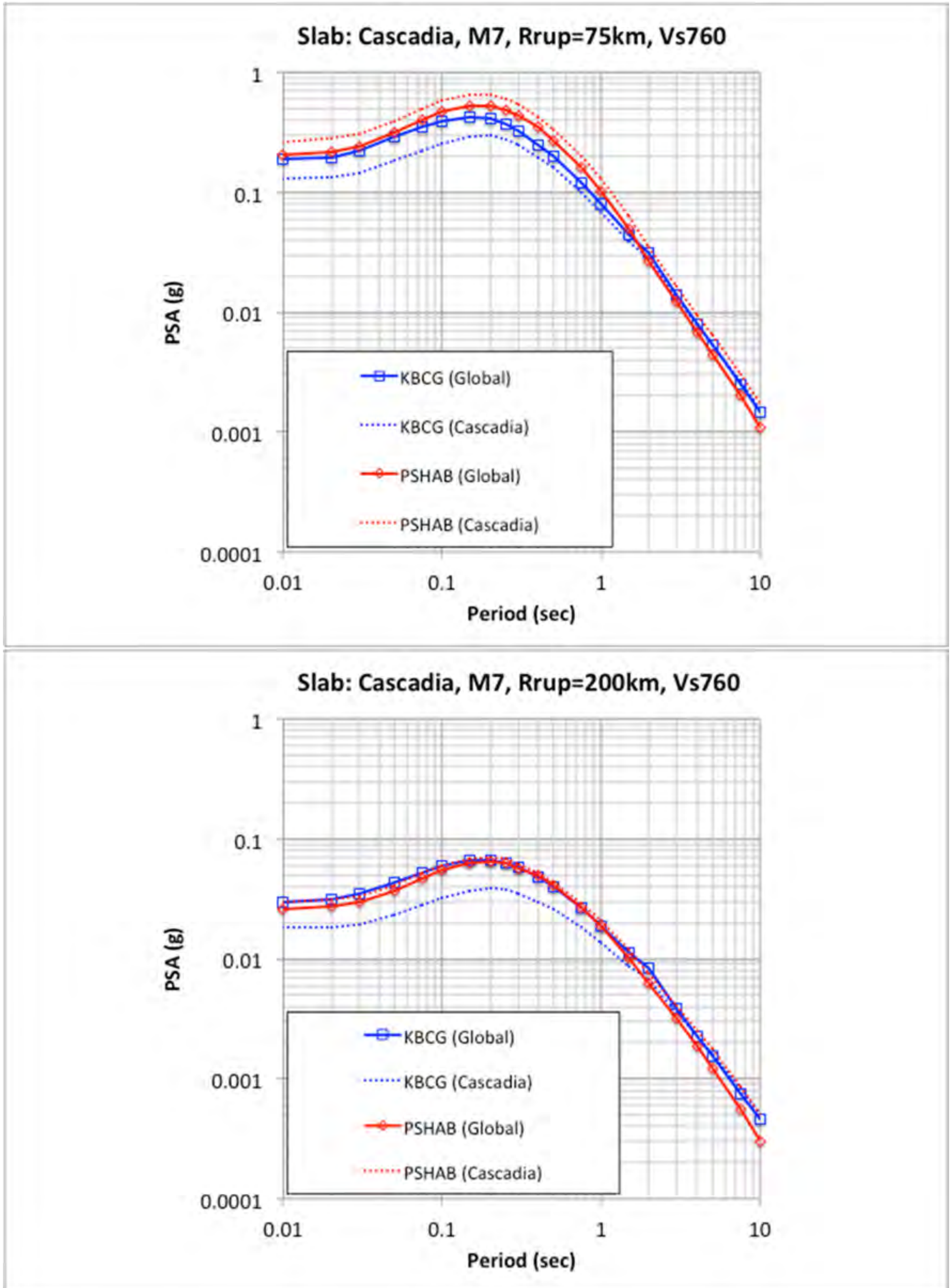

Figure 3.95 **Comparison of Cascadia regional M7 (slab) for distances of 75 km (top) and 200 km (bottom) spectra for V_{S30} = 760 m/sec.**

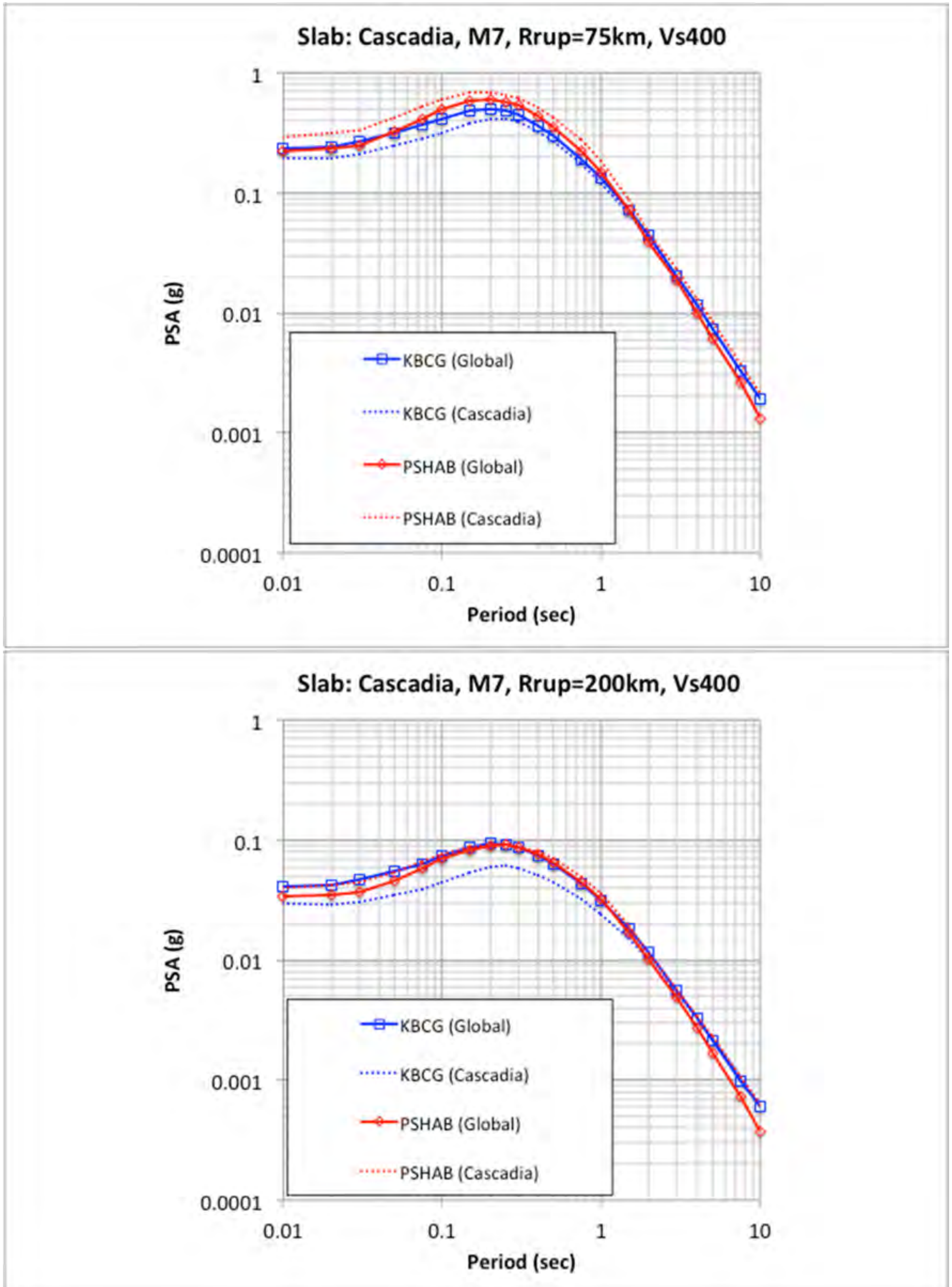

Figure 3.96 **Comparison of Cascadia regional M7 (slab) for distances of 75 km (top) and 200 km (bottom) spectra for V_{S30} = 400 m/sec.**

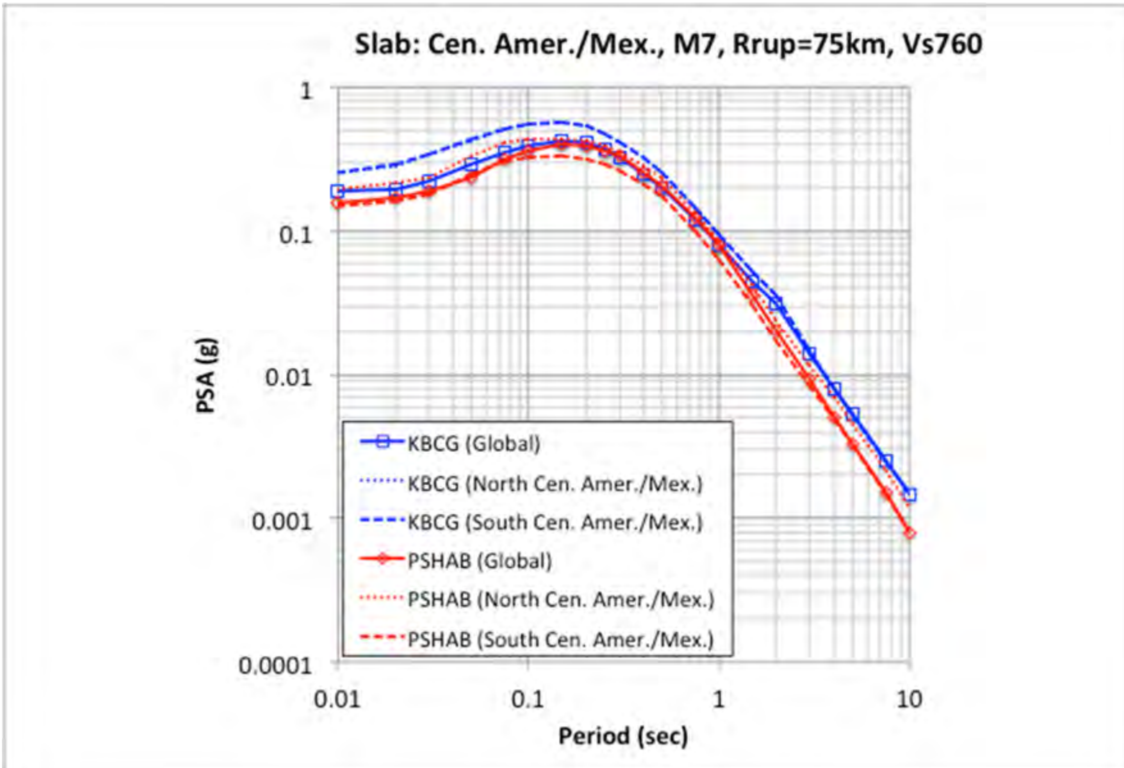

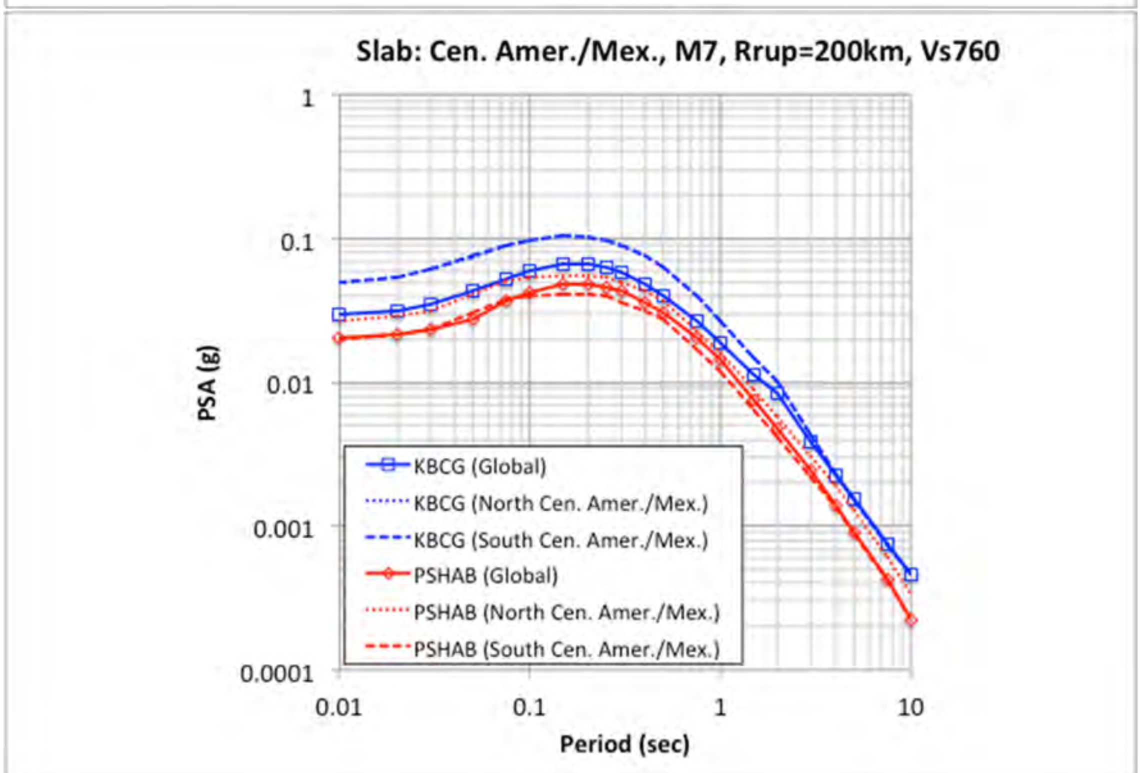

Figure 3.97 **Comparison of Central America and Mexico regional M7 (slab) for distances of 75 km (top) and 200 km (bottom) spectra for V_{S30} = 760 m/sec.**

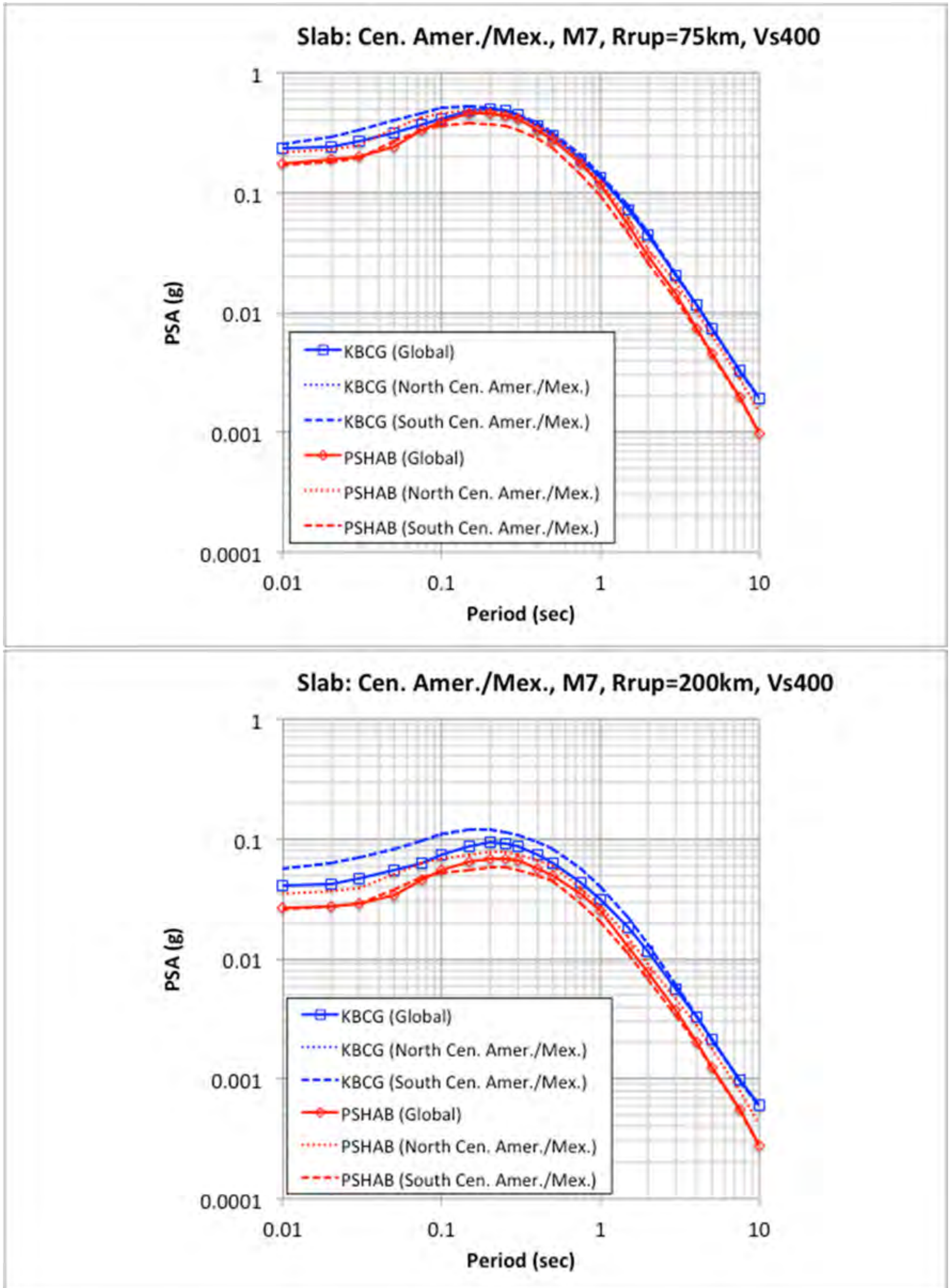

Figure 3.98 **Comparison of Central America and Mexico regional M7 (slab) for distances of 75 km (top) and 200 km (bottom) spectra for V_{S30} = 400 m/sec.**

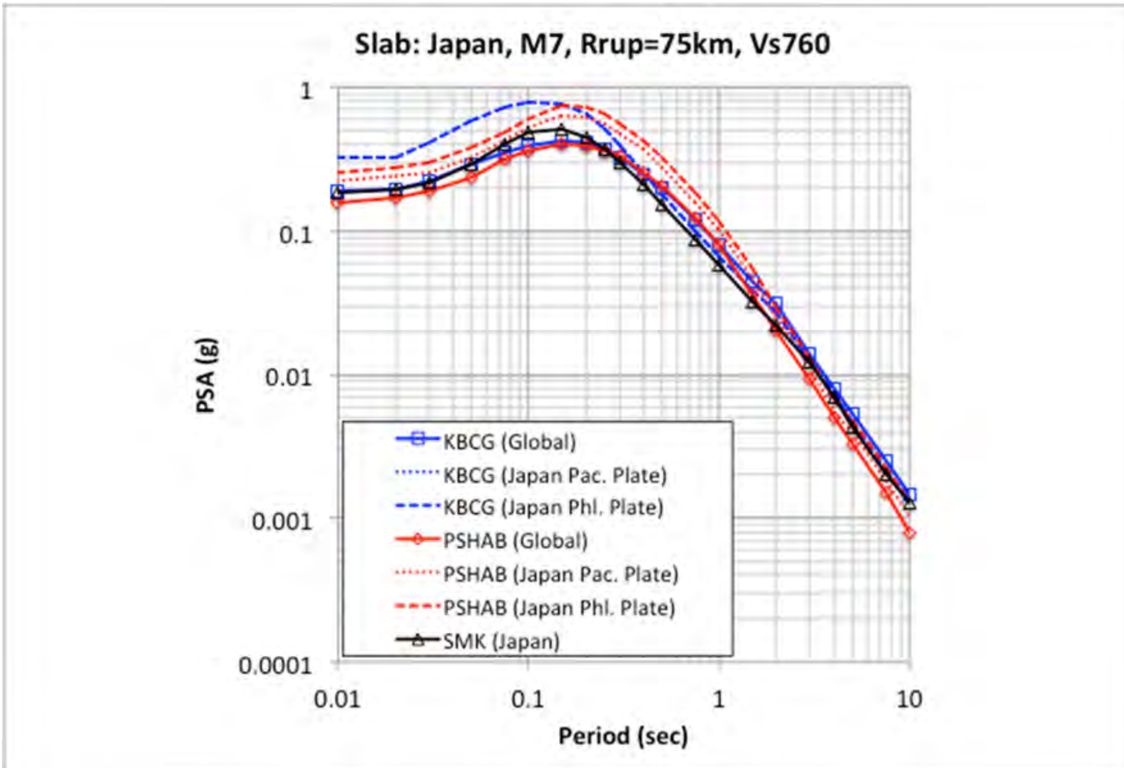

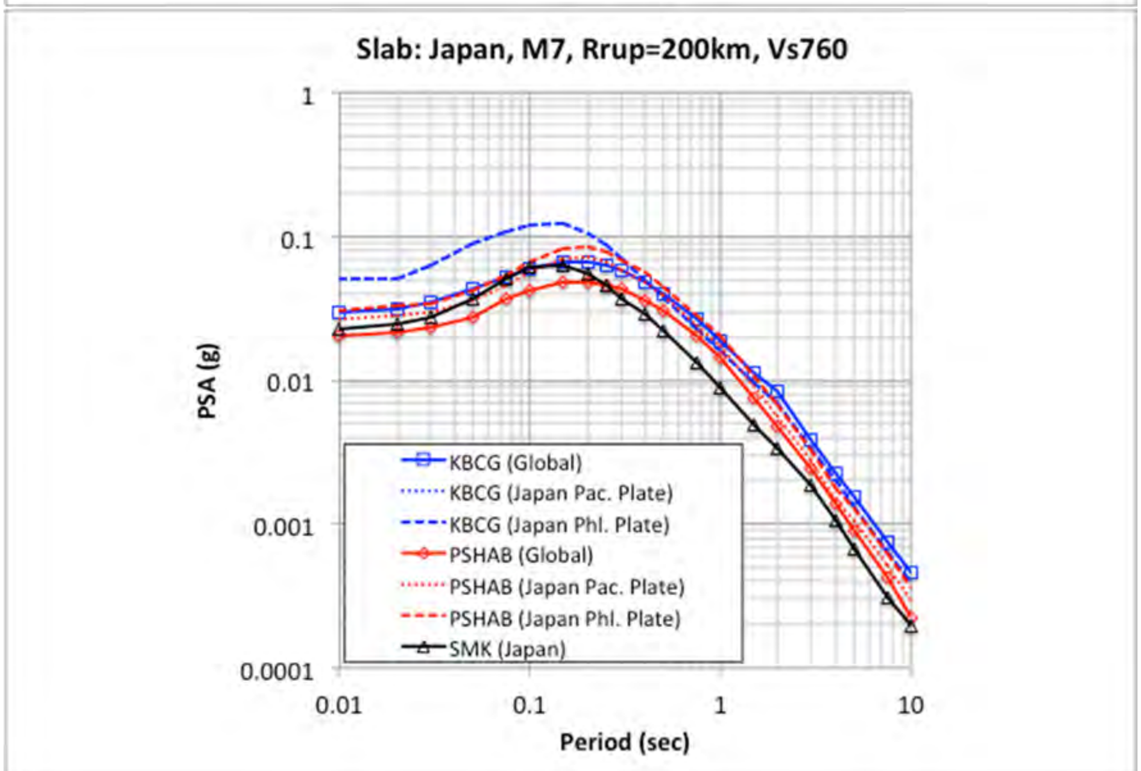

Figure 3.99 **Comparison of Japan regional M7 (slab) for distances of 75 km (top) and 200 km (bottom) spectra for V_{S30} = 760 m/sec.**

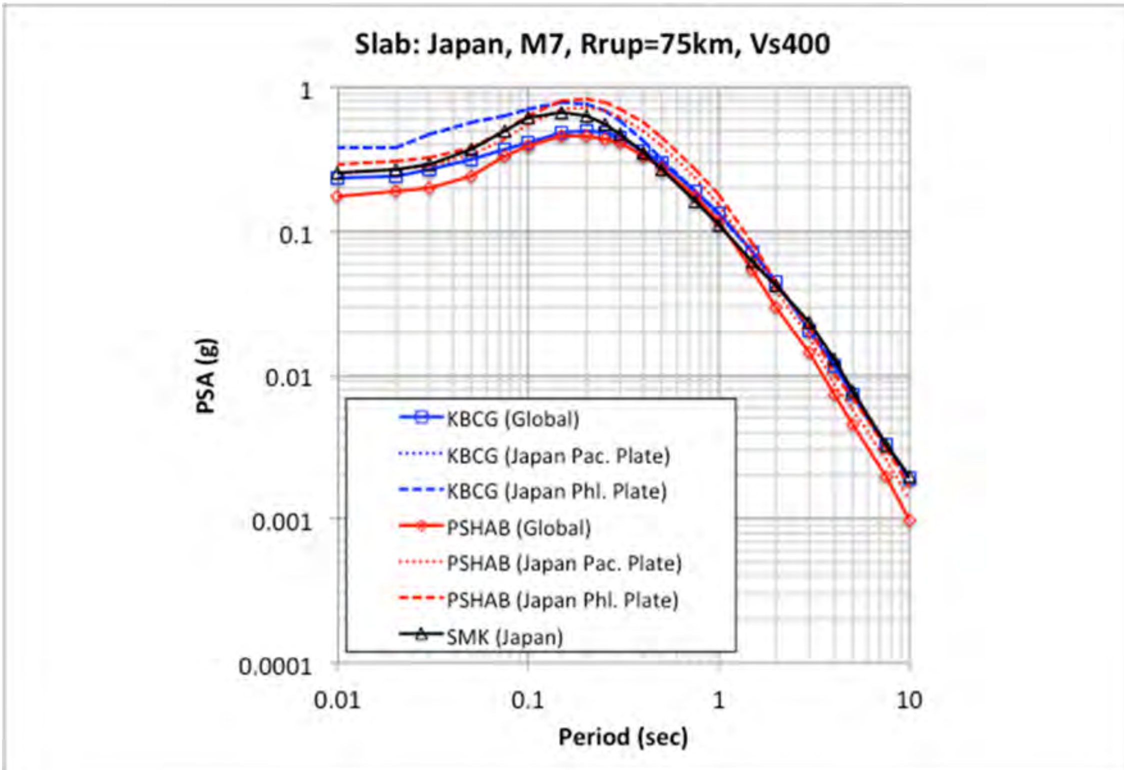

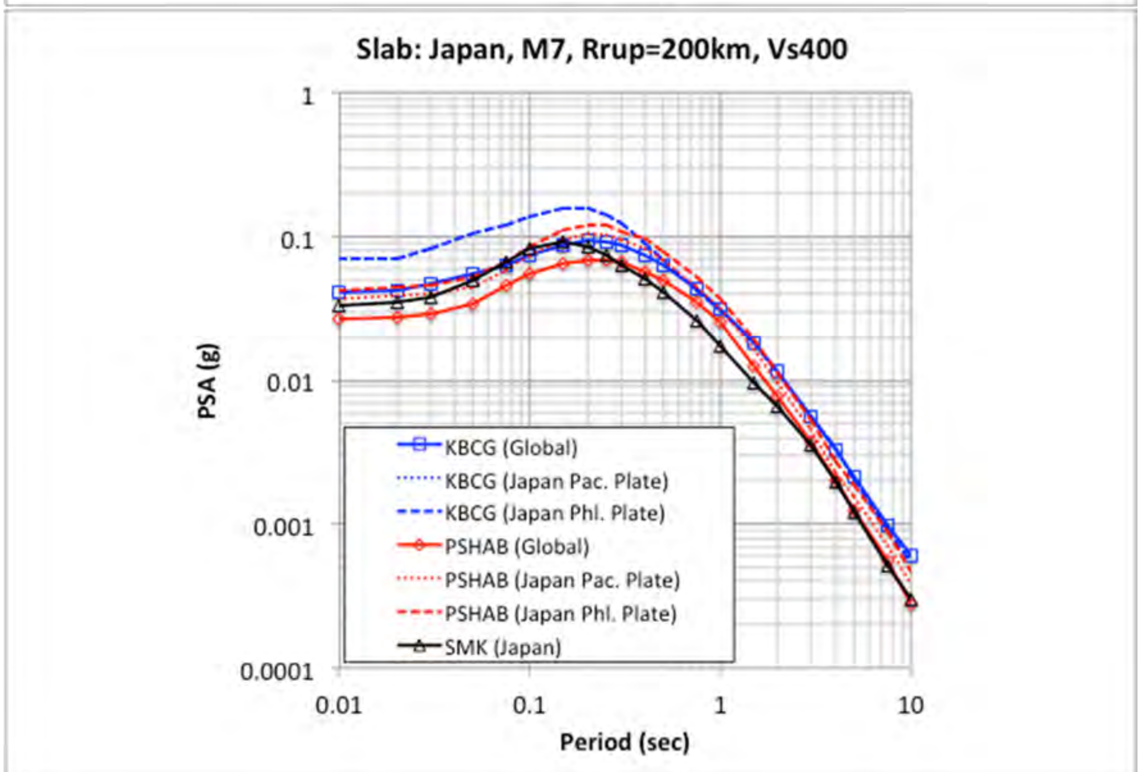

Figure 3.100 Comparison of Japan regional M7 (slab) for distances of 75 km (top) and 200 km (bottom) spectra for V_{S30} = 400 m/sec.

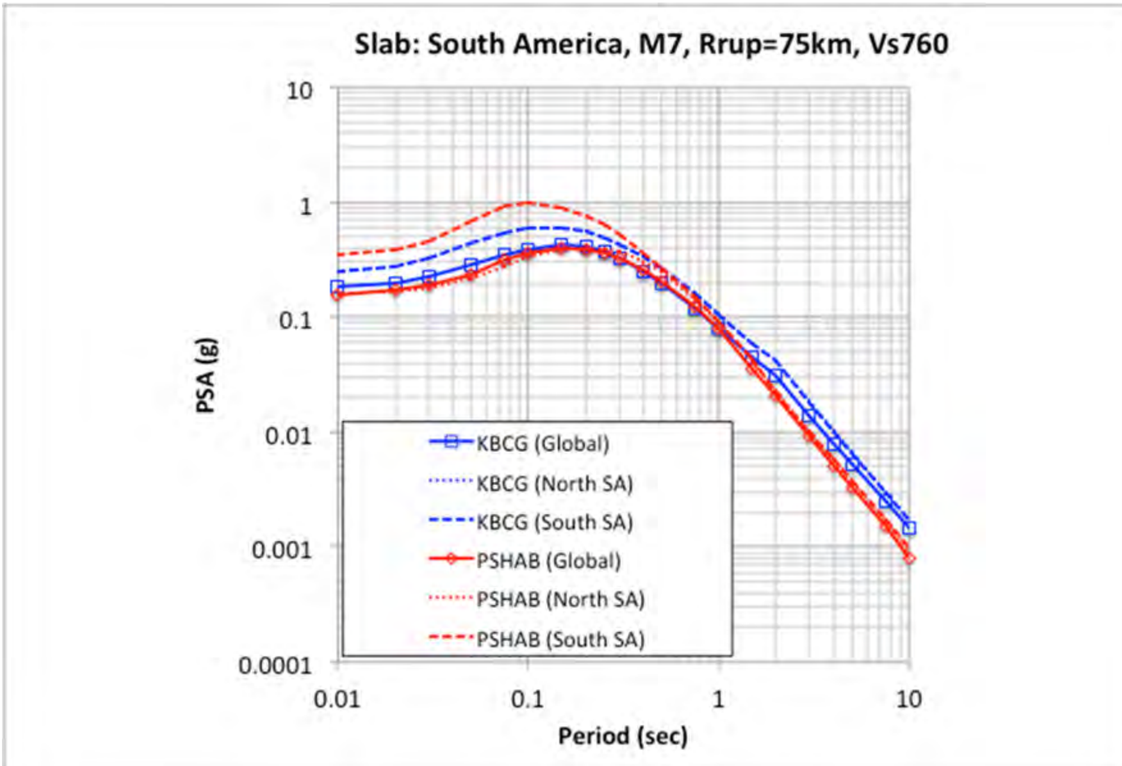

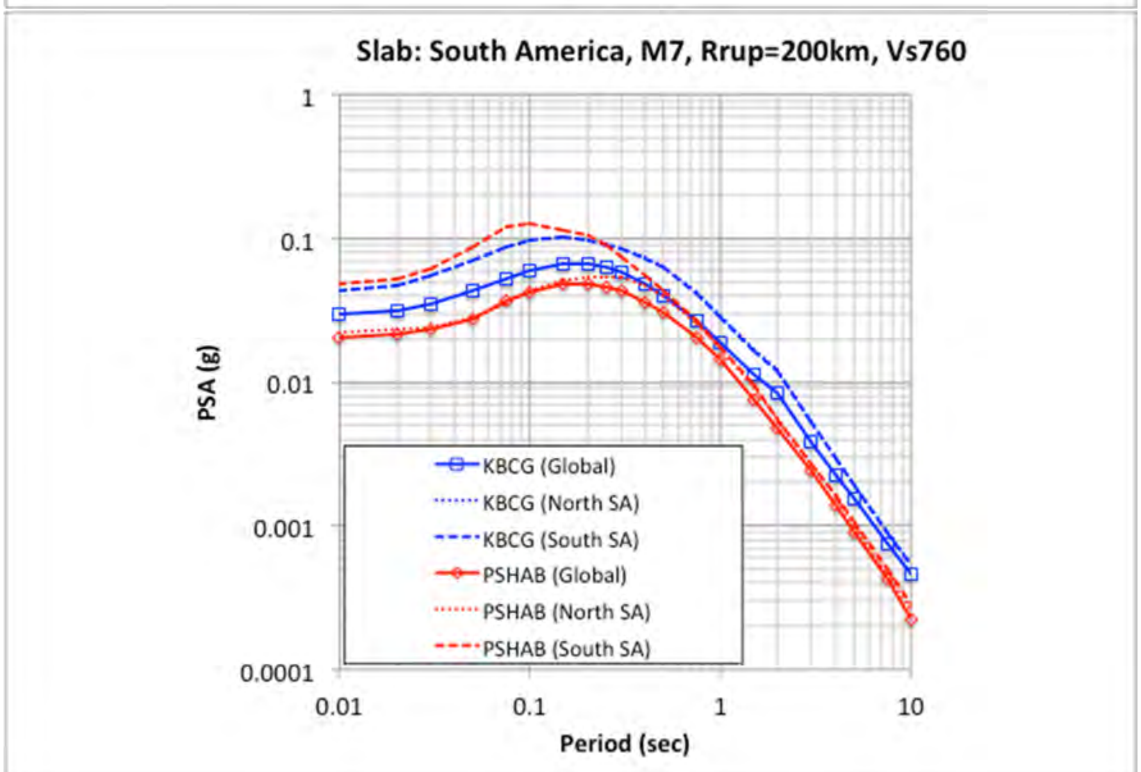

Figure 3.101 **Comparison of South America regional M7 (slab) for distances of 75 km (top) and 200 km (bottom) spectra for V_{S30} = 760 m/sec.**

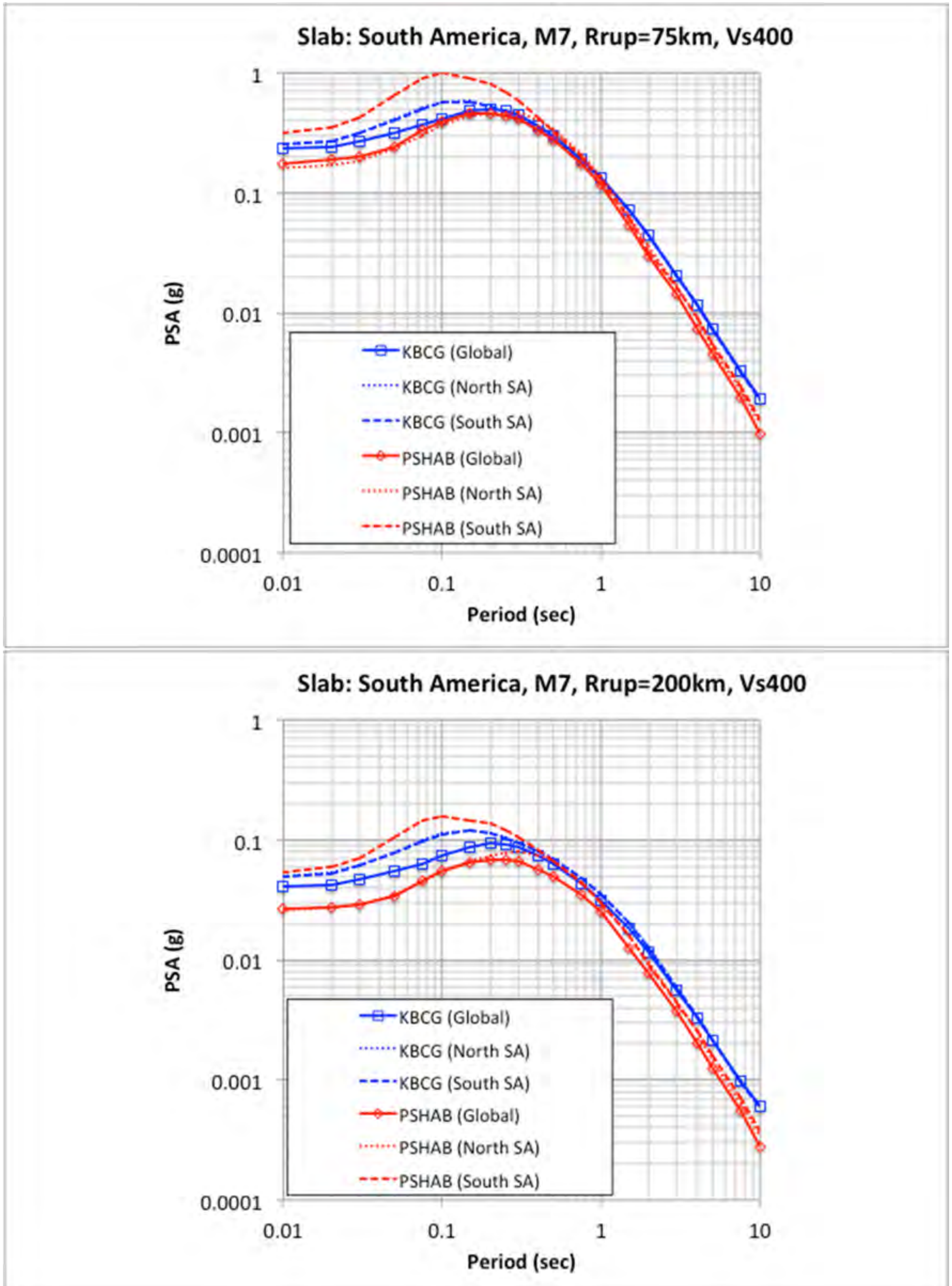

Figure 3.102 Comparison of South America regional M7 (slab) for distances of 75 km (top) and 200 km (bottom) spectra for V_{S30} = 400 m/sec.

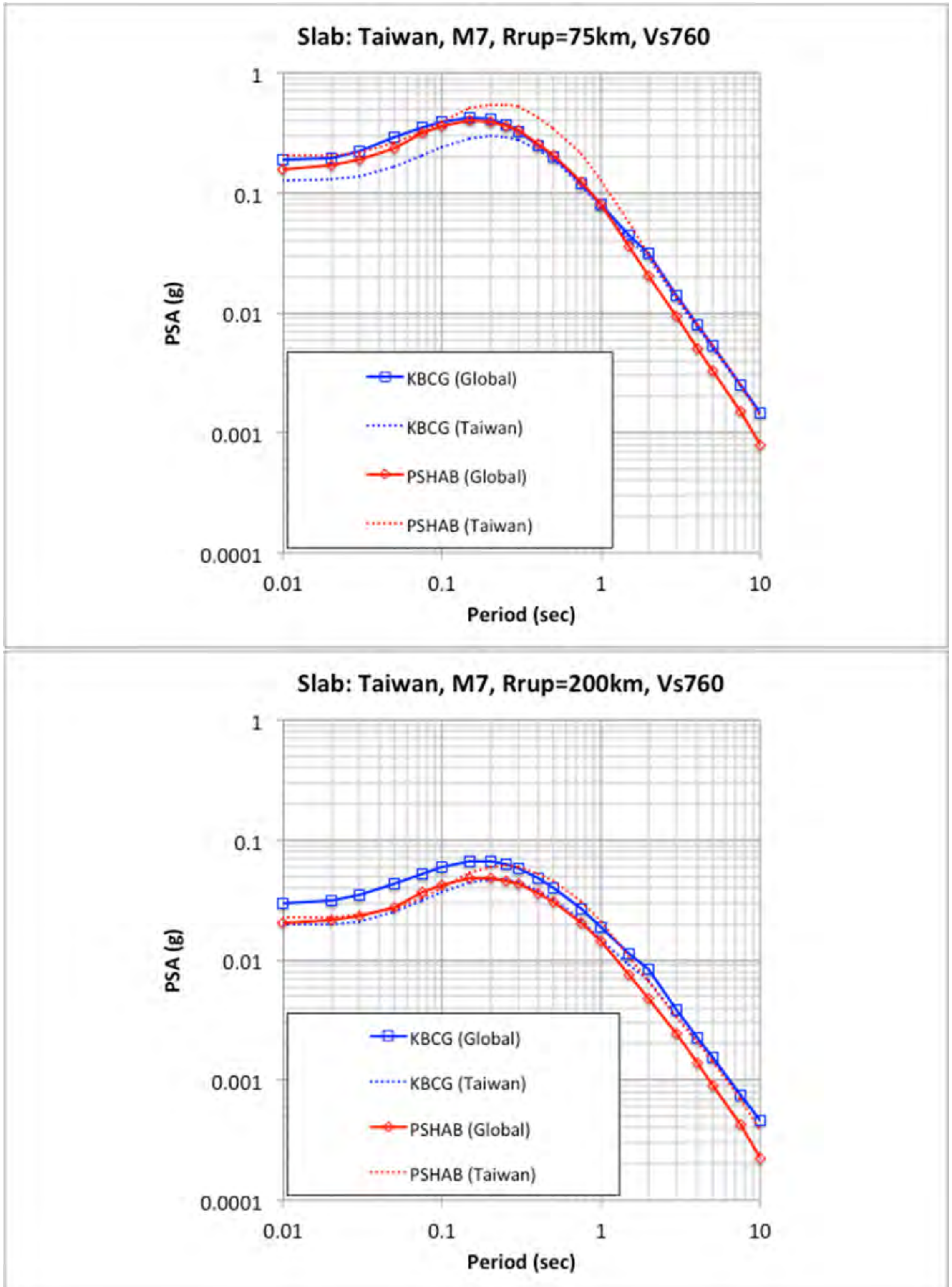

Figure 3.103 Comparison of Taiwan regional M7 (slab) for distances of 75 km (top) and 200 km (bottom) spectra for V_{S30} = 760 m/sec.

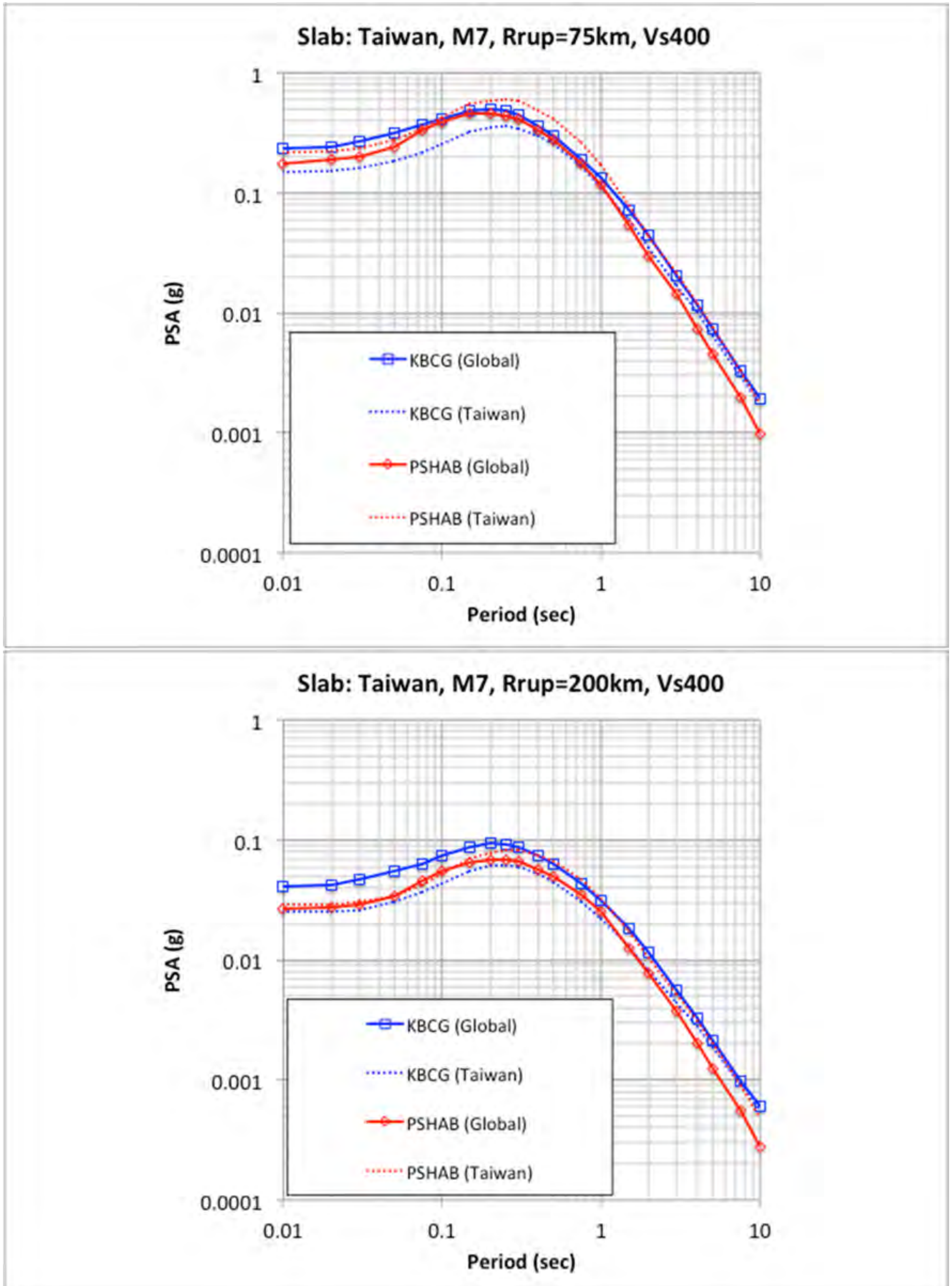

Figure 3.104 **Comparison of Taiwan regional M7 (slab) for distances of 75 km (top) and 200 km (bottom) spectra for V_{S30} = 400 m/sec.**

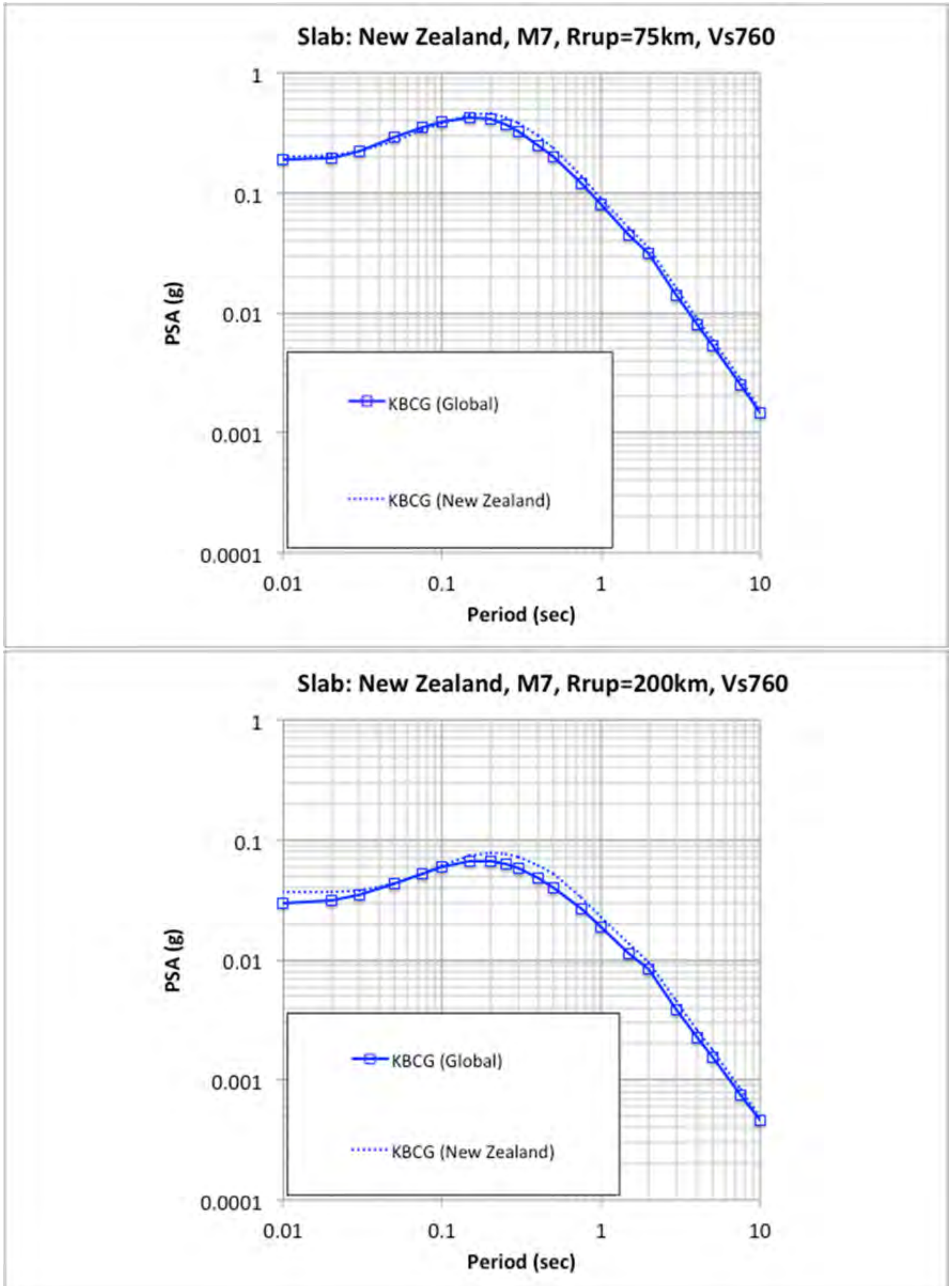

Figure 3.105 Comparison of New Zealand regional M7 (slab) for distances of 75 km (top) and 200 km (bottom) spectra for V_{S30} = 760 m/sec.

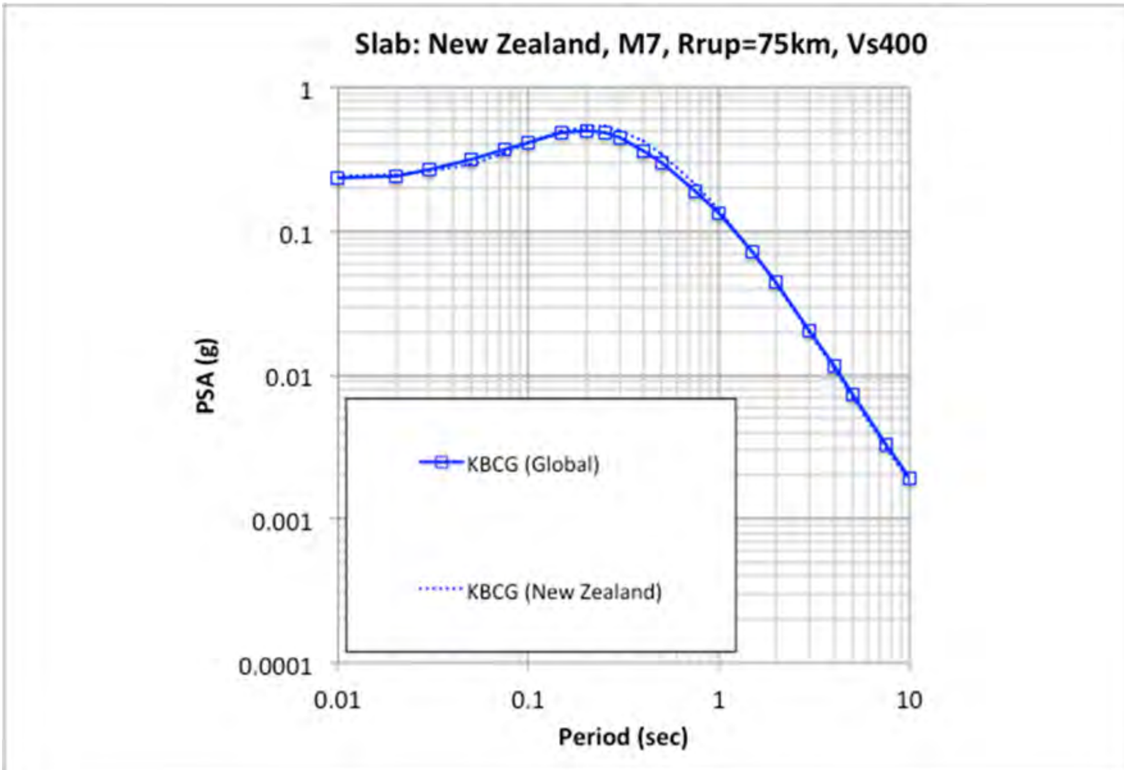

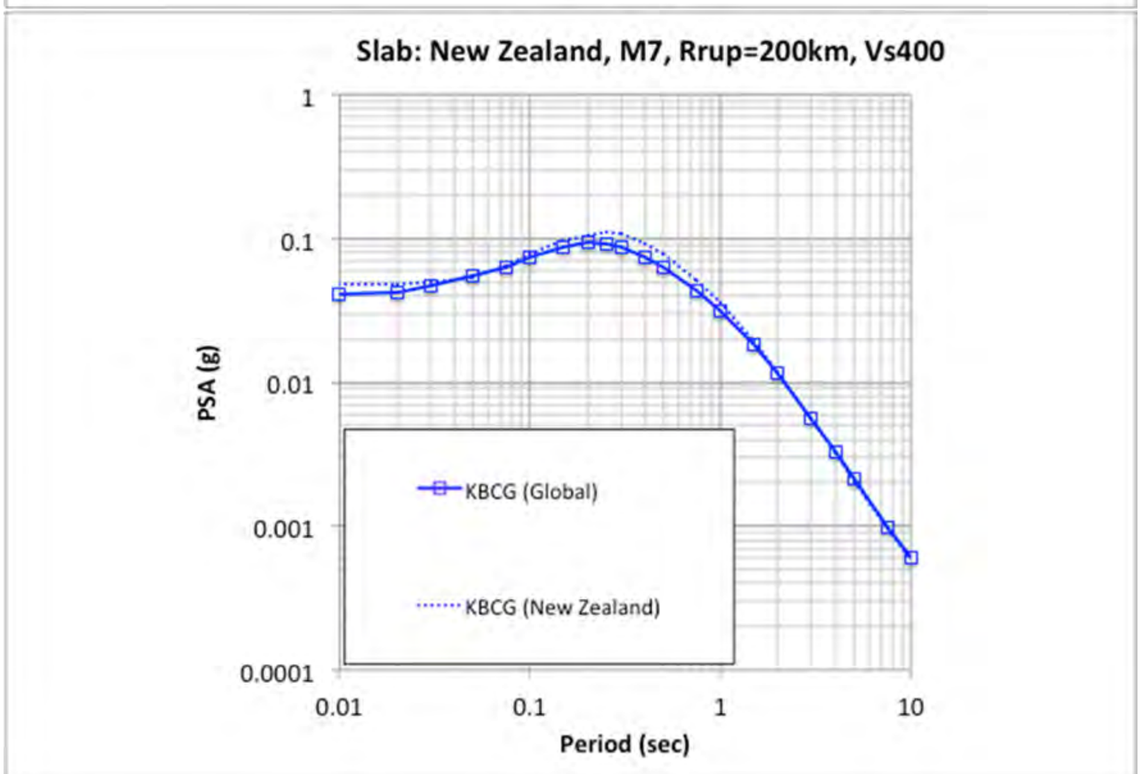

Figure 3.106 **Comparison of New Zealand regional M7 (slab) for distances of 75 km (top) and 200 km (bottom) spectra for V_{S30} = 400 m/sec.**

3.2.3 Slab Magnitude Scaling

Similar to the interface versions of the GMMs, all three of the NGA-Sub GMMs have a magnitude breakpoint where there is a change in the slab magnitude scaling; see Table 2.2. Although the magnitude-scaling breakpoint is based on a single magnitude value, the impact on the calculated ground motions is spectral period dependent. Both the KBCG and PSHAB models assign a global slab magnitude-scaling breakpoint of 7.6 although the functional formulation within each model is different.

Comparisons of the median ground motions from a slab earthquake at a distance of 75 km for a V_{S30} value of 760 m/sec are plotted in Figure 3.107 through Figure 3.111 for PGA (T = 0.01 sec) and spectral periods of 0.2, 1.0, 3.0, and 5.0 sec. The results from the KBCG and PSHAB models are for the global version of their models. The SMK results are also included in these comparison figures, along with the results from the suite of previously developed GMMs.

With a few noted exceptions, there is relative agreement between the results from the three NGA-Sub GMMs and the other published models. The models have a wider distribution for the smaller and largest magnitude values, which would be expected based on the limited distribution of data contained and used in the individual model development for these magnitude ranges. The BCHU model shows a lower magnitude-scaling dependency than the other models across all spectral periods, which leads to lower estimated ground motions for the larger magnitude cases. The AB08 model is modeled with complete saturation for slab events for earthquake with **M**8 and larger, which is similar to the complete saturation for the interface events for this GMM. The SMK model, however, does not completely saturate for the largest magnitude slab events unlike for the interface events. The SMK model does show a change in the magnitude scaling that is consistent with the other GMMs.

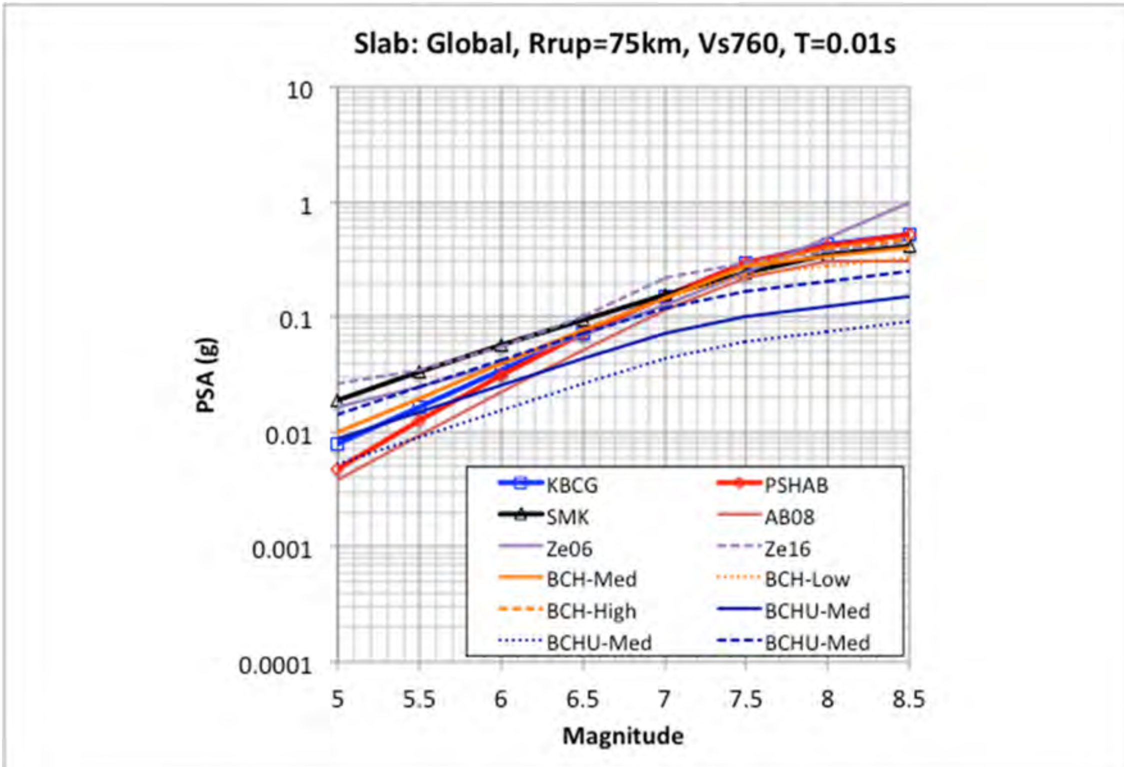

Figure 3.107 Comparison of PGA magnitude scaling for slab events at a distance of 75 km for V_{S30} = 760 m/sec.

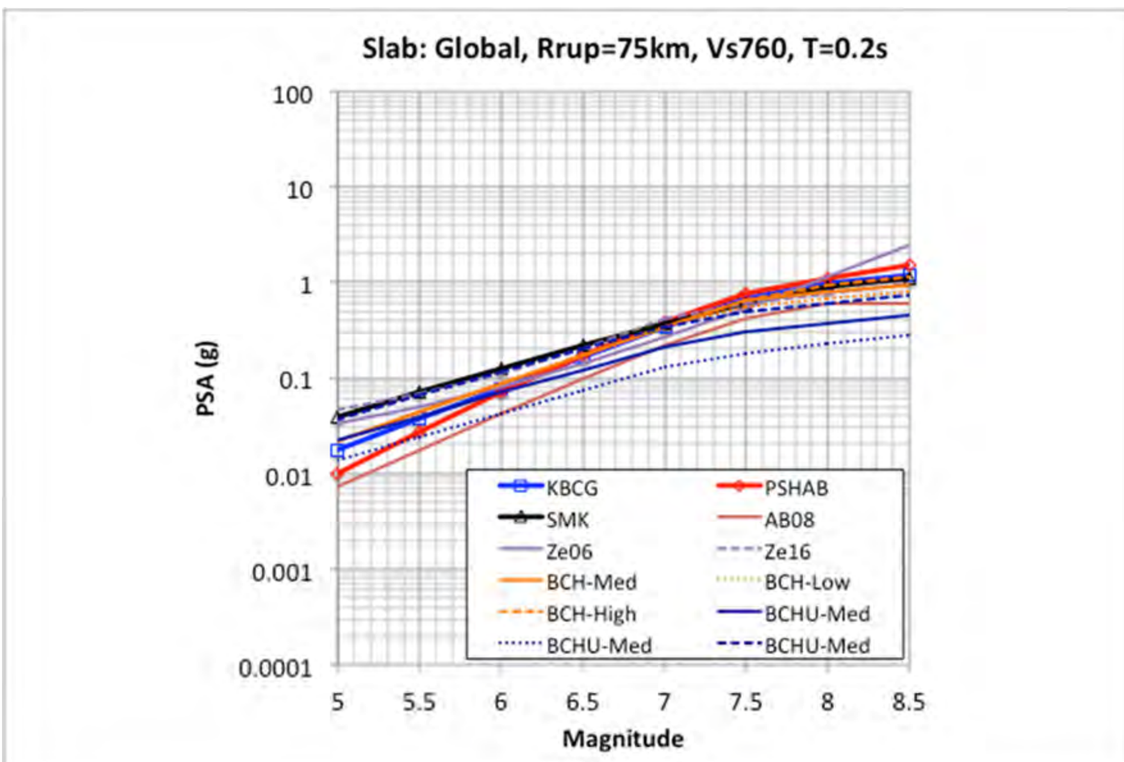

Figure 3.108 Comparison of T = 0.2 sec spectral acceleration magnitude scaling for slab events at a distance of 75 km for V_{S30} = 760 m/sec.

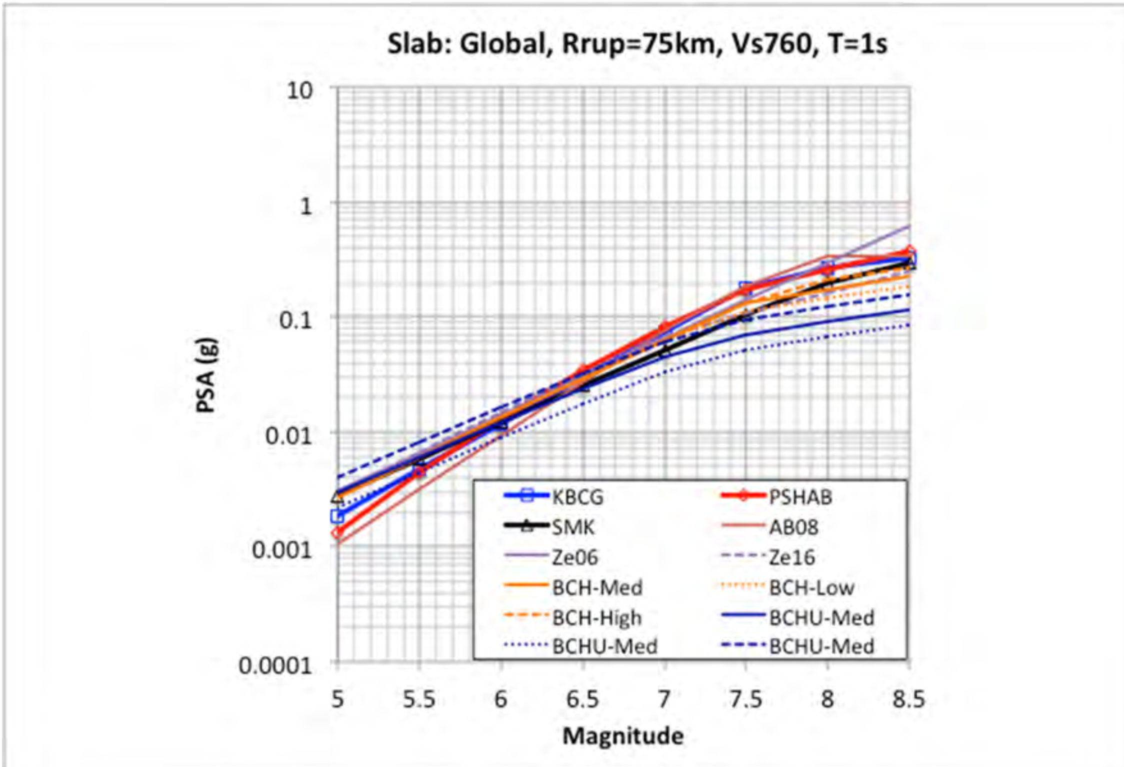

Figure 3.109 Comparison of T = 1.0 sec spectral acceleration magnitude scaling for slab events at a distance of 75 km for V_{S30} = 760 m/sec.

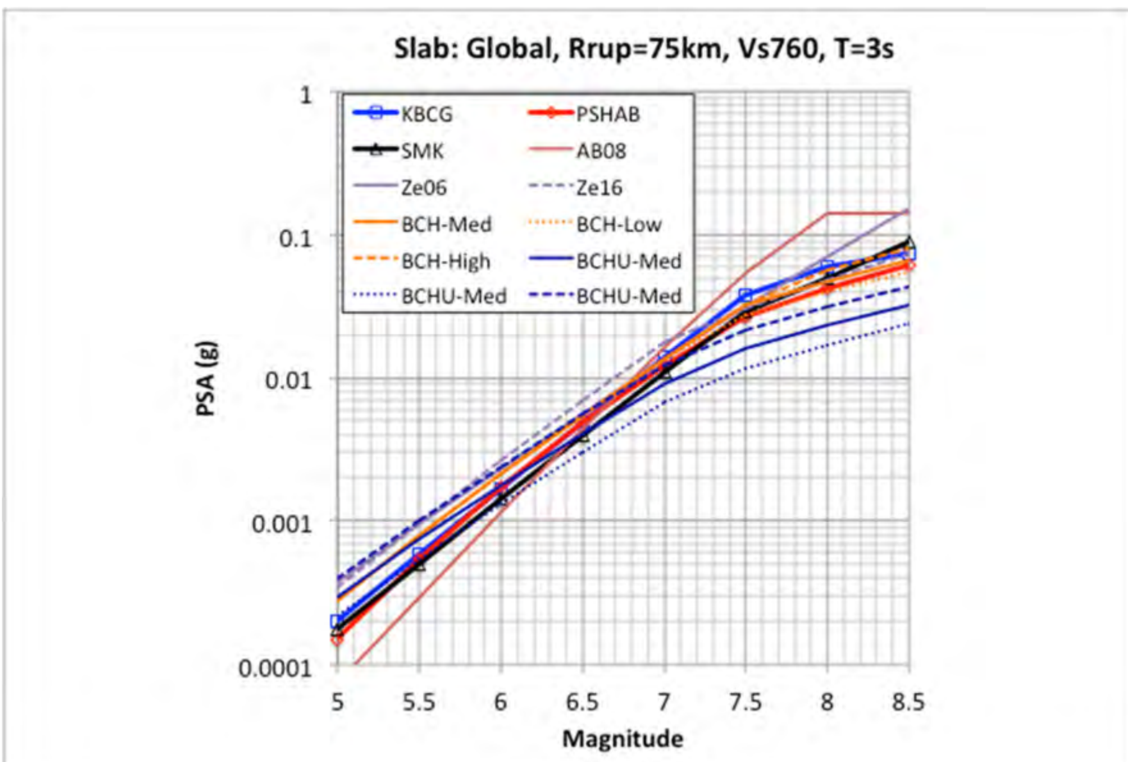

Figure 3.110 Comparison of T = 3.0 sec spectral acceleration magnitude scaling for slab events at a distance of 75 km for V_{S30} = 760 m/sec.

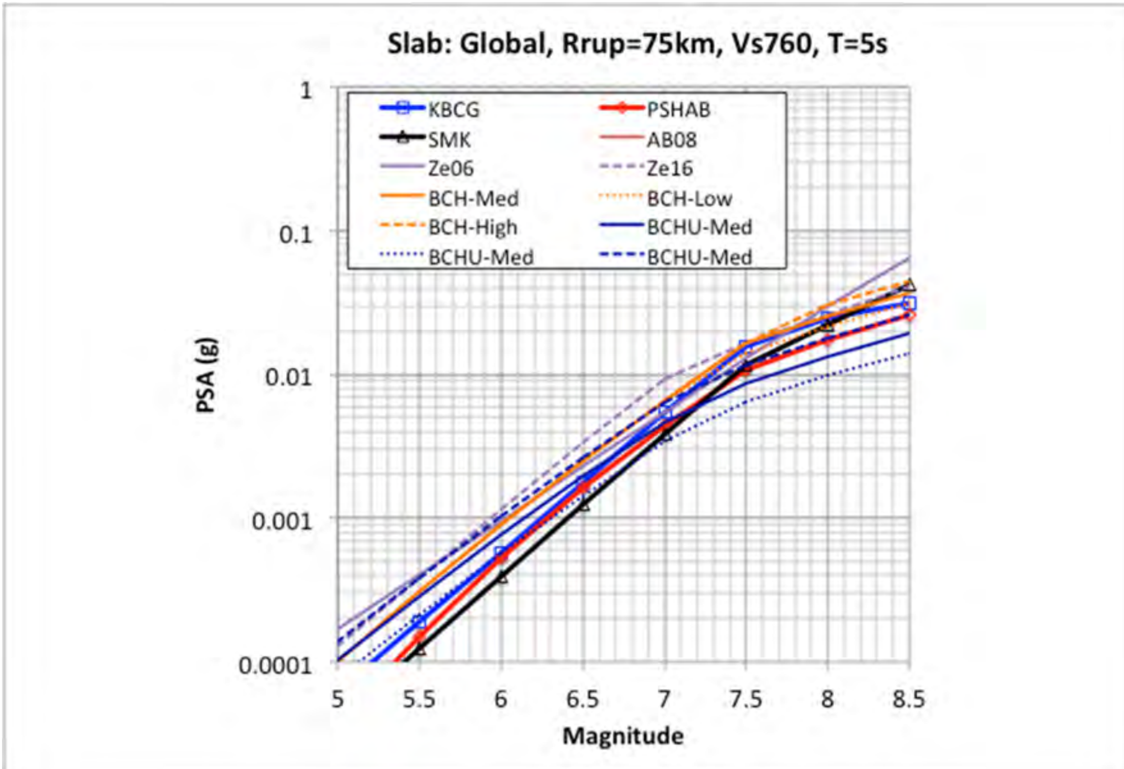

Figure 3.111 **Comparison of *T* = 5.0 sec spectral acceleration magnitude scaling for slab events at a distance of 75 km for V_{S30} = 760 m/sec.**

3.2.4 Slab Depth Dependence

The depth dependence of slab ground motions has been previously observed to be a strong feature of deeper slab earthquakes [Abrahamson et al. 2016]. This is captured in the three NGA-Sub GMMs and as well in the previous GMMs evaluated in these comparisons. The comparison of the estimated ground motions from the global KBCG and PSHAB models, and the SMK model and other GMMs are provided in Figure 3.112 through Figure 3.116. These ground-motion curves are plotted as a function of Z_{tor} for slab earthquakes at a distance of 75 km and with a V_{S30} value of 760 m/sec. For these comparisons, the Z_{tor} for the KBCG model and the hypocentral depth for the PSHAB model were assumed to be equal. For the three NGA-Sub GMMs, this depth dependence is spectral period dependent with a stronger impact at the shorter to intermediate spectral periods compared to the longer spectral periods. For the KBCG and PSHAB models, saturation is observed for the depths greater than about 65 km for spectral periods of 1.0 sec and less. For the longer spectral periods, this depth dependency is observed to be approximately constant over the range of depth values.

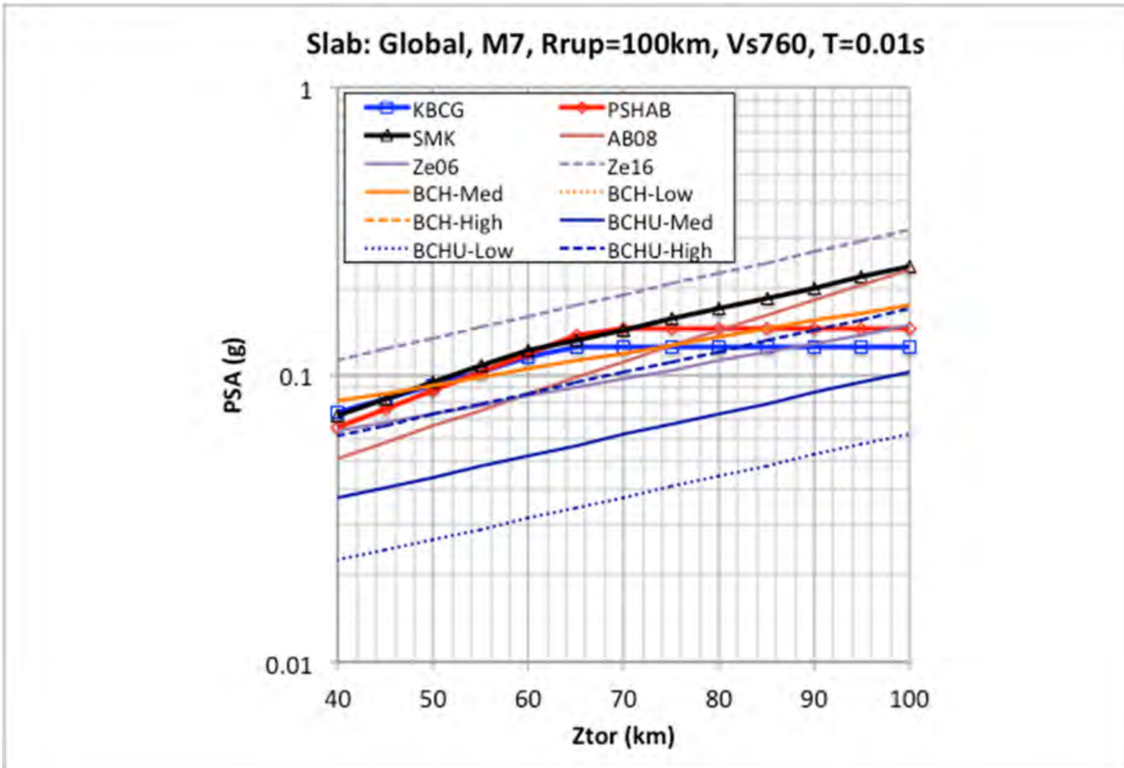

Figure 3.112 Comparison of PGA (*T* = 0.01 sec) Z_{tor} scaling for a M7 slab event at a distance of 75 km for V_{S30} = 760 m/sec.

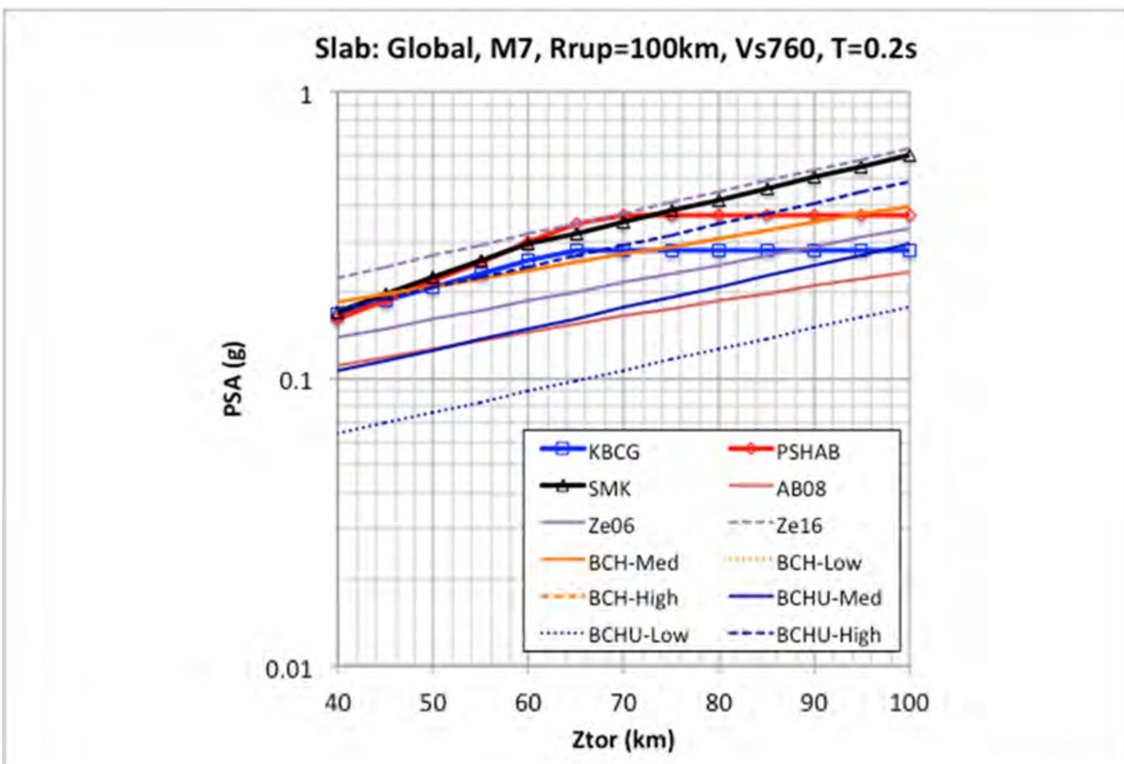

Figure 3.113 Comparison of *T* = 0.2 sec Z_{tor} scaling for a M7 slab event at a distance of 75 km for V_{S30} = 760 m/sec.

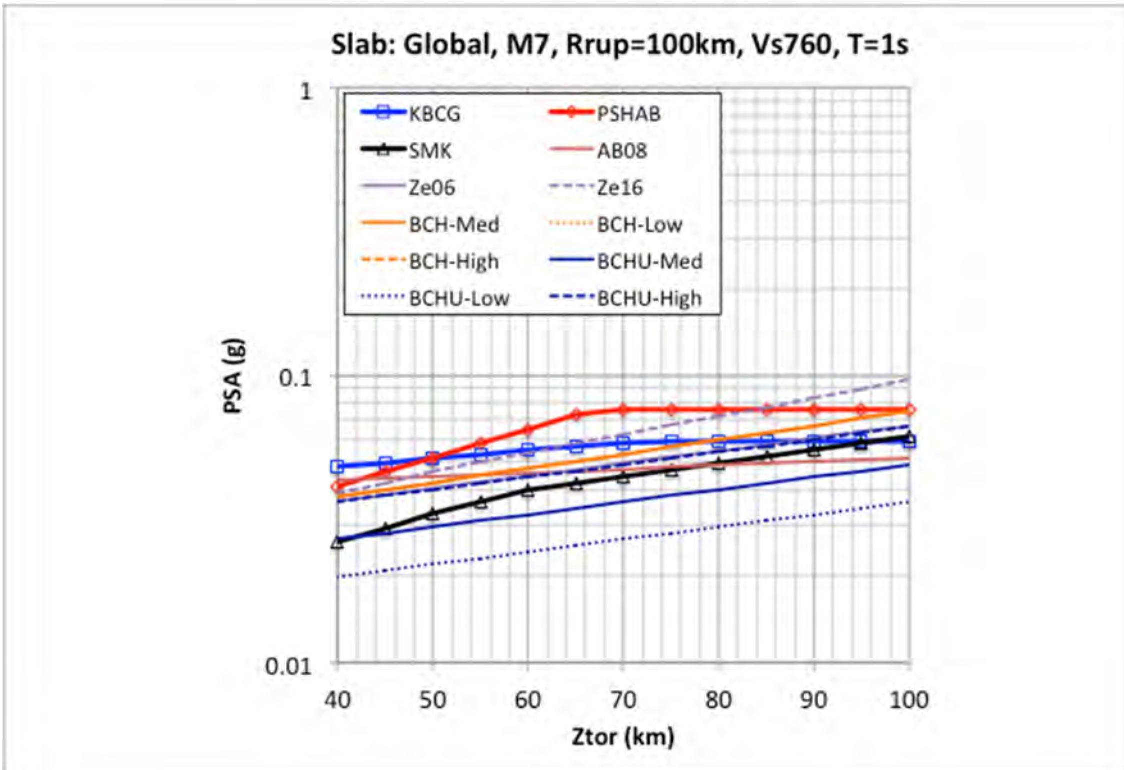

Figure 3.114 Comparison of T = 1.0 sec Z_{tor} scaling for a M7 slab event at a distance of 75 km for V_{S30} = 760 m/sec.

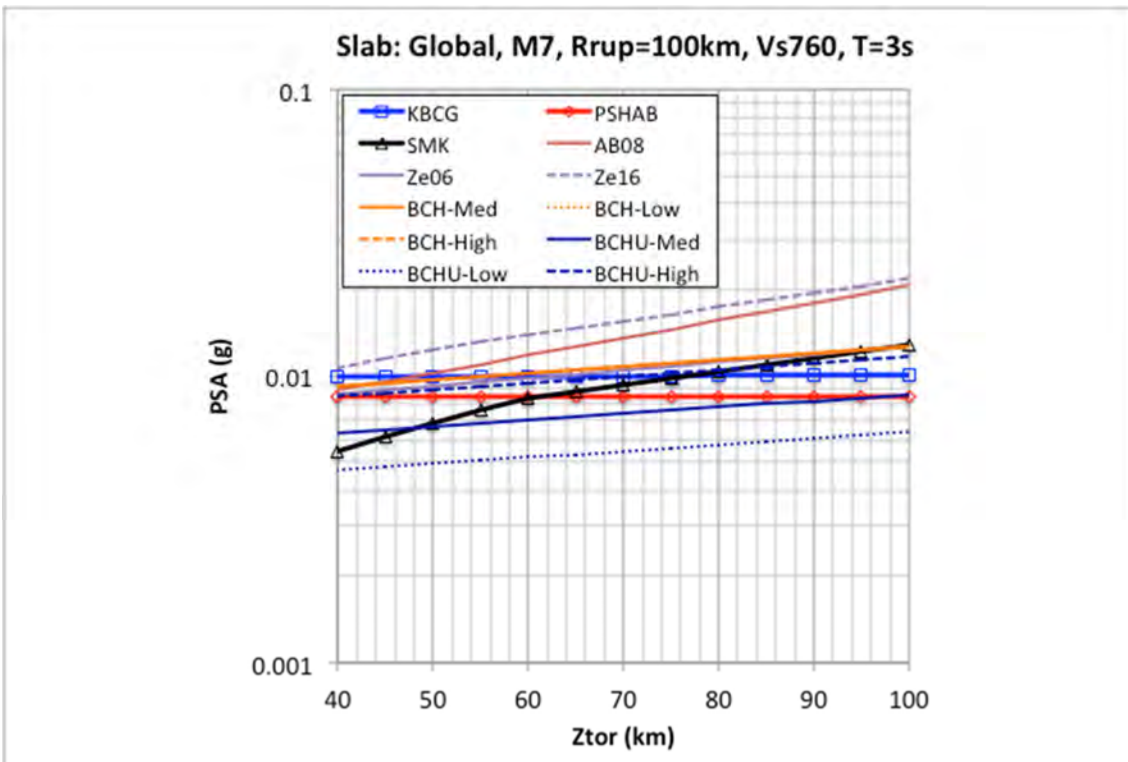

Figure 3.115 Comparison of T = 3.0 sec Z_{tor} scaling for a M7 slab event at a distance of 75 km for V_{S30} = 760 m/sec.

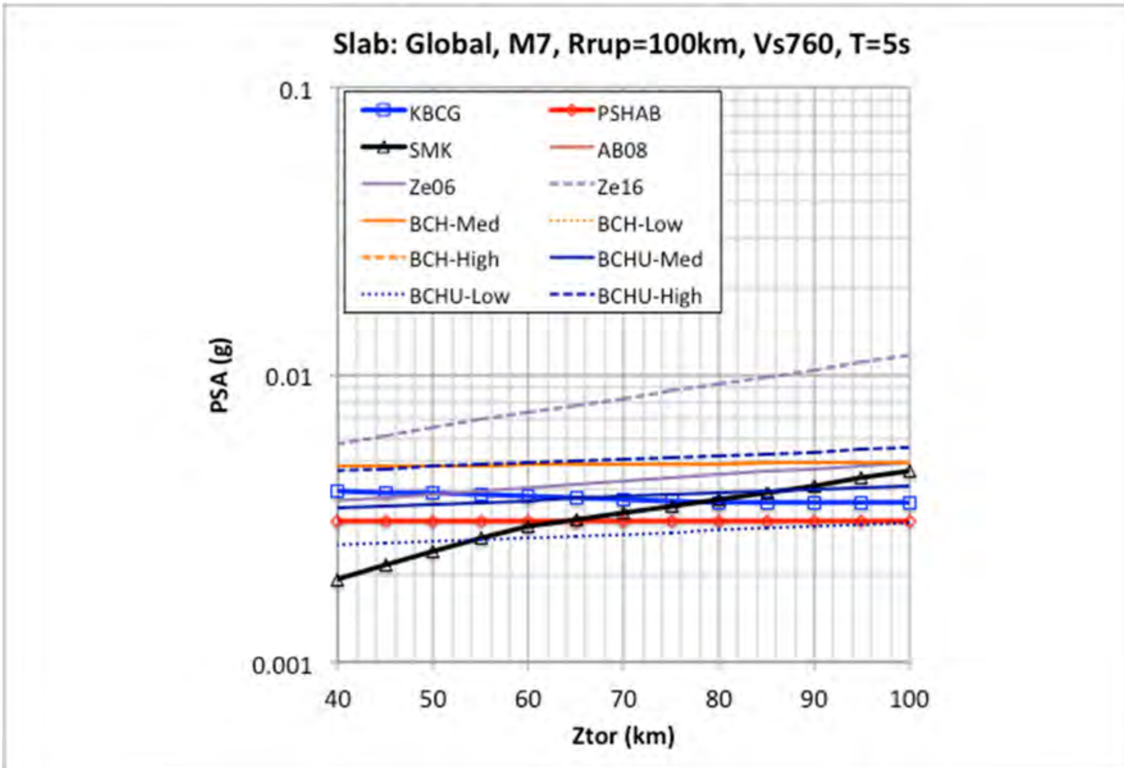

Figure 3.116 Comparison of T = 5.0 sec Z_{tor} scaling for a M7 slab event at a distance of 75 km for V_{S30} = 760 m/sec.

3.3 BASIN AMPLIFICATION

In addition to the site response model contained in each of the NGA-Sub GMMs, an additional term is included for the deeper structure associated with sedimentary basins. All three models include this feature for Japan and both the KBCG and PSAHB models for sites located in Cascadia. The KBCG model also includes a term for basins in New Zealand and Taiwan. These basin-amplification functions are independent of the earthquake type and would apply to both interface and slab events for a given region.

For sites in Japan, the basin amplification is dependent on the $Z_{2.5}$ depth. For the SMK model, this basin amplification is a linear function of $Z_{2.5}$, whereas for the KBCG and PSHAB models, the functional form is centered based on the difference between the site-specific $Z_{2.5}$ value and the median predicted $Z_{2.5}$ value given the V_{S30} value and the empirical relationship developed from the database. These specific $Z_{2.5}$ and V_{S30} empirical relationships for the different regions and GMMs are presented in the separate PEER report for each model. The same centering approach is applied for sites in the Pacific Northwest for both the KBCG and PSHAB models. Note that since the SMK model is only developed from Japanese data, it is not applicable for sites in the Pacific Northwest. The empirical relationships from the two NGA-Sub models for Japan and Cascadia are plotted in Figure 3.117. The two models are very similar for Japan but show a large difference for Cascadia, especially in the higher V_{S30} range. These differing results are attributable to the large dispersion in the empirical data from sites in the Pacific Northwest region.

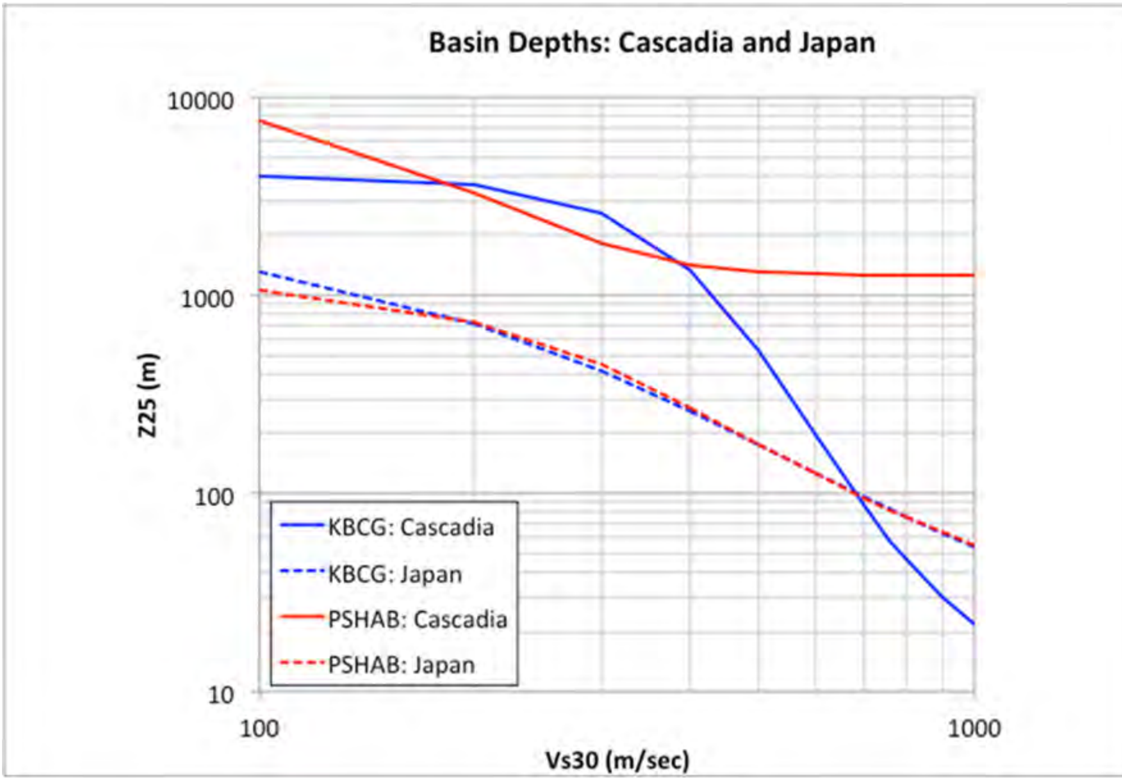

Figure 3.117 Empirical relationships between V_{S30} and $Z_{2.5}$ for Japan and Cascadia from the KBCG and PSHAB models.

For the Cascadia region, both the KBCG and PSHAB further differentiate the basin response as being located within the Seattle basin, within other basins in the region (e.g., Tacoma), or for the PSHAB model, being located outside of a basin but in Cascadia with the amplification based on the $Z_{2.5}$ relationship. The centering relationships plotted in Figure 3.117 are the same for all of these additional cases, but the specific basin-amplification response is varied depending on the specific basin location. For a V_{S30} value of 600 m/sec, the median $Z_{2.5}$ values are 0.20 km and 1.28 km from the KBCG and PSHAB models, respectively.

As an example, a series of comparisons plots are provided in Figure 3.118 through Figure 3.121 for a **M**8 interface earthquake at a distance of 100 km with a V_{S30} value of 600 m/sec. These plots are for the spectral ratio of the acceleration response spectra from the defined $Z_{2.5}$ value divided by the ground motions from the median $Z_{2.5}$ value. Thus, a ratio of unity would be computed for a defined $Z_{2.5}$ of 0.20 km for the KBCG model and 1.28 km for the PSHAB model.

The results for the KBCG model are presented for both Seattle basin sites (dashed blue lines) and non-Seattle basin sites (solid blue lines). This model has an additional constraint in that any basin-amplification factors for non-Seattle basin sites cannot exceed the factors from the Seattle basin sites, which are independent of the $Z_{2.5}$ term. For this reason, the non-Seattle basin-amplification ratios are equal to the Seattle amplification ratios for those longer spectral periods for $Z_{2.5}$ greater than 1 km.

The results or the PSHAB model show similar basin-amplification factors for the deeper $Z_{2.5}$ values. For the shallowest $Z_{2.5}$ value, the PSHAB shows minimal basin amplification for all three potential sites. Also note that for the range of $Z_{2.5}$ values presented in the comparison figures, the basin amplification for sites outside of a basin (solid red line) is near unity, especially in the longer spectral period range. Another observation from both models is the predicted de-amplification of ground motions for basin sites in the spectral period range around 0.1 sec, especially for the larger $Z_{2.5}$ values.

Given the potential importance of expected increase in the ground motions response for longer spectral periods in the greater Seattle area, a recent basin-amplification adjustment function has been adopted by the City of Seattle [SDCI 2018]. This adopted amplification function is based on **M**9 simulation results [Wirth et al. 2018] for a Cascadia interface earthquake. The amplification function plotted in Figure 3.121 was developed based on the spectral ratio from sites in and around the Seattle area located within the Seattle basin. The simulations are based on a V_{S30} of 600 m/sec, and the computed ratios are for a $Z_{2.5}$ value of 6 km for the Seattle basin. Overall, the comparison between the SDCI-recommended amplification function [2018] and the two results from NGA-Sub model is favorable, with the noted observation that the SDCI [2018] factors envelope the NGA-Sub model factors.

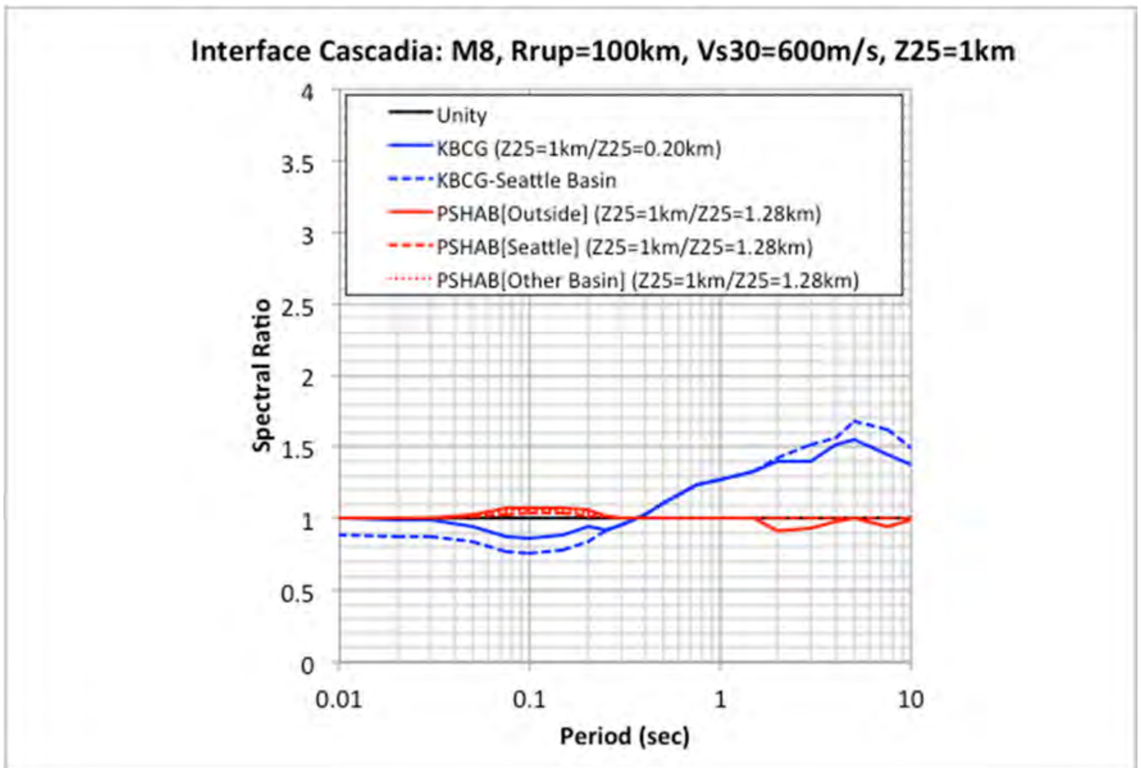

Figure 3.118 Basin amplification factors for Cascadia from a M8 interface event at a distance of 100 km and with V_{S30} = 600 m/sec and $Z_{2.5}$ value of 1 km.

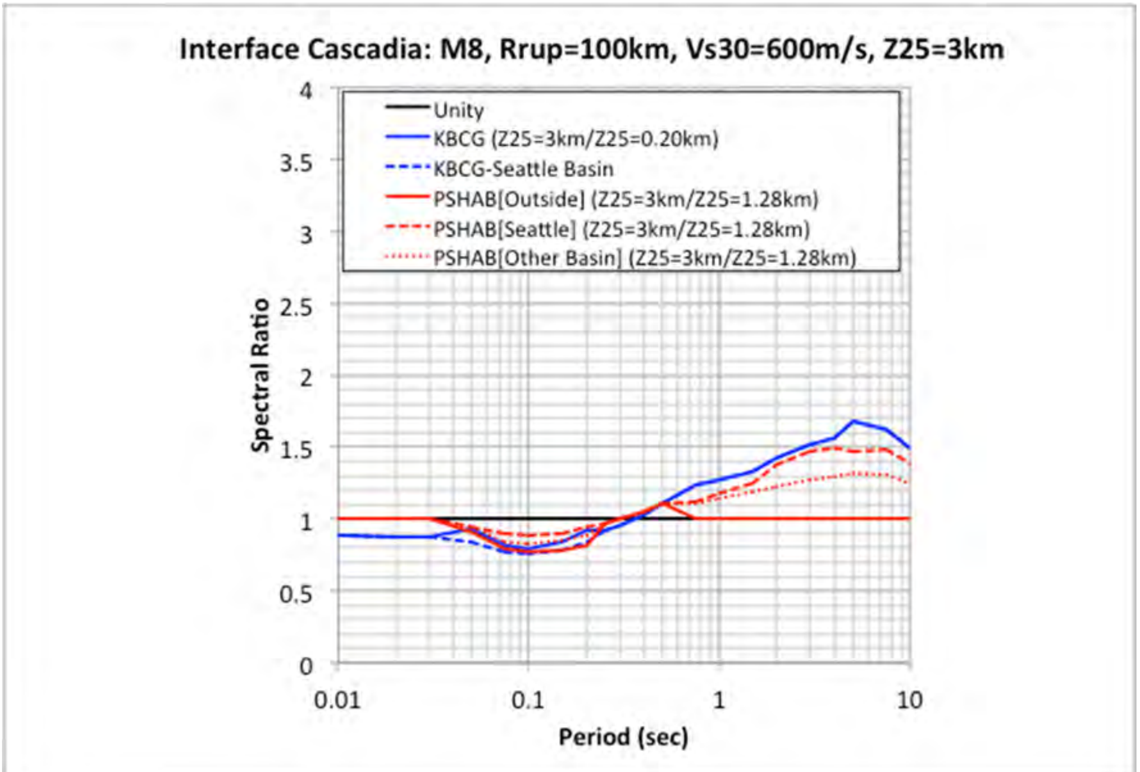

Figure 3.119 **Basin amplification factors for Cascadia from a M8 interface event at a distance of 100 km and with V_{S30} = 600 m/sec and $Z_{2.5}$ value of 3 km.**

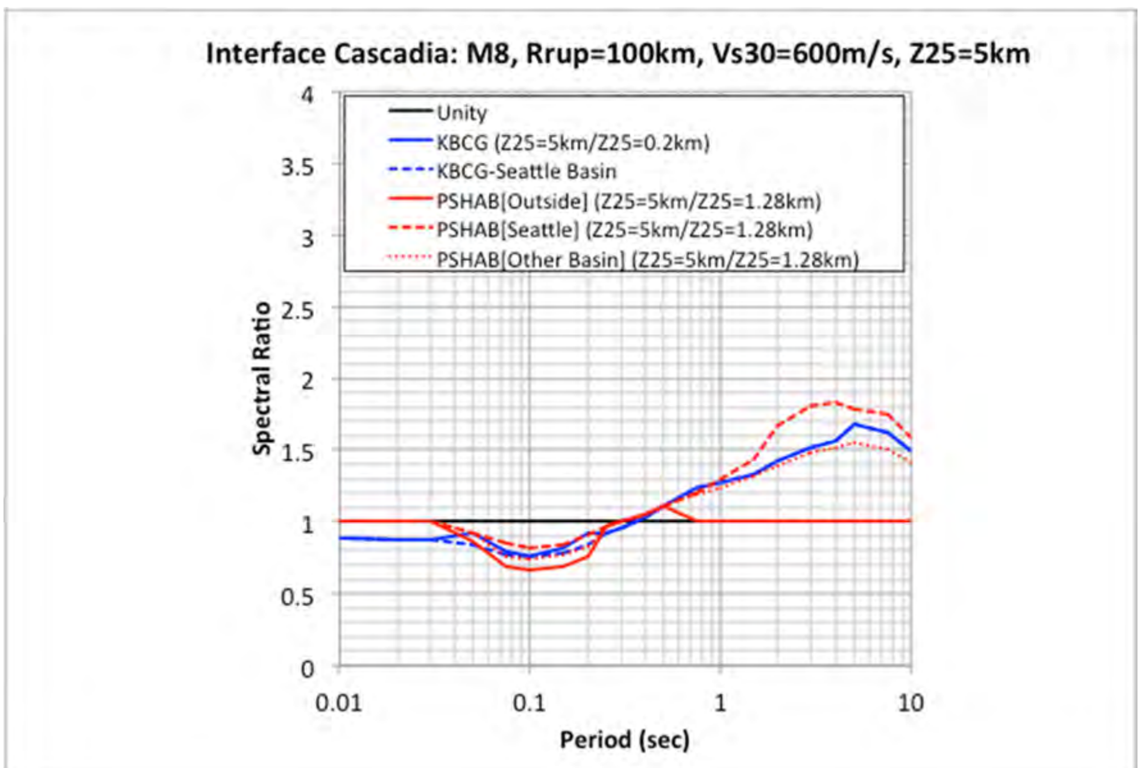

Figure 3.120 **Basin amplification factors for Cascadia from a M8 interface event at a distance of 100 km and with V_{S30} = 600 m/sec and $Z_{2.5}$ value of 5 km.**

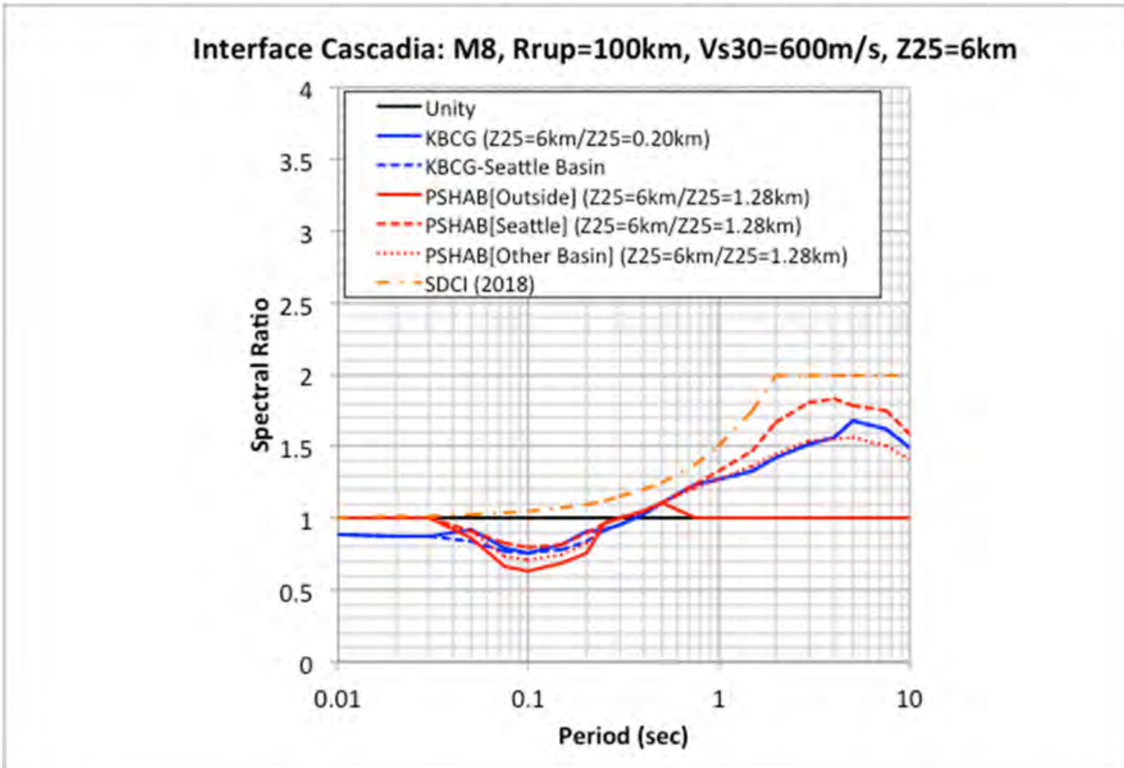

Figure 3.121 Basin amplification factors for Cascadia from a M8 interface event at a distance of 100 km and with V_{S30} = 600 m/sec and $Z_{2.5}$ value of 6 km.

For Japan, comparisons are presented for all three NGA-Sub models given a **M**8 interface event at a distance of 100 km with an assigned V_{S30} value of 400 m/sec. The median $Z_{2.5}$ values are 0.259 km and 0.272 km from the KBCG and PSHAB models, respectively. For the SMK model, a reference $Z_{2.5}$ value of 0.28 km was selected for the spectral ratio. Spectral ratio values are plotted in Figure 3.122 through Figure 3.125. For the lowest $Z_{2.5}$ value, the models predict a de-amplification in the ground motions for intermediate to long spectral periods. As the $Z_{2.5}$ value increases, however, the models predict amplification from this basin modeling function for the intermediate to longer spectral periods.

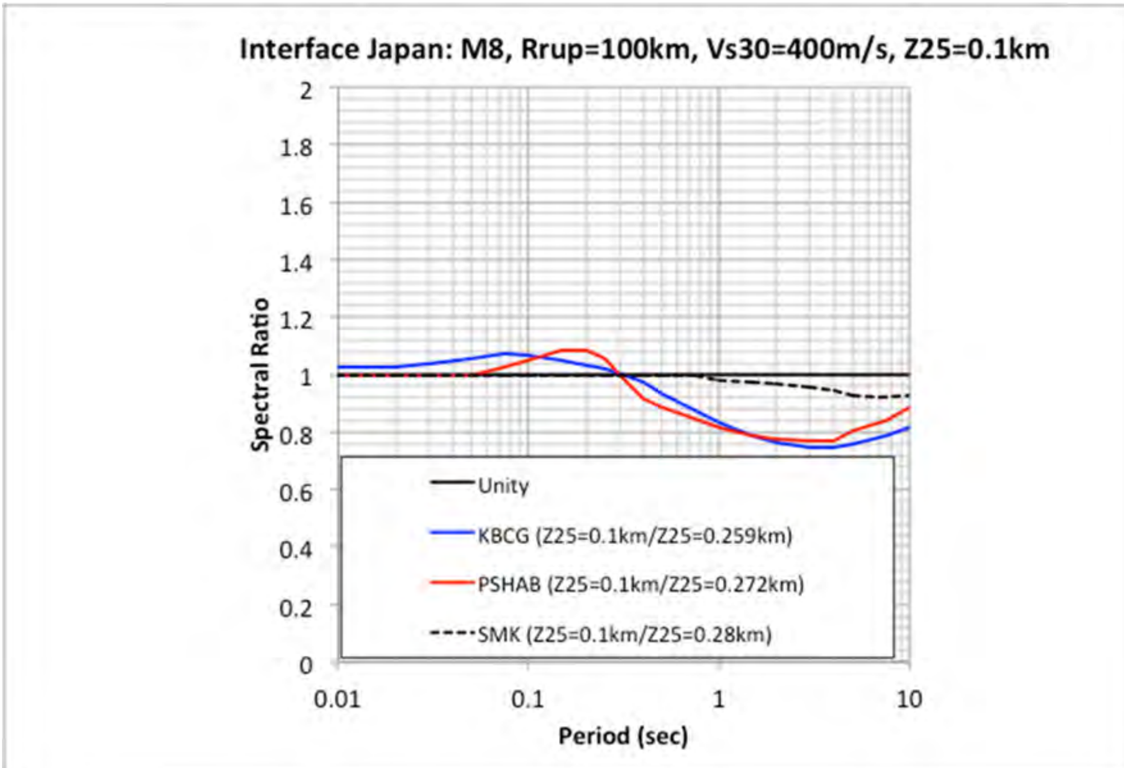

Figure 3.122 Basin-amplification factors for Japan from a M8 interface event at a distance of 100 km with V_{S30} = 400 m/sec and $Z_{2.5}$ value of 0.1 km.

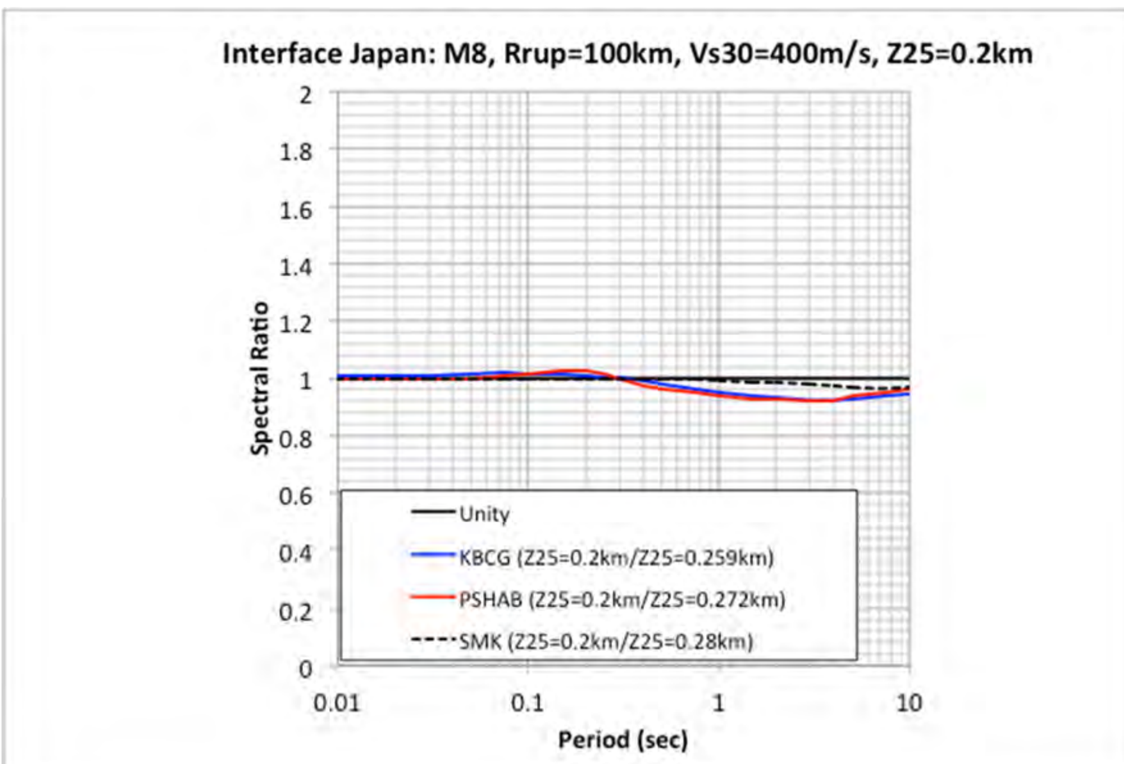

Figure 3.123 Basin-amplification factors for Japan from a M8 interface event at a distance of 100 km with V_{S30} = 400 m/sec and $Z_{2.5}$ value of 0.2 km.

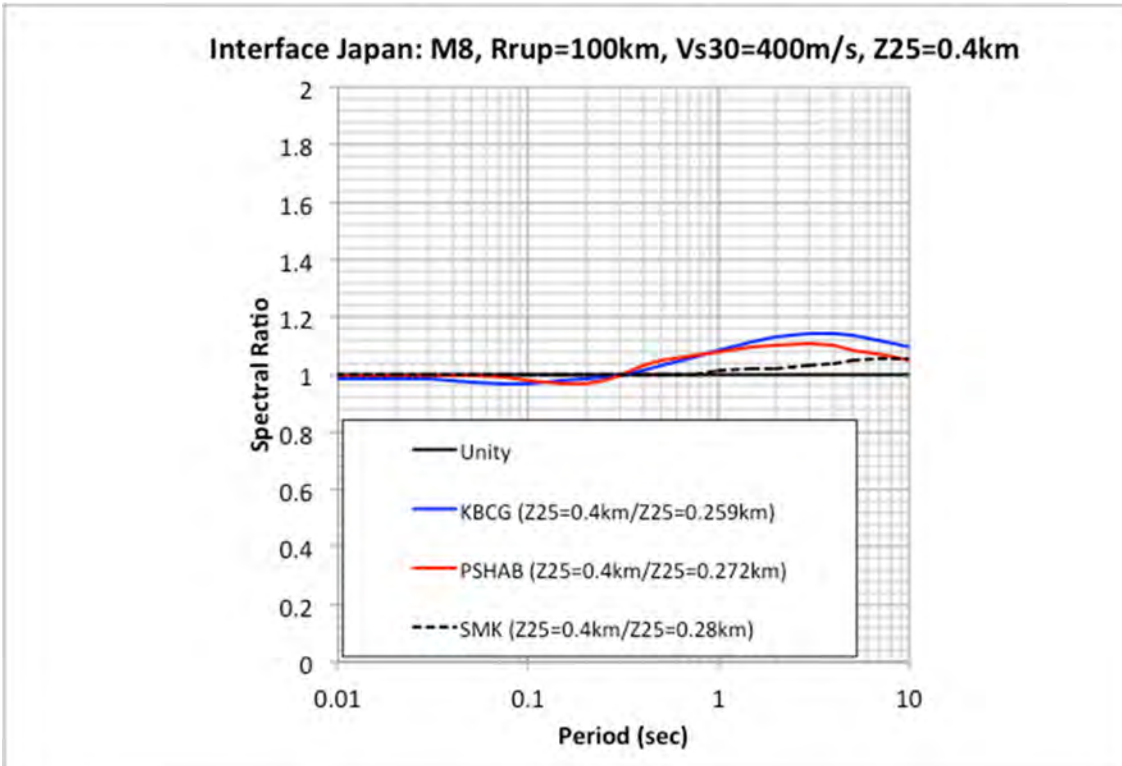

Figure 3.124 Basin-amplification factors for Japan from a M8 interface event at a distance of 100 km with V_{S30} = 400 m/sec and $Z_{2.5}$ value of 0.4 km.

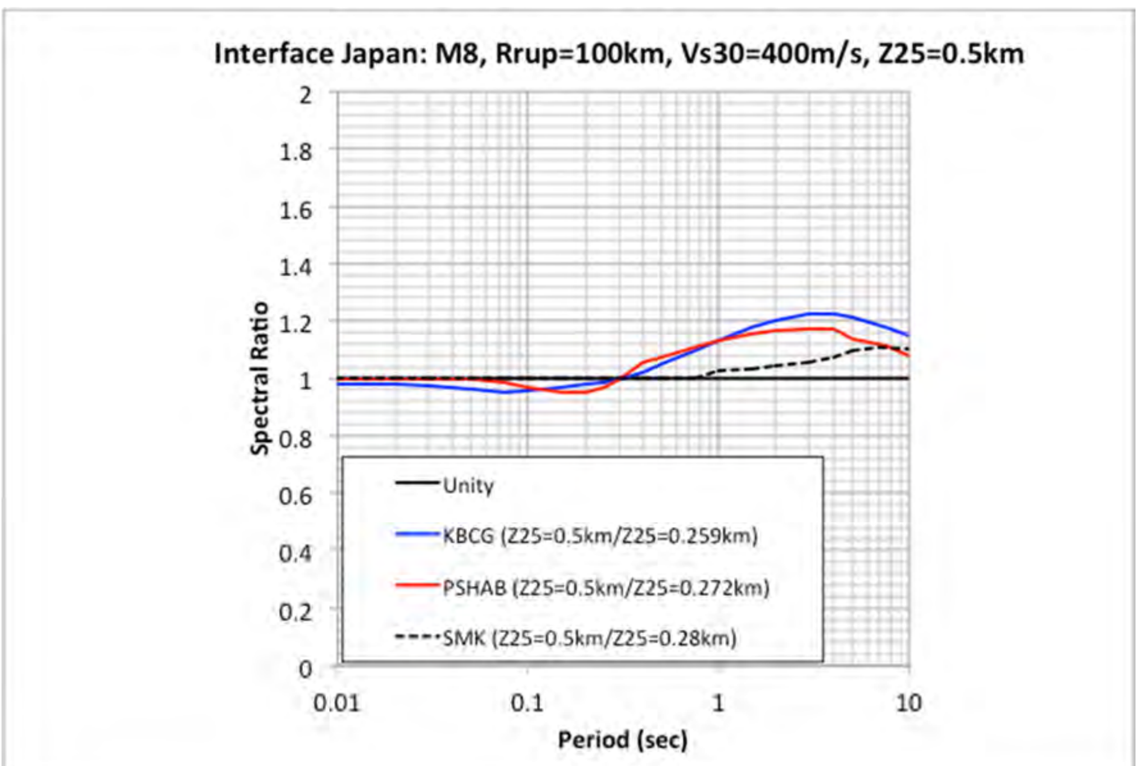

Figure 3.125 Basin-amplification factors for Japan from a M8 interface event at a distance of 100 km with V_{S30} = 400 m/sec and $Z_{2.5}$ value of 0.5 km.

For the KBCG mode, the basin-amplification model for Taiwan and New Zealand is defined in terms of the $Z_{1.0}$ value. The empirical median estimates given a V_{S30} value are shown in Figure 3.126 for the two regions of New Zealand and Taiwan. For a V_{S30} value of 400 m/sec, the median $Z_{1.0}$ values are 0.072 km and 0.097 km for New Zealand and Taiwan, respectively. Based on these $Z_{1.0}$ values, the comparison of spectral ratio values for a **M**8 interface earthquake at a distance of 100 km with a V_{S30} value of 400 m/sec are presented in Figure 3.127 to Figure 3.129 for New Zealand and Figure 3.130 to Figure 3.132 for Taiwan. For New Zealand, the model predicts de-amplification for spectral periods less than 0.8 sec and amplification for the longer spectral periods. For Taiwan, the KBCG model predicts amplification across all spectral periods with an increase in the longer spectral period range.

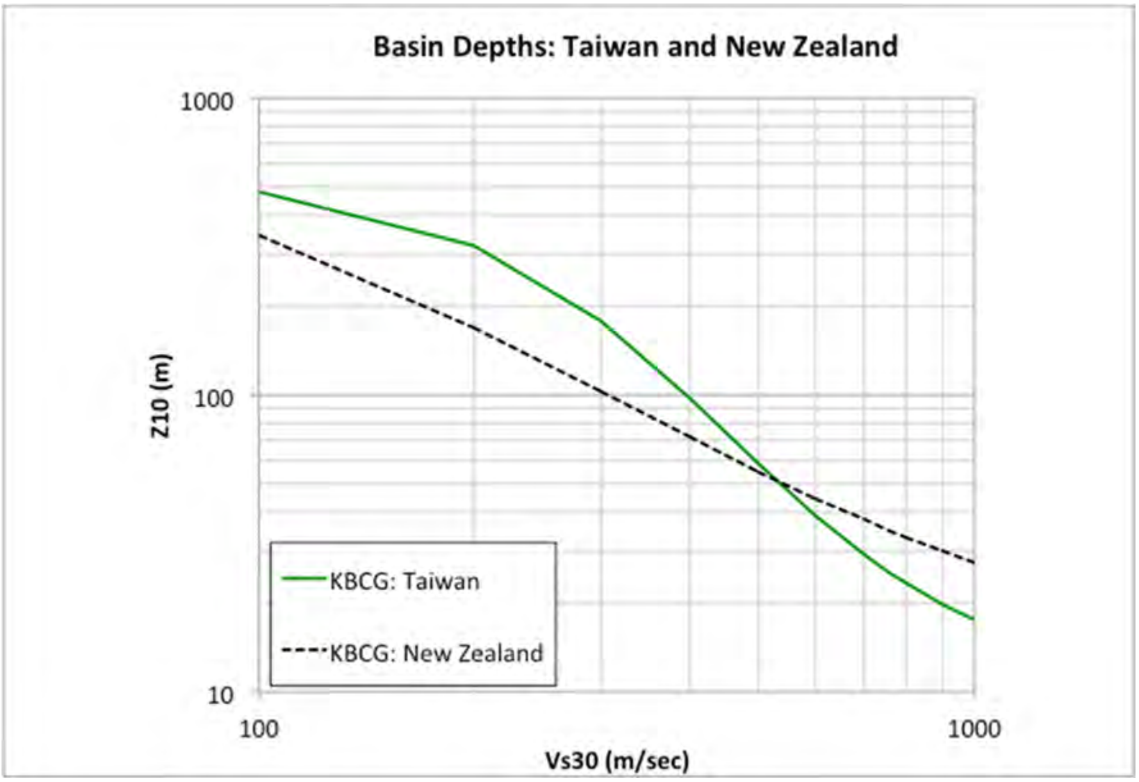

Figure 3.126 Empirical relationships between V_{S30} and $Z_{1.0}$ for Taiwan and New Zealand from the KBCG model.

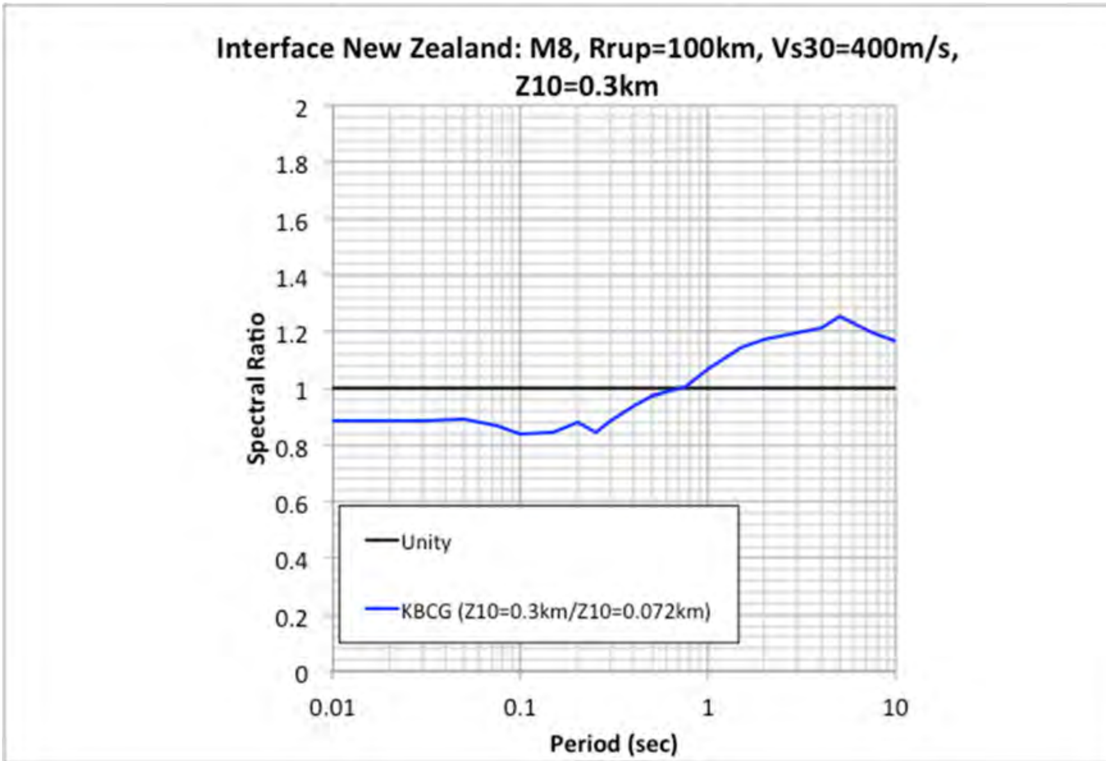

Figure 3.127 Basin-amplification factors for New Zealand from a M8 interface event at a distance of 100 km and with V_{S30} = 400 m/sec and $Z_{1.0}$ value of 0.3 km.

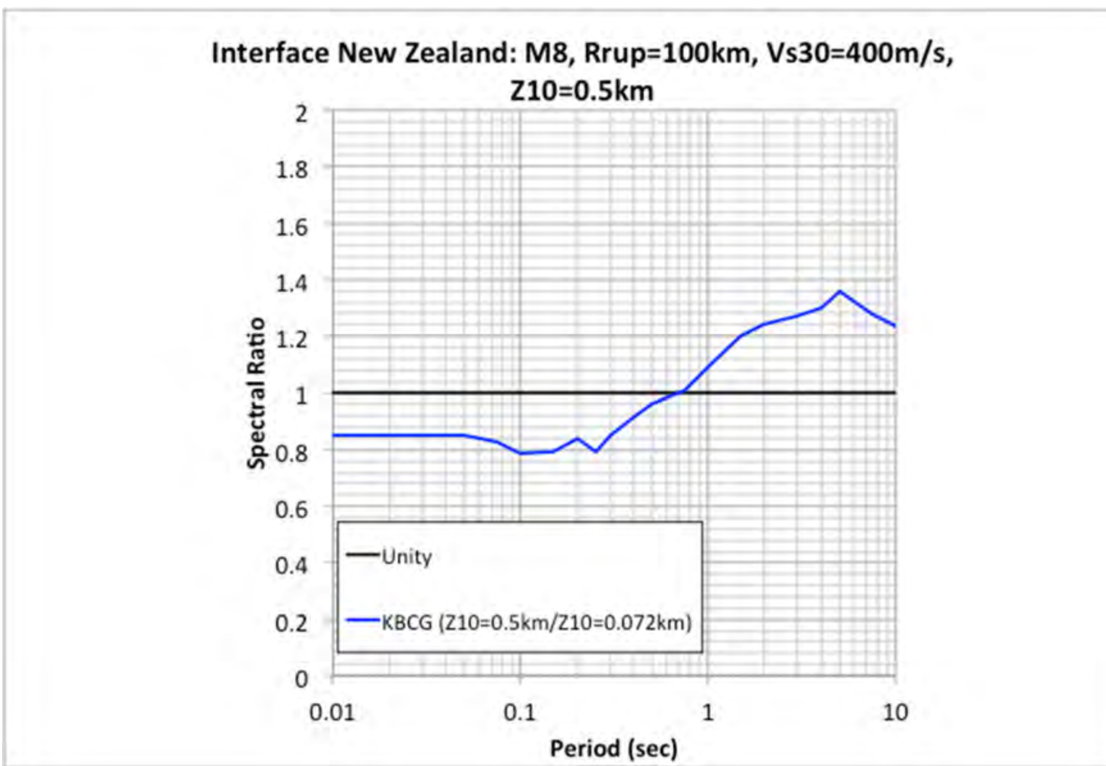

Figure 3.128 Basin-amplification factors for New Zealand from a M8 interface event at a distance of 100 km and with V_{S30} = 400 m/sec and $Z_{1.0}$ value of 0.5 km.

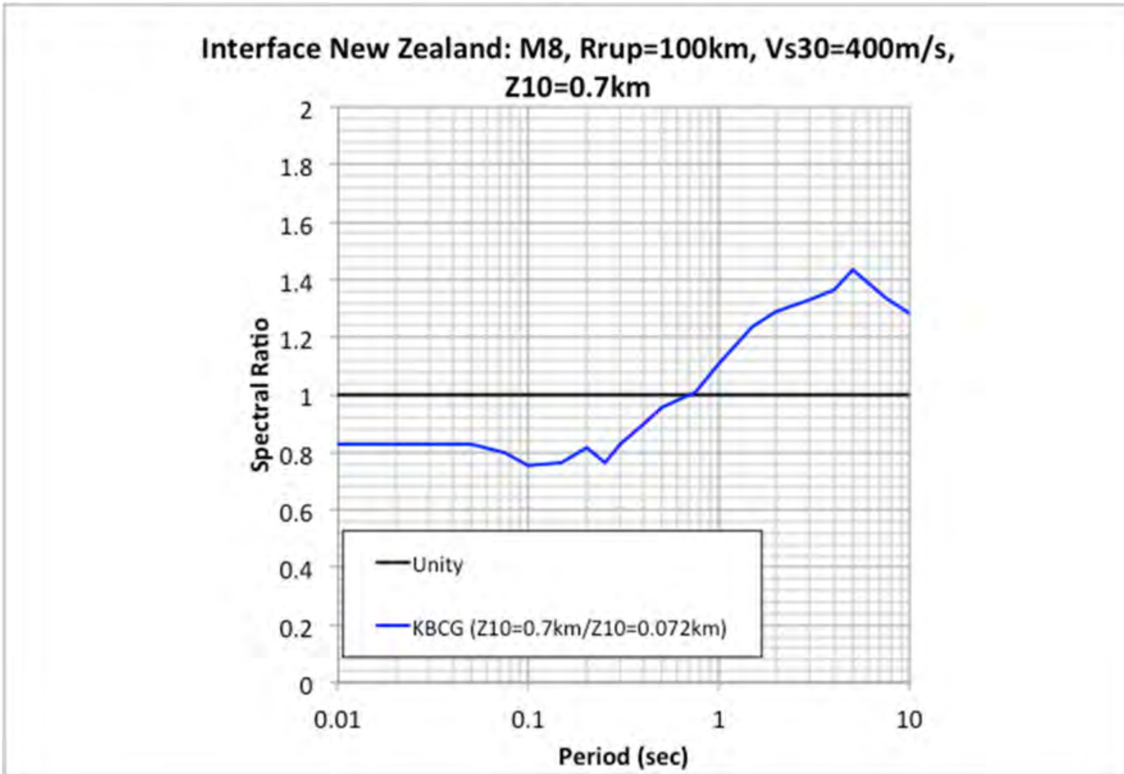

Figure 3.129 Basin-amplification factors for New Zealand from a M8 interface event at a distance of 100 km and with V_{S30} = 400 m/sec and $Z_{1.0}$ value of 0.7 km.

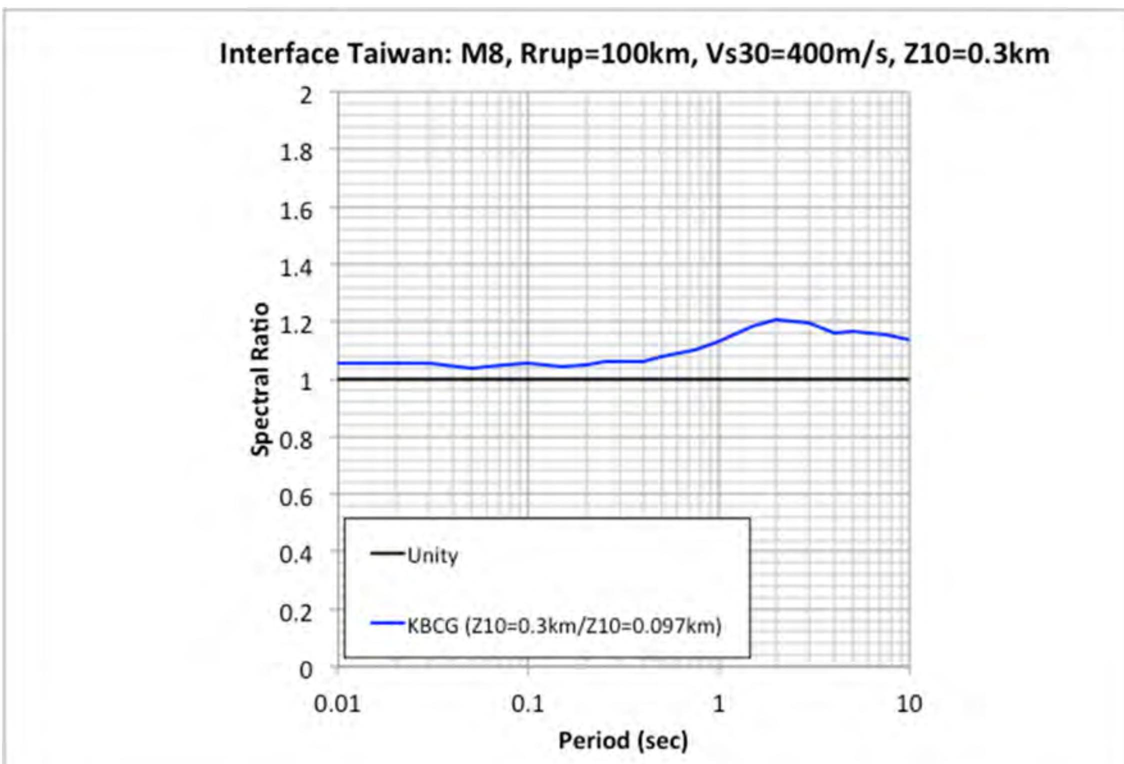

Figure 3.130 Basin amplification factors for Taiwan from a M8 interface event at a distance of 100 km and with V_{S30} = 400 m/sec and $Z_{1.0}$ value of 0.3 km.

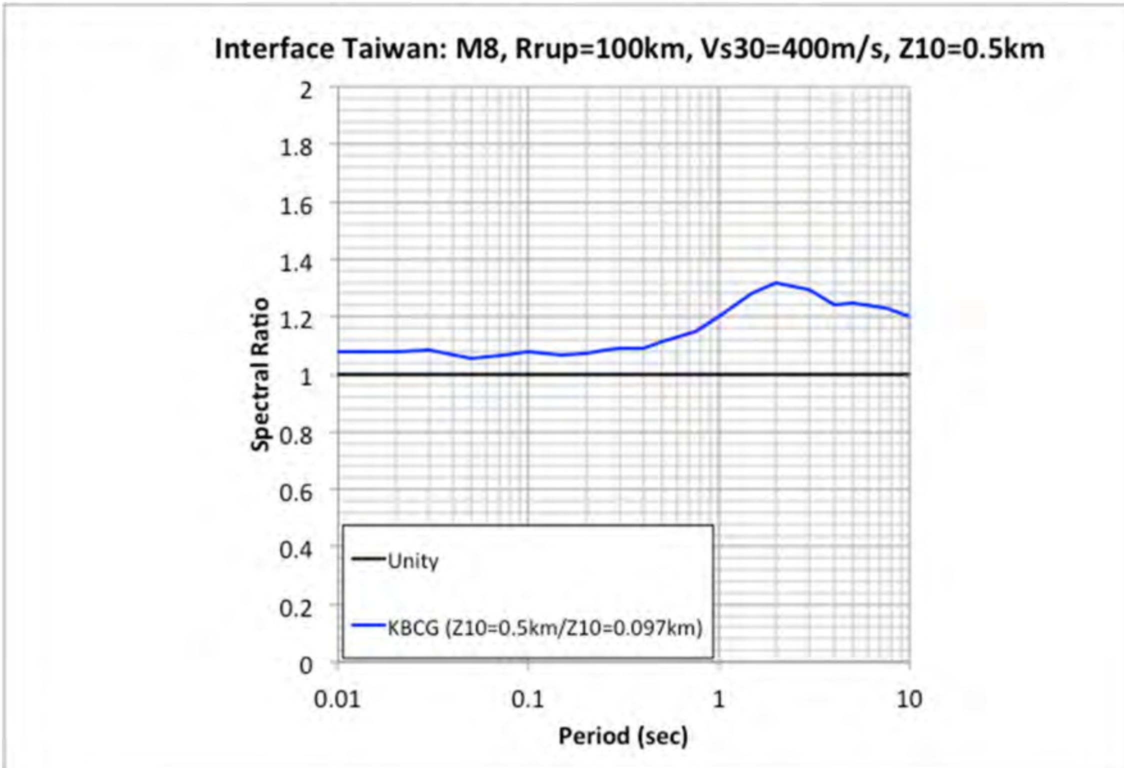

Figure 3.131 Basin-amplification factors for Taiwan from a M8 interface event at a distance of 100 km and with V_{S30} = 400 m/sec and $Z_{1.0}$ value of 0.5 km.

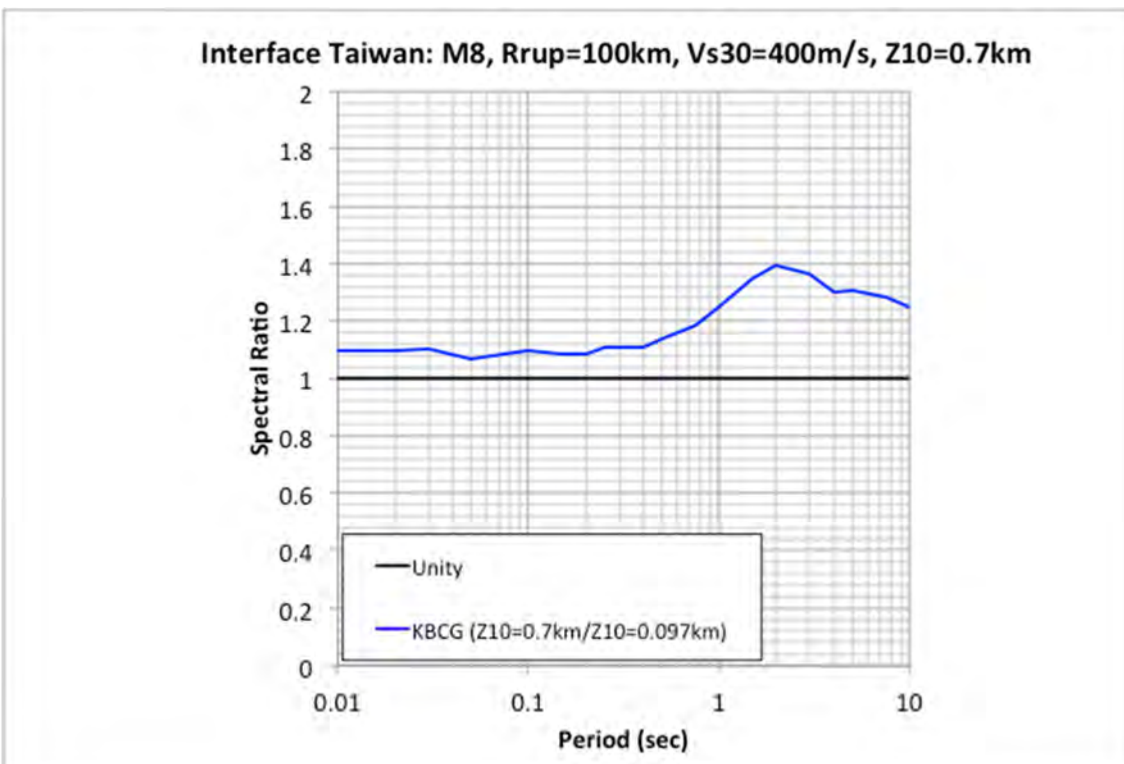

Figure 3.132 Basin-amplification factors for Taiwan from a M8 interface event at a distance of 100 km and with V_{S30} = 400 m/sec and $Z_{1.0}$ value of 0.7 km.

3.4 EPISTEMIC UNCERTAINTY

Both the KBCG and PSHAB models provide estimates of the associated epistemic uncertainty in the median ground motion. The SMK model does not currently provide such estimates. The expanded discussion and details on the epistemic models for the KBCG and PSHAB models are contained in their respective reports [Kuehn et al. 2020; Parker et al. 2020]. For the KBCG model, the epistemic uncertainty can be estimated from the sample of 800 posterior distributions of the model coefficients. These 800 sample cases are provided at each spectral period; however, the sampling is not correlated across each spectral period. For a given spectral period, the ground motions from the 800 sample coefficients can be computed, ranked, and the epistemic uncertainty calculated. In repeating this process for all spectral periods, epistemic uncertainty for a given scenario event can be computed. For the PSHAB model, a functional model is provided that can be applied to the median ground-motion estimates. For both models, the epistemic uncertainties are based on region and earthquake type (i.e., interface or slab), and are spectral period dependent.

As an example, the epistemic uncertainty for interface events in Cascadia from the two models is plotted in Figure 3.133. Both models show a larger uncertainty in the short-period range relative to the longer spectral periods, with the PSHAB model having higher overall epistemic uncertainty. Applying these epistemic models to a **M**9 Cascadia (no basin) interface earthquake at a distance of 75 km with a Z_{tor} value of 10 km and a V_{S30} value of 760 m/sec, the resulting median, epistemic 16^{th} and 84^{th} percentile response spectra are plotted in Figure 3.134.

In addition to this regional epistemic uncertainty models associated with the KBCG and PSHAB models, it is expected that an evaluation of the model-to-model uncertainty will be performed upon completion of the other NGA-Sub GMMs. This will allow for the potential development of an applicable epistemic model that could be implemented for seismic hazard studies that is similar to how the Al Atik and Youngs [2014] model is typically implemented for the NGA-West2 GMMs.

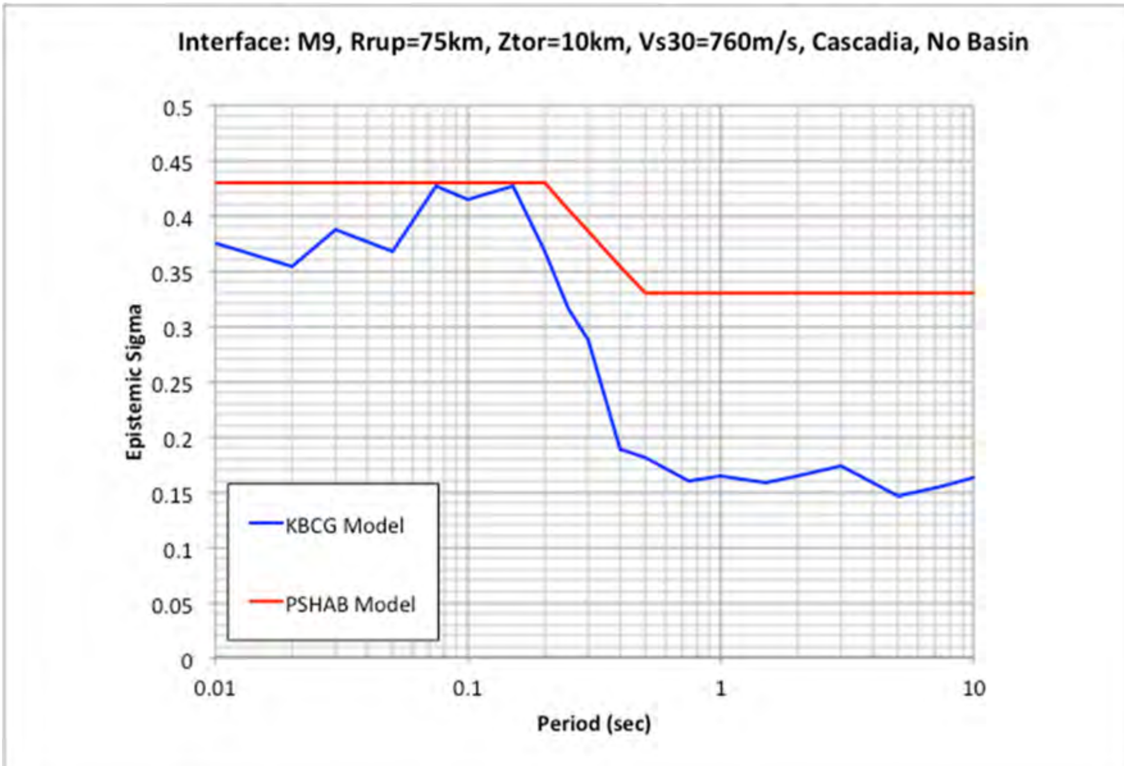

Figure 3.133 Epistemic uncertainty from the KBCG (blue line) and PSHAB (red line) models for interface events in Cascadia.

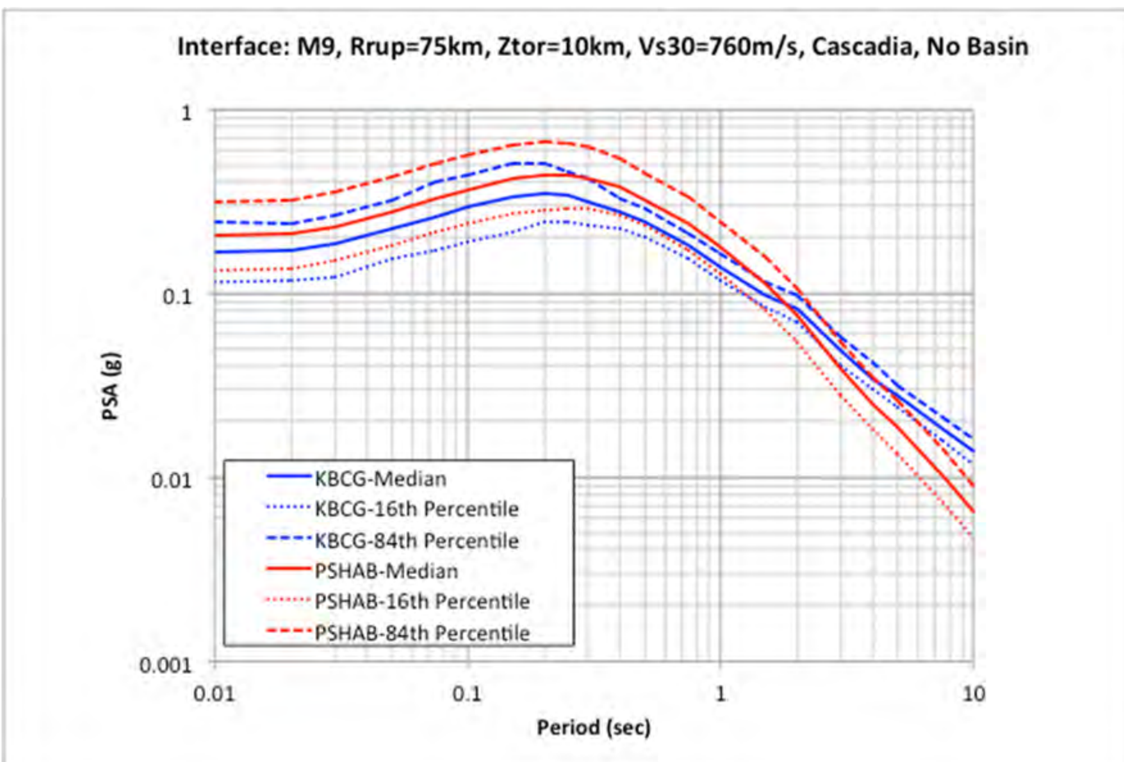

Figure 3.134 Comparison of median and epistemic 16th and 84th percentile spectra for a M9 Cascadia (no basin) interface event at a distance of 75 km (Z_{tor} = 10 km) for V_{S30} = 760 m/sec.

4 Aleatory Uncertainty

The aleatory uncertainty is based on the between-event (τ) and within-event uncertainty (ϕ) following the structure of Al Atik et al. [2010]. Similar to the development of the median GMM, each modeler team investigated, evaluated, and developed an aleatory uncertainty model based on the between-event and within-event variations. For the KBCG and SMK models, these variations are independent of prediction parameters such as distance, magnitude, and or site conditions. For the PSHAB model, the within-event model is defined as a function of distance and V_{S30} site conditions. Note that a single-station model is also developed for the PSHAB model but is not currently developed for the other two NGA-Sub models. The between-event variation is independent of these variables for the PSHAB model, which is consistent with the other two models. All three models are equal for both interface and slab events and are the same for the global and regionalized models.

A comparison of the within-event variability models from the three NGA-Sub GMMs and the BCH and BCHU models is presented in Figure 4.1. For the PSHAB model, the bounding distance and V_{S30} values outside of which the values are constant are plotted individually. For distance and V_{S30} values between these bounding values, the within-event variation would be interpolated consistent with Parker et al. [2020]. For spectral periods of 2 sec and longer, the variation based on distance and V_{S30} values is constant, and the four bounding results are equal. For shorter spectral periods, the low V_{S30} values (i.e., less than 200 m/sec) at distances less than 200 km yields the lowest within-event variation with values around 0.5. For distances less than 200 km but larger V_{S30} values, the within-event variation is similar to the results from the other models in addition to both the BCH and BCHU models. Finally, for the two cases for the larger distances of 500 km and larger, the results are the highest for the PSHAB model and exceed the results from the other models.

The between-event comparisons are presented in Figure 4.2 for the same set of models. Overall, there is good agreement between the KBCG and PSHAB models, and a large variation with the SMK model. As was noted earlier, the SMK model is based solely on data from Japan, whereas the other two models are based a more global dataset. Also note that BCHU model is also based on this larger global dataset, whereas the BCH model was based on a smaller global dataset.

Given these two components of the uncertainty, the total aleatory uncertainty is compared in Figure 4.3 for the same suite of models. For the PSHAB model, the combinations of the bounding cases are again plotted in the comparison. Focusing on the cases for distances less than 200 km and V_{S30} values in the range of 400–500 m/sec, the aleatory uncertainty noted in the KBCG and PSHAB models is observed to be similar. These results are also generally similar to the BCHU model results, which are all higher than the BCH model results. The results from the SMK model are higher. Note that the final results for BCH and BCHU models presented in the comparison plots are smoothed model values, which will lead to a smoother spectrum compared to the other NGA-Sub models when the uncertainty model is applied.

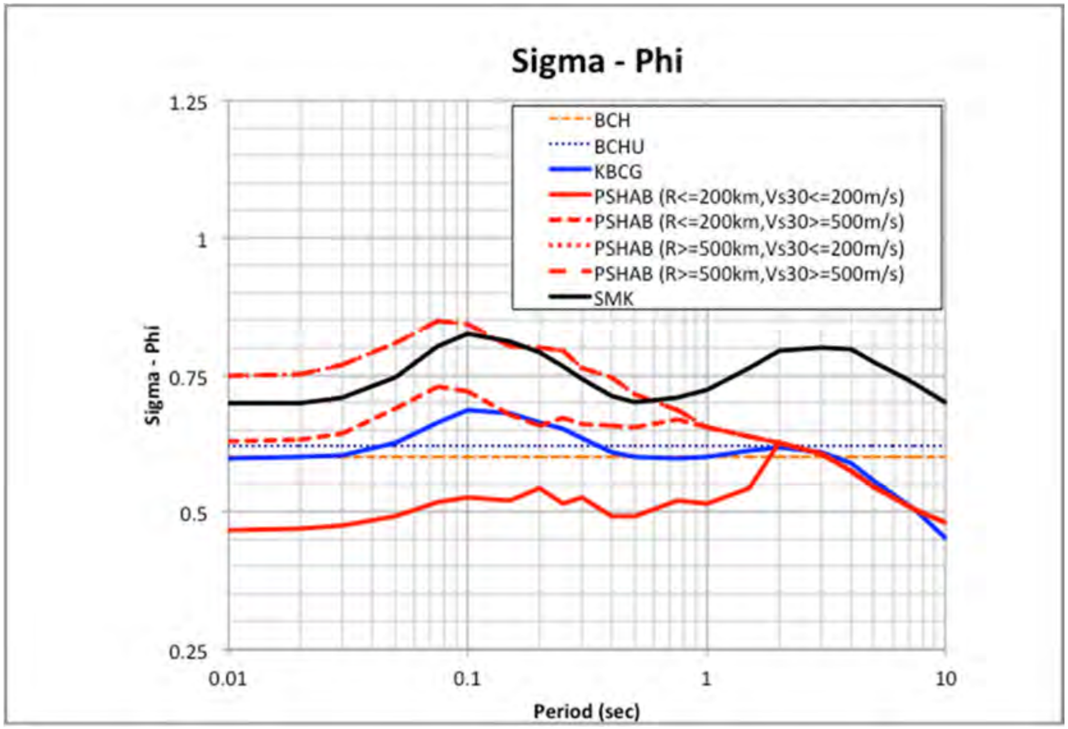

Figure 4.1 Comparison of within-event uncertainty (ϕ) from the three new NGA-Sub GMMs and the BCH and BCHU models.

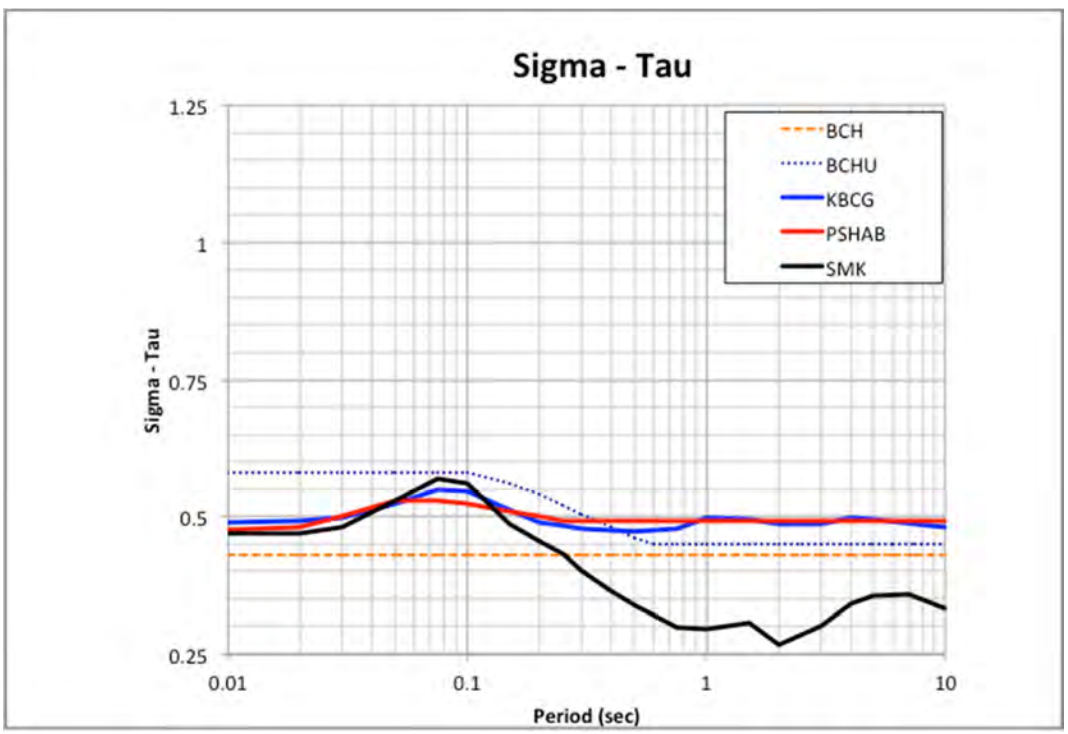

Figure 4.2 Comparison of between-event uncertainty (τ) from the three new NGA-Sub GMMs and the BCH and BCHU models.

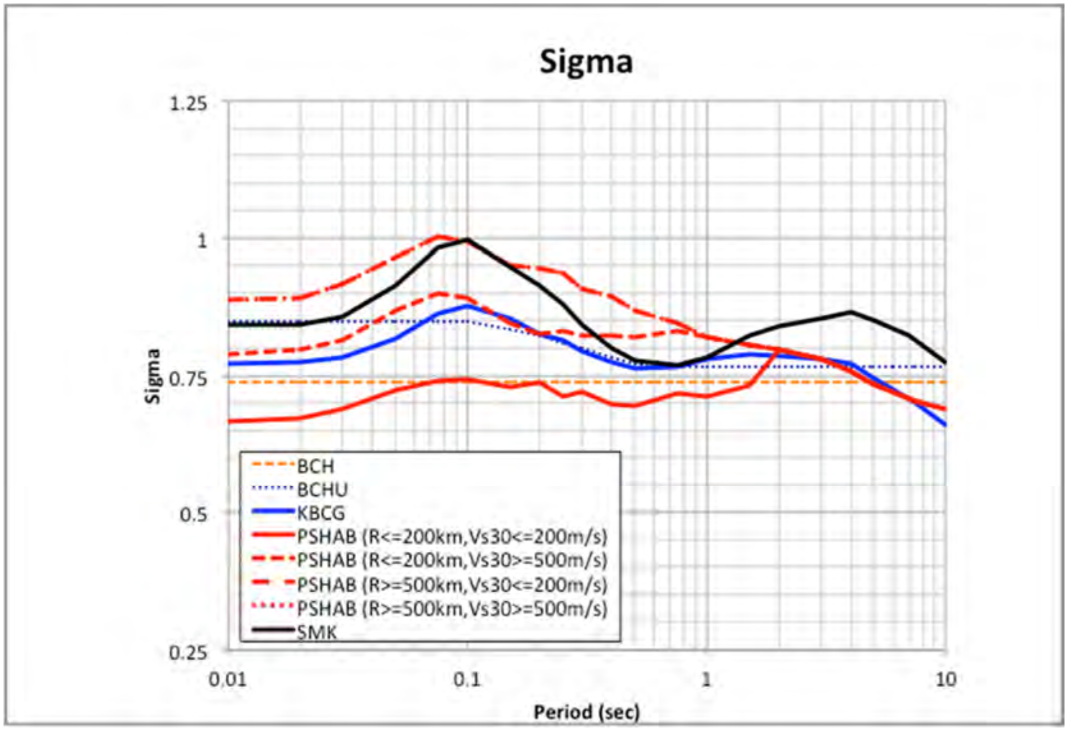

Figure 4.3 **Comparison of aleatory uncertainty from the three new NGA-Sub GMMs and the BCH and BCHU models.**

5 Example PSHA Calculation

Given the development of the NGA-Sub GMMs, their implementation can be expected to have an impact on the resulting ground motions within a standard PSHA analysis. To illustrate the potential impacts given the incorporation of these new models, PSHA calculations are performed for two sites in Washington state, in the Pacific Northwest region of the U.S. The first site is for a general location in the city of Seattle; the second site is located in the town of Centralia. The chosen site latitude and longitude values for these two cities are listed in Table 5.1. The location of these two sites is also plotted in Figure 5.1. The PSHA results presented in this section for these two sites are only meant to illustrate the potential impact from the use of these new models. It is expected that as part of the implementation of these new NGA-Sub GMMs for either sites in the Pacific Northwest or other global sites, sensitivity studies should be conducted to provide technical support for the use of these new models and any associated logic-tree weights.

Results are computed following a standard PSHA methodology [EERI 1989] using the seismic-source model from the 2014 USGS national seismic hazard maps for the region [Petersen et al. 2014]. This source model consists of crustal faults (e.g., the Seattle fault and other regional faults), and both large interface events and deeper slab events associated with the Cascadia subduction zone. For the Seattle site, the contribution to the total seismic hazard is based on a combination of the local Seattle crustal fault and both the interface and slab events. The Centralia site is located closer to the coast; therefore, the influence from the crustal faults is diminished, and the relative contribution from the interface events is larger than from the deeper slab events.

For the ground-motion characterization (GMC) model, four separate cases are performed: one base case and three separate subduction GMMs. For all crustal seismic sources, the suite of five NGA-West2 models are used with the weighting scheme used in the USGS [2014] National Seismic Hazard Maps. These weights are listed along with the five models in Table 5.2. No additional epistemic model (e.g., Al Atik and Youngs [2014]) is applied to these crustal GMMs in the PSHA calculations. The four subduction GMMs that are used in this example analyses are the BCH, BCHU, KBCG, and PSHAB models. Since the SMK model is developed solely for application in Japan, it was not considered in these example calculations.

Table 5.1 Locations of sites used in the PSHA analyses.

City	*Latitude*	*Longitude*
Seattle	47.60	-122.35
Centralia	46.72	-122.95

Table 5.2 GMC model weights for base case.

GMM Model	Source Type	Weight
Abrahamson et al. [2014]	Crustal	0.22
Boore et al. [2014]	Crustal	0.22
Campbell and Bozorgnia [2014]	Crustal	0.22
Chiou and Youngs [2014]	Crustal	0.22
Idriss [2014]	Crustal	0.12
Abrahamson et al. [2016] (BCH)	Subduction	1.0

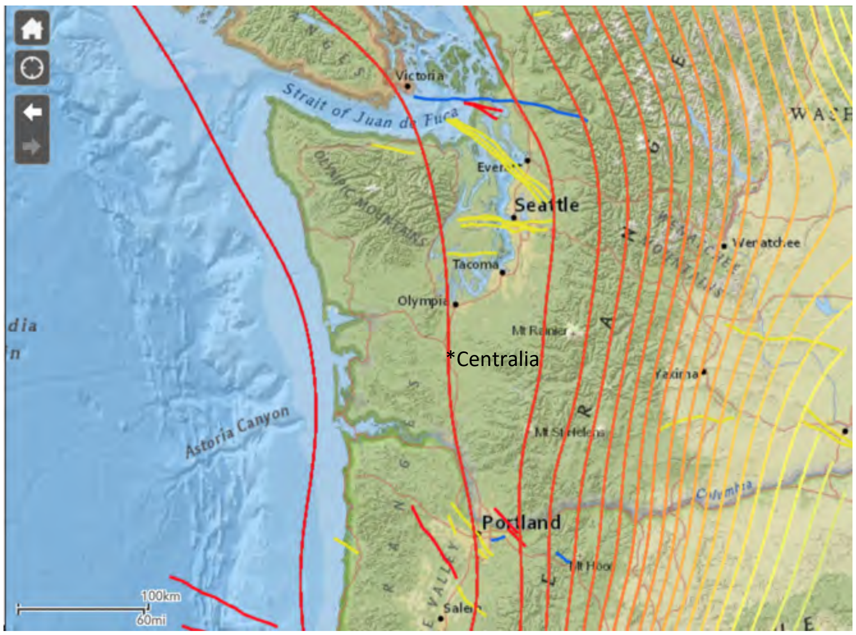

Figure 5.1 Map showing the location of the two site (Seattle and Centralia) used in the PSHA calculation along with the crustal faults (red and yellow lines) and subducting Cascadia subduction zone plate depth contours.

For the base case example using the BCH model, only the central branch of the model is used rather than the full suite of upper and lower branches. For the slab events, however, both the global and Cascadia branches of the logic tree with their respective weights of 0.7 and 0.3 are implemented. All calculations are performed for V_{S30} value of 760 m/sec. For the KBCG and PSHAB models, it is assumed that the sites are not located in a basin. Note that the Seattle site is clearly located in the Seattle basin; however, given that the previous BCHU and BCH models do not include an adjustment for basin locations, the PSHA calculations are based on the site not being located within the Seattle basin. The crustal model default values for $Z_{1.0}$ and $Z_{2.5}$ given the V_{S30} value of 760 m/sec are applied for the NGA-West2 models. Note that if the example calculations were to be computed for sites located within a basin, the default $Z_{2.5}$ values given a V_{S30} value of 760 m/sec would be different for both the KBCG and PSHAB models, and the crustal models and would need to be accounted for within a PSHA calculation.

For each site, hazard curves are computed for PGA (T = 0.01 sec) and spectral periods of 0.2, 1.0, 3.0, and 5.0 sec. Comparisons of these hazard curves–separated by source type and GMMs–are presented in this report. A minimum magnitude of 5 and a sigma truncation value of 6 is implemented for the PSHA calculations. Uniform hazard spectrum (UHS) ground-motion values are computed for the different GMC cases for return period hazard levels of 500, 1000, 2475, 5000, and 10,000 years. Finally, comparisons of the deaggregation results for the 500- and 2475-year-return-period levels are presented for the two sites.

To further isolate the impact of the new GMMs, an additional set of PSHA calculations is performed using the median ground-motion estimates from the BCHU, KBCG, and PSHAB models with the aleatory sigma model from the BCH model. Since the sigma models are identical, this combination of the median and sigma models allows for the direct comparison of the impact on the ground motions from the differences in the median estimates. The results from these example PSHA calculations are presented below.

5.1 SEATTLE SITE EXAMPLE PSHA

The representative Seattle site is located close to the Seattle fault; see Figure 5.1. For the base case (i.e., BCH subduction GMM), the resulting mean annual frequency of exceedance (MAFE) hazard curves are plotted in Figure 5.2 through Figure 5.6. In each of these plots, the contribution from the seismic sources are separated by the Seattle fault (dotted line), combined other crustal faults (long dashed green line), combined background gridded seismicity (short dashed line), slab sources (solid blue line), and interface source (solid green line). These plots show that the Seattle fault, slab, and interface events all contribute significantly to the total hazard, and the specific variation of their contribution is based on the hazard level of interest and the spectral period of consideration. For the longer return period hazard levels and longer spectral periods, the contribution from the Seattle fault increases.

Given these base case hazard curves, the same PSHA calculation is performed by swapping out the BCH subduction GMM with the BCHU, KBCG, and PSHAB subduction GMMs. The same NGA-West2 crustal models are used for these additional example calculations. Comparisons are presented in Figure 5.10 through Figure 5.21 for the total hazard curve, interface, and slab hazard curves plotted as a function of the different subduction GMMs. These figures provide insight on the impact between the different subduction GMMs. The largest impact is observed in the differences between the models in the estimation of ground motions for slab events. Specifically for the PGA and spectral period cases of 0.2 and 1.0 sec, the larger ground motion estimates from the PSHAB model relative to the other models is noted, which is the cause of the differences (i.e., larger) results for the total hazard. For the longer spectral periods, the differences in the slab ground motions is reduced as well as the contribution from the slab sources to the total hazard such that the differences in the resulting ground motions is reduced given the different subduction GMMs.

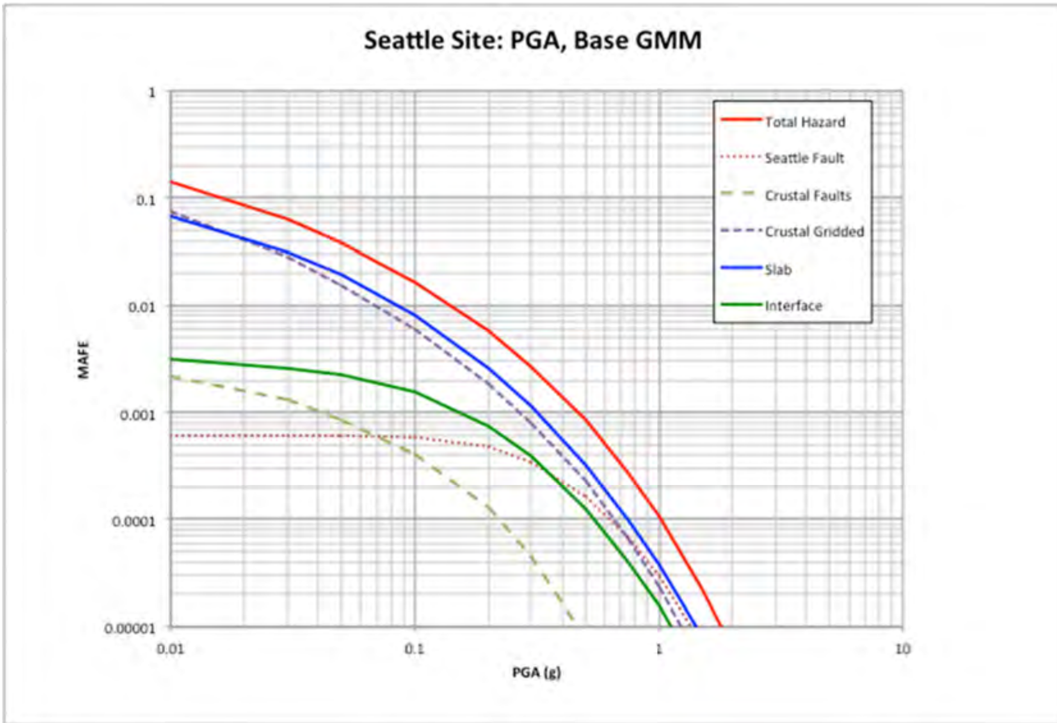

Figure 5.2 Total hazard curve (solid red line) and hazard curves differentiated by seismic source for the Seattle site for PGA (*T* = 0.01 sec).

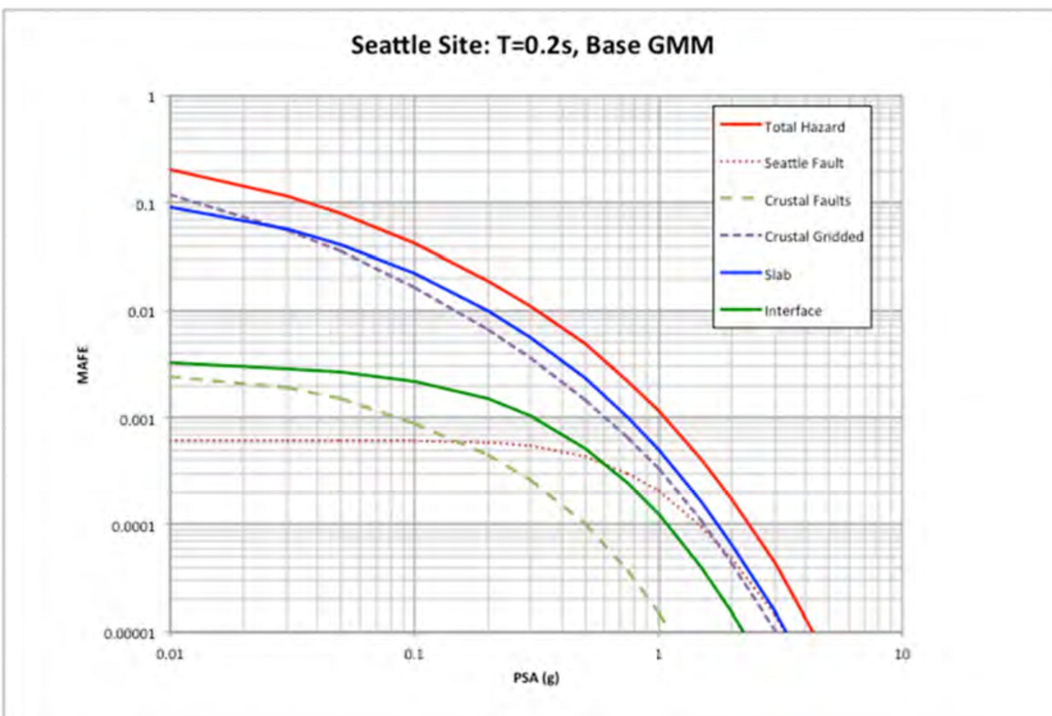

Figure 5.3 Total hazard curve (solid red line) and hazard curves differentiated by seismic source for the Seattle site for spectral period of 0.2 sec.

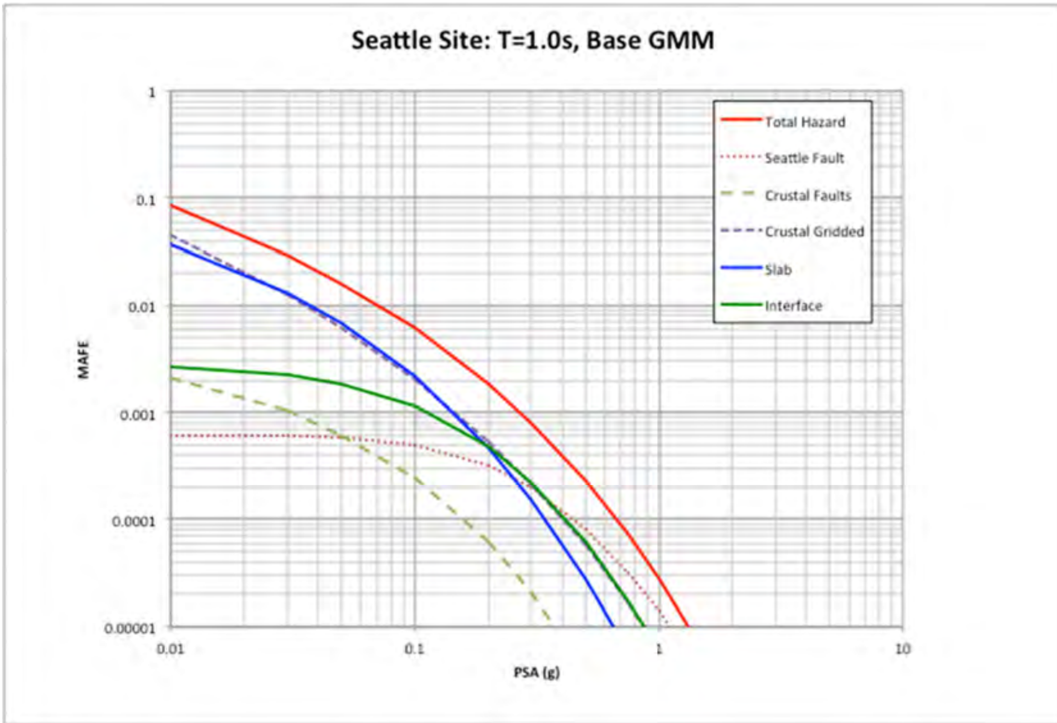

Figure 5.4 Total hazard curve (solid red line) and hazard curves differentiated by seismic source for the Seattle site for spectral period of 1.0 sec.

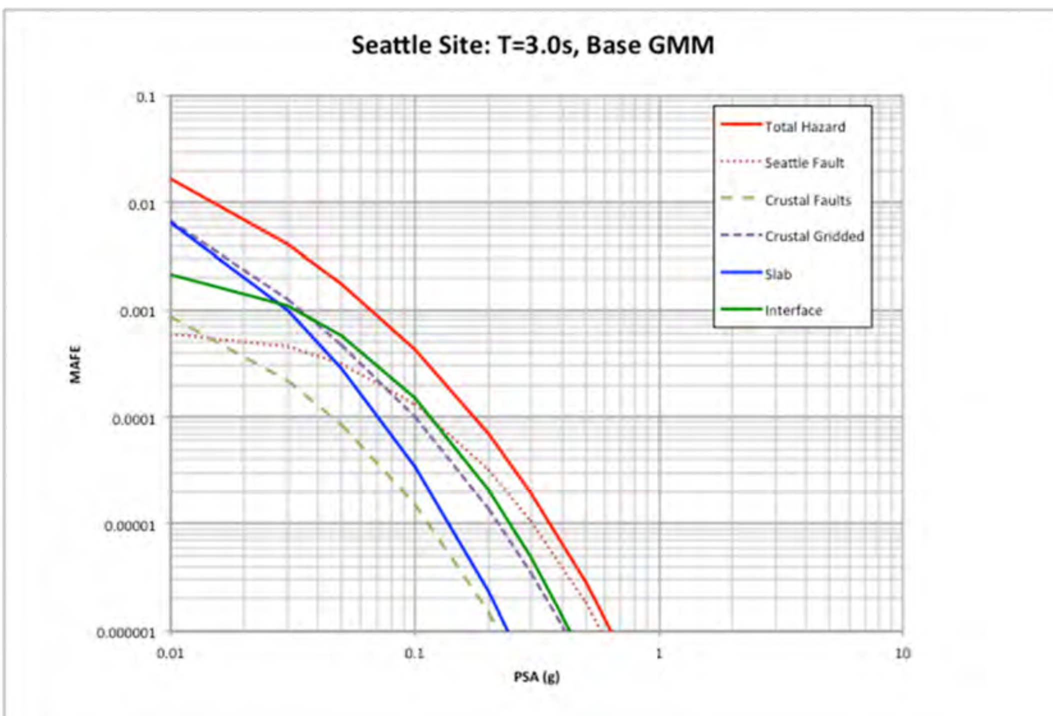

Figure 5.5 Total hazard curve (solid red line) and hazard curves differentiated by seismic source for the Seattle site for spectral period of 3.0 sec.

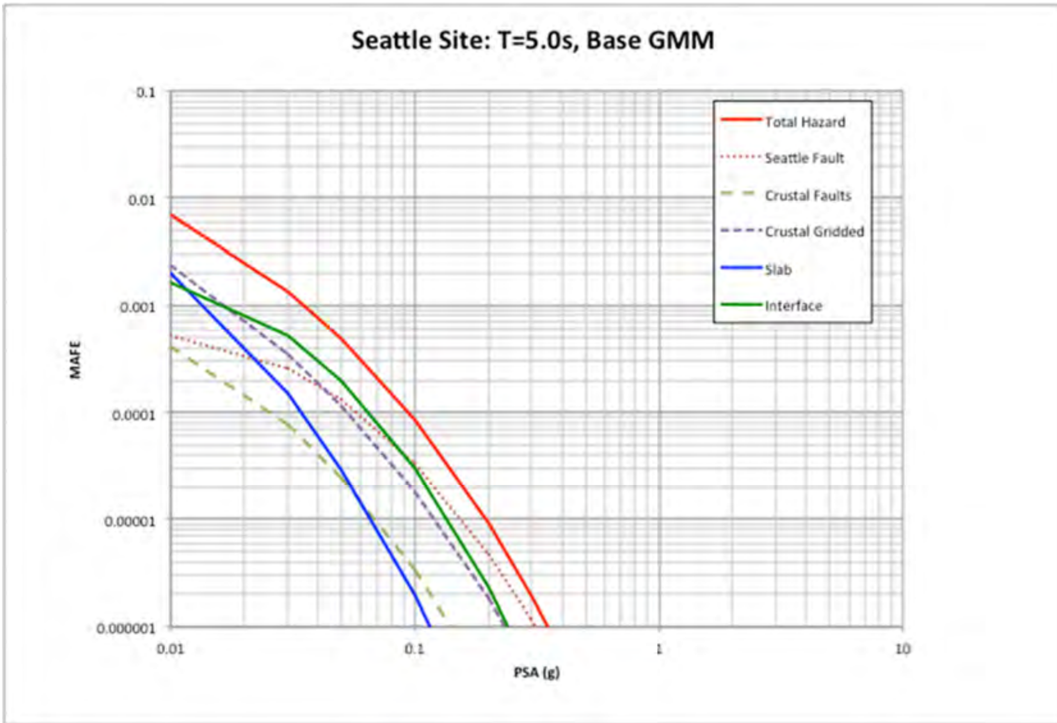

Figure 5.6 Total hazard curve (solid red line) and hazard curves differentiated by seismic source for the Seattle site for spectral period of 5.0 sec.

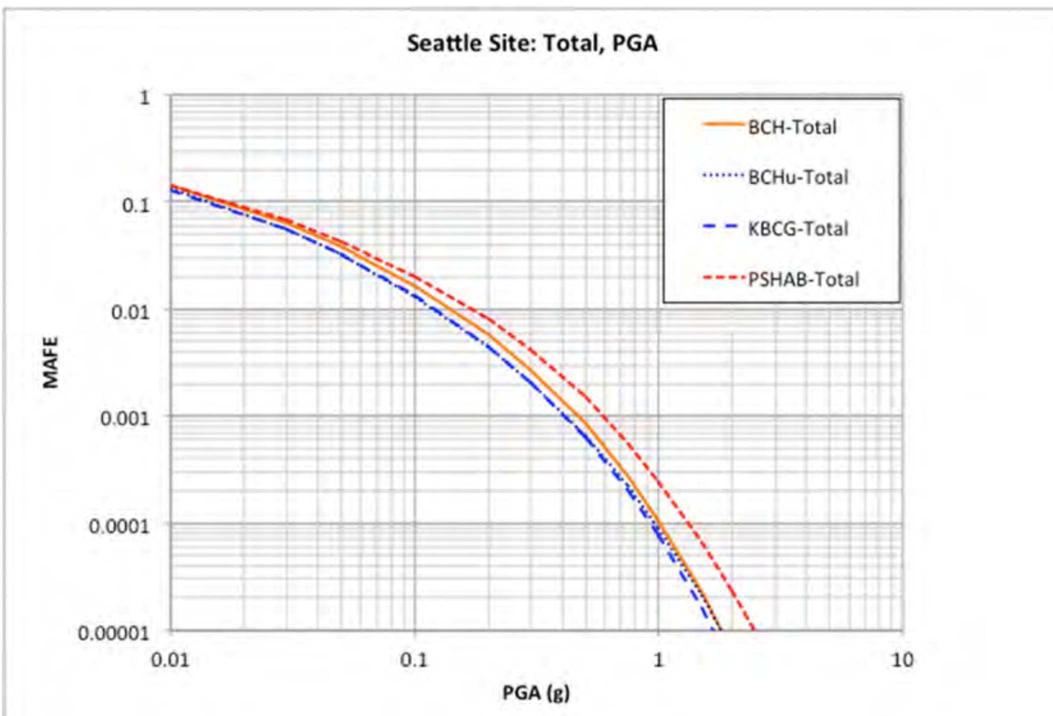

Figure 5.7 Comparison of the total hazard curve using BCH (solid orange line), BCHU (dotted line), KBCG (long dashed blue line), and PSHAB (short dashed red line) for the Seattle site for PGA (*T* = 0.01 sec).

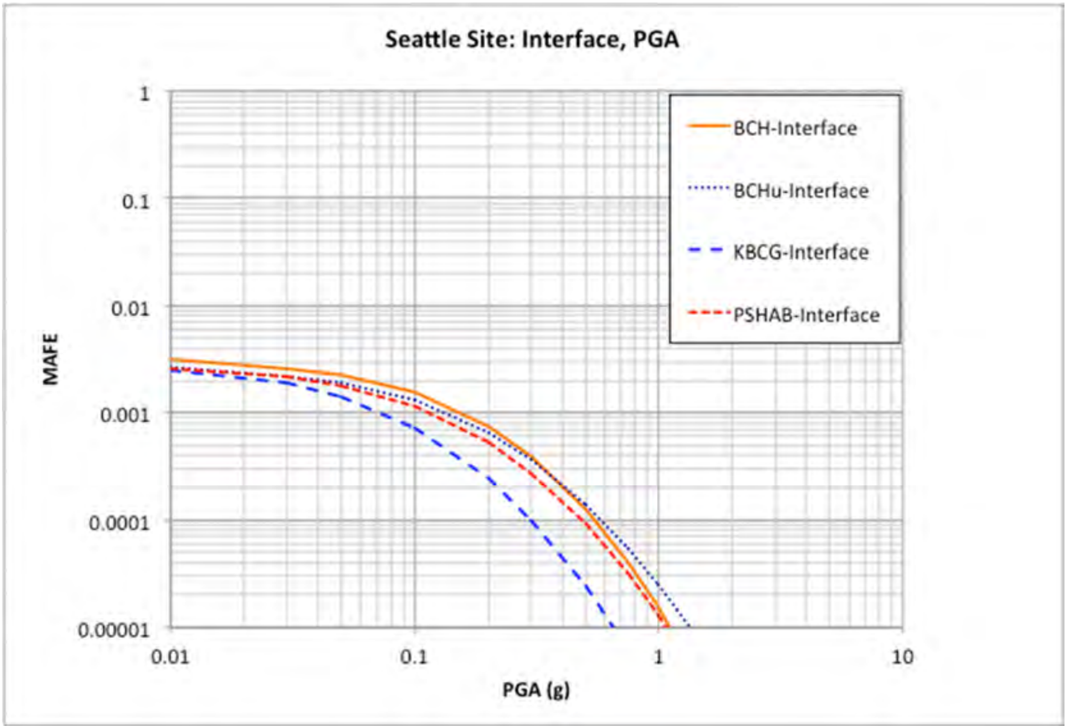

Figure 5.8 **Comparison of the interface hazard curve using BCH (solid orange line), BCHU (dotted line), KBCG (long dashed blue line), and PSHAB (short dashed red line) for the Seattle site for PGA (*T* = 0.01 sec).**

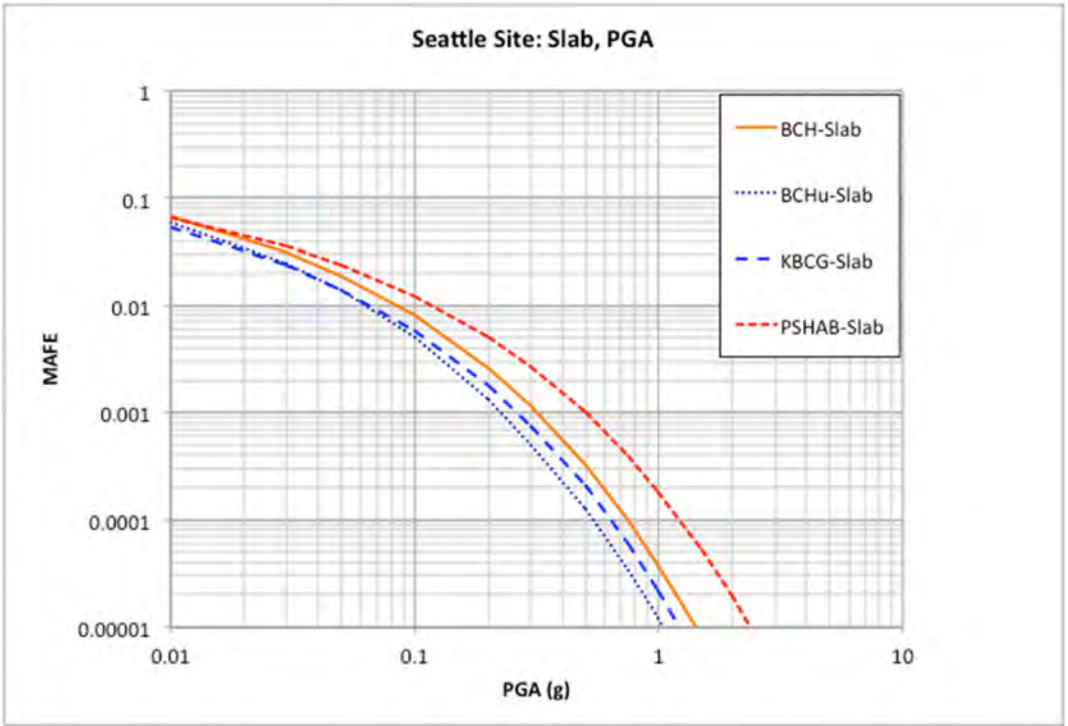

Figure 5.9 **Comparison of the slab hazard curve using BCH (solid orange line), BCHU (dotted line), KBCG (long dashed blue line), and PSHAB (short dashed red line) for the Seattle site for PGA (*T* = 0.01 sec).**

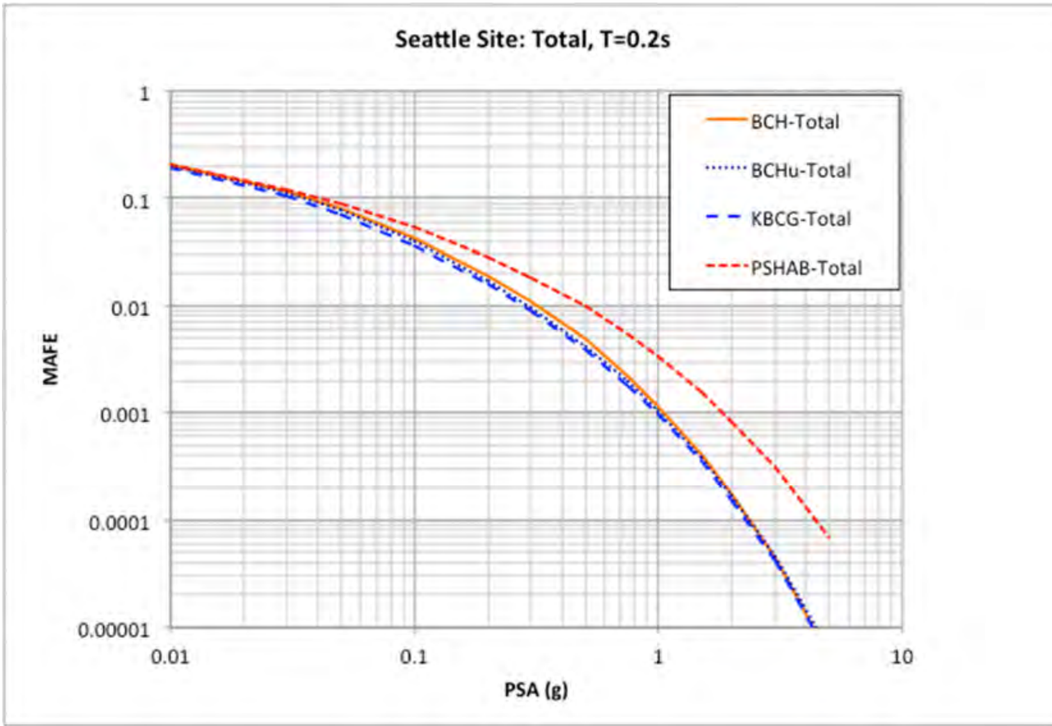

Figure 5.10 Comparison of the total hazard curve using BCH (solid orange line), BCHU (dotted line), KBCG (long dashed blue line), and PSHAB (short dashed red line) for the Seattle site for spectral period of *T* = 0.2 sec.

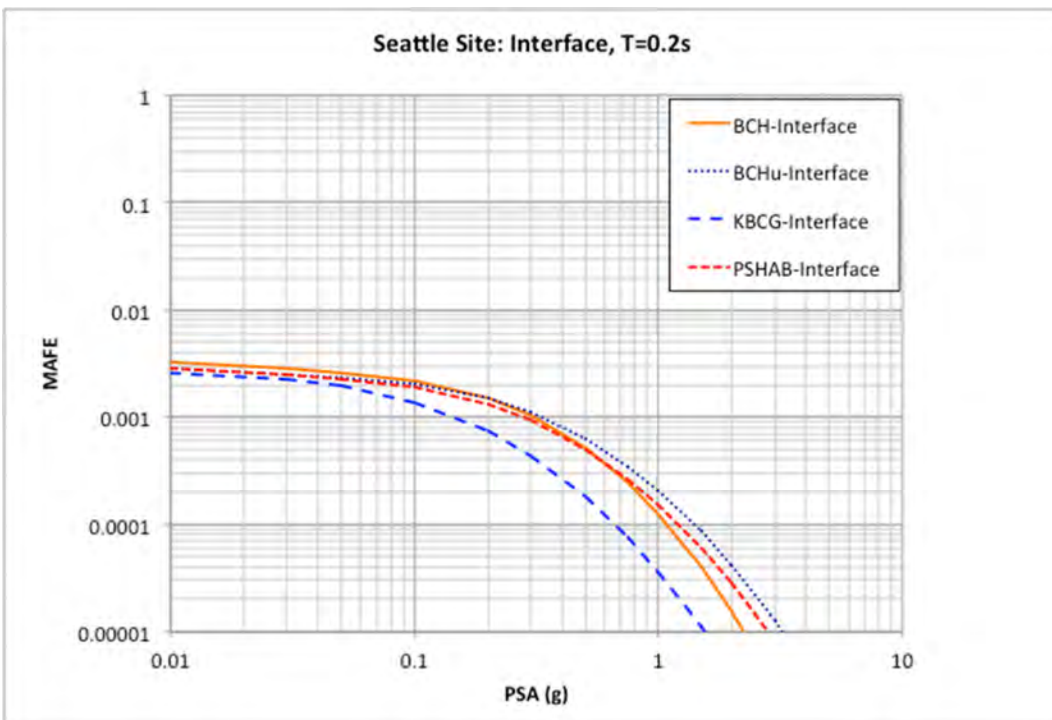

Figure 5.11 Comparison of the interface hazard curve using BCH (solid orange line), BCHU (dotted line), KBCG (long dashed blue line), and PSHAB (short dashed red line) for the Seattle site for spectral period of *T* = 0.2 sec.

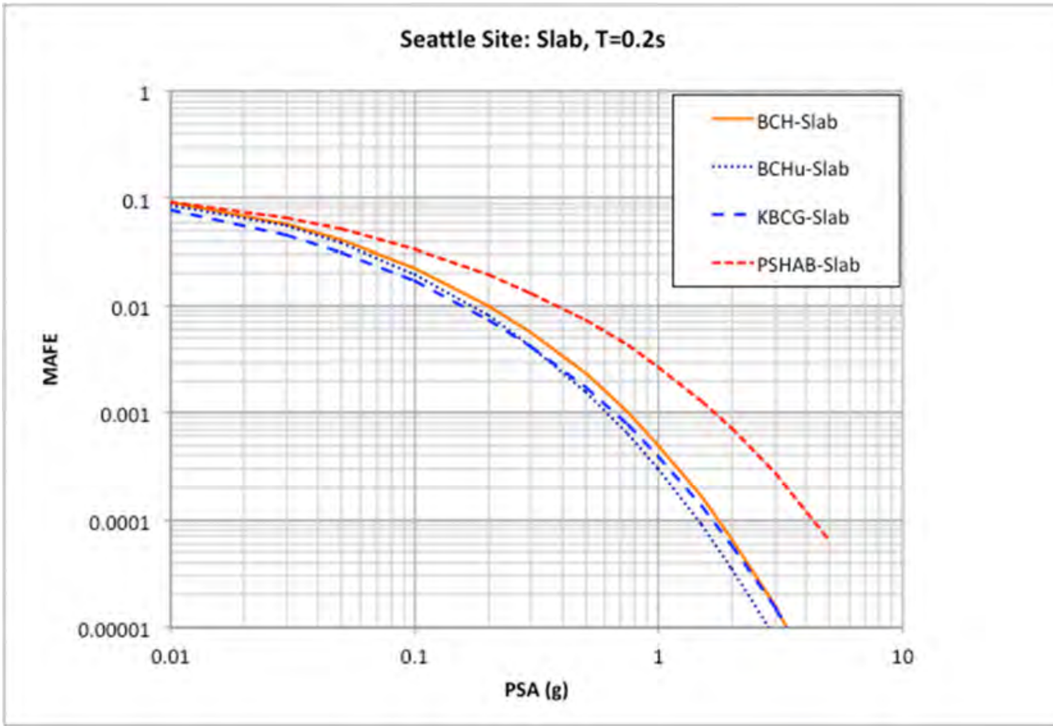

Figure 5.12 Comparison of the slab hazard curve using BCH (solid orange line), BCHU (dotted line), KBCG (long dashed blue line), and PSHAB (short dashed red line) for the Seattle site for spectral period of *T* = 0.2 sec.

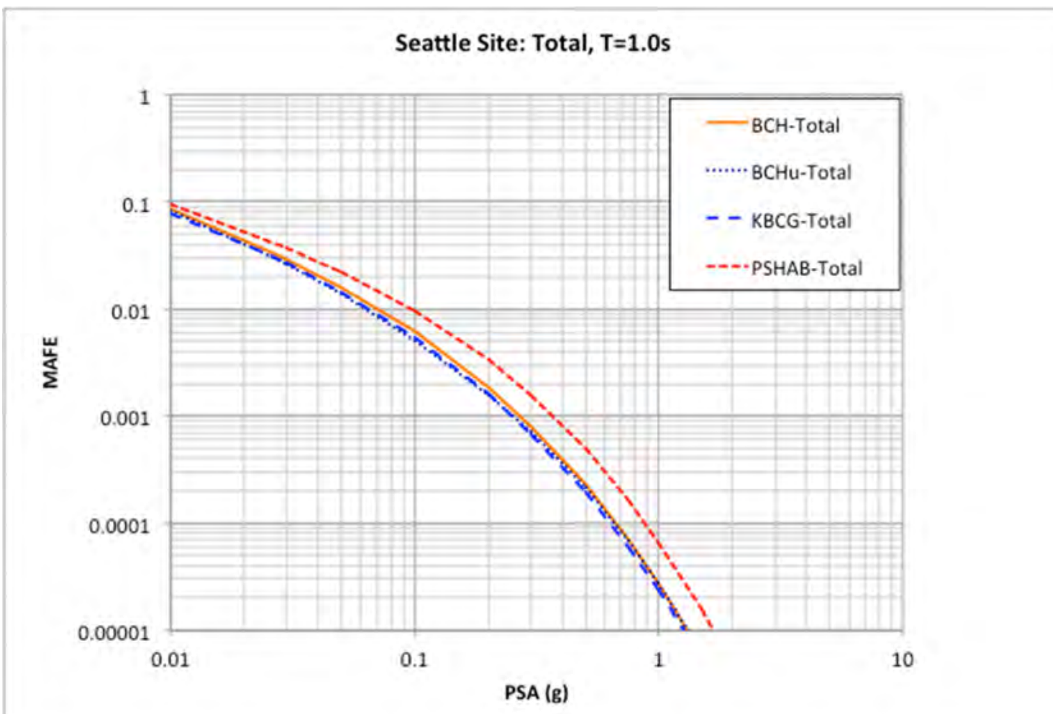

Figure 5.13 Comparison of the total hazard curve using BCH (solid orange line), BCHU (dotted line), KBCG (long dashed blue line), and PSHAB (short dashed red line) for the Seattle site for spectral period of *T* = 1.0 sec.

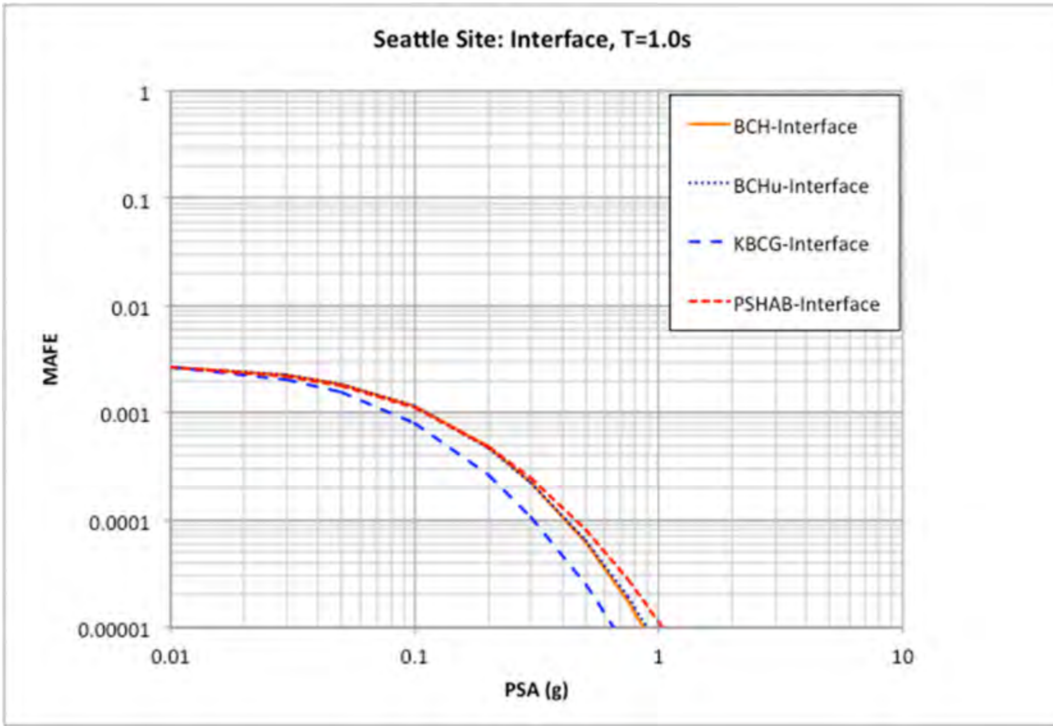

Figure 5.14 **Comparison of the interface hazard curve using BCH (solid orange line), BCHU (dotted line), KBCG (long dashed blue line), and PSHAB (short dashed red line) for the Seattle site for spectral period of *T* = 1.0 sec.**

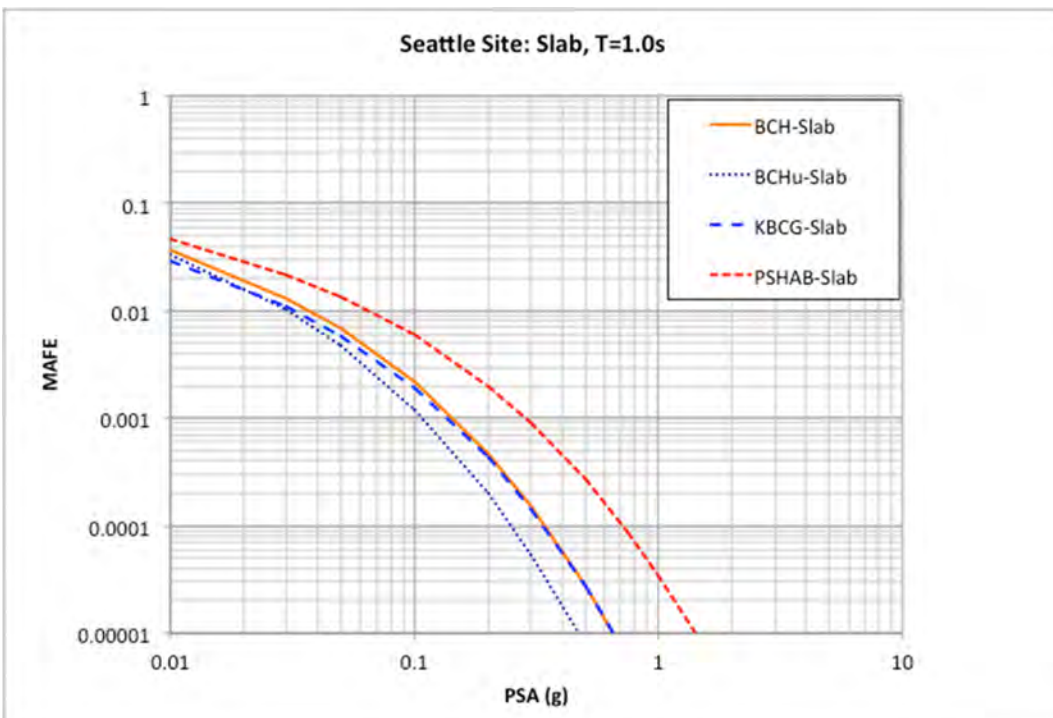

Figure 5.15 **Comparison of the slab hazard curve using BCH (solid orange line), BCHU (dotted line), KBCG (long dashed blue line), and PSHAB (short dashed red line) for the Seattle site for spectral period of *T* = 1.0 sec.**

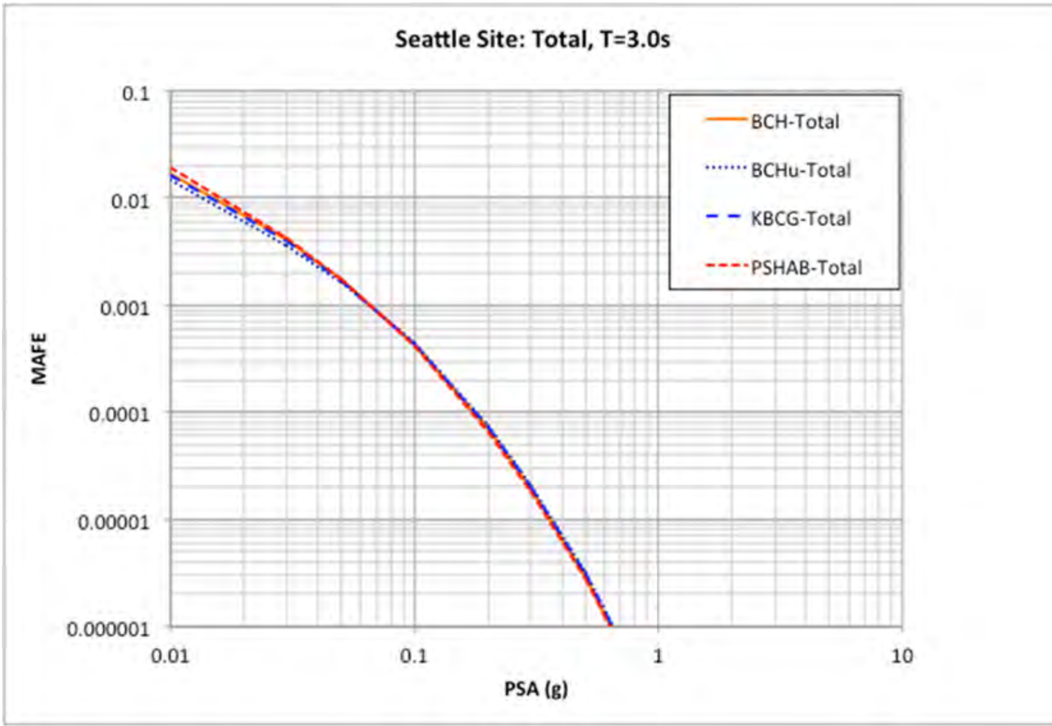

Figure 5.16 **Comparison of the total hazard curve using BCH (solid orange line), BCHU (dotted line), KBCG (long dashed blue line), and PSHAB (short dashed red line) for the Seattle site for spectral period of *T* = 3.0 sec.**

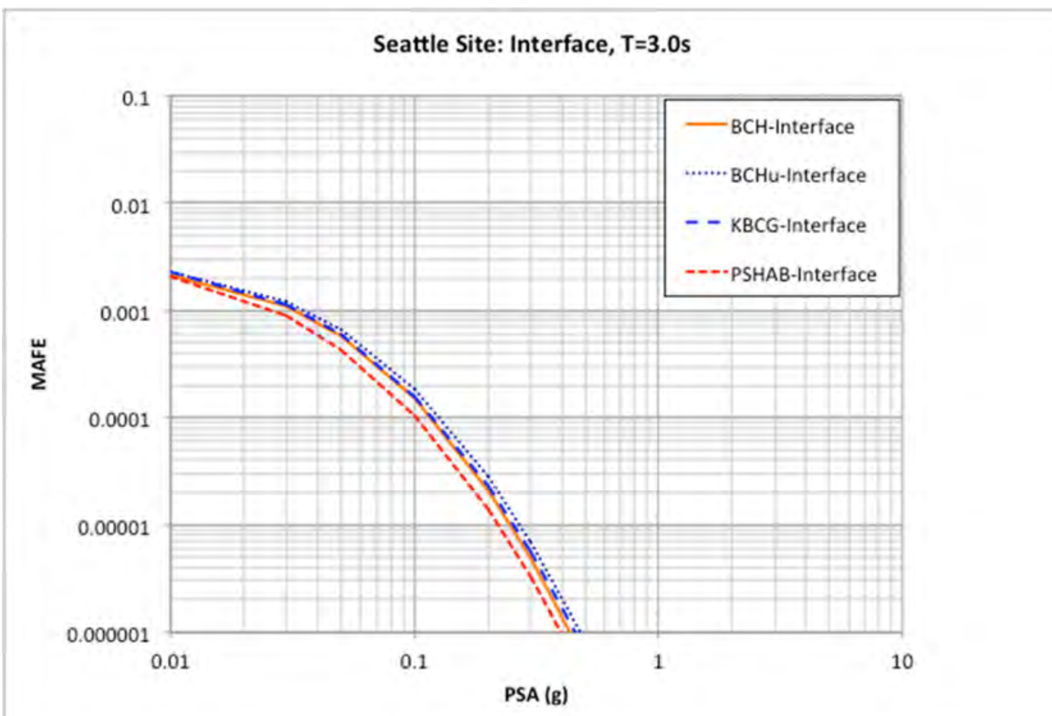

Figure 5.17 **Comparison of the interface hazard curve using BCH (solid orange line), BCHU (dotted line), KBCG (long dashed blue line), and PSHAB (short dashed red line) for the Seattle site for spectral period of *T* = 3.0 sec.**

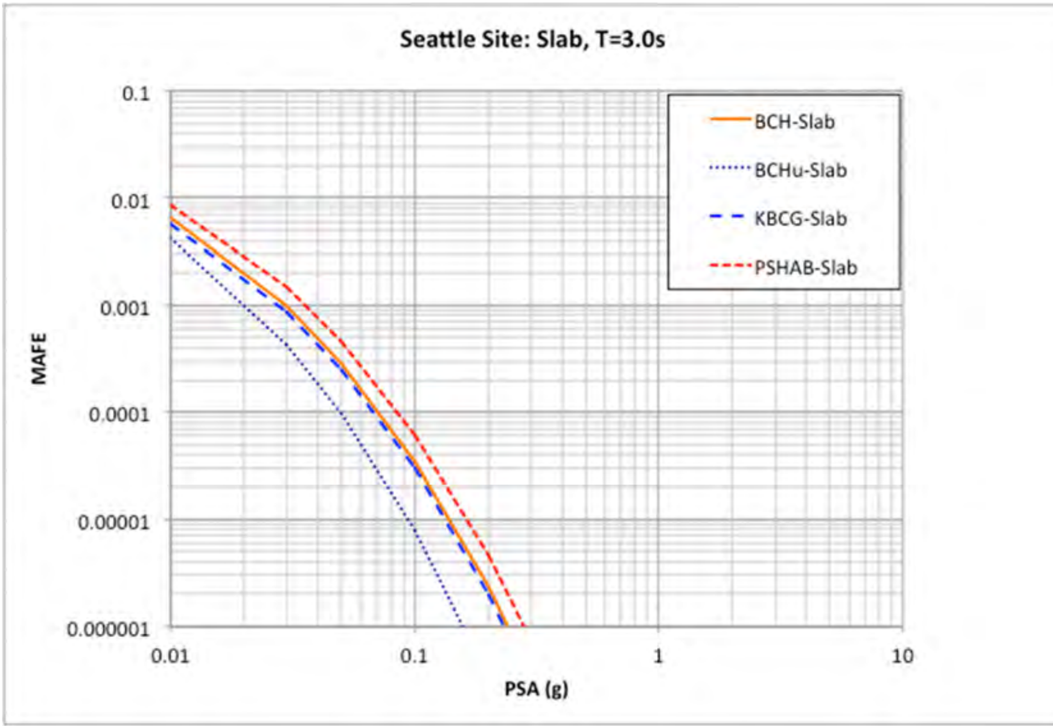

Figure 5.18 **Comparison of the slab hazard curve using BCH (solid orange line), BCHU (dotted line), KBCG (long dashed blue line), and PSHAB (short dashed red line) for the Seattle site for spectral period of *T* = 3.0 sec.**

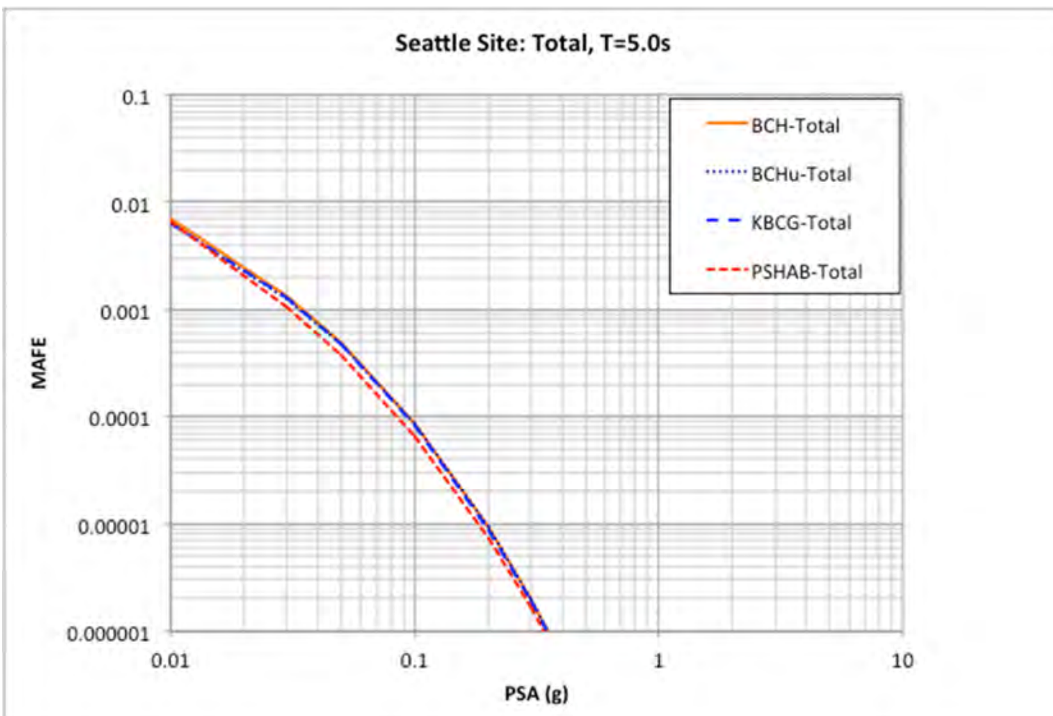

Figure 5.19 **Comparison of the total hazard curve using BCH (solid orange line), BCHU (dotted line), KBCG (long dashed blue line), and PSHAB (short dashed red line) for the Seattle site for spectral period of *T* = 5.0 sec.**

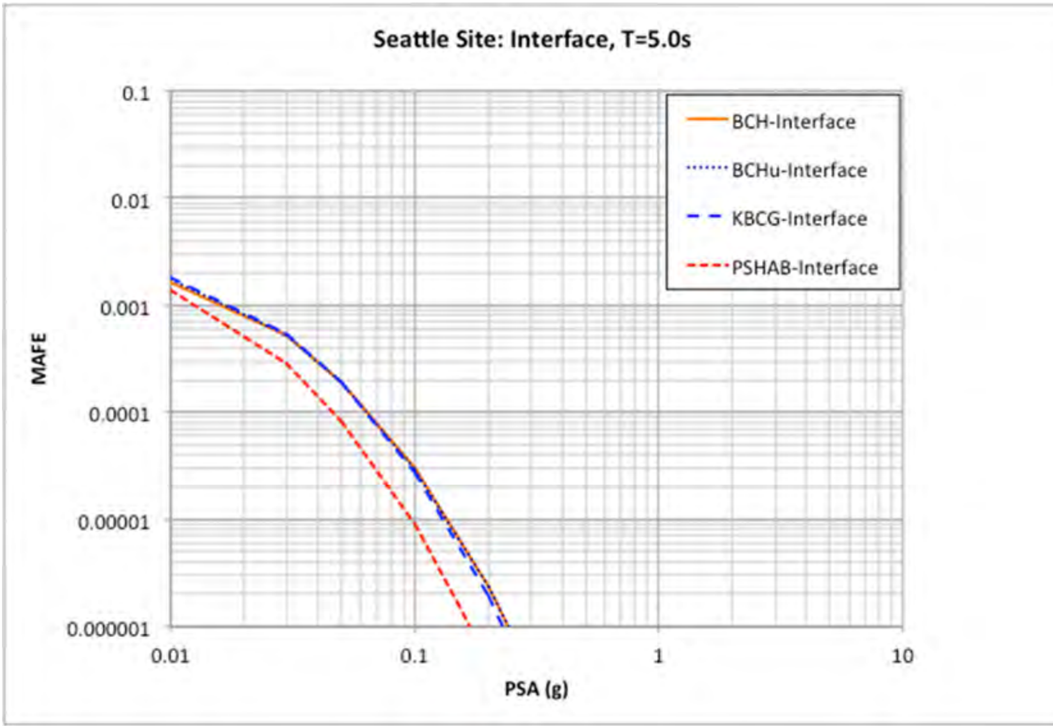

Figure 5.20 **Comparison of the interface hazard curve using BCH (solid orange line), BCHU (dotted line), KBCG (long dashed blue line), and PSHAB (short dashed red line) for the Seattle site for spectral period of *T* = 5.0 sec.**

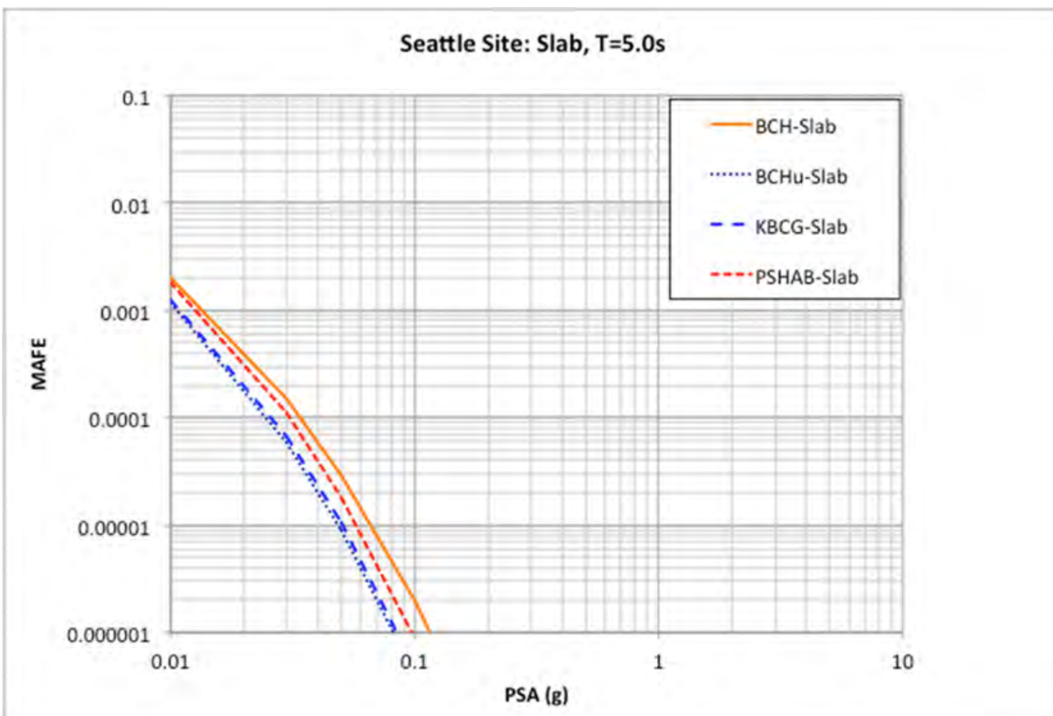

Figure 5.21 **Comparison of the slab hazard curve using BCH (solid orange line), BCHU (dotted line), KBCG (long dashed blue line), and PSHAB (short dashed red line) for the Seattle site for spectral period of *T* = 5.0 sec.**

The UHS ground motions for the suite of five return-period hazard levels consistent with the hazard curves plotted in the previous figures are listed in Table 5.3 through Table 5.6. The ground-motion results are plotted graphically in Figure 5.22 through Figure 5.26. As noted earlier, the largest difference in the ground motions is observed for the spectral period of 0.2 sec, with the results from the PSHAB model being higher by about 87% at the 10,000-year hazard level. Over all spectral periods and return period levels, the results from the PSHAB model are approximately 25% larger than the results from the BCH model. For the KBCG model, the average results are about 5% lower than the BCH model results.

Table 5.3 Ground motions for the mean total hazard at the Seattle site using the BCH subduction GMM for the subduction seismic sources.

Period (sec)	500-year PSA (*g*)	1000-year PSA (*g*)	2475-year PSA (*g*)	5000-year PSA (*g*)	10,000-year PSA (*g*)
PGA (0.010)	0.342	0.464	0.650	0.822	1.014
0.200	0.783	1.061	1.508	1.911	2.354
1.000	0.191	0.270	0.397	0.525	0.667
3.000	0.046	0.066	0.103	0.134	0.175
5.000	0.023	0.035	0.054	0.072	0.094

Table 5.4 Ground motions for the mean total hazard at the Seattle site using the BCHU subduction GMM for the subduction seismic sources.

Period (sec)	500-year PSA (*g*)	1000-year PSA (*g*)	2475-year PSA (*g*)	5000-year PSA (*g*)	10,000-year PSA (*g*)
PGA (0.010)	0.303	0.415	0.600	0.775	0.968
0.200	0.737	1.018	1.470	1.889	2.355
1.000	0.174	0.252	0.381	0.512	0.656
3.000	0.044	0.065	0.103	0.136	0.179
5.000	0.022	0.034	0.053	0.071	0.093

Table 5.5 Ground motions for the mean total hazard at the Seattle site using the KBCG subduction GMM for the subduction seismic sources.

Period (sec)	500-year PSA (*g*)	1000-year PSA (*g*)	2475-year PSA (*g*)	5000-year PSA (*g*)	10,000-year PSA (*g*)
PGA (0.010)	0.302	0.408	0.583	0.748	0.923
0.200	0.710	0.986	1.421	1.829	2.282
1.000	0.176	0.250	0.371	0.494	0.630
3.000	0.046	0.066	0.103	0.135	0.176
5.000	0.022	0.034	0.053	0.070	0.092

Table 5.6 Ground motions for the mean total hazard at the Seattle site using the PSHAB subduction GMM for the subduction seismic sources.

Period (sec)	500-year PSA (*g*)	1000-year PSA (*g*)	2475-year PSA (*g*)	5000-year PSA (*g*)	10,000-year PSA (*g*)
PGA (0.010)	0.430	0.588	0.838	1.066	1.322
0.200	1.313	1.840	2.678	3.469	4.405
1.000	0.263	0.366	0.536	0.693	0.874
3.000	0.047	0.066	0.101	0.131	0.171
5.000	0.021	0.031	0.048	0.064	0.084

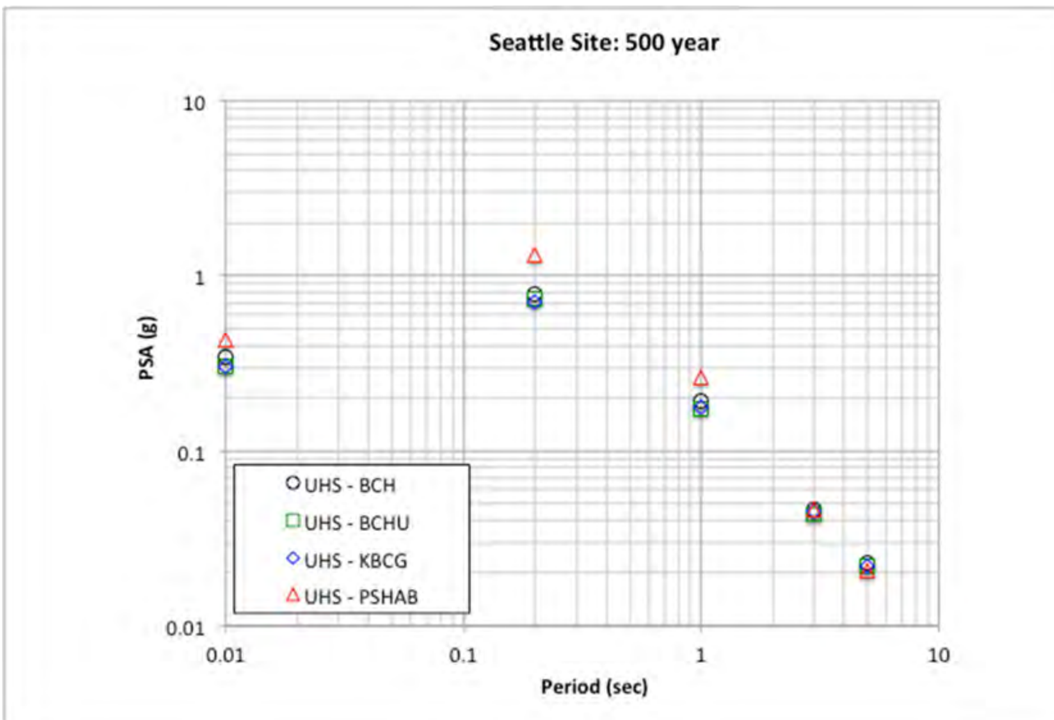

Figure 5.22 Comparison of UHS ground motions for the Seattle site based on the four separate subduction GMMs for the subduction seismic sources at the 500-year-return-period hazard level.

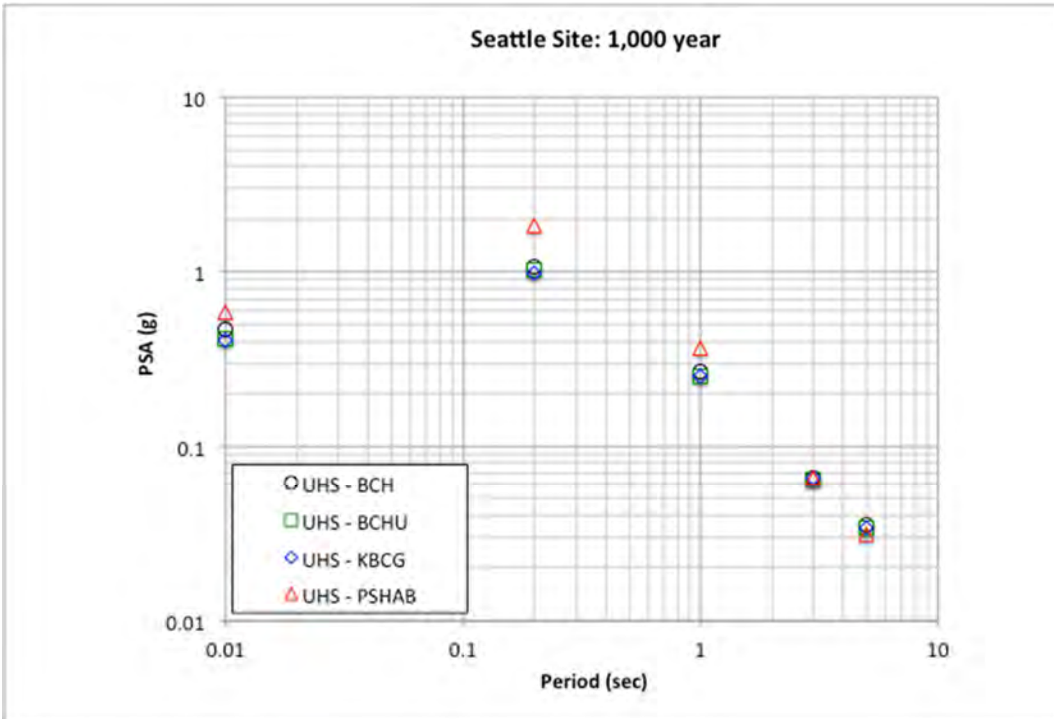

Figure 5.23 **Comparison of UHS ground motions for the Seattle site based on the four separate subduction GMMs for the subduction seismic sources at the 1000-year-return-period hazard level.**

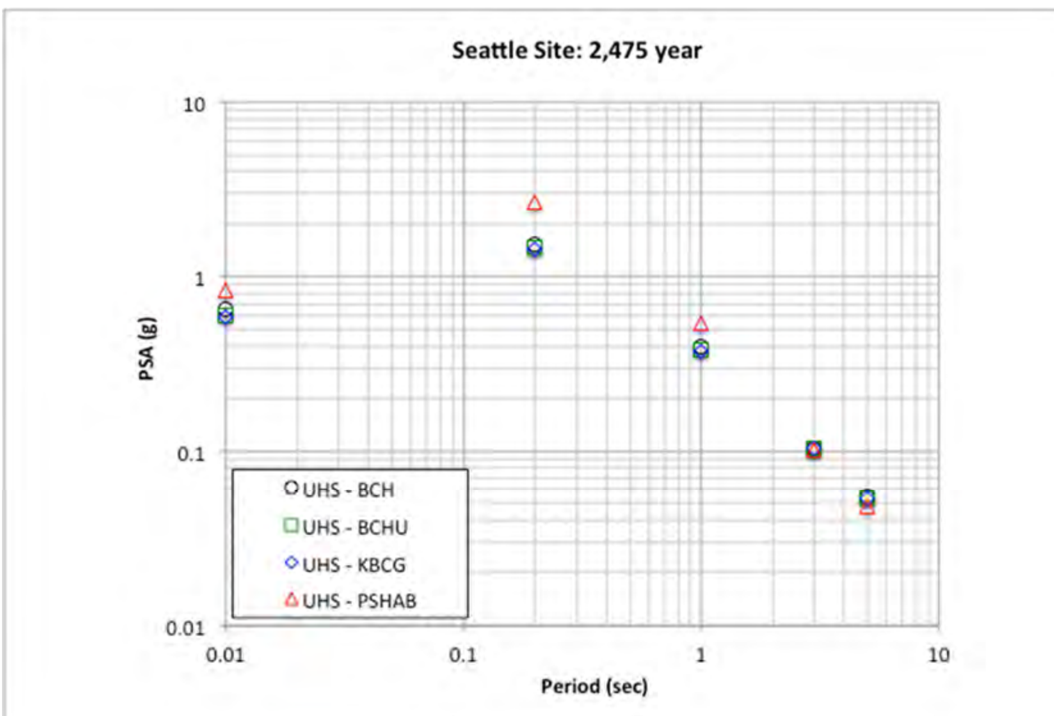

Figure 5.24 **Comparison of UHS ground motions for the Seattle site based on the four separate subduction GMMs for the subduction seismic sources at the 2475-year-return-period hazard level.**

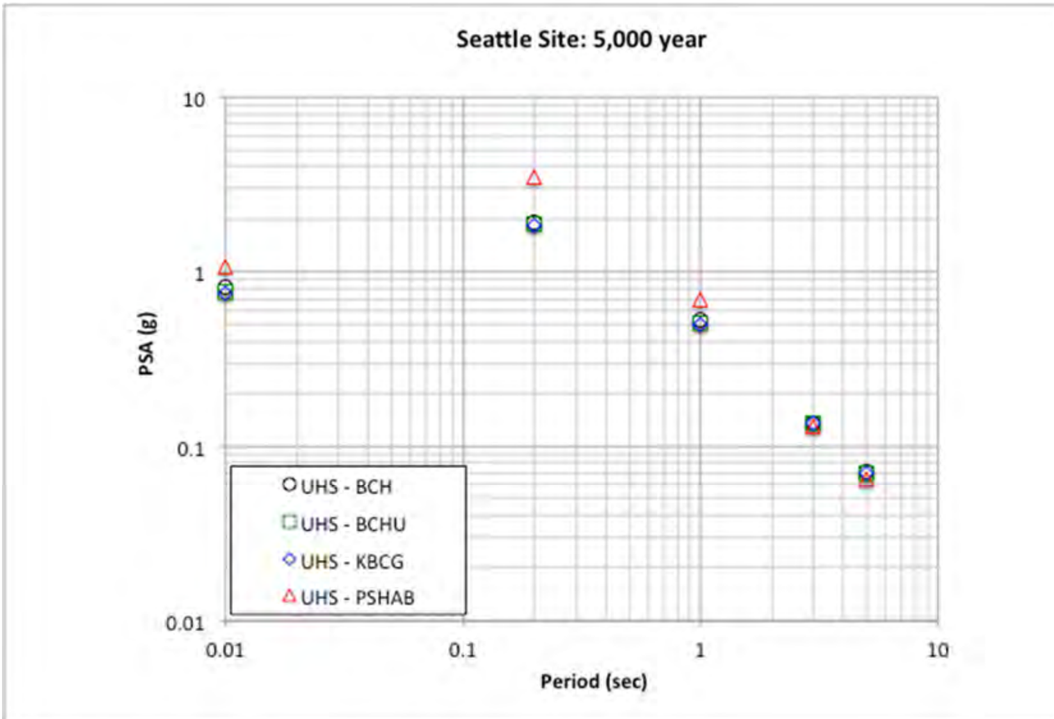

Figure 5.25 Comparison of UHS ground motions for the Seattle site based on the four separate subduction GMMs for the subduction seismic sources at the 5000-year-return-period hazard level.

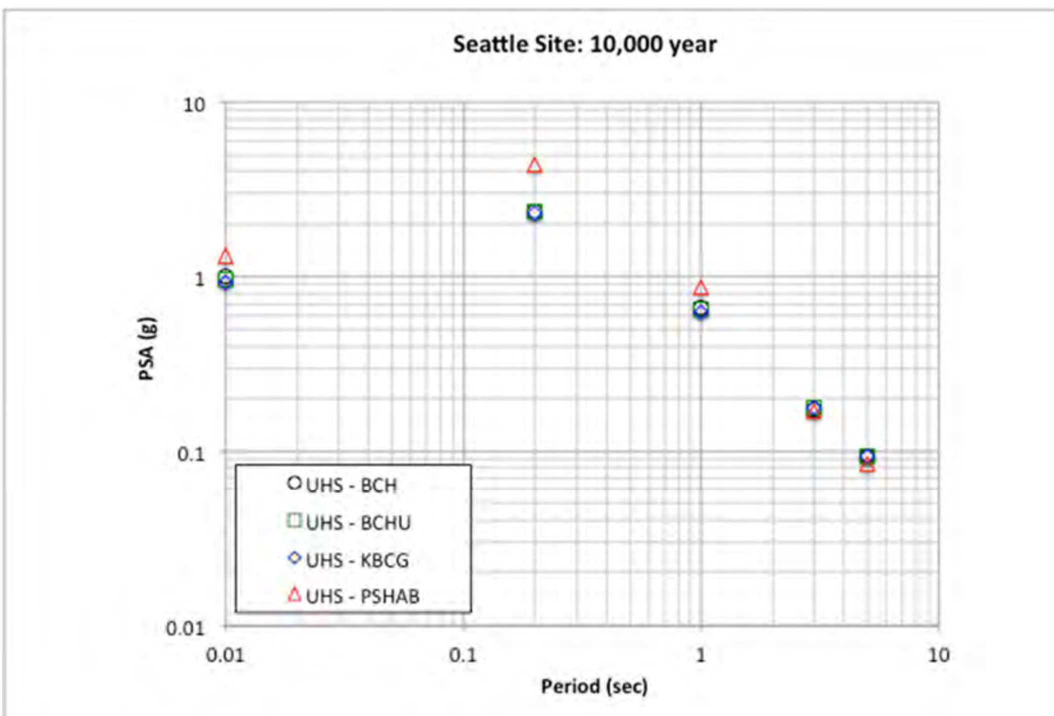

Figure 5.26 Comparison of UHS ground motions for the Seattle site based on the four separate subduction GMMs for the subduction seismic sources at the 10,000-year-return-period hazard level.

The binned deaggregation results are summarized in Figure 5.27 through Figure 5.36 for the four subduction GMMs and for the return periods of 500 and 2475 years. These results show the contribution from the three controlling sources: (1) crustal faults for shorter distances and small to moderate magnitudes; (2) slab events with distances greater than 100 km and intermediate magnitudes; and (3) larger magnitude interface events at larger distances. Similar results and observations are noted for the other return-period levels. These plots are consistent with the previous hazard curve plots showing similar results for the BCH, BCHU, and KBCG models and an increase in contribution for slab events from the PSHAB model for PGA, 0.2, and 1.0 sec spectral periods.

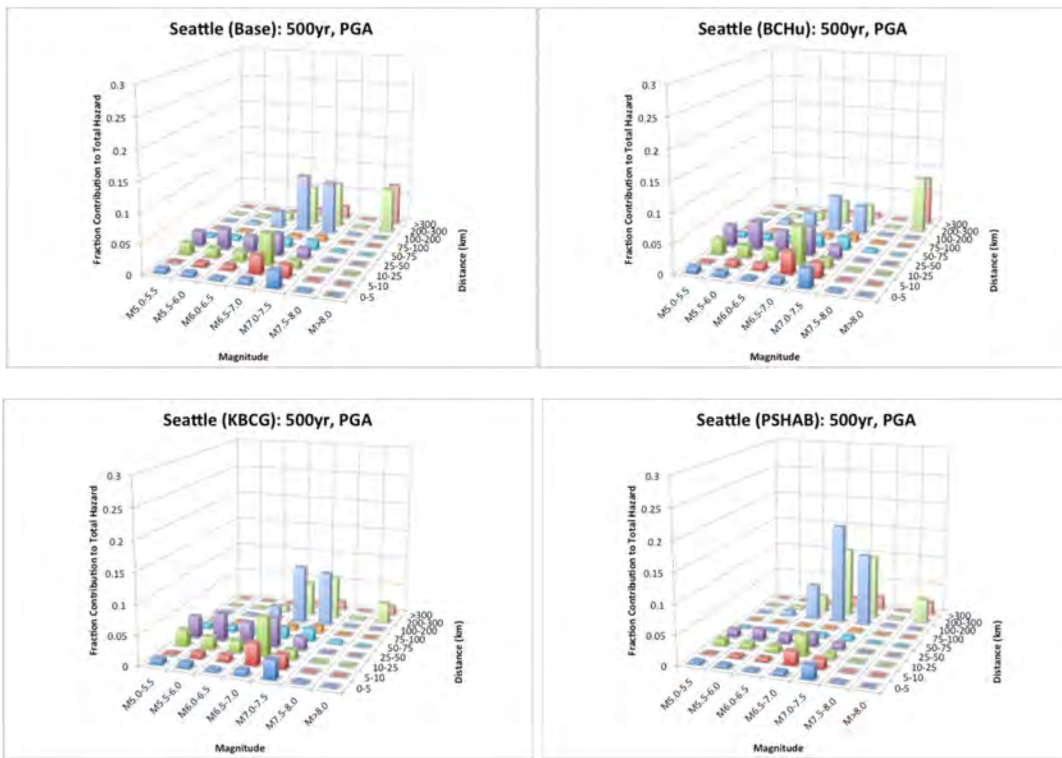

Figure 5.27 Binned deaggregation results for the Seattle site at the 500 year return period level for PGA (*T* = 0.01 sec) for the BCH (upper left), BCHU (upper right), KBCG (lower left) and PSHAB (lower right) models.

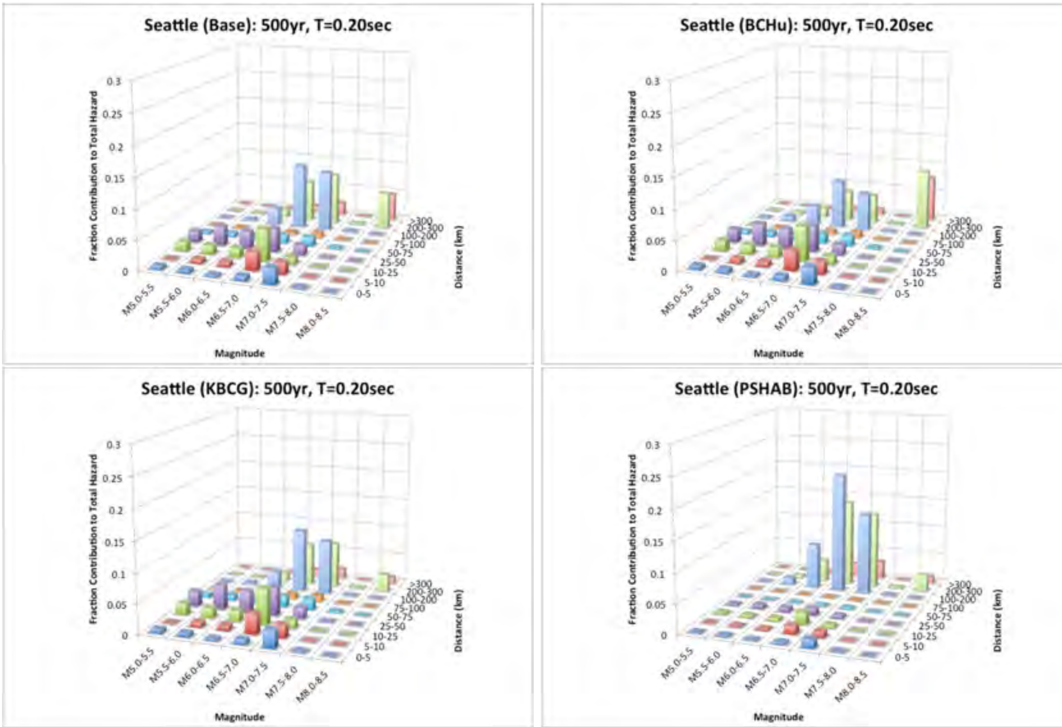

Figure 5.28 **Binned deaggregation results for the Seattle site at the 500 year return period level for *T* = 0.2 sec for the BCH (upper left), BCHU (upper right), KBCG (lower left), and PSHAB (lower right) models.**

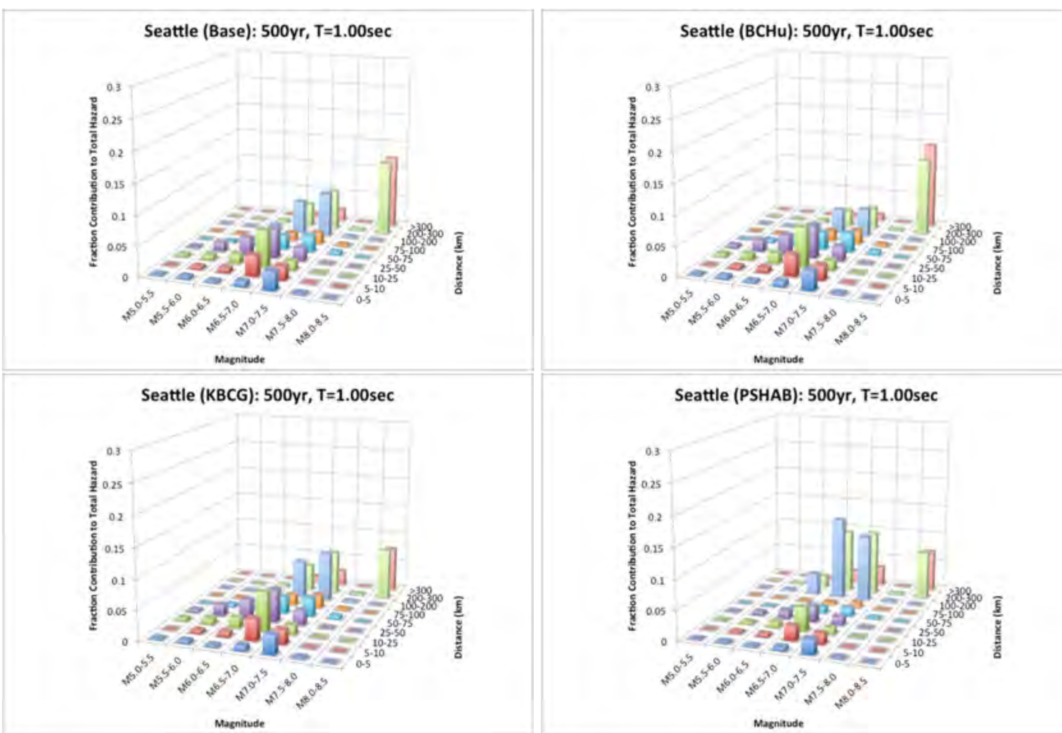

Figure 5.29 **Binned deaggregation results for the Seattle site at the 500 year return period level for *T* = 1.0 sec for the BCH (upper left), BCHU (upper right), KBCG (lower left), and PSHAB (lower right) models.**

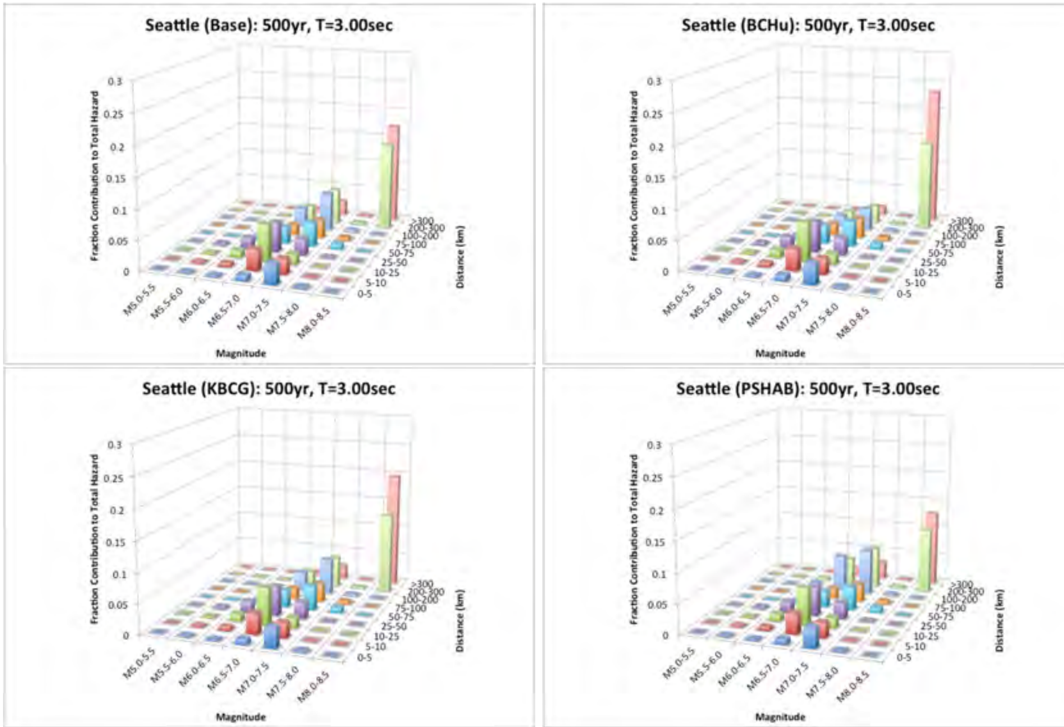

Figure 5.30 Binned deaggregation results for the Seattle site at the 500 year return period level for T = 3.0 sec for the BCH (upper left), BCHU (upper right), KBCG (lower left), and PSHAB (lower right) models.

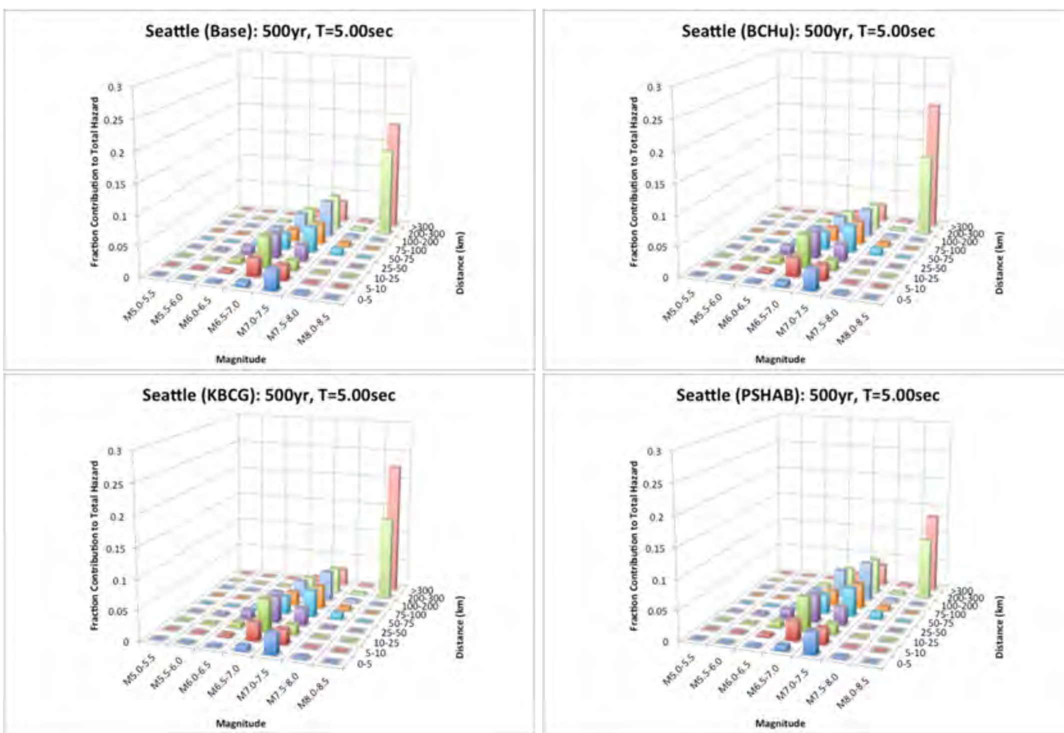

Figure 5.31 Binned deaggregation results for the Seattle site at the 500 year return period level for T = 5.0 sec for the BCH (upper left), BCHU (upper right), KBCG (lower left), and PSHAB (lower right) models.

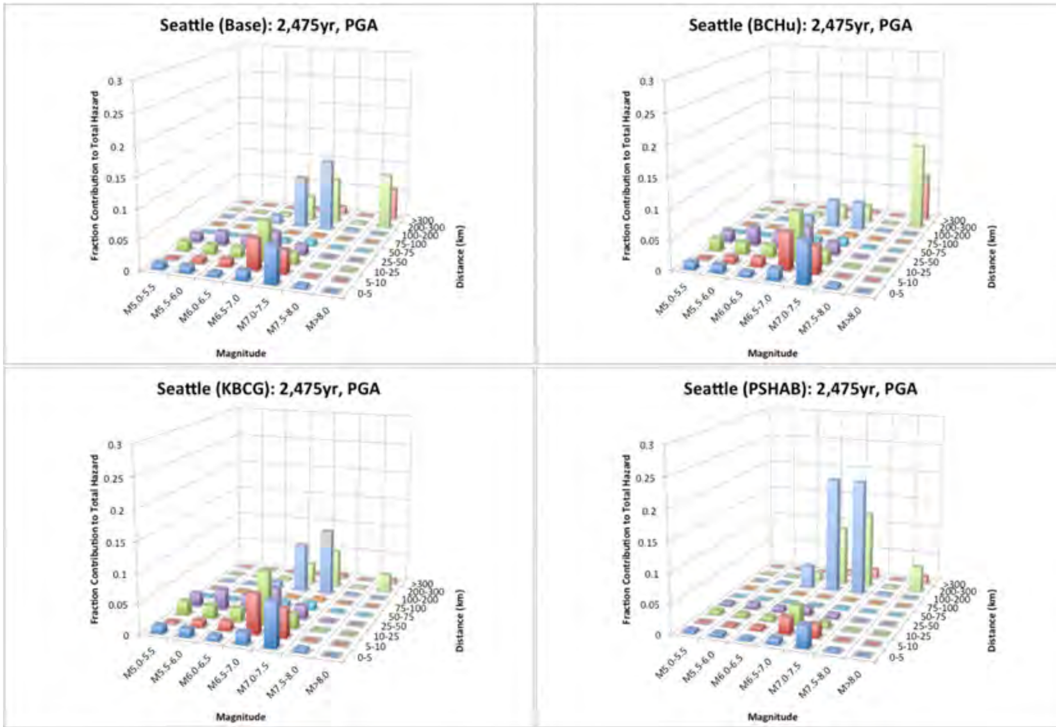

Figure 5.32 **Binned deaggregation results for the Seattle site at the 2475-year-return-period level for PGA (*T* = 0.01 sec) for the BCH (upper left), BCHU (upper right), KBCG (lower left), and PSHAB (lower right) models.**

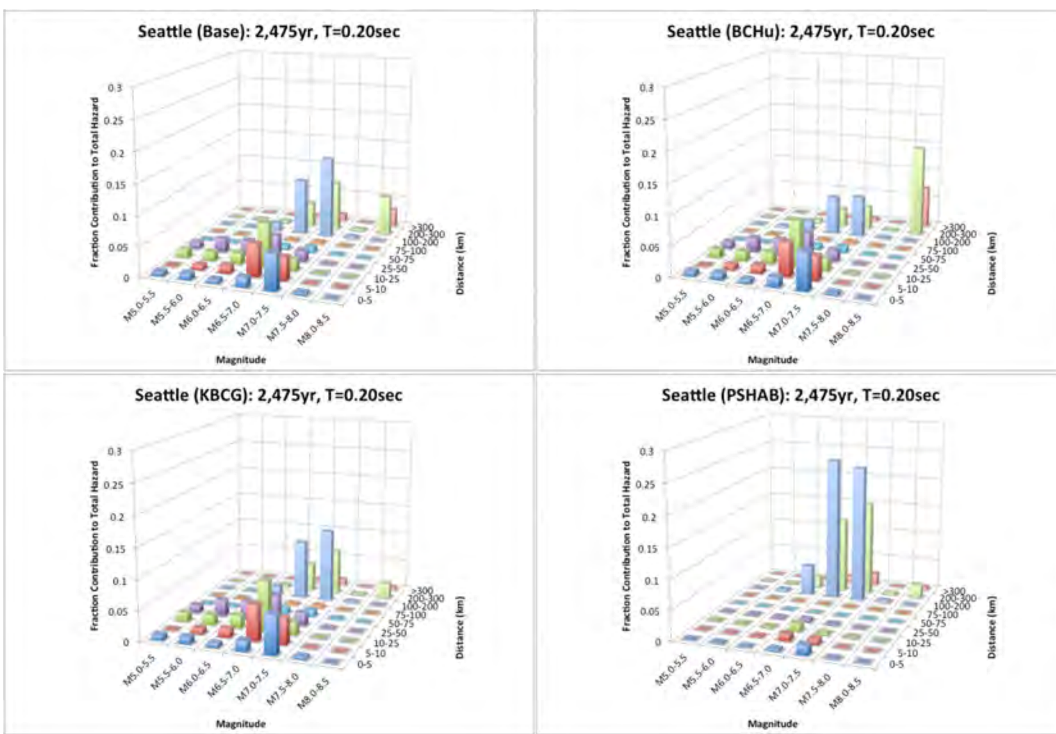

Figure 5.33 **Binned deaggregation results for the Seattle site at the 2475-year-return-period level for *T* = 0.2 sec for the BCH (upper left), BCHU (upper right), KBCG (lower left), and PSHAB (lower right) models.**

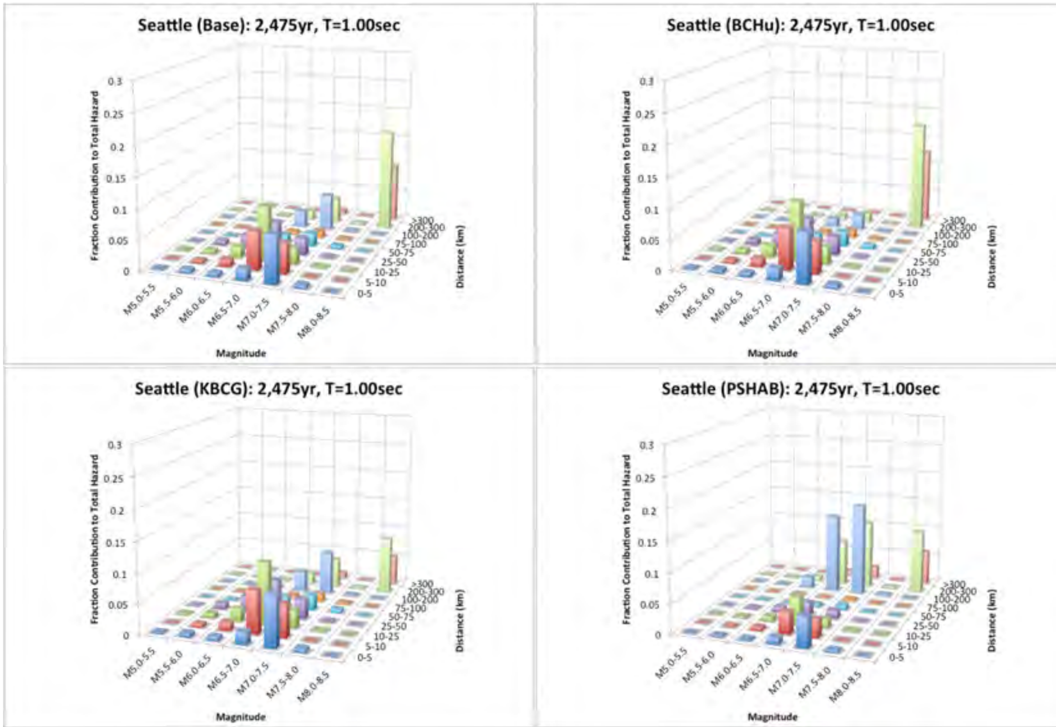

Figure 5.34 **Binned deaggregation results for the Seattle site at the 2475-year-return-period level for *T* = 1.0 sec for the BCH (upper left), BCHU (upper right), KBCG (lower left), and PSHAB (lower right) models.**

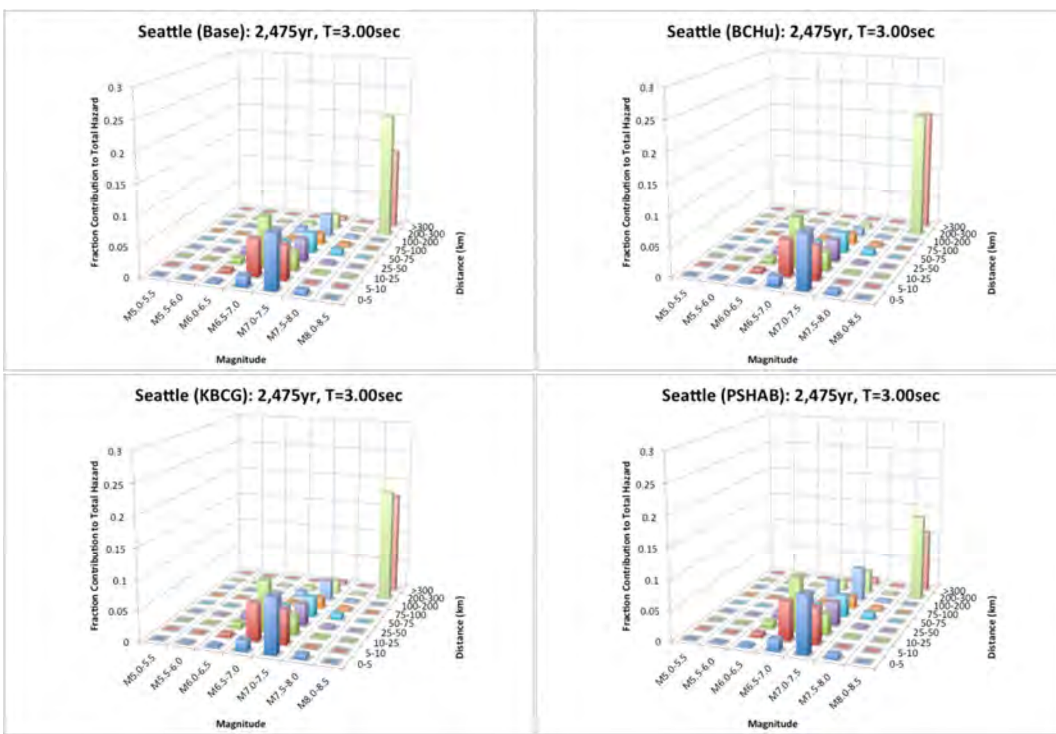

Figure 5.35 **Binned deaggregation results for the Seattle site at the 2475-year-return-period level for *T* = 3.0 sec for the BCH (upper left), BCHU (upper right), KBCG (lower left), and PSHAB (lower right) models.**

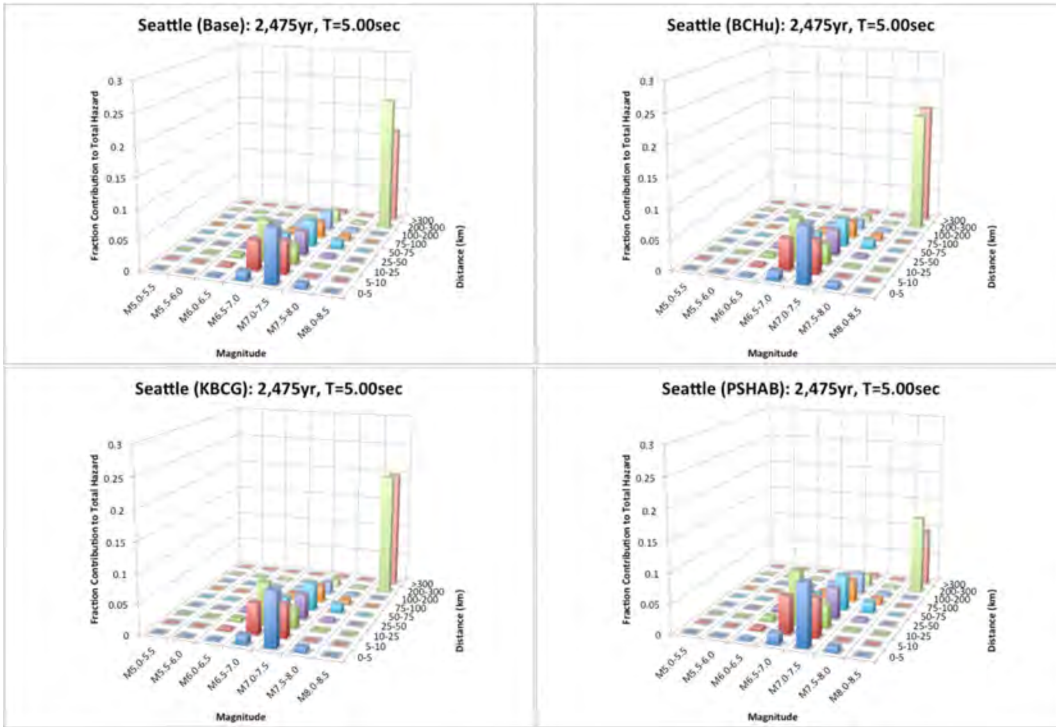

Figure 5.36 Binned deaggregation results for the Seattle site at the 2475-year-return-period level for *T* = 5.0 sec for the BCH (upper left), BCHU (upper right), KBCG (lower left), and PSHAB (lower right) models.

An addition set of PSHA calculations is performed to isolate the impact of the median ground-motion differences between the four subduction GMMs. For these calculations, the aleatory sigma model from the BCH model is applied with the median ground-motion estimates from the other three GMMs. Given this approach, the observed differences are fully attributable to the differences in the median ground-motion estimates. The resulting UHS ground motions are listed in Table 5.7 through

Table 5.9 for the three GMMs (note that the base case UHS ground-motion results based on the BCH model are listed in Table 5.3). Overall, the observed differences are less for the three models than those observed using both the median and aleatory sigma adjustments from the three subduction GMMs. The average reduction in ground motions for the BCHU and KBCG models is about 7%; however, the PSHAB model shows an observed average increase of about 16%, with the largest increase (i.e., approximately 55%) occurring for the *T* = 0.2 sec spectral periods. The ground-motion values are plotted in Figure 5.37 through Figure 5.41.

Table 5.7 Ground motions for the mean total hazard at the Seattle site using the BCHU subduction GMM with BCH aleatory sigma for the subduction seismic sources.

Period (sec)	500-year PSA (*g*)	1000-year PSA (*g*)	2475-year PSA (*g*)	5000-year PSA (*g*)	10,000-year PSA (*g*)
PGA (0.010)	0.281	0.384	0.556	0.714	0.887
0.200	0.689	0.951	1.362	1.749	2.183
1.000	0.171	0.248	0.374	0.503	0.643
3.000	0.043	0.064	0.102	0.133	0.174
5.000	0.021	0.033	0.052	0.069	0.091

Table 5.8 Ground motions for the mean total hazard at the Seattle site using the KBCG subduction GMM with BCH aleatory sigma for the subduction seismic sources.

Period (sec)	500-year PSA (*g*)	1000-year PSA (*g*)	2475-year PSA (*g*)	5000-year PSA (*g*)	10,000-year PSA (*g*)
PGA (0.010)	0.295	0.398	0.569	0.728	0.899
0.200	0.662	0.915	1.313	1.692	2.119
1.000	0.172	0.244	0.362	0.482	0.616
3.000	0.044	0.064	0.100	0.131	0.170
5.000	0.022	0.034	0.053	0.070	0.092

Table 5.9 Ground motions for the mean total hazard at the Seattle site using the PSHAB subduction GMM with BCH aleatory sigma for the subduction seismic sources.

Period (sec)	500-year PSA (*g*)	1000-year PSA (*g*)	2475-year PSA (*g*)	5000-year PSA (*g*)	10,000-year PSA (*g*)
PGA (0.010)	0.409	0.557	0.784	0.989	1.208
0.200	1.203	1.655	2.346	3.011	3.701
1.000	0.244	0.336	0.484	0.616	0.775
3.000	0.045	0.064	0.097	0.127	0.165
5.000	0.021	0.031	0.048	0.064	0.084

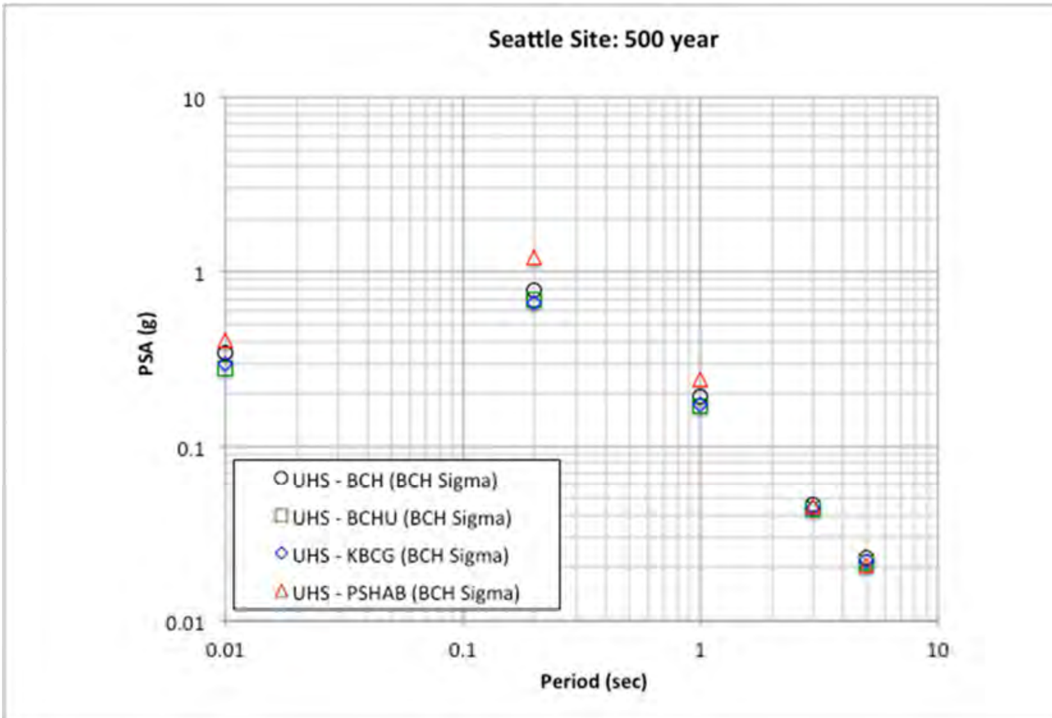

Figure 5.37 **Comparison of UHS ground motions for the Seattle site based on the four separate subduction GMMs, with the BCH aleatory sigma model for the subduction seismic sources at the 500-year-return-period hazard level.**

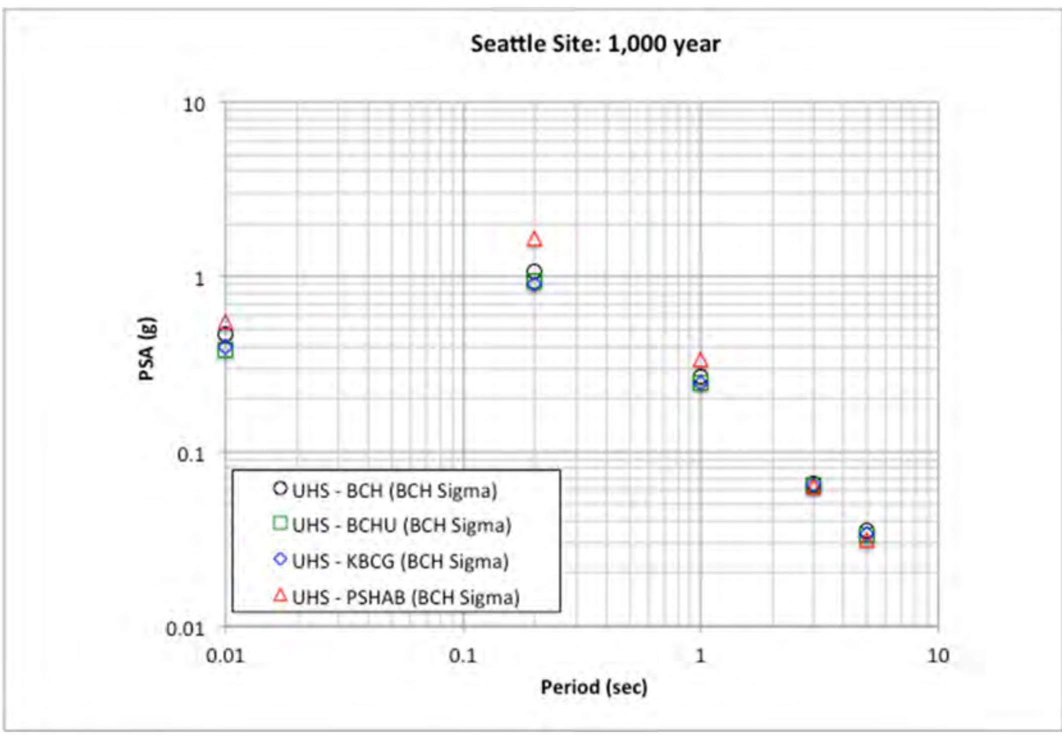

Figure 5.38 **Comparison of UHS ground motions for the Seattle site based on the four separate subduction GMMs, with the BCH aleatory sigma model for the subduction seismic sources at the 1000-year-return-period hazard level.**

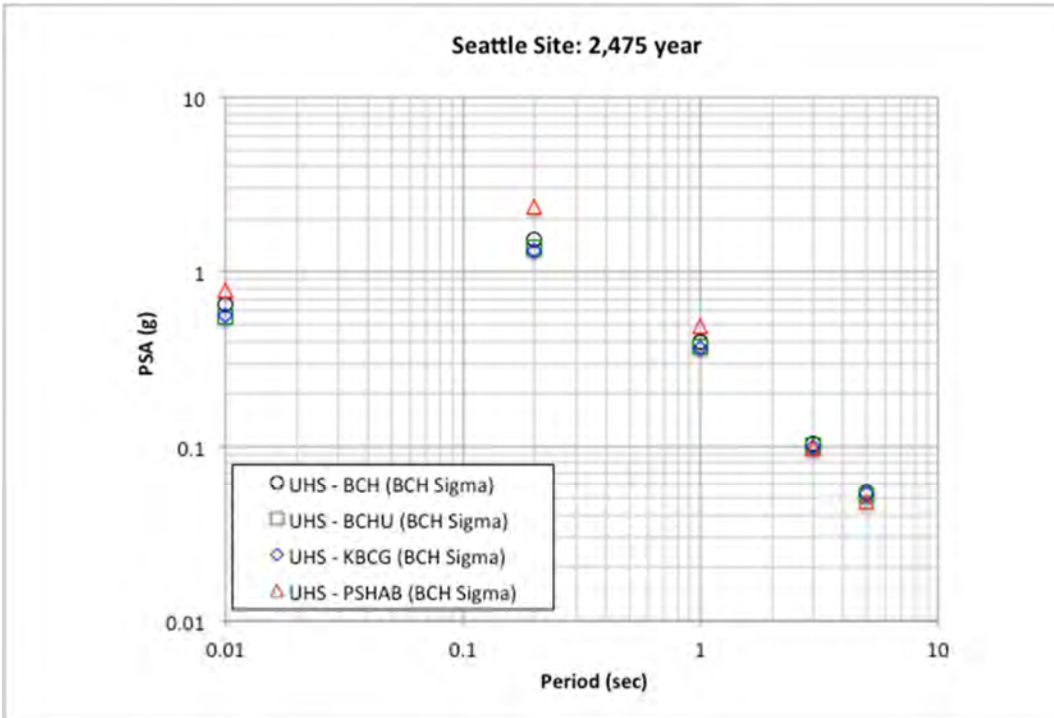

Figure 5.39 **Comparison of UHS ground motions for the Seattle site based on the four separate subduction GMMs, with the BCH aleatory sigma model for the subduction seismic sources at the 2475-year-return-period hazard level.**

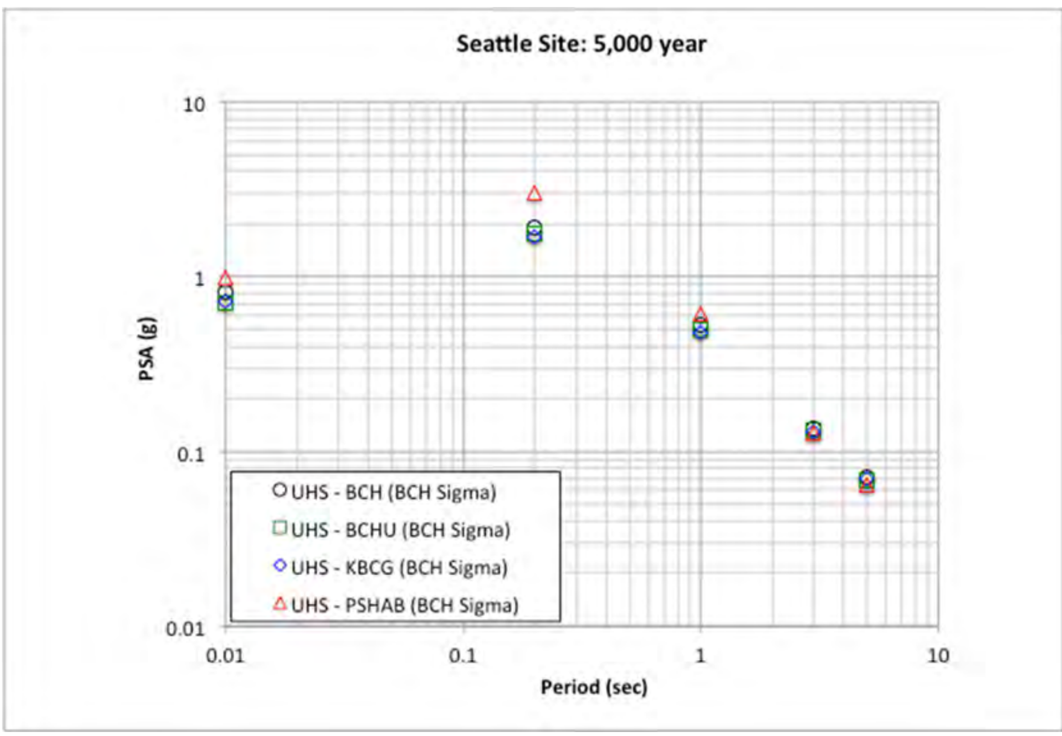

Figure 5.40 **Comparison of UHS ground motions for the Seattle site based on the four separate subduction GMMs for the subduction seismic sources at the 5000-year-return-period hazard level.**

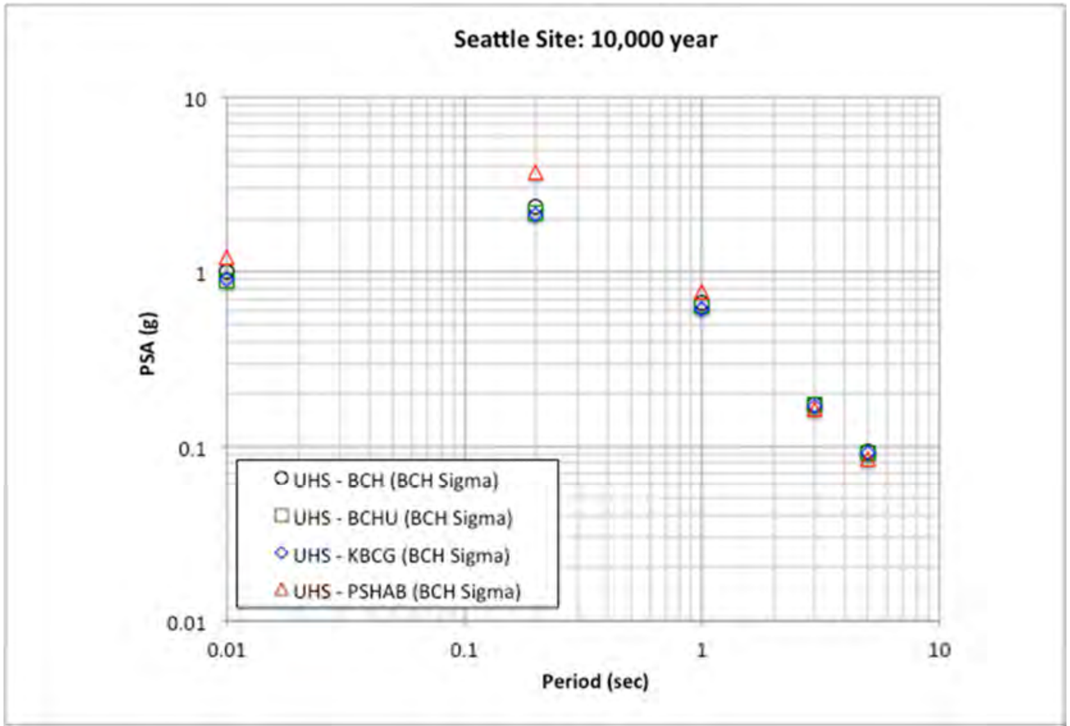

Figure 5.41 **Comparison of UHS ground motions for the Seattle site based on the four separate subduction GMMs, with the BCH aleatory sigma model for the subduction seismic sources at the 10,000-year-return-period hazard level.**

5.2 CENTRALIA SITE EXAMPLE PSHA

The city of Centralia was selected for the second example PSHA calculation; see Figure 5.1. This location is more distant from any crustal fault than the Seattle site and is closer to the coast of Washington where the contribution from the Cascadia interface source can be expected to be larger than the contribution from the deeper slab events. This assumption is observed in the hazard curves for the base case (i.e., BCH subduction GMM) plotted in Figure 5.42 through Figure 5.46. In each of these plots, the contribution from the seismic sources are separated by the Seattle fault (dotted line), combined other crustal faults (long dashed green line), combined background gridded seismicity (short dashed line), slab sources (solid blue line), and interface source (solid green line). For return periods shorter than about 1000 years for PGA and $T = 0.2$ sec, the slab source is the controlling seismic source. For longer return periods, the Cascadia interface source controls. At the longer spectral periods of 1.0, 3.0, and 5.0 sec, the total hazard is controlled by the Cascadia interface source.

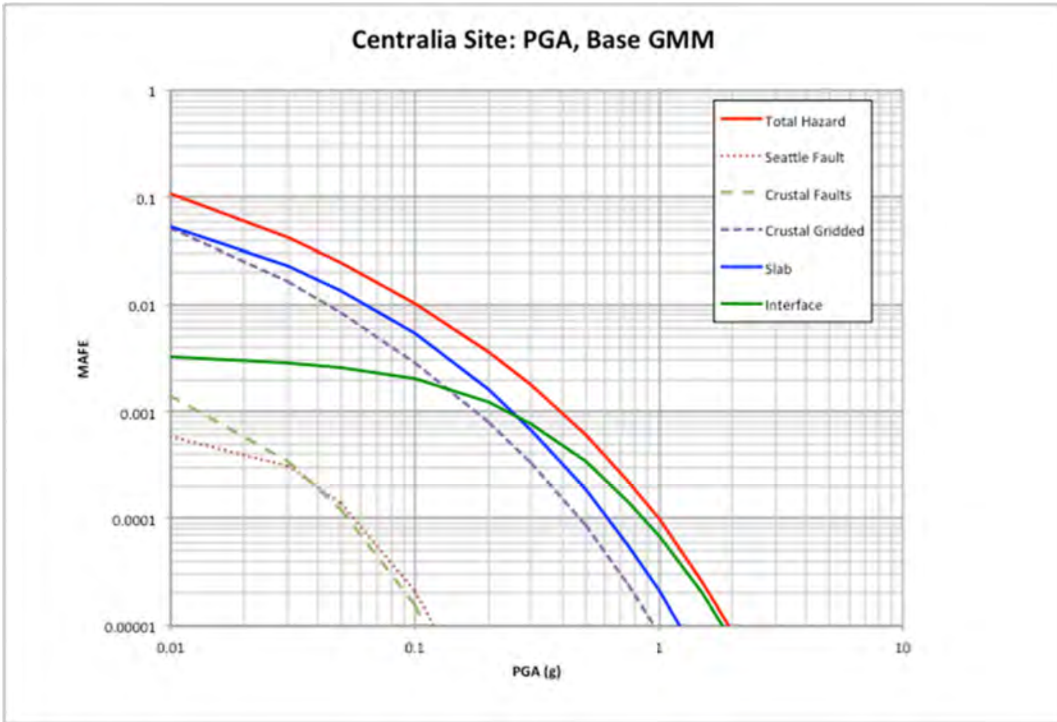

Figure 5.42 Total hazard curve (solid red line) and hazard curves differentiated by seismic source for the Centralia site for PGA (*T* = 0.01 sec).

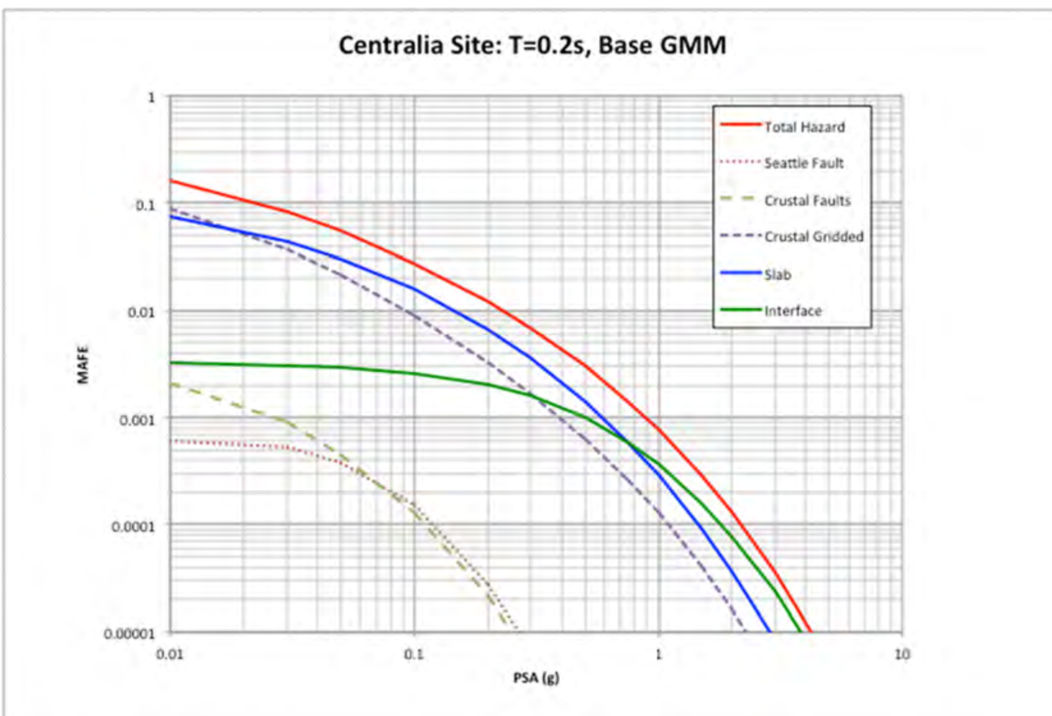

Figure 5.43 Total hazard curve (solid red line) and hazard curves differentiated by seismic source for the Centralia site for spectral period of 0.2 sec.

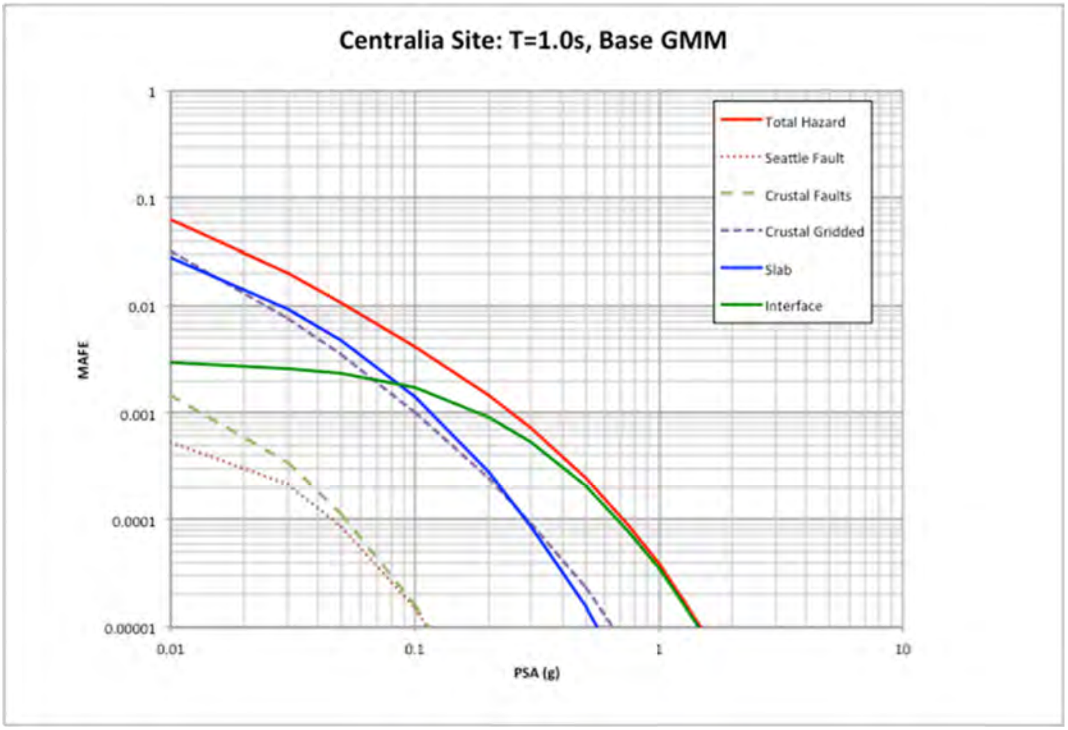

Figure 5.44 Total hazard curve (solid red line) and hazard curves differentiated by seismic source for the Centralia site for spectral period of 1.0 sec.

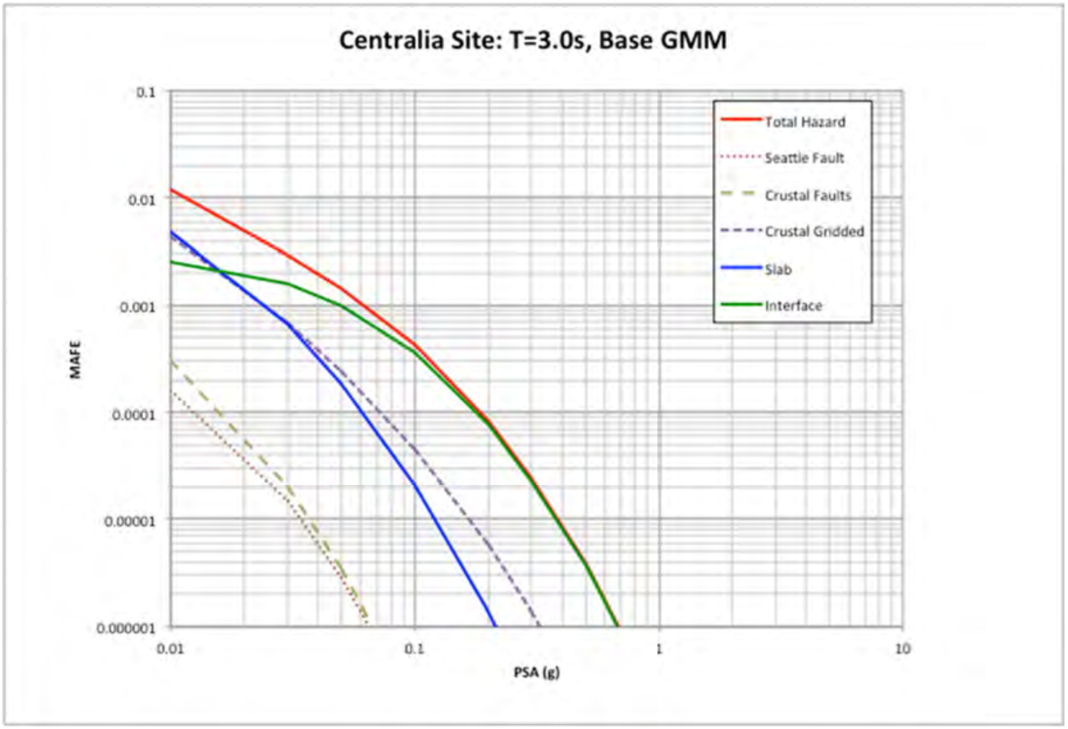

Figure 5.45 Total hazard curve (solid red line) and hazard curves differentiated by seismic source for the Centralia site for spectral period of 3.0 sec.

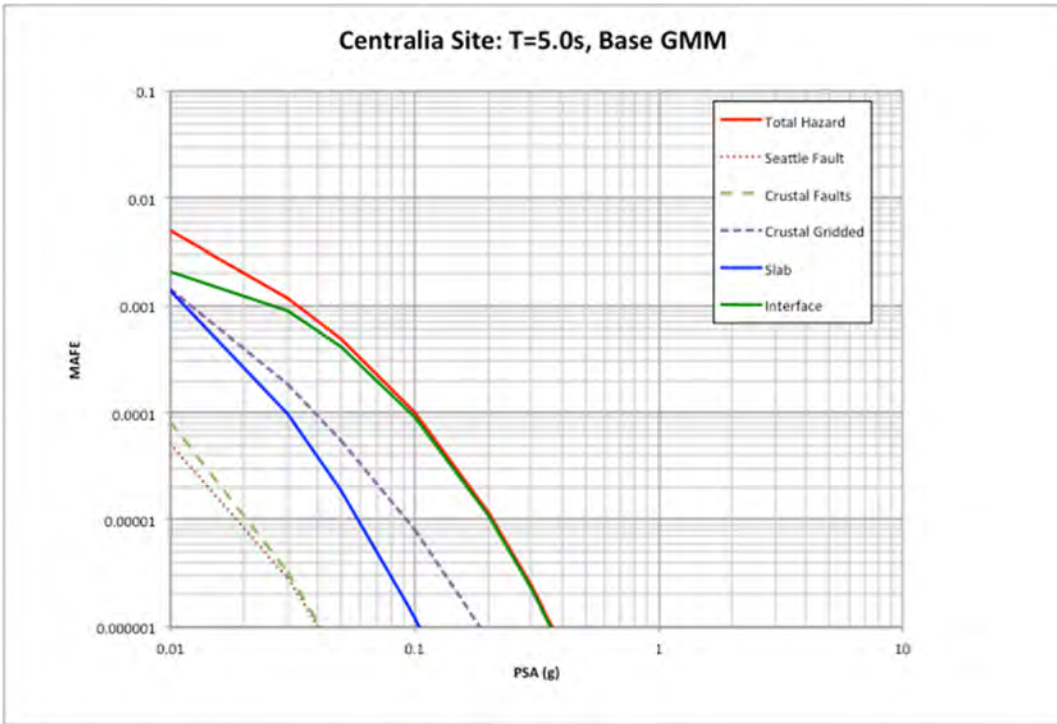

Figure 5.46 **Total hazard curve (solid red line) and hazard curves differentiated by seismic source for the Centralia site for spectral period of 5.0 sec.**

The same approach that was used for the Seattle site is performed for the Centralia site, where the BCH subduction GMM is replaced with the BCHU, KBCG, and PSHAB subduction GMMs. The same NGA-West2 crustal models are used for these additional example calculations for the crustal sources. Comparisons are presented in Figure 5.47 through Figure 5.61 for the total hazard curve, interface, and slab hazard curves plotted as a function of the different subduction GMMs. These figures provide the observations on the impact between the different subduction GMMs. Variations are observed for the interface, slab, and resulting total hazard curves depending on the individual GMMs. For the longer spectral periods, the change in the total hazard is smaller than the observed changes in the PGA and T = 0.2 sec cases. The change in the slope of the total hazard curve for the BCHU model shown in the plots is based on the relative change in the individual hazard for the interface (i.e., approximately equal or higher) and slab (i.e., lower values) sources rather than a change in the sigma model. Consistent with the results for the Seattle site, the PSHAB model has higher results for PGA and T = 0.2 sec from slab events, and the KBCG model is lower for interface events. At the longer spectral periods, the agreement between the models is more favorable.

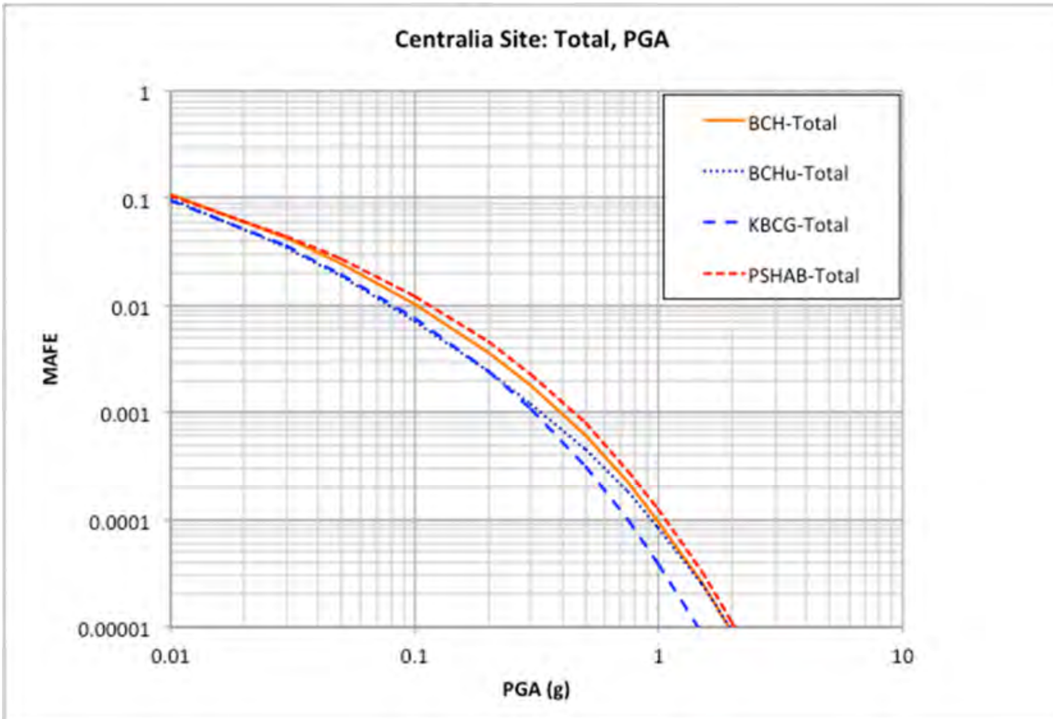

Figure 5.47 Comparison of the total hazard curve using BCH (solid orange line), BCHU (dotted line), KBCG (long dashed blue line), and PSHAB (short dashed red line) for the Centralia site for PGA (*T* = 0.01 sec).

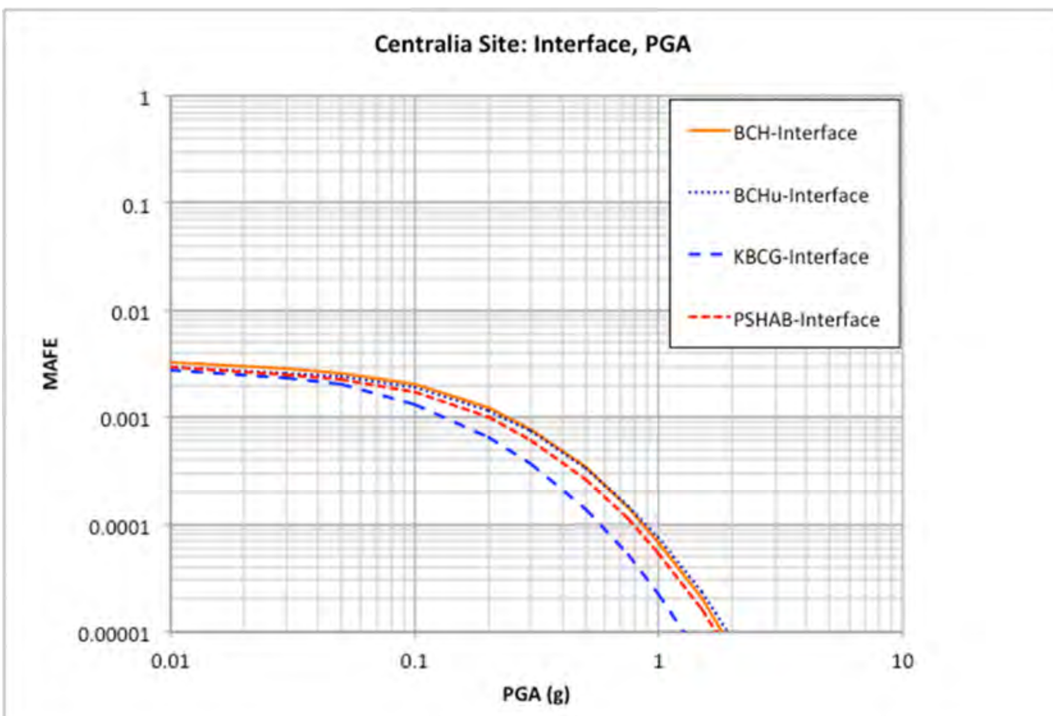

Figure 5.48 Comparison of the interface hazard curve using BCH (solid orange line), BCHU (dotted line), KBCG (long dashed blue line), and PSHAB (short dashed red line) for the Centralia site for PGA (*T* = 0.01 sec).

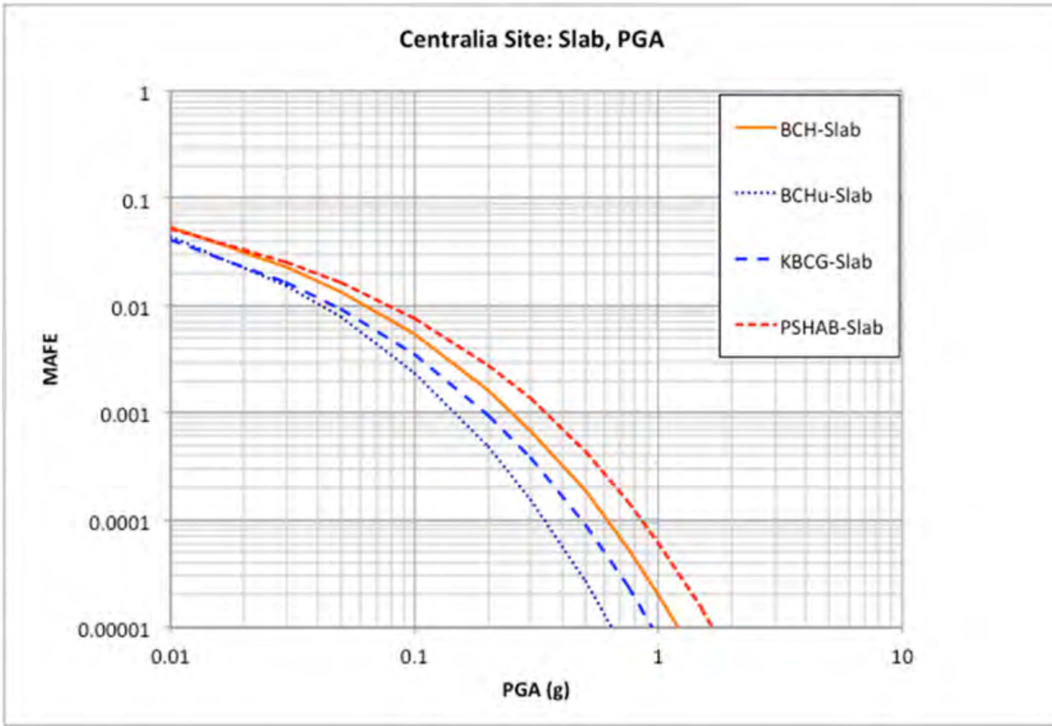

Figure 5.49 Comparison of the slab hazard curve using BCH (solid orange line), BCHU (dotted line), KBCG (long dashed blue line), and PSHAB (short dashed red line) for the Centralia site for PGA (*T* = 0.01 sec).

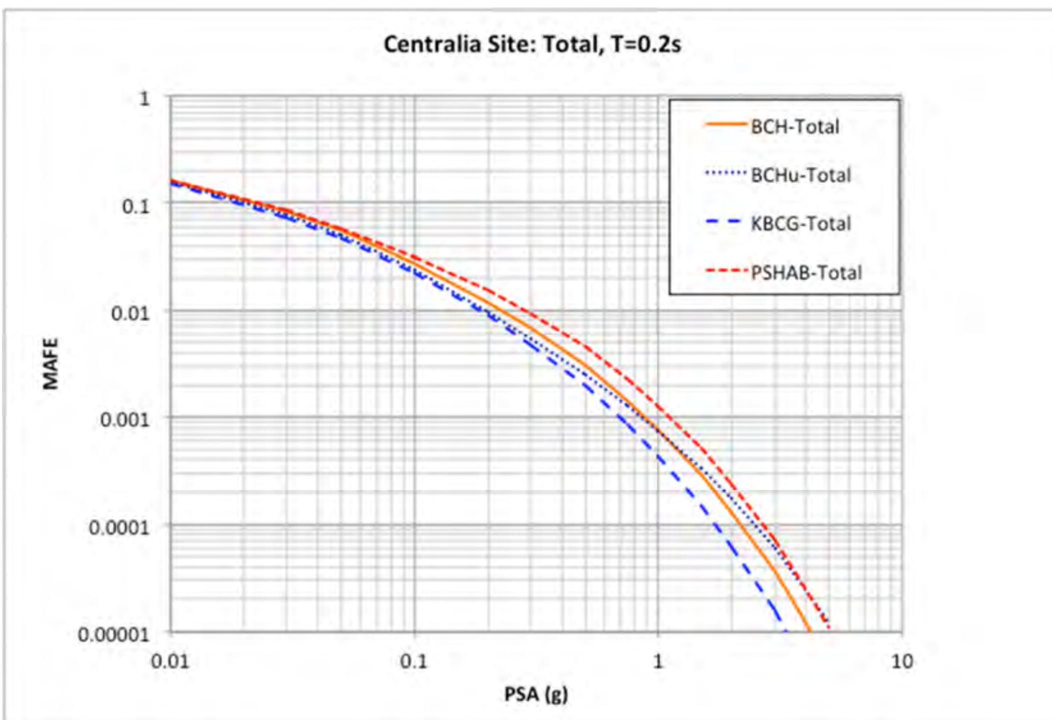

Figure 5.50 Comparison of the total hazard curve using BCH (solid orange line), BCHU (dotted line), KBCG (long dashed blue line), and PSHAB (short dashed red line) for the Centralia site for spectral period of *T* = 0.2 sec.

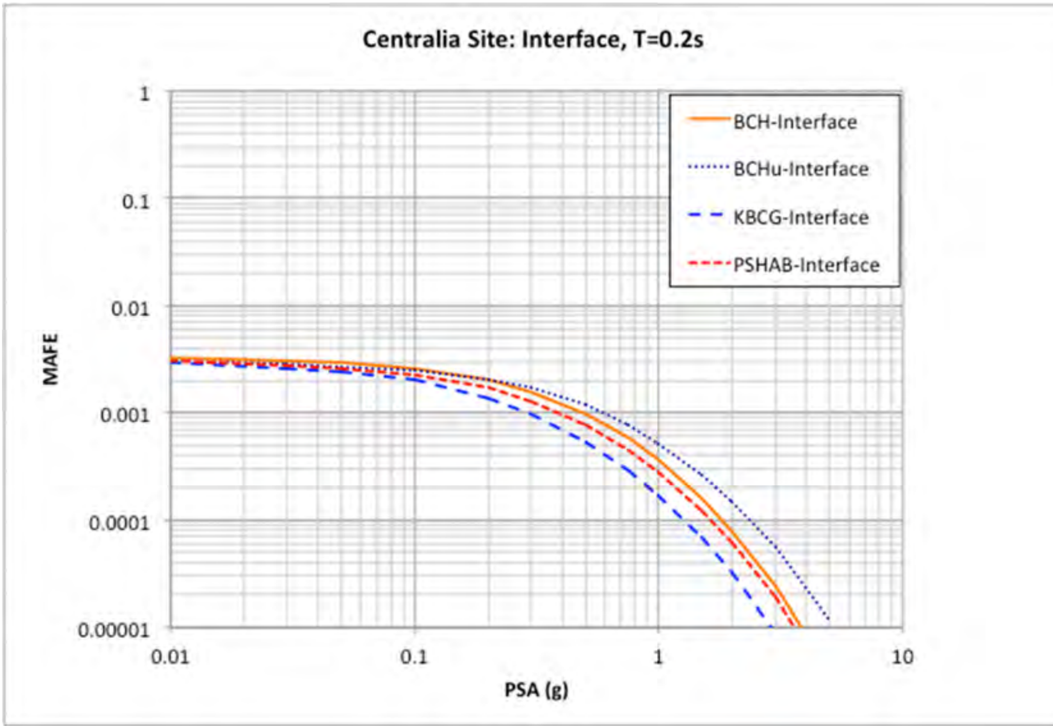

Figure 5.51 **Comparison of the interface hazard curve using BCH (solid orange line), BCHU (dotted line), KBCG (long dashed blue line), and PSHAB (short dashed red line) for the Centralia site for spectral period of *T* = 0.2 sec.**

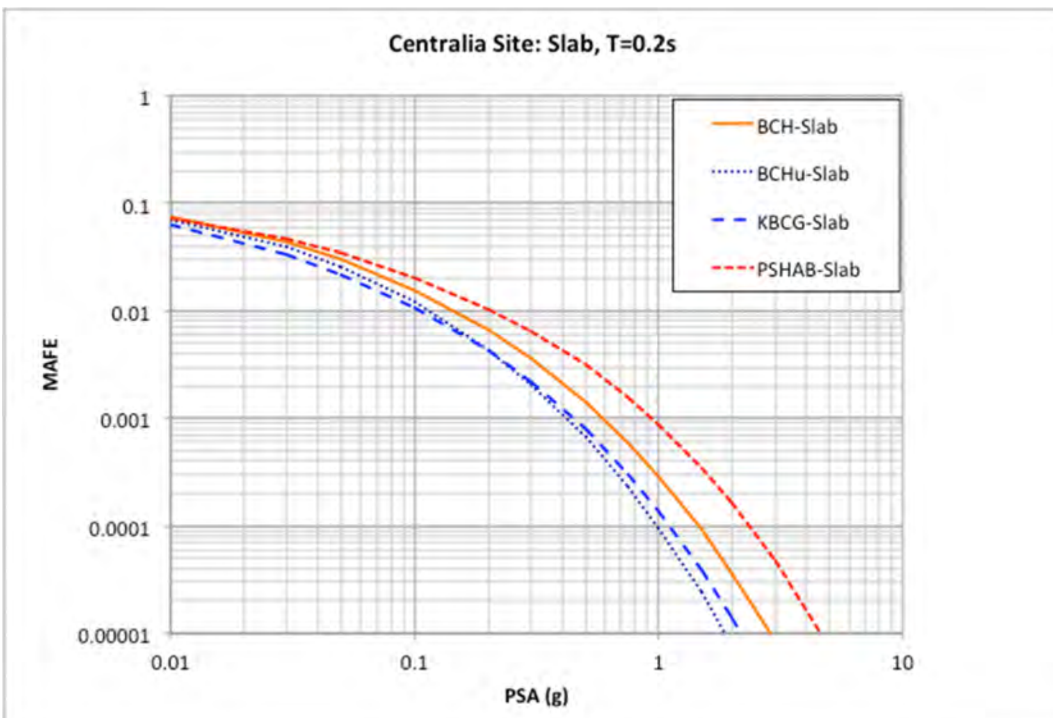

Figure 5.52 **Comparison of the slab hazard curve using BCH (solid orange line), BCHU (dotted line), KBCG (long dashed blue line), and PSHAB (short dashed red line) for the Centralia site for spectral period of *T* = 0.2 sec.**

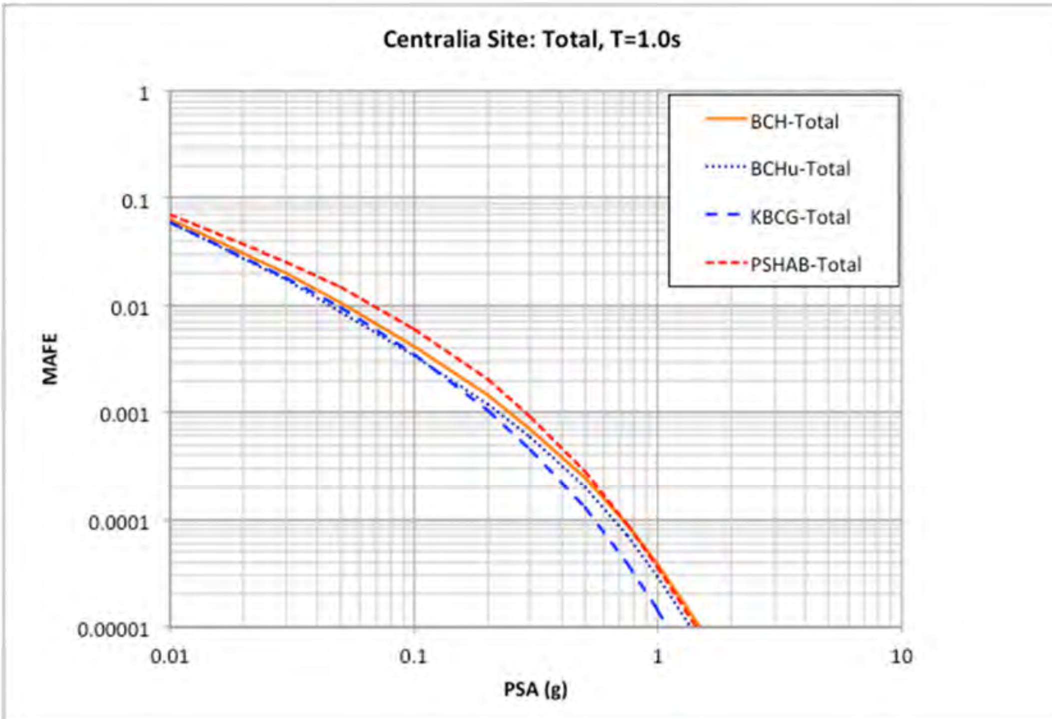

Figure 5.53 Comparison of the total hazard curve using BCH (solid orange line), BCHU (dotted line), KBCG (long dashed blue line), and PSHAB (short dashed red line) for the Centralia site for spectral period of *T* = 1.0 sec.

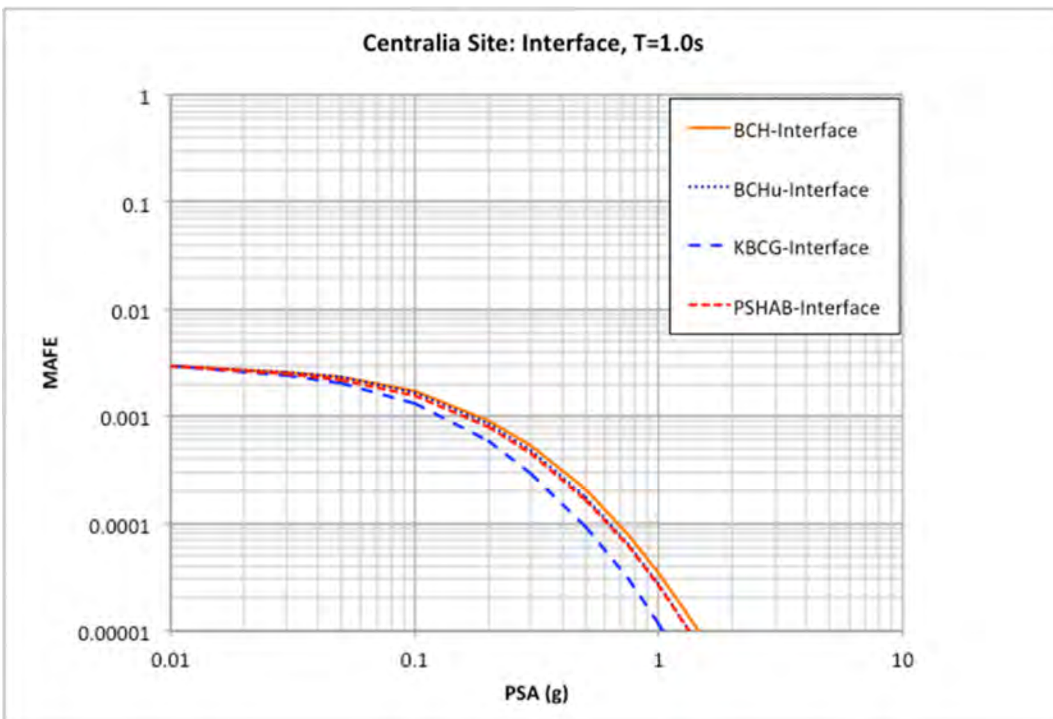

Figure 5.54 Comparison of the interface hazard curve using BCH (solid orange line), BCHU (dotted line), KBCG (long dashed blue line), and PSHAB (short dashed red line) for the Seattle site for spectral period of *T* = 1.0 sec.

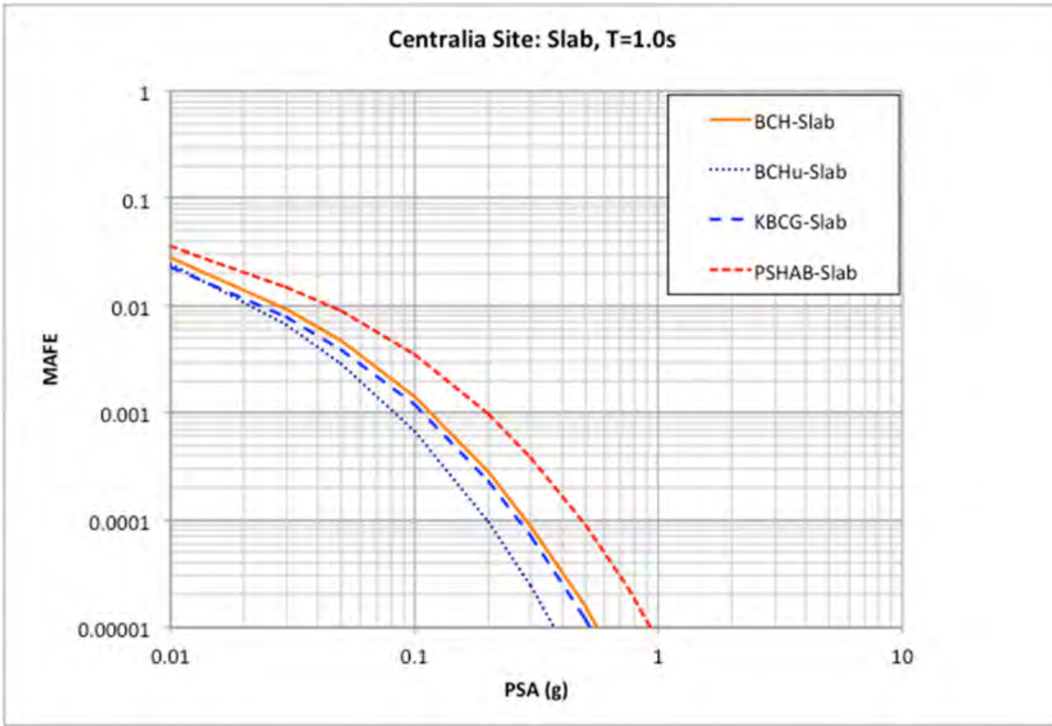

Figure 5.55 **Comparison of the slab hazard curve using BCH (solid orange line), BCHU (dotted line), KBCG (long dashed blue line), and PSHAB (short dashed red line) for the Centralia site for spectral period of *T* = 1.0 sec.**

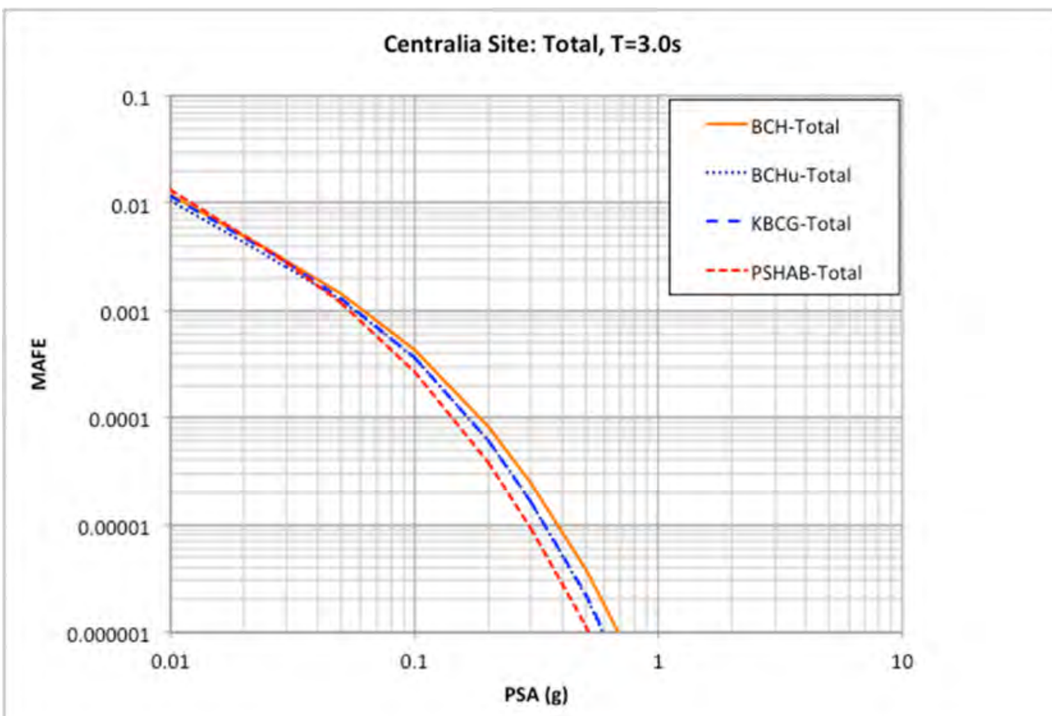

Figure 5.56 **Comparison of the total hazard curve using BCH (solid orange line), BCHU (dotted line), KBCG (long dashed blue line), and PSHAB (short dashed red line) for the Centralia site for spectral period of *T* = 3.0 sec.**

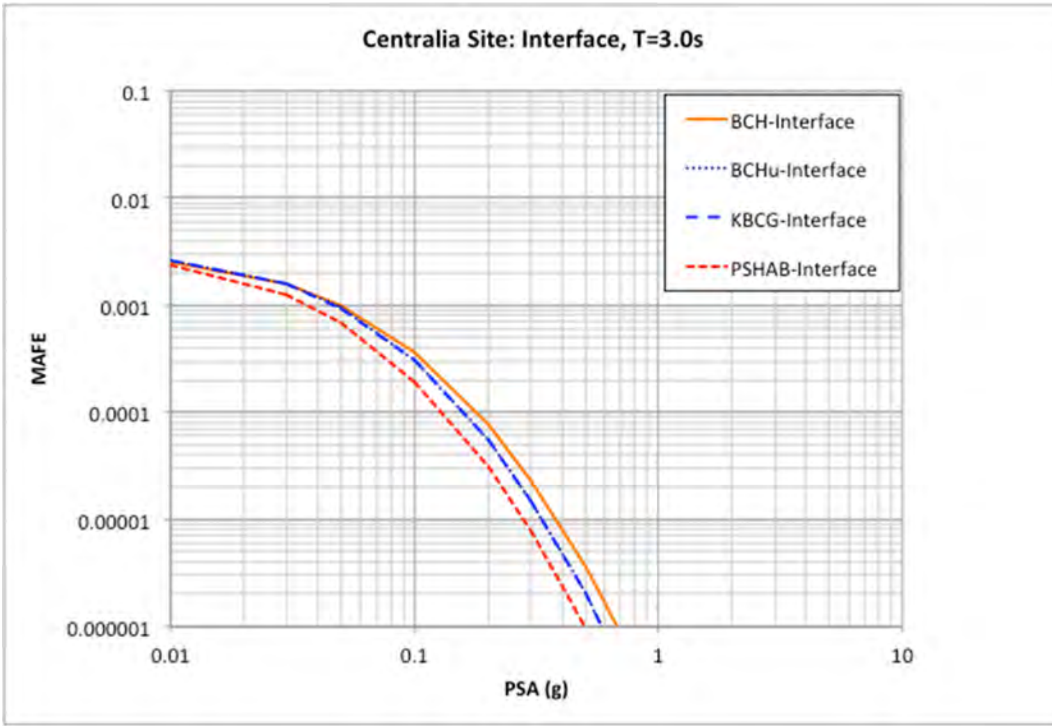

Figure 5.57 **Comparison of the interface hazard curve using BCH (solid orange line), BCHU (dotted line), KBCG (long dashed blue line), and PSHAB (short dashed red line) for the Centralia site for spectral period of *T* = 3.0 sec.**

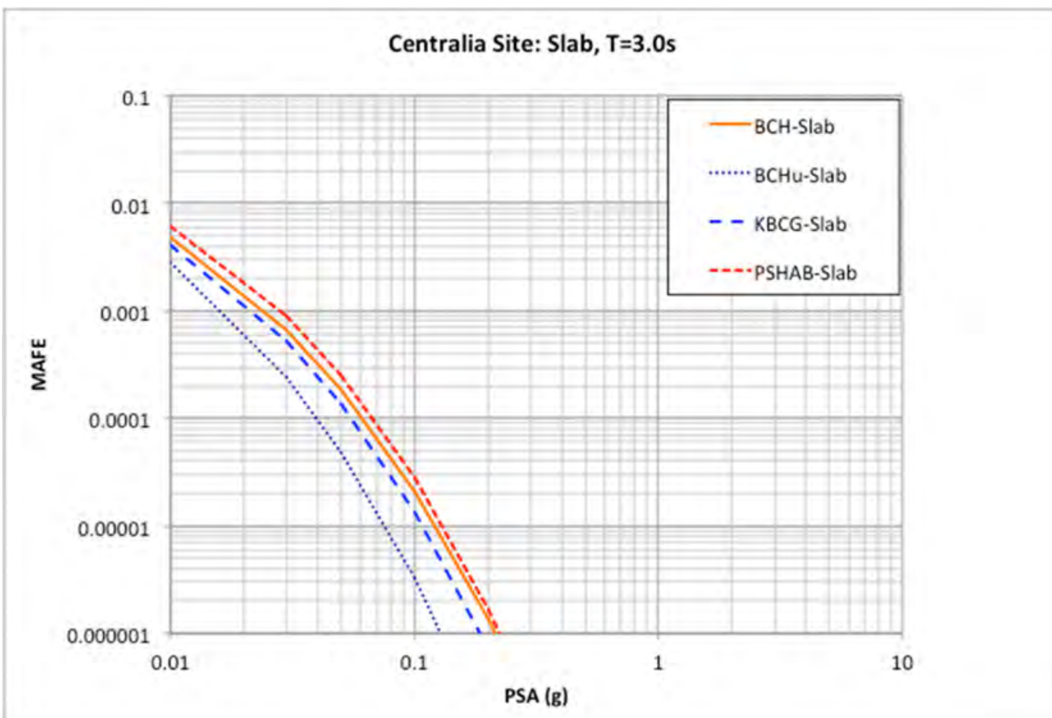

Figure 5.58 **Comparison of the slab hazard curve using BCH (solid orange line), BCHU (dotted line), KBCG (long dashed blue line), and PSHAB (short dashed red line) for the Centralia site for spectral period of *T* = 3.0 sec.**

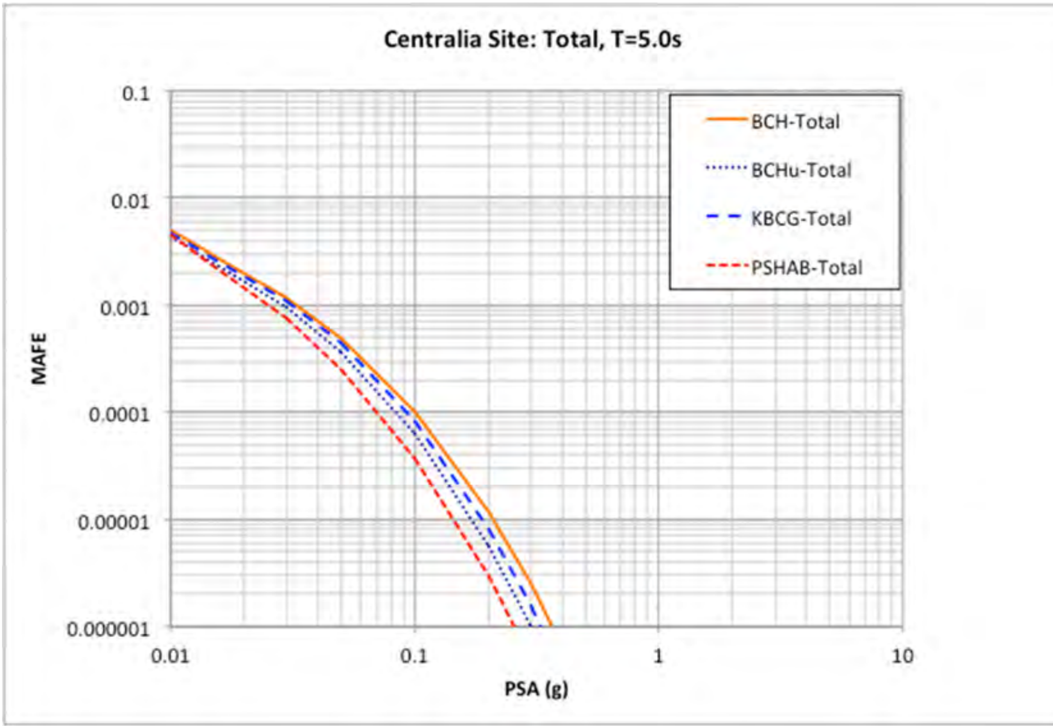

Figure 5.59 Comparison of the total hazard curve using BCH (solid orange line), BCHU (dotted line), KBCG (long dashed blue line), and PSHAB (short dashed red line) for the Centralia site for spectral period of *T* = 5.0 sec.

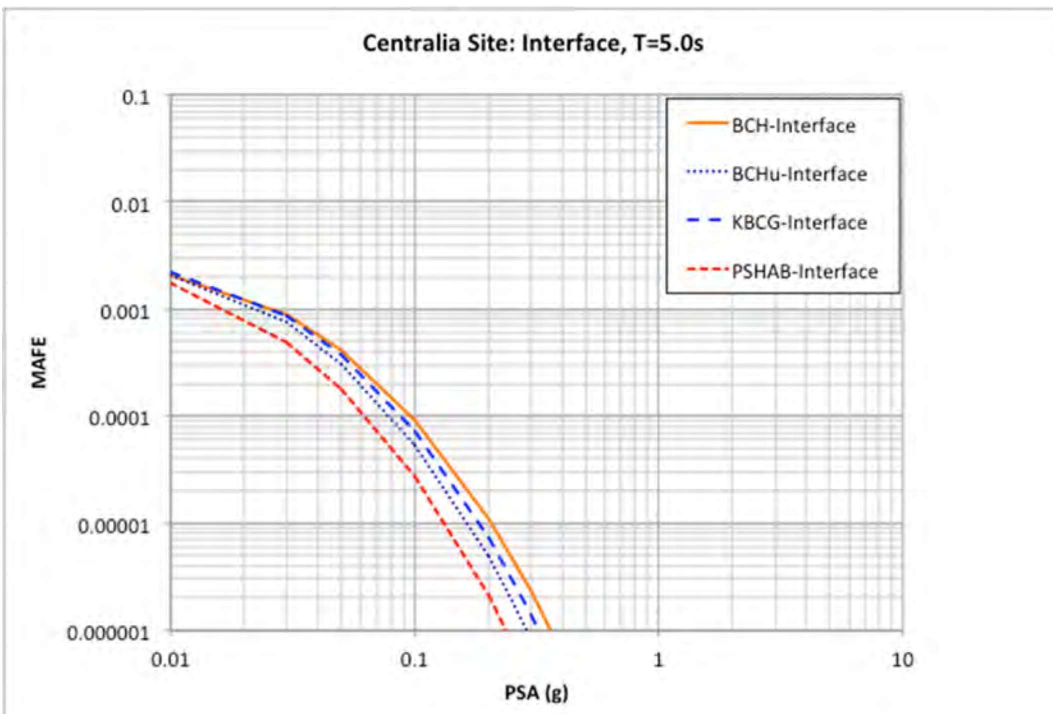

Figure 5.60 Comparison of the interface hazard curve using BCH (solid orange line), BCHU (dotted line), KBCG (long dashed blue line), and PSHAB (short dashed red line) for the Centralia site for spectral period of *T* = 5.0 sec.

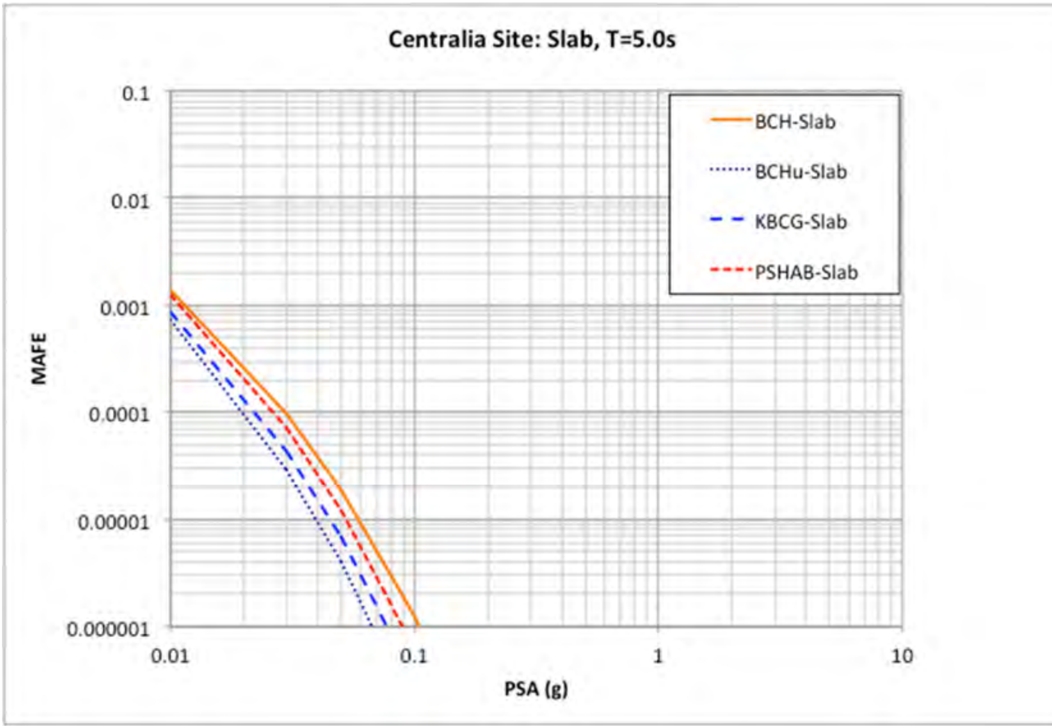

Figure 5.61 Comparison of the slab hazard curve using BCH (solid orange line), BCHU (dotted line), KBCG (long dashed blue line), and PSHAB (short dashed red line) for the Centralia site for spectral period of *T* = 5.0 sec.

The UHS ground motions for the suite of five return-period hazard levels are consistent with the hazard curves plotted in the previous figures are listed in Table 5.10 through Table 5.13. The ground-motion results are shown graphically in Figure 5.62 through Figure 5.66. The largest difference in the ground motions is observed for the spectral period of 0.2 sec, with the results from the PSHAB model being higher by about 45% at the 10,000-year hazard level. These observed differences are less than the results for the Seattle site based on the overall contribution of the slab source being less at the Centralia site than at the Seattle site. Over all spectral periods and return period levels, the results from the PSHAB model are approximately 10% larger than the results from the BCH model. For the KBCG model, the average results are about 12% lower than the BCH model results primarily due to the interface ground motion being lower than for the BCH model. For the BCHU model, the results on average are about 3% lower than the results from the BCH model.

Table 5.10 Ground motions for the mean total hazard at the Centralia site using the BCH subduction GMM for the subduction seismic sources.

Period (sec)	500-year PSA (*g*)	1000-year-PSA (*g*)	2475-year PSA (*g*)	5000-year PSA (*g*)	10,000-year PSA (*g*)
PGA (0.010)	0.280	0.394	0.589	0.776	0.989
0.200	0.624	0.887	1.310	1.717	2.179
1.000	0.161	0.246	0.392	0.541	0.712
3.000	0.039	0.061	0.102	0.138	0.185
5.000	0.020	0.033	0.054	0.074	0.100

Table 5.11 Ground motions for the mean total hazard at the Centralia site using the BCHU subduction GMM for the subduction seismic sources.

Period (sec)	500-year PSA (*g*)	1000-year-PSA (*g*)	2475-year PSA (*g*)	5000-year PSA (*g*)	10,000-year PSA (*g*)
PGA (0.010)	0.239	0.358	0.579	0.811	1.092
0.200	0.602	0.911	1.482	2.073	2.797
1.000	0.143	0.226	0.369	0.517	0.683
3.000	0.036	0.057	0.096	0.130	0.173
5.000	0.018	0.030	0.049	0.065	0.087

Table 5.12 Ground motions for the mean total hazard at the Centralia site using the KBCG subduction GMM for the subduction seismic sources.

Period (sec)	500-year PSA (*g*)	1000-year-PSA (*g*)	2475-year PSA (*g*)	5000-year PSA (*g*)	10,000-year PSA (*g*)
PGA (0.010)	0.224	0.316	0.467	0.610	0.782
0.200	0.528	0.758	1.138	1.521	1.966
1.000	0.141	0.210	0.324	0.435	0.568
3.000	0.038	0.059	0.098	0.132	0.176
5.000	0.019	0.031	0.052	0.069	0.092

Table 5.13 Ground motions for the mean total hazard at the Centralia site using the PSHAB subduction GMM for the subduction seismic sources.

Period (sec)	500-year PSA (*g*)	1000-year-PSA (*g*)	2475-year PSA (*g*)	5000-year PSA (*g*)	10,000-year PSA (*g*)
PGA (0.010)	0.333	0.474	0.704	0.925	1.175
0.200	0.866	1.238	1.867	2.456	3.164
1.000	0.214	0.313	0.480	0.641	0.835
3.000	0.038	0.056	0.087	0.117	0.152
5.000	0.017	0.025	0.040	0.054	0.069

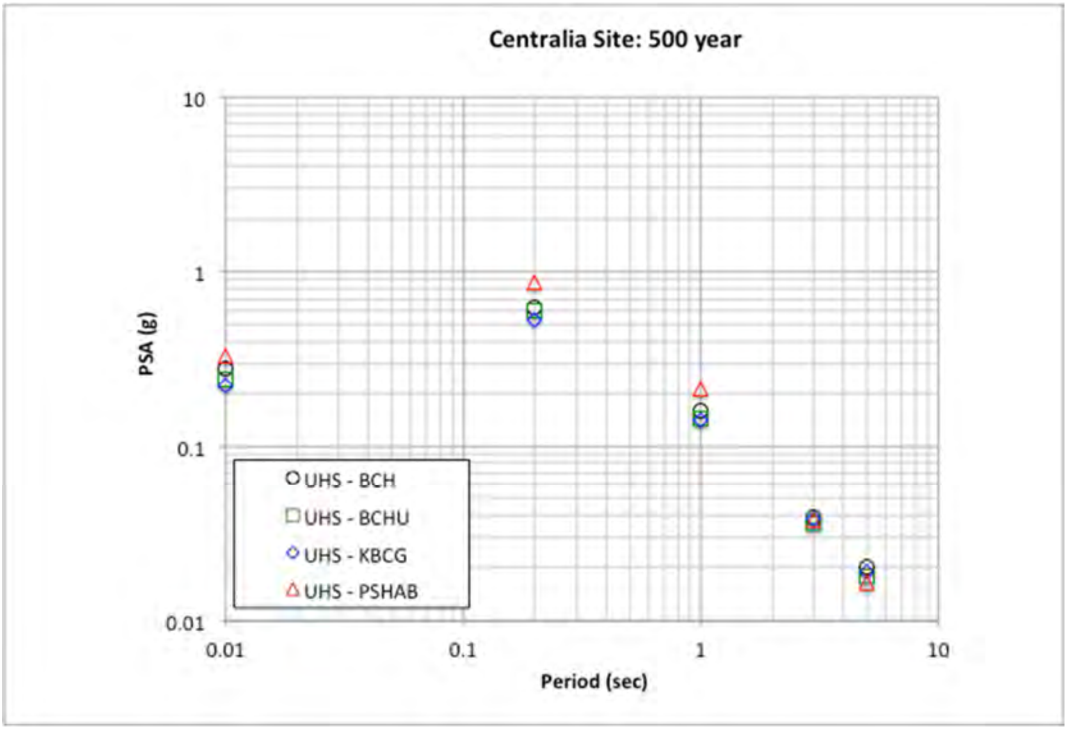

Figure 5.62 Comparison of UHS ground motions for the Centralia site based on the four separate subduction GMMs for the subduction seismic sources at the 500-year-return-period hazard level.

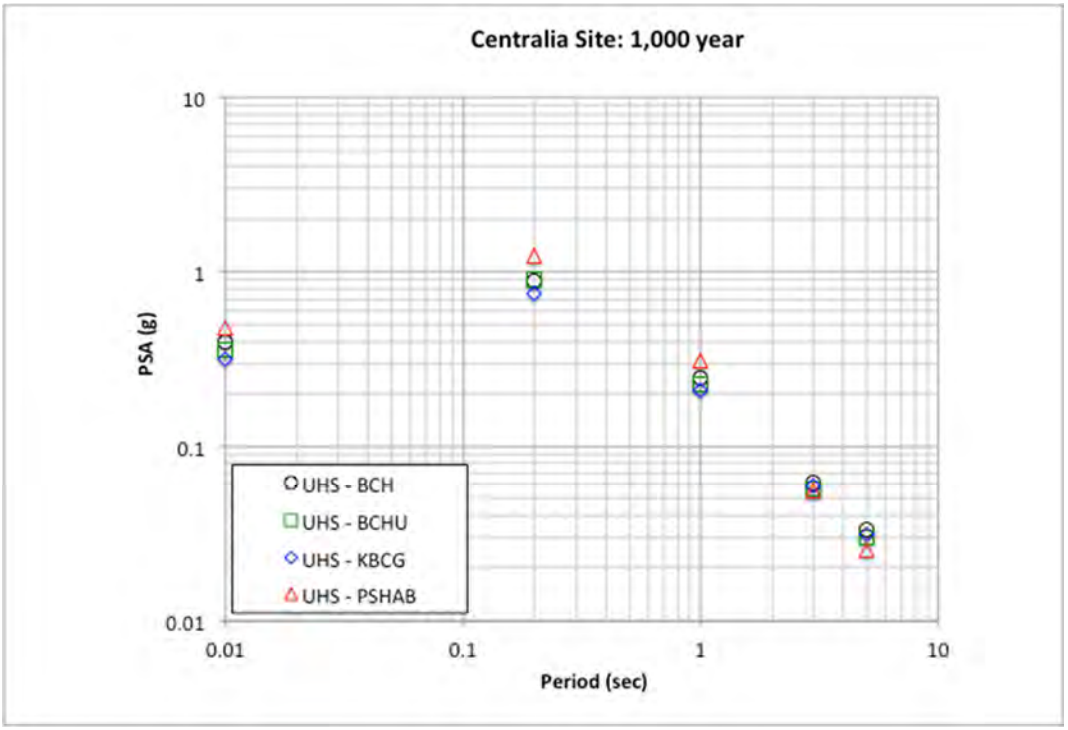

Figure 5.63 Comparison of UHS ground motions for the Centralia site based on the four separate subduction GMMs for the subduction seismic sources at the 1000-year-return-period hazard level.

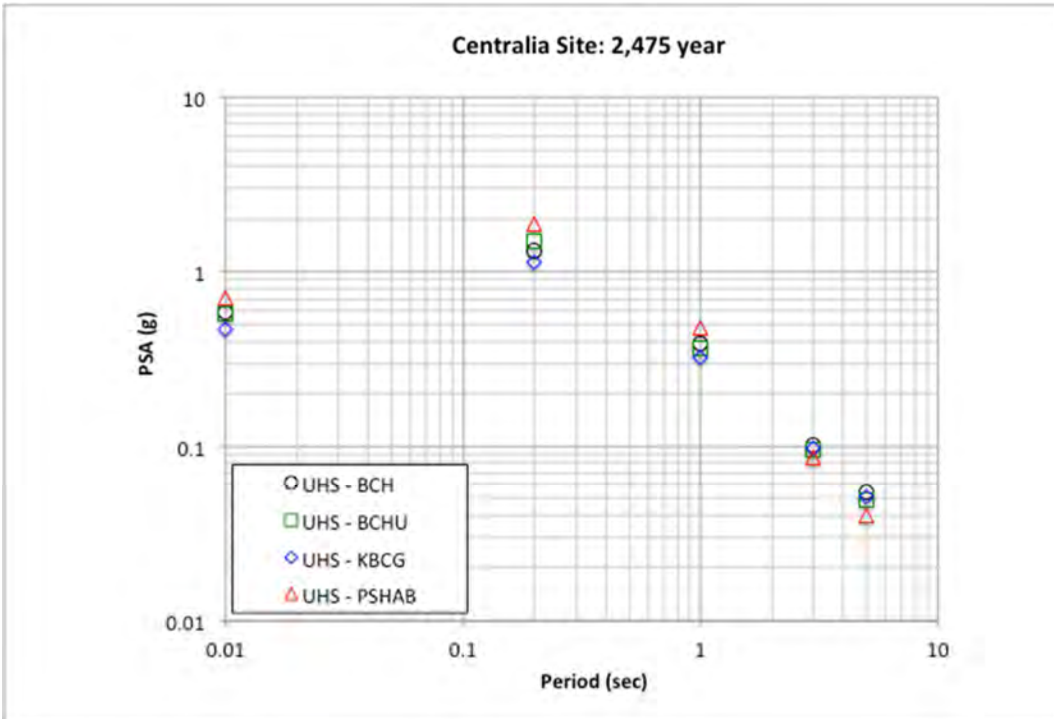

Figure 5.64 Comparison of UHS ground motions for the Centralia site based on the four separate subduction GMMs for the subduction seismic sources at the 2475-year-return-period hazard level.

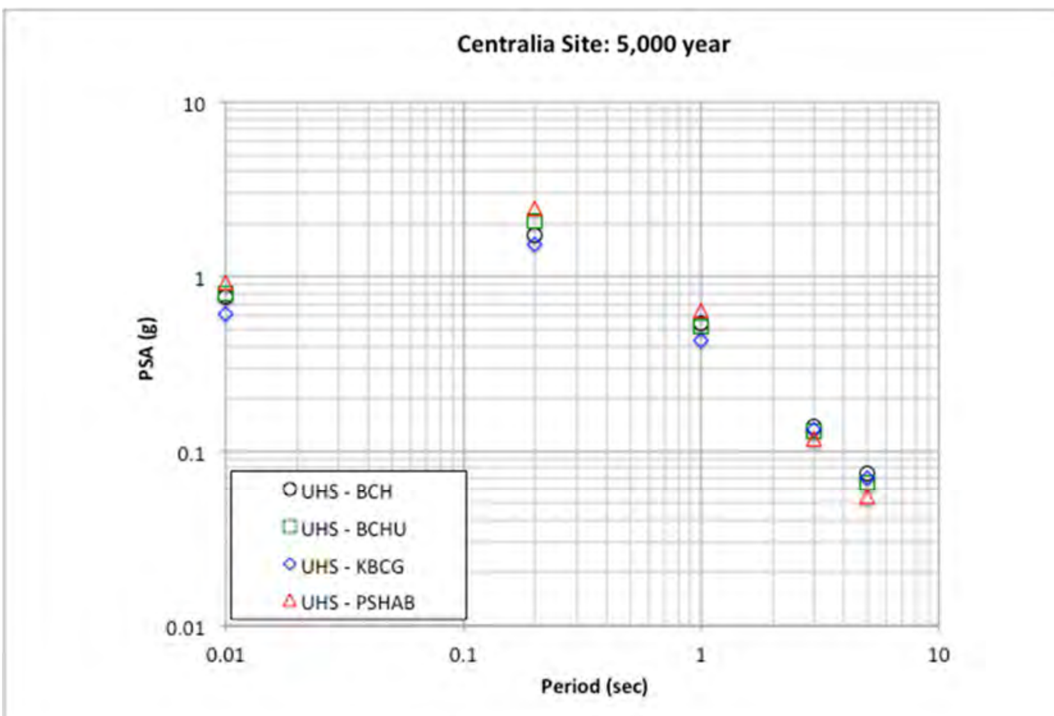

Figure 5.65 Comparison of UHS ground motions for the Centralia site based on the four separate subduction GMMs for the subduction seismic sources at the 5000-year-return-period hazard level.

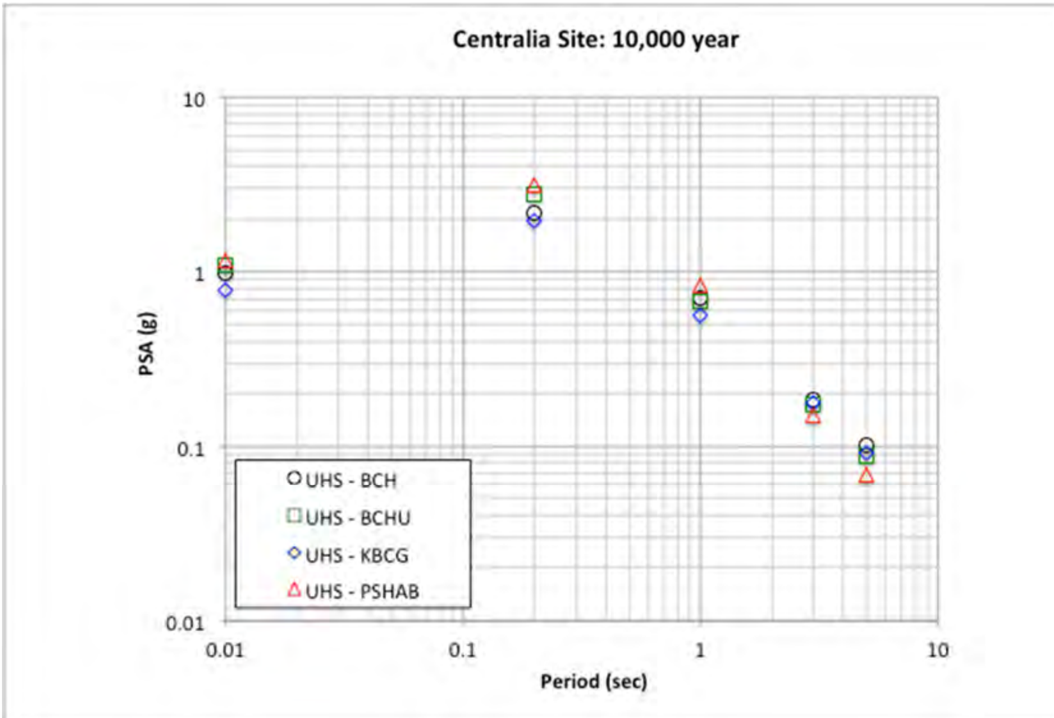

Figure 5.66 Comparison of UHS ground motions for the Centralia site based on the four separate subduction GMMs for the subduction seismic sources at the 10,000 year return period hazard level.

The binned deaggregation results are summarized in Figure 5.67 through Figure 5.76 for the four subduction GMMs and for the return periods of 500 and 2475 years. For the Centralia site, the distribution is more bi-modal than for the Seattle site, with a limited contribution from the crustal sources for the 500-year and short-period cases. For the other spectral periods and the 2475-year cases, the distribution is controlled by the slab and interface sources. Overall, the comparison across the four GMM cases is in agreement with similar controlling magnitude and distance bins.

Following the same approach for the Seattle site, an additional set of PSHA calculations is performed to isolate the impact of the median ground-motion estimate differences between the four subduction GMMs for the Centralia site. For these calculations, the aleatory sigma model from the BCH model is applied with the median ground-motion estimates from the other three GMMs. Given this approach, the observed differences are fully attributable to the differences in the median ground-motion estimates. The resulting UHS ground motions are listed in Table 5.14 through

Table 5.16 for the three GMMs (note that the base case UHS ground-motion results based on the BCH model are listed in Table 5.10). Overall, the observed differences are approximately similar (i.e., KBCG) or less (i.e., BCHU and PSHAB) for the three models than those observed using both the median and aleatory sigma adjustments from the three subduction GMMs. The average reduction in ground motions for the BCHU and KBCG models is about 9% and 16%, respectively. The PSHAB model shows an observed average increase of about 1%, with the largest increase—approximately 25%—occurring for the T = 0.2 sec spectral periods based on the slab model differences and the largest reduction of about 25% at T = 5.0 sec spectral period based on the interface model differences. The comparisons of the ground-motion values are plotted in Figure 5.77 through Figure 5.81.

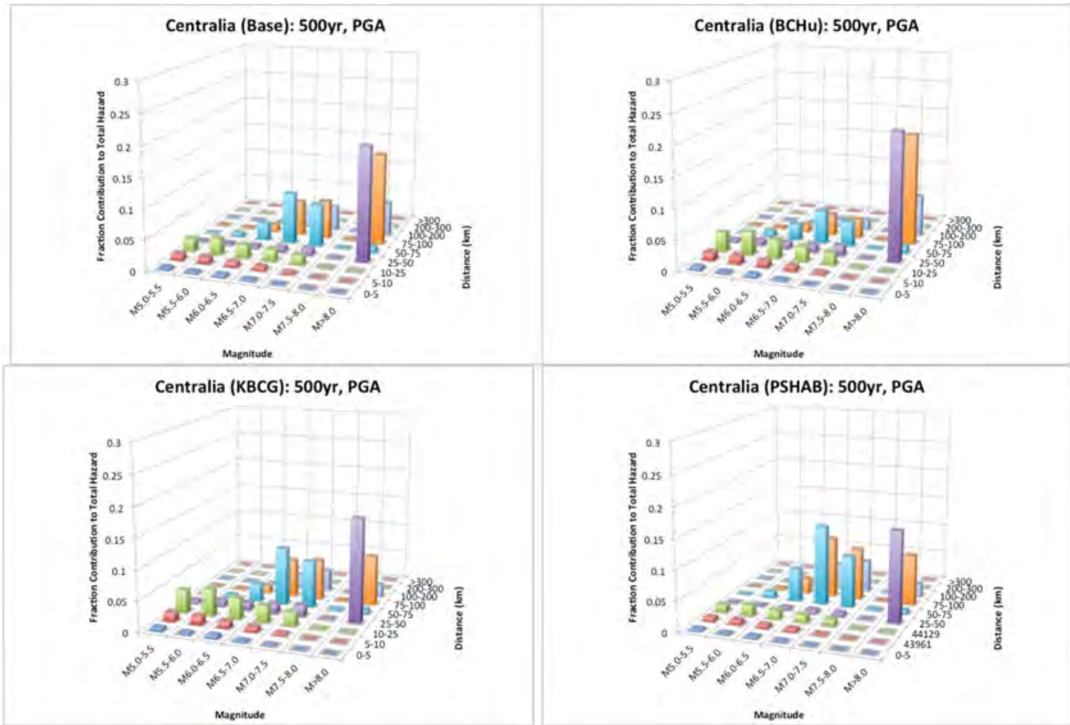

Figure 5.67 Binned deaggregation results for the Centralia site at the 500-year-return-period level for PGA (*T* = 0.01 sec) for the BCH (upper left), BCHU (upper right), KBCG (lower left), and PSHAB (lower right) models.

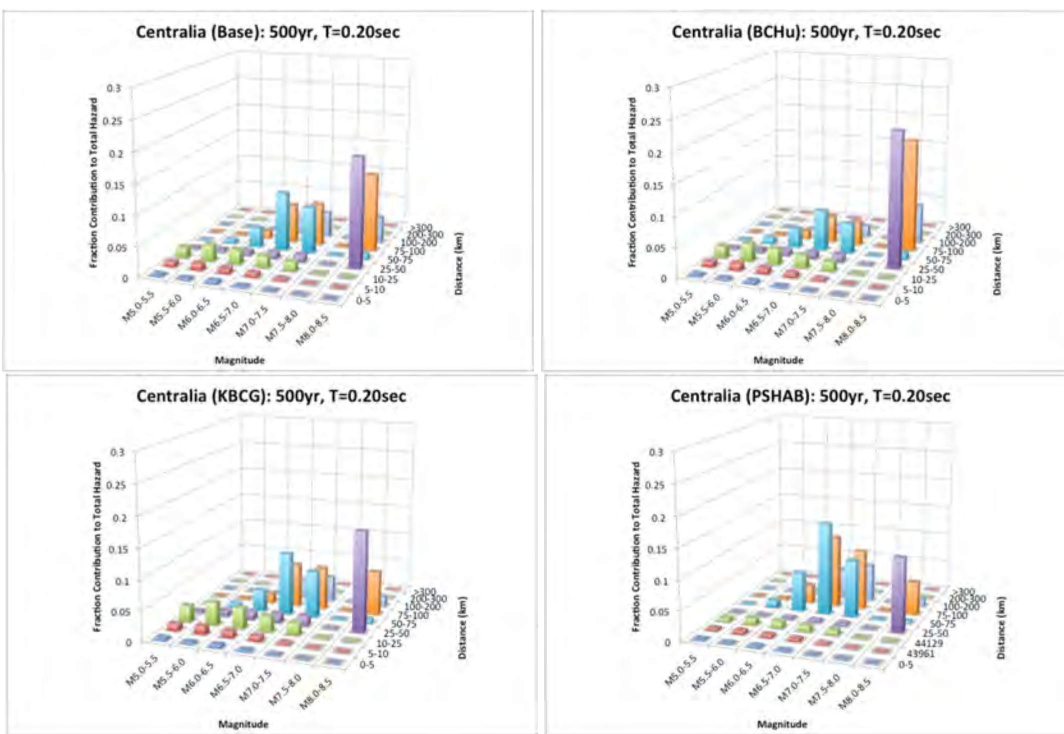

Figure 5.68 Binned deaggregation results for the Centralia site at the 500 year return period level for *T* = 0.2 sec for the BCH (upper left), BCHU (upper right), KBCG (lower left), and PSHAB (lower right) models.

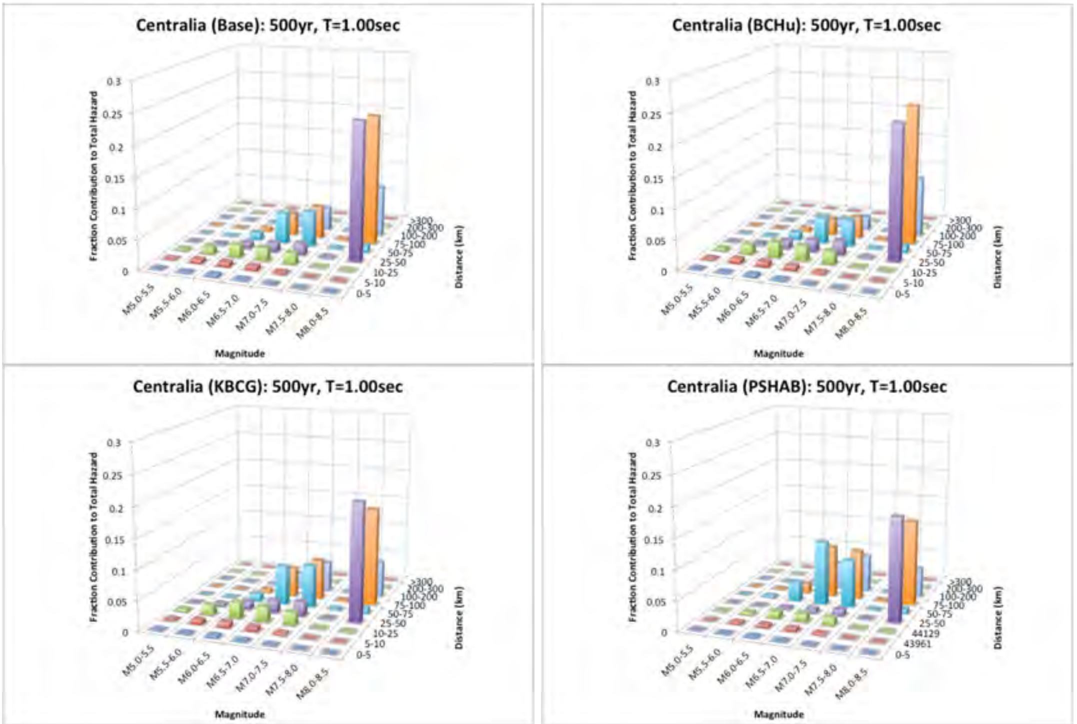

Figure 5.69 **Binned deaggregation results for the Centralia site at the 500-year-return-period level for *T* = 1.0 sec for the BCH (upper left), BCHU (upper right), KBCG (lower left), and PSHAB (lower right) models.**

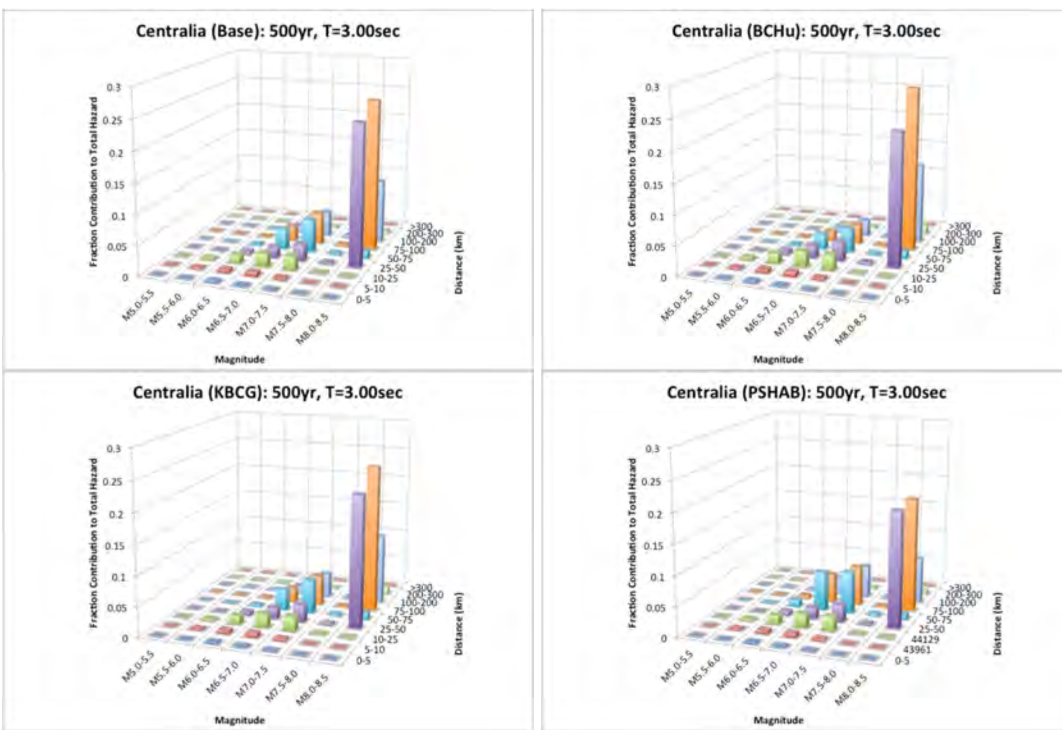

Figure 5.70 **Binned deaggregation results for the Centralia site at the 500-year-return-period level for *T* = 3.0 sec for the BCH (upper left), BCHU (upper right), KBCG (lower left), and PSHAB (lower right) models.**

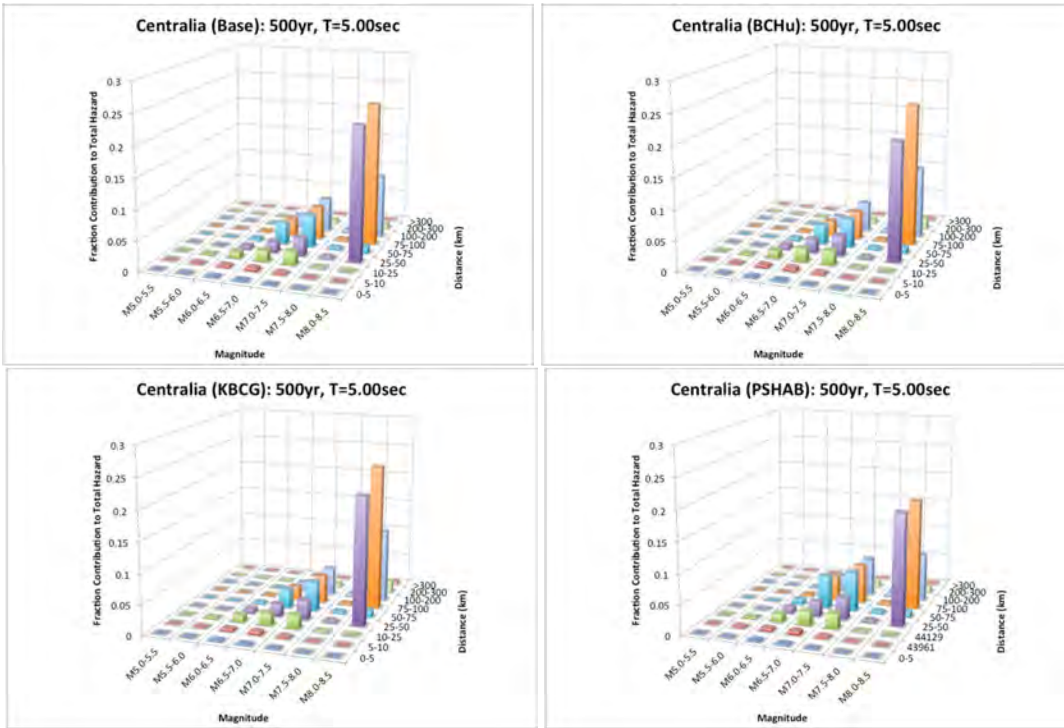

Figure 5.71 Binned deaggregation results for the Centralia site at the 500-year-return-period level for *T* = 5.0 sec for the BCH (upper left), BCHU (upper right), KBCG (lower left), and PSHAB (lower right) models.

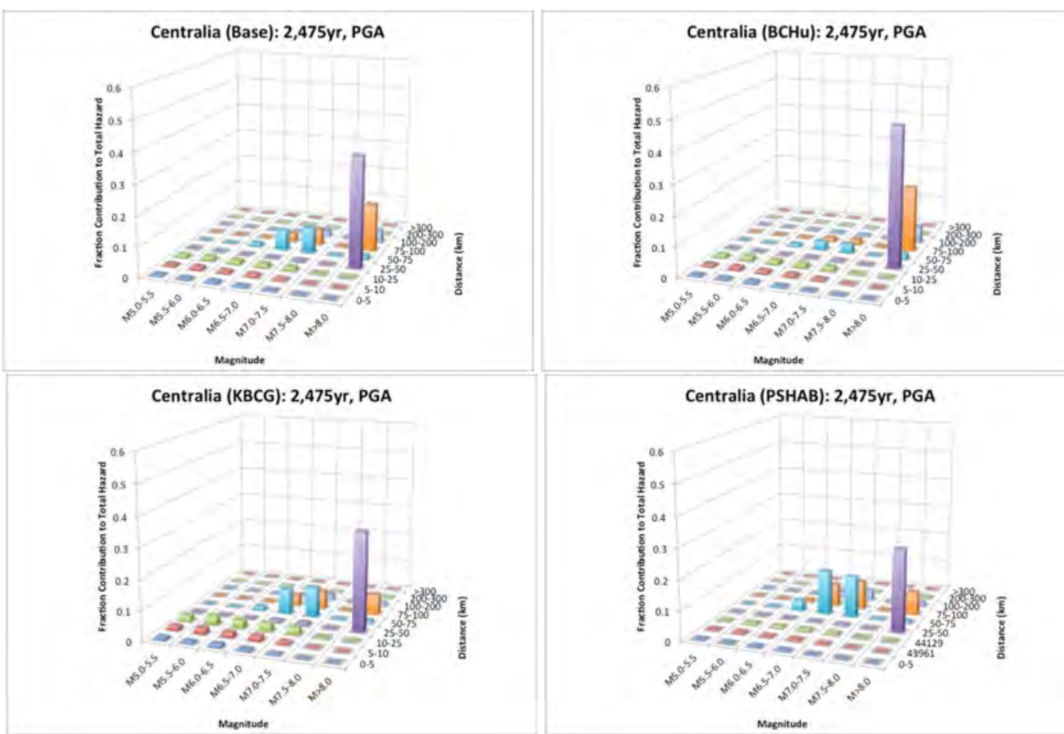

Figure 5.72 Binned deaggregation results for the Centralia site at the 2475-year-return-period level for PGA (*T* = 0.01 sec) for the BCH (upper left), BCHU (upper right), KBCG (lower left), and PSHAB (lower right) models.

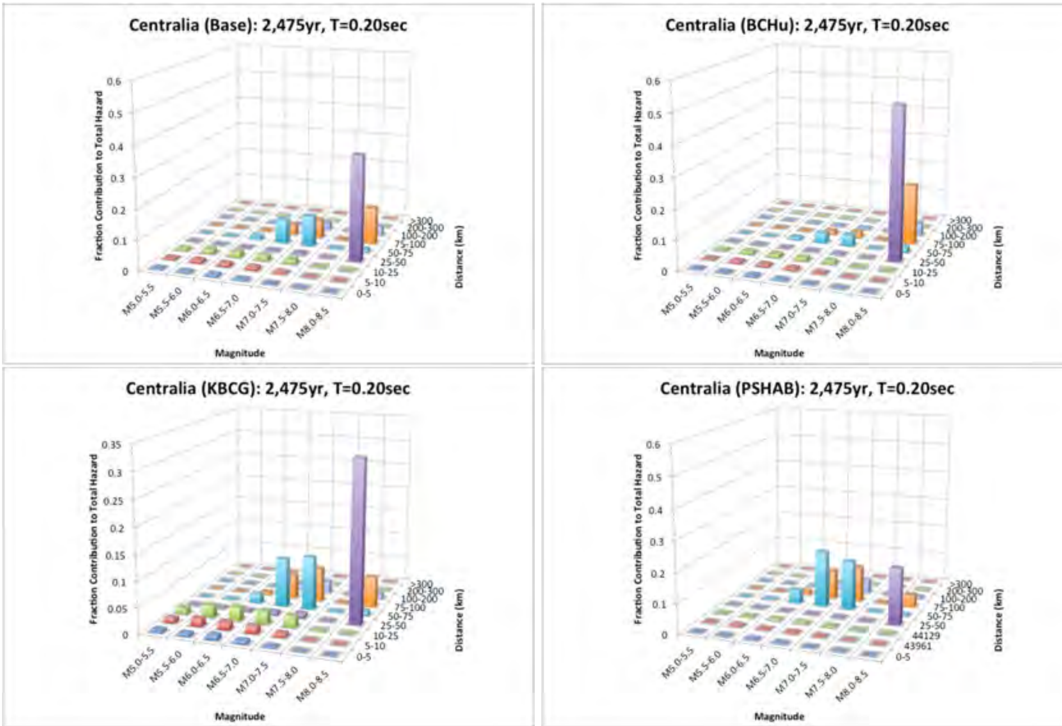

Figure 5.73 **Binned deaggregation results for the Centralia site at the 2475-year-return-period level for *T* = 0.2 sec for the BCH (upper left), BCHU (upper right), KBCG (lower left), and PSHAB (lower right) models.**

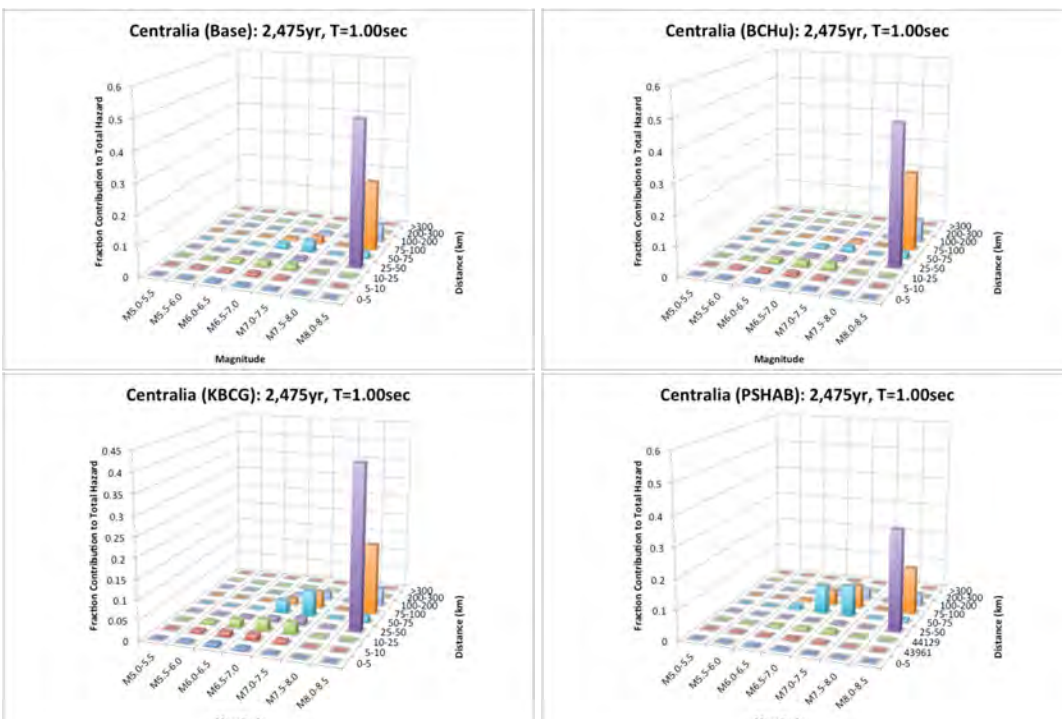

Figure 5.74 **Binned deaggregation results for the Centralia site at the 2475-year-return-period level for *T* = 1.0 sec for the BCH (upper left), BCHU (upper right), KBCG (lower left), and PSHAB (lower right) models.**

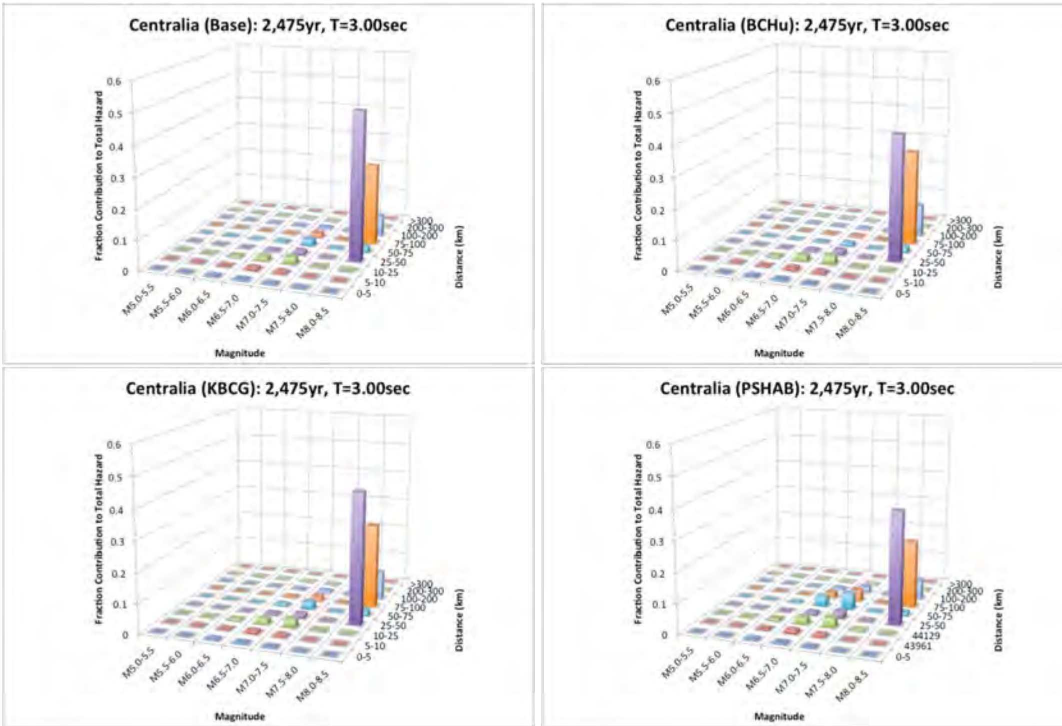

Figure 5.75 Binned deaggregation results for the Centralia site at the 2475-year-return-period level for *T* = 3.0 sec for the BCH (upper left), BCHU (upper right), KBCG (lower left), and PSHAB (lower right) models.

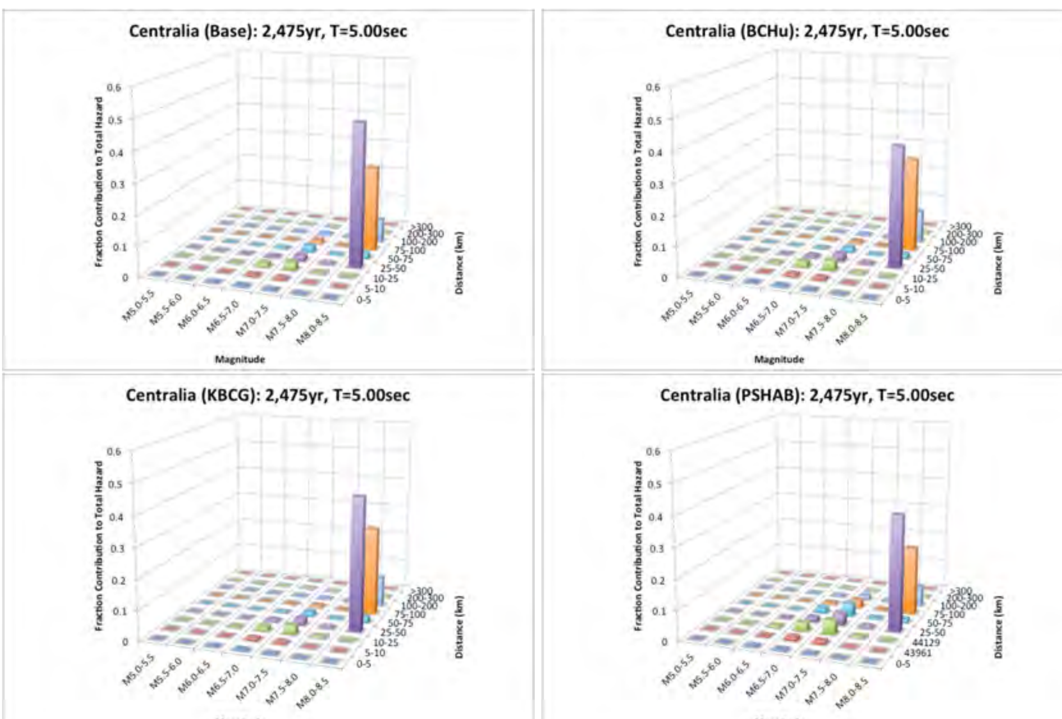

Figure 5.76 Binned deaggregation results for the Centralia site at the 2475-year-return-period level for *T* = 5.0 sec for the BCH (upper left), BCHU (upper right), KBCG (lower left), and PSHAB (lower right) models.

Table 5.14 Ground motions for the mean total hazard at the Centralia site using the BCHU subduction GMM with BCH aleatory sigma for the subduction seismic sources.

Period (sec)	500-year PSA (*g*)	1000-year-PSA (*g*)	2475-year PSA (*g*)	5000-year PSA (*g*)	10,000-year PSA (*g*)
PGA (0.010)	0.223	0.331	0.523	0.713	0.936
0.200	0.567	0.851	1.358	1.874	2.469
1.000	0.141	0.222	0.360	0.502	0.655
3.000	0.036	0.057	0.094	0.126	0.165
5.000	0.018	0.029	0.048	0.063	0.083

Table 5.15 Ground motions for the mean total hazard at the Centralia site using the KBCG subduction GMM with BCH aleatory sigma for the subduction seismic sources.

Period (sec)	500-year PSA (*g*)	1000-year-PSA (*g*)	2475-year PSA (*g*)	5000-year PSA (*g*)	10,000-year PSA (*g*)
PGA (0.010)	0.219	0.308	0.450	0.586	0.748
0.200	0.493	0.694	1.029	1.342	1.710
1.000	0.138	0.205	0.315	0.418	0.544
3.000	0.037	0.058	0.094	0.126	0.165
5.000	0.019	0.031	0.052	0.069	0.092

Table 5.16 Ground motions for the mean total hazard at the Centralia site using the PSHAB subduction GMM with BCH aleatory sigma for the subduction seismic sources.

Period (sec)	500-year PSA (*g*)	1000-year-PSA (*g*)	2475-year PSA (*g*)	5000-year PSA (*g*)	10,000-year PSA (*g*)
PGA (0.010)	0.318	0.445	0.651	0.847	1.068
0.200	0.798	1.118	1.639	2.120	2.664
1.000	0.200	0.287	0.426	0.563	0.722
3.000	0.037	0.054	0.082	0.111	0.142
5.000	0.017	0.025	0.040	0.054	0.069

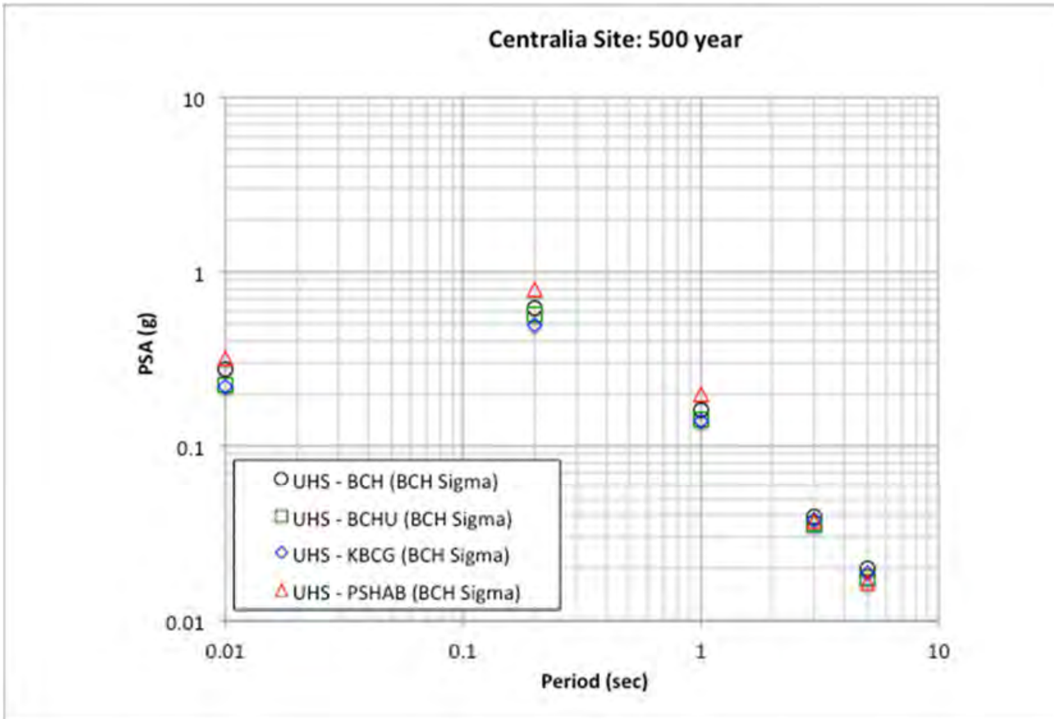

Figure 5.77 **Comparison of UHS ground motions for the Centralia site based on the four separate subduction GMMs, with the BCH aleatory sigma model for the subduction seismic sources at the 500-year-return-period hazard level.**

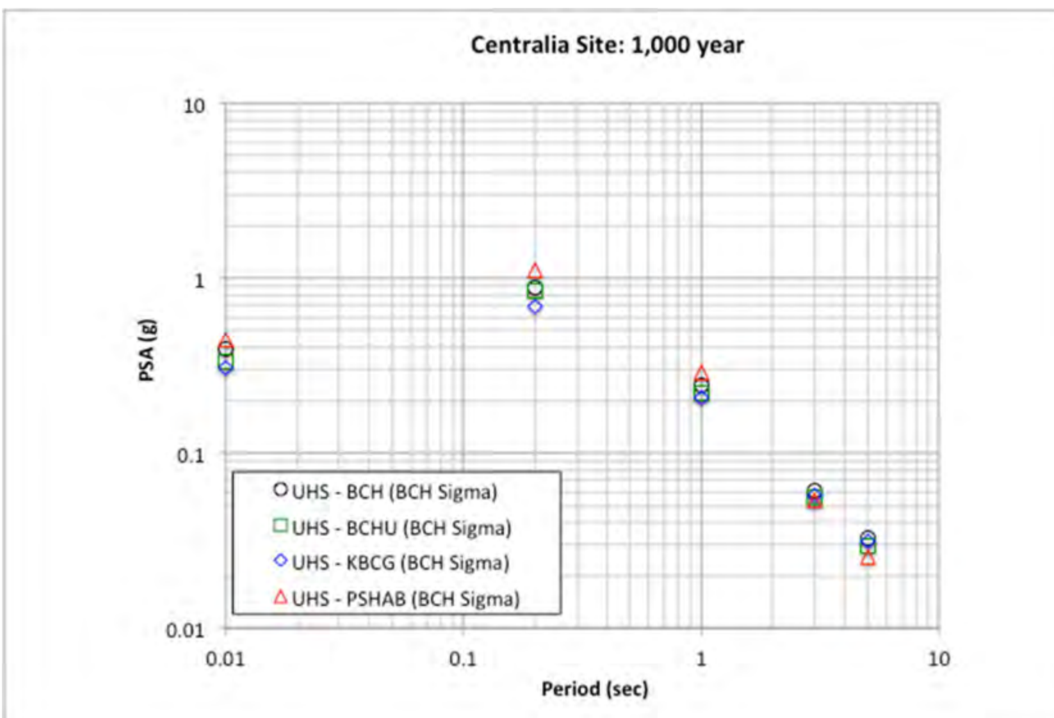

Figure 5.78 **Comparison of UHS ground motions for the Centralia site based on the four separate subduction GMMs, with the BCH aleatory sigma model for the subduction seismic sources at the 1000-year-return-period hazard level.**

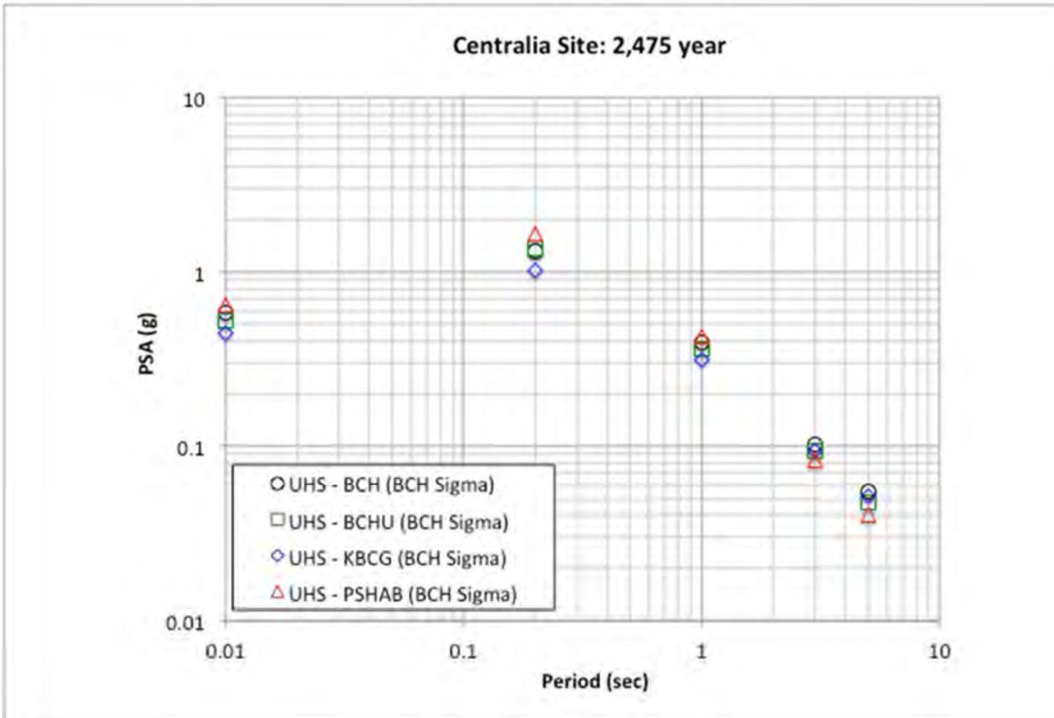

Figure 5.79 Comparison of UHS ground motions for the Centralia site based on the four separate subduction GMMs, with the BCH aleatory sigma model for the subduction seismic sources at the 2475-year-return-period hazard level.

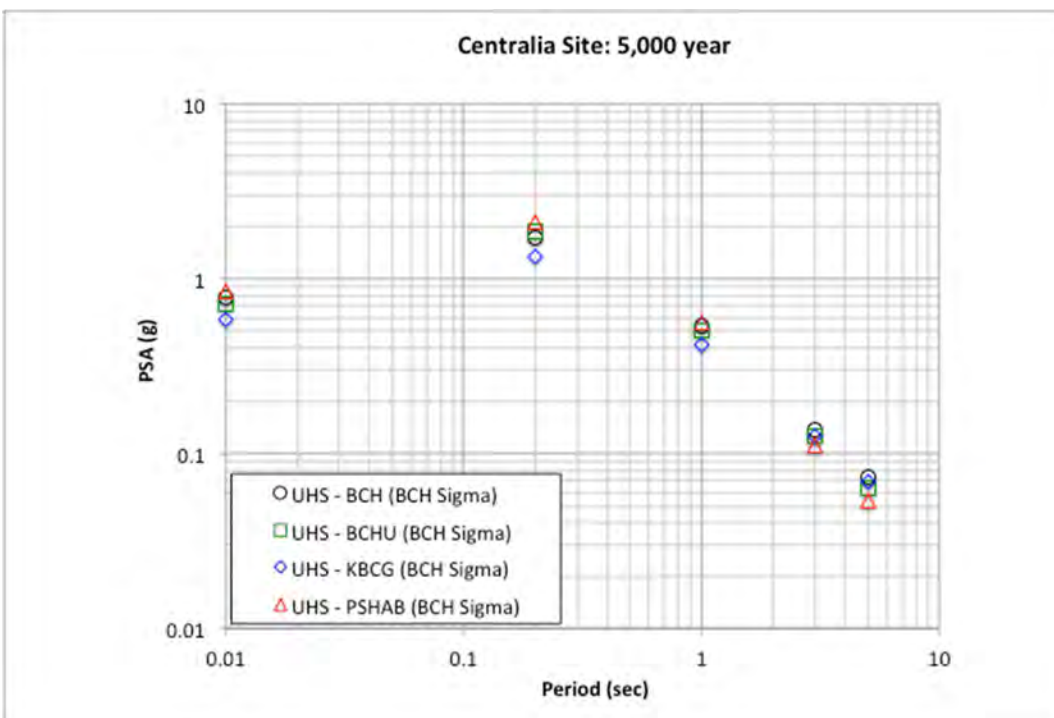

Figure 5.80 Comparison of UHS ground motions for the Centralia site based on the four separate subduction GMMs for the subduction seismic sources at the 5000-year-return-period hazard level.

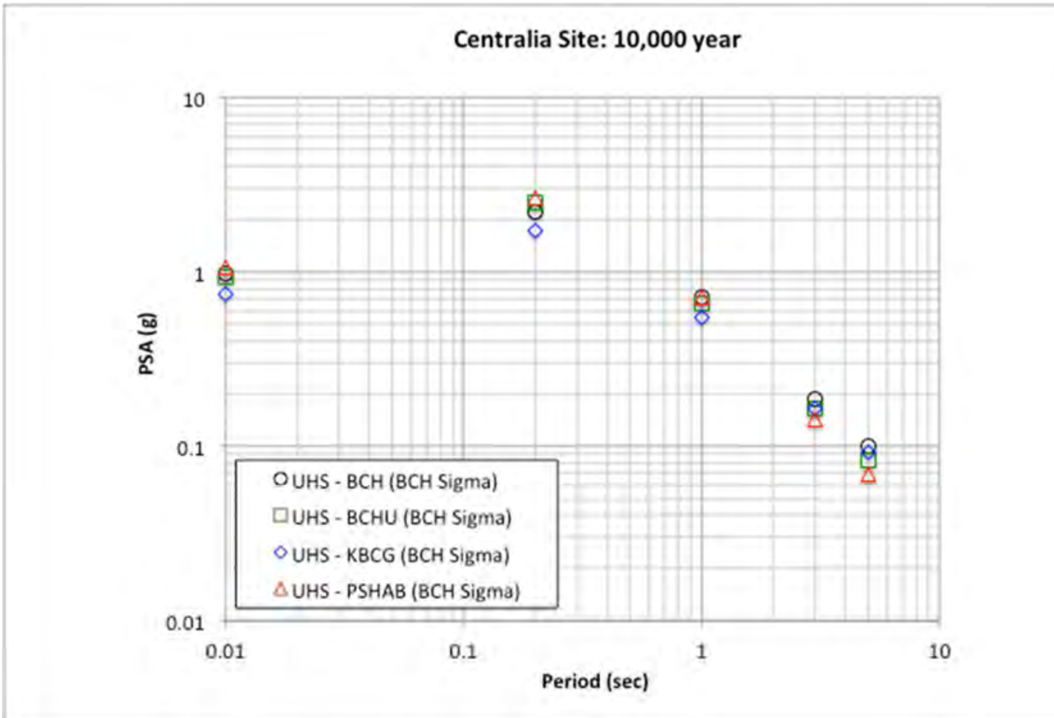

Figure 5.81 Comparison of UHS ground motions for the Centralia site based on the four separate subduction GMMs, with the BCH aleatory sigma model for the subduction seismic sources at the 10,000-year-return-period hazard level.

6 Summary

Currently three new subduction GMMs have been developed as part of the NGA-Sub program. These new GMMs are based on the NGA-Sub dataset [Bozorgnia and Stewart 2020], which represents a significant increase in the amount of empirical subduction ground-motion data. Two of the models, KBCG and PSHAB, have global and regionalized versions based on the regional datasets contained in the larger NGA-Sub database. The third newly developed model, SMK, is based on data from Japan and as such is applicable for seismic hazard studies for sites in Japan.

To assist with the understanding of these new models and their comparisons to previously published GMMs, this report shows various comparisons of the models. These comparisons are primarily in the form of attenuation curves and spectral response comparisons for a select set of scenario events. As noted in the report, these selected scenario events are not meant to capture the full range of the models or their expected implementation, but rather provide a small sample of representative scenario cases with a focus on the events controlling hazard in the Pacific Northwest region. Additional plots and the digital values for the attenuation curves and response spectra presented in this report are provided as part of the electronic supplement for this report; see Appendix A.

In addition to these attenuation curves and spectra comparisons, separate comparisons are provided for specific features contained in these models. Specifically, comparisons are provided for magnitude scaling, source depth and basin response.

In reviewing the various comparisons, observed differences are noted between the new GMMs and the previous published GMMs across different subduction source types (i.e., interface and slab events), magnitude, distance, site conditions, basin conditions, and spectral periods. Differences are also observed between the different aleatory models from the new and previous GMMs. Overall, the KBCG and PSHAB models estimate similar ground motions for the global cases (e.g., Figure 3.33 and Figure 3.34 for interface events and Figure 3.91 and Figure 3.92 for slab cases). For certain regionalized cases, such as Japan, the comparisons show a larger variation between the models along with the SMK model (see Figure 3.41 and Figure 3.42 for interface and Figure 3.99 and Figure 3.100 for slab) than observed for the global cases.

Two example sites are presented in the report for an example PSHA calculation. These sites—located in the state of Washington in the Pacific Northwest—highlight the potential impact of these new NGA-Sub GMMs. Given that the SMK model is developed for Japan, it was not included in these PSHA calculations.

Based on these limited comparisons and noted observations, it is expected that the implementation of these newly developed NGA-Sub GMMs will be supported by the types of comparisons presented in this report. For specific applications, additional comparison may and should be performed allowing for technical justifications for the implementation of these new models, including for the development of logic-tree weights. It is also expected in the future that additional NGA-Sub GMMs will be released, and these comparisons can be updated to include those new models in the future.

REFERENCES

Abrahamson N., Kuehn N., Gregor N., Bozorgnia Y., Parker G.A., Stewart J.P., Chiou B.-S.J., Campbell K.W., Youngs R. (2018). Update of the BC Hydro subduction ground-motion model using the NGA-subduction dataset, *PEER Report No. 2018/02*, Pacific Earthquake Engineering Research Center, University of California, Berkeley, CA.

Abrahamson N.A., Gregor N., Addo K. (2016). BC Hydro ground motion prediction equations for subduction earthquakes, *Earthq. Spectra*, 32: 23–44.

Abrahamson N.A., Silva W.J., Kamai R. (2014). Summary of the ASK14 ground motion relation for active crustal regions, *Earthq. Spectra*, 30: 1025–1055.

Al Atik L., Abrahamson N., Bommer J.J., Scherbaum F., Cotton F., Kuehn N. (2010). The variability of ground-motion prediction models and its components, *Seismol. Res. Lett.*, 81(5): 794–801.

Al Atik L., Youngs R.R. (2014). Epistemic uncertainty for NGA-West2 models. *Earthq. Spectra*, 30(3): 1301–1318.

Atkinson G.M., Boore D.M. (2003). Empirical ground-motion relations for subduction-zone earthquakes and their application to Cascadia and other regions, *Bull. Seismol. Soc. Am.*, 93: 1703–1729.

Atkinson G.M., Boore D.M. (2008). Erratum to Empirical ground-motion relations for subduction zone earthquakes and their application to Cascadia and other regions, *Bull. Seism. Soc. Am.*, 98(5): 2567–2569.

Atkinson G.M., Macias M. (2009). Predicted ground motions for great interface earthquakes in the Cascadia Subduction Zone, *Bull. Seism. Soc. Am.*, 99(3)1552–1578.

Boore D.M., Stewart J.P., Seyhan E., Atkinson G.M. (2014). NGA-West 2 equations for predicting PGA, PGV, and 5%-damped PSA for shallow crustal earthquakes, *Earthq. Spectra*, 30: 1057–1085.

Bozorgnia Y., Stewart J.P. (2020). Data resources for NGA-Subduction Project, *PEER No. Report 2020/02*, Pacific Earthquake Engineering Research Center, University of California, Berkeley, CA.

Building Seismic Safety Council (2009). *NEHRP Recommended Seismic Provisions for New Buildings and Other Structures FEMA Report P-750.* (Also available at *http://www.fema.gov/media-library/assets/documents/18152?id=4103.*)

Campbell K.W. (2020). Proposed methodology for estimating the magnitude at which subduction megathrust ground motions and source dimensions exhibit a break in magnitude scaling: Example for 79 global subduction zones, *Earthq. Spectra*, 36: *https://doi.org/10.1177/8755293019899957.*

Campbell K.W., Bozorgnia Y. (2014). NGA-West2 ground motion model for the average horizontal components of PGA, PGV, and 5% damped linear acceleration response spectra, *Earthq. Spectra*, 30: 1087–1115.

Chiou B.S.-J., Youngs R.R. (2014). Update of the Chiou and Youngs NGA model for the average horizontal component of peak ground motion and response spectra, *Earthq. Spectra*, 30, 1117–1153.

Earthquake Engineering Research Institute (1989). The basics of seismic risk analysis, *Earthq. Spectra*, (5): 675–699.

Gregor N., Abrahamson N.A., Atkinson G.M., Boore D.M., Bozorgnia Y., Campbell K.W., Chiou B. S-J, Idriss I.M., Kamai R., Seyhan E., Silva W.J., Stewart J.P. Youngs R.R. (2014). Comparison of NGA-West2 GMPEs, *Earthq. Spectra*, 30(3): 1179–1197.

Idriss I.M. (2014). An NGA-West2 empirical model for estimating the horizontal spectral values generated by shallow crustal earthquakes, *Earthq. Spectra*, 30(3) 1155–1177.

Ji C., Archuleta R. (2018). Scaling of PGA and PGV deduced from numerical simulations of intraslab earthquakes, Department of Earth Science, University of California, Santa Barbara, CA.

Kuehn N., Bozorgnia Y., Campbell K.W., Gregor N. (2020). Partially nonergodic ground-motion model for subduction regions using NGA-Subduction database, *PEER Report No. 2020/04*, Pacific Earthquake Engineering Research Center, University of California, Berkeley, CA.

Parker G.A., Stewart J.P., Boore D.M., Atkinson G.M., Hassani B. (2020). NGA-subduction global ground-motion model with regional adjustment factors, *PEER Report No. 2020/03*, Pacific Earthquake Engineering Research Center, University of California, Berkeley, CA.

Petersen M.D., Moshetti, M.P., Powers P.M., Mueller C.S., Haller K.M., Frankel A.D., Zeng Y., Rezaeian S., Harmsen S.C., Boyd O.S., Field E.H., Chen R., Rukstales K.S., Luco N., Wheeler R.L., Williams R.A., Olsen A.H. (2014). Documentation for the 2014 Update of the United States National Seismic Hazard Maps, *USGS. Open File Report 2014-1091*, U.S. Geological Survey, Reston, VA.

Petersen M.D, Shumway A.M., Powers P.M., Mueller C.S., Moschetti M.P., Frankel A.D., Rezaeian S., McNamara D.E., Luco N., Boyd O.S., Rukstales K.S., Hoover S.M., Clayton B.S., Field E.H., Zang Y. (2020). The 2018 update of the US National Seismic Hazard Model: Overview of model and implications, *Earthq. Spectra*, 36(1): 5–41.

SDCI (2018). Implementation of March 22, 2018 USGS/SDCI Basin Amplification Workshop Results, City of Seattle Department of Construction and Inspections, *Director's Rule 20-2018*, Seattle, WA.

Si H., Midorikawa S., Kishida T. (2020). Development of NGA-sub ground motion model of 5%-damped pseudo-spectral acceleration based on database for subduction earthquakes in Japan, PEER Report, *in press*, Pacific Earthquake Engineering Research Center, University of California, Berkeley, CA.

Wirth E.A., Chang S.W., Frankel A.D. (2018). 2018 report on incorporating sedimentary basin response into the design of tall buildings in Seattle, Washington, *U.S. Geological Survey Open-File Report 2018–1149*, Reston, VA, *https://doi.org/10.3133/ofr20181149*.

Zhao J.X., Jiang F., Shi P., Xing H., Huang H., Hou R., Zhang Y., Yu P., Lan X., Rhoades D.A., Somerville P.G. (2016b). Ground-motion prediction equations for subduction slab earthquakes in Japan using site class and simple geometric attenuation functions, *Bull. Seismol. Soc. Am.*, 106: 1535–1551.

Zhao J.X., Liang X., Jiang F., Xing H., Zhu M., Hou R., Zhang Y., Lan X., Rhoades D.A., Irikura K., Fukushima Y. (2016a). Ground-motion prediction equations for subduction interface earthquakes in Japan using site class and simple geometric attenuation functions, *Bull. Seismol. Soc. Am.*, 106: 1518–1534.

Zhao J.X., Zhang J., Asano A., Ohno Y., Oouchi T., Takahashi T., Ogawa H., Irikura K., Thio H.K., Somerville P.G., Fukushima Y. (2006). Attenuation relations of strong ground motion in Japan using site classification based on predominant period, *Bull. Seismol. Soc. Am.*, 96: 898–913.

APPENDIX A Description of Electronic Supplement Excel files for Digital GMM Values and Additional Comparison Plots

Several comparison plots are presented in the report for attenuation curves and spectra. These plots are separated based on interface and slab events and as well for global and regional versions of the models. For the interface cases, the comparisons are plotted for **M**8 events and for the slab cases only the **M**7 cases are plotted. As noted in the main report, the additional two magnitude values for both cases and all digital values are provided in the supplement electronic files associated with this report. This appendix presents the specific files and their format that contain these additional plots and digital values.

The electronic files provided as an electronic supplement for this report are separated into two folders: Interface and Slab. Within these folders, a similar sub-folder structure and file nomenclature is presented. The file and folder structure is:

Interface Cases – Attenuation Curves

Interface\Attenuation\Interface-Atten-Global-Rev001.xlsx

Interface\Attenuation\Interface-Atten-Alaska-Rev001.xlsx

Interface\Attenuation\Interface-Atten-CA&M-Rev001.xlsx

Interface\Attenuation\Interface-Atten-Cascadia-Rev001.xlsx

Interface\Attenuation\Interface-Atten-Japan-Rev001.xlsx

Interface\Attenuation\Interface-Atten-NewZealand-Rev001.xlsx

Interface\Attenuation\Interface-Atten-SA-Rev001.xlsx

Interface\Attenuation\Interface-Atten-Taiwan-Rev001.xlsx

Interface Cases – Spectra

Interface\Attenuation\Interface-Spectra-Global-Rev001.xlsx

Interface\Attenuation\Interface-Spectra-Alaska-Rev001.xlsx

Interface\Attenuation\Interface-Spectra-CA&M-Rev001.xlsx

Interface\Attenuation\Interface-Spectra-Cascadia-Rev001.xlsx

Interface\Attenuation\Interface-Spectra-Japan-Rev001.xlsx

Interface\Attenuation\Interface-Spectra-NewZealand-Rev000.xlsx

Interface\Attenuation\Interface-Spectra-SA-Rev001.xlsx

Interface\Attenuation\Interface-Spectra-Taiwan-Rev001.xlsx

Slab Cases – Attenuation Curves

Slab\Attenuation\Slab-Atten-Global-Rev001.xlsx

Slab\Attenuation\Slab-Atten-Alaska-Rev001.xlsx

Slab\Attenuation\Slab-Atten-CA&M-Rev001.xlsx

Slab\Attenuation\Slab-Atten-Cascadia-Rev001.xlsx

Slab\Attenuation\Slab-Atten-Japan-Rev001.xlsx

Slab\Attenuation\Slab-Atten-NewZealand-Rev001.xlsx

Slab\Attenuation\Slab-Atten-SA-Rev001.xlsx

Slab\Attenuation\Slab-Atten-Taiwan-Rev001.xlsx

Slab Cases – Spectra

Slab\Attenuation\Slab-Spectra-Global-Rev001.xlsx

Slab\Attenuation\Slab-Spectra-Alaska-Rev001.xlsx

Slab\Attenuation\Slab-Spectra-CA&M-Rev001.xlsx

Slab\Attenuation\Slab-Spectra-Cascadia-Rev001.xlsx

Slab\Attenuation\Slab-Spectra-Japan-Rev001.xlsx

Slab\Attenuation\Slab-Spectra-NewZealand-Rev001.xlsx

Slab\Attenuation\Slab-Spectra-SA-Rev001.xlsx

Slab\Attenuation\Slab-Spectra-Taiwan-Rev001.xlsx

The regional versions of the comparisons are differentiated in the filename. Within each of these files there are several data pages, summary data pages (indicated with blue tabs), a plot summary sheet (green tab), and numerous comparison plots. The specific models and plots are indicated on the abbreviated tabs names for each data sheet and chart plot.

PEER REPORTS

PEER reports are available as a free PDF download from https://peer.berkeley.edu/peer-reports. In addition, printed hard copies of PEER reports can be ordered directly from our printer by following the instructions at https://peer.berkeley.edu/peer-reports. For other related questions about the PEER Report Series, contact the Pacific Earthquake Engineering Research Center, 325 Davis Hall, Mail Code 1792, Berkeley, CA 94720. Tel.: (510) 642-3437; and Email: peer_center@berkeley.edu.

PEER 2020/06 *Development of NGA-Sub Ground-Motion Model of 5%-Damped Pseudo-Spectral Acceleration based on Database for Subduction Earthquakes in Japan.* Hongjun Si, Saburoh Midorikawa, and Tadahiro Kishida. November 2020.

PEER 2020/05 *Conditional Ground-Motion Model for Peak Ground Velocity for Active Crustal Regions.* Norman A. Abrahamson and Sarabjot Bhasin. October 2020.

PEER 2020/05 *Conditional Ground-Motion Model for Peak Ground Velocity for Active Crustal Regions.* Norman A. Abrahamson and Sarabjot Bhasin. October 2020.

PEER 2020/04 *Partially Non-Ergodic Ground-Motion Model for Subduction Regions using the NGA-Subduction Database.* Nicolas Kuehn, Yousef Bozognia, Kenneth W. Campbell, and Nicholas Gregor. September 2020.

PEER 2020/03 *NGA-Subduction Global Ground-Motion Models with Regional Adjustment Factors.* Grace A. Parker, Jonathan P. Stewart, David M. Boore, Gail M. Atkinson, and Behzad Hassani. September 2020.

PEER 2020/02 *Data Resources for NGA-Subduction Project.* Yousef Bozorgnia (PI) and Jonathan P. Stewart (Editor). March 2020.

PEER 2020/01 *Modeling Viscous Damping in Nonlinear Response History Analysis for Steel Moment-Frame Buildings.* Xin Qian, Anil K. Chopra, and Frank McKenna. June 2020.

PEER 2019/09 Seismic Behavior of Special Concentric Braced Frames under Short- and Long-Duration Ground Motions. Ali Hammad and Mohamed A. Moustafa. December 2019.

PEER 2019/08 Influence of Vertical Ground Motion on Bridges Isolated with Spherical Sliding Bearings. Rushil Mojidra and Keri L. Ryan. December 2019.

PEER 2019/07 *PEER Hub ImageNet* (ϕ-Net): *A Large-Scale Multi-Attribute Benchmark Dataset of Structural Images*. Yuqing Gao, and Khalid. M. Mosalam. November 2019.

PEER 2019/06 *Fluid-Structure Interaction and Python-Scripting Capabilities in OpenSees*. Minjie Zhu and Michael H. Scott. August 2019.

PEER 2019/05 *Expected Earthquake Performance of Buildings Designed to the California Building Code (California Alfred E. Alquist Seismic Safety Publication 19-01).* Grace S. Kang, Sifat Muin, Jorge Archbold, Bitanoosh Woods, and Khalid Mosalam. July 2019.

PEER 2019/04 *Aftershock Seismic Vulnerability and Time-Dependent Risk Assessment of Bridges*. Sujith Mangalathu, Mehrdad Shokrabadi, and Henry V. Burton. May 2019.

PEER 2019/03 *Ground-Motion Directivity Modeling for Seismic Hazard Applications.* Jennifer L. Donahue, Jonathan P. Stewart, Nicolas Gregor, and Yousef Bozorgnia. Review Panel: Jonathan D. Bray, Stephen A. Mahin, I. M. Idriss, Robert W. Graves, and Tom Shantz. May 2019.

PEER 2019/02 *Direct-Finite-Element Method for Nonlinear Earthquake Analysis of Concrete Dams Including Dam–Water–Foundation Rock Interaction.* Arnkjell Løkke and Anil K. Chopra. March 2019.

PEER 2019/01 *Flow-Failure Case History of the Las Palmas, Chile, Tailings Dam.* R. E. S. Moss, T. R. Gebhart, D. J. Frost, and C. Ledezma. January 2019.

PEER 2018/08 *Central and Eastern North America Ground-Motion Characterization: NGA-East Final Report*. Christine Goulet, Yousef Bozorgnia, Norman Abrahamson, Nicolas Kuehn, Linda Al Atik, Robert Youngs, Robert Graves, and Gail Atkinson. December 2018.

PEER 2018/07 *An Empirical Model for Fourier Amplitude Spectra using the NGA-West2 Database*. Jeff Bayless, and Norman A. Abrahamson. December 2018.

PEER 2018/06 *Estimation of Shear Demands on Rock-Socketed Drilled Shafts subjected to Lateral Loading*. Pedro Arduino, Long Chen, and Christopher R. McGann. December 2018.

PEER 2018/05 *Selection of Random Vibration Procedures for the NGA-East Project*. Albert Kottke, Norman A. Abrahamson, David M. Boore, Yousef Bozorgnia, Christine Goulet, Justin Hollenback, Tadahiro Kishida, Armen Der Kiureghian, Olga-Joan Ktenidou, Nicolas Kuehn, Ellen M. Rathje, Walter J. Silva, Eric Thompson, and Xiaoyue Wang. December 2018.

PEER 2018/04 *Capturing Directivity Effects in the Mean and Aleatory Variability of the NGA-West 2 Ground Motion Prediction Equations.* Jennie A. Watson-Lamprey. November 2018*.*

PEER 2018/03 *Probabilistic Seismic Hazard Analysis Code Verification*. Christie Hale, Norman Abrahamson, and Yousef Bozorgnia. July 2018.

PEER 2018/02 *Update of the BCHydro Subduction Ground-Motion Model using the NGA-Subduction Dataset.* Norman Abrahamson, Nicolas Kuehn, Zeynep Gulerce, Nicholas Gregor, Yousef Bozorgnia, Grace Parker, Jonathan Stewart, Brian Chiou, I. M. Idriss, Kenneth Campbell, and Robert Youngs. June 2018.

PEER 2018/01 *PEER Annual Report 2017–2018*. Khalid Mosalam, Amarnath Kasalanati, and Selim Günay. June 2018.

PEER 2017/12 *Experimental Investigation of the Behavior of Vintage and Retrofit Concentrically Braced Steel Frames under Cyclic Loading*. Barbara G. Simpson, Stephen A. Mahin, and Jiun-Wei Lai, December 2017.

PEER 2017/11 *Preliminary Studies on the Dynamic Response of a Seismically Isolated Prototype Gen-IV Sodium-Cooled Fast Reactor* (*PGSFR*). Benshun Shao, Andreas H. Schellenberg, Matthew J. Schoettler, and Stephen A. Mahin. December 2017.

PEER 2017/10 *Development of Time Histories for IEEE693 Testing and Analysis (including Seismically Isolated Equipment).* Shakhzod M. Takhirov, Eric Fujisaki, Leon Kempner, Michael Riley, and Brian Low. December 2017.

PEER 2017/09 *“”R” Package for Computation of Earthquake Ground-Motion Response Spectra.* Pengfei Wang, Jonathan P. Stewart, Yousef Bozorgnia, David M. Boore, and Tadahiro Kishida. December 2017.

PEER 2017/08 *Influence of Kinematic SSI on Foundation Input Motions for Bridges on Deep Foundations*. Benjamin J. Turner, Scott J. Brandenberg, and Jonathan P. Stewart. November 2017.

PEER 2017/07 *A Nonlinear Kinetic Model for Multi-Stage Friction Pendulum Systems*. Paul L. Drazin and Sanjay Govindjee. September 2017.

PEER 2017/06 *Guidelines for Performance-Based Seismic Design of Tall Buildings, Version 2.02*. TBI Working Group led by co-chairs Ron Hamburger and Jack Moehle: Jack Baker, Jonathan Bray, C.B. Crouse, Greg Deierlein, John Hooper, Marshall Lew, Joe Maffei, Stephen Mahin, James Malley, Farzad Naeim, Jonathan Stewart, and John Wallace. May 2017.

PEER 2017/05 *Recommendations for Ergodic Nonlinear Site Amplification in Central and Eastern North America*. Youssef M.A. Hashash, Joseph A. Harmon, Okan Ilhan, Grace A. Parker, and Jonathan P. Stewart. March 2017.

PEER 2017/04 *Expert Panel Recommendations for Ergodic Site Amplification in Central and Eastern North America*. Jonathan P. Stewart, Grace A. Parker, Joseph P. Harmon, Gail M. Atkinson, David M. Boore, Robert B. Darragh, Walter J. Silva, and Youssef M.A. Hashash. March 2017.

PEER 2017/03 *NGA-East Ground-Motion Models for the U.S. Geological Survey National Seismic Hazard Maps*. Christine A. Goulet, Yousef Bozorgnia, Nicolas Kuehn, Linda Al Atik, Robert R. Youngs, Robert W. Graves, and Gail M. Atkinson. March 2017.

PEER 2017/02 *U.S.–New Zealand–Japan Workshop: Liquefaction-Induced Ground Movements Effects, University of California, Berkeley, California, 2–4 November 2016.* Jonathan D. Bray, Ross W. Boulanger, Misko Cubrinovski, Kohji Tokimatsu, Steven L. Kramer, Thomas O’Rourke, Ellen Rathje, Russell A. Green, Peter K. Robinson, and Christine Z. Beyzaei. March 2017.

PEER 2017/01 *2016 PEER Annual Report*. Khalid M. Mosalam, Amarnath Kasalanati, and Grace Kang. March 2017.

PEER 2016/10 *Performance-Based Robust Nonlinear Seismic Analysis with Application to Reinforced Concrete Bridge Systems*. Xiao Ling and Khalid M. Mosalam. December 2016.

PEER 2017/09 *Detailing Requirements for Column Plastic Hinges subjected to Combined Flexural, Axial, and Torsional Seismic Loading.* Gabriel Hurtado and Jack P. Moehle. December 2016.

PEER 2016/08 *Resilience of Critical Structures, Infrastructure, and Communities*. Gian Paolo Cimellaro, Ali Zamani-Noori, Omar Kamouh, Vesna Terzic, and Stephen A. Mahin. December 2016.

PEER 2016/07 *Hybrid Simulation Theory for a Classical Nonlinear Dynamical System*. Paul L. Drazin and Sanjay Govindjee. September 2016.

PEER 2016/06 *California Earthquake Early Warning System Benefit Study*. Laurie A. Johnson, Sharyl Rabinovici, Grace S. Kang, and Stephen A. Mahin. July 2006.

PEER 2016/05 *Ground-Motion Prediction Equations for Arias Intensity Consistent with the NGA-West2 Ground-Motion Models.* Charlotte Abrahamson, Hao-Jun Michael Shi, and Brian Yang. July 2016.

PEER 2016/04 *The M_W 6.0 South Napa Earthquake of August 24, 2014: A Wake-Up Call for Renewed Investment in Seismic Resilience Across California.* Prepared for the California Seismic Safety Commission, Laurie A. Johnson and Stephen A. Mahin. May 2016.

PEER 2016/03 *Simulation Confidence in Tsunami-Driven Overland Flow.* Patrick Lynett. May 2016.

PEER 2016/02 *Semi-Automated Procedure for Windowing time Series and Computing Fourier Amplitude Spectra for the NGA-West2 Database.* Tadahiro Kishida, Olga-Joan Ktenidou, Robert B. Darragh, and Walter J. Silva. May 2016.

PEER 2016/01 *A Methodology for the Estimation of Kappa (κ) from Large Datasets: Example Application to Rock Sites in the NGA-East Database and Implications on Design Motions.* Olga-Joan Ktenidou, Norman A. Abrahamson, Robert B. Darragh, and Walter J. Silva. April 2016.

PEER 2015/13 *Self-Centering Precast Concrete Dual-Steel-Shell Columns for Accelerated Bridge Construction: Seismic Performance, Analysis, and Design*. Gabriele Guerrini, José I. Restrepo, Athanassios Vervelidis, and Milena Massari. December 2015.

PEER 2015/12 *Shear-Flexure Interaction Modeling for Reinforced Concrete Structural Walls and Columns under Reversed Cyclic Loading*. Kristijan Kolozvari, Kutay Orakcal, and John Wallace. December 2015.

PEER 2015/11 *Selection and Scaling of Ground Motions for Nonlinear Response History Analysis of Buildings in Performance-Based Earthquake Engineering*. N. Simon Kwong and Anil K. Chopra. December 2015.

PEER 2015/10 *Structural Behavior of Column-Bent Cap Beam-Box Girder Systems in Reinforced Concrete Bridges Subjected to Gravity and Seismic Loads. Part II: Hybrid Simulation and Post-Test Analysis*. Mohamed A. Moustafa and Khalid M. Mosalam. November 2015.

PEER 2015/09 *Structural Behavior of Column-Bent Cap Beam-Box Girder Systems in Reinforced Concrete Bridges Subjected to Gravity and Seismic Loads. Part I: Pre-Test Analysis and Quasi-Static Experiments*. Mohamed A. Moustafa and Khalid M. Mosalam. September 2015.

PEER 2015/08 *NGA-East: Adjustments to Median Ground-Motion Models for Center and Eastern North America*. August 2015.

PEER 2015/07 *NGA-East: Ground-Motion Standard-Deviation Models for Central and Eastern North America*. Linda Al Atik. June 2015.

PEER 2015/06 *Adjusting Ground-Motion Intensity Measures to a Reference Site for which V_{S30} = 3000 m/sec*. David M. Boore. May 2015.

PEER 2015/05 *Hybrid Simulation of Seismic Isolation Systems Applied to an APR-1400 Nuclear Power Plant.* Andreas H. Schellenberg, Alireza Sarebanha, Matthew J. Schoettler, Gilberto Mosqueda, Gianmario Benzoni, and Stephen A. Mahin. April 2015.

PEER 2015/04 *NGA-East: Median Ground-Motion Models for the Central and Eastern North America Region*. April 2015.

PEER 2015/03 *Single Series Solution for the Rectangular Fiber-Reinforced Elastomeric Isolator Compression Modulus*. James M. Kelly and Niel C. Van Engelen. March 2015.

PEER 2015/02 *A Full-Scale, Single-Column Bridge Bent Tested by Shake-Table Excitation.* Matthew J. Schoettler, José I. Restrepo, Gabriele Guerrini, David E. Duck, and Francesco Carrea. March 2015.

PEER 2015/01 *Concrete Column Blind Prediction Contest 2010: Outcomes and Observations.* Vesna Terzic, Matthew J. Schoettler, José I. Restrepo, and Stephen A Mahin. March 2015.

PEER 2014/20 *Stochastic Modeling and Simulation of Near-Fault Ground Motions for Performance-Based Earthquake Engineering*. Mayssa Dabaghi and Armen Der Kiureghian. December 2014.

PEER 2014/19 *Seismic Response of a Hybrid Fiber-Reinforced Concrete Bridge Column Detailed for Accelerated Bridge Construction*. Wilson Nguyen, William Trono, Marios Panagiotou, and Claudia P. Ostertag. December 2014.

PEER 2014/18 *Three-Dimensional Beam-Truss Model for Reinforced Concrete Walls and Slabs Subjected to Cyclic Static or Dynamic Loading*. Yuan Lu, Marios Panagiotou, and Ioannis Koutromanos. December 2014.

PEER 2014/17 *PEER NGA-East Database.* Christine A. Goulet, Tadahiro Kishida, Timothy D. Ancheta, Chris H. Cramer, Robert B. Darragh, Walter J. Silva, Youssef M.A. Hashash, Joseph Harmon, Jonathan P. Stewart, Katie E. Wooddell, and Robert R. Youngs. October 2014.

PEER 2014/16 *Guidelines for Performing Hazard-Consistent One-Dimensional Ground Response Analysis for Ground Motion Prediction*. Jonathan P. Stewart, Kioumars Afshari, and Youssef M.A. Hashash. October 2014.

PEER 2014/15 *NGA-East Regionalization Report: Comparison of Four Crustal Regions within Central and Eastern North America using Waveform Modeling and 5%-Damped Pseudo-Spectral Acceleration Response*. Jennifer Dreiling, Marius P. Isken, Walter D. Mooney, Martin C. Chapman, and Richard W. Godbee. October 2014.

PEER 2014/14 *Scaling Relations between Seismic Moment and Rupture Area of Earthquakes in Stable Continental Regions*. Paul Somerville. August 2014.

PEER 2014/13 *PEER Preliminary Notes and Observations on the August 24, 2014, South Napa Earthquake*. Grace S. Kang and Stephen A. Mahin, Editors. September 2014.

PEER 2014/12 *Reference-Rock Site Conditions for Central and Eastern North America: Part II – Attenuation (Kappa) Definition*. Kenneth W. Campbell, Youssef M.A. Hashash, Byungmin Kim, Albert R. Kottke, Ellen M. Rathje, Walter J. Silva, and Jonathan P. Stewart. August 2014.

PEER 2014/11 *Reference-Rock Site Conditions for Central and Eastern North America: Part I - Velocity Definition*. Youssef M.A. Hashash, Albert R. Kottke, Jonathan P. Stewart, Kenneth W. Campbell, Byungmin Kim, Ellen M. Rathje, Walter J. Silva, Sissy Nikolaou, and Cheryl Moss. August 2014.

PEER 2014/10 *Evaluation of Collapse and Non-Collapse of Parallel Bridges Affected by Liquefaction and Lateral Spreading*. Benjamin Turner, Scott J. Brandenberg, and Jonathan P. Stewart. August 2014.

PEER 2014/09 *PEER Arizona Strong-Motion Database and GMPEs Evaluation*. Tadahiro Kishida, Robert E. Kayen, Olga-Joan Ktenidou, Walter J. Silva, Robert B. Darragh, and Jennie Watson-Lamprey. June 2014.

PEER 2014/08 *Unbonded Pretensioned Bridge Columns with Rocking Detail*. Jeffrey A. Schaefer, Bryan Kennedy, Marc O. Eberhard, and John F. Stanton. June 2014.

PEER 2014/07 *Northridge 20 Symposium Summary Report: Impacts, Outcomes, and Next Steps*. May 2014.

PEER 2014/06 *Report of the Tenth Planning Meeting of NEES/E-Defense Collaborative Research on Earthquake Engineering*. December 2013.

PEER 2014/05 *Seismic Velocity Site Characterization of Thirty-One Chilean Seismometer Stations by Spectral Analysis of Surface Wave Dispersion*. Robert Kayen, Brad D. Carkin, Skye Corbet, Camilo Pinilla, Allan Ng, Edward Gorbis, and Christine Truong. April 2014.

PEER 2014/04 Effect of Vertical Acceleration on Shear Strength of Reinforced Concrete Columns. Hyerin Lee and Khalid M. Mosalam. April 2014.

PEER 2014/03 *Retest of Thirty-Year-Old Neoprene Isolation Bearings.* James M. Kelly and Niel C. Van Engelen. March 2014.

PEER 2014/02 *Theoretical Development of Hybrid Simulation Applied to Plate Structures.* Ahmed A. Bakhaty, Khalid M. Mosalam, and Sanjay Govindjee. January 2014.

PEER 2014/01 *Performance-Based Seismic Assessment of Skewed Bridges.* Peyman Kaviani, Farzin Zareian, and Ertugrul Taciroglu. January 2014.

PEER 2013/26 *Urban Earthquake Engineerin*g. Proceedings of the U.S.-Iran Seismic Workshop. December 2013.

PEER 2013/25 *Earthquake Engineering for Resilient Communities: 2013 PEER Internship Program Research Report Collection.* Heidi Tremayne (Editor), Stephen A. Mahin (Editor), Jorge Archbold Monterossa, Matt Brosman, Shelly Dean, Katherine deLaveaga, Curtis Fong, Donovan Holder, Rakeeb Khan, Elizabeth Jachens, David Lam, Daniela Martinez Lopez, Mara Minner, Geffen Oren, Julia Pavicic, Melissa Quinonez, Lorena Rodriguez, Sean Salazar, Kelli Slaven, Vivian Steyert, Jenny Taing, and Salvador Tena. December 2013.

PEER 2013/24 *NGA-West2 Ground Motion Prediction Equations for Vertical Ground Motions*. September 2013.

PEER 2013/23 *Coordinated Planning and Preparedness for Fire Following Major Earthquakes*. Charles Scawthorn. November 2013.

PEER 2013/22 *GEM-PEER Task 3 Project: Selection of a Global Set of Ground Motion Prediction Equations.* Jonathan P. Stewart, John Douglas, Mohammad B. Javanbarg, Carola Di Alessandro, Yousef Bozorgnia, Norman A. Abrahamson, David M. Boore, Kenneth W. Campbell, Elise Delavaud, Mustafa Erdik, and Peter J. Stafford. December 2013.

PEER 2013/21 *Seismic Design and Performance of Bridges with Columns on Rocking Foundations*. Grigorios Antonellis and Marios Panagiotou. September 2013.

PEER 2013/20 *Experimental and Analytical Studies on the Seismic Behavior of Conventional and Hybrid Braced Frames*. Jiun-Wei Lai and Stephen A. Mahin. September 2013.

PEER 2013/19 *Toward Resilient Communities: A Performance-Based Engineering Framework for Design and Evaluation of the Built Environment.* Michael William Mieler, Bozidar Stojadinovic, Robert J. Budnitz, Stephen A. Mahin, and Mary C. Comerio. September 2013.

PEER 2013/18 *Identification of Site Parameters that Improve Predictions of Site Amplification*. Ellen M. Rathje and Sara Navidi. July 2013.

PEER 2013/17 *Response Spectrum Analysis of Concrete Gravity Dams Including Dam-Water-Foundation Interaction*. Arnkjell Løkke and Anil K. Chopra. July 2013.

PEER 2013/16 *Effect of Hoop Reinforcement Spacing on the Cyclic Response of Large Reinforced Concrete Special Moment Frame Beams.* Marios Panagiotou, Tea Visnjic, Grigorios Antonellis, Panagiotis Galanis, and Jack P. Moehle. June 2013.

PEER 2013/15 *A Probabilistic Framework to Include the Effects of Near-Fault Directivity in Seismic Hazard Assessment*. Shrey Kumar Shahi, Jack W. Baker. October 2013.

PEER 2013/14 *Hanging-Wall Scaling using Finite-Fault Simulations.* Jennifer L. Donahue and Norman A. Abrahamson. September 2013.

PEER 2013/13 *Semi-Empirical Nonlinear Site Amplification and its Application in NEHRP Site Factors*. Jonathan P. Stewart and Emel Seyhan. November 2013.

PEER 2013/12 *Nonlinear Horizontal Site Response for the NGA-West2 Project.* Ronnie Kamai, Norman A. Abramson, Walter J. Silva. May 2013.

PEER 2013/11 *Epistemic Uncertainty for NGA-West2 Models.* Linda Al Atik and Robert R. Youngs. May 2013.

PEER 2013/10 *NGA-West 2 Models for Ground-Motion Directionality.* Shrey K. Shahi and Jack W. Baker. May 2013.

PEER 2013/09 *Final Report of the NGA-West2 Directivity Working Group.* Paul Spudich, Jeffrey R. Bayless, Jack W. Baker, Brian S.J. Chiou, Badie Rowshandel, Shrey Shahi, and Paul Somerville. May 2013.

PEER 2013/08 *NGA-West2 Model for Estimating Average Horizontal Values of Pseudo-Absolute Spectral Accelerations Generated by Crustal Earthquakes*. I. M. Idriss. May 2013.

PEER 2013/07 *Update of the Chiou and Youngs NGA Ground Motion Model for Average Horizontal Component of Peak Ground Motion and Response Spectra*. Brian Chiou and Robert Youngs. May 2013.

PEER 2013/06 *NGA-West2 Campbell-Bozorgnia Ground Motion Model for the Horizontal Components of PGA, PGV, and 5%-Damped Elastic Pseudo-Acceleration Response Spectra for Periods Ranging from 0.01 to 10 sec.* Kenneth W. Campbell and Yousef Bozorgnia. May 2013.

PEER 2013/05 *NGA-West 2 Equations for Predicting Response Spectral Accelerations for Shallow Crustal Earthquakes*. David M. Boore, Jonathan P. Stewart, Emel Seyhan, and Gail M. Atkinson. May 2013.

PEER 2013/04 *Update of the AS08 Ground-Motion Prediction Equations Based on the NGA-West2 Data Set*. Norman Abrahamson, Walter Silva, and Ronnie Kamai. May 2013.

PEER 2013/03 *PEER NGA-West2 Database.* Timothy D. Ancheta, Robert B. Darragh, Jonathan P. Stewart, Emel Seyhan, Walter J. Silva, Brian S.J. Chiou, Katie E. Wooddell, Robert W. Graves, Albert R. Kottke, David M. Boore, Tadahiro Kishida, and Jennifer L. Donahue. May 2013.

PEER 2013/02 *Hybrid Simulation of the Seismic Response of Squat Reinforced Concrete Shear Walls*. Catherine A. Whyte and Bozidar Stojadinovic. May 2013.

PEER 2013/01 *Housing Recovery in Chile: A Qualitative Mid-program Review*. Mary C. Comerio. February 2013.

PEER 2012/08 *Guidelines for Estimation of Shear Wave Velocity.* Bernard R. Wair, Jason T. DeJong, and Thomas Shantz. December 2012.

PEER 2012/07 *Earthquake Engineering for Resilient Communities: 2012 PEER Internship Program Research Report Collection.* Heidi Tremayne (Editor), Stephen A. Mahin (Editor), Collin Anderson, Dustin Cook, Michael Erceg, Carlos Esparza, Jose Jimenez, Dorian Krausz, Andrew Lo, Stephanie Lopez, Nicole McCurdy, Paul Shipman, Alexander Strum, Eduardo Vega. December 2012.

PEER 2012/06 *Fragilities for Precarious Rocks at Yucca Mountain.* Matthew D. Purvance, Rasool Anooshehpoor, and James N. Brune. December 2012.

PEER 2012/05 *Development of Simplified Analysis Procedure for Piles in Laterally Spreading Layered Soils.* Christopher R. McGann, Pedro Arduino, and Peter Mackenzie–Helnwein. December 2012.

PEER 2012/04 *Unbonded Pre-Tensioned Columns for Bridges in Seismic Regions.* Phillip M. Davis, Todd M. Janes, Marc O. Eberhard, and John F. Stanton. December 2012.

PEER 2012/03 *Experimental and Analytical Studies on Reinforced Concrete Buildings with Seismically Vulnerable Beam-Column Joints*. Sangjoon Park and Khalid M. Mosalam. October 2012.

PEER 2012/02 *Seismic Performance of Reinforced Concrete Bridges Allowed to Uplift during Multi-Directional Excitation*. Andres Oscar Espinoza and Stephen A. Mahin. July 2012.

PEER 2012/01 *Spectral Damping Scaling Factors for Shallow Crustal Earthquakes in Active Tectonic Regions.* Sanaz Rezaeian, Yousef Bozorgnia, I. M. Idriss, Kenneth Campbell, Norman Abrahamson, and Walter Silva. July 2012.

PEER 2011/10 *Earthquake Engineering for Resilient Communities: 2011 PEER Internship Program Research Report Collection*. Heidi Faison and Stephen A. Mahin, Editors. December 2011.

PEER 2011/09 *Calibration of Semi-Stochastic Procedure for Simulating High-Frequency Ground Motions*. Jonathan P. Stewart, Emel Seyhan, and Robert W. Graves. December 2011.

PEER 2011/08 *Water Supply in regard to Fire Following Earthquake*. Charles Scawthorn. November 2011.

PEER 2011/07 *Seismic Risk Management in Urban Areas*. Proceedings of a U.S.-Iran-Turkey Seismic Workshop. September 2011.

PEER 2011/06 *The Use of Base Isolation Systems to Achieve Complex Seismic Performance Objectives*. Troy A. Morgan and Stephen A. Mahin. July 2011.

PEER 2011/05 *Case Studies of the Seismic Performance of Tall Buildings Designed by Alternative Means.* Task 12 Report for the Tall Buildings Initiative. Jack Moehle, Yousef Bozorgnia, Nirmal Jayaram, Pierson Jones, Mohsen Rahnama, Nilesh Shome, Zeynep Tuna, John Wallace, Tony Yang, and Farzin Zareian. July 2011.

PEER 2011/04 *Recommended Design Practice for Pile Foundations in Laterally Spreading Ground.* Scott A. Ashford, Ross W. Boulanger, and Scott J. Brandenberg. June 2011.

PEER 2011/03 *New Ground Motion Selection Procedures and Selected Motions for the PEER Transportation Research Program*. Jack W. Baker, Ting Lin, Shrey K. Shahi, and Nirmal Jayaram. March 2011.

PEER 2011/02 *A Bayesian Network Methodology for Infrastructure Seismic Risk Assessment and Decision Support*. Michelle T. Bensi, Armen Der Kiureghian, and Daniel Straub. March 2011.

PEER 2011/01 *Demand Fragility Surfaces for Bridges in Liquefied and Laterally Spreading Ground.* Scott J. Brandenberg, Jian Zhang, Pirooz Kashighandi, Yili Huo, and Minxing Zhao. March 2011.

PEER 2010/05 *Guidelines for Performance-Based Seismic Design of Tall Buildings.* Developed by the Tall Buildings Initiative. November 2010.

PEER 2010/04 *Application Guide for the Design of Flexible and Rigid Bus Connections between Substation Equipment Subjected to Earthquakes.* Jean-Bernard Dastous and Armen Der Kiureghian. September 2010.

PEER 2010/03 *Shear Wave Velocity as a Statistical Function of Standard Penetration Test Resistance and Vertical Effective Stress at Caltrans Bridge Sites.* Scott J. Brandenberg, Naresh Bellana, and Thomas Shantz. June 2010.

PEER 2010/02 *Stochastic Modeling and Simulation of Ground Motions for Performance-Based Earthquake Engineering.* Sanaz Rezaeian and Armen Der Kiureghian. June 2010.

PEER 2010/01 *Structural Response and Cost Characterization of Bridge Construction Using Seismic Performance Enhancement Strategies.* Ady Aviram, Božidar Stojadinović, Gustavo J. Parra-Montesinos, and Kevin R. Mackie. March 2010.

PEER 2009/03 *The Integration of Experimental and Simulation Data in the Study of Reinforced Concrete Bridge Systems Including Soil-Foundation-Structure Interaction.* Matthew Dryden and Gregory L. Fenves. November 2009.

PEER 2009/02 *Improving Earthquake Mitigation through Innovations and Applications in Seismic Science, Engineering, Communication, and Response*. Proceedings of a U.S.-Iran Seismic Workshop. October 2009.

PEER 2009/01 *Evaluation of Ground Motion Selection and Modification Methods: Predicting Median Interstory Drift Response of Buildings*. Curt B. Haselton, Editor. June 2009.

PEER 2008/10 *Technical Manual for Strata.* Albert R. Kottke and Ellen M. Rathje. February 2009.

PEER 2008/09 *NGA Model for Average Horizontal Component of Peak Ground Motion and Response Spectra.* Brian S.-J. Chiou and Robert R. Youngs. November 2008.

PEER 2008/08 *Toward Earthquake-Resistant Design of Concentrically Braced Steel Structures*. Patxi Uriz and Stephen A. Mahin. November 2008.

PEER 2008/07 *Using OpenSees for Performance-Based Evaluation of Bridges on Liquefiable Soils*. Stephen L. Kramer, Pedro Arduino, and HyungSuk Shin. November 2008.

PEER 2008/06 *Shaking Table Tests and Numerical Investigation of Self-Centering Reinforced Concrete Bridge Columns*. Hyung IL Jeong, Junichi Sakai, and Stephen A. Mahin. September 2008.

PEER 2008/05 *Performance-Based Earthquake Engineering Design Evaluation Procedure for Bridge Foundations Undergoing Liquefaction-Induced Lateral Ground Displacement*. Christian A. Ledezma and Jonathan D. Bray. August 2008.

PEER 2008/04 *Benchmarking of Nonlinear Geotechnical Ground Response Analysis Procedures.* Jonathan P. Stewart, Annie On-Lei Kwok, Youssef M. A. Hashash, Neven Matasovic, Robert Pyke, Zhiliang Wang, and Zhaohui Yang. August 2008.

PEER 2008/03 *Guidelines for Nonlinear Analysis of Bridge Structures in California.* Ady Aviram, Kevin R. Mackie, and Božidar Stojadinović. August 2008.

PEER 2008/02 *Treatment of Uncertainties in Seismic-Risk Analysis of Transportation Systems*. Evangelos Stergiou and Anne S. Kiremidjian. July 2008.

PEER 2008/01 *Seismic Performance Objectives for Tall Buildings.* William T. Holmes, Charles Kircher, William Petak, and Nabih Youssef. August 2008.

PEER 2007/12 *An Assessment to Benchmark the Seismic Performance of a Code-Conforming Reinforced Concrete Moment-Frame Building.* Curt Haselton, Christine A. Goulet, Judith Mitrani-Reiser, James L. Beck, Gregory G. Deierlein, Keith A. Porter, Jonathan P. Stewart, and Ertugrul Taciroglu. August 2008.

PEER 2007/11 *Bar Buckling in Reinforced Concrete Bridge Columns.* Wayne A. Brown, Dawn E. Lehman, and John F. Stanton. February 2008.

PEER 2007/10 *Computational Modeling of Progressive Collapse in Reinforced Concrete Frame Structures*. Mohamed M. Talaat and Khalid M. Mosalam. May 2008.

PEER 2007/09 *Integrated Probabilistic Performance-Based Evaluation of Benchmark Reinforced Concrete Bridges*. Kevin R. Mackie, John-Michael Wong, and Božidar Stojadinović. January 2008.

PEER 2007/08 *Assessing Seismic Collapse Safety of Modern Reinforced Concrete Moment-Frame Buildings*. Curt B. Haselton and Gregory G. Deierlein. February 2008.

PEER 2007/07 *Performance Modeling Strategies for Modern Reinforced Concrete Bridge Columns*. Michael P. Berry and Marc O. Eberhard. April 2008.

PEER 2007/06 *Development of Improved Procedures for Seismic Design of Buried and Partially Buried Structures*. Linda Al Atik and Nicholas Sitar. June 2007.

PEER 2007/05 *Uncertainty and Correlation in Seismic Risk Assessment of Transportation Systems*. Renee G. Lee and Anne S. Kiremidjian. July 2007.

PEER 2007/04 *Numerical Models for Analysis and Performance-Based Design of Shallow Foundations Subjected to Seismic Loading.* Sivapalan Gajan, Tara C. Hutchinson, Bruce L. Kutter, Prishati Raychowdhury, José A. Ugalde, and Jonathan P. Stewart. May 2008.

PEER 2007/03 *Beam-Column Element Model Calibrated for Predicting Flexural Response Leading to Global Collapse of RC Frame Buildings*. Curt B. Haselton, Abbie B. Liel, Sarah Taylor Lange, and Gregory G. Deierlein. May 2008.

PEER 2007/02 *Campbell-Bozorgnia NGA Ground Motion Relations for the Geometric Mean Horizontal Component of Peak and Spectral Ground Motion Parameters*. Kenneth W. Campbell and Yousef Bozorgnia. May 2007.

PEER 2007/01 *Boore-Atkinson NGA Ground Motion Relations for the Geometric Mean Horizontal Component of Peak and Spectral Ground Motion Parameters*. David M. Boore and Gail M. Atkinson. May 2007.

PEER 2006/12 Societal Implications of Performance-Based Earthquake Engineering. Peter J. May. May 2007.

PEER 2006/11 *Probabilistic Seismic Demand Analysis Using Advanced Ground Motion Intensity Measures, Attenuation Relationships, and Near-Fault Effects*. Polsak Tothong and C. Allin Cornell. March 2007.

PEER 2006/10 *Application of the PEER PBEE Methodology to the I-880 Viaduct*. Sashi Kunnath. February 2007.

PEER 2006/09 *Quantifying Economic Losses from Travel Forgone Following a Large Metropolitan Earthquake*. James Moore, Sungbin Cho, Yue Yue Fan, and Stuart Werner. November 2006.

PEER 2006/08 *Vector-Valued Ground Motion Intensity Measures for Probabilistic Seismic Demand Analysis*. Jack W. Baker and C. Allin Cornell. October 2006.

PEER 2006/07 *Analytical Modeling of Reinforced Concrete Walls for Predicting Flexural and Coupled–Shear-Flexural Responses*. Kutay Orakcal, Leonardo M. Massone, and John W. Wallace. October 2006.

PEER 2006/06 *Nonlinear Analysis of a Soil-Drilled Pier System under Static and Dynamic Axial Loading*. Gang Wang and Nicholas Sitar. November 2006.

PEER 2006/05 *Advanced Seismic Assessment Guidelines.* Paolo Bazzurro, C. Allin Cornell, Charles Menun, Maziar Motahari, and Nicolas Luco. September 2006.

PEER 2006/04 *Probabilistic Seismic Evaluation of Reinforced Concrete Structural Components and Systems*. Tae Hyung Lee and Khalid M. Mosalam. August 2006.

PEER 2006/03 *Performance of Lifelines Subjected to Lateral Spreading.* Scott A. Ashford and Teerawut Juirnarongrit. July 2006.

PEER 2006/02 *Pacific Earthquake Engineering Research Center Highway Demonstration Project.* Anne Kiremidjian, James Moore, Yue Yue Fan, Nesrin Basoz, Ozgur Yazali, and Meredith Williams. April 2006.

PEER 2006/01 *Bracing Berkeley. A Guide to Seismic Safety on the UC Berkeley Campus.* Mary C. Comerio, Stephen Tobriner, and Ariane Fehrenkamp. January 2006.

PEER 2005/17 *Earthquake Simulation Tests on Reducing Residual Displacements of Reinforced Concrete Bridges.* Junichi Sakai, Stephen A Mahin, and Andres Espinoza. December 2005.

PEER 2005/16 *Seismic Response and Reliability of Electrical Substation Equipment and Systems.* Junho Song, Armen Der Kiureghian, and Jerome L. Sackman. April 2006.

PEER 2005/15 *CPT-Based Probabilistic Assessment of Seismic Soil Liquefaction Initiation.* R. E. S. Moss, R. B. Seed, R. E. Kayen, J. P. Stewart, and A. Der Kiureghian. April 2006.

PEER 2005/14 *Workshop on Modeling of Nonlinear Cyclic Load-Deformation Behavior of Shallow Foundations.* Bruce L. Kutter, Geoffrey Martin, Tara Hutchinson, Chad Harden, Sivapalan Gajan, and Justin Phalen. March 2006.

PEER 2005/13 *Stochastic Characterization and Decision Bases under Time-Dependent Aftershock Risk in Performance-Based Earthquake Engineering*. Gee Liek Yeo and C. Allin Cornell. July 2005.

PEER 2005/12 *PEER Testbed Study on a Laboratory Building: Exercising Seismic Performance Assessment.* Mary C. Comerio, Editor. November 2005.

PEER 2005/11 *Van Nuys Hotel Building Testbed Report: Exercising Seismic Performance Assessment.* Helmut Krawinkler, Editor. October 2005.

PEER 2005/10 *First NEES/E-Defense Workshop on Collapse Simulation of Reinforced Concrete Building Structures.* September 2005.

PEER 2005/09 *Test Applications of Advanced Seismic Assessment Guidelines.* Joe Maffei, Karl Telleen, Danya Mohr, William Holmes, and Yuki Nakayama. August 2006.

PEER 2005/08 *Damage Accumulation in Lightly Confined Reinforced Concrete Bridge Columns.* R. Tyler Ranf, Jared M. Nelson, Zach Price, Marc O. Eberhard, and John F. Stanton. April 2006.

PEER 2005/07 *Experimental and Analytical Studies on the Seismic Response of Freestanding and Anchored Laboratory Equipment.* Dimitrios Konstantinidis and Nicos Makris. January 2005.

PEER 2005/06 *Global Collapse of Frame Structures under Seismic Excitations*. Luis F. Ibarra and Helmut Krawinkler. September 2005.

PEER 2005//05 *Performance Characterization of Bench- and Shelf-Mounted Equipment.* Samit Ray Chaudhuri and Tara C. Hutchinson. May 2006.

PEER 2005/04 *Numerical Modeling of the Nonlinear Cyclic Response of Shallow Foundations.* Chad Harden, Tara Hutchinson, Geoffrey R. Martin, and Bruce L. Kutter. August 2005.

PEER 2005/03 *A Taxonomy of Building Components for Performance-Based Earthquake Engineering.* Keith A. Porter. September 2005.

PEER 2005/02 *Fragility Basis for California Highway Overpass Bridge Seismic Decision Making*. Kevin R. Mackie and Božidar Stojadinović. June 2005.

PEER 2005/01 *Empirical Characterization of Site Conditions on Strong Ground Motion.* Jonathan P. Stewart, Yoojoong Choi, and Robert W. Graves. June 2005.

PEER 2004/09 *Electrical Substation Equipment Interaction: Experimental Rigid Conductor Studies.* Christopher Stearns and André Filiatrault. February 2005.

PEER 2004/08 *Seismic Qualification and Fragility Testing of Line Break 550-kV Disconnect Switches.* Shakhzod M. Takhirov, Gregory L. Fenves, and Eric Fujisaki. January 2005.

PEER 2004/07 *Ground Motions for Earthquake Simulator Qualification of Electrical Substation Equipment.* Shakhzod M. Takhirov, Gregory L. Fenves, Eric Fujisaki, and Don Clyde. January 2005.

PEER 2004/06 *Performance-Based Regulation and Regulatory Regimes.* Peter J. May and Chris Koski. September 2004.

PEER 2004/05 *Performance-Based Seismic Design Concepts and Implementation: Proceedings of an International Workshop.* Peter Fajfar and Helmut Krawinkler, Editors. September 2004.

PEER 2004/04 *Seismic Performance of an Instrumented Tilt-up Wall Building.* James C. Anderson and Vitelmo V. Bertero. July 2004.

PEER 2004/03 *Evaluation and Application of Concrete Tilt-up Assessment Methodologies.* Timothy Graf and James O. Malley. October 2004.

PEER 2004/02 *Analytical Investigations of New Methods for Reducing Residual Displacements of Reinforced Concrete Bridge Columns.* Junichi Sakai and Stephen A. Mahin. August 2004.

PEER 2004/01 *Seismic Performance of Masonry Buildings and Design Implications.* Kerri Anne Taeko Tokoro, James C. Anderson, and Vitelmo V. Bertero. February 2004.

PEER 2003/18 *Performance Models for Flexural Damage in Reinforced Concrete Columns.* Michael Berry and Marc Eberhard. August 2003.

PEER 2003/17 *Predicting Earthquake Damage in Older Reinforced Concrete Beam-Column Joints.* Catherine Pagni and Laura Lowes. October 2004.

PEER 2003/16 *Seismic Demands for Performance-Based Design of Bridges.* Kevin Mackie and Božidar Stojadinović. August 2003.

PEER 2003/15 *Seismic Demands for Nondeteriorating Frame Structures and Their Dependence on Ground Motions.* Ricardo Antonio Medina and Helmut Krawinkler. May 2004.

PEER 2003/14 *Finite Element Reliability and Sensitivity Methods for Performance-Based Earthquake Engineering*. Terje Haukaas and Armen Der Kiureghian. April 2004.

PEER 2003/13 *Effects of Connection Hysteretic Degradation on the Seismic Behavior of Steel Moment-Resisting Frames.* Janise E. Rodgers and Stephen A. Mahin. March 2004.

PEER 2003/12 *Implementation Manual for the Seismic Protection of Laboratory Contents: Format and Case Studies*. William T. Holmes and Mary C. Comerio. October 2003.

PEER 2003/11 *Fifth U.S.-Japan Workshop on Performance-Based Earthquake Engineering Methodology for Reinforced Concrete Building Structures*. February 2004.

PEER 2003/10 *A Beam-Column Joint Model for Simulating the Earthquake Response of Reinforced Concrete Frames.* Laura N. Lowes, Nilanjan Mitra, and Arash Altoontash. February 2004.

PEER 2003/09 *Sequencing Repairs after an Earthquake: An Economic Approach.* Marco Casari and Simon J. Wilkie. April 2004.

PEER 2003/08 *A Technical Framework for Probability-Based Demand and Capacity Factor Design (DCFD) Seismic Formats*. Fatemeh Jalayer and C. Allin Cornell. November 2003.

PEER 2003/07 *Uncertainty Specification and Propagation for Loss Estimation Using FOSM Methods.* Jack W. Baker and C. Allin Cornell. September 2003.

PEER 2003/06 *Performance of Circular Reinforced Concrete Bridge Columns under Bidirectional Earthquake Loading*. Mahmoud M. Hachem, Stephen A. Mahin, and Jack P. Moehle. February 2003.

PEER 2003/05 *Response Assessment for Building-Specific Loss Estimation.* Eduardo Miranda and Shahram Taghavi. September 2003.

PEER 2003/04 *Experimental Assessment of Columns with Short Lap Splices Subjected to Cyclic Loads*. Murat Melek, John W. Wallace, and Joel Conte. April 2003.

PEER 2003/03 *Probabilistic Response Assessment for Building-Specific Loss Estimation*. Eduardo Miranda and Hesameddin Aslani. September 2003.

PEER 2003/02 *Software Framework for Collaborative Development of Nonlinear Dynamic Analysis Program*. Jun Peng and Kincho H. Law. September 2003.

PEER 2003/01 *Shake Table Tests and Analytical Studies on the Gravity Load Collapse of Reinforced Concrete Frames.* Kenneth John Elwood and Jack P. Moehle. November 2003.

PEER 2002/24 *Performance of Beam to Column Bridge Joints Subjected to a Large Velocity Pulse.* Natalie Gibson, André Filiatrault, and Scott A. Ashford. April 2002.

PEER 2002/23 *Effects of Large Velocity Pulses on Reinforced Concrete Bridge Columns.* Greg L. Orozco and Scott A. Ashford. April 2002.

PEER 2002/22 *Characterization of Large Velocity Pulses for Laboratory Testing.* Kenneth E. Cox and Scott A. Ashford. April 2002.

PEER 2002/21 *Fourth U.S.-Japan Workshop on Performance-Based Earthquake Engineering Methodology for Reinforced Concrete Building Structures*. December 2002.

PEER 2002/20 *Barriers to Adoption and Implementation of PBEE Innovations.* Peter J. May. August 2002.

PEER 2002/19 *Economic-Engineered Integrated Models for Earthquakes: Socioeconomic Impacts.* Peter Gordon, James E. Moore II, and Harry W. Richardson. July 2002.

PEER 2002/18 *Assessment of Reinforced Concrete Building Exterior Joints with Substandard Details.* Chris P. Pantelides, Jon Hansen, Justin Nadauld, and Lawrence D. Reaveley. May 2002.

PEER 2002/17 *Structural Characterization and Seismic Response Analysis of a Highway Overcrossing Equipped with Elastomeric Bearings and Fluid Dampers: A Case Study*. Nicos Makris and Jian Zhang. November 2002.

PEER 2002/16 *Estimation of Uncertainty in Geotechnical Properties for Performance-Based Earthquake Engineering*. Allen L. Jones, Steven L. Kramer, and Pedro Arduino. December 2002.

PEER 2002/15 *Seismic Behavior of Bridge Columns Subjected to Various Loading Patterns*. Asadollah Esmaeily-Gh. and Yan Xiao. December 2002.

PEER 2002/14 *Inelastic Seismic Response of Extended Pile Shaft Supported Bridge Structures.* T.C. Hutchinson, R.W. Boulanger, Y.H. Chai, and I.M. Idriss. December 2002.

PEER 2002/13 *Probabilistic Models and Fragility Estimates for Bridge Components and Systems.* Paolo Gardoni, Armen Der Kiureghian, and Khalid M. Mosalam. June 2002.

PEER 2002/12 *Effects of Fault Dip and Slip Rake on Near-Source Ground Motions: Why Chi-Chi Was a Relatively Mild M7.6 Earthquake*. Brad T. Aagaard, John F. Hall, and Thomas H. Heaton. December 2002.

PEER 2002/11 *Analytical and Experimental Study of Fiber-Reinforced Strip Isolators*. James M. Kelly and Shakhzod M. Takhirov. September 2002.

PEER 2002/10 *Centrifuge Modeling of Settlement and Lateral Spreading with Comparisons to Numerical Analyses***.** Sivapalan Gajan and Bruce L. Kutter. January 2003.

PEER 2002/09 *Documentation and Analysis of Field Case Histories of Seismic Compression during the 1994 Northridge, California, Earthquake*. Jonathan P. Stewart, Patrick M. Smith, Daniel H. Whang, and Jonathan D. Bray. October 2002.

PEER 2002/08 *Component Testing, Stability Analysis and Characterization of Buckling-Restrained Unbonded Braces^{TM}*. Cameron Black, Nicos Makris, and Ian Aiken. September 2002.

PEER 2002/07 *Seismic Performance of Pile-Wharf Connections.* Charles W. Roeder, Robert Graff, Jennifer Soderstrom, and Jun Han Yoo. December 2001.

PEER 2002/06 *The Use of Benefit-Cost Analysis for Evaluation of Performance-Based Earthquake Engineering Decisions*. Richard O. Zerbe and Anthony Falit-Baiamonte. September 2001.

PEER 2002/05 *Guidelines, Specifications, and Seismic Performance Characterization of Nonstructural Building Components and Equipment*. André Filiatrault, Constantin Christopoulos, and Christopher Stearns. September 2001.

PEER 2002/04 *Consortium of Organizations for Strong-Motion Observation Systems and the Pacific Earthquake Engineering Research Center Lifelines Program: Invited Workshop on Archiving and Web Dissemination of Geotechnical Data, 4–5 October 2001*. September 2002.

PEER 2002/03 *Investigation of Sensitivity of Building Loss Estimates to Major Uncertain Variables for the Van Nuys Testbed*. Keith A. Porter, James L. Beck, and Rustem V. Shaikhutdinov. August 2002.

PEER 2002/02 *The Third U.S.-Japan Workshop on Performance-Based Earthquake Engineering Methodology for Reinforced Concrete Building Structures*. July 2002.

PEER 2002/01 *Nonstructural Loss Estimation: The UC Berkeley Case Study.* Mary C. Comerio and John C. Stallmeyer. December 2001.

PEER 2001/16 *Statistics of SDF-System Estimate of Roof Displacement for Pushover Analysis of Buildings.* Anil K. Chopra, Rakesh K. Goel, and Chatpan Chintanapakdee. December 2001.

PEER 2001/15 *Damage to Bridges during the 2001 Nisqually Earthquake.* R. Tyler Ranf, Marc O. Eberhard, and Michael P. Berry. November 2001.

PEER 2001/14 *Rocking Response of Equipment Anchored to a Base Foundation.* Nicos Makris and Cameron J. Black. September 2001.

PEER 2001/13 *Modeling Soil Liquefaction Hazards for Performance-Based Earthquake Engineering*. Steven L. Kramer and Ahmed-W. Elgamal. February 2001.

PEER 2001/12 *Development of Geotechnical Capabilities in OpenSees*. Boris Jeremić. September 2001.

PEER 2001/11 *Analytical and Experimental Study of Fiber-Reinforced Elastomeric Isolators*. James M. Kelly and Shakhzod M. Takhirov. September 2001.

PEER 2001/10 *Amplification Factors for Spectral Acceleration in Active Regions.* Jonathan P. Stewart, Andrew H. Liu, Yoojoong Choi, and Mehmet B. Baturay. December 2001.

PEER 2001/09 *Ground Motion Evaluation Procedures for Performance-Based Design.* Jonathan P. Stewart, Shyh-Jeng Chiou, Jonathan D. Bray, Robert W. Graves, Paul G. Somerville, and Norman A. Abrahamson. September 2001.

PEER 2001/08 *Experimental and Computational Evaluation of Reinforced Concrete Bridge Beam-Column Connections for Seismic Performance*. Clay J. Naito, Jack P. Moehle, and Khalid M. Mosalam. November 2001.

PEER 2001/07 *The Rocking Spectrum and the Shortcomings of Design Guidelines.* Nicos Makris and Dimitrios Konstantinidis. August 2001.

PEER 2001/06 *Development of an Electrical Substation Equipment Performance Database for Evaluation of Equipment Fragilities*. Thalia Agnanos. April 1999.

PEER 2001/05 *Stiffness Analysis of Fiber-Reinforced Elastomeric Isolators.* Hsiang-Chuan Tsai and James M. Kelly. May 2001.

PEER 2001/04 *Organizational and Societal Considerations for Performance-Based Earthquake Engineering*. Peter J. May. April 2001.

PEER 2001/03 *A Modal Pushover Analysis Procedure to Estimate Seismic Demands for Buildings: Theory and Preliminary Evaluation*. Anil K. Chopra and Rakesh K. Goel. January 2001.

PEER 2001/02 *Seismic Response Analysis of Highway Overcrossings Including Soil-Structure Interaction*. Jian Zhang and Nicos Makris. March 2001.

PEER 2001/01 *Experimental Study of Large Seismic Steel Beam-to-Column Connections.* Egor P. Popov and Shakhzod M. Takhirov. November 2000.

PEER 2000/10 *The Second U.S.-Japan Workshop on Performance-Based Earthquake Engineering Methodology for Reinforced Concrete Building Structures*. March 2000.

PEER 2000/09 *Structural Engineering Reconnaissance of the August 17, 1999 Earthquake: Kocaeli (Izmit), Turkey.* Halil Sezen, Kenneth J. Elwood, Andrew S. Whittaker, Khalid Mosalam, John J. Wallace, and John F. Stanton. December 2000.

PEER 2000/08 *Behavior of Reinforced Concrete Bridge Columns Having Varying Aspect Ratios and Varying Lengths of Confinement*. Anthony J. Calderone, Dawn E. Lehman, and Jack P. Moehle. January 2001.

PEER 2000/07 *Cover-Plate and Flange-Plate Reinforced Steel Moment-Resisting Connections.* Taejin Kim, Andrew S. Whittaker, Amir S. Gilani, Vitelmo V. Bertero, and Shakhzod M. Takhirov. September 2000.

PEER 2000/06 *Seismic Evaluation and Analysis of 230-kV Disconnect Switches.* Amir S. J. Gilani, Andrew S. Whittaker, Gregory L. Fenves, Chun-Hao Chen, Henry Ho, and Eric Fujisaki. July 2000.

PEER 2000/05 *Performance-Based Evaluation of Exterior Reinforced Concrete Building Joints for Seismic Excitation*. Chandra Clyde, Chris P. Pantelides, and Lawrence D. Reaveley. July 2000.

PEER 2000/04 *An Evaluation of Seismic Energy Demand: An Attenuation Approach*. Chung-Che Chou and Chia-Ming Uang. July 1999.

PEER 2000/03 *Framing Earthquake Retrofitting Decisions: The Case of Hillside Homes in Los Angeles.* Detlof von Winterfeldt, Nels Roselund, and Alicia Kitsuse. March 2000.

PEER 2000/02 *U.S.-Japan Workshop on the Effects of Near-Field Earthquake Shaking*. Andrew Whittaker, Editor. July 2000.

PEER 2000/01 *Further Studies on Seismic Interaction in Interconnected Electrical Substation Equipment.* Armen Der Kiureghian, Kee-Jeung Hong, and Jerome L. Sackman. November 1999.

PEER 1999/14 *Seismic Evaluation and Retrofit of 230-kV Porcelain Transformer Bushings*. Amir S. Gilani, Andrew S. Whittaker, Gregory L. Fenves, and Eric Fujisaki. December 1999.

PEER 1999/13 *Building Vulnerability Studies: Modeling and Evaluation of Tilt-up and Steel Reinforced Concrete Buildings*. John W. Wallace, Jonathan P. Stewart, and Andrew S. Whittaker, Editors. December 1999.

PEER 1999/12 *Rehabilitation of Nonductile RC Frame Building Using Encasement Plates and Energy-Dissipating Devices*. Mehrdad Sasani, Vitelmo V. Bertero, James C. Anderson. December 1999.

PEER 1999/11 *Performance Evaluation Database for Concrete Bridge Components and Systems under Simulated Seismic Loads*. Yael D. Hose and Frieder Seible. November 1999.

PEER 1999/10 *U.S.-Japan Workshop on Performance-Based Earthquake Engineering Methodology for Reinforced Concrete Building Structures*. December 1999.

PEER 1999/09 *Performance Improvement of Long Period Building Structures Subjected to Severe Pulse-Type Ground Motions*. James C. Anderson, Vitelmo V. Bertero, and Raul Bertero. October 1999.

PEER 1999/08 *Envelopes for Seismic Response Vectors.* Charles Menun and Armen Der Kiureghian. July 1999.

PEER 1999/07 *Documentation of Strengths and Weaknesses of Current Computer Analysis Methods for Seismic Performance of Reinforced Concrete Members*. William F. Cofer. November 1999.

PEER 1999/06 *Rocking Response and Overturning of Anchored Equipment under Seismic Excitations*. Nicos Makris and Jian Zhang. November 1999.

PEER 1999/05 *Seismic Evaluation of 550 kV Porcelain Transformer Bushings.* Amir S. Gilani, Andrew S. Whittaker, Gregory L. Fenves, and Eric Fujisaki. October 1999.

PEER 1999/04 *Adoption and Enforcement of Earthquake Risk-Reduction Measures.* Peter J. May, Raymond J. Burby, T. Jens Feeley, and Robert Wood. August 1999.

PEER 1999/03 *Task 3 Characterization of Site Response General Site Categories*. Adrian Rodriguez-Marek, Jonathan D. Bray and Norman Abrahamson. February 1999.

PEER 1999/02 *Capacity-Demand-Diagram Methods for Estimating Seismic Deformation of Inelastic Structures: SDF Systems*. Anil K. Chopra and Rakesh Goel. April 1999.

PEER 1999/01 *Interaction in Interconnected Electrical Substation Equipment Subjected to Earthquake Ground Motions*. Armen Der Kiureghian, Jerome L. Sackman, and Kee-Jeung Hong. February 1999.

PEER 1998/08 *Behavior and Failure Analysis of a Multiple-Frame Highway Bridge in the 1994 Northridge Earthquake*. Gregory L. Fenves and Michael Ellery. December 1998.

PEER 1998/07 *Empirical Evaluation of Inertial Soil-Structure Interaction Effects.* Jonathan P. Stewart, Raymond B. Seed, and Gregory L. Fenves. November 1998.

PEER 1998/06 *Effect of Damping Mechanisms on the Response of Seismic Isolated Structures*. Nicos Makris and Shih-Po Chang. November 1998.

PEER 1998/05 *Rocking Response and Overturning of Equipment under Horizontal Pulse-Type Motions*. Nicos Makris and Yiannis Roussos. October 1998.

PEER 1998/04 *Pacific Earthquake Engineering Research Invitational Workshop Proceedings, May 14–15, 1998: Defining the Links between Planning, Policy Analysis, Economics and Earthquake Engineering*. Mary Comerio and Peter Gordon. September 1998.

PEER 1998/03 *Repair/Upgrade Procedures for Welded Beam to Column Connections*. James C. Anderson and Xiaojing Duan. May 1998.

PEER 1998/02 *Seismic Evaluation of 196 kV Porcelain Transformer Bushings.* Amir S. Gilani, Juan W. Chavez, Gregory L. Fenves, and Andrew S. Whittaker. May 1998.

PEER 1998/01 *Seismic Performance of Well-Confined Concrete Bridge Columns.* Dawn E. Lehman and Jack P. Moehle. December 2000.

PEER REPORTS: ONE HUNDRED SERIES

PEER 2012/103 *Performance-Based Seismic Demand Assessment of Concentrically Braced Steel Frame Buildings.* Chui-Hsin Chen and Stephen A. Mahin. December 2012.

PEER 2012/102 *Procedure to Restart an Interrupted Hybrid Simulation: Addendum to PEER Report 2010/103.* Vesna Terzic and Bozidar Stojadinovic. October 2012.

PEER 2012/101 *Mechanics of Fiber Reinforced Bearings.* James M. Kelly and Andrea Calabrese. February 2012.

PEER 2011/107 *Nonlinear Site Response and Seismic Compression at Vertical Array Strongly Shaken by 2007 Niigata-ken Chuetsu-oki Earthquake.* Eric Yee, Jonathan P. Stewart, and Kohji Tokimatsu. December 2011.

PEER 2011/106 *Self Compacting Hybrid Fiber Reinforced Concrete Composites for Bridge Columns.* Pardeep Kumar, Gabriel Jen, William Trono, Marios Panagiotou, and Claudia Ostertag. September 2011.

PEER 2011/105 *Stochastic Dynamic Analysis of Bridges Subjected to Spacially Varying Ground Motions.* Katerina Konakli and Armen Der Kiureghian. August 2011.

PEER 2011/104 *Design and Instrumentation of the 2010 E-Defense Four-Story Reinforced Concrete and Post-Tensioned Concrete Buildings.* Takuya Nagae, Kenichi Tahara, Taizo Matsumori, Hitoshi Shiohara, Toshimi Kabeyasawa, Susumu Kono, Minehiro Nishiyama (Japanese Research Team) and John Wallace, Wassim Ghannoum, Jack Moehle, Richard Sause, Wesley Keller, Zeynep Tuna (U.S. Research Team). June 2011.

PEER 2011/103 *In-Situ Monitoring of the Force Output of Fluid Dampers: Experimental Investigation.* Dimitrios Konstantinidis, James M. Kelly, and Nicos Makris. April 2011.

PEER 2011/102 *Ground-Motion Prediction Equations 1964–2010.* John Douglas. April 2011.

PEER 2011/101 *Report of the Eighth Planning Meeting of NEES/E-Defense Collaborative Research on Earthquake Engineering.* Convened by the Hyogo Earthquake Engineering Research Center (NIED), NEES Consortium, Inc. February 2011.

PEER 2010/111 *Modeling and Acceptance Criteria for Seismic Design and Analysis of Tall Buildings.* Task 7 Report for the Tall Buildings Initiative - Published jointly by the Applied Technology Council. October 2010.

PEER 2010/110 *Seismic Performance Assessment and Probabilistic Repair Cost Analysis of Precast Concrete Cladding Systems for Multistory Buildlings.* Jeffrey P. Hunt and Božidar Stojadinovic. November 2010.

PEER 2010/109 *Report of the Seventh Joint Planning Meeting of NEES/E-Defense Collaboration on Earthquake Engineering. Held at the E-Defense, Miki, and Shin-Kobe, Japan, September 18–19, 2009.* August 2010.

PEER 2010/108 *Probabilistic Tsunami Hazard in California.* Hong Kie Thio, Paul Somerville, and Jascha Polet, preparers. October 2010.

PEER 2010/107 *Performance and Reliability of Exposed Column Base Plate Connections for Steel Moment-Resisting Frames.* Ady Aviram, Božidar Stojadinovic, and Armen Der Kiureghian. August 2010.

PEER 2010/106 *Verification of Probabilistic Seismic Hazard Analysis Computer Programs.* Patricia Thomas, Ivan Wong, and Norman Abrahamson. May 2010.

PEER 2010/105 *Structural Engineering Reconnaissance of the April 6, 2009, Abruzzo, Italy, Earthquake, and Lessons Learned.* M. Selim Günay and Khalid M. Mosalam. April 2010.

PEER 2010/104 *Simulating the Inelastic Seismic Behavior of Steel Braced Frames, Including the Effects of Low-Cycle Fatigue.* Yuli Huang and Stephen A. Mahin. April 2010.

PEER 2010/103 *Post-Earthquake Traffic Capacity of Modern Bridges in California.* Vesna Terzic and Božidar Stojadinović. March 2010.

PEER 2010/102 *Analysis of Cumulative Absolute Velocity (CAV) and JMA Instrumental Seismic Intensity (I_{JMA}) Using the PEER–NGA Strong Motion Database.* Kenneth W. Campbell and Yousef Bozorgnia. February 2010.

PEER 2010/101 *Rocking Response of Bridges on Shallow Foundations.* Jose A. Ugalde, Bruce L. Kutter, and Boris Jeremic. April 2010.

PEER 2009/109 *Simulation and Performance-Based Earthquake Engineering Assessment of Self-Centering Post-Tensioned Concrete Bridge Systems.* Won K. Lee and Sarah L. Billington. December 2009.

PEER 2009/108 *PEER Lifelines Geotechnical Virtual Data Center.* J. Carl Stepp, Daniel J. Ponti, Loren L. Turner, Jennifer N. Swift, Sean Devlin, Yang Zhu, Jean Benoit, and John Bobbitt. September 2009.

PEER 2009/107 *Experimental and Computational Evaluation of Current and Innovative In-Span Hinge Details in Reinforced Concrete Box-Girder Bridges: Part 2: Post-Test Analysis and Design Recommendations.* Matias A. Hube and Khalid M. Mosalam. December 2009.

PEER 2009/106 *Shear Strength Models of Exterior Beam-Column Joints without Transverse Reinforcement.* Sangjoon Park and Khalid M. Mosalam. November 2009.

PEER 2009/105 *Reduced Uncertainty of Ground Motion Prediction Equations through Bayesian Variance Analysis.* Robb Eric S. Moss. November 2009.

PEER 2009/104 *Advanced Implementation of Hybrid Simulation.* Andreas H. Schellenberg, Stephen A. Mahin, Gregory L. Fenves. November 2009.

PEER 2009/103 *Performance Evaluation of Innovative Steel Braced Frames.* T. Y. Yang, Jack P. Moehle, and Božidar Stojadinovic. August 2009.

PEER 2009/102 *Reinvestigation of Liquefaction and Nonliquefaction Case Histories from the 1976 Tangshan Earthquake.* Robb Eric Moss, Robert E. Kayen, Liyuan Tong, Songyu Liu, Guojun Cai, and Jiaer Wu. August 2009.

PEER 2009/101 *Report of the First Joint Planning Meeting for the Second Phase of NEES/E-Defense Collaborative Research on Earthquake Engineering.* Stephen A. Mahin et al. July 2009.

PEER 2008/104 *Experimental and Analytical Study of the Seismic Performance of Retaining Structures.* Linda Al Atik and Nicholas Sitar. January 2009.

PEER 2008/103 *Experimental and Computational Evaluation of Current and Innovative In-Span Hinge Details in Reinforced Concrete Box-Girder Bridges. Part 1: Experimental Findings and Pre-Test Analysis.* Matias A. Hube and Khalid M. Mosalam. January 2009.

PEER 2008/102 *Modeling of Unreinforced Masonry Infill Walls Considering In-Plane and Out-of-Plane Interaction.* Stephen Kadysiewski and Khalid M. Mosalam. January 2009.

PEER 2008/101 *Seismic Performance Objectives for Tall Buildings.* William T. Holmes, Charles Kircher, William Petak, and Nabih Youssef. August 2008.

PEER 2007/101 *Generalized Hybrid Simulation Framework for Structural Systems Subjected to Seismic Loading*. Tarek Elkhoraibi and Khalid M. Mosalam. July 2007.

PEER 2007/100 *Seismic Evaluation of Reinforced Concrete Buildings Including Effects of Masonry Infill Walls*. Alidad Hashemi and Khalid M. Mosalam. July 2007.

The Pacific Earthquake Engineering Research Center (PEER) is a multi-institutional research and education center with headquarters at the University of California, Berkeley. Investigators from over 20 universities, several consulting companies, and researchers at various state and federal government agencies contribute to research programs focused on performance-based earthquake engineering.

These research programs aim to identify and reduce the risks from major earthquakes to life safety and to the economy by including research in a wide variety of disciplines including structural and geotechnical engineering, geology/seismology, lifelines, transportation, architecture, economics, risk management, and public policy.

PEER is supported by federal, state, local, and regional agencies, together with industry partners.

PEER Core Institutions

University of California, Berkeley (Lead Institution)
California Institute of Technology
Oregon State University
Stanford University
University of California, Davis
University of California, Irvine
University of California, Los Angeles
University of California, San Diego
University of Nevada, Reno
University of Southern California
University of Washington

PEER reports can be ordered at https://peer.berkeley.edu/peer-reports or by contacting

Pacific Earthquake Engineering Research Center
University of California, Berkeley
325 Davis Hall, Mail Code 1792
Berkeley, CA 94720-1792
Tel: 510-642-3437
Email: peer_center@berkeley.edu

ISSN 1547-0587X